

Evaluating Spatial and Seasonal Variability of Wetlands in Eastern Ontario
using Remote Sensing and GIS

By

Laura Dingle Robertson, B.A. (Hons.), M.Sc.

A thesis submitted to
the Faculty of Graduate and Postdoctoral Affairs
in partial fulfillment of the requirements of the degree of

Doctor of Philosophy

Department of Geography and Environmental Studies

Carleton University

Ottawa, Ontario

May, 2014

© Laura Dingle Robertson, 2014

ABSTRACT

Wetlands provide many ecological services, but are under threat from climate change and land modification amongst other stressors. The Ontario Ministry of Natural Resources (OMNR) currently uses the field-based Ontario Wetland Evaluation System (OWES) to assign scores to wetlands for planning and conservation purposes. These evaluations have been primarily from the field observer's viewpoint, but were often augmented using analog air photo and/or digital ortho-photo interpretation. With such an approach overall spatial and temporal wetland dynamics were often overlooked or under represented. This research evaluated attributes in four wetland complexes through three seasons using remote sensing data. Landsat 5 Thematic Mapper (TM, 30m) Radarsat-2 (8m), and WorldView-2 (0.5-2m) imagery were acquired, and several types of image metrics (e.g. vegetation indices, texture, and object metrics) were evaluated in mapping 14 OWES attributes. Differences were found in overall and specific class related accuracies for all 14 attributes of interest depending upon time of year, location, and/or data used. Eight attributes were successfully assessed using existing data or data developed using the methods of this research. Scores derived for four of those attributes were equivalent to the OWES field-measured scores. Some general technical conclusions from the research were that high resolution optical imagery provided higher overall accuracies for most attributes of interest. Coarse resolution optical imagery had higher overall accuracy for the attribute Open Water Type. Radar-based variables did not improve overall accuracies, but the addition of these variables to the optical imagery object-based image analysis (OBIA) improved some individual class accuracies. With respect to season of image acquisition, spring or summer imagery produced the highest accuracies. These results support an overview perspective with a top-down investigative

approach for wetlands analysis in that they expose the inconsistencies and some consistencies in results between sites, between imagery types and/or at different times of year.

ACKNOWLEDGEMENTS

This research was funded by the Ontario Ministry of Natural Resources (C. Davies) and by an NSERC Discovery Grant to D. King. Radarsat-2 imagery and additional student funding were provided by the Landscape Science and Technology Division of Environment Canada.

My many thanks are given to Dr. Douglas J. King for his advice and guidance. Thanks for sticking with me and letting me ‘enjoy’ the process, because I’ve always said it’s about the journey; I’m happy to finally have arrived! Further thanks are given to my committee, Dr. Chris Davies, Dr. Murray Richardson, Dr. Scott Mitchell, and Dr. Sean Carey for their insight and dedication to this work.

Fieldwork would not have been possible without the assistance of Blair Kennedy, Valerie Torontow, Chris Czerwinski, Victoria Putinski and Brook Beaulieu. Thank you for the support and camaraderie, especially in some really uncomfortable places.

To my friends and family thank you for your ongoing support and encouragement. Thank you to Alistair Robertson for your continued belief in me and for all those nights up with the boys. You’ve once again shown that you are my greatest friend and biggest supporter.

“It’s been a hard day’s night, and I’ve been working like a dog...”

Lennon/McCartney

TABLE OF CONTENTS

ABSTRACT	ii
ACKNOWLEDGEMENTS	iv
TABLE OF CONTENTS	v
LIST OF TABLES	ix
LIST OF FIGURES.....	xiv
LIST OF APPENDICES	xxii
LIST OF ACRONYMS.....	xxiii
1.0 Introduction	1
1.1 Research goal.....	3
1.2 Research objectives.....	4
1.3 Research contributions.....	4
1.4 Thesis structure	5
2.0 Background	8
2.1 Functional description of wetlands	8
2.2 Wetlands of Ontario	11
2.2.1 History of wetlands in Ontario	11
2.2.2 OMNR role in wetland management.....	12
2.3 Methods to evaluate wetlands	13
2.3.1 Ontario wetland inventory schemes.....	13
2.3.2 Ontario wetland evaluations	15
2.4 Wetland attributes typically measured in the field that have shown potential for estimation using remote sensing.....	18
2.5 Scale.....	22
2.5.1 The pattern-attribute-process relationship: influences of scale.....	24
2.6 Remote sensing of wetlands.....	24
2.6.1 Previous reviews of wetland remote sensing.....	24
2.6.2 GIS analyses of wetlands.....	42
2.6.3 Sensors used for wetland attribute analysis pertinent to this research	44
2.7 Remote sensing of hydrology and forestry as it relates to wetland research.....	49
2.7.1 Hydrology.....	49
2.7.2 Forestry.....	50
2.8 Remote sensing methods for the mapping the 14 selected OWES attributes.....	51
2.8.1 Object-based image analysis	52
2.8.2 Linear Spectral Unmixing (LSU)	57
2.8.3 Classification of remote sensing imagery	60
2.8.4 Radar imagery analyses.....	64
2.9 Selection of OWES attributes for image modelling and classification	73
2.9.1 Wetland Type (Biological and Special Feature components).....	81

2.9.2	Vegetation Community Forms (VCFs, Biological component)	83
2.9.3	Open Water Type (Biological component)	85
2.9.4	Inundation Extent (Hydrologic component)	85
2.9.5	Number of Wetland Types (Biological component)	89
2.9.6	Diversity of Surrounding Habitat (Biological component)	90
2.9.7	Proximity to Other Wetlands (Biological component)	90
2.9.8	Wetland Size (Biological component)	91
2.9.9	Hunting (Social component)	92
2.9.10	Ownership Patterns (Social component)	93
2.9.11	Wetland Basin Size (Hydrologic component)	93
2.9.12	Rarity of Wetland in the Landscape (Special Features component)	94
2.9.13	Anthropogenic Disturbance (Social component)	96
3.0	Study areas and remotely sensed imagery	98
3.1	Study region and study areas	98
3.1.1	Selection of wetland complexes	100
3.2	Remotely sensed imagery	112
3.2.1	WorldView-2	113
3.2.2	Landsat TM 5	114
3.2.3	Radarsat-2	115
4.0	Methods	117
4.1	Methods to segment, classify, and map Wetland Type using optical and radar imagery	117
4.1.1	Field analysis for Wetland Type	119
4.1.2	OBIA using spring 2010 WorldView-2 imagery	120
4.1.3	OBIA using 2010 spring Landsat 5 TM imagery	127
4.1.4	Radarsat-2 image processing, classification and analyses for Wetland Type	130
4.1.5	Wetland Type classification accuracy assessment	133
4.2	Methods to segment, classify, and map VCFs using optical and radar imagery	135
4.2.1	Segmentation methods using spring 2010 WorldView-2 imagery	135
4.2.2	Classification methods using spring 2010 WorldView-2 imagery	136
4.2.3	Segmentation and classification methods using spring 2010 Landsat 5 TM imagery	137
4.2.4	Radarsat-2 image processing and analysis for VCFs	137
4.3	Methods to segment, classify, and map Open Water Types using optical imagery	137
4.4	Methods to segment, classify, and map Inundation Extent using optical imagery	138
4.4.1	Field analysis	139
4.4.2	Semi-variogram analysis of VWC	139
4.4.3	Pixel-based image processing	141
4.5	GIS analysis of derived imagery and existing LIO layers	143
4.5.1	Number of Wetland Types for the Biological component	143
4.5.2	Diversity of Surrounding Habitat for the Biological component	143
4.5.3	Proximity to Other Wetlands for the Biological component	144
4.5.4	Wetland Size for the Biological component	144
4.5.5	Hunting Pattern mapping for the Social component	144
4.5.6	Ownership Patterns for the Social component	144
4.5.7	Wetland Basin Size for the Hydrologic component	145
4.5.8	Rarity of Wetlands and Rarity in Landscape for the Special Feature component	145
4.6	Compare the scores derived from the geo-spatial analysis to the OWES field-based scores	145

4.7	Review of temporal remote sensing data in classification of wetland attributes and analysis of attribute changes over the long term	146
4.7.1	Wetland Type, VCFs, and Open Water Types	146
4.7.2	Inundation Extent	147
4.7.3	Anthropogenic Disturbance	147
5.0	Results	149
5.1	Wetland Types	152
5.1.1	Segmentation and classification of Wetland Type using optical and radar imagery	152
5.1.2	Results from OBIA using spring 2010 Landsat 5 TM imagery for Wetland Type	169
5.1.3	Radarsat-2 image processing, classification and analyses for Wetland Type	176
5.1.4	Summary of main findings for Wetland Type	198
5.2	VCFs	200
5.2.1	VCF classification using OBIA and 2010 spring WorldView-2 imagery	201
5.2.2	VCF classification using OBIA and 2010 spring Landsat 5 TM imagery	205
5.2.3	VCF classification using Radarsat-2 data	207
5.2.4	Summary of main findings for VCF classification	211
5.3	Open Water Type	212
5.3.1	Open Water Type classification using OBIA and 2010 spring WorldView-2 imagery	212
5.3.2	Open Water Type OBIA classification using 2010 spring Landsat 5 TM imagery	216
5.3.3	Summary of main findings for Open Water Type	218
5.4	Inundation Extent	219
5.4.1	Pixel-based analysis of spring 2010 WorldView-2 imagery vegetation index relationships with VWC thresholds as an indicator of Inundation Extent	219
5.4.2	Summary of main findings for Inundation Extent	226
5.5	GIS analysis of derived imagery and existing LIO layers for selected OWES attributes	226
5.5.1	Number of Wetland Types	226
5.5.2	Diversity of Surrounding Habitat	228
5.5.3	Proximity to Other Wetlands	230
5.5.4	Hunting Pattern mapping	232
5.5.5	Ownership Patterns for the Social category	234
5.5.6	Wetland area and basin area measurements for Wetland Attenuation Factor	234
5.5.7	Rarity of Wetlands and Rarity in Landscape for the Special Feature category	235
5.5.8	Summary of main findings of the GIS analysis of maps created in this research and existing LIO layers for OWES attributes	236
5.6	Comparative analyses of wetland attribute scores derived from geo-spatial data, and OWES scores	236
5.6.1	Wetland Type	237
5.6.2	VCFs and Number of VCF	238
5.6.3	Open Water Type	239
5.6.4	Number of Wetland Types	239
5.6.5	Diversity of Surrounding Habitat	240
5.6.6	Proximity to Other Wetlands	240
5.6.7	Wetland Size for the Biological component	241
5.6.8	Hunting Pattern method and Ownership Patterns for the Social component and Wetland Attenuation Factor for the Hydrologic component	243
5.6.9	Rarity of Wetland Type and Rarity in Landscape for the Special Feature category	243

5.6.10	Summary of main findings for the comparison of attribute scores derived from geo-spatial data to OWES scores.....	245
5.7	Assessing seasonal and inter-annual differences in the OWES attributes.....	245
5.7.1	Temporal analysis for Wetland Type	246
5.7.2	Temporal analyses for VCFs	253
5.7.3	Temporal analyses for Open Water Type	259
5.7.4	Temporal analyses for Inundation Extent.....	263
5.8	Two-date temporal comparison of fraction maps as an indicator of Anthropogenic Influence.	267
5.8.1	Summary of the main findings for the two-date temporal comparison of fraction maps ...	271
6.0	Discussion and conclusions.....	273
6.1	Findings and contributions of this research	273
6.1.1	Contributions of the research to wetland and remote sensing science	273
6.1.2	Technical successes and contributions	279
6.1.3	OBIA segmentation for object creation	284
6.1.4	Radar analysis.....	288
6.1.5	Vegetation index thresholding for wet extent mapping	294
6.1.6	GIS thematic map analyses and scoring	294
6.1.7	Temporal analyses	297
6.2	Recommendations.....	300
6.3	Overall limitations of this research	304
6.4	Further research directions	307
6.4.1	Technical research directions	308
6.5	Conclusions.....	309
7.0	References	311
8.0	Appendices	338

LIST OF TABLES

Table 2.1. Wetland Type classifications highlighting the hydrologic, biological and physical/geochemical influences (OWES, 2002).	17
Table 2.2. A synopsis of the types of remote sensing and GIS analyses methods for wetlands in general.	37
Table 2.3. Sensors used for remote sensing of wetlands in this research. MS is multi-spectral, PAN is panchromatic, and TIR is thermal infrared.	45
Table 2.4. OWES components and wetland attributes selected for this research.	74
Table 2.5. A synopsis of the 14 selected OWES attributes, their synonyms in geomatics literature and corresponding remote sensing and GIS methods applied in previous studies.	76
Table 2.6. OWES scoring system for VCFs by Number of Forms (OWES Southern Manual, 2002).	84
Table 2.7. Eight OWES Open Water Types and their associated scores (OWES Southern Manual, 2002).	86
Table 2.8. Connections and scores for measuring the Proximity to Other Wetlands.	91
Table 2.9. Table for size score (Biological Component) (after Table 5 in OWES Southern Manual, 2013).	92
Table 2.10. Scores given for wetland presence within the landscape and by Wetland Type in the three site districts representing the area of interest (after Table 4, OWES Southern Manual, 2002).	94
Table 3.1 Field investigation dates and time spent in the field for the OWES field-based evaluations.	102
Table 3.2. Summary of the four wetlands selected for this research.	102
Table 3.3. Detailed list of the imagery used in this research including season, date acquired and details related to the type of imagery.	112
Table 4.1. Summary of the field sites presented in detail in Appendix B and presented on the Figure 4.3.	120
Table 4.2. Experimental design matrix showing shape/colour and compactness/ smoothness tests implemented after Tian and Chen (2007).	121

Table 4.3. The average and minimum Bhattacharyya Distance separabilities for the class training data.	124
Table 5.1. Summary of the key findings of the results in structural order of this chapter.	149
Table 5.2A. Error matrix for the spring 2010 Loch GarryWorldView-2 and DEM object-based MLC (7-classes).	159
Table 5.2B. Accuracy statistics (%) for the spring 2010 Loch GarryWorldView-2 and DEM OBIA MLC (7-classes).	159
Table 5.3A. Error matrix for the spring 2010 Loch Garry WorldView-2 and DEM object-based MLC (5-classes).	160
Table 5.3B. Accuracy statistics (%) for the spring 2010 Loch Garry WorldView-2 and DEM object-based MLC (5-classes).	161
Table 5.4. Accuracy statistics for 5-class CTA (GINI algorithm) of segmented spring 2010 WorldView-2 imagery and DEM at all study sites.	165
Table 5.5A. Error matrix for the spring 2010 Loch Garry WorldView-2 and DEM object-based GINI CTA (5-classes).	168
Table 5.5B. Accuracy statistics (%) for the spring 2010 Loch Garry WorldView-2 and DEM object-based GINI CTA (5-classes).	168
Table 5.6. Wetland Type accuracies (%) per combination of data type and segmentation (yes/no) for spring Landsat TM imagery. The highest accuracy per site is highlighted in yellow.	171
Table 5.7. Accuracy statistics (%)for Wetland Type CTA classifications using the spring 2010 Landsat TM data and the DEM, original and unmixed, segmented and not segmented, at Marlborough Forest. Highest accuracy was achieved for test 5 (orange highlight). Other highlights of the best and worst results for some classes are described in the text.	174
Table 5.8. Error matrix for the spring 2010 Marlborough Forest Landsat 5 TM GINI CTA of the 5 EM derived fraction maps, no segmentation, no DEM.	175
Table 5.9. Marlborough Forest CTA accuracies (%) utilizing the segmented WorldView-2 imagery (four spectral bands), the DEM, HH and HV images, and Landsat 5 TM unsegmented 5 EM fraction images. Orange highlights the class (Swamp) that improved with the addition of the HH, HV images.	182
Table 5.10. Minimum, maximum and average co- and cross-pol pedestal heights from training areas from the steep incidence angle spring/fall and summer imagery.	192

Table 5.11. Minimum, maximum and average summed co- and cross-pol pedestal heights for samples extracted from the steep incidence angle summer imagery.	194
Table 5.12. Accuracies (%) for Loch Garry utilizing the WorldView-2 imagery (four spectral bands), the DEM, summer CP variables images for a Wishart unsupervised, MLC, and CTA classifiers. Orange highlight shows that the Fen improved with the addition of the CP variables.	199
Table 5.13. CTA accuracies (%) for Number of VCFs for the four sites. Input data were: segmented spring WorldView-2 imagery (four spectral bands) and the DEM. Classes A, B and C represent 1 to 3, 4 to 5, and 6 or more forms, respectively.	203
Table 5.14. CTA accuracy statistics for the VCFs including accuracies (%) for the four sites. Input data were the segmented spring WorldView-2 imagery (four spectral bands) and the DEM (see Section 2.9.2 for descriptions of each class).	206
Table 5.15. Summary of the Landsat CTA accuracy statistics for the 3 form (A, B, C) and VCFs providing accuracies (%) for the four sites. Loch Garry, Mer Bleue Bog and Marlborough Forest were processed using an April 2010 image and Westport Bog was processed using a March 2010 image. Yellow shading highlights the highest accuracy per site.	207
Table 5.16. OBIA CTA results for Open Water Type providing accuracies (%) for the four sites. Input imagery included the segmented spring 2010 WorldView-2 imagery (four spectral bands) and a DEM.	215
Table 5.17. OBIA CTA results for Open Water Type providing accuracies (%) per site for the four sites. Input data included 5 fraction maps not segmented and the original segmented data both including the DEM. Yellow highlights the best results per class.	216
Table 5.18. Number and type of wetlands from OWES evaluations and from the image classification of this research.	227
Table 5.19. Land cover types within 1.5km of the wetland complex boundaries: OWES field evaluation and those derived from the land cover maps created or obtained for this research.	229
Table 5.20. Hydrological Proximity to Other Wetlands as measured during the OWES evaluation and derived from geospatial data.	231
Table 5.21. OWES Wetland Type field observed fractional areas and scores (columns 2, 3); Wetland Type mapping fractional areas and scores (columns 4, 5).	237
Table 5.22. Scores derived for Open Water Types were based upon the image-derived thematic map and compared to those listed in the OWES field evaluations. See Section 2.9.3 for type descriptions.	239

Table 5.23. OWES and thematic map scores derived for the Number of Wetland Types.	240
Table 5.24. Scores for the hydrological Proximity to Other Wetlands as measured in the field and derived from geospatial data.....	241
Table 5.25a. Scores for the Wetland Size attribute evaluated in the OWES.....	242
Table 5.25b. Scores for the Wetland Size attribute derived from geospatial data.....	243
Table 5.26. Rarity of Wetland Type and Rarity of Wetlands in the Landscape observed from OWES and geospatial data.	244
Table 5.27. OBIA CTA accuracy statistics for the Wetland Type class accuracies (%) for the four sites using the various combinations of seasonal data.	249
Table 5.28. Landsat TM 5 CTA accuracies (%) A) best spring result; B) summer results using same configuration of data; and C) best summer results.	251
Table 5.29. CTA accuracy statistics (%) for the Number of VCFs for the combinations of seasonal imagery for Mer Bleue Bog. Class A, B, and C represent 1 to 3, 4 to 5 forms, and 6 or more forms, respectively (Section 2.9.2).	255
Table 5.30. CTA error matrices for the Number of VCFs for A) spring; B) summer; C) fall; D) spring/fall; E) summer/fall for Mer Bleue Bog. Class A, B, C representing 1 to 3, 4 to 5, and 6 or more forms, respectively (Section 2.9.2).	256
Table 5.31. CTA accuracy statistics (%) for the VCFs for the combinations of seasonal WorldView-2 imagery for Mer Bleue Bog.	258
Table 5.32. CTA accuracy statistics (%) for the Open Water Types for Mer Bleue Bog for the combinations of seasonal WorldView-2 imagery.	259
Table 5.33. CTA accuracy statistics for the Open Water Types providing accuracies (%) for seasonal Landsat TM 5 imagery for Loch Garry.....	260
Table 6.1. List of the highest accuracies obtained for Wetland Type (Bog, Fen, Marsh, Swamp); VCFs (overall accuracy only); # of VCFs (A = 3 or less forms, B = 4 -5 forms, C = 6 or more); and Open Water Types (refer to Table 2.7 for Type definitions). OA (%) is Overall Accuracy and, under each individual class, PA (%) / UA(%) are presented. Definitions of codes of data types and seasons are: WV (WorldView-2); L(Landsat TM-5); R2 (Radarsat-2); DEM (DEM); 5EM (5 Automatically selected EM); 3EM (3 manually selected EM); HH & HV (HH and HV backscatter) CP (Cloude-Pottier components); SU (Summer); SP(Spring); F(Fall); and where seasons were combined, '/' means both/all were used. All of the best accuracies were obtained using some form of OBIA and CTA, or pixel-based CTA alone (for EM classifications).	282

Table 6.2. Recommendations for selection of data based upon the majority results presented in this research. 283

Table 6.3. Recommendations for OMNR to utilize results from this research..... 301

LIST OF FIGURES

Figure 1.0. Conceptual flow chart of the overall thesis.....	7
Figure 2.1. Components of wetlands and how the components interact. Solid lines are a direct influence while dotted/dashed lines represent feedback mechanisms (after Mitsch and Gosselink, 2007). The wetness and overall flow paths (hydrology) affect the physiochemical environment (e.g. causing anaerobic conditions and changing water levels), which then influences the vegetation as specific species will be present or absent depending on these factors.....	10
Figure 2.2. Simplified object-based hierarchy with the lowest level representing pixels and the top level representing the whole scene. Mid-levels represent segmented object levels. Examples of classes at mid-levels are for illustrative purposes only.....	55
Figure 2.3. A simple classification tree. Red and NIR represent spectral bands.....	61
Figure 2.4. A conceptual representation of different scattering mechanisms in a wetland complex for C-band data (after Bourgeau-Chavez <i>et al.</i> , 2010; Fernandez-Ordonez <i>et al.</i> , 2010; OWES, 2002). A = Volume scattering; B = Surface scattering; C = Double bounce.....	65
Figure 2.5. Typical polarimetric signatures for (A) Sphere, flat plane or trihedral corner reflector (often representing surface scattering)); (B) Bragg model; (C) Dihedral corner reflector (double-bounce scattering); (D) Multiple, dissimilar scatterers. After Figures 5.1 – 5.4, (NRCAN.gc.ca/earth-sciences/node/2163, 2008).	70
Figure 2.6. Scattering regions of the α - H plane. Physical characteristics of each zone are described in Cloude and Pottier, 1997.....	71
Figure 2.7. Wetland vegetation VCFs and symbols (after Figure 11, OWES Southern Manual, 2013).....	84
Figure 2.8. Open Water Type drawings (after Figure 17, OWES Southern Manual, 2013).	86
Figure 2.9. Eastern Ontario Subsection of Site Regions and Site Districts in Southern Ontario (after Figure 16, OWES Southern Manual, 2002).....	95
Figure 3.1. Eastern Ontario and the position of the four wetland complex study areas in Kemptville area. Study areas are red squares.....	99
Figure 3.2. Loch Garry Wetland Complex: CIR (colour infrared) WorldView-2 composite (Summer 2010) with OMNR wetland layer (2013) overlaid. Black outline highlights the focussed area of interest where field work was performed. Light blue colour is CIR representation of some of the water in this image; an indication the image is potentially substandard.....	103

Figure 3.3. Marlborough Forest Wetland Complex: CIR WorldView-2 composite (Spring 2010) with OMNR wetland layer (2013) overlaid. Black outline highlights the focussed area of interest where field work was performed. Red circle highlights Bog on OMNR wetland layer. Light blue in this image is the CIR representation of bare fields.	107
Figure 3.4. Mer Bleue Conservation Area: CIR WorldView-2 composite (Spring 2010) with OMNR wetland layer (2013) overlaid. Black outline highlights the area of focus where field work was performed.	108
Figure 3.5. Photographs near the public boardwalk at Mer Bleue Bog. Yellow circles highlight the presence of tamarack (sparse, and denser) that in the 2013 OWES would indicate this area is fen or swamp.	109
Figure 3.6. Westport-Nelson Wetland Complex: CIR WorldView-2 composite (Spring 2010) with OMNR wetland layer (2013) overlaid. Black outline highlights the area of interest where field work was performed.	111
Figure 3.7. True colour composite of WorldView-2 imagery at Westport Bog.	115
Figure 4.1. Detailed workflow of the entire methods structure (Provided digitally with thesis).	
Figure 4.2. A workflow of the methods used to segment, classify and map Wetland Type using optical and radar imagery.	118
Figure 4.3. Location of field sites at each wetland site.	125
Figure 4.4. A simple classification tree. Red and NIR represent spectral bands.	127
Figure 4.5. Example of the training site monitoring graph for the GINI splitting tree on the Loch Garry spring training sites for the Landsat TM imagery (X-axis represents classes: Class 1-Water; Class 2-Upland; Class 3-Fen; Class 4-Swamp; Class 5-Marsh).	129
Figure 4.6. Theoretical display of created objects. Once rasterized, (e.g. pixel values B) all pixels within an object maintain the original object value. The blue square in pixel values B is an example of the location of a validation sample. The red square outlines the complete MMU of the validation site (e.g. 90 x 90 m).	134
Figure 4.7. A workflow of the methods used to segment, classify, and map VCFs using optical and radar imagery.	136
Figure 4.8. A workflow of the methods used to segment, classify and map Open Water Type using optical and radar imagery.	138

Figure 4.9. A workflow of the methods used to segment, classify and map Inundation Extent using optical and radar imagery. 140

Figure 4.10. A workflow of the methods used to segment, classify and map Anthropogenic Disturbance using optical imagery. 148

Figure 5.1. (A) CIR composite of the spring 2010 Loch Garry WorldView-2 image showing the created objects using scale value of 45, shape value of 0.1 and compactness value of 0.75; and in red (B) objects that make up the boundaries of a known fen; (C) objects that form a known channel; and (D) objects that mimic the shoreline of Loch Garry. 153

Figure 5.2. (A) CIR composite of the spring Loch Garry WorldView-2 image where several segmented objects are within a known fen. The field images show: (B) swamp area that grades into (C) less dense treed fen which grades into (D) grassier fen area... 154

Figure 5.3. Example of the effects of different scale parameter values on segmentation of objects for known features. A) WorldView-2 spring CIR composite sub set of Westport Bog. Yellow outlines in B through D highlight bog lagg objects created with scale values of 45, 40, and 50 respectively. Important features such as the bog lagg are well defined using a scale value of 45, whereas objects for larger and smaller scale values include non-lagg areas (blue circles and red arrows; erroneously incorporated non-lagg at all scales are circled in green. All shape and compactness values were maintained at 0.1 and 0.75, respectively). 156

Figure 5.4. Lagg at Westport Bog. Yellow circle highlights presence of vegetation showing that the bog is not necessarily a simple linear water feature but a transition zone between the bog and upland. 157

Figure 5.5. MLC Thematic map of Loch Garry developed from spring 2010 WorldView-2 and DEM images segmented (scale value = 45; shape value = 0.1; compactness value = 0.75). Red circles show areas of erroneously classified Marsh. 158

Figure 5.6. 5-class thematic maps of Loch Garry derived from object-based classification of spring 2010 WorldView-2 image and DEM data. A) CTA; B) MLC. Red circles show areas that were well-classified using CTA as compared to MLC. Black dashed lines shows route travelled in the field on foot and by canoe to visually inspect areas with limited access..... 164

Figure 5.7. A) 5-Class GINI classification tree using spring 2010 WorldView-2 imagery and the DEM for Loch Garry. B through E) are maps representing the leaves (end nodes) where class contributions are greater than 80%. In these maps, green represents the assigned pixels, and black represents the unassigned (or previously assigned) pixels. Blue underlines represent the contributing end nodes for Marsh class. 167

- Figure 5.8. (A) Mer Bleue Bog study site segmented fraction map images (5 EMs, no DEM) derived from spring 2010 Landsat 5 TM imagery (scale value = 2; shape value = 0.1; compactness value = 0.1). Yellow highlighted objects represent land cover spatial features. (B) Includes the DEM in the segmentation process (same parameter values). Blue circles show areas where finer objects were segmented due to the addition of the DEM data..... 170
- Figure 5.9. 5-Class pixel based GINI CTA map for Marlborough Forest derived using Landsat TM imagery acquired in April 2010. Red circles highlight known water bodies (Roger Stevens Pond and Steven’s Creek). Black circle highlights known Fen area. 175
- Figure 5.10. Comparison between the best (test 5) and worst (test 8) classification of Marlborough Forest using CTA with spring 2010 Landsat 5 TM imagery. Column A provides CIR sub sets of the overall Marlborough Forest image, with Columns B and C showing the corresponding subsets of the test 5 and test 8 maps, respectively. The black arrows point to areas where detail present in the pixel-based test 5 is not present in the object-based test 8 classification. The red arrows show the excessive amounts of Marsh that were erroneously classified in test 8. 176
- Figure 5.11. Loch Garry summer 2010 Radarsat-2 backscatter for Wetlands (yellow), Uplands (green) and Water (blue) at steep incidence angles (29.1°– 30.9°)..... 178
- Figure 5.12. Marlborough Forest spring 2010 Radarsat-2 backscatter for Fen (Green), Marsh (Yellow) and Swamp (Purple) at A) steep (18.4° - 20.4°), and B) shallow (46.8°- 48.0°) incidence angles..... 179
- Figure 5.13. All sites spring 2010 Radarsat-2 backscatter for Fen (Green), Marsh (Yellow), Swamp (Purple), and Bog (blue) at steep (18.4 ° - 27.6°) incidence angles with A) Marsh compared to Swamp; B) Marsh compared to Fen; and C) Fen compared to Bog. 180
- Figure 5.14. Comparison of 5-class CTA Wetland Type thematic maps using A) WorldView-2 optical imagery, DEM and HH and HV images; B) WorldView-2 optical imagery and DEM only; and C) Landsat TM unsegmented fraction maps. 184
- Figure 5.15. Polarimetric signatures for (A) typical water (surface scattering) at Westport Bog; and (B) atypical water (double -bounce model (double-bounce scattering)) at Marlborough Forest. Yellow circles on the CIR composites show the area from which training data were extracted..... 186
- Figure 5.16. Representative polarimetric signatures for Marsh A) in the spring, (Westport Bog); and B) in the fall (Mer Bleue Bog)..... 187

Figure 5.17. Polarimetric signatures for (A1 & B1) Swamp at steep (18.4° - 20.4°) incidence angles and (A2 & B2) at shallow (46.8° - 48.0°) incidence angles at Marlborough Forest in the spring 2010.	189
Figure 5.18. Polarimetric signatures for (A1 & B1) Fen at steep incidence angles and (A2 & B2) at shallow incidence angles at Marlborough Forest in the spring 2010.	190
Figure 5.19. Polarimetric signatures for Bog in the fall (A, Mer Bleue Bog) and in the spring (B, Westport Bog) at steep incidence angles. Red circle highlights presence of sporadic tamarack.	191
Figure 5.20. (A & C) Spring/fall co- and cross-pol pedestal maximum and minimum heights; (B&D) Summer co- and cross-pol pedestal maximum and minimum heights. Black dashes represent the median. Pedestal height is normalized to 1.00 (vertical axis); land cover type (horizontal axis).	193
Figure 5.21. The summation of the summer co- and cross-pol minimum pedestal heights (lower red dots) and maximum heights (upper red dots). Black dashes represent the median. Pedestal height was normalized to 1.00 (vertical axis). Group 1 is Bog and Fen, Group 2 is Marsh and Water and Group 3 is Swamp and Upland as described in the text.	195
Figure 5.22. A) WorldView-2 CIR composite and CP variables of B) entropy, C) alpha and D) anisotropy derived from summer 2010 Loch Garry Radarsat-2 imagery.	197
Figure 5.23. A) Spring 2010 WorldView-2 true colour composite of Westport Bog; B) WorldView-2 and DEM segmented imagery (scale = 25, shape = 0.1; compactness = 0.75) with yellow outlines of objects representing vegetation communities; C) field photograph of open, bare rock/lichen covered rock that grades to shrubs/saplings, a small tree stand and then water; and D) grassier open community surrounded by a deciduous forest stand. Yellow arrows point to locations of photos. Red arrows indicate the view direction of the photos.	202
Figure 5.24. A) Number of VCFs (Class A: 1-3; B: 4-5; C: > 6) classification of Westport Bog; B) the same area with an Upland and Water Mask. The Marsh class of the Wetland Type classification (Appendix F, Figure F6) was considerably over-classified, and thus it has been masked as well.	204
Figure 5.25. Spring steep incidence angle backscatter for different bog plant types/groups. The only noticeably separate plant type/group is treed bogs (green circle).	208
Figure 5.26. Comparison of backscatter obtained for different plant types/groups at marshes. There is distinct separation between all three plant types using summer imagery.	209
Figure 5.27. Comparison of backscatter obtained for different plant types/groups at fens. There is separation between the two groups using spring imagery. HH and HV values derived from summer imagery acquired at steep incidence angles.	210

Figure 5.28. Comparison of backscatter obtained for different plant types/groups at swamps during spring. There is separation between hardwood and mixed swamp communities.	211
Figure 5.29. Object-based CTA Open Water Type classification of Loch Garry using spring 2010 WorldView-2 imagery and the DEM. The Water and Upland classes are taken from the Wetland Type classification (Section 5.1). Red, yellow and black circles highlight field-assessed areas that were well classified.	214
Figure 5.30. Loch Garry Open Water Type CTA classification. A) spring WorldView-2 imagery and DEM; B) Landsat TM imagery (3 EM fraction maps with DEM not segmented; and C) Landsat TM imagery (original bands and a DEM segmented). Water and Upland classes are from the WorldView-2 5-Class Wetland Type classification (Section 5.1). Yellow circles show detail lost at the Landsat scale around a boardwalk. Red circles show an ephemeral wetland captured in all three classifications.	217
Figure 5.31. Four examples of field measured VWC (%) compared to NDVI _{Green} derived from spring 2010 WorldView-2 imagery for Mer Bleue Bog. Yellow areas give an approximation of the NDVI _{Green} threshold range that relates to 100% or greater VWC.	221
Figure 5.32. Four examples of field measured VWC (%) compared to NDVI derived from spring 2010 WorldView-2 imagery for Mer Bleue Bog. Yellow circles show overlap of NDVI values at varying moisture. There are not distinct ranges/separation at the high (100% or more) end of the VWC as found for NDVI _{Green}	222
Figure 5.33. A) Spring 2010 WorldView-2 CIR composite of Mer Bleue Bog; B) orange is the 100% saturated boundary derived from the NDVI _{Green} range of -0.025 to -0.075; C) is a close up showing yellow transects measured in 2010 meeting with the orange boundary (red circle); and D) the blue saturated lines mimicking the derived boundary on the north side, but being slightly off on the south side.	224
Figure 5.34. A) CIR composite of the WorldView-2 spring image of Mer Bleue Bog; B) orange is the 100% saturated boundary derived from the pixel-based NDVI _{Green} threshold range of -0.025 to 0.075; C) shows the 100% saturated boundaries (pink and green) derived from the segmented imagery.	225
Figure 5.35. The Diversity of Surrounding Habitat surrounding the Marlborough Forest wetland subset (black boundary). The data layers include the WorldView-2 image derived Wetland Type layer, the 2011 AAFC Crop Type Map of Canada (2011); the OMNR water bodies layer, and the OMNR contour layer.	231
Figure 5.36. Hydrological proximity of the Loch Garry wetland complex to surrounding wetlands. The data layers include the OMNR Wetland Type layer, the OHN	

watercourses layer; the OMNR water bodies layer, and original Loch Garry boundary layer.	232
Figure 5.37. Hunting layers available through the LIO and one field observed attribute (deer blinds). Very little coverage is available in far eastern Ontario. Further to the west and north the coverage is denser which may allow for mapping of the intensity of hunting use in those areas.	233
Figure 5.38. WorldView-2 CIR composites of A) Loch Garry in the summer showing specular reflectance of water and B) Westport Bog with vegetation present (yellow circles).	247
Figure 5.39. Comparison of A) spring B) summer; C) combined spring & summer; and D) fall only Wetland Type classifications as derived from segmented WorldView-2 imagery and a DEM at Mer Bleue Bog. Blue circles highlight areas of illogical class assignment. Table provides area (ha) per class type.	250
Figure 5.40: Loch Garry Open Water Type classification A) spring WorldView-2 imagery, DEM and CTA analyses; B) spring Landsat TM imagery (original bands segmented with DEM and CTA analyses); and C) summer Landsat TM imagery (original bands segmented with DEM and CTA analyses) Water and Upland class are from WorldView-2 5-Class Wetland Type classification.	261
Figure 5.41. Monthly total precipitation for Ottawa-McDonald Cartier Airport, revealing the drought (less precipitation) that occurred before the spring imagery were acquired (February, March for April acquisition) and the greater accumulation that occurred before the summer imagery were acquired (June for July acquisition (Environment Canada, 2013)).	262
Figure 5.42. Spring and summer field measured VWC transects measured at A) Marlborough Forest, where spring had a larger wet extent then B) Westport Bog, where summer had larger wet extent.	264
Figure 5.43. 2011 Field measured wet extent compared to the 2010 field measured soil moisture transects. A) Marlborough Forest with B) subset of transects and boundaries measured in the field in 2010 and 2011. C) is a field photo of the marsh.	265
Figure 5.44. A) Summer WorldView-2 CIR composite of a section of Mer Bleue Bog; B) orange is the 100% saturated boundary derived from the NDVI _{Green} threshold with the red lines representing the transects measured in the summer of 2010.	266
Figure 5.45. Fraction images from 1984 and 2010 for Loch Garry. Yellow circle highlights an area which, for both years, appears as bare with low vegetation values. Purple circles highlight areas where the vegetation fraction was higher in 2010, and the moisture fraction was higher in 1984. (Red display = 2010; Green display = 1984; and Blue display = 1984).	269

Figure 5.46. A) 1984 CIR composite of Landsat TM image; B) 2010 CIR composite of Landsat TM image; and C) temporal composite (Red display = 2010; Green display = 1984; and Blue display = 1984) of vegetation fractions derived from the previous two images. The yellow circle highlights the change from water body to vegetation; and the yellow arrow points to a flooded area. 271

Figure 6.1. Workflow for six OWES attributes that can be implemented immediately or with some investigation (Wet Extent with existing QuickBird data). 303

LIST OF APPENDICES

APPENDIX A. Wetland Attenuation Factor scoring method.....	338
APPENDIX B. Field data including sites and photographs.....	339
APPENDIX C. Training separabilities for Loch Garry spring, summer and combined imagery and segmentation scale parameter values of 25, 45 and 75.....	365
APPENDIX D. Results from Wetland Type segmentations for Marlborough Forest, Mer Bleue Bog and Westport Bog.....	368
APPENDIX E. Results from CTA testing of GINI, Gain Ratio and Entropy algorithms...	370
APPENDIX F. Results from Wetland Type classifications for Marlborough Forest, Mer Bleue Bog and Westport Bog.....	371
APPENDIX G. LSU details for all four sites.....	380
APPENDIX H. Sites and polarimetric signatures for Bog, Fen, Marsh, Swamp, Water and Upland.....	396
APPENDIX I. Pedestal height analysis for spring and summer radar imagery.....	407
APPENDIX J. Field-measured VWC% for all four sites and two seasons.....	411
APPENDIX K. GIS analysis for Diversity of the Surrounding Habitat and the Proximity of Other Wetlands attributes for Loch Garry, Mer Bleue Bog and Westport Bog.....	412
APPENDIX L. Multi-season WorldView-2 CTA results for Number of VCFs, VCFs and Open Water Types for Loch Garry, Marlborough Forest and Westport Bog.....	418
APPENDIX M. Relative calibration data for temporal analysis of Landsat 5 TM vegetation fraction images	421

LIST OF ACRONYMS

AIRSAR	Airborne Synthetic Aperture Radar
ALOS	Advanced Land Observing Satellite
ANN	Artificial Neural Network
ASTER	Advanced Spaceborne Thermal Emission and Reflection Radiometer
AVHRR	Advanced Very High Resolution Radiometer
BRDF	Bidirectional Reflectance Distribution Function
CA	Conservation Authority
CAA	Conservation Authorities Act
CART	Classification and Regression Tree
CIR	Colour-infrared
COA	Canada-Ontario Agreement Respecting the Great Lakes Basin Ecosystem
Co-Pol	Co-polarisation
CP	Cloude-Pottier
Cross-Pol	Cross-polarisation
CTA	Classification Tree Analysis
CWI	Canadian Wetland Inventory
DEM	Digital Elevation Model
DRAPE	Digital Raster Acquisition Project for the East
DTW	Depth to Water
EM	Endmembers
ERS-1	European Remote Sensing Satellite

ET	Evapotranspiration
ETM+	Enhanced Thematic Mapper +
ESP	Estimation of Scale Parameter
FNEA	Fractal Net Evolution Approach
GIS	Geographic Information Systems
GLWCAP	Great Lakes Wetland Conservation Action Plan
GPS	Global Positioning System
GLCM	Grey level co-occurrence matrix
HEP	Habitat Evaluation Procedure
HGM	Hydrogeomorphic Classification for Wetlands
HH, HV, VH, VV	Various forms of co- and cross-polarisation (H=Horizontal, V=Vertical)
IEA	Iterative Error Analysis
IRS	Indian Remote Sensing
ISODATA	Iterative Self-Organizing Data Analysis Technique
JERS-1	Japanese Earth Resources Satellite
LiDAR	Light detection and ranging
LIO	Land Information Ontario
LSU	Linear Spectral Unmixing
LULC	Land use land cover
MCARI	Modified Chlorophyll Absorption Ratio Index
MEIS-II	Multispectral Electro optical Imaging Scanner
MERIS	MEDium Resolution Imaging Spectrometer
MIR	Mid-infrared
MLC	Maximum Likelihood Classification

MMU	Minimum Mapping Unit
MODIS	Moderate Resolution Imaging Spectroradiometer
MSS	Multi-spectral scanner
NAPP	Net Aerial Primary Production
NASA	National Aeronautics and Space Administration
NDVI	Normalized Difference Vegetation Index
NDWI	Normalized Difference Water Index
NHIC	Natural Heritage Information Centre
NIR	Near-infrared
NRVIS	Natural Resources Values and Information System
OBIA	Object-based Image Analysis
OBM	Ontario Base Maps
OMNR	Ontario Ministry of Nature Resources
OWES	Ontario Wetland Evaluation System
PA	Producer's Accuracy
PAD	Peace-Athabasca River Delta
PALSAR	Phased Array L-band Synthetic Aperture Radar
PAN	Panchromatic
PCC	Pixels Correctly Classified
PIF	Pseudo-invariant Features
RF	Random Forest
RMSE	Root Mean Square Error
SAR	Synthetic Aperture Radar
SIR	Shuttle Imaging Radar

SOLRIS	Southern Ontario Land Resources Information Systems
SOWCA	Southern Ontario Wetland Conversion Analysis
SPOT	Système Pour l'Observation de la Terre
SRTM	Shuttle Radar Topography Mission
SVM	Support Vector Machine
SWI	Soil Water Index
SWIR	Short-Wavelength Infrared
TM	Thematic Mapper
TP	Total Power
TPH	Total Petroleum Hydrocarbons
TSI	Topographic Soils Index
UA	User's Accuracy
UTM	Universal Transverse Mercator
VCF	Vegetation Community Forms
VIS	Visible portion of the electromagnetic spectrum
VWC	Volumetric soil water content
VWI	Vegetation-water index
WGS	World Geodetic System

1.0 Introduction

Wetlands are dynamic ecosystems with climatic, geomorphologic, biological and hydrologic influences (National Wetlands Working Group, 1997). Through these natural and anthropogenic forces wetlands are constantly changing (Foley *et al.*, 2005; Mitsch and Gosselink, 2007). Wetlands provide benefits including functions that are described as “the things that wetlands do” (Bartoldus, 1999) such as: flood water control, ground water recharge and discharge, nutrient, sediment, and contaminant retention, food web support, shoreline stabilization, erosion control, storm protection, stabilization of local climatic conditions, water transport, wildlife habitat, etc. (Lodge *et al.*, 1995; Hruby *et al.*, 1998; Thiesing, 2001; OWES, 2002; Carletti *et al.*, 2004; Papas and Holmes, 2007). Wetlands also provide values such as products or services which include recreational, cultural, heritage, educational, and aboriginal use, fisheries, water supply, wildlife, forage, agricultural, and forest resources, etc. (Roth *et al.*, 1996; Bartoldus, 1999; OWES, 2002; Carletti *et al.*, 2004; Papas and Holmes, 2007). These many functions and values and the dynamic nature of wetlands highlight the need to monitor and manage wetlands at the local, national, and global levels. Evaluating wetlands hierarchically top-down from the general to the more specific, from ecological processes to wetland attributes to spatial patterns is one approach. This is in contrast to bottom-up from the specific to the general, linking spatial pattern to wetland attributes to ecological processes.

Ecological processes in wetlands operate over multiple spatial, temporal, and organizational scales and include such things as nutrient cycling, succession, hydrologic

functioning (Smith *et al.*, 2008; Castaneda and Herrero, 2008; Lang and Kasischke, 2008; Pavelsky and Smith, 2008; Dewan and Yamaguchi, 2009). Attributes such as flood attenuation, wetland diversity, etc. are used as indicators of these processes. Attributes can also be indicators of site characteristics. High biomass such as peat can indicate a mature ecosystem (Mitsch and Gosselink, 2007). Pattern can be used to assess these attributes. For example, attributes of wetlands, vegetation composition and structure, etc. are used as indicators of wetland diversity. Therefore through mapping of the attributes, knowledge about the processes that are occurring within wetland complexes can be obtained. Wetland complexes can be described as dense and/or proximal groupings of wetland types (e.g. bog, fen, swamp, marsh) with functional relationships where each wetland unit contributes to the whole complex, thus making it important to consider all units together (OWES, 2002). A key assumption is that wetland processes can be used as indicators of wetland health and functioning and therefore, in wetland evaluation systems, the presence or degree of presence of these processes can be used in land management.

The Ontario Wetland Evaluation System (OWES) is used by the Ontario Ministry of Natural Resources (OMNR) for the evaluation and scoring of wetlands in Ontario. The method assesses functions of wetlands in ecological processes, and the social and economic values wetlands provide to humans in four major components: Biological, Hydrologic, Social and Special Features. Components are comprised of sub-components and ‘attributes’ and in the OWES some attributes describe ecological processes directly, while others describe wetland characteristics from which a process or an evaluation of the state of a

process can be inferred. The current system is costly, and evaluations quickly become obsolete. Remote sensing is one way that wetland attributes can be monitored across wetlands and has many advantages over traditional field based methods (Lee and Lunetta, 1995; Ramsey, 1998; Ozesmi and Bauer, 2002; Mitsch and Gosselink, 2007). This research, in collaboration with the OMNR, was designed to develop and review remote sensing and geographic information systems (GIS) methods for wetland attribute classification. The attributes considered in this research and selected from the OWES included: Wetland Type, Vegetation Community Forms (VCFs), Open Water Type, Inundation Extent, Number of Wetland Types, Diversity of Surrounding Habitat, Proximity to Other Wetlands, Wetland Size, Hunting, Ownership Patterns, Wetland Basin Size, Rarity of the Wetland in the Landscape, Rarity of Wetland, and Anthropogenic Disturbance. The selection of these 14 attributes was made based upon their potential to be assessed using remote sensing and GIS and their overall contribution to the OWES score for a given wetland.

1.1 Research goal

The overall goal of this research was to determine the potential to map OWES attributes in wetland complexes using spatial patterns extracted from remote sensing and other geospatial data using two imagery types, optical and radar, at multiple spatial, spectral and temporal resolutions and extents. From this, knowledge gained on how the mapping of the attributes differ with changing spatial, spectral and temporal resolution can be applied to wetland status evaluation and land management planning.

1.2 Research objectives

Objective 1 of this research was to map selected OWES attributes that have known wetland pattern-attribute associations. The spatial and spectral resolutions and extents for which the results were most accurate were then determined.

Objective 2 was to compare and relate the scores determined for each of these attributes to field-evaluated OWES scores to determine if these methods can be related to, and/or integrated into the existing evaluation system.

Objective 3 was to assess temporal remote sensing data in classification of the wetland attributes and analyze attribute changes over two decades.

1.3 Research contributions

The overall scope of this research is large and unique as it includes multiple attributes across varying natural and human-constructed components of wetlands incorporating analyses of imagery type, resolution and spatial extent; seasonality and temporal change; remote sensing and GIS methods; and applying this information to an existing wetland management system for a spatially diverse region. This research contributes to the general body of knowledge of wetland science and in particular, the use of remote sensing and GIS to map wetlands attributes. This research also provided direction and contributions to the existing wetland status evaluation methodology currently in use in Ontario, Canada.

1.4 Thesis structure

This thesis follows a traditional structure beginning with this introductory chapter. Chapter 2 contains the background information on wetlands in general, including an understanding of wetlands worldwide, in Canada and in particular the history and management of wetlands in Ontario. The chapter next provides an overview of the existing field-based methods to classify wetlands. Chapter 2 continues with an overview on remote sensing of wetlands, GIS analysis of wetlands, and remote sensing of hydrology and forestry as it relates to this research. Next, more specific background is given for general remote sensing and GIS methods and data types used for this wetland analyses. Finally, the remote sensing methods used to assess the 14 attributes are described, the general background on the methods chosen for this research is provided, and a description of the OWES attributes scoring methods for analysis is given. Chapter 3 provides the details on the study sites, and the remote sensing and GIS data used for this research.

For clarity and consistency all further chapters are organized in modular format by objective as listed above. For any repetitive information (e.g. method used), the reader will be instructed to review the pertinent area of the previous section that contained the same information. Chapter 4 provides the methods that were carried out for each objective. Chapter 5 presents the results of the attribute mapping, the findings in relation to the application of these methods in the OWES evaluation system and the temporal analysis. The discussion of these findings is found in Chapter 6, with a complete appraisal of the benefits

and limitations of this research and recommendations for implementation of the findings. Chapter 6 then summarizes the thesis and provides the conclusions and future directions. Figure 1.1 provides a conceptual flow chart of the research and thesis structure.

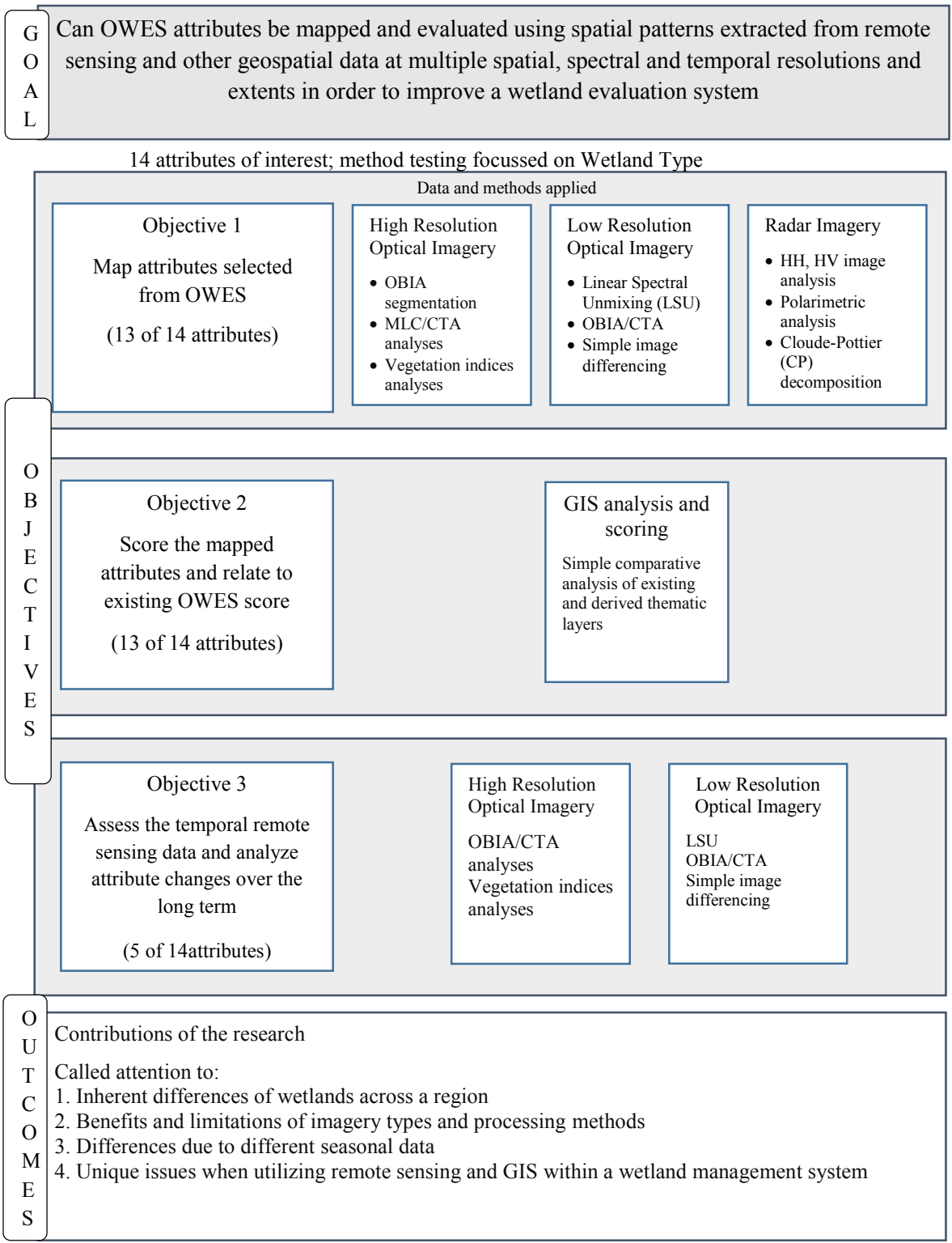


Figure 1.0. Conceptual flow chart of the overall thesis.

2.0 Background

This chapter gives the definitions of wetlands and common wetland types, and it describes the overall function of wetlands in the context of the OWES. Scale is defined as it relates to this research, and describes the pattern-attribute-process relationship. The chapter then reviews the literature on sensor and imagery types as well as the image analyses and GIS methods that have been used in past efforts to map the 14 wetland attributes of this research, with emphasis on those sensors and methods that were employed in this research.

2.1 Functional description of wetlands

The Convention on Wetlands is an intergovernmental treaty that was developed at Ramsar, Iran in 1971. It provides a framework for the conservation of wetlands globally (Ramsar Convention Secretariat, 2006). The Ramsar Convention Manual (2006) gives a definition of wetlands as “Areas where water is the primary factor controlling the environment and the associated plant and animal life. They occur where the water table is at or near the surface of the land, or where the land is covered by shallow water.” Wetland types are specifically defined as “Areas of marsh, fen, peatland or water, whether natural or artificial, permanent or temporary, with water that is static or flowing, fresh, brackish or salt, including areas of marine water, the depth of which at low tide does not exceed six metres” (Ramsar Convention Secretariat, 2006).

Canada has had a national interest in wetlands since the 1960s and is a contracting party of the Ramsar Convention (Ramsar Convention Secretariat, 2006). As a contracting

party, Canada has agreed to work towards the “wise use” of all wetlands through management, policy and legislation; to designate suitable wetlands for the Ramsar List; and to cooperate internationally on shared wetlands and wetland policy (Ramsar Convention Secretariat, 2006). In total, Canada has an estimated 24% of the world’s wetlands representing approximately 150 million hectares (National Wetlands Working Group, 1997). Losses to Canadian wetlands are dependent upon their location. Those wetlands located in less populated areas are less impacted than those located in more populated regions. Overall, losses range across Canada from an estimated 65 to 85% of pre-settlement area (National Wetlands Working Group, 1988).

In Canada, wetland management falls under the jurisdiction of the provinces while the territories share their responsibility with the federal government, and aboriginal agencies (Lynch-Stewart, 1994). The federal government of Canada has had a wetlands policy since March 1992. This policy aims to ensure the conservation of wetlands to sustain both ecological and socio-economic functions (Government of Canada, 1991). The Canadian government defines a wetland as “land that is saturated with water long enough to promote wetland or aquatic processes as indicated by poorly drained soils, hydrophytic vegetation and various kinds of biological activity which are adapted to a wet environment. Wetlands in Canada include bogs, fens, marshes, swamps and shallow waters (usually 2 m deep or less)” (National Wetlands Working Group, 1997). This definition has been adopted by the OWES (excluding shallow waters, OWES, 2002).

There are three key components of the ecological functioning of wetlands; hydrologic, physical/chemical (biogeochemistry) and biological (Cronk and Fennessy, 2001; Mitsch and Gosselink, 2007). Each of these has an impact on the others and the relationship between the three components is illustrated in Figure 2.1 (after Mitsch and Gosselink, 2007). The hydrologic component has greatest overall influence on wetland ecological processes and the water level regime and fluctuations known as the “hydroperiod” are often used to classify wetlands (National Wetlands Working Group, 1997; Cronk and Fennessy, 2001; Mitsch and Gosselink, 2007).

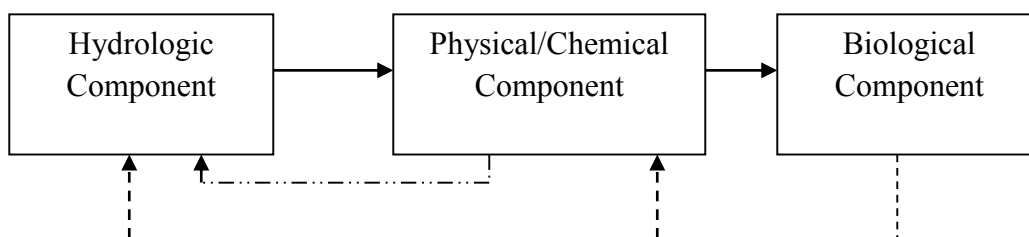


Figure 2.1. Components of wetlands and how the components interact. Solid lines are a direct influence while dotted/dashed lines represent feedback mechanisms (after Mitsch and Gosselink, 2007). The wetness and overall flow paths (hydrology) affect the physiochemical environment (e.g. causing anaerobic conditions and changing water levels), which then influences the vegetation as specific species will be present or absent depending on these factors.

The Canadian Wetland Classification System categorizes wetlands into two main hydrologic systems, the ombrogenous system and the minerogenous system (National Wetlands Working Group, 1997). The minerogenous system is subdivided into several wetland types, whereas the ombrogenous system only contains bogs (Figure 2, page 7, National Wetlands Working Group, 1997). Ombrogenous systems only receive input from

precipitation and are hydrologically isolated (National Wetlands Working Group, 1997). The minerogenous wetland types are categorized by influences of the biological component (e.g. vegetation present) which is affected by the physical/chemical component.

The physical/chemical component (biogeochemical cycling) of wetlands is concerned with chemical conversions and chemical movement. These can include movement within the soil profile, or through conversions to gases (e.g. denitrification) and release into the atmosphere. Many of these movements, cycles and transformations are caused by the lack of soil oxygen (i.e. anaerobic conditions) because of the overwhelming presence of water (Smith *et al.*, 2003). The changes and cycles then effect the vegetation present in the system.

The biological component includes both plants and animals; however for classification of wetlands, the focus is on the vegetative elements. For multi-cellular vegetation, the main distinction between wetlands and other areas is the adaptation of wetland plants (e.g. hydrophytes) to saturated conditions (Cronk and Fennessy, 2001). The types of adapted vegetation are often used in the classification of wetlands.

2.2 Wetlands of Ontario

2.2.1 History of wetlands in Ontario

Approximately 29.2 million hectares of wetlands, approximately 20% of Canadian and approximately 5% of the world's wetlands are located in Ontario, the majority of which are located in the north (National Wetlands Working Group, 1988). The losses in Ontario

include destruction along the Great Lakes Water Basin of approximately 72% of pre-settlement area (National Wetlands Working Group, 1988; GLWCAP, 2012). Around major cities in Ontario wetland losses range from approximately 37% around Kitchener up to 97% around the city of Windsor (National Wetlands Working Group, 1988). The largest losses were found in southwestern Ontario and some parts of eastern Ontario. Historically, wetlands were believed to be unsuitable for use and were converted to agricultural lands, hydro right-of ways, edge of transportation corridors and forest clearings (GLWCAP, 2012). Several methods have been used to assess these land conversions, and the spatial trends of wetlands in Ontario from pre-settlement to more recent times. The Snell Report (Environment Canada, 1987) assessed these types of conversions from approximately 1800 to 1982. The Southern Ontario Wetland Conversion Analysis (SOWCA) converted the Snell methodology to GIS-based analysis and further assessed the spatial trends in wetlands from pre-settlement to 2002 (SOWCA, 2010). From that analysis it was found that there continues to be losses of wetland area in Ontario of up to 0.12% per year (SOWCA, 2010).

2.2.2 OMNR role in wetland management

OMNR's role in wetland management is a partnership between the OMNR and wetland conservation associates such as Ducks Unlimited Canada, Nature Conservancy, Ontario Nature, etc. Wetland protection and conservation in Ontario falls under the Provincial Policy Statement, the Ontario government's statement on land use planning, and the Conservation Authorities Act (CAA). The CAA is administered by 36 Conservation Authorities (CAs) that regulate development and activities adjacent to, and within wetlands

(Conservation Ontario, 2009). The OMNR wetland conservation staff is responsible for providing policy advice and support, assisting in the development of several conservation plans, including the Great Lakes Wetland Conservation Action Plan (GLWCAP), the North American Waterfowl Management Plan and the Canada-Ontario Agreement Respecting the Great Lakes Basin Ecosystem (COA), as well as in maintaining and providing training on the existing OWES (OMNR, 2013).

2.3 Methods to evaluate wetlands

There are many different methods that are used to identify (e.g. Hydrogeomorphic (HGM) Classification for Wetlands (Brinson, 1993)); inventory (e.g. Canadian Wetland Inventory (CWI, Milton and Hélie, 2003)); and evaluate wetlands (e.g. Habitat Evaluation Procedure (HEP, US Fish and Wildlife Service, 1980), among others). See Dingle Robertson and King, 2008 for a complete review of these and other methods to that time (available digitally with this thesis)). These methods provide information about wetland functions and values for land management purposes (Thiesing, 2001). For the purposes of this research, the focus is on methods used in Ontario.

2.3.1 Ontario wetland inventory schemes

The main objective of wetland inventory is to provide a visual representation, count or catalogue of the extent and/or type of wetlands (such as bog, fen, marsh, swamp) that are present in a landscape (Thiesing, 2001; Dahl and Watmough, 2007).

The Natural Resources Values and Information System (NRVIS) layers provide coverage of the province of Ontario (NRVIS, 2002). This information was published as OMNR Ontario Base Maps (OBM) at 1:10,000 (southern Ontario) and 1:20,000 scales (northern Ontario) and included manually interpreted wetlands assessed from aerial photography obtained in the spring. Newer layers include OWES evaluated wetlands that were taken from the OMNR's evaluated wetland files (OWES, 2002, e.g., NRVIS Wetland Unit).

The Southern Ontario Land Resource Information System (SOLRIS, 2003) land use/land cover classification follows the ecological land classification system for southern Ontario (Lee *et al.*, 1998; SOLRIS, 2008). Ecological land classifications include all components of earth systems (e.g. air, water, land, biota, etc.) and are based upon the hierarchical structure of ecosystems that are nested within other ecosystems (Environment Canada, 2005). This inventory used remote sensing and spatial modelling techniques to identify and classify wetland features at the community series level to delineate wetlands not previously inventoried by NRVIS ("Unevaluated Wetlands") and to identify ephemeral wetlands. Data used included Landsat, Radarsat, and Indian Remote Sensing (IRS) imagery (23 m, multispectral), OMNR Forest Resources Inventory photos, CIR (colour-infrared) aerial photos, high and medium precision DEMs (Digital Elevation Models), a topographic soils index (TSI) derived from OBM contours and a quaternary geology layer, and the NRVIS layers for Wetlands, Open Water and Wooded Area, (SOLRIS, 2003). This adaptive method was applied to a reference site to compare with wetland evaluations obtained through

fieldwork, OWES derived maps, and the NRVIS Wetland layer. The overall accuracy between the two classes of Wetland and Upland was approximately 90% utilizing one reference site near Bolton, Ontario (906 ha). Using only the high precision DEM method, overall accuracy was for the two classes were 82%. The research presented in this thesis was designed to classify individual Wetland Types such as Bog, Fen, Marsh and Swamp through the use of higher resolution imagery.

SOLRIS layers are currently used in the Canadian Wetland Inventory (<http://maps.ducks.ca/cwi/>). The OMNR has merged all existing wetland layers for Ontario (specifically NRVIS and SOLRIS) to create one layer representing the most up-to-date, accurate wetland information.

2.3.2 Ontario wetland evaluations

Functional wetland evaluations investigate the functions that wetlands provide. They are often model-based and allow for a high degree of reproducibility and predictable outcomes (Thiesing, 2001). The methods and models applied can be based on current/recent field data, existing archived data or a combination of both. Other components that are not considered to be wetland functions can be included, but the majority of elements assessed are functional. The general expertise needed to perform these evaluations ranges from trained lay persons to specialists in geology, hydrology and/or ecology (wetland scientists) (Smith *et al.*, 1995; Bartoldus, 1999). These methods can assess individual wetlands to wetland-complexes across regions.

To respond to the illustrated conversion of wetland land cover, and wetland losses modeled in the Snell Report (Environment Canada, 1987), the OMNR developed the OWES. This functional method assessed ecological processes, with the addition of several social and economic values, evaluated in four categories: Biological, Hydrologic, Social and Special Features. Each category's particular functions and/or values were selected based upon consultation with experts and are typically characteristic of Ontario wetland ecosystems (OWES, 2002). Scores are derived for each function/value and are subsequently summed for each category and then for the entire wetland. Provincial 'significance' is given based upon the total score for all four categories (or if the total value of the "Special Features" category is higher than 250). The significance designation allows for the protection of the wetland and for special consideration to be given during development. The OWES adopted generalized categories of four Wetland Types outlined in Table 2.1.

The Biological component of the OWES consists of three sub-components: productivity, biodiversity and size. The Social component evaluates the values that wetlands provide to humans including economically valuable products, recreational activities, landscape aesthetics, education and public awareness, proximity to areas of human settlement, ownership, aboriginal values and cultural heritage. The Hydrologic component has categories of flood attenuation, water quality improvement, carbon sink, shoreline erosion control, groundwater recharge. The Special Features component contains classes of rarity, significant features and habitat, ecosystem age, and Great Lakes coastal wetlands. Under each of these subcategories there are attributes that are assessed in the field or through

a manual interpretation of aerial imagery. Limitations of the current evaluation method are that it is pre-dominantly field-based, not temporally repeatable, and the physical viewpoint of the assessor is highly oblique, looking out across the wetland as opposed to an overhead viewpoint.

Table 2.1. Wetland Type classifications highlighting the hydrologic, biological and physical/geochemical influences (OWES, 2002).

Bogs	<ul style="list-style-type: none"> • peat-covered areas and/or peat-filled depressions • surface carpet of mosses (Sphagnum) • closed drainage, strongly acidic surface waters and peat • treed or treeless (tree cover does not exceed 25%) • layer of shrubs from the heather family
Fens	<ul style="list-style-type: none"> • poorly to moderately decomposed peat • mosses with narrow pH tolerance (Sphagnum may or may not be present) • covered by dominant component of sedges (with grasses and reeds in local pools) • often low to medium height shrub cover (~sparse tree cover (white cedar, tamarack)) • water and peats less acidic than bogs
Swamps	<ul style="list-style-type: none"> • wooded wetlands ($\geq 25\%$ cover trees and tall shrubs) • standing to gently flowing water (pools and channels indicate subsurface flow) • characteristically flooded in spring with relic pools later in summer • sometimes has a strong low shrub community, but tall shrub component must be present/dominant • can be sub-classed as treed swamps or shrub swamps • treed swamps <ul style="list-style-type: none"> ○ conifer swamps (white cedar, tamarack, black spruce) ○ deciduous swamps (silver maple, elm, black ash, yellow birch)
Marshes	<ul style="list-style-type: none"> • vigorous, non-woody emergents (rushes, reeds, reed grasses, sedges with anchored floating plants) and submergents • wet areas periodically and/or permanently inundated • zones/mosaics of vegetation interspersed with channels or pools of water

Some of the categories and scoring methods are qualitative and subjective, and some of the attributes that have been historically scored in the OWES cannot be detected directly or indirectly using remotely sensed imagery. Additionally, OWES evaluations are limited to a single measurement and observational scale, and depending upon the location in Ontario and the availability of funds, there has been little temporal repetition of these evaluations over the last 20-30 years.

2.4 Wetland attributes typically measured in the field that have shown potential for estimation using remote sensing

There are many methods used in the field to measure different wetland attributes. Bio-assessments are based on the premise that the biotic community found in a wetland reflects its overall health or condition (Papas and Holmes, 2007). As wetlands are altered, the diversity of the biotic component typically declines and the species composition changes. Often, terms such as “biotic integrity”, “ecological integrity”, “biological condition” (Adamus, 1995) are associated with bio-assessments. These types of methods are most commonly based on metrics that characterize the abundance, diversity and distribution of plants and animals. Although habitat maps derived from remote sensing and GIS are used in conjunction with field-based data, generally it is not possible to assess other information about animals with geo-spatial data. One of the most straightforward and common attributes that can be detected and analysed using remotely sensed images are the biomass, abundance, diversity and distribution of vegetation.

For example, Hardisky *et al.* (1984) used a hand-held spectroradiometer to mimic three of the Landsat TM (Thematic Mapper) 4 bands (red, NIR (near-infrared), MIR (mid-infrared)) and regressed spectral indices such as NDVI (Normalized Difference Vegetation Index), and an infrared index where MIR was substituted for RED in the traditional NDVI equation, against biomass found in salt-marshes. They then used the models to predict above-ground biomass derived from clipped samples of live and dead vegetation, and net aerial primary production (NAPP). The MIR-based index provided a better biomass model for sampling done from May through July while NDVI was better for biomass sampled between August to October, however both indices underestimated NAPP.

Li *et al.* (2007) had found in the literature that there were strong positive and linear correlations between biomass and backscatter of SAR (synthetic aperture radar). They compared Radarsat-1 backscatter and Landsat TM NDVI in regression modelling of mangrove biomass in the Pearl River Delta region of China. Overall, Radarsat-1 provided a more accurate model and increasing backscatter was well correlated with increasing biomass.

Dillabaugh and King (2008) used IKONOS imagery to model field sampled biomass in three riparian marshes, in eastern Ontario. They extracted GLCM (Grey level co-occurrence matrix) image textures such as Homogeneity, Contrast, Dissimilarity, etc. using two window sizes (3 x 3 and 5 x 5) and several vegetation indices from the imagery. Using stepwise regression they obtained a highly significant model that was subsequently used to map continuous biomass distribution in the three wetlands. However, due to an RMSE (root

mean square error) of about 40% (relative to the mean field measured biomass), they aggregated the data into three classes of biomass (high, medium, low) to produce a map that corresponded well to the known spatial distribution of biomass in the wetlands. Biomass mapping was not undertaken in this research

There have been many studies that have attempted to map Wetland Types and vegetation abundance, diversity, structure and distribution to varying degrees of success using methods such as pattern prediction of plant species, habitat quality assessment and diversity, interpolation of soil pH distribution in combination with thematic maps to assess species distribution of mangroves, mapping wetland area using a Bayesian probability model as a post-classifier to improve the quality of a thematic map, and using DEMs derived from high resolution LiDAR data to improve classification of Wetland Type mapping (Pope *et al.*, 1997; Baghdadi *et al.*, 2001; Harvey and Hill, 2003; O'Hara *et al.*, 2003; Berberoglu *et al.*, 2004; Rogers and Kearney, 2004; Racine *et al.*, 2005; Schmid *et al.*, 2005; Belluco *et al.*, 2006; Chiu and Couloigner, 2006; Filippi and Jensen, 2006; Durieux *et al.*, 2007; Grenier *et al.*, 2007; Ghioca-Robrecht *et al.*, 2008; Laba *et al.*, 2008; Bourgeau-Chavez *et al.*, 2010; Melendez-Pastor *et al.*, 2010; Dribault *et al.*, 2012; Bourgeau-Chavez *et al.*, 2013; Evans and Costa, 2013). Accuracies for these studies range from 70% to 100% depending on the image type, method used and number of class types. Further description of some of these studies are found in Tables 2.2 and 2.3.

For wetland hydrologic function, attributes that are commonly assessed in the field such as soil moisture and wet extent have also been successfully mapped using remote

sensing. For example, Quinton *et al.* (2003) determined the relationships between fen and bog cover types and runoff discharged from the Liard river drainage basin in the Northwest Territories, Canada. Land cover was classified using IKONOS and Landsat images. Additional data layers included topographic data to compute drainage area, density and average slope. Stream discharge was monitored at gauging stations. Using both land cover classifications, the overall area covered by fens and bogs was estimated, as well as the connectivity of wetland pixels in the drainage basin system. These measures were subsequently correlated to the amount of annual runoff and a small degree of correlation was found between annual runoff and percent cover (fens and bogs). Individually these relations were correlated in opposite directions due to the unique hydrologic functioning of each wetland type.

Harris *et al.* (2005) related changes in surface and near-surface soil moisture to spectral characteristics of *Sphagnum* moss in a Welsh bog, (Cors Fochno, Britain). The samples were saturated and kept in environmental cabinets and were allowed to dry over 15 days. They were gradually re-hydrated using rainfall simulators for 6 days until reaching full saturation. A handheld spectroradiometer was used with wavebands between 0.35 to 2.50 μ m. They found that decreasing soil moisture increased VIS (visible), NIR and MIR reflectance and there were strong correlations between soil moisture and water and vegetation indices. Water indices (WBI, bands in the NIR), and Moisture Stress Index (MSI) were sensitive to reductions in soil moisture but not as sensitive to re-wetting for one of the species. MSI gave a good indication of soil moisture conditions although that was

dependent on the target species. Both vegetation indices showed some indication of plant-water stress associated with drying.

Pavelsky and Smith (2008) assessed the relationship between floodplain inundation and river level fluctuations using MODIS (Moderate Resolution Imaging Spectroradiometer) time series data in the Peace-Athabasca River Delta (PAD), a Ramsar Convention wetland. Water surface elevation at four locations in the PAD was highly correlated with MODIS inundated area generated from the NIR band for 2007 when water levels, inundation and connectivity were high, as compared to 2006 when water levels were lower.

2.5 Scale

Scale is central to understanding the complexity of the world's ecosystems and ecosystem processes (Marceau and Hay, 1999). Scale can be defined as the spatial or temporal elements of an attribute that display discernible levels of organization (Turner *et al.*, 2001). It is linked to the attribute of interest and is often described as the “window” of perception (Marceau, 1999; Marceau and Hay, 1999; Hay *et al.*, 2003). In ecology, scale is often characterized by the ‘grain’ which refers to the smallest spatial resolution in observed data and the ‘extent’, which is the size of an area of interest such as the study area “window” (Turner *et al.*, 2001). In digital remote sensing, the nominal ground pixel size, often referred to as the spatial resolution, is essentially interchangeable with grain (Lillesand *et al.*, 2008). Wu and Loucks (1995) state that the scale of observation of an attribute can act as a “blinder,

magnifier or filter”. The challenge is to determine the most appropriate window size or spatial extent in which an observed attribute is most indicative of a physical ecosystem, or of wetland attributes and processes. This research is concerned with the concepts of measurement (resolution) scale and observational (extent) scale (Quattrochi and Goodchild, 1997). Wu and Li (2009) use a similar definition, but consider observation scale to be resolution and geographic scale as extent. To avoid confusion, this research utilized the definition from Quattrochi and Goodchild (1997), but in either case it is concerned with changing resolution and extent. For example, if an attribute such as wetland type or wetland edge/boundary is mapped from remotely sensed imagery, how does that change if the measurement (resolution) and observational (extent) scales change? Another form of scale that is used in geomatics is geographic scale which is the relationship between a distance or point on a map to that on the earth’s surface. Wu and Li (2009) refer to this as the cartographic scale. This research did not address geographical scale in a theoretical manner, however it was considered when changing the measurement and observational scales.

Historically, scale issues were not addressed in investigations of ecological attributes and processes (Marceau and Hay, 1999), however more recently there has been increasing interest in scale and scale issues (e.g. Nagabhatia, *et al.*, 2010; Di Sabatino *et al.*, 2013; Muster *et al.*, 2013, among others). There are two main components of the scale issue (Marceau, 1999; Marceau and Hay, 1999; Wilbanks 2006). First, an appropriate measurement and observational scale (resolution and/or extent) must be selected when trying to map a particular geographical or ecological attribute or process and second, an

understanding of the relationships between scales and the rules that govern them (e.g. cross-scale interactions) is also necessary (Marceau and Hay, 1999; Wilbanks, 2006; Schooley and Branch, 2007).

2.5.1 The pattern-attribute-process relationship: influences of scale

Ecological processes operate over multiple spatial and temporal scales. Nutrient cycling, succession, flood attenuation can be described as ecological processes (Castaneda and Herrero, 2008; Lang and Kasischke, 2008; Dewan and Yamaguchi, 2009). Wetland attributes are often used as indicators of these processes. Patterns in geospatial and/or temporal data can be used to estimate or indicate these attributes, which, in turn, can contribute to assessment of a given ecological process. For example, mapping of the attribute ‘wet extent’ may be accomplished through detection of edge patterns derived from classifications of water or vegetation, or from edges derived from model-based prediction of soil moisture and the saturation extent. Such mapping of wet extent then contributes to improving the understanding of the overall ability of a wetland to attenuate floods (Odum and Barrett, 2005).

2.6 Remote sensing of wetlands

2.6.1 Previous reviews of wetland remote sensing

As stated above, remote sensing can provide spatial and temporal data at different scales that are used to extract patterns indicative of wetland attributes. Many remote sensing studies have linked observed pattern to processes that occur in wetlands, although in general

the assessed attributes related to only one of the wetland components such as the Biological, Hydrologic, Social and Special Features etc. and, in many cases, such studies have only been concerned with one measurement and observational scale. Through a review of the literature, this section outlines and synthesizes results obtained in previous studies that were used to inform the selection of the remotely sensed imagery and methods of this research. Results are included where they are included in the reviews.

Rundquist *et al.* (2001) reviewed the current state of remote sensing of wetlands to that date by listing the imagery types and methods used in previous studies, including air photos to delineate wetlands, or the use of temporal photo sequences to assess vegetation growth over time. They discussed airborne multispectral imaging and the use of such imagery to derive wetland type thematic maps, map wetland conditions, relate wetland vegetation to water temperature using a thermal band, and estimate vegetation structure. Satellite multispectral imaging at multiple spatial and spectral resolutions had been used successfully to delineate wetlands, estimate open water using spectral unmixing, and thermal imagery had been used to discern floating vegetation. Finally, they discussed radar imaging and found that L-band data best discriminated the land-water interface, combinations of Landsat and radar imagery were best for wetland mapping and radar imagery better detected stands of emergent, floating and submerged macrophytes. Shorter radar wavelengths were best for detection of open surface water and to estimate soil-moisture levels.

Following their review of image types, Rundquist *et al.* (2001) reviewed typical wetland applications using remotely-sensed data in a similar manner as those listed in Table

2.2. First, they listed different inventory and mapping applications including the two national surveys made by the U.S. Fish and Wildlife Service to map four broad wetland types: inland-fresh, inland-saline, coastal freshwater and coastal-saline. With the addition of further data, they categorized wetlands into a hierarchical system similar to the Canadian Wetland Classification system. For measuring vegetative biomass, they reviewed several studies that correlated biomass with radiance in specific spectral bands and with indices derived from combinations of spectral bands. The third category they assessed was detection of change and that included studies that used image algebra to delineate and quantify seasonal change in particular vegetation. At that time it was suggested that further investigation into all of these types of research was warranted. Rundquist *et al.* (2001) concluded that the majority of the research in the literature had been on identifying and classifying wetlands, and measuring biomass. The authors suggested that research on spectral reflectance characteristics of wetland species was limited, therefore the research presented in this thesis aimed to look at the spectral reflectance characteristics of wetland vegetation with a variety of sensors such as WorldView-2, Landsat TM and Radarsat-2. Rundquist *et al.* (2001) also stated that information on environmental factors such as wet soils and standing water were limited. This research consequently investigated relationships of soil moisture to different spectral variables such as vegetation indices or radar backscatter. Finally, the authors suggested that basic research into controlled, experimental settings was warranted. This was out of the scope of this research as it did not fit the mandate from the OMNR and the OWES.

Ozesmi and Bauer (2002) reviewed the current state of satellite remote sensing of wetlands to that date. In contrast to Rundquist *et al.* (2001), they first described the types of wetlands that had been studied using satellite remote sensing and concluded that the simplest types to assess were permanently flooded or open water, and then marshes, swamps, (deciduous then coniferous), and shrub-scrub wetlands. All of these types of wetlands have been well studied worldwide. Ozesmi and Bauer (2002) next reviewed the types of imagery that were most useful and, similarly to Rundquist *et al.* (2001), found that satellite multispectral imagery such as Landsat MSS (Multi-Spectral Scanner)/TM, SPOT (Système Pour l'Observation de la Terre), IRS, AVHRR (Advanced Very High Resolution Radiometer) were useful to identify wetland types while radar, including Radarsat-1 and ERS-1 (European Remote Sensing Satellite) C-band data were found to be useful to detect the difference between flooded and non-flooded areas. Ozesmi and Bauer (2002) also listed the types of techniques used for wetlands identification, which included: visual interpretation, unsupervised classification such as ISODATA (Iterative Self-Organizing Data Analysis Technique), principal component analysis, supervised classification such as maximum likelihood classification (MLC), hybrid classification through combinations of supervised and unsupervised classification, vegetation indices such as NDVI, spectral mixture analysis along with sub-pixel classification, and rule-based classifiers. Ozesmi and Bauer (2002) concluded that the techniques that improved classification of wetlands were those that used multi-temporal data and ancillary data. The research presented in this thesis utilized multi-temporal data obtained for different seasons, and through years to ensure that

classifications of wetlands would be optimized. Additionally, the research presented here added ancillary data such as DEM and other geospatial data from the LIO (Land Information Ontario) to improve upon classification accuracies. Ozesmi and Bauer (2002) suggested that layer or rule-based method had better results over typical statistical classification methods. The research presented in this thesis selected the newer rule-based method of CTA (Classification Tree Analysis) to compare to a typical statistical classifier such as MLC to see if these trends continued. The authors suggested that combination of radar and optical research had not been fully explored. This research aimed to add to the literature by exploring the combinations of radar variables with optical imagery to determine if it would improve classification results.

Davidson and Finlayson (2007) reviewed remote sensing for wetland inventory and assessment, which determines the status of a wetland, and wetland monitoring to implement management techniques. Landsat and ASTER (Advanced Spaceborne Thermal Emission and Reflection Radiometer) data were cited as being particularly useful due to their low/free cost, long time series, and global coverage. They identified that few studies to that time had undertaken to identify wetlands across large extents, such as continent-scale or globally. Davidson and Finlayson (2007) acknowledged that with the increasing availability of new satellites and sensors, there was an increased ability to investigate time-series aspects of wetland extent and individual wetland features. The research presented in this thesis aimed to take advantage of these data, such as the long-term Landsat datasets and to investigate vegetation trends in wetlands. Davidson and Finlayson (2007) also suggested that the Earth

Observation techniques may improve the understanding of the biogeochemical cycles, however this was out of the scope of this research, and the researcher's expertise.

More specifically, Silva *et al.* (2008) reviewed remote sensing for the mapping of aquatic vegetation. They reviewed optical remote sensing methods to distinguish between submerged, floating, and emergent plants. The green region of the spectrum was considered to be the most useful followed by the red and red-edge regions. The main challenge of the work was to reduce the influence from the water component, the presence of material such as plankton, sediment or organic material, and organisms that cover plant surfaces. They indicated that the optical spectral reflectance in blue, green, red and NIR, of emergent species would typically be higher than the submerged species. Sensors that could be used to detect these species included air photography, digital camera and videographic sensors, airborne or satellite hyperspectral systems, general satellite sensors such as Landsat, SPOT and IKONOS, and SAR sensors such as JERS-1 (Japanese Earth Resources Satellite), Radarsat-1, ERS-1/2. Methods to assess vegetation biomass included principal component analysis, percent cover, leaf area index and model-predicted physiological characteristics such as chlorophyll concentration, etc. Results included R^2 values from 0.79 to 0.85. For radar mapping of macrophytes, accuracies were indicated to be between 65 to 97% and some specific species could be determined. Silva *et al.* (2008) concluded that hyperspectral data appeared to be very promising for wetland vegetation analysis, however the cost and extent of that type of imagery meant that it was not conducive for a regional program such as the OWES and therefore was not used in this research. Silva *et al.* (2008) also suggested that

combining Radarsat-2 imagery and optical imagery could provide a good data set for investigating emergent wetland vegetation. The research presented in this thesis aimed to combine optical imagery (WorldView-2 and Landsat TM) with derived Radarsat-2 variables to see if that would improve classification of wetland vegetation.

More recently, Adams *et al.* (2010) reviewed multispectral and hyperspectral remote sensing for wetland vegetation mapping. A wide variety studies used multi-spectral data such as SPOT, Landsat and IKONOS data to map vegetation types in wetlands. Techniques included supervised and unsupervised classification, vegetation index clustering and change detection. Levels of accuracy ranged to a maximum of 80% with IKONOS data and it was found that Landsat and SPOT data were insufficient for mapping vegetation species in great detail. To improve upon these accuracies, further techniques had been developed including knowledge-based classifications and combining GIS with remotely sensed data. Accuracies ranged from 81% with digital aerial imagery to 53% with Landsat imagery. Other methods that improved overall classification accuracies included the use of non-parametric artificial neural networks, fuzzy, and decision tree classifiers. Adams *et al.* (2010) concluded that mapping with higher resolution imagery would improve upon classification accuracies. The research presented here aimed to determine if this held true by using higher resolution imagery from a newer optical sensor, WorldView-2. Adams *et al.* (2010) also found that using knowledge-based classification methods and combining these with ancillary data improved upon classification accuracies. This research attempted to explore these findings by combining optical imagery, radar imagery, DEMs and other ancillary geospatial data to

improve upon wetland mapping. Although Adams *et al.* (2010) found that in the literature there were relationships between remotely sensed variables and leaf-area index and other biophysical variables, these were deemed out of scope for this research due to the intensive nature of field assessment for reference data for these types of variables such as clipping and processing biomass in the field. They also suggested that more classification techniques needed to be adopted to improve spatial accuracies. This research aimed to investigate this by combining OBIA with CTA which, at that time, was limited in the literature, and comparing that to traditional knowledge-based methods like MLC.

Radar has been the subject of several reviews of its utility in mapping wetlands. Kasischke *et al.* (1997) reviewed the use of radar for ecological applications. Most studies to evaluated single or multiple polarizations in single or multiple wavelengths. Long wave bands, such as L and P were generally found to interact with large branches or trunks while shorter wavelengths such as C or X, interact with small branches, leaves or needles. The presence of water such as in wetlands often produced double-bounce scattering from the water surface and vegetation edge, producing a stronger ground-vegetation response. The polarization state of the backscatter is measurable and dependent upon the orientation of the scattering elements present in the vegetation. Kasischke *et al.* (1997) next discussed methods used with SAR data to map land cover types. Classifications included manual image interpretation, and unsupervised and supervised classification. Classification accuracies with MLC were greater than 90%. Using multi-temporal SAR data or multi-frequency SAR data was one manner to identify vegetation types. Surface characteristics that could be detected

with SAR included inundation, and differences between marshes and flooded forests. Particularly for wetland inundation and vegetation, SAR data backscatter increases had been shown in flooded forest, but this was typically only detected with L- or P-band data. Where there was no woody vegetation, such as in marshes, specular (forward) scattering resulted in a decrease in backscatter. Kasischke *et al.* (1997) concluded to that time that the utility of polarimetric data as compared to multispectral data still required investigation for land cover classification. They particularly indicated that like-band HH and VV imagery radars could detect flooding under vegetation and for that, L- and P- band were most optimal. They indicated that C-band data worked best for wetlands dominated with herbaceous vegetation. For this research, C-band Radarsat-2 data was obtained for free and additionally several of the wetland complexes in the study area included herbaceous vegetation wetlands. Therefore it was decided to investigate the utility of the C-band Radarsat-2 imagery. The fully polarimetric nature of the Radarsat-2 imagery also allowed for further investigation into the co-polarisation (co-pol) and cross-polarisation (cross-pol) variables. Kasischke *et al.* (1997) finally concluded that the temporal ability of radar imagery would be useful for variations in soil moisture and variations in flooding in non-wooded wetlands. It was decided to investigate this type of temporal analysis by utilizing multi-season Radarsat-2 imagery.

More recently, Henderson and Lewis (2008) reviewed the overall state of wetland detection using radar imagery. They reviewed the five previous major reviews, including Kasischke *et al.* (1997) and then subsequently reviewed the remaining 60 plus studies that had been published between 1998 and their publication date. Studies during that time period

included research using sensors such as Radarsat-1, JERS-1, SIR-C (shuttle imaging radar), AIRSAR (National Aeronautics and Space Administration's Airborne Synthetic Aperture Radar P-, L- and C-band) and ERS data. Classes of Wetland Types and vegetation that had been classified in these studies included: mangrove forest, various tidal subclasses of mangrove, flooded forests, outer and inner salt marsh as well as other coastal marsh types, swamps, various coastal and interior fen types, including treed fen and shrub fen, and bog, with many other variations listed. Methods included: conventional manual interpretation through tone and texture, classification of wetland classes using radar backscatter and various classifiers, statistically modelling vegetation parameters such as tree height, diameter, density, and basal area against backscatter (best correlation to biomass (0.94)); and combining radar with optical imagery in classification (class accuracies ranged from 71 – 92%). As a conclusion, Henderson and Lewis (2008) indicated that as more studies are published there is less consistency between results indicating that many methods and combinations of image types and locations have been used, but results and recommendations vary for all. Henderson and Lewis (2008) also concluded that C-band data would be useful for herbaceous wetland discrimination, but both L- and C- band were needed for separating forest from herbaceous. This research, as noted, freely obtained Radarsat-2 data and it was decided to investigate the utility of the Radarsat-2 imagery alone, and combined with the optical imagery. Henderson and Lewis (2008) suggested that multi-polarization data were good as, or better than multi-temporal imagery. One benefit of this research was the acquisition of both multi-polarized, and temporal data and the ability to assess both of these.

The authors also suggested that while steep incident angle imagery was preferable, more information would be provided with multiple incident angles. It was attempted in this research to obtain multiple incident angle imagery, although the main request was for steep incident angle imagery which had been shown to be preferred for wetland discrimination. Finally, for analysis techniques Henderson and Lewis (2008) indicated that the success of the technique was highly dependent upon the site location, sensor specifications and environmental characteristics, making it difficult to narrow down the preferred methodology. However, what they did find is that radar and optical combinations always produced better results, however without a consistent set of combination(s). This research attempted to confirm and add to the literature by combining optical and radar variables with CTA and OBIA, newer analysis methods that had not yet been fully explored in the literature.

A final article that warrants review in the context of this thesis is Touzi *et al.* (2007), which gives an indication of wetland classification potential utilizing newer polarimetric capabilities, specifically of Radarsat-2 imagery. For a specific wetland, Mer Bleue Bog, which is also one of the study sites of this research, they showed that there was limited capability of single-polarization C-band data and discussed the use of the Cloude-Pottier (1997) and Touzi (2007) decompositions for mapping Wetland Types of marsh, treed bog, shrub bog, and fen as well as upland classes of deciduous forest and agricultural fields. They found that the Touzi decomposition parameters distinguished these classes well, improving slightly on the Cloude-Pottier decomposition parameters, although accuracy statistics for the thematic map produced were not provided. The paper suggests that the Cloude-Pottier alpha

and entropy combined alone does not allow for discrimination of wetland vegetation species (Touzi *et al.*, 2007) and that Touzi decomposition would be preferable.

This section now focusses on the literature on remote sensing methods that are directly pertinent to this research. There are many methods that can be used to map wetland attributes that have been described above and a further brief synopsis is provided in Table 2.2 following the structure of Rundquist *et al.* (2002). This synopsis overlaps with Henderson and Lewis (2008) and Adams *et al.* (2010) as it was completed at the beginning of this research to inform the overall directions taken and selection of appropriate methods.

General analyses performed with remotely sensed imagery can be broken down into three broad categories including: attribute mapping, biophysical modeling and temporal analysis. Table 2.2 summarizes these including the scale of the study, the method used, and the potential applications. There is some overlap between categories as certain types of classifiers or analysis techniques can be applied in more than one category (1st column of Table 2.2). The accuracies of the varying classifications listed in the table range from about 30% to 100%. Typically classifications with 4 or more class types had lower accuracies (30 to 75%), whereas classifications with 1 to 3 classes had higher accuracies (85 to 100%). For statistical relations between geospatial and biophysical variables, R^2 values were typically moderate (0.5-0.7) to high (near 0.9), depending on the sensor, resolution, attribute precision, environmental conditions, etc. Biophysical variables typically had lower R^2 values ranging 0.5-0.6 whereas some hydrological variables such as flooded extent had higher R^2 values such as 0.9 or higher. Specific accuracies related to the 14 Wetland Type attributes

found in the literature are discussed in Table 2.5. This research was designed to improve on or meet these general accuracies using a different, newer high resolution imagery type (WorldView-2) and by combining existing variables from moderate resolution image types such as Radarsat-2 polarimetric data with Landsat TM-5 derived variables.

There are both benefits and limitations to employing remote sensing analyses for wetland mapping. The key benefits include that remote sensing provides spatially extensive coverage including adjacent upland areas. This means all points within an area have associated data compared to field sampling techniques where only a sub-portion of an area can be sampled. With remote sensing repeatable data acquisition at varying temporal scales is achievable and the digital nature of satellite remote sensing products allowing for complex analyses (Ozesmi and Bauer, 2002).

Limitations of remote sensing for wetland assessment include wetland temporal dynamics (both seasonally and annually), which make it difficult to represent all possible wetland characteristics with only one date of imagery or with individual dates of imagery over several years as phenology and hydrology vary from year to year due to environmental conditions. Therefore, even images obtained on anniversary dates are affected by differences in snowpack and weather occurring before they were acquired. Remote sensing analysis is based on image representation of surface reflectance, which is an indirect indicator of many surface attributes.

Table 2.2. A synopsis of the types of remote sensing and GIS analyses methods for wetlands in general.

Overall Category	Type of Technique	Scale	Example Applications and Comments	Representative Studies
Mapping	Classification: Parametric techniques (supervised and unsupervised)	Local for plant species to regional for wetland type classification.	Plant species, especially for determination of rare species.	<ul style="list-style-type: none"> • Harvey and Hill (2003) • O'Hara <i>et al.</i> (2003) • Belluco <i>et al.</i> (2006) • Laba <i>et al.</i> (2008)
	Classification: Non-parametric techniques (fuzzy classification, sub-pixel unmixing classification, Artificial Neural Networks (ANN), OBIA	Local for plant species to regional for wetland type classification	<p>As above, and for some classifiers such as neural networks and OBIA multiple sources of data can be used (e.g. DEMs, multi-sources of imagery; other data (e.g. quaternary geological layers).</p> <p>Most of these methods are proving to be more accurate than traditional parametric methods.</p>	<ul style="list-style-type: none"> • Berberoglu <i>et al.</i> (2004) • Rogers and Kearney (2004) • Schmid <i>et al.</i> (2005) • Chiu and Couloigner (2006) • Filippi and Jensen (2006) • Durieux <i>et al.</i> (2007) • Grenier <i>et al.</i> (2007) • Melendez-Pastor <i>et al.</i> (2010)
	Classification: Nonmetric (decision/ classification trees)	Landscape to regional although theoretically should be able to classify at the local level	As above. Most studies show accuracy improvements with the addition of ancillary data.	<ul style="list-style-type: none"> • Li and Chen (2005) • Wright and Gallant (2007)
Biophysical Modelling	Hydrologic	Local to landscape to regional	<ul style="list-style-type: none"> • Relations between runoff and percent cover or runoff and cover type; • Changes assessed in surface/near surface soil; • Image-based indices as indicators of soil moisture conditions and vegetation stress; • Radar backscatter and flood mapping; and 	<ul style="list-style-type: none"> • Quinton <i>et al.</i> (2003) • Harris <i>et al.</i> (2005) • Lang and Kasischke (2008)

			<ul style="list-style-type: none"> • Water surface elevation correlated with inundated area (generated from NIR band). These studies showed the value of vegetation and moisture indices and the ability to assess hydrologic features/functions (e.g. surface water, flooding inundation, etc.). 	
	Biogeochemical	Local to landscape	<p>High potential to assess soil properties that may be useful in predicting some wetland functions (e.g. substrate/soil composition; organic material composition, ecological integrity of the wetland, etc.).</p> <p>These studies showed strong relationships between indices derived from imagery, total soil phosphorus and distance to water control structures.</p>	<ul style="list-style-type: none"> • Rivero <i>et al.</i> (2007; 2009)
	Biological	Local to landscape	<ul style="list-style-type: none"> • Predictions of above-ground biomass and net primary productivity are possible using image-based indices; and • Relationships between tide height and vegetation indices (negative correlations). <p>These studies have shown the ability to produce other spatial distribution maps that may be used to aid in the understanding of wetlands (e.g. functions such as ecological integrity; dominant land use; amount of impervious surface; overall wetland condition; overall biological condition, etc.).</p>	<ul style="list-style-type: none"> • Hardisky <i>et al.</i> (1984) • Tan <i>et al.</i> (2003) • Li <i>et al.</i> (2007) • Dillabaugh and King (2008) • Yan <i>et al.</i> (2008)
Change detection of wetlands	Seasonal change	Landscape	Assess flooding extent and water level changes within a season and link to key hydrologic functions.	<ul style="list-style-type: none"> • Pope <i>et al.</i> (1997) • Lu and Kwoun (2008)

			<p>These studies used seasonal change in polarimetric backscatter magnitude and phase; and used interferometric synthetic aperture radar (InSAR) to assess water level changes with great detail.</p>	
Annual change	Local, landscape and regional	<ul style="list-style-type: none"> • Presence/absence of vegetation or changes in percent cover; • Annual changes in evapotranspiration (ET) and spatial distribution of ET; • Soil moisture related to percent cover (e.g. unsaturated, saturated, inundated); and • Hydrologic dynamics of wetlands. <p>These studies aid in the knowledge of the overall “health” of wetlands and trends in wetland dynamics using: classification change analysis to assess change in wetland size; estimations of evapotranspiration from multiple optical images to assess restoration activities (planting, ditch closures); change vector analysis to assess change over decades; SAR data over long period to assess surface hydrological patterns.</p>	<ul style="list-style-type: none"> • Munyati (2000) • Melesse <i>et al.</i> (2006) • Baker <i>et al.</i> (2007) • Sass and Creed (2008) 	
Combined seasonal and annual change	Local, landscape and regional	<ul style="list-style-type: none"> • Change in total wetland area and rates of wetland loss; • Correlations between functional traits and principal components of image data; • Defined ecosystem functioning types; • Annual and seasonal NDVI trends; • Mapping recharge and discharge per season; and 	<ul style="list-style-type: none"> • Kent and Nystrom Mast (2005) • Alcaraz <i>et al.</i> (2006) • Beerli and Phillips (2007) 	

			<ul style="list-style-type: none"> • Determine surface water trends over multiple years. <p>These types of methods using aerial, AVHRR, and Landsat imagery can provide important seasonal hydrologic information that may be missing from many evaluation systems because of singular field site visits. They provide additional information on functions (e.g. rates of change, trends, etc.).</p>	
GIS analyses of wetlands	Mapping	Local, landscape and regional	<ul style="list-style-type: none"> • Interpolation of soil pH distribution in combination with thematic maps to assess species distribution of mangroves; • Using GIS and a combination of data, beaver pond occurrence and their correlation with stream order, elevation, deciduous cover and amphibians can be statistically assessed; • Mapping wetland area using a Bayesian probability model as a post-classifier to improve the quality of a thematic map; and • DEMs derived from high resolution LiDAR data to improve classification of Wetland Type mapping. <p>Strong potential for use of multiple data sources including non-remotely sensed data (e.g. soil data) to map wetland characteristics. Also the ability to improve upon products derived from remotely sensed data.</p>	<ul style="list-style-type: none"> • Vaiphasa <i>et al.</i> (2006) • Hogg and Todd (2007) • Hogg and Holland (2008) • Murphy <i>et al.</i> (2007) • Stevens <i>et al.</i> (2007)
	Change analyses	Local, landscape and regional	<ul style="list-style-type: none"> • Decadal change in total soil phosphorous (P); • Extent of increase in total soil P; 	<ul style="list-style-type: none"> • DeBusk <i>et al.</i> (2001) • Papastergiadou <i>et al.</i> (2008) • Wilcox <i>et al.</i> (2008)

			<ul style="list-style-type: none"> • Change in land cover types in wetlands; • Changes in wetland plant communities; and • Changes in water levels. <p>These studies have shown that hydrologic dynamics of wetlands and soil properties can be monitored effectively using GIS.</p>	
	Biophysical modeling	Local, landscape and regional	<ul style="list-style-type: none"> • Predicting patterns of plant species; • Assessing habitat quality and diversity; and • Impacts of human activity by characterization of activities and water chemistry. <p>These studies have accurately assessed biophysical properties of wetlands.</p>	<ul style="list-style-type: none"> • van Horssen <i>et al.</i> (1999) • Berberoglu <i>et al.</i> (2004) • Morrice <i>et al.</i> (2008)
	Population analyses and habitat conservation	Local, and landscape	<ul style="list-style-type: none"> • Calculation of population and habitat requirement statistics; • Habitat suitability assessment; • Connectivity of core areas assessment; and • Assessment of breeding bird wetland habitat. <p>These studies were able to assess fauna population statistics and information when remote sensing is not readily available or applicable.</p>	<ul style="list-style-type: none"> • Beazley <i>et al.</i> (2005) • Connor and Gabor (2006)

As it can be seen from the review above it is well accepted that the advantages of using remote sensing for wetland analysis outweigh the limitations (Lee and Lunetta, 1995; Ozesmi and Bauer, 2002; Davidson and Finlayson, 2007; Moffett and Gorelick, 2013). In this research to address these limitations, especially temporal issues, analyses were conducted on image date selection and long term differences in image variables.

2.6.2 GIS analyses of wetlands

As a broader framework and set of tools to represent, process and analyze geo-spatial and temporal data, GIS is useful because of its capability to integrate a number of data types, including remotely sensed data (e.g. thematic maps, change statistics, biophysically modelled variables, etc.) and other geo-spatial data types such as soils data, topographic, and census data, etc. Rather than derive metrics directly from imagery (e.g. using band brightness/reflectance or radar backscatter), information is derived from products previously created such as thematic maps, DEMs, etc., many which may have been derived from remotely sensed imagery. To maintain consistency with the presentation of the remote sensing methods in this chapter, focus is placed on GIS methods utilized in this research. More generalized methods are outlined in Table 2.2.

Many of the attributes of interest for this research require boundaries be identified. There have been many GIS-based studies that have used both remotely sensed data and other geo-spatial data to map wetlands and wetland boundaries. Topography is a key component for mapping and evaluating wetlands. It acts as a major control on wetland distribution (Murphy *et al.*, 2007) and influences many of the processes that occur within wetlands, specifically the hydrologic functioning, distribution of soil carbon stocks, decomposition, net primary production, among others (Ferone and Devito, 2004; Ju and Chen, 2005; Murphy

et al., 2007; Murphy *et al.*, 2009). DEMs, as representations of topography, are often used to derive wetland variables. Topographic indices, such as the soil wetness index (SWI) and depth-to-water (DTW) index (Murphy *et al.*, 2009) are often derived from DEMs that are, in turn, generally created with remotely sensed imagery (e.g. LiDAR, optical imagery, interferometric radar, etc.).

Hogg and Todd (2007) compared three methods to delineate the boundaries of wetlands in Ontario. They used a DEM to derive wetland terrain variables (topographic index, contributing area and slope, standard deviation of slope, planform curvature, profile curvature, amongst others). Logistic regression was used to determine which variables should be retained for subsequent mapping. The first model was the visual derivative threshold method (where topographic index and positive mass balance hydraulic slope (two uncorrelated variables) were used in a density slicing approach; the second model was a logistic regression model of the variables; and the third model used a classification and regression tree (CART) statistical analysis. Using the visual derivative threshold method, the overall accuracy was 99% however 37% of upland was also mapped as wetland. With reduction of the threshold values, the wetland mapping accuracy decreased significantly. For the CART method, the overall validation accuracy was 84%.

Hogg and Holland (2008) compared the use of a high resolution DEM that was derived from LiDAR data to a coarser DEM (20m resolution) to classify wetland types using the CART methodology described above (Hogg and Todd, 2007). They found that the addition of the high resolution DEM improved the overall mapping of Wetland Types.

Many layers containing information on hunting, recreation and land ownership are available from the OMNR. These types of layers can be used as predictor variables in

analyses of current and potential wetland land-use change in a GIS. For example, Allen *et al.* (2002) attempted to determine suitable predictors of potential land use change around the South Carolina coastal area. Using spatial logistic regression analysis, they found that land ownership variables and primary roads were strong predictors of commercial development, while beachfront, open view, private ownership data were indicators of residential development. Prediction success for the model was 90% for residential, and 92% for non-residential parcel use. For the social features and features relating to human constructs such as ownership there is fewer studies that relate to this work. Available such studies are listed in Table 2.5.

2.6.3 Sensors used for wetland attribute analysis pertinent to this research

The sensors used for wetland mapping can be categorized by the measurement and observational scale at which imagery is obtained. For this research, wetland analyses were conducted using two measurement and observational scales of optical imagery and one of radar imagery (Table 2.3). The following section outlines the capabilities of the sensors to record particular listed aspects of wetland vegetation structure and form, wetland hydrology and general land use land cover configuration as well as previous studies that have used such imagery for wetland analyses. For specific methods selected for this research more detail is provided in sections 2.8.1 to 2.8.4.

Optical imagery may include the spectral bands in the ultraviolet, visible, and infrared portions of the electromagnetic spectrum. The spectral bands and spectral resolution (the bandwidth of each spectral band) impact the type and precision/accuracy of information derived for wetlands. Healthy vegetation reflects strongly in the NIR (approximately 0.7 to

1.1 μm) portion of the spectrum (Jensen, 2005), and live and dead plants can be discriminated (Lyon, 2001).

Table 2.3. Sensors used for remote sensing of wetlands in this research. MS is multi-spectral, PAN is panchromatic, and TIR is thermal infrared.

	Satellite/ Sensor	Dates of Service	Spectral Range (μm)	Approximate Spatial Resolution (pixel size, m)	Approximate Swath (km)
Fine Optical Imaging Sensors	WorldView-2	Launch 2009- present	8 bands (0.45-1.04) plus PAN	0.50 MS, 1.84 PAN	18
Medium Optical Imaging Sensors	Landsat TM-5	1984-June 2013	7 bands (0.45-2.35 plus thermal (10.4-12.5)) plus PAN	30 MS, 120 TIR	180
Radar	Radarsat-2	December 2007- present	C-band Dual/single/ quad polarisation	3-100	3-500 depending on resolution

Distinction can be made between submerged plants with extremely low NIR as water absorbs NIR to a depth of 5 cm in comparison to floating or emergent vegetation in non-laboratory settings (Silva *et al.*, 2008). Soil types and soil moisture display reflectance variation in the visible portion of the spectrum, but are better assessed using the short-wavelength infrared (SWIR, 1.1 to 2.4 μm) (Lyon, 2001), which is absorbed strongly by water. This portion of the spectrum can be used in the identification of hydric soils (Lyon, 2001). The edges of water bodies can be identified well using the NIR (e.g., the boundary of water/soil/vegetation) due to the significant contrast between water with almost no NIR reflectance and adjacent land with reflectance of about 30-60% for soil, rock, or vegetation. In the visible portion of the spectrum, sediment loaded water reflects more in the green and

red than clear water. Shallow water may also reflect more in the visible than deep water if radiation can penetrate to the bottom of the water body and reflect back to the sensor. Vegetation and water indices (some calculation/combination of several spectral bands) can often improve discrimination of water, soil and vegetation and model their condition (Rivero *et al.*, 2009; Satyanarayana *et al.*, 2011; Kim *et al.*, 2012).

Although there are no strict definitions, high resolution optical imagery typically has minimum pixel sizes in the range of a few centimetres to approximately 5 m with swaths covering up to 20 km. Such images can cover individual wetlands (e.g. a marsh within a wetland complex) or small wetland complexes, and can provide information about spatial characteristics within wetlands (e.g., classify specific salt-marsh vegetation (Belluco *et al.*, 2006); relate remotely sensed derived metrics to biomass (Dillabaugh and King, 2008); examine the distribution of beaver dams (Stevens *et al.*, 2007); identify dredged soil disposal sites, and sites colonized by the common reed (Hudon *et al.*, 2005)). High resolution optical imagery has been used to map Wetland Types on an island in Yueqing Bay China (Zhang *et al.*, 2011) and to estimate biomass in densely vegetated wetlands in South Africa (Mutanga *et al.*, 2012). In the latter, normalized difference indices using the same formulation NDVI were calculated from all possible two-band combinations of the eight bands for WorldView-2 imagery. These indices were the same form as the common NDVI derived as:

$$NDVI_i = \frac{(NIR-R)}{(NIR+R)} \quad \text{Eq.2.1}$$

- where NIR is the near-infrared spectral band of a sensor; and
- R represents the red spectral band of same sensor.

A model was constructed relating these values to field sampled biomass using random forest (RF) regression (an ensemble learning method, also known as bagging or

bootstrap aggregation). They were able to identify the smallest number of index images that provided the best biomass prediction model (R^2 0.76; RMSE = 12.9% of mean biomass). The indices included red-edge and NIR1 bands, red-edge and NIR2 bands and the green and NIR2 bands).

For optical imagery with moderate resolutions, minimum pixel sizes are typically in the tens of metres and swaths of up to 200 km. Such images encompass whole wetland complexes (landscape level) and cover regional areas (e.g. eastern or southern Ontario). Minimum wetland sizes for mapping are greater than 1 ha at these scales (Jensen, 2005) and applications include landscape level analysis such as mapping of the Prairie Potholes Regions (Mita *et al.*, 2007); estimation of carbon emissions from peat along the coastal plain in North Carolina, USA (Poulter *et al.*, 2007); and delineation of plant functional types at Poyang Lake, China (Dronova *et al.*, 2012).

The potential for mapping wetlands at landscape to regional scales has been shown with radar imagery for very broad land cover classes (e.g. wetland and non-wetland), and broad wetland vegetation classes (e.g. shrub, forested, etc.) (Hess *et al.*, 2003; Racine *et al.*, 2005; Durieux *et al.*, 2007; Grenier *et al.*, 2007; Touzi *et al.*, 2007; Henderson and Lewis, 2008; Marechal *et al.*, 2012). It works well in detecting seasonal changes, including flooding (Pope *et al.*, 1997; Lu and Kwoun, 2008). SAR sensors emit microwave pulses in wavelengths that are generally unaffected by atmospheric moisture, dust or clouds. They are also not limited by time of day sun-angle acquisition issues that impact optical imagery (Fernandez-Ordonez *et al.*, 2010). Wavelengths are also longer than traditional optical analysis allowing for different information to be derived from the landscape. Strong positive and linear correlations have been found between radar backscatter and wetland vegetation

biomass (Li *et al.*, 2007). Radar imagery has proven useful for mapping Wetland Type classes and specific wetland vegetation, including invasive species (Li and Chen, 2005; Racine *et al.*, 2005; Grenier *et al.*, 2007). Radarsat-2 has been used to identify and delineate seasonal flooded extent in a time series for a wetland in Brittany, France (Marechal *et al.*, 2012).

Wavelengths that work well for the detection of wetlands include C-band (approximately 5.6 cm wavelength) and L-band (approximately 20 cm wavelength) at landscape to regional scales. Longer wavelengths penetrate deeper into vegetation canopies than shorter wavelengths and are better suited to modelling and mapping of forested wetlands and swamps with standing dead trees. C-band has been shown to detect herbaceous wetlands (Henderson and Lewis, 2008) and to detect open smooth water due to specular reflectance of the pulse away from the sensor, which creates a black object in the imagery. Depending on the spatial resolution, incidence angle and canopy openness, radar signals may 'double bounce' or corner reflect off trunks, such as standing snags in open swamps or emergent vegetation (e.g. reeds) (Karszenbaum *et al.*, 2000; Kandus *et al.*, 2001) producing bright point signals. Radar can also be polarized in both the emitted and received signals. In general in the literature, HH polarisation was generally used more than VV, but cross-pol (HV or VH) was also useful (Li and Chen, 2005; Henderson and Lewis, 2008; Lu and Kwoun, 2008). HH polarisation was better correlated with soil moisture and inundation than VV polarisation (Dobson and Ulaby, 1988; Lang and Kasischke, 2008), however, at shallower incidence angle, soil moisture was less influential on all polarisations (HH, HV, VH, VV) (McNairn *et al.*, 2002). Many Wetland Types (bog, fen, saline and freshwater marsh) have been better discriminated with HH polarisation than with VV (Li and Chen,

2005; Henderson and Lewis, 2008; Lu and Kwoun, 2008), however VV has been shown to be useful for cattail and low density marshes (Henderson and Lewis, 2008). The swath of satellite-based radar images can range from 20 km to 500 km and can cover similar areas as high to moderate resolution optical imagery. Polarimetric decompositions, either coherent or incoherent, express the scattering matrix as some combination or summation of the scattering responses from the surface (Touzi, 2007). These variables have been used to categorize Wetland Types (bog, treed bog, fen, marsh) (Touzi *et al.*, 2007).

2.7 Remote sensing of hydrology and forestry as it relates to wetland research

Hydrology has a significant role in wetlands, and forest structure has sometimes been found to be similar to the structure of swamp vegetation, therefore it is important to consider some of the literature as it relates to the wetland analysis in this research.

2.7.1 Hydrology

Pietroniro and Leconte (2005) reviewed the research in remote sensing for hydrological applications in Canada. The particular sensors found to be most useful included Radarsat-1, AQUA and ENVISAT for soil moisture, Landsat for vegetation and SPOT, ERS-1/2, Radarsat-1 and Landsat for surface water. In one study, near surface soil moisture could be extracted from SAR data using linear regression between backscatter and measured soil moisture, however, they noted that these models could not be transferred between sites of interest. In another study, using polarimetric data from the Canadian Convair-580 C-band SAR system, it was not possible to develop a conclusive relationship between soil moisture and backscatter response. For surface water, Pietroniro and Leconte (2005) discussed the use of the near and mid-infrared portion of the spectrum as important to contrast between

water and vegetation. Additionally, SAR systems showed utility in differentiating between open water and vegetation, however these results are complicated by the Bragg effect, which produces backscattering from surface waves.

More recently, Klemas (2011) reviewed remote sensing in hydrology and showed the utility of using LiDAR for discrimination of flooded marsh types and separation between plant species as well as multi- and hyper-spectral imagery for discrimination of Wetland Types and bio-chemical and bio-physical properties of wetland vegetation. Methods used included common pixel-based classification such as MLC, but it was also shown that OBIA was frequently being used as a means to capture spatial pattern of spectrally mixed land covers, like submerged vegetation.

2.7.2 Forestry

Govender *et al.* (2009) reviewed the use of remote sensing data and the development of spectral reflectance indices to detect plant water stress. The spectral bands that proved useful to detect plant stress included those in the visible, near- and short-wave infrared portions of the spectrum. Particularly, they found research that related changes in the green band due to chloroplast deterioration. They also reviewed studies that showed green and NIR ratios to be highly correlated with chlorophyll concentration. In addition, they summarized research that used Landsat bands 5 and 7, representing the short-wave infrared portion of the spectrum, to model and map soil and vegetation water content.

Roberts *et al.* (2007) reviewed the current literature to that time to assess the state of the remote sensing of forest structure. Categories of detectable variables were given for different satellite resolutions. Contextual forest attributes such as leaf area index, timber volume, above-ground biomass and basal area could be well estimated with Landsat TM and

ETM+ sensors utilizing regression or classification methods. Accuracies were given as mostly R^2 values ranging from 0.67 to 0.83. For variables such as forest age class, individual tree detection and crown detection, and mangrove species mapping, high resolution multispectral or hyperspectral sensors were required (e.g. satellite sensors such as IKONOS; airborne hyperspectral sensors such as the CASI). With such high resolution imagery, image spatial information such as image texture, and object-based classification were found to improve biophysical estimates with R^2 values of 0.76 to 0.82, and species classifications with overall accuracies ranging from 67% to 89%.

2.8 Remote sensing methods for the mapping the 14 selected OWES attributes

The remote sensing image analyses methods applied to map the 14 attributes in this research used the spectral bands of the imagery, mathematical combinations and decompositions of that spectral information, additional geo-spatial data including DEMs, and social spatial information. The overall methods that were used to derive data are described in this section as background information. Equations numbers are only given for those equations used in this research; other equations given in the text are for definition purposes only. Metrics that have potential to be evaluated through remote sensing and other geospatial data are of interest for this research and include: object and sub-pixel spatial configuration; vegetation indices thresholds, classification methods, and radar-based variables (Ju and Chen, 2005; Artigas and Yang, 2006; Frieswyk and Zedler, 2007; Rivero *et al.*, 2007). Some of these particular methods were repeatedly used for mapping several of the attributes and are noted as such in each particular attribute section following the methods descriptions and backgrounds in sections 2.8.1 to 2.8.2.

2.8.1 Object-based image analysis

The main intent of OBIA is to segment imagery into objects representing relative spatial homogeneity in reflectance and then classify the segmented objects as land cover classes (e.g. bogs, upland forest, streams) of interest.

The technical objective in segmentation is to define objects that have minimized within-object variability, and maximized between-object variability. The creation of objects from individual pixels is based upon the spectral and spatial properties of neighbouring pixels and subsequently created objects (Burnett and Blaschke, 2003). Segmentation algorithms are categorized as edge-based and area-based (Jensen, 2005). Edges occur where there are sharp changes in brightness values. In edge-based segmentation the growth of objects is based upon the edges and linked edges that may signify borders. Problems can occur if edges are not present where a real border exists, or if edges are present where no real border exists. Area-based (also known as region-based or region growing) segmentation compares pixels or groups of pixels (the 'seed') and merges comparable areas as long as they are homogenous within a defined tolerance. Large heterogeneous areas can also be split into smaller homogenous units. Some segmentation algorithms use a combination of splitting and merging.

The following discussion focuses on the aspects of eCognition Developer 64 (8.64) which is a widely available object-based software suite that was used in this research. It includes the most common algorithm for object segmentation, the area-based algorithm known as multi-resolution segmentation. Marpu *et al.* (2010) showed that this algorithm was one of the two best from a comparison of 12 segmentation algorithms in terms of positional accuracy of segmentation of land cover objects using IKONOS imagery in an urban setting

and vegetative area. The evaluation of the 12 algorithms was completed by comparing created objects with reference segments for 10 reference areas. The algorithms were assessed based upon lost pixels and extra pixels in relation to the reference data. The other algorithm that performed well was SEGEN (Gofman, 2006). eCognition was chosen for this research because it performed as well as the SEGEN algorithm in this study, it performed well in other studies of land cover classification (Benz *et al.*, 2004; Yu *et al.*, 2006; Dingle Robertson and King, 2011; Barker and King, 2012), and it was available for this research.

The key parameter in multi-resolution segmentation is a unitless variable of scale that is correlated to the image's pixel size and is related to the parameters of colour (spectral (or other pixel value (e.g. DEM)) information) and shape (the physical characteristics of the image features (Laliberte *et al.*, 2004) further defined by smoothness and compactness). Most researchers follow a "trial and error" process in order to determine the best scale, shape and compactness values (Ouyang *et al.*, 2011; Duro *et al.*, 2012; Aguilar *et al.*, 2013). Traditionally, this has been through comparison of how well the segmented object boundaries align with visually interpreted objects. Tian and Chen (2007) utilized a matrix format and visual interpretation to test scale parameter selection. Dronova *et al.* (2012) used nine scale parameters (2 to 10) to create wetland objects varying of sizes based upon field observations, and assessed the scale parameter accuracy based upon the accuracy obtained in classification. More recently, the estimation of scale parameter (ESP) tool developed by Dragut *et al.* (2010) was proposed as a means to automatically and quantitatively optimize scale parameter value selection. This tool creates objects at a variety of scale parameter values and calculates the local variance of the object heterogeneity. Subsequently, the local variance is plotted against the change in scale parameter value and the rate of change is

calculated. They found that the tool enabled an accurate selection of a scale parameter value for a variety of image types. As this tool by Dragut *et al.*, (2010) was developed during this research, and subsequently published after OBIA had been completed for this research it was not employed. Instead, this research followed the `trial and error` matrix method proposed by Tian and Chen (2007) and qualitatively assessed the accuracy of the scale parameter value based upon assessed overall classification accuracy.

Once the scale parameter has been selected, objects are segmented based upon similarity of pixels, contrast of an object with neighbouring objects and object shape characteristics. In general, the larger the value of the scale parameter the larger the resulting image objects (Benz *et al.*, 2004). Objects are grown evenly and simultaneously across the entire scene. Colour and shape (smoothness and compactness) can be weighted by the user (Laliberte *et al.*, 2004). As objects are created they are merged together following the scale, shape, colour, smoothness and compactness parameter values. The process ends once the growth of the objects satisfy the values of scale, colour and compactness defined (Laliberte *et al.*, 2004). This creates one object level in a hierarchy (Figure 2.2). The multi-resolution segmentation process can be applied again with a different scale parameter value to the first object level to obtain a second level of objects at a higher or lower level in the hierarchy. Once segmented, objects can be classified at any level within the developed hierarchy.

In previous research it has been found that OBIA produces more useful thematic maps showing land cover entities as humans perceive them as compared to pixel-based thematic maps (Dingle Robertson and King, 2011; Brenner *et al.*, 2012; Dronova *et al.*, 2012; Duro *et al.*, 2012; Meneguzzo *et al.*, 2013).

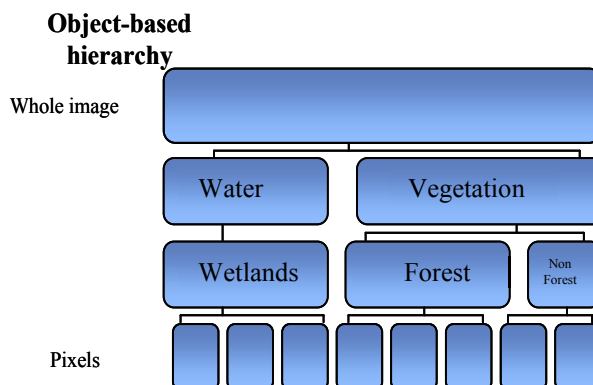


Figure 2.2. Simplified object-based hierarchy with the lowest level representing pixels and the top level representing the whole scene. Mid-levels represent segmented object levels. Examples of classes at mid-levels are for illustrative purposes only.

Accuracies assessed using pixel-based sampling are sometimes higher than pixel-based accuracies, however, in some cases (Dingle Robertson and King, 2011 and Duro *et al.*, 2012) OBIA accuracies are found to be not significantly better. OBIA classification accuracy assessment is more appropriate on an object-basis and thus accuracies cannot be compared in a simple manner to pixel-based classification accuracies. The benefit of OBIA is that through qualitative assessment it proves to provide more useful and accurate maps. There has been little investigation with OBIA and WorldView-2 imagery. However, there has been research with other high resolution imagery. For example, Ouyang *et al.* (2011) used OBIA with Quickbird imagery to map saltmarsh plants and were able to classify two classes of salt marsh vegetation, and a non-vegetation class with an overall accuracy of 87%. Moffett and Gorelick (2012) used OBIA with IKONOS imagery to derive vegetation zones, patches and surface water channels for salt marshes in San Francisco Bay. Through testing, they were able to determine the best scale, colour, shape (smoothness and compactness) parameter values to derive these features.

For combining optical and radar imagery with OBIA, Grenier *et al.* (2007) used Landsat ETM+ and Radarsat-1 imagery to map wetlands in two sites for the Canadian Wildlife Service Canadian Wetland Inventory (CWI) with the five classes of Bog, Fen, Marsh, Swamp and Shallow Water. Objects were found at each of three segmentation levels and were subsequently merged back into the five classes of interest. Accuracy was assessed both thematically and spatially based on interpretation of Landsat colour composites and use of photos taken from a helicopter. For thematic accuracy, all wetlands were combined into one wetlands class versus 'other' (open water was not validated as confusion was thought to be very low), resulting in 82% and 90% accuracy for the two study sites. In addition, accuracy was assessed between the five wetland classes, resulting in 76% and 68%, respectively

Durieux *et al.* (2007) used 300 m pixel MEdium Resolution Imaging Spectrometer Instrument (MERIS) data, 100 m pixel JERS-1 radar data, and SRTM (Shuttle Radar Topography Mission) to classify wetland complexes (seven classes: river, riparian vegetation, lichen and mosses, lakes, dark taiga, broadleaf forest, bogs and anthropic area/bare soil) in western Siberia. A Landsat TM derived pixel-based thematic map with an accuracy of 89% was used for validation. The object-based technique used was the fractal net evolution approach (FNEA) which segments images simultaneously at two levels and then subsequently builds semantics between the levels and the corresponding level units (patches). The first object level was created using multi-resolution segmentation solely based upon the radar backscatter coefficient and the second object level was created using the spectral difference algorithm for three MERIS bands (555-565 nm, green; 677.5-685 nm, red; and 855-875 nm, NIR). A classification rule set was defined using the three levels of

segmentation (e.g. objects that overlapped SRTM water bodies and areas with low backscatter on the radar image were considered lakes). The overall accuracy for this classification was 72.5%.

Based upon the literature, it was expected that OBIA applied to WorldView-2 imagery and combinations of other data types (including radar) would improve upon accuracies in the literature which, for example, ranged from 68% to 76% when more than two Wetland Types were classified using lower spatial resolution imagery. Similarly, it was expected that these data and methods would improve upon accuracies reported in the literature for VCFs, which ranged from 76-91%. It was hoped that OBIA would prove to be useful with higher resolution imagery alone and combined with radar imagery, which has not been shown in the literature for Open Water Type.

2.8.2 Linear Spectral Unmixing (LSU)

Individual pixels are often comprised of more than one land cover class (e.g., 25% water, 30% soil, 45% vegetation). While fuzzy classification and resulting membership scores may indicate the degree of similarity of pixel values to individual class training data, and the scores may be related to proportion of each land cover type in a pixel, LSU or spectral mixture analysis is a technique directly linked to reflectance theory of linear mixing of radiance from land cover types within a pixel area (Jensen, 2005).

Endmembers (EMs) represent the major radiometric land covers such as water, asphalt, concrete, healthy vegetation canopy, etc. present in an image (Neville *et al.*, 1998). These can be manually selected using known training areas of pure pixels, however a limitation is that there are often few known sites where an area would be completely pure. Other more automated methods of choosing EMs have been developed; one of the most

common that was used in this research is the iterative error analysis (IEA) algorithm. An initial vector (the mean spectrum of the data) is chosen to start the process. A constrained unmixing (where each fraction must fall between 0 and 1 (Neville *et al.*, 1998)) is then performed and an error image is developed. The process chooses the EM as that which minimizes the remaining error in the unmixed image, therefore the average of the vectors with the largest error (distance from the initial vector) is assumed to be the first EM. Another constrained unmixing occurs and the error image is found again. The average of the vectors with the largest distance from the first EM is considered the second EM. This process continues until all EMs are found or a specified number is reached.

From the location of EMs within an n-dimensional space, a linear mixing model (Rogers and Kearney, 2004) is used to determine the proportion of each EM in each pixel. The most commonly used model (and associated with most remote sensing software) is the Least-Squares Mixing Model (Shimabukuro and Smith, 1991), which defines the spectral signature of a pixel per spectral band as the sum of the reflectance of each land cover type within that pixel and the associated error:

$$\rho_{i,j,k} = \sum_{m=1,p} F_{i,j,m} * \rho_{m,k} * e_{i,j} \quad \text{Eq. 2.2}$$

- where $\rho_{i,j,k}$ is the total reflectance of a pixel for row i , column j ;
- band k ; $F_{i,j,m}$ is the proportion of each pure component m of a pixel for row i , column j ;
- $\rho_{m,k}$ is the reflectance for that pure component m in band k ; and
- e is the error associated with the estimation of each of the components for each pixel $e_{i,j}$.

The constraint of this model ensures that pure EM proportions range between 0 and 1. This means that the proportions of the components are normalized to a common range of

potential values. The assumption of this model is that the sum of the fractions with a pixel is equal to the total pixel surface; i.e., that there is no other radiance that is unaccounted for (Shimabukuro and Smith, 1991). There have been only two or three studies found on research conducted utilizing LSU for wetlands and only one study found that used fraction maps as input to OBIA for any type of land cover mapping.

Schmid *et al.* (2005) used spectral unmixing of hyperspectral aerial imagery, Landsat and ASTER imagery to detect changes in wetlands in La Mancha Alta, Spain. Five EMs were derived from the higher resolution hyperspectral imagery including: hydrophytic vegetation, wetland soils A (dried, exposed soil surface with seasonal flooding) and B (cultivation practices bare soil: fallow or sowed with crops), wet salt crust and upland soil. The EMs were transferred to the coarser multispectral satellite data (Landsat and ASTER) showing that their spectral characteristics remained relatively stable in this process. This subsequently allowed for the temporal comparison and determination of change using the multi-date medium resolution multispectral imagery.

Melendez–Pastor *et al.* (2010) used land cover components (vegetation, soil, water) from LSU of Landsat 5 imagery to compare temporal changes at El Hondo Natural Park wetland, Spain. Their results showed a significant increase (+123.8%) in the soil fraction between a non-drought year (2001) and a drought year (2004/05).

The ability of the land cover fractions to indicate change based upon climatic differences (Schmid *et al.*, 2005; Melendez-Pastor *et al.*, 2010) or human-based changes in other ecosystems such as slash and burn in the Amazon (Adams *et al.*, 1995) or tundra land cover change (Olthof and Fraser, 2007) led to the selection of this attribute to classify imagery and assess change through time based upon these fractions. Additionally, the lack

of previous studies on LSU applied in OBIA suggested this could be a significant contribution to the literature. It is also hoped that this type of analysis will improve upon the existing assessment of anthropogenic disturbance in the literature with accuracies that ranged from 85 to 89%. Finally, LSU was also selected for the potential of the sub-pixel information, while maintaining the coverage and cost of a product like Landsat which would be practical and cost-effective for a regionally diverse monitoring system like OWES.

2.8.3 Classification of remote sensing imagery

A traditional parametric method, supervised MLC is often used as a base comparison for other classification methods (Flanders *et al.*, 2003) and was selected for the same purpose in this thesis. For selected classes such as Bog, Fen, Marsh, etc., training pixels are selected from the image that are representative of the spectral and/or spatial characteristics of a class of interest. MLC is generally an optimal classifier if pixels forming a training class are normally distributed and there is some previous knowledge regarding the landscape (Jensen, 2005). Given this condition, the statistical probability (the Bayesian likelihood) can be calculated that an unknown pixel (or object) belongs to a particular land cover category. The separability of the training data can be analyzed using multivariate inverse variance-covariance weighted measures of distance between class means, such as the Bhattacharyya Distance (Haralick and Fu, 1983). In this research, the algorithm scaled the resultant distance into a range between 0 and 2, where 0 indicates complete overlap of two classes and 2 indicates a complete separation between the two classes. As Bhattacharyya Distance is non-linear, values of 1.9 and greater are often used to indicate good separability and values of 1.7-1.9 may indicate potential for accurate classification. Following the training

stage, the statistical information in the training data is used to assign each image pixel to the class to which it has the highest probability of belonging.

Classification trees can be used with remotely sensed and ancillary data to develop land cover maps. They are non-parametric and do not require assumptions regarding data distributions (Friedl and Brodley, 1997) and can incorporate data from multiple measurement scales (e.g. nominal, ordinal, interval and ratio (Wright and Gallant, 2007)). Trees are composed of branches that represent the attributes whereas the leaves (end nodes) are the decisions (Figure 2.3). Classification trees are thought to be ‘transparent’ as all decisions are shown in the resulting tree.

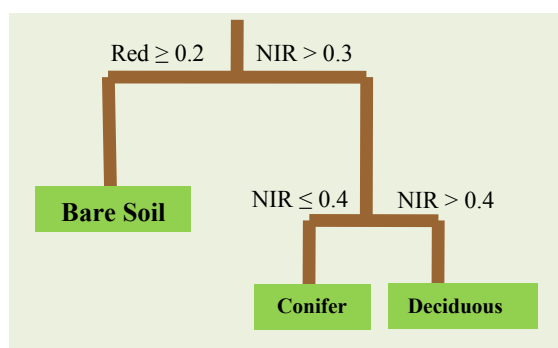


Figure 2.3. A simple classification tree.
Red and NIR represent spectral bands.

Using training data, splits in the tree are determined through recursive partitioning, where at each node the data splits until the data are only from one class or there is one acceptable level of class dominance within the leaf. A commonly used algorithm is C4.5 (Quinlan, 1993); a univariate classifier that has three splitting options, (entropy, gain ratio and GINI). The entropy ratio (the measure of homogeneity at a node) has been known to oversplit with the gain ratio employed to correct for that oversplitting. Research has found that, in general, there is no statistical difference between the splitting methods, however, through testing, it

is recommended to use GINI over the other two options (Zambon *et al.*, 2006; Duro, pers. comm. 2012). The GINI algorithm was selected for this research.

GINI measures the impurity at a given node that is at a maximum when all the pixels are equally distributed among all classes. The main splitting criterion is the reduction of that impurity. GINI starts by finding the largest homogenous class within a dataset and isolates it, and repeats until all data are parsed (Zambon *et al.*, 2006).

$$GINI(t) = \sum_i p_i(1 - p_i) \quad \text{Eq. 2.3}$$

- where p_i is the relative frequency at node t , (determined by dividing the total number of observations of the class $_i$ by the total number of observations); and
- t represents any node (parent or child) at which a given split of the data is performed (Apte and Weiss, 1997).

Subsequent nodes are then segregated in the same manner until further divisions are not possible. Auto-pruning, which removes any leaves with pixel counts less than or equal to a defined within-class proportion, can be implemented.

Overfitting occurs when a classification tree model follows the structure of the training data too closely (Khoshgoftaar and Allen, 2001). The model appears to be accurate in classifying the training data, but is much less accurate when it comes to non-training pixels or objects. Boosting and bagging are methods of training sample manipulation (Du *et al.*, 2010). Boosting applies the classification tree model with each subsequent classification dependent upon the previous. Classes that are incorrectly predicted in the previous classification can be weighted more heavily in the training data. Boosting sometimes results in overfitting of the training data. Bagging (bootstrap aggregation), trains the classification tree by selecting random subsets of the training data and repeating the classification (Du *et*

al., 2010). An example of bagging is the RF classification algorithm (Breiman, 2001; Mutanga *et al.*, 2012).

Wright and Gallant (2007) assessed palustrine wetlands in Yellowstone National Park using Landsat 5 TM for various data from 1988 to 2002. The classes of interest included two levels, one level for palustrine wetlands and non-wetlands (uplands) and one level for the five classes within the wetlands. Canonical discriminant analysis was used with multiple spectral, and spatial data inputs. Error was assessed using 100,000 pixels sampled from locations not used for training or decision tree pruning. Overall, they found the addition of the non-spectral data (GIS, terrain, and image texture) halved the overall error rate in detection of palustrine wetlands for the coarser wetlands/no wetlands model. Additionally, the classification tree technique improved the discrimination between emergent wetlands and other classes. Wright and Gallant (2007) listed kappa coefficients for each model to detect palustrine wetlands that ranged from 0.41 to 0.68.

Davranche *et al.*, (2010) used a binary classification tree algorithm from R software, (RPart) using multi-spectral indices as data input derived from SPOT-5 data to classify reeds and submerged macrophytes. Their overall accuracies ranged 85% to 98%.

In other land cover studies, Jiao *et al.* (2011) used a C4.5-based classification tree to improve MODIS land cover classification by combining spectral data and reflectance anisotropy (BRDF, Bidirectional Reflectance Distribution Function) over the Canadian Boreal Forest resulting in an increase in overall accuracy by 2.92% with UA (User's Accuracy) and PA (Producer's Accuracy) improving by 8.64% and 7.81%, respectively.

Zhao *et al.* (2012) tested four classification tree algorithms (Model-10, Model-09, CT_{m-1}, CT_{m-2}) with Landsat ETM+ imagery to classify aquatic vegetation of emergent, floating-leaf, submerged vegetation and open water testing a variety of spectral indices such as NDVI, NDWI, etc. as input. The best classification tree was Model-10 and had class accuracies ranging from 88 to 98%.

2.8.4 Radar imagery analyses

Radar image analysis was not a central focus of this research; methods were selected that were straightforward to implement and combine with optical imagery, in order to determine the potential for integration into an operational wetland evaluation system such as OWES. Radarsat-2 data were selected because they were provided at no cost, thus other data types, including those at different wavelengths were not considered. Radar imagery has proven useful for assessing wetland classes and vegetation (Li and Chen, 2005; Racine *et al.*, 2005; Grenier *et al.*, 2007; Marechal *et al.*, 2012). Scattering mechanisms of the ground cover are an important component of radar analysis and include surface scattering, volume scattering, and double-bounce/multiple scattering which are represented conceptually for C-band data in Figure 2.4 (after Bourgeau-Chavez *et al.*, 2010; Fernandez-Ordonez *et al.*, 2010) for wetlands.

Particularly well understood is the relationship between radar backscatter and a variety of land covers and/or other ground-based measures. The radar backscatter coefficient is an indication of the average backscattered power in relation to the incident power and is represented as σ° (Ulaby *et al.*, 1988), measured in decibels (dB).

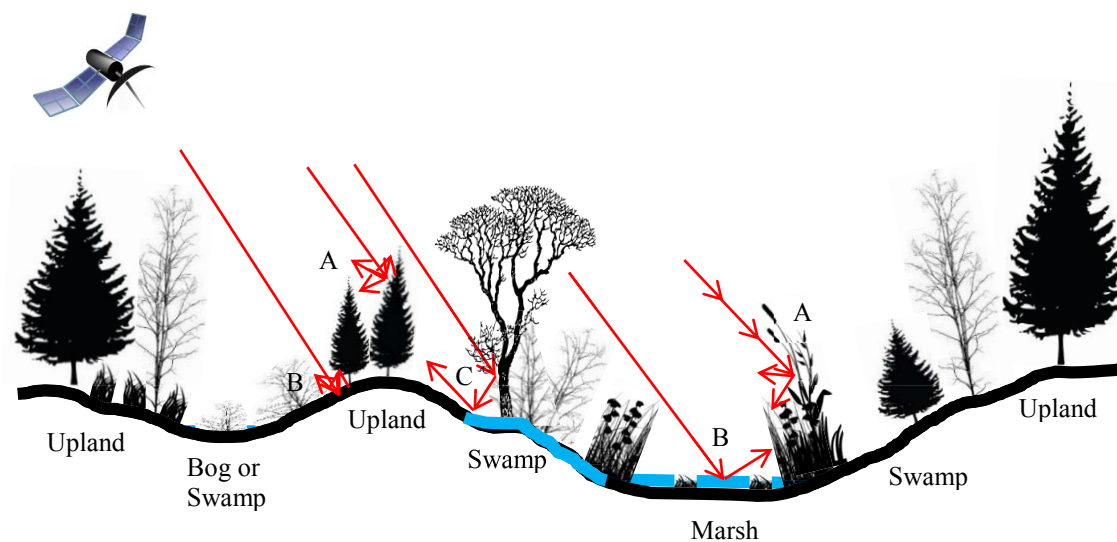


Figure 2.4. A conceptual representation of different scattering mechanisms in a wetland complex for C-band data (after Bourgeau-Chavez *et al.*, 2010; Fernandez-Ordonez *et al.*, 2010; OWES, 2002). A = Volume scattering; B = Surface scattering; C = Double bounce.

For example, Lang and Kasischke (2008) assessed the relationships between radar backscatter and soil moisture and inundation. There was a positive linear relationship between flooding and backscatter coefficients for both C-HH and C-VV data with C-HH performing well in leaf-off and leaf-on seasons, while C-VV data could detect flooding during the leaf-off season. Pope *et al.* (1997) used SIR-C images acquired in the dry and wet seasons over the Yucatan Peninsula to assess seasonal differences in marshes. Increased flooding produced increased backscatter in taller, densely covered marshes and decreases in backscatter in sparsely covered marshes. What is less understood is the relationship between wetland target response/response mechanisms and other radar variables, such as backscatter, pedestal height and polarimetric variables of decomposition. Additionally, the benefits of using different scattering mechanism representations to classify wetland types and vegetation communities have not been fully explored. Both of these techniques were addressed in this research.

A full review of the HH, VV and HV abilities are listed under the discussion of Radar imagery in general. In particular, Banks *et al.* (2011) were able to discriminate between some classes of arctic shoreline land cover by comparing the HH and HV on a scatterplot particularly from imagery with shallow incidence angles. Baghdadi *et al.* (2001) assessed Radarsat-1 backscatter coefficients of six land covers in Mer Bleue Bog by plotting the HH, VV, and HV response for various incidence angles over three months in 1995. The cross-pol response provided the best discrimination between the six classes. Several wetland studies have utilized this graphical relationship of polarisation response at various incidence angles to discriminate classes (Baghdadi *et al.*, 2001; Horitt *et al.*, 2003; Marti-Cardona *et al.*, 2010).

Bartsch *et al.* (2007) assessed the suitability of using satellite radar imagery for monitoring wetlands in the boreal and sub-arctic in Russia. They used ENVISAT SAR to relate backscatter to scatterometer data from SeaWinds/QuikScat by comparing the diurnal effects within the backscatter data to map soil moisture and freeze/thaw boundaries. They determined the permanent detectable thaw lake size to be 2 ha. They also presented representative monthly backscatter values for wetlands.

Polarimetric radar measures the polarisation properties of a surface. Surfaces respond to incident polarized radiation by reflecting partially polarized and depolarized radiation (van Zyl *et al.*, 1987). The response gives an indication of the properties of the surface and allows for types of scattering to be distinguished. Fully polarimetric radar systems measure the characteristics of the surface for all configurations (e.g. HH, VV, HV, VH) as well as providing phase information. They improve upon data acquired in single polarisations, for which it is difficult to distinguish between different types of scatterers. Stokes parameters

describe the polarisation state and phase. Coherency matrices are the second order statistical representation of the variations and correlations of that polarisation state and phase (van Zyl *et al.*, 1987).

The polarimetric information of the wave is measured (or referenced) in relation to a global 3-dimensional Cartesian coordinate system with the origin situated within the scatterer (van Zyl *et al.*, 1987; Banks *et al.*, 2011). Information measured includes: power (backscatter), ellipticity (χ), and orientation angle (ψ). As a backscattered wave travels, at each point in space, the electric vector of the wave rotates in a plane perpendicular to the direction of the wave (creating a shape). If the wave appears to be rotating clockwise it is denoted as right-handed; left-handed waves rotate counter clockwise (van Zyl *et al.*, 1987). This “handedness” provides the sign (+ or -) of the ellipticity, while the angular values of ellipticity are an indication of the wave rotation shape (circular (45°), linear (0°), or elliptical). The orientation angle is the angle between the backscattered wave and either the horizontal (0 or 180°) or vertical plane (90°). Polarimetric signatures are the graphical representation of surface response and can aid in understanding of the scattering mechanisms at those targets. Pedestal height is a way to measure randomness in the scattering process (Lee and Pottier, 2009). Measuring pedestal height is the same as the ratio of the minimum eigenvalue to the maximum eigenvalue, which is also a ratio of the unpolarized component in the average return (Lee and Pottier, 2009). As pedestal height increases, diffuse scattering increases and depolarization increases (Evans *et al.*, 1988; Boerner *et al.*, 1998; McNairn *et al.*, 2002; Touzi *et al.*, 2004).

There are four types of models expected for polarimetric signatures: (A) sphere, flat plane or trihedral corner reflector (often representing surface scattering)); (B) Bragg Model

(defines ocean wavelengths as a function of radar wavelength and incident angle; pedestal height is close to zero); (C) dihedral corner reflector (double-bounce scattering); (D) multiple, dissimilar scatterers, which look typically like the shapes found in the graphs in Figure 2.5.

Evans *et al.* (1988) related differences in polarimetric signatures for five varied samples of landcover including ocean, park and three urban sites. The ocean with waves followed the Bragg Model and had low pedestal height (more polarized return), while the park, with a variety of vegetation including grassy, shrubby and forest areas, had the highest pedestal height, indicating multiple scatterers and a depolarized return signal. Boerner *et al.* (1998) described the pedestal heights for a variety of crop areas from bare soil, with the lowest pedestal height, potato with an intermediate pedestal height to corn with the highest pedestal height. The signature plot for bare soil was smooth and flat (representing surface scattering), that for potato more peaked but still relatively smooth, representing surface scattering, while the corn plot showed multiple scattering due to its lower spatial uniformity and the variation in the corn leaves and between corn rows (Boerner *et al.*, 1998).

Several techniques extract different representations of scattering mechanisms of the coherency matrix (Liao and Wang 2009). These variables can then be compared in a plane to determine classes of interest, or utilized with classifications to determine the land cover classes on the ground. One common technique is the Cloude-Pottier (CP) method (Cloude and Pottier, 1996, 1997; Touzi *et al.*, 2007; Liao and Wang, 2010; Sartori *et al.*, 2011; Schmitt and Brisco, 2013). Targets contain not only radar response but speckle (noise) and random scattering (from surface and volume components), therefore the analysis to determine the underlying (or true) scattering of the target requires multivariate statistical

description through matrix mathematics (Cloude and Pottier, 1996). The CP decomposition theorem starts with a 3x3 (square) matrix which contains the eigenvalues from which entropy and anisotropy are derived, and the 3x3 unitary (orthogonal) matrix, from which the alpha angle is derived. These three components relate to the physical scattering mechanisms (surface, volume and double bounce/multiple scattering) of the target.

Entropy (H , between 0 and 1) represents the degree of randomness:

$$H = \sum_{i=1}^3 p_i \log_3(p_i) \quad \text{Eq. 2.4}$$

where p_i is the probability of the eigenvalue λ_i .

$$p_i = \frac{\lambda_i}{\sum_{k=1}^3 \lambda_k} \quad \text{Eq. 2.5}$$

When $H = 0$ there it implies a non-depolarizing scattering process and generally relates to one dominant scattering mechanism and $H=1$ relates to depolarizing surfaces (Liao and Wang, 2009; Cloude and Pottier, 1996, 1997).

Anisotropy (A , between 0 and 1) represents defines the relation between the second and third eigenvalues and is a measure of the difference between the secondary scattering mechanisms.

$$A = \frac{\lambda_2 - \lambda_3}{\lambda_2 + \lambda_3} \quad \text{Eq. 2.6}$$

where $A=0$ the two mechanism are mixed in equal proportions and the associated eigenvalues are equal. When A is close to 1, the second eigenvalue is much larger than the third eigenvalue and the second mechanism is dominant over the third. This provides information complementary to the entropy and allows for interpretation of the surface scatterers.

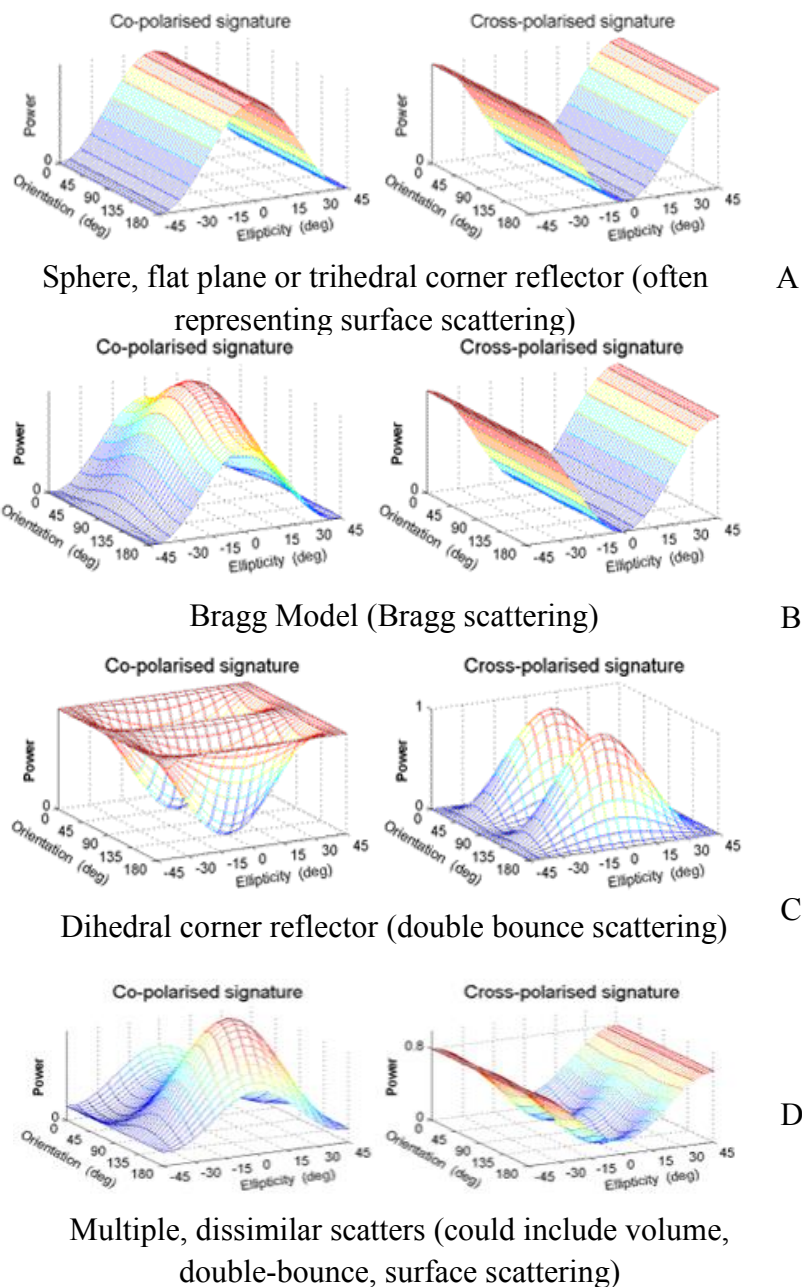


Figure 2.5. Typical polarimetric signatures for (A) Sphere, flat plane or trihedral corner reflector (often representing surface scattering)); (B) Bragg model; (C) Dihedral corner reflector (double-bounce scattering); (D) Multiple, dissimilar scatterers. After Figures 5.1 – 5.4, (NRCAN.gc.ca/earth-sciences/node/2163, 2008).

Alpha angle (α), is the main component for identifying the dominant scattering mechanism (Cloude and Potier, 1997) and the resultant value determines the type of

scattering mechanism for a given eigenvector.

$$\bar{\alpha} = \sum_{i=1}^3 p_i \alpha_i \quad \text{Eq. 2.7}$$

when $\alpha=0^\circ$ indicates a surface scatterer; when $\alpha=45^\circ$ is representative of a volume scatterer; and when $\alpha=90^\circ$ indicates a double bounce/multiple scattering mechanism (Cloude and Pottier, 1996, 1997; Liao and Wang, 2009). Once the three secondary parameters are derived they can be compared on an α/H 2-dimensional plane resulting in 8 classes, which depict potential scatterers/combinations of scatters (Figure 2.6, after Cloude and Pottier, 1997).

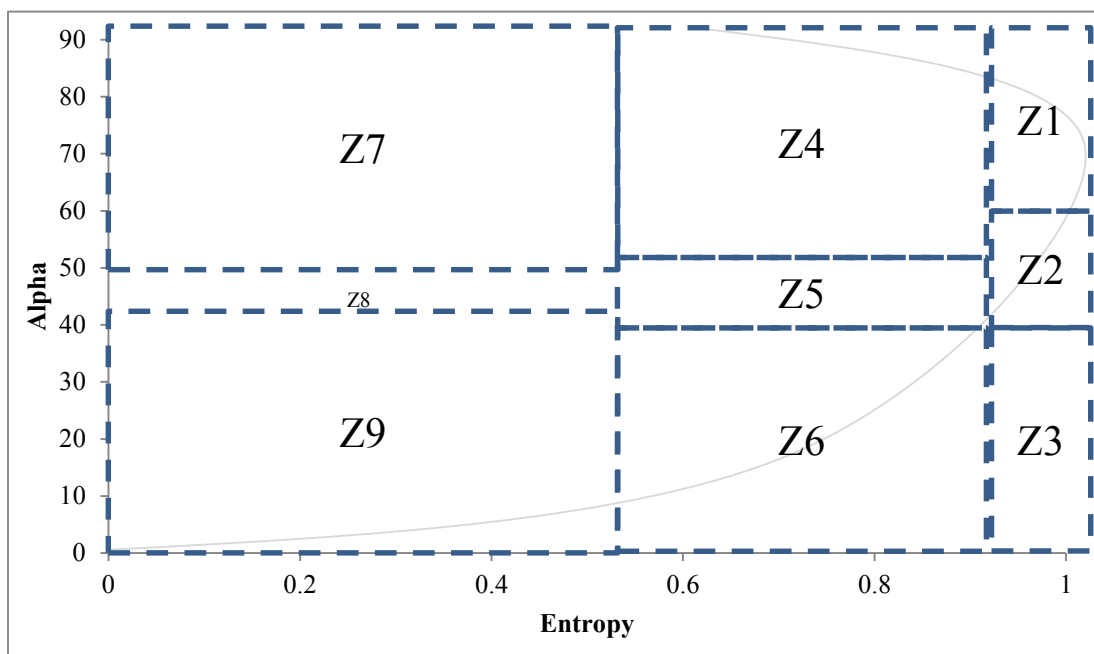


Figure 2.6. Scattering regions of the α - H plane. Physical characteristics of each zone are described in Cloude and Pottier, 1997.

Zones 9, 6 and 3 all represent surface scatterers with low alpha and low, medium and high entropy, respectively; zone 8 shows isolated dipole scatterers and some vegetation scattering; and zones 5 and 2 are indicators of vegetation scattering. Finally, zones 7, 4, and 1 correspond to double-bounce or multiple scattering events (Cloude and Pottier, 1997). The addition of anisotropy allows for further partitioning of the plane (each zone is subsequently

split into two ((resulting in 16 potential zones of scattering) Cloude and Pottier, 1997). The Wishart unsupervised classification utilizes these zones (either 8 or 16) as training areas. Wishart unsupervised classifier assigns pixels to classes similarly in a process to a k-means algorithm (Anfinsen *et al.*, 2007), but rather than using the sample-cluster mean vector distance to cluster the data, Wishart uses a matrix derived distance (Anfinsen *et al.*, 2007).

Sartori *et al.* (2011), using ALOS (Advanced Land Observing Satellite) PALSAR (Phased Array L-band Synthetic Aperture Radar) data, compared a rule-based classification to the CP decomposition variables, the H/α plane + Wishart classifications, and other polarimetric variables to map macrophyte species in the Amazon floodplain wetlands in Brazil. They found that the CP decomposition variables (the H/α plane) were able to separate the floodplain from the upland, macrophytes from floodable (affected by the annual flood pulse) areas of trees and shrubs, but they could not distinguish between the macrophyte species. The Wishart H/α classifier was not able to separate the floodplain from the upland, but was able to separate floodable trees and shrubs from macrophyte species.

Touzi *et al.* (2007) compared the Touzi decomposition (Touzi, 2007) to the CP decomposition and found that the Touzi variables were better in discrimination of wetland vegetation. This study was conducted at Mer Bleue Bog, one of the sites for this research. As others have found that CP components can distinguish between classes such as upland, wetland, forest and shrub (Sartori *et al.*, 2011) or that higher alpha values indicated flooded vegetation (Schmitt and Brisco, 2013), and instead of repeating the methods in Touzi *et al.* (2007), it was decided to evaluate the potential of addition of the CP components to other imagery types or variables in improving wetland classifications.

Based upon the literature review in the previous sections it was expected that utilizing radar and optical variables together in classification with OBIA and CTA would improve upon overall accuracies presented as 86 – 89% for Wetland Type classification, and greater than 76% for VCFs. For Open Water Type, using with OBIA optical imagery with radar and DEM information using a non-parametric classifier was expected to improve upon results from other studies that have used one data type, and/or pixel-based classification, and/or parametric classifiers.

2.9 Selection of OWES attributes for image modelling and classification

Chisholm *et al.* (1997) developed predictive linear regression models to identify whether different combinations OWES attributes contributed more to the overall wetland score. Eight variables were identified that contributed most to the overall score and included wetland size (log), wetland type rarity, recreational activities, flood attenuation, open water types, proximity to human settlement, proximity to other wetlands, and education and public awareness. In conjunction with this, and after review of the OWES with OMNR experts and users, a subset of the OWES attributes were selected based on their potential for detection, estimation or classification in remotely sensed imagery and/or their potential to be derived from existing GIS data. These were selected prior to in-depth review of the remote sensing literature. The second criterion was that selected attributes had to contribute most to an overall OWES wetland score (Chisholm *et al.*, 1997). Table 2.4 lists, from the 2002 Southern Ontario Evaluation manual (2002), each of the OWES components, the sub-component and the selected attribute to be mapped in this research. In some cases, attributes were duplicated under different OWES components. The methods used for each attribute are listed in the rightmost column and described in Chapter 4. The description of each attribute and its

associated score follows, including a summary table of the literature as it relates to the particular attributes. The weights given for particular scoring methods by the OWES vary between districts. Explicit justification for the weighting selection was not published in the OWES but was the result of expert consultations.

Following the tables are descriptions and definitions of each attribute taken from the OWES Southern Manual (2002). The text has been revised for clarity and brevity, but much of the scoring explanations remain the same or similar to the 2002 OWES manual. Table 2.5 lists the generalized methods that are used in the literature to map these attributes.

Table 2.4. OWES components and wetland attributes selected for this research.

OWES component	Sub-component	Attribute	Total maximum OWES score	Methods used
Biological	Productivity	Wetland Type	15	<ul style="list-style-type: none"> • WV-2: segmentation and classification (OBIA) with MLC & CTA • L-TM5: OBIA with LSU (MLC & CTA) • R-2: classification: (backscatter; pedestal height, polarimetric signatures CP variables) • Combined optical and radar variables with OBIA
	Biodiversity	Number of Wetland Types	30	Assess the Numbers Of Wetland Types (GIS analysis based upon different classifications as above)
		Number of Vegetation Community Forms (VCFs)	45	<ul style="list-style-type: none"> • Classification: as above • Assess best VCF classification • Assess numbers of VCFs
		Open Water Types	30	Classification as above
		Diversity of Surrounding Habitat	7	GIS analysis of classifications above; compare to existing layers

		Proximity to Other Wetlands	8	GIS analysis of classifications above
	Size	Wetland Size	50	GIS analysis of classifications above
Total maximum Biological score			185	
Social	Recreational Activities	Hunting, Recreation Areas	40/80	GIS analysis of existing recreational layers
	Landscape aesthetics	Lack of Anthropogenic Disturbance	40	Classify disturbance and compare over decades
	Ownership	'Ownership Patterns' – who owns the property on which the wetland is situated	10	GIS analysis of existing ownership layers
Total maximum Social score			90	
Hydrologic	Flood attenuation	Inundation Extent/ Seasonally Flooded Extent	100*	<ul style="list-style-type: none"> WV-2 – pixel based vegetation indices compared to field measures L-TM5 – NDVI compared to field measures
		Wetland Basin Size	100*	GIS analysis of existing hydrological layers
Total maximum Hydrologic score *The total possible score of 100 has other contributing factors not assessed here (see OWES Southern Manual, 1993)			100*	
Special Feature	Rarity	Wetland Type	80	GIS analysis of created classification layers
		Rarity of Wetland In Landscape	80	GIS analysis of created classification layers
Total maximum Special Feature score			160	

Table 2.5. A synopsis of the 14 selected OWES attributes, their synonyms in geomatics literature and corresponding remote sensing and GIS methods applied in previous studies.

Attribute	Synonyms in geomatics literature	Types of methods	Imagery types	Highest accuracies	Authors
<p>Wetland Type (Bog, Fen, Marsh, Swamp)</p> <p>Related to these types of studies are the attributes: Number of Wetland Types, Wetland Size, and Rarity of Wetland</p>	<p>Water, Mudflat, Vegetation, Sand; Codes relating to state of soil, type of vegetation and water presence; Saline wetlands; Bottomlands Swamp forests; peatlands; woody wetlands, shrubby wetlands</p>	<p><u>Optical</u></p> <ul style="list-style-type: none"> • OBIA with supervised classification, and with watershed algorithms and decision trees • manual image interpretation • neural networks classification • supervised and unsupervised classification • linear spectral unmixing <p><u>Radar</u></p> <ul style="list-style-type: none"> • seasonally averaged backscatter coefficients alone and with NDVI • decomposition parameters (van Zyl, Touzi, Cloude-Pottier) • canonical discriminant analysis • radar backscatter coefficients with maximum likelihood classification <p><u>Overall analysis trend toward:</u> OBIA more recently with optical and SAR imagery alone;</p>	<p>Bejing-1 microsatellite QuickBird IKONOS SPOT Landsat TM & ETM+ MODIS</p> <p>SRTM DEM ERS-2 & ERS1/2 RADARSAT-1 ENVISAT ASAR</p>	<p>Overall accuracies optical: 71 – 92%</p> <p>Radar overall accuracies: 65.5-75.2%</p> <p>Radar and optical: 86 – 89% (Pixels Correctly Classified (PCC))</p>	<p>Schmitt and Brisco, (2013) Dribault <i>et al.</i> (2012) Ricaurte <i>et al.</i> (2012) Dronova <i>et al.</i> (2011) Jiao <i>et al.</i> (2011) Waleska <i>et al.</i> (2011) Castaneda and Ducrot, (2009) Kwoun and Lu (2009) Durieux <i>et al.</i> (2007) Grenier <i>et al.</i> (2007) Touzi <i>et al.</i> (2007) Wright and Gallant (2007) Racine <i>et al.</i> (2005) Li and Chen (2005) Rogers and Kearney (2004) Bernier <i>et al.</i> (2003)</p>

		Previously tended to be standard (e.g. MLC) pixel-based classification			
Vegetation Community Form	Plant functional types; C3 forbs; grasses; C4/C3 reeds; C4 short grasses; emergent aquatic macrophytes; Submerged macrophytes emergent vegetation; floating leaf vegetation, submerged vegetation; Phragmites, tamarix, wet meadows; species levels names; mangrove separated by dead, healthy and height; Vegetation patterns	<ul style="list-style-type: none"> • OBIA with six statistical machine-learning classifiers; NDVI • Classification trees with spectral indices • Boosted Genetic Fuzzy Classifier (BGFC) (e.g. AdaBoost) with textures, wavelets and intensity, hue and saturation • seasonally averaged backscatter coefficients • maximum likelihood classification • incidence angle changes for flooding in particular forest types • Random Forests <p><u>Overall analysis trends toward:</u> OBIA with SAR data; combination of SAR with optical data</p>	Bejing-1 microsatellite WorldView-1 QuickBird SPOT-4 IKONOS Landsat TM & ETM+ ALOS-AVNIR-2 ERS1/2 RADARSAT-1 alone and combined ENVISAT ASAR alone and combined with Landsat TM JERS L-band	Overall accuracies in general: 78 - 98% 88-96% for emergent vegetation 54% ASAR alone but 76% for combined 85-92% with other radar	Dronova <i>et al.</i> (2012) Wang <i>et al.</i> (2012) Jiang <i>et al.</i> (2012) Zhao <i>et al.</i> (2012) Atkinson and Treitz (2012) Frick <i>et al.</i> (2011) Stavrakoudis <i>et al.</i> (2011) Davranche <i>et al.</i> (2010) Kovacs <i>et al.</i> (2008) Lang <i>et al.</i> 2008 Toyra and Pietroniro (2005) Hess <i>et al.</i> (2003)
Open Water Type	Surface water; permanent water	<ul style="list-style-type: none"> • polarized brightness temperature 	Landsat TM & Landsat ETM+ AMSR-E	R ² = 0.84	Campos <i>et al.</i> (2012) Watts <i>et al.</i> (2012) Bartsch <i>et al.</i> (2008)

	bodies; seasonal water bodies	<ul style="list-style-type: none"> • SAR data over long period to assess surface hydrological patterns • threshold-based classification • water indices <p><u>Overall analysis trends toward:</u> Analysis with SAR data</p>	ENVISAT ScanSAR		Sass and Creed (2008)
Inundation Extent	Soil moisture, flood mapping; wet area; flood pulsing; wetland extent Inundation patterns	<ul style="list-style-type: none"> • satellite brightness temperature • principal component analysis; cluster analysis • stepwise regression between inundation and hydrometeorological data • GPS field measures • density slicing and fuzzy thresholding and radar backscatter • backscatter coefficients for three classes (open water, flooded vegetation, and dry land) <p><u>Overall analysis trends toward:</u> Analysis with SAR data</p>	Landsat ETM+ AMSR-E RADARSAT-1, LiDAR PALSAR ASAR WSM	R ² = 0.96 100% overall accuracy	Chen <i>et al.</i> (2013) Kuenzer <i>et al.</i> (2013) Zhang <i>et al.</i> (2012) Gala and Melesse (2012) van der Velde <i>et al.</i> (2009) Rebelo <i>et al.</i> (2009) Lang <i>et al.</i> (2008) Lang and Kasischke, (2008) Bourgeau-Chavez <i>et al.</i> (2005)
Number of Wetland Types	Related to Wetland Type				
Diversity of Surrounding Habitat	Upland types	<ul style="list-style-type: none"> • OBIA with classification • Buffering with thematic maps 	Thematic maps	Similar accuracies to the ability to classify Wetland Type	Ruan and Ustin (2012) Begley <i>et al.</i> (2012) Tufford <i>et al.</i> (1998)

		<ul style="list-style-type: none"> in addition studies of Wetland Types usually have some Upland component <p><u>Overall analysis trends toward:</u> Buffering (with thematic maps created through Wetland Type analysis)</p>			
Proximity to Other Wetlands	Hydrological connectivity; Surface water connectivity	<ul style="list-style-type: none"> topography modelling with high resolution DEM to determine flow pathways and barriers <p><u>Overall analysis trends toward:</u> Topography modelling</p>	LiDAR; field surveyed stream data (rivers)	Able to determine connectivity between wetlands	Karim <i>et al.</i> (2012)
Wetland Size	Related to Wetland Type				
Hunting		<ul style="list-style-type: none"> -GPS tracking of hunters to estimate movement <p><u>Overall analysis trends toward:</u> GPS tracking</p>	-GPS	Can determine hunter movement with GPS	Broseth and Pedersen (2000)
Ownership Patterns	Tax parcels	<ul style="list-style-type: none"> Hedonic property price model including recreational quality models with buffering -using tax parcel data to assess ownership with buffering -regression analysis <p><u>Overall analysis trends toward:</u> Buffering existing data layers</p>	-tax parcel data -road files -private ownership data	Prediction success of 90 – 92%	Tapsuwan <i>et al.</i> (2012) Allen <i>et al.</i> (2002) Waddell <i>et al.</i> (1998)
Wetland Basin Size	Drainage basin	<ul style="list-style-type: none"> drainage basin delineation with DEM 	DEM	Can derive drainage basin	Schwanghart and Heckmann (2012)

		<ul style="list-style-type: none"> • using fuzzy methodology • Shannon Entropy) 			Reuter <i>et al.</i> (2009)
Rarity of Wetland in Landscape	Related to Wetland Type				
Anthropogenic Disturbance	Human influence; deforestation, agriculture expansion (Land use land cover change)	<ul style="list-style-type: none"> • Cellular Automata (CA)-Markov model • GIS assessment of thematic data to determine change in polygons • aerial photointerpretation • linear spectral mixture analysis • assessment of forest cover change through thematic maps derived through tasselled cap transformation and unsupervised classification • maximum likelihood classification and change detection • GIS classification model using Basin Buffer Index and Hydric Vegetation Index <p><u>Overall analysis trends toward:</u> Optical based change detection</p>	Thematic maps (derived from satellite data) Landsat TM -Landsat ETM+ -Landsat TM SPOT-5 data	Overall accuracy: 85% - 89%	<p>Yang <i>et al.</i> (2013) Behera <i>et al.</i> (2012) Dubovyk <i>et al.</i> (2012) Dyukarev <i>et al.</i> (2011) Sunderman and Weisburg (2011) Papastergiadou <i>et al.</i> (2008) Stuart <i>et al.</i> (2006) Phillips <i>et al.</i> (2005) Hostert <i>et al.</i> (2003) Wilcox (1995)</p>

2.9.1 Wetland Type (Biological and Special Feature components)

Wetland Types in the literature may be any relevant class name such as water, mudflat, vegetation, sand, saline wetlands, swamp forests, bottomlands, wood wetlands, shrubby wetlands, etc. In this research, Wetland Type refers the National Wetland Classification System classes of Bog, Fen, Marsh and Swamp (National Wetlands Working Group, 1988), as used by the OWES. Overall classification accuracy for these types of classes have ranged from 66% to 92%, depending on the number of classes and their specificity, the data, and the methods used (Bernier *et al.*, 2003; Rogers and Kearney, 2004; Li and Chen, 2005; Racine *et al.*, 2005; Wright and Gallant, 2007; Touzi *et al.*, 2007; Grenier *et al.*, 2007; Durieux *et al.*, 2007; Castaneda and Ducrot, 2009; Kwoun and Lu, 2009; Jiao *et al.*, 2011; Dronova *et al.*, 2011; Ricaurte *et al.*, 2012). The overall trend in the research is toward utilizing OBIA combined with variations of optical and radar images, as well as derived image variables. This research was designed to contribute to this growing body of work.

The methods selected to map Wetland Types and reasons for selecting them are outlined in section 2.8.1 through 2.8.4 because those methods are used repeatedly for 5 of the 14 attributes. In relation to SOLRIS (2003), which is the current method used to inventory wetlands in Southern Ontario, these methods were employed to minimize the data used, use newer higher resolution optical imagery and newer fully polarimetric radar variables, and determine if the overall accuracies (82% to 95%) could be maintained or improved for more than one reference site.

Based upon the overall literature analysis of this chapter, it was expected that using OBIA with WorldView-2 imagery and combinations of other imagery types such as Radarsat-2 polarimetric variables, Landsat 5 data and CTA, would improve upon the accuracies listed in the literature which range in overall accuracy from 71 – 92%. Additionally, the potential for application of LSU fractions with OBIA and/or CTA and moderate resolution data such as Landsat to derive subpixel land cover and land cover change information was deemed to be high. The minimal literature on this topic suggested that this approach may contribute significantly to advancement of wetland mapping and monitoring.

For scoring Wetland Type for the OWES, the proportion of each Wetland Type to the whole wetland complex, known as Fractional Area (FA = area Wetland Type/total wetland area), is calculated and then multiplied by a weight for the given wetland type as follows:

$$\text{Bog} = \text{FA} \times 3$$

$$\text{Fen} = \text{FA} \times 6$$

$$\text{Swamp} = \text{FA} \times 8$$

$$\text{Marsh} = \text{FA} \times 15$$

The complete score for Wetland Type (category) is determined by summing the individual scores per individual type of wetland.

2.9.2 Vegetation Community Forms (VCFs, Biological component)

The OWES categorizes VCFs in 14 potential dominant classes (Figure 2.7). A form must represent approximately 25% of the vegetation community to be recorded. Although combinations of vegetation forms may occur more than once within a wetland complex, these combinations can only be scored once. In the literature, VCFs are also known by specific vegetation species names, C3/C4 categorization of forbs, grasses, etc., by separation of vegetation by health and life, and by particular vegetation patterns. Methods used to assess VCFs include OBIA classification with optical and/or radar data, seasonally averaged backscatter coefficients, supervised, unsupervised and random forest classification with accuracies that range from 78 – 98% in general, 88 to 96% for emergent vegetation, and 76% for combined variables (Hess *et al.*, 2003; Toyra and Pietroniro, 2005; Lang *et al.*, 2008; Kovacs *et al.*, 2008; Davranche *et al.*, 2010; Stavrakoudis *et al.*, 2011; Frick *et al.*, 2011; Atkinson and Treitz,, 2012; Dronova *et al.*, 2012; Jiang *et al.*, 2012; Wang *et al.*, 2012; Zhao *et al.*, 2012). The overall trend in the research is toward utilizing OBIA combined with variations of optical and radar images, and various image derived variables. Based upon the literature it was expected that using radar and optical variables together with OBIA and CTA would improve upon the overall accuracies currently presented as greater than 76% for VCFs. The numbers of different combinations of communities present are assessed to estimate a score. Table 2.6 outlines the scoring method of these forms.

Table 2.6. OWES scoring system for VCFs by Number of Forms (OWES Southern Manual, 2002).

# of communities with 1-3 forms		# of communities with 4-5 forms	# of communities with 6 or more forms
#	Score	Score	Score
1	1.5	2.0	3
2	2.5	3.5	5
3	3.5	5.0	7
4	4.5	6.5	9
5	5.0	7.5	10.5
6	5.5	8.5	12
7	6.0	9.5	13.5
8	6.5	10.5	15
9	7.0	11.5	16.5
10	7.5	12.5	18
11	8.0	13.0	19
+0.5 for each additional community		+0.5 for each additional community	+0.5 for each additional community

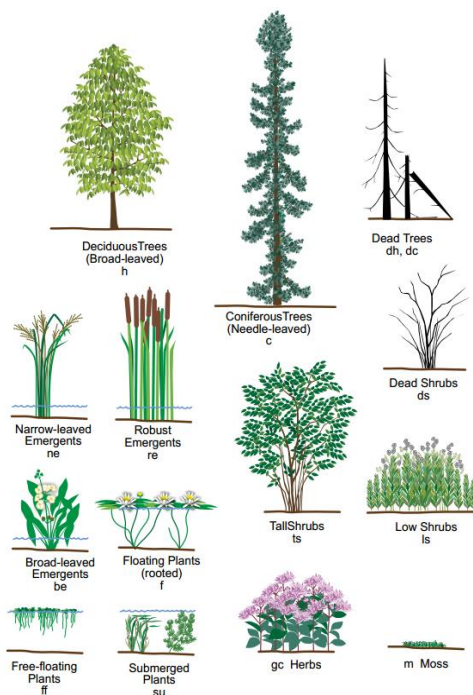


Figure 2.7. Wetland vegetation VCFs and symbols (after Figure 11, OWES Southern Manual, 2013).

2.9.3 Open Water Type (Biological component)

The relative proportion and areal configuration of permanent open water to adjacent emergent vegetation is important to many species of wildlife. There are eight categories of Open Water Types outlined in the OWES manual (Table 2.7). If there is no permanent open water, the wetland obtains zero points for this attribute. Figure 2.8 provides a visual representation of the Open Water Types.

Open Water Type is also known in the literature as surface water, permanent surface bodies, and seasonal water bodies. Much of literature focuses on the detection of these attributes using radar data and methods such as temporal analysis to assess the hydrological water patterns, threshold-based analysis with R^2 values of 0.84 and utilizing water indices to classify water patterns (Bartsch *et al.*, 2007; Sass and Creed, 2008; Campos *et al.*, 2012; Watts *et al.*, 2012). The generalized trend for these types of attributes focuses on radar data, and/or with optical spectral indices. For Open Water Type it was hoped that using OBIA with optical and radar imagery would prove to be useful with higher resolution imagery alone, and/or combined with radar imagery, which has not been shown in the literature. It was hoped that Open Water Type can be assessed using optical imagery alone and combined with Radarsat-2 variables in OBIA with CTA.

2.9.4 Inundation Extent (Hydrologic component)

Determining the wet extent (Inundation Extent) of a wetland is important in relation to its capacity to attenuate or reduce flood peaks in downstream areas;

Table 2.7. Eight OWES Open Water Types and their associated scores (OWES Southern Manual, 2002).

Open Water Type	Description	Score
Type 1	Open water occupies less than 5% of the wetland area	8
Type 2	Open water occupies 5-25% of the wetland area, occurring in a central area.	8
Type 3	Open water occupies 5-25% of the wetland area, occurring in ponds of various sizes; vegetation occurs in dense patches or diffuse open stands	14
Type 4	Open water occupies 26-75% of the wetland area, occurring over a central area	20
Type 5	Open water occupies 26-75% of the wetland area, occurring in a pattern where small ponds and "embayments" are common	30
Type 6	Open water occupies 76-95% of the wetland area, occurring in a large central area; vegetation is peripheral	8
Type 7	Open water occupies 76-95% of the wetland area; vegetation occurs in patches or diffuse, open stands	14
Type 8	Open water occupies more than 95% of the wetland area	3

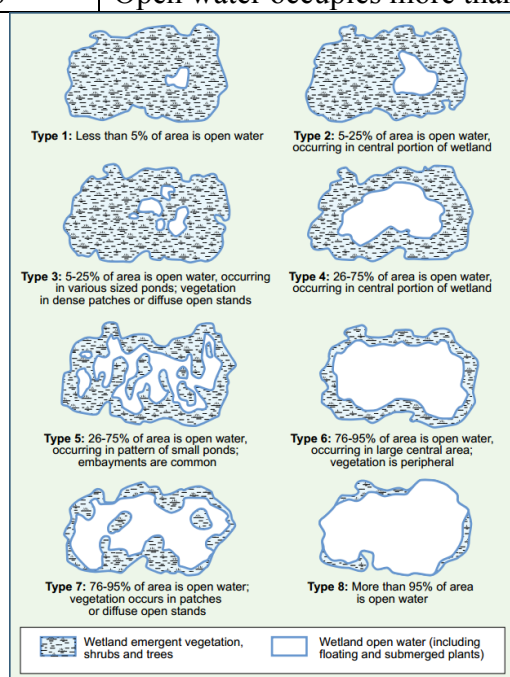


Figure 2.8. Open Water Type drawings (after Figure 17, OWES Southern Manual, 2013).

this is an important ecological function, as well as providing obvious human value function (OWES, 2002). Inundation extent could be considered the maximum size of a wetland when considering its hydrological function to attenuate flood peaks.

The specific use of vegetation indices selected for this research is presented here as it only relates to this one attribute. There are approximately 150 different types of vegetation indices (Asner, 1998) proposed in a wide variety of studies that support the use of the different indices to establish different patterns in wetlands. Mathematical combinations of two or more spectral bands have been shown to be reliable indicators of vegetation health/primary productivity such as NDVI (Eq. 2.1); moisture content in the canopy (NDWI, Normalized Difference Water Index)(Gao, 1996)); or through inference, of soil composition (MCARI, Modified Chlorophyll Absorption Ratio Index best estimated soil Total Petroleum Hydrocarbons (TPH) (Zhu *et al.*, 2013).

As a variant of NDVI, $NDVI_{green}$ is derived as:

$$NDVI_{green} = \frac{(NIR-G)}{(G+NIR)} \quad \text{Eq. 2.8}$$

- where NIR is the near-infrared spectral band of a sensor; and
- G represents the green spectral band of same sensor.

$NDVI_{Green}$ has not been shown to determine wet extents of wetlands, habitat, or wetland type in the literature. $NDVI_{Green}$ was developed as a way to estimate plant chlorophyll (Gitelson and Merzlyak, 1997), which changes throughout a plant's lifespan and as it reacts to stressors (such as soil moisture levels). Similar indices have been used to map habitat, wetland type and plant functional types in the literature. Delgado and Marin (2013) utilized

Landsat-derived NDVI values to map swan habitat in a southern Chilean wetland. They found they were able to estimate habitat area, but not determine individual vegetation species.

Wang *et al.* (2012) classified plant functional types at Poyang Lake, China (freshwater lake-wetland) using time series of NDVI and another of the vegetation-water index (VWI = time series NDVI/Submersion Time Index) derived from Beijing-1 microsatellite (32m pixels with 3 spectral bands, green (0.52-0.62 μm ; red (0.63-0.69 μm) and NIR (0.76-0.09 μm)). They obtained an overall accuracy of 81.3% for 3 plant functional types (and 3 general classes, water, mudflat and sand).

Campos *et al.* (2012) detected seasonal and permanent surface water utilizing $\text{NDWI}_{\text{Green/MIR}}$ (Gao, 1996) and $\text{NDWI}_{\text{NIR/MIR}}$ (Xu, 2006) derived from multi-temporal series of Landsat 5 TM and 7 ETM+ (Enhanced Thematic Mapper Plus) imagery over Mauritania.

Lang *et al.* (2008) used multi-date C-band data from ERS-2 and ENVISAT to compare with field observation of inundation and soil moisture, deriving principal components from both leaf-off and leaf-on data sets. The comparative analysis resulted in R^2 for soil moisture from 0.55 to 0.90 and for inundated area R^2 values from 0.06 to 0.81.

van der Velde *et al.* (2009) assessed the backscatter signatures derived from single polarized (HH, VV) ASAR WSM imagery of grassland and a wetland to conduct multi-variate analysis of soil moisture, soil temperature and vegetation biomass against SPOT

NDVI. The correlation calculated between backscatter and wetland soil moisture were 0.62; with wetland NDVI was 0.56 and with soil temperatures was 0.64.

This research builds on the literature by: 1) evaluating various vegetation indices derived from more recent imagery such as WorldView-2 as well as Landsat TM imagery to determine an optimal index for mapping the wet extent boundary, and 2) to correlate radar parameters against transect measured soil moisture and to use that relationship to estimate the location of wet extent. (Lang *et al.*, 2008; van der Velde *et al.*, 2009).

The scoring of flood attenuation is complex and requires knowledge of the wetland of interest and the surrounding wetlands within the same basin. The complete outline of this scoring method is given in Appendix A.

2.9.5 Number of Wetland Types (Biological component)

For this and the following attributes up to Anthropogenic Disturbance, the main requirement of the collaboration with the OMNR was to assess the LIO data and use it in simple GIS applications as described in section 2.6.2 to determine if these data and methods were sufficient to map these attributes. There are methods in the remote sensing and GIS literature that are used to derive new thematic data to map these variables and these are listed in Table 2.5, however, they were out of the scope of this research.

The OWES assumes that for every additional Wetland Type present in a wetland or wetland complex, species presence should increase by 50%, therefore the score increases incrementally by a factor of ~1.5 with each additional Wetland Type, resulting in scores as

follows (maximum of 30 points): One Wetland Type = 9 points, Two Wetland Types = 13 points, Three Wetland Types = 20 points, Four Wetland Types = 30 points.

2.9.6 Diversity of Surrounding Habitat (Biological component)

Surrounding habitat can act as both a buffer to wetlands (e.g. providing access to the wetlands) or as a deterrent to use (e.g. intense human activity). Surrounding habitats were assessed as those that were within 1.5 km straight line distance to the edge of the wetland and that had a MMU of 0.5 ha or greater (following the criteria as the OWES, 2002). The OWES scoring of these habitats gives one point to each of the following (maximum of 7 points): row crop, pasture, abandoned agricultural land, deciduous forest, coniferous forest, mixed forest, abandoned pits and quarries, open lake or deep river, fence rows with deep cover, or shelterbelts, terrain appreciably undulating, hilly or with ravines, creek flood plain.

2.9.7 Proximity to Other Wetlands (Biological component)

When wetlands are located close to one another wildlife can move between them allowing for extended use of habitat, breeding areas, food sources among others, and therefore the associated value of the wetland is increased (OWES, 2002). The most valuable wetlands are those that are connected hydrologically via surface water, even if that surface water is seasonal. The scoring of proximity is made from the boundary of the entire wetland complex, and not for wetlands within the complex, which are assumed to have proximity of 0 km. The scores for this category are assessed for the highest valued category (maximum of 8 points) and are outlined in Table 2.8.

Table 2.8. Connections and scores for measuring the Proximity to Other Wetlands.

Type of Connection	Number of Points
Hydrologically connected by surface water to other wetlands (different dominant Wetland Type), or open lake or deep river within 1.5 km	8
Hydrologically connected by surface water to other wetlands (same dominant Wetland Type) within 0.5 km	8
Hydrologically connected by surface water to other wetlands (different dominant Wetland Type), or open lake or deep river from 1.5 to 4 km away	5
Hydrologically connected by surface water to other wetlands (same dominant Wetland Type) from 0.5 to 1.5 km away	5
Within 0.75 km of other wetlands (different dominant Wetland Type) or open lake or deep river, but not hydrologically connected by surface water	5
Within 1 km of other wetlands, but not hydrologically connected by surface water	2
No wetland within 1 km	0

2.9.8 Wetland Size (Biological component)

Generally, larger wetlands obtain higher scores in the OWES because they will have more of the features that are considered valuable. The Wetland Size score is directly related to the scores received for Number of Wetland Types, VCFs, Diversity of Surrounding Habitat, Proximity to Other Wetlands and Open Water Types. The total score for those categories (plus Interspersion, which was not measured for this research because of the lack of validation data) is assessed in relation to the physical size of the wetland. The breakdown of the total score is given in Table 2.9 (after OWES, 2013); and the scores earned by the above attributes are used along with the size of the wetland to determine the overall size score. The maximum possible score is 50 points.

Table 2.9. Table for size score (Biological Component) (after Table 5 in OWES Southern Manual, 2013).

		Total Score for Biodiversity Subcomponent									
		<37	37-47	48-60	61-72	73-84	85-96	97-108	109-120	121-132	>132
Wetland size (ha)	<20 ha	1	5	7	8	9	17	25	34	43	50
	20-40	5	7	8	9	10	19	28	37	46	50
	41-60	6	8	9	10	11	21	31	40	49	50
	61-80	7	9	10	11	13	23	34	43	50	50
	81-100	8	10	11	13	15	25	37	46	50	50
	101-120	9	11	13	15	18	28	40	49	50	50
	121-140	10	13	15	17	21	31	43	50	50	50
	141-160	11	15	17	19	23	34	46	50	50	50
	161-180	13	17	19	21	25	37	49	50	50	50
	181-200	15	19	21	23	28	40	50	50	50	50
	201-400	17	21	23	25	31	43	50	50	50	50
	401-600	19	23	25	28	34	46	50	50	50	50
	601-800	21	25	28	31	37	49	50	50	50	50
	801-1000	23	28	31	34	40	50	50	50	50	50
	1001-1200	25	31	34	37	43	50	50	50	50	50
	1201-1400	28	34	37	40	46	50	50	50	50	50
	1401-1600	31	37	40	43	49	50	50	50	50	50
	1601-1800	34	40	43	46	50	50	50	50	50	50
	1801-2000	37	43	47	49	50	50	50	50	50	50
>2000	40	46	50	50	50	50	50	50	50	50	

2.9.9 Hunting (Social component)

In the existing OWES, the intensity of use of the area by hunters is evaluated using classes of high, moderate, and low as follows (OWES, 2002):

- High Intensity (40 points): Evidence of heavy use includes at least 10 duck blinds, or known concentrations of waterfowl hunters or deer hunters (in the wetland); if numbers are available, then 100 or more hunter-days of recreation.
- Moderate Intensity (20 points): Evidence of two to nine duck blinds or hunters checked regularly by Conservation Officers; if numbers are available, 21-99 hunter-days of recreation.
- Low Intensity (8 points): Evidence of one duck blind, shotgun shells, reported use by on-agency sources; if numbers are available, up to 20 hunter-days of recreation.

2.9.10 Ownership Patterns (Social component)

Ownership of a wetland is an indicator of the value of a wetland to humans. Privately held lands have less value than publicly owned wetlands (OWES, 2002) due to lack of accessibility and inability to direct conservation. The scoring of this attribute is made by estimating the percentage (fractional area, FA) of ownership of a wetland and multiplying it by a factor depending upon the ownership pattern, to a maximum of 10 points.

Private or Crown lands, held under contract or in trust for wetland protection	FA x 10
Public land	FA x 8
Private land	FA x 4

2.9.11 Wetland Basin Size (Hydrologic component)

Upstream detention attributes are often used to determine the net benefit of the wetland in relation to the all the other possible detention areas upstream of the wetland. Theoretically, if there are detention areas (other wetlands, especially riverine wetlands, rivers and lakes, etc.) upstream of the evaluated wetland, the overall hydrological detention value of the downstream wetland is reduced. However, with the removal of the upstream areas (anthropogenic disturbance/development) the value of the downstream area will obviously increase. As well, if a wetland represents 50% of total storage or more in its basin (based on area), it will provide maximum detention benefits regardless of its position (Adamus and Stockwell, 1983). Three factors need to be determined to assess the overall effectiveness for flood attenuation of a wetland complex: wetland basin size, size of the wetland, and size of other detention areas in the basin.

2.9.12 Rarity of Wetland in the Landscape (Special Features component)

Wetlands often contain rare vegetation (e.g. snake-mouth orchid (*Pogonia ophioglossoides*) or provide habitat for rare animal species (e.g. Blanding's Turtle (*Emydoidea blandingii*)). When wetlands are rare within the landscape their value as potential habitat for rare species is high. For example, wetlands isolated within upland can contain rare flora species, and act as habitat for fauna where major wetlands have been removed (Flinn *et al.*, 2008). This attribute assesses both the rarity of wetlands in the landscape in general, and rarity of each of the four Wetland Types within particular site regions broken down into Site Districts (Hills, 1959; Hills 1961). Figure 2.9 provides the visual depiction of the site regions and site districts in eastern Ontario.

Scores are assigned for rarity ranging from 0 (not rare) to 80 (very rare) (Snell, 1987), with a maximum of 80 points for rarity within the landscape and 80 points for Rarity of the Wetland Type. Table 2.10 gives the breakdown of the scores per site district.

Table 2.10. Scores given for wetland presence within the landscape and by Wetland Type in the three site districts representing the area of interest (after Table 4, OWES Southern Manual, 2002).

Site District	Rarity within the Landscape	Rarity of Wetland Type			
		Marsh	Swamp	Fen	Bog
6-10	20	0	20	80	80
6-11	0	30	0	80	80
6-12	0	30	0	60	80

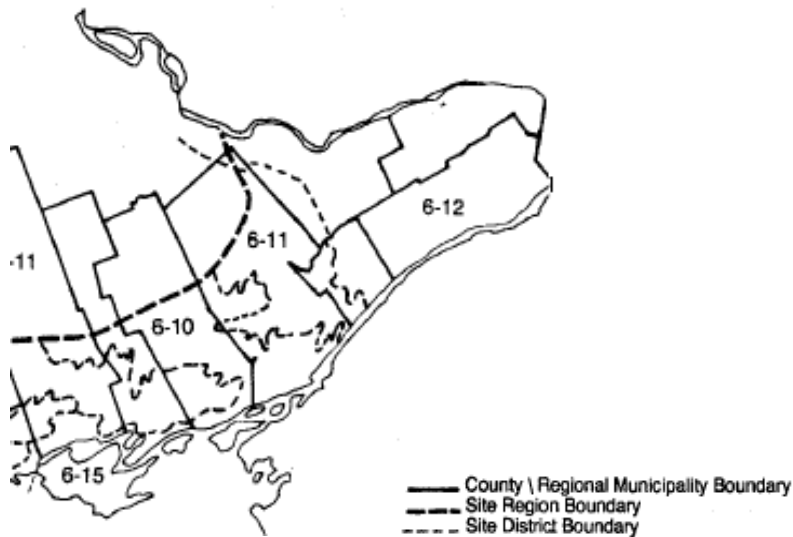


Figure 2.9. Eastern Ontario Subsection of Site Regions and Site Districts in Southern Ontario (after Figure 16, OWES Southern Manual, 2002).

The scores are assessed by comparing the Wetland Type attribute, the existing OMNR wetland layer and using the ecodistrict layers. The first portion of the score is based upon the percentage of the total evaluated wetland area that each particular Wetland Type represents. Any type with greater than 40% of the total area received a score of 0. Wetland Types representing less than 40% of total area were scored as follows: 0-10% = 80, 11-20% = 60, 21-30% = 40, 31-40% = 20. These scores were reduced by 50% for all Wetland Types represented in more than 40% by number of the evaluated wetlands.

2.9.13 Anthropogenic Disturbance (Social component)

This attribute indicates human impacts on the aesthetics of a wetland (OWES, 2002). Impacts include: roads, utility corridors, buildings, dumps, fill, channelization, dredging, drainage ditches, control dams and other human uses.

In the literature, Anthropogenic Disturbance is also known as human influence, deforestation, agriculture expansion, and land use land cover (LULC) change. Methods used to assess these changes include GIS assessment of thematic data to determine change in polygons, aerial photointerpretation, LSU, assessment of forest cover change through thematic maps derived through tasselled cap transformation, unsupervised classification, MLC and change detection, and GIS classification models using Basin Buffer Index and Hydric Vegetation Index, and Cellular Automata-Markov Chain modelling. Data types used with these methods have included Landsat TM and ETM+, and SPOT-5 data. Overall accuracies range from 85% to 89% (Wilcox, 1995; Phillips *et al.*, 2005; Stuart *et al.*, 2006; Papastergiadou *et al.*, 2008; Dyukarev *et al.*, 2011; Behera *et al.*, 2012; Yang *et al.*, 2013).

Previous studies using unmixed image fractions in land cover change analysis based upon climatic differences (Schmid *et al.*, 2005; Melendez-Pastor *et al.*, 2010) or human-based changes in other ecosystems such as slash and burn in the Amazon (Adams *et al.*, 1995) or tundra land cover change (Olthof and Fraser, 2007) led to the selection in the research of LSU to assess anthropogenic change through time. There is little literature on the use of such fractions with OBIA and none that was found for wetland applications, suggesting that, if successful, this could be a novel contribution. It was also hoped that this

type of analysis would improve upon the existing assessment of anthropogenic disturbance in the literature with accuracies ranging from 85 to 89%.

For OWES scoring, the areal extent of disturbances is estimated as localized situations are separated from more widespread disturbances. The amount of water pollution is also assessed in this category.

This attribute is scored as follows (maximum of 7 points):

Human disturbances absent or nearly so =	7
One or several localized disturbances =	4
Moderate disturbance; localized water pollution =	2
Wetland intact but impairment of ecosystem quality intense in some areas =	1
Extreme ecological degradation, or water pollution severe and widespread =	0

3.0 Study areas and remotely sensed imagery

This chapter provides a description of the study areas and then discusses the optical and radar satellite imagery used for this research.

3.1 Study region and study areas

This research was carried out in eastern Ontario, Canada (Figure 3.1), a region of approximately 15,500 km² which is a mix of agricultural, forest, and urban lands including the city of Ottawa on the northern edge. Wetlands are distributed throughout the region and are predominantly swamps and marshes with fewer bogs and fens (National Wetlands Working Group, 1997). Agriculture is dominant near the St. Lawrence and Ottawa Rivers, and in the flat landscapes from Ottawa east towards the Québec border. In the northwest of the area, and along the Frontenac Axis (a strip of the Canadian shield linking to the Adirondacks in the south), there are generally thin soils over igneous and metamorphic bedrock with limited agriculture potential (Baldwin *et al.*, 2000).

There are many lakes on the shield portion of study region, allowing for wetland formation in bays, and along shores. Around Westport Bog the area of lakes is approximately 11,686 hectares (116 km²). Some lakes along the axis are marl-based resulting kettle hole-type formations (Keddy, 1995). Forest covers about 38% of the eastern Ontario region, and varies from about 60% on the shield in the northwest, to less than 30% in the east.

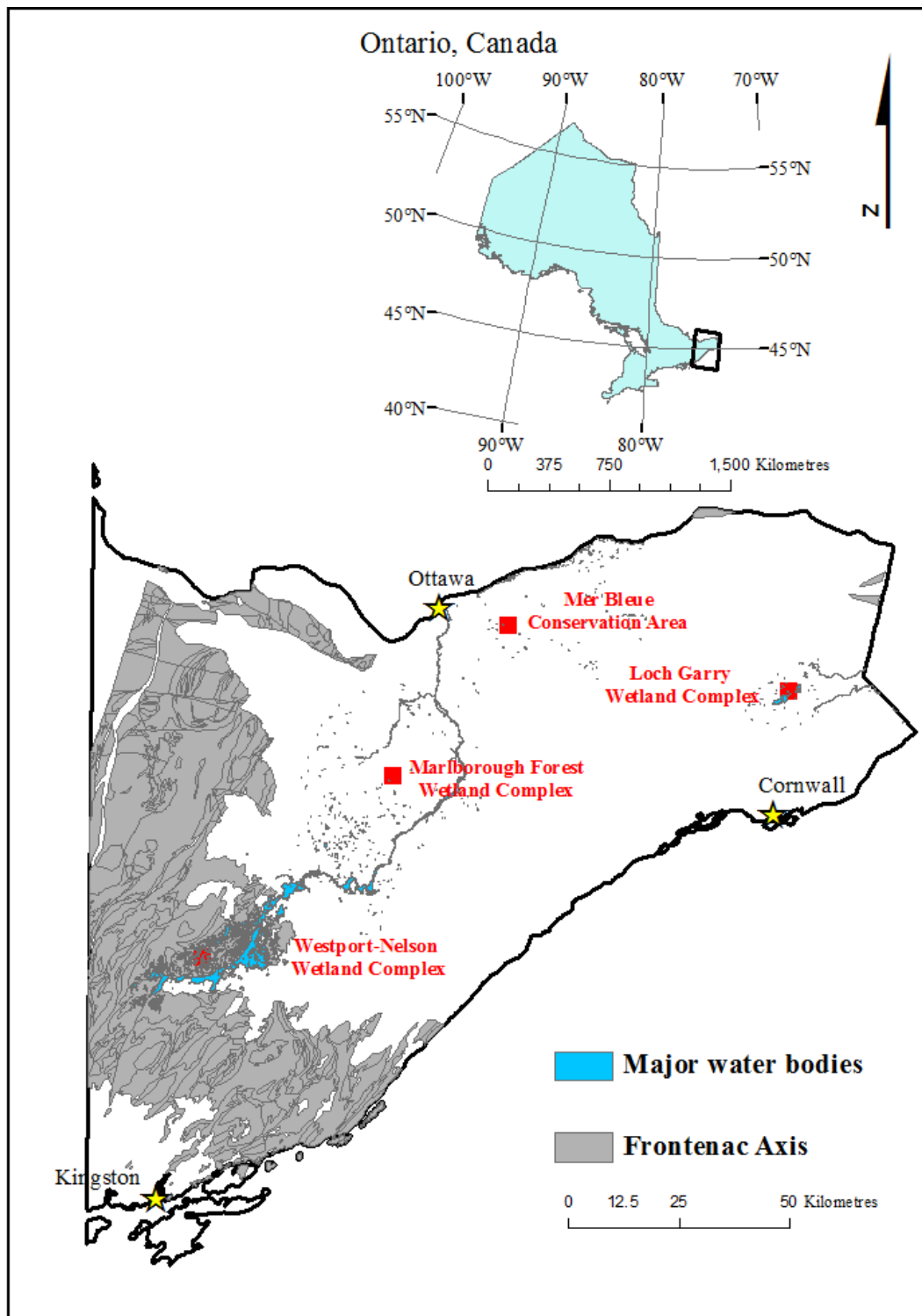


Figure 3.1. Eastern Ontario and the position of the four wetland complex study areas in Kemptville area. Study areas are red squares.

Most forests are deciduous or mixed deciduous-coniferous and are dominated by sugar maple (*Acer saccharum* Marsh), with lesser amounts of other temperate species (e.g., American beech (*Fagus grandifolia* Ehrh.), red oak (*Quercus rubra* L.), red pine (*Pinus resinosa* Sol. Ex Aiton); low-lying wetter areas are often dominated by white cedar (*Thuja occidentalis* L.) (Thompson, 2000; EOMF, 2006). Detailed descriptions of species composition at each site are given in following sections.

The eastern Ontario region was selected as there are many wetland complexes present. OWES (2002) criteria for defining a wetland complex includes: the complex does not extend across watersheds (except in rare conditions where a functional flora and/or fauna linkage can be shown), and that the maximum distance between the units of a complex does not exceed 0.75 km (OWES, 2002). Another edition of the OWES (3rd edition, version 3.2, 2013) has since been released. Significant differences between criteria from 2002 to 2013 are noted in the following sections.

3.1.1 Selection of wetland complexes

The selection of the wetland complexes was made through an investigation of the OMNR NHIC (Natural Heritage Information Centre) database, on the advice of the OMNR, which included wetland specialists and district ecologists of four Ontario districts (Kemptville, Peterborough, Aurora, Pembroke) and through the review of Chisholm *et al.* (1997). The on-line NHIC database provides information on the size of the wetland complex, its location, whether or not it has provincial significance, the types of wetlands and vegetation present and the landform of the wetland, including soils and site type (e.g.

riverine, lacustrine, palustrine, moraine etc.). The following criteria also aided in site selection:

- The wetland complex must be provincially significant;
- Wetland complex size must be suitable for analysis using coarse resolution imagery (> 30 m pixels), but must be smaller than one or two high resolution satellite scenes (e.g., approximately 16 km swath) to minimize the cost of image acquisition and processing/correction time;
- Maximize the number of wetland types within a complex; and
- Must be located close to Ottawa, Ontario for logistical reasons.

Four wetlands complexes within the Kemptville district met the criteria, including Loch Garry Wetland Complex ('Loch Garry'), Marlborough Forest Wetland Complex ('Marlborough Forest'), Mer Bleue Conservation Area ('Mer Bleue Bog'), and Westport-Nelson Wetland Complex ('Westport Bog') (Figure 3.1). Descriptions of each of these wetland complexes is based on existing information as well as fieldwork and remote sensing analysis conducted for this research. The OWES field evaluations were last completed in the mid-1980s and early 1990s. Table 3.1 lists the field investigation dates and all four field-based evaluation reports are scanned and included digitally with this thesis. Table 3.2 provides a summary of the details of the four wetlands. They are all large with respect to typical wetland sizes, and thus are considered rare in the landscape in eastern Ontario. However, each was a wetland complex with different Wetland Types (Table 3.2), VCFs, and hydrological conditions in a mosaic of subareas. As such these four sites presented an

excellent opportunity for analysis of image and wetland attribute variability both within each wetland and between the four wetland study sites.

Table 3.1 Field investigation dates and time spent in the field for the OWES field-based evaluations.

Wetland Complex	Date visited			Total person hours
Loch Garry	July 1983			198 (3 investigators)
Marlborough Forest	July 9, 1991	August 8, 1991	September 6 & 11, 1991	65 (2 investigators)
Mer Bleue Bog	July 5 & 6, 1983			Unknown (2 investigators)
Westport Bog		August 27/28, 1985		38 (3 investigators)

Table 3.2. Summary of the four wetlands selected for this research.

Name	Area (ha)	Wetland Types	OWES Designation	Change in Wetland Types
Loch Garry	1,281	Fen, Marsh, Swamp	Significant	Bog present
Marlborough Forest	1,099	Fen, Marsh, Swamp	Significant	Bog present
Mer Bleue Bog	3,500	Bog, Marsh	Significant	Swamp present
Westport Bog	356	Bog, Marsh	Significant	Swamp present

Situated north of Cornwall, Ontario the Loch Garry Wetland Complex is found within fragmented farmland and located along the shores of a large lake, Loch Garry (Figure 3.2). The lake is 1 to 5 m deep and is about 3.8 km² (380 ha). The wetland complex is located within the Garry River watershed (3,400 ha), is about 1,281 ha, and contains 3 Wetland

Types of fen, marsh and swamp. This site was given provincial significance during a 1983 field-based evaluation due to a strong Special Features component score with the presence of a rare wetland assessed at that time as bog. The lake is hydrologically isolated with water being supplied to the Garry River watershed by precipitation. Hydrological isolation is a defining feature of bogs (National Wetlands Working Group, 1997), which is why it is believed the 1983 field assessors classified much of the area as bog.

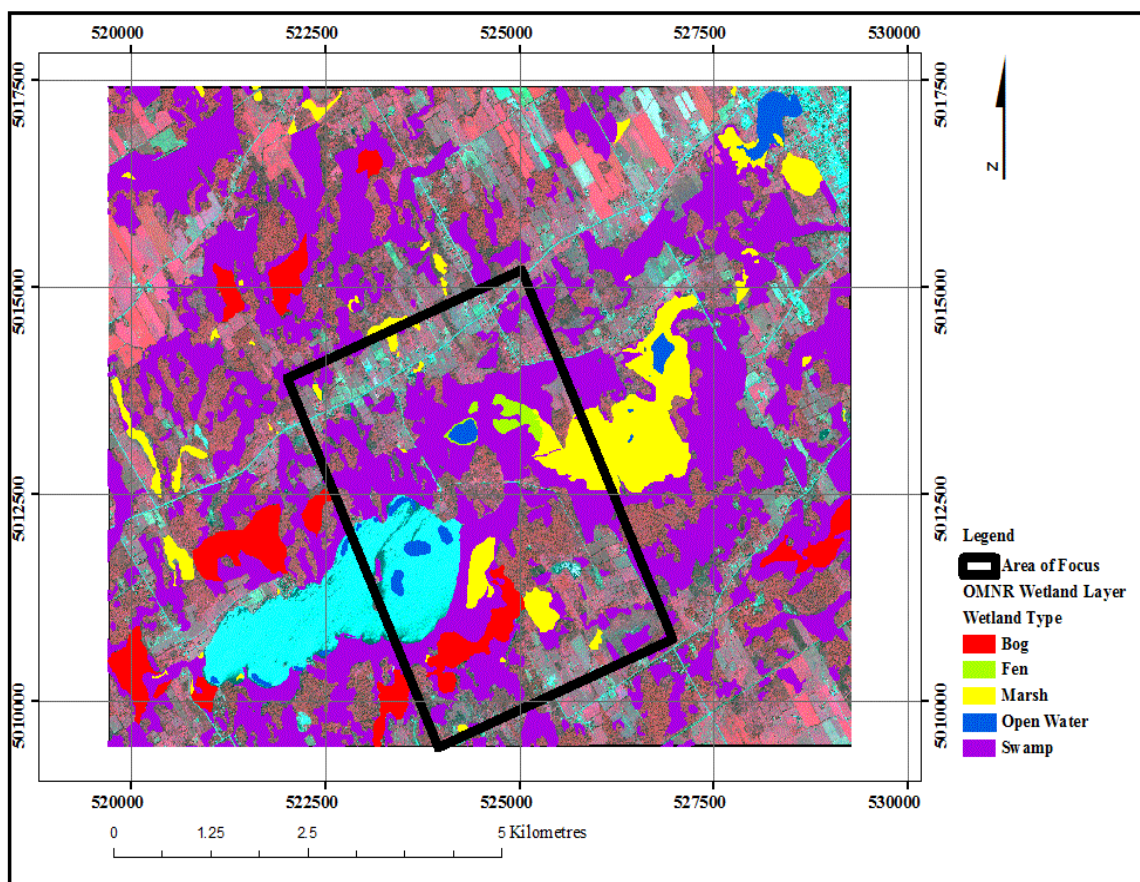


Figure 3.2. Loch Garry Wetland Complex: CIR (colour infrared) WorldView-2 composite (Summer 2010) with OMNR wetland layer (2013) overlaid. Black outline highlights the focussed area of interest where field work was performed. Light blue colour is CIR representation of some of the water in this image; an indication the image is potentially substandard.

Based upon this research (e.g. field observed vegetation, and spectral response in imagery), the Wetland Type originally identified as bog (bright red in Figure 3.2) is thought to be Fen. Fen vegetation identified in the field included: stunted tamarack (*Larix laricina* (Du Roi) K.Koch), low shrubs such as sweet gale (*Myrica gale* L.), dwarf birch (*Betula pumila* L.), bog willow (fen indicator species, *Salix pedicellaris* Pursh); herbs including pitcher plant (*Sarracenia purpurea* L.), buckbean (fen indicator species, *Menyanthes trifoliata* L.), ferns (*Dryopteris* spp.) and numerous narrow leaved emergents (including sedges (*Carex* spp.) and rushes (*Juncus* spp.)). Also present as a minor component were cattails (*Typha latifolia* L.). Sphagnum moss (*Sphagnum* spp.) and brown mosses (*Campylium stellatum* Hedw., *Drepanocladus revolvens* (Sm.) Warnst, *Tomenthyphnum nitens* Hedw., *Scorpidium scorpioides*, Hedw.) were abundantly present. An expert field ecologist at OMNR agreed this area most resembles Fen, but the SOLRIS classification shows it as mostly Bog.

Marsh-dominant vegetation identified in the field consisted mainly of robust emergents (cattails, common reeds (*Phragmites australis* (Cav.) Trin. Ex Steud, subspecies *australis*, *Phragmites australis* (Cav.) Trin. Ex Steud subspecies *americanus*), bulrushes (*Scirpus* spp.) etc.), components of free-floating plants (duckweed (*Lemna* spp.)), rooted floating plants (yellow pond lily (*Nuphar variegatum* Engelm. Ex Durand), fragrant white water lily (*Nymphaea odorata* Aiton) and watershield (*Brasenia schreberi* J.F. Gmel)). In ecotonal areas such as marsh and swamp, and/or marsh and fen, swamp and fen vegetation were present (to a minor degree) and included: tall shrubs of red-osier dogwood (*Cornus*

stolonifera L.), speckled alder (*Alnus incana* (L.) Moench), willow (*Salix* spp.); herbs such as ferns, spotted joe-pye weed (*Eupatorium maculatum* (L.) E.E. Lamont), purple loosestrife (*Lythrum salicaria* L.); narrow leaved emergents such as sedges and Canada bluejoint (*Calamagrostis Canadensis* (Michx.) P. Beauv.); and broad-leaved emergents such as wild calla (*Calla palustris* L.).

Swamp vegetation included large components of dead coniferous (particularly dead eastern white cedar) along with live cedar, tamarack, white pine (*Pinus strobus* L.), black spruce (*Picea mariana* (Mill.) Britton, Stems & Poggenburg), hemlock (*Tsuga Canadensis* (L.) Carrière), and balsam fir (*Abies balsamea* (L.) Mill). In areas of mixed-forest swamp, hardwood vegetation included black ash and maple. White spruce (*Picea glauca* (Moench) Voss) was present along with aspen (*Populus* spp.), jack pine (*Pinus banksiana* Lamb.) and red and white pine in drier sites; wetter sites had black spruce with eastern white cedar and black ash.

The Marlborough Forest Wetland Complex (Figure 3.3) of approximately 1,099 ha is located south-west of Ottawa, within less fragmented farmland but near industrial land uses (e.g. quarrying). With extensive hunting, ATV and snowmobile use, this complex is recreationally active. For the purposes of this research some components of the Richmond Wetland and Steven Creek Wetland Complex were also included. The complex was OWES assessed in 1991 and was given provincial significance due to the presence of rare Wetland Types (Fen and Bog) and rare vegetation species (e.g. orchids). During field work for this research, an attempt was made to locate the assessed bog (0.03% of the area, OMNR wetland

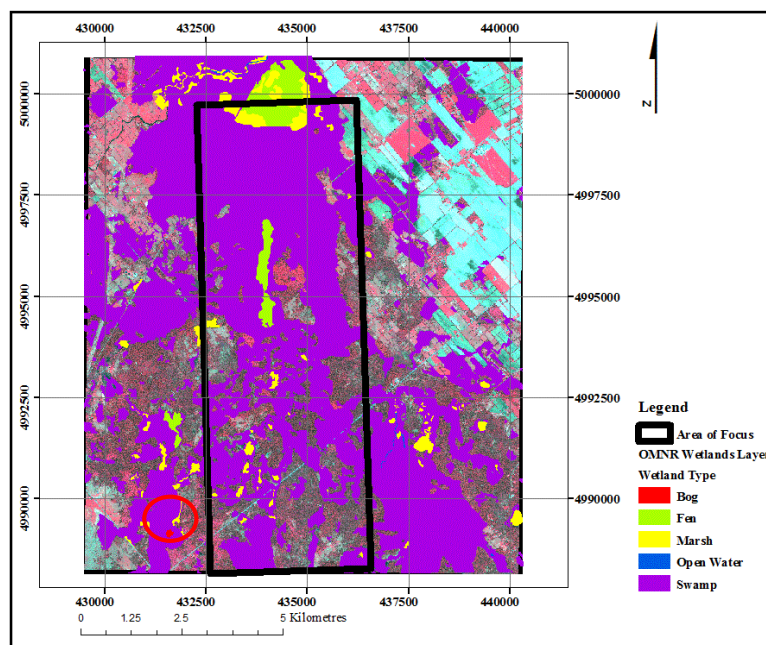
layer; see red circle Figure 3.3), but there was not a wetland of any type visible in that area in either spring or summer.

The fen vegetation included extensive sedge in wide open meadows with pitcher plants, some orchid species (unidentified) and, along the ecotone zone with swamps, low shrubs of creeping snowberry (*Gaultheria hispidula* (L.) Muhl. Ex Bigelow), leatherleaf (*Chamaedaphne calyculata* (L.) Moench), and willow species.

Marsh vegetation was largely sedges and cattails with some floating and free-floating plants such as yellow pond lily, duckweed and watershield. Coniferous swamps were dominant in this region, primarily cedar with minor tamarack, fern and grass components. In areas of standing water there was dead cedar as well as floating species such as duckweed, water shield and pondweed (*Potamogeton* spp.). In dryer areas, or later in the season, the understorey often consisted of grasses such as marsh timothy (*Muhlenbergia glomerata* (Willd.) Trin.), reeds and canary grasses (*Phalaris arundinacea* L.) and herbs such as ferns and poison ivy (*Rhus radicans* (L.) Kuntze). In mixed or predominantly hardwood swamps the tree species included black ash and maple with similar understoreys. In some minor cases there was the presence of cattails, especially in marsh/swamp ecotonal areas.

The Mer Bleue Conservation Area ('Mer Bleue Bog', Figure 3.3) is found within the city limits of Ottawa, with extensive suburban development to the north, and surrounded by farmland to the south and east. This well-studied area of approximately 3,500 ha is a wetland of international importance (Ramsar-designated, Ramsar, 2006) and is also provincially

significant. The bog is approximately 7,700 years old and representative of a northern boreal landscape, including flora and fauna species that are common to boreal bogs. Bog vegetation identified in the field included dominant areas of low shrubs such as cotton grass (*Eriophorum vaginatum* L.), Labrador tea (*Ledum groenlandicum* (Oeder) Kron & Judd), leatherleaf, velvet leaf blueberry (bog indicator species, *Vaccinium myrtilloides* Michx.) and bog laurel (bog indicator species, *Kalmia polifolia* Wangenh.).



3.3. Marlborough Forest Wetland Complex: CIR WorldView-2 composite (2010) with OMNR wetland layer (2013) overlaid. Black outline highlights the field area of interest where field work was performed. Red circle highlights Bog OMNR wetland layer. Light blue in this image is the CIR representation of bare

There was also a strong sphagnum component. In treed areas there were birch and maple along with tamarack/tamarack saplings, black spruce (bog indicator species), red pine, and white pine. The OWES (2002) indicates that bogs can be 25% treed with no height restriction. Black spruce is listed as an indicator species of bog, and tamarack is listed as having a potential presence in bogs (with no indication of rarity). A significant change in OWES (2013) is a height restriction where trees must be <6 m tall, and that black spruce occurs in bog and fen, and tamarack is no longer present in bogs.

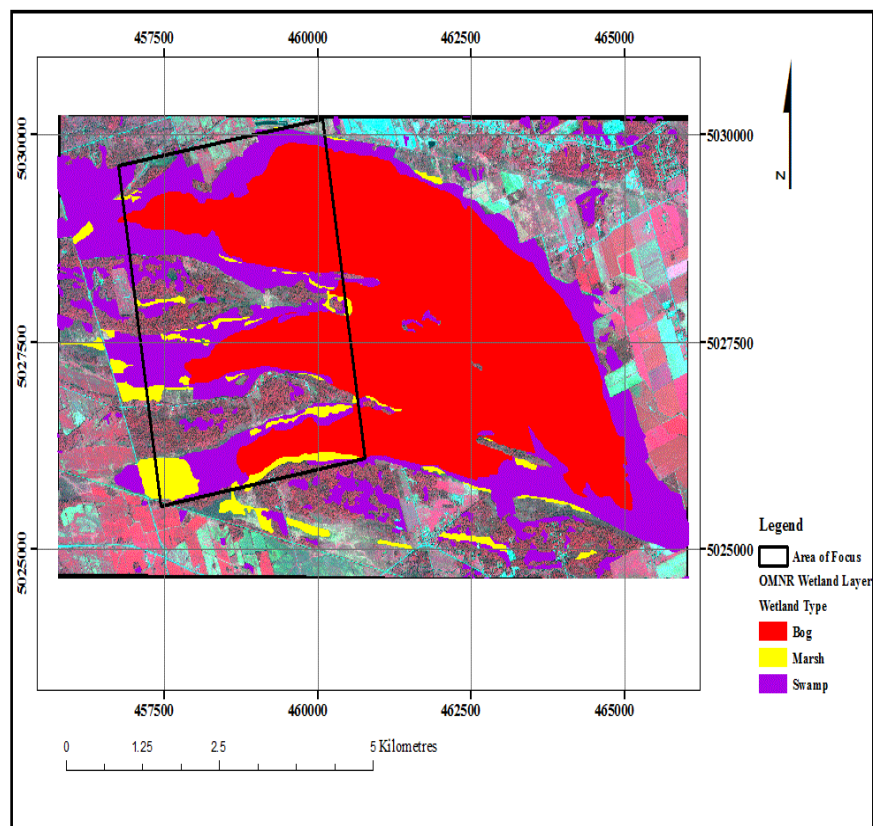


Figure 3.4. Mer Bleue Conservation Area: CIR WorldView-2 composite (Spring 2010) with OMNR wetland layer (2013) overlaid. Black outline highlights the area of focus where field work was performed.

In the field near the public boardwalk at Mer Bleue Bog the presence of tamarack was recorded and some trees that were greater than 6 m were also observed (see Figure 3.5 A and B, yellow circles).

Marsh vegetation included large areas of cattails, with some ecotone marsh/bog, marsh/upland areas containing speckled alder, sweet gale, spotted joe-pye weed, purple loosestrife, Canada bluejoint, and wild calla. Duckweed and watershield were also found in some areas. Swamp and fen vegetation were not observed during the field visits. There is a small portion of fen vegetation located in the northwest corner of the north arm of the bog (Touzi, 2007; Humphreys *pers.comm*, 2010). Accessing this area damages bog vegetation and therefore it was not considered for this research.

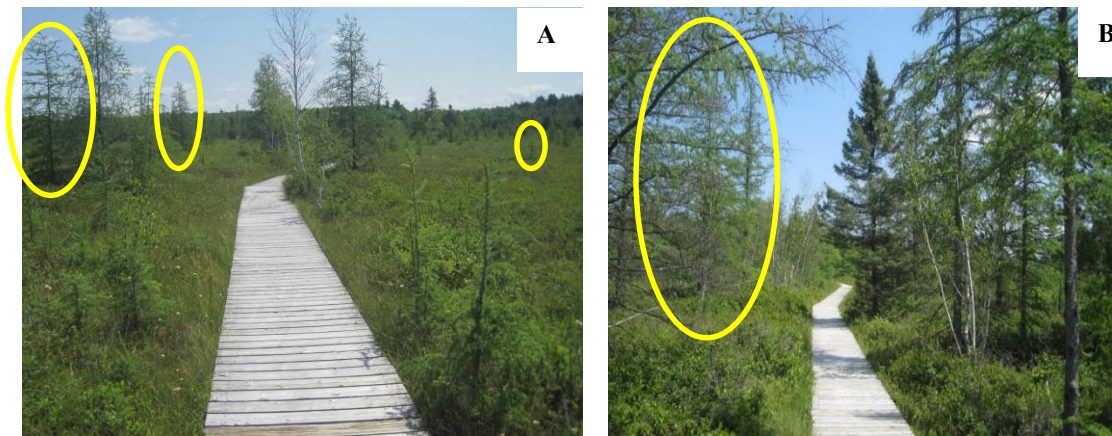


Figure 3.5. Photographs near the public boardwalk at Mer Bleue Bog. Yellow circles highlight the presence of tamarack (sparse, and denser) that in the 2013 OWES would indicate this area is fen or swamp.

Westport-Nelson Wetland Complex ('Westport Bog', Figure 3.6) is located on the Frontenac Axis, approximately 120 km southwest of Ottawa and 60 km north of Kingston.

The axis divides the St. Lawrence lowlands and the Great Lakes lowlands. Bedrock is often found to be exposed at the surface, or covered with thin soils (Keddy, 1995). The area was forested in the past, but logging has depleted most areas of old-growth (Keddy, 1995). Current forest vegetation generally contains northern hardwoods (maple, beech, birch) mixed with spruce, pine and fir (Keddy, 1995). Irregular topography and marl-based ponds and lakes restrict the hydrology of the area (Keddy, 1995). Wetlands present include bog, marsh and swamp with some poor fen (not observed, and very rare (Keddy, 1995)). Bogs listed and confirmed in the field included open and treed bogs (<25% (very minor component overall)) with treed areas containing some minor deciduous saplings such as birch, and minor tamarack along with some dead coniferous.

In open bog areas the vegetation included willow, black chokeberry (*Aronia melanocarpa* (Michx) Elliott), cotton grass, sweet gale, rushes, tall and short grasses. The bog area of observation was surrounded by a well-defined lagg. A lagg is a transition zone where runoff collects from both the bog and the surrounding upland area (Howie and Tromp-van Meervald, 2011), and is a strong indicator of a raised bog. The vegetation observed in the lagg was fen- or marsh-like in nature and included cattails, wild calla and rooted-floating and free-floating plants such as duckweed and watershield. Vegetation present in a lagg often has fen characteristics and “raised bogs that are physically constrained by basins often develop a “moat-like” lagg” (Howie and Tromp-van Meervald, 2011).

Marsh vegetation included homogenous areas of rushes, cattails, and some sedge species along with duckweed, watershield, yellow pond lily and wild calla. There was a

strong presence of ferns as well. In some ecotonal areas between marsh and upland there were tall and low shrubs of willow and meadowsweet (*Spiraea alba* Du Roi). Swamp and fen vegetation were not observed on this site. Swamp is more common in the Westport Bog area while fen is very rare (Keddy, 1995). Westport Bog was last assessed under the OWES in 1985.

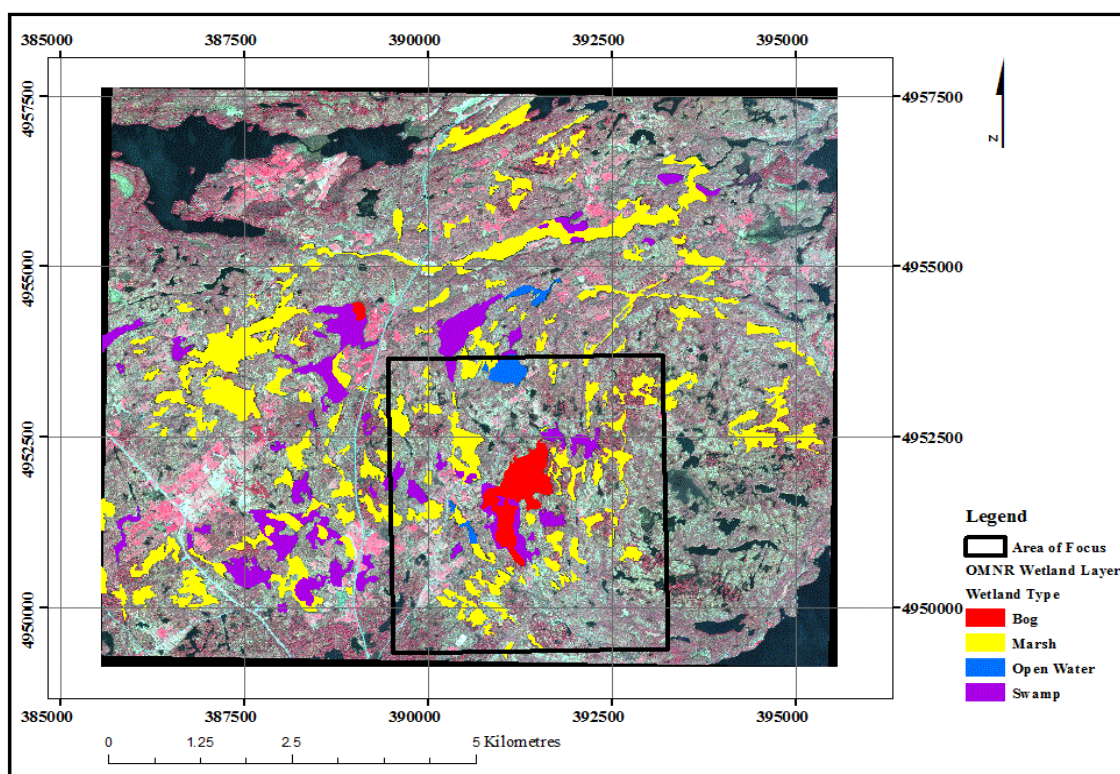


Figure 3.6. Westport-Nelson Wetland Complex: CIR WorldView-2 composite (Spring 2010) with OMNR wetland layer (2013) overlaid. Black outline highlights the area of interest where field work was performed.

3.2 Remotely sensed imagery

Two types of optical imagery were used in this research: high resolution WorldView-2 and coarser resolution Landsat TM 5. SAR imagery from Radarsat-2 was also used. A generalized description of these imagery types and justification for their selection is given here; a detailed list of the imagery used in this research is given in Table 3.2.

Table 3.3. Detailed list of the imagery used in this research including season, date acquired and details related to the type of imagery.

Season	Image Type	Site (s)	Date	Details		
Spring	Landsat TM 5	Loch Garry	April 13, 2010			
		Mer Bleue Bog				
		Marlborough Forest				
		Westport Bog	March 19, 2010	Just outside of the swath for the other sites		
	Radarsat-2	Marlborough Forest		March 29, 2010	FQ1	Incidence Angle (Near – Far) 18.4° – 20.4°
				April 9, 2010	FQ29	46.8° – 48.0°
		Westport Bog		April 8, 2010	FQ7	25.7° – 27.6°
		WorldView-2	Loch Garry	April 25, 2010		
			Mer Bleue Bog	April 25, 2010		
	Marlborough Forest		May 17, 2010			
	Westport Bog		April 28, 2010			
	Summer	Landsat TM 5	Loch Garry	July 2, 2010		
Mer Bleue Bog						
Marlborough Forest						
Westport Bog			September 11, 2010	Just outside of the swath for the other sites		
		Loch Garry	July 10, 1984			
		Mer Bleue Bog				
		Westport Bog	August 18, 1984			
		Marlborough Forest	August 22, 1991			Different field-based OWES evaluation dates

	Radarsat-2	Loch Garry	June 23, 2010	FQ10	29.1° – 30.9°
		Mer Bleue Bog	June 26, 2010	FQ 7	25.7° – 27.6°
			August 2, 2011	FQ 28	46.0° – 47.2°
		Marlborough Forest	July 3, 2010	FQ 5	23.4° – 25.3°
		Westport Bog	June 26, 2010	FQ 2	20.0° – 21.8°
	WorldView-2	Loch Garry	July 27, 2010		
		Marlborough Forest	June 19, 2011	**no summer acquisition in 2010	
		Mer Bleue Bog	September 1, 2010		
		Westport Bog	September 1, 2010		
	Fall	WorldView-2	Marlborough Forest	November 2011	
Mer Bleue Bog			November 2011		
Radarsat-2		Mer Bleue Bog	November 10 2010	FQ 12	31.3° – 33.0°

3.2.1 WorldView-2

WorldView-2 imagery was selected for detailed, high resolution analysis at the local extent. The nominal ground pixel size is 46 cm and 1.8 m pixels for the PAN band and the eight multispectral bands, respectively, over a swath of approximately 17.7 km. The eight bands include: blue (400 – 450 nm), blue-green (450-510 nm) green (510-580 nm), yellow (585-625 nm), red (630 – 690 nm), red edge (705-745 nm), near-infra red (NIR) 1 (770 – 895 nm) and NIR 2 (860 – 1040 nm). Imagery acquired for this research included only the primary wavelengths of blue-green, green, red and NIR 1 due to its lower cost and because it was not certain if the additional bands would provide significant additional information (e.g., bands within the same portion of the spectrum (e.g. visible or NIR) are commonly highly correlated). Figure 3.7 is an example colour composite of the spring WorldView-2

image of Westport Bog. The data were delivered in GeoTIFF format and had been geometrically corrected to the world geodetic survey 1984 datum (WGS84) and the universal transverse mercator (UTM) coordinate system (zone 18, row T) prior to delivery. The accuracy of these corrections was assessed using image registration of one of the images to the OMNR road vector file. Overall root mean square positional error (RMSE) was less than $\frac{1}{2}$ pixel, so it was deemed unnecessary for further geometric correction.

3.2.2 Landsat TM 5

Landsat 5 was launched in 1984 and continually acquired imagery using the TM instrument until June 2013. Landsat TM acquired images on a 16-day revisit basis at nominal ground pixel sizes of 30 metres over a 185 x 185 km area. It had spectral bands similar to WorldView-2 in the blue-green (450 – 520 nm), green (520-600 nm), red (630-690 nm), and NIR (760-900 nm), as well as two MIR bands, MIR1 (1550 – 1750 nm) and MIR2 (2080-2350nm) and a thermal band (10400 – 12500nm, 120m pixels). The thermal band was not used for this research due to its coarse spatial resolution which would increase the minimum mapping unit (MMU taken to be 3 x 3 pixels) for validation and reference to 360 m by 360 m approximately 13 hectares. Landsat TM 5 imagery was selected for this research because it is free and therefore attractive to operational mapping programs such as the OWES. The temporal archive surpasses most other imagery currently available, and the regional extent of this imagery allowed for multiple sites to be encompassed within one image, thereby minimizing processing time while maximizing spectral consistency compared to the use of

multiple images, which has been shown to degrade classification accuracy (Pax-Lenney *et al.*, 2001; Dingle Robertson and King, 2011).

Although Landsat 7 ETM+ data were available, in 2003 the satellite's scan line corrector failed, resulting in reduced quality of data.

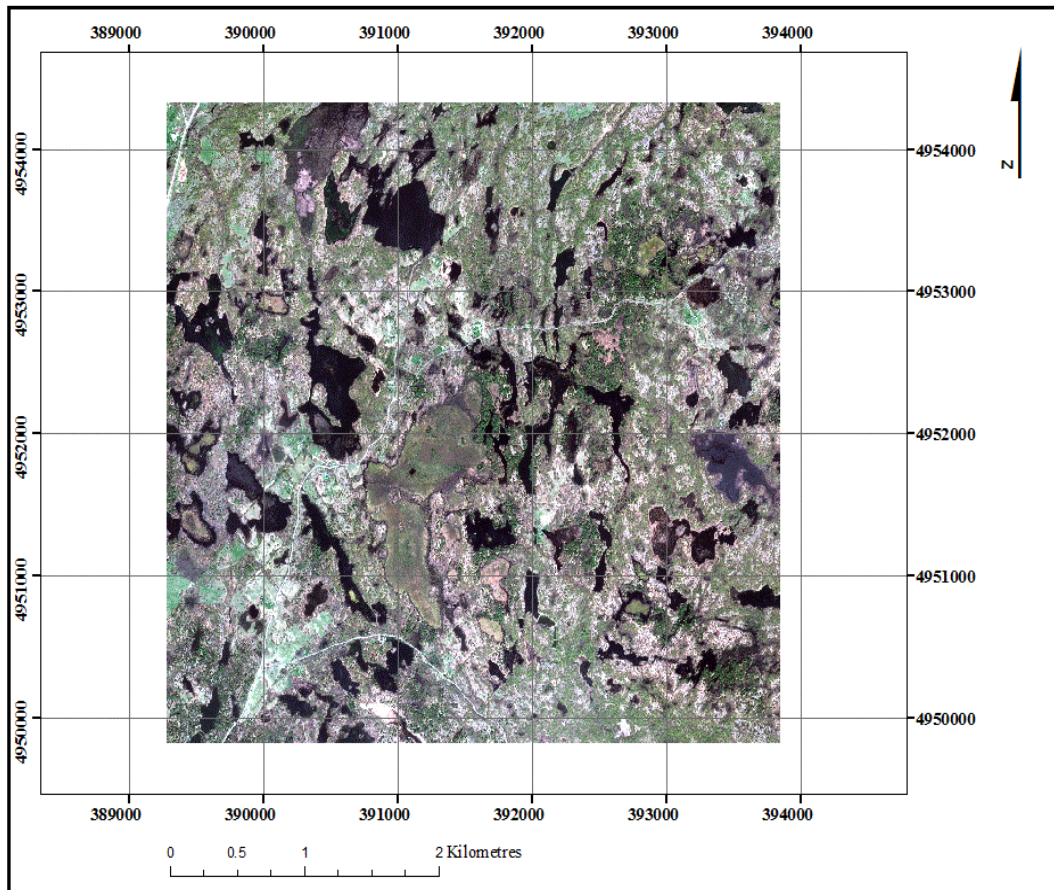


Figure 3.7. True colour composite of WorldView-2 imagery at Westport Bog.

3.2.3 Radarsat-2

Radarsat-2 is a C-band sensor with advanced polarimetric capabilities and multiple possible resolutions and image swaths that have proven advantageous in wetland mapping.

Radarsat-2 imagery used in this research was acquired in descending mode in fine quad-polarisation (Henderson and Lewis, 2008). The nominal ground pixel size is theoretically 8 m at the steepest incidence angle and as most of the imagery was acquired with steep incidence angles (low FQs (fine quad) beams) the general nominal ground pixel size of the raw radar imagery is about 9.5 m. This resolution is hereafter called ‘medium’ resolution (between WorldView-2 and Landsat TM 5) with a local spatial extent of approximately 25 x 25 km². Due to the noisy nature of raw radar imagery and the general requirement to filter it prior to processing, the nominal ground pixel size of the filtered imagery is degraded and can be considered ‘coarse’ resolution, in the same class as Landsat imagery.

Radarsat-2 imagery was selected for this research because the imagery swath covered each wetland complex, it has been shown to work well in detecting open water and herbaceous wetlands, and it has been previously used to detect wetland types at Mer Bleue Bog (Touzi *et al.*, 2007). It is also relatively simple for Canadian government organizations to acquire. The imagery of this research was acquired through the assistance of Environment Canada, and the potential for inter-governmental collaboration with the Ontario government made the use of this imagery appealing. Additionally, the different spectral nature and information content of radar imagery compared to optical imagery made these data a compelling addition to this research. All other data including a 10 m digital elevation model (DEM, Version 2.0.0, horizontal accuracy +/- 10m; vertical accuracy +/- 5 m, (LIO, OMNR, 2006) were obtained from the LIO.

4.0 Methods

This chapter is structured to follow the three main objectives of this research: map the selected OWES attributes for one season which was selected as spring; score the mapped attributes and then compare those scores to OWES scores; and assess the temporal remote sensing data in classification of wetland attributes, and analyze attribute changes over the long term. Under each objective, the methods are described by attribute, including the field work completed to obtain reference data. Where the methods are repeated, the reader is directed to the section in Chapter 4 where that information is located. Figure 4.1 (provided digitally with this thesis) provides a detailed workflow of the entire methods structure. Portions of Figure 4.1 accompany each attribute section as workflow diagrams.

Objective 1 Methods: Map the selected OWES attributes for one season

4.1 Methods to segment, classify, and map Wetland Type using optical and radar imagery

Figure 4.2 provides the workflow for the methods used to segment, classify and map Wetland Type. Potential for mapping Wetland Type was assessed as it is important in both the Biological and Special Features components. OWES Wetland Types were defined in Table 2.1 and included Marsh, Fen, Bog and Swamp. In addition, a survey was made of the surrounding landforms and areas that were transition zones (ecotones) between Wetland Types, or between Wetland Type and Upland. Upland types included: Coniferous Forest, Hardwood Forest, Mixed Forest, Open Grassy Field, Agriculture, Shrub Area, Impervious

(Roads) and Water which follow typical USGS landcover classification categories (Anderson *et al.*, 1976).

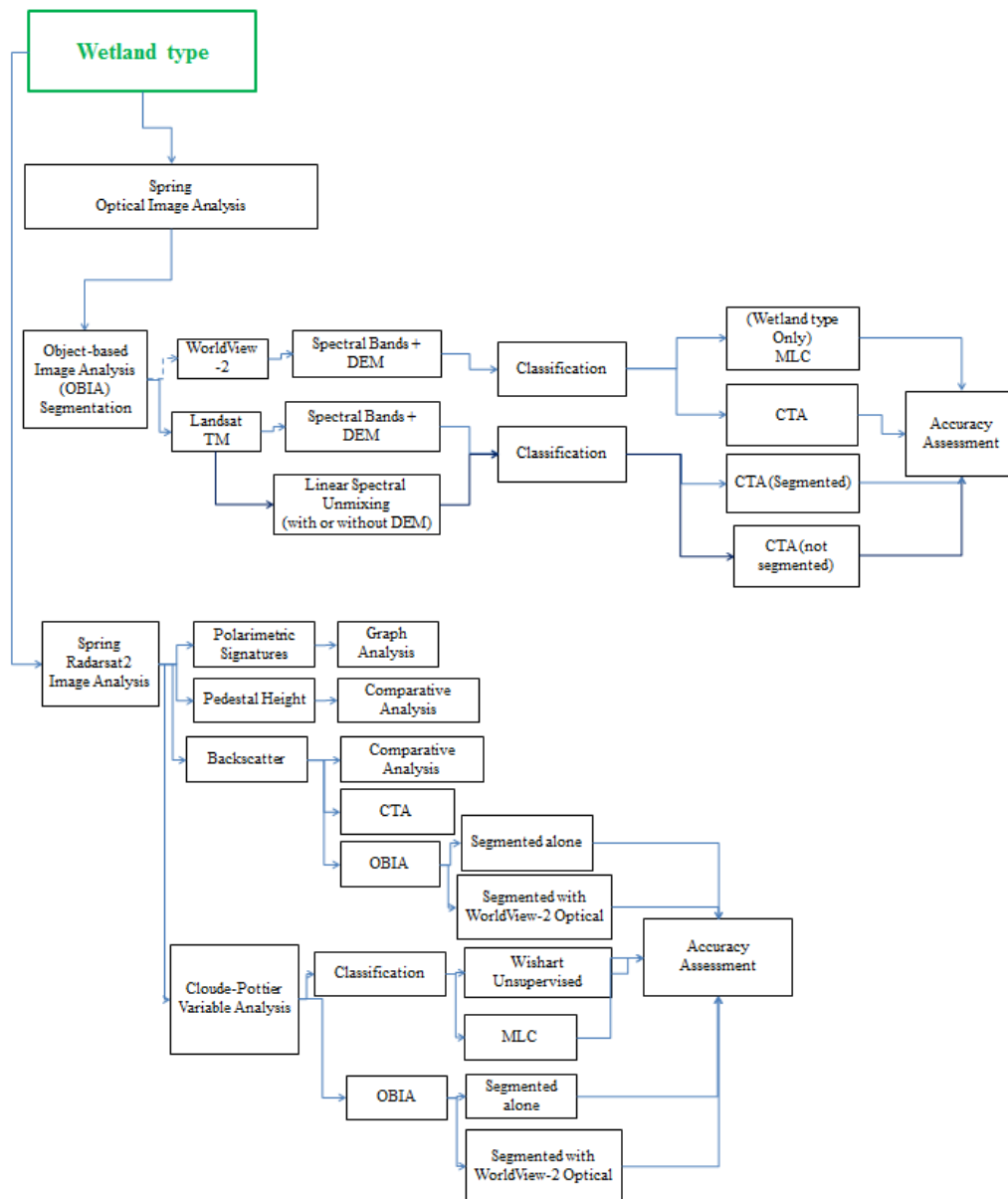


Figure 4.2. A workflow of the methods used to segment, classify and map Wetland Type using optical and radar imagery.

4.1.1 Field analysis for Wetland Type

Defining characteristics of the attribute 'Wetland Type' were based upon vegetation present, hydrologic conditions, and their spatial arrangement, both which have the potential to be assessed using remote sensing. In the spring and summer of 2010 and 2011, in the four study areas, validation sites of a MMU of 90 x 90 m (3 x 3 Landsat pixels) were established using a tape measure or visually using a laser range finder (e.g. at the edge of marsh, deep swamp, unstable bog/fen, protected bog, etc.). A survey was made of the land cover types present, and a GPS (Global Positioning System) waypoint was taken at the edge of the site using a Trimble Juno SB (expected real time accuracy of approximately 2-5 m (www.trimble.com, 2013)). Where there was confusion between Wetland Types (e.g. Fen and Bog), the vegetation present was assessed to determine if there were indicator species present (as outlined in the OWES Southern Manual, 2002). Effort was made to accumulate multiple samples for each land cover type (e.g., 15 to 50 (Jensen, 2000; Foody, 2002; Lillesand *et al.*, 2008), but for rare wetlands of fen and bog it was often impossible to find more than one or two examples within a particular wetland complex. In addition, all four Wetland Types were not observed in each wetland. The size of the MMU also limited the number of samples of Wetland Type(s) that could be recorded; smaller areas were observed but could not be used in calibration and training. In addition to these field data, calibration and validation training areas for the Water class were supplemented by visual interpretation of high resolution DRAPE (Digital Raster Acquisition Project for the East, Ontario Geospatial Data Exchange (OGDE, ©2008 Queen's Printer)) imagery. This aerial CIR

imagery has 20 cm pixels and was acquired over eastern Ontario in the spring of 2008 and 2009 in leaf-off conditions (Aero-Photo (1961) Inc.). A list of the 156 field surveyed land cover types can be found in Appendix B, Table B1. Figure 4.3 provides an overview of the location of the field sites per wetland. Table 4.1 provides a summary of the field data found in Appendix B.

Table 4.1. Summary of the field sites presented in detail in Appendix B and presented on the Figure 4.3.

Wetland	Wetland Types				VCF		
	# of Bog	# of Fen	# of Swamp	# of Marsh	Form A (1 to 3)	Form B (4 – 5)	Form C (6 or more)
Loch Garry	n/a	5	8	6	3	11	5
Marlborough Forest	n/a	6	11	11	17	9	2
Mer Bleue Bog	9	n/a	n/a	11	9	10	1
Westport Bog	9	n/a	n/a	11	8	11	1
	18	11	19	37	37	41	9

4.1.2 OBIA using spring 2010 WorldView-2 imagery

All OBIA segmentation was completed using eCognition Developer 64 8.64. Segmentation testing was accomplished using one sample WorldView-2 image (Loch Garry, spring) with four spectral bands and a 10 m digital elevation model (DEM, Version 2.0.0, horizontal accuracy +/- 10m; vertical accuracy +/- 5 m, Land Information Ontario (LIO), OMNR, 2006). Additional DEM-derived products (e.g. slope) did not improve results and in some cases worsened them, therefore, only the original DEM elevation data were used in segmentation analyses. Multi-resolution segmentation was selected as it has been shown to create objects that match real landscape entities (Dingle Robertson and King, 2011;

Ouyang *et al.*, 2011; Duro *et al.*, 2012). This research followed a qualitative trial and error analysis by testing several scale parameter values and visually assessing the segmented objects to choose the best scale parameter values for further analysis. This resulted in one scale parameter value for WorldView-2 imagery of 45 that visually and qualitatively best represented Wetland Type objects and other land form objects at that scale. The visual criteria for such objects were that they met boundaries such as water/land interfaces, and created visually apparent features such as linear roads, rectangular fields, and rounded shorelines. These represented real entities comprised of a minimal number of segmented objects. Some areas included objects representing transition zones within a given Wetland Type, for example, where shrubby Fen graded into grassier Fen. Such segmentations for Wetland Type classification were considered successful if the entire boundary around the Fen was consistent and did not include areas from surrounding land covers. Then, for the selected optimal scale value, following Tian and Chen (2007), an experimental design matrix (Table 4.2) was used to visually evaluate segmentation results for each combination of the shape and compactness parameter values. This testing method attempts to impose a thorough and consistent review of objects created at each permutation.

Table 4.2. Experimental design matrix showing shape/colour and compactness/ smoothness tests implemented after Tian and Chen (2007).

	Compactness Parameter (Compactness + Smoothness = 1.00)			
Shape (1.00 – Colour)	0.25	0.50	0.75	0.90
0.10	Test 1	Test 2	Test 3	Test 4
0.25	Test 5	Test 6	Test 7	Test 8
0.50	Test 9	Test 10	Test 11	Test 12
0.75	Test 13	Test 14	Test 15	Test 16
0.90	Test 17	Test 18	Test 19	Test 20

OBIA classification of Wetland Type classes was completed using PCI Geomatica (MLC) and IDRISI Taiga (CTA, (C4.5, Quinlan, 1993)). Training areas were derived from the field data and in some cases, such as for Water, were supplemented from the DRAPE imagery. Training data were generated for classes of Water, Upland, and the Wetland Types that were present. Individual examples (Appendix B, Tables B2 to B5) are given for each of the four study areas, however for comprehensive training, several samples from across each wetland complex were selected to represent the variety in each class. In some cases, the class of Uplands was separated into more specific classes containing forests, agricultural fields, urban land covers, etc. due to spectral reflectance differences. The band data were visually assessed as normal to very slightly positively skewed (see also Table 4.3) using the mean:median ratio. Values close to 1.0 indicate a normal distribution, which is an important assumption of parametric classifiers such as the MLC.

The mean:median ratio was checked for all training samples in each band for each Wetland Type. Values differing from 1.0 by a large amount such as 0.1-0.2 or more (Jensen, 2005) indicate non-normal data. The range for training samples data at Loch Garry was normally distributed. The other three sites were expected to also have normally distributed training data for the Worldview-2 imagery.

The spectral reflectance curves of each training sample group followed general curves of Wetland Types and underlying vegetation found in the literature (Mertes *et al.*, 1993, Anderson and Perry, 1996; Silva *et al.*, 2008; Govender *et al.*, 2009). Differences in

the visible reflection are found with higher green band reflection which relates the changes in the chlorophyll concentration, and lower values in blue and red due to pigment absorption. (Anderson and Perry, 1996; Govender *et al.*, 2009). Highest values in NIR were related to the cell structure (Mertes *et al.*, 1993; Anderson and Perry, 1996). Additionally the presence of water resulted in higher, but still significantly low values in the blue band, and the addition of sediments, or flora in the water resulted in increasing values of the red or red-edge (Mertes *et al.*, 1993; Silva *et al.*, 2008).

Separability of training data for the Wetland Types of interest in the WorldView-2 spring Loch Garry segmented image with a scale parameter of 45 were next tested for the spring data, the summer data and the spring and summer data combined. The common separability metric Bhattacharyya Distance (Haralick and Fu, 1983) was selected. It is non-linear: values of 1.9 and greater are often used to indicate good separability and values of 1.7-1.9 may indicate potential for accurate classification. The Loch Garry image was selected for testing as there were three Wetland Types in Loch Garry representing the greatest variety of the four study sites, as well as for logistical reasons as it was the first image to be delivered. Holding the shape and compactness parameter values constant at 0.1 and 0.75, respectively, the first test evaluated class separability for a scale parameter value of 45 for the spring imagery. This was repeated using the summer imagery, and the spring and summer imagery combined. The average and minimum separabilities for each test are given in Table 4.3. These values show that separability of the training data for all class pairs

was high, indicating strong potential for accurate classification. Separabilities for all five classes and all test cases are provided in Appendix C, Tables C1-C5.

Table 4.3. The average and minimum Bhattacharyya Distance separabilities for the class training data.

Scale	Season	Test Complex	# of classes	Average	Minimum	Minimum Pair
45	Spring	Loch Garry	5	1.951148	1.835126	Fen and Marsh
	Summer	Loch Garry	5	1.943180	1.838589	Upland and Swamp
	Combined	Loch Garry	5	1.991326	1.972173	Swamp and Marsh
25	Spring	Loch Garry	5	1.936777	1.792341	Fen and Marsh
75	Spring	Loch Garry	5	1.964748	1.886956	Fen and Marsh

MLC was used for comparison to CTA using a sample set of WorldView-2 spring segmented imagery. MLC, being one of the first classification techniques utilized with remotely sensed data, and a classifier that is considered optimal if data are normally distributed, has been widely used as a comparison method in the literature (Paola and Schowendgerdt, 1995; Berendes *et al.*, 1999; Rogan *et al.*, 2002; Kavzoglu and Mather, 2003; Joshi *et al.*, 2004; Lu *et al.*, 2007; Gao, 2008; Dingle Robertson and King, 2011, etc.). The mean brightness values of the spectral bands plus the mean DEM value were obtained for each segmented object. These objects were subsequently rasterized however each pixel within each object maintained the original object value (Figure 4.4).

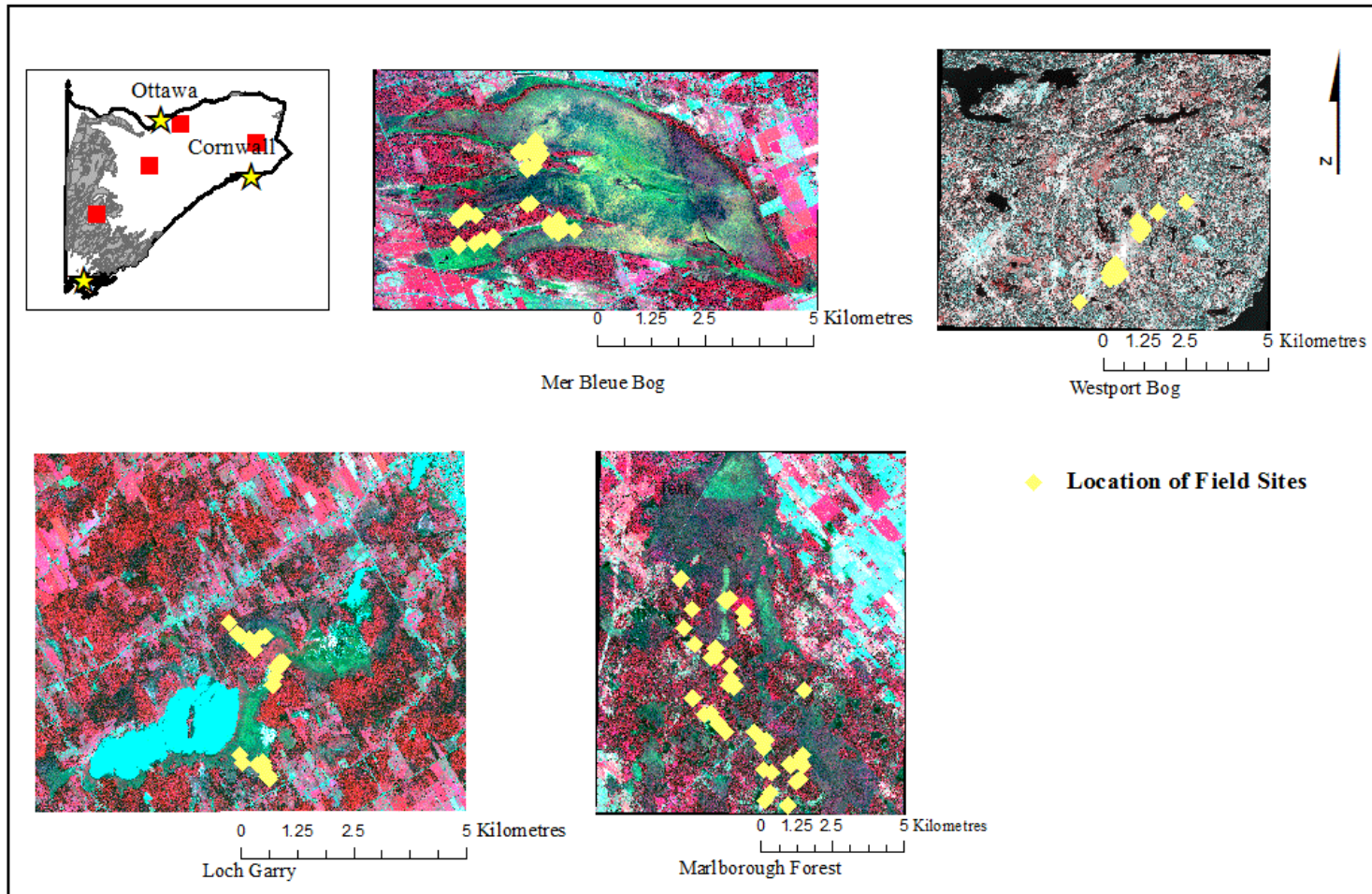


Figure 4.3. Location of field sites at each wetland site.

CTA was selected for this research as it has been shown in the literature to improve upon the discrimination of Wetland Types with accuracies ranging 85% to 98% and kappa coefficients ranging from 0.41 to 0.68 (Wright and Gallant, 2007; Davranche *et al.*, 2010; Jiao *et al.*, 2011; Zhao *et al.*, 2012). A commonly used CTA algorithm is C4.5 (Quinlan, 1993). In CTA, it has been recommended to use GINI splitting algorithm over the entropy and gain ratio algorithms (Zambon *et al.*, 2006; Duro, pers. comm. 2012). The GINI algorithm measures the impurity at a given node that is at a maximum when all the pixels are equally distributed among all classes.

The GINI algorithm is given as (Zambon *et al.*, 2006):

$$GINI(t) = \sum_i p_i(1 - p_i) \quad \text{Eq. 4.1}$$

- where p_i is the relative frequency at node t , (determined by dividing the total number of observations of class $_i$ by the total number of observations); and
- t represents any node (parent or child) at which a given split of the data is performed (Apte and Weiss, 1997).

Auto-pruning was set at 1%, which removes any leaves with pixel counts less than or equal to a defined within-class proportion. Figure 4.4 provides a simple diagram of the classification tree process. Using the same training data derived above, the GINI splitting algorithm was tested on the spring Worldview-2 Loch Garry image objects derived.

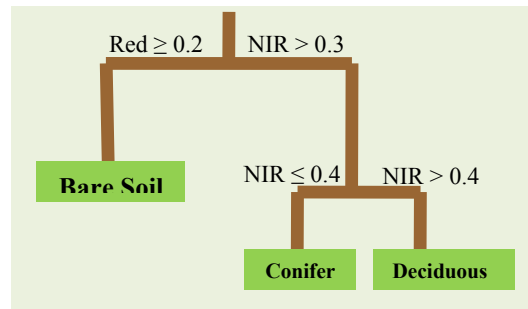


Figure 4.4. A simple classification tree. Red and NIR represent spectral bands.

During classification, the accuracy of the training data was assessed by observing a monitoring graph that shows the proportion of misclassified or re-assigned training pixels in a given iteration. The final graph that is produced indicates the stability of the training data: positive values indicate a class has obtained training pixels from another class and negative values indicate training pixels have been lost to another class. In the case of Loch Garry spring training sites, there was minimal (+/- 1%) deviation from 0 indicating that the training classes were well trained and classified. There is no quantitative measure of how many training pixels have been lost or gained during the process.

4.1.3 OBIA using 2010 spring Landsat 5 TM imagery

Segmentation testing was completed as outlined in section 4.1.2. The Landsat image was clipped to match the WorldView-2 images for each focus area at each wetland complex. This minimized the unknown variability found in those areas outside the study complexes. Previous testing (Dingle Robertson and King, 2011) with the eCognition multi-resolution segmentation algorithm has shown that a scale parameter value of 10 (shape parameter value of 0.1 and compactness parameter value of 0.5) works well for Landsat 5 TM imagery in eastern Ontario landscapes so it was used for this research as well. The spring 2010 image with six spectral bands and the DEM were used as inputs.

Segmentation was also completed using LSU fraction maps. LSU was selected for this portion of the research as land cover fractions have been shown to be able to provide subpixel information in moderate and coarse resolution imagery to be useful in identification of land cover change over time (Adams *et al.*, 1995; Schmid *et al.*, 2005; Olthof and Fraser, 2007; Melandez-Pastor *et al.*, 2010). To derive the LSU fraction maps, three manually-selected EMs were trained. DRAPE imagery was used with the field survey data to select the pure sites of bare ground, water and vegetation. The Least-Squares Mixing Model (Shimabukuro and Smith, 1991) defines the spectral reflectance in a pixel of a given spectral band as the sum of the reflectance of each land cover type within that pixel and the associated error.

The Least Squares Mixing Model (Shimabukuro and Smith, 1991) is given as:

$$\rho_{i,j,k} = \sum_{m=1,p} F_{i,j,m} * \rho_{m,k} * e_{i,j} \quad \text{Eq. 4.2}$$

- where $\rho_{i,j,k}$ is the total reflectance of a pixel for row i , column j , band k ;
- $F_{i,j,m}$ is the proportion of each pure component (end member) m of a pixel for row i , column j ;
- $\rho_{m,k}$ is the reflectance for that pure component m in band k ; and
- e is the error associated with the estimation of each of the components for each pixel $e_{i,j}$.

The above process was repeated using five EMs automatically selected using the IEA algorithm, which iteratively finds the average of the vectors with the largest errors for a specified number of EMs. Each fraction and the sum of the fractions are constrained to a values between 0 and 1 (Neville *et al.*, 1998).

Training data were assessed in the same manner as the WorldView-2 imagery. Landsat 5 TM data were also normally distributed and therefore MLC would be an appropriate choice for classification, but as CTA was shown to produce higher accuracies than MLC for WorldView-2/DEM classification of Wetland Types, CTA was used with the segmented Landsat images. In separate tests, inputs were the original spectral bands, three EM fraction maps, or five EM fraction maps, each with or without the DEM. A thematic map was derived for each of the three classifications. An example of the monitoring graph is given as Figure 4.5. The negative values for the Fen class and the positive values for the Swamp class indicate that some of the Fen training pixels more closely resembled Swamp training data and they were moved to that class. In Loch Garry, in the field, it was observed that swamps often merged into fen areas and, in some areas of the classified map that could be considered transition zones between the two types of wetlands, objects were incorrectly classified as one or the other class (especially using the coarser Landsat imagery). However, as there was not complete reference data for these transition areas, the total area of such misclassifications could not be quantified.

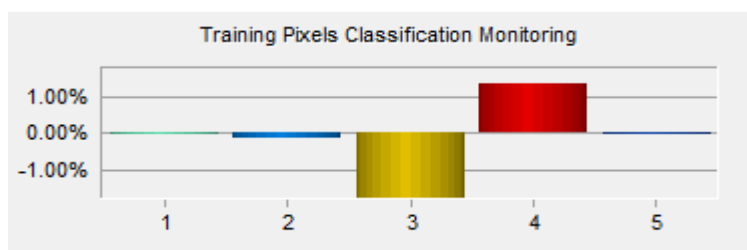


Figure 4.5. Example of the training site monitoring graph for the GINI splitting tree on the Loch Garry spring training sites for the Landsat TM imagery (X-axis represents classes: Class 1-Water; Class 2-Upland; Class 3-Fen; Class 4-Swamp; Class 5-Marsh).

4.1.4 Radarsat-2 image processing, classification and analyses for Wetland Type

Radar imagery analyses were not a central focus of the thesis; as such methods were selected that were straightforward to implement and combine with optical imagery, in order to evaluate the potential for integration into an operational wetland evaluation system such as OWES. Radarsat-2 processing was completed using PolSarPro_v4.2.0, NEST4C-1.1, and Polarimetric Workstation Software (PWSv5r5.3, Touzi *et al.*, 2010). Raw radar imagery was processed to sigma nought values and extracted to full resolution. Using these data, the polarimetric signatures were first generated from training polygons at the same field sites used for the optical imagery. The polarimetric graphs for Wetland Type were subsequently analyzed in terms of their shape, position of peaks and troughs, and pedestal height. Based on the literature, polarimetric plots were analyzed for the dominant type(s) of scattering mechanism such as surface, Bragg, double bounce, and volume, as depicted in Figure 2.5. Pedestal height gave an indication of the degree of depolarization in the target response, with a low value representing polarized response and increasing values representing increased depolarization (Evans *et al.*, 1988; Boerner *et al.*, 1998; McNairn *et al.*, 2002; Touzi *et al.*, 2004; Touzi *et al.*, 2010).

The radar data, including the HH, HV, VH, VV images and CP decomposition variables were geocorrected using NEST4C-1.1 allowing for comparison to the validation data, and to use in segmentation and classifications with the geocorrected optical imagery. The four corners (longitude and latitude) were obtained, and the scene boundaries were set. Next the range and azimuth were determined and, target image pass times were calculated. Tie points (geolocation points) were developed from the latitude/longitude and slant range time derived from the geolocation grid from the original product. The correction occurred

individually at each cell where latitude and longitude for corrected cell is related to the corresponding position of the cell in the original image and four pixels immediately adjacent to it.

Slant range (R) was calculated for the cell using the slant range time and bi-quadratic interpolation; zero Doppler Time (T) was computed and then bias-corrected zero Doppler time ($T_c = T + R^2/C$) where C is the speed of light; finally the azimuth index (Ia) was computed using zero Doppler time and the range image index (Ir) was computed using slant range (R). The corrected cell value was computed with Ia and Ir using bilinear interpolation, and corrected to a WGS84 UTM (zone 18 row T) ellipsoid. The corrected images were assessed through a comparison to the OMNR road vector file. These corrections showed minimal positional error (approximately less than 1 pixel) and therefore, these final images were deemed suitable for addition to, and use with the optical imagery (segmentation) and for accuracy assessment of products derived directly from the radar imagery. The normality of the radar data was not assessed, as based on results from the Worldview tests of classification, CTA was selected over MLC, and CTA does not require normal distributions.

A 7 x 7 enhanced Lee adaptive filter was then applied to the raw radar data to reduce speckle while maintaining edges or sharp features in the image. This filter and window size was selected following De Leeuw (2009) who found that they outperformed about 20 other speckle filters/window size combinations and had speckle reduction rates up to 70%. Once the radar data, were filtered they were used for a variety of analyses as follows.

HV and HH images were derived and samples were taken at field validation locations for all land cover types (up to 5 depending upon the study area), at all study areas (4), for all seasons of data (3), and for all incidence angles (ranging from steep (18.4°) to shallow (48.0°)). The literature has shown that HH has proven useful for distinguishing Bog, Fen,

freshwater versus saline marsh, and forested areas with water, and that, in general, HH is preferable over VV data (Li and Chen, 2005; Henderson and Lewis, 2008; Lang *et al.*, 2008; Lang and Kasischke, 2008; Lu and Kwoun, 2008). HV has also been shown to produce high accuracies for certain wetland classifications (Baghdadi *et al.*, 2001; Henderson and Lewis, 2008). These data were plotted on scatter graphs to determine if Wetland Type could be distinguished based upon backscatter for this polarisation combination. HV and HH images were then used to classify the Wetland Types using CTA. Finally, the HV and HH images were added to the OBIA segmentation/CTA classification along with the WorldView-2 spring imagery and the DEM to determine if they improved the Wetland Type classification accuracy. OBIA parameter values were the same as for the WorldView-2 data (scale value = 45; shape value = 0.1; compactness value = 0.75).

Decomposition of polarimetric radar data was selected for this research because previous studies had found that decomposition components provided significant discrimination between Wetland Types (Touzi, 2007; Touzi *et al.*, 2007; Sartori *et al.*, 2011; Bourgeau-Chavez *et al.*, 2013; Schmitt and Brisco, 2013). Of the various decomposition techniques that have been proposed, CP components have been shown to distinguish between Wetland Type classes such as Upland, Wetland, Forest and Shrub (Sartori *et al.*, 2011), and that higher alpha values distinguished greater flooding in vegetated areas compared to areas with less flooding and lower alpha values (Schmitt and Brisco, 2013). Other studies have found other decomposition techniques to perform well in wetland mapping for various purposes and in some cases comparisons were made between techniques. For example, Touzi (2007) and Touzi *et al.* (2007), working in a single wetland, Mer Bleue Bog, which was also a site of this research, found that the Touzi decomposition components provided better discrimination of the Wetland Types than CP components.

However, based on the availability and ease of implementation of the CP decomposition technique, it was selected to determine if the addition of the CP components to other imagery types or variables could improve the overall classification.

The CP decomposition process starts with a 3x3 (square) matrix that contains the eigenvalues from which entropy and anisotropy are derived, and the 3x3 unitary (orthogonal) matrix, from which the alpha angle is derived. These three components relate to the physical scattering mechanisms (surface, volume and double bounce/multiple scattering) of the target. The components are given as: entropy (H , between 0 and 1) representing the degree of randomness; anisotropy (A , between 0 and 1) represents the relation between the second and third eigenvalues and is a measure of the difference between the secondary scattering mechanisms; and alpha which identifies the dominant scattering mechanism (Cloude and Pottier, 1997).

The components entropy, anisotropy and alpha were derived from the Loch Garry summer image and used as inputs to a Wishart unsupervised eight-class classification, and to a MLC using the same training sites as for the WorldView-2 and Landsat TM classifications. The CP components were also assessed in classification using the CTA method (pixel-based), and using OBIA segmentation/CTA classification, combined with the WorldView-2 imagery and the DEM.

4.1.5 Wetland Type classification accuracy assessment

Thematic map accuracies were assessed using standard error matrices and accuracy statistics, which are well known and used in remote sensing. An error matrix compares validation (reference) data with the classification data (Congalton and Green, 1993; Foody, 2002) and provides information regarding the errors of omission (exclusion of pixels from

a class, or conversely the Producer's Accuracy (PA) = 100% - % errors of omission) and errors of commission (erroneous inclusion of pixels into a class, or conversely the User's Accuracy (UA) = 100% - % errors of commission (Congalton and Green, 1993; Foody, 2002)).

Another measure of accuracy is the kappa (k) coefficient of agreement which indicates the accuracy of the map beyond that which would be obtained through a random assignment of pixels to land cover classes (Congalton and Green, 1993; Foody, 2002). Unlike overall accuracy, kappa incorporates the errors of commission and omission and can be used to compare confusion matrices. For all OBIA classifications, because the objects had been rasterized, the accuracy assessments were based upon selection of only one pixel sample value per validation object centred within the 90 x 90 m (or larger) MMU (Figure 4.6). Accuracy was assessed in relation to a common threshold of 75% deemed to be useful for operational mapping (Foody, 2002).

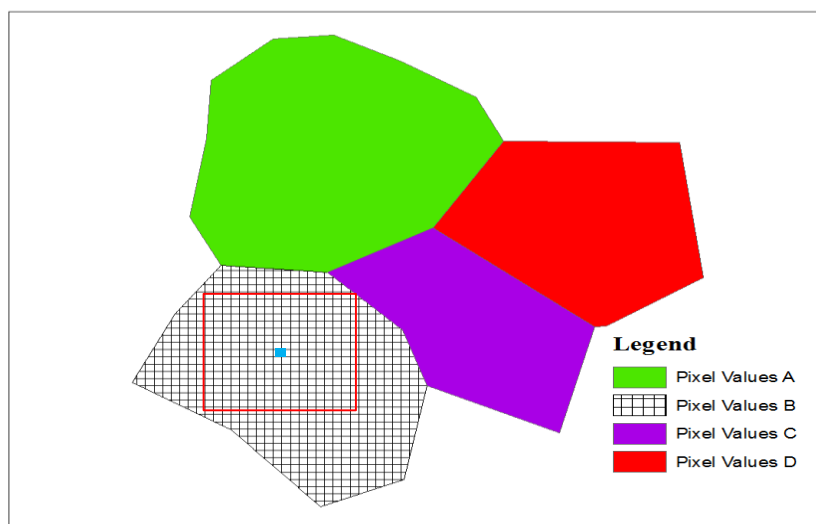


Figure 4.6. Theoretical display of created objects. Once rasterized, (e.g. pixel values B) all pixels within an object maintain the original object value. The blue square in pixel values B is an example of the location of a validation sample. The red square outlines the complete MMU of the validation site (e.g. 90 x 90 m).

Separate groups of field and image-based reference data were used for both training and validation, generally in a ratio of 30:70%, respectively, between training and validation samples (Foody, 2002; McCoy, 2005). The field-based reference data sets were particularly small; by splitting them 30:70% this ensured a large enough representative training set, while maintaining a large representative portion to generate accuracy statistics. However, due to the aforementioned issue of small reference sample sizes, in some cases, these splits were not possible for Open Water Types, which was a relatively rare class in the landscape.

4.2 Methods to segment, classify, and map VCFs using optical and radar imagery

Part of the challenge of this research was minimizing the number of methods while maximizing the outcomes and accuracies of the attributes mapped. After determining that the method that obtained the best results for Wetland Type mapping was OBIA segmentation followed by CTA classification this method was applied for the VCFs. Figure 4.7 provides the workflow for the methods used to segment, classify and map VCFs.

4.2.1 Segmentation methods using spring 2010 WorldView-2 imagery

WorldView-2 imagery were segmented using the four spectral bands and the DEM with the multi-resolution segmentation algorithm and a scale parameter value of 25, shape parameter value of 0.1 and compactness parameter value of 0.75 which, visually represented these types of classes best.

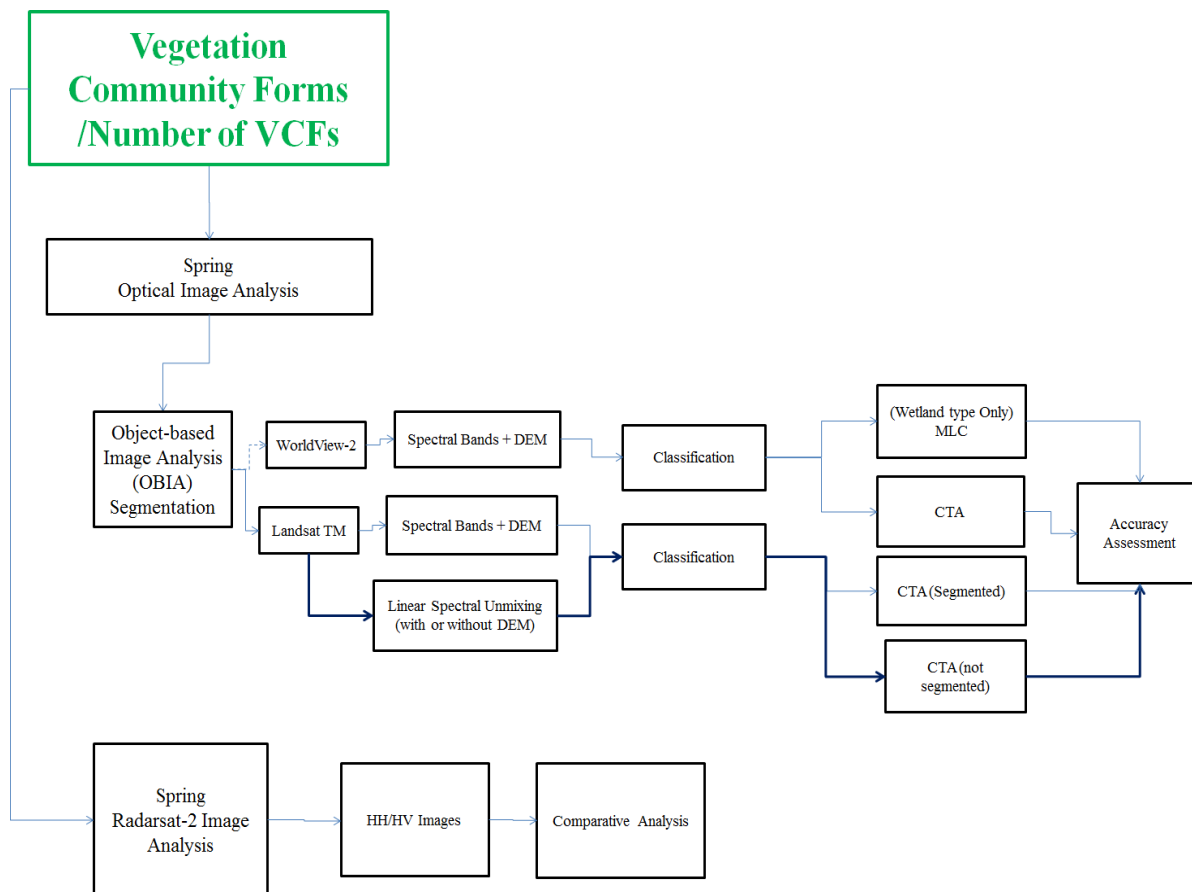


Figure 4.7. A workflow of the methods used to segment, classify, and map VCFs using optical and radar imagery.

4.2.2 Classification methods using spring 2010 WorldView-2 imagery

For VCFs, training data were extracted for a minimum six classes of interest (C, H, GC, DH/DC, water and Other, see Figure 3.8). If the ‘Other’ class had enough subclass representations (e.g. emergents, shrubs, floating) training data for these classes were also extracted. The images were first masked to remove water and upland using the results from the Wetland Type classification. Examples of training sites used for the VCF classes are listed in Appendix B in Tables B6-9, with accompanying photographs.

Once the imagery were classified, the numbers of communities present needed to be assessed. This was done by classifying each into one of three classes (Class A, B or C: # of

communities with 1-3, 4-5, or more than 6 forms, respectively). Examples of training sites for these three classes are given for each wetland complex in Appendix B in Tables B6-C9.

Classifications of VCFs and Number of Forms were completed using the field data and a CTA using the GINI splitting algorithm with trees auto-pruned (1%). Accuracy was assessed using the same methodology as noted in section 4.1.5.

4.2.3 Segmentation and classification methods using spring 2010 Landsat 5 TM imagery

The segmentation parameters were kept the same as for the attribute Wetland Type (see section 4.1.3) as a smaller scale parameter value did not appear to create any meaningful objects related to VCFs. Similar classification analyses were also completed as noted in 4.2.2.

4.2.4 Radarsat-2 image processing and analysis for VCFs

Samples were taken from the HV and HH images at field validation locations for particular VCFs and vegetation types per Wetland Type at all complexes (4), for all seasons of data (3), and for all incidence angles (ranging from steep (18.4°) to shallow (48.0°)). These data were plotted on scatter graphs to determine if VCFs could be distinguished using these data.

4.3 Methods to segment, classify, and map Open Water Types using optical imagery

The same segmentation and classification methods were used for this attribute type as noted for VCFs (Section 4.2) with the following additional information. Figure 4.8. provides a workflow of these methods.

In classification, there were approximately five classes that could be assessed depending upon the wetland complex study area (see Appendix B, Table B1). The images were first masked using the results from the Wetland Type classification (Section 4.1.2), removing Water and Upland classes. Calibration for the CTA was completed on the segmented imagery and DEM. Examples of some training sites used for the five Open Water Type classes are given in Appendix B, Tables B2-B5.

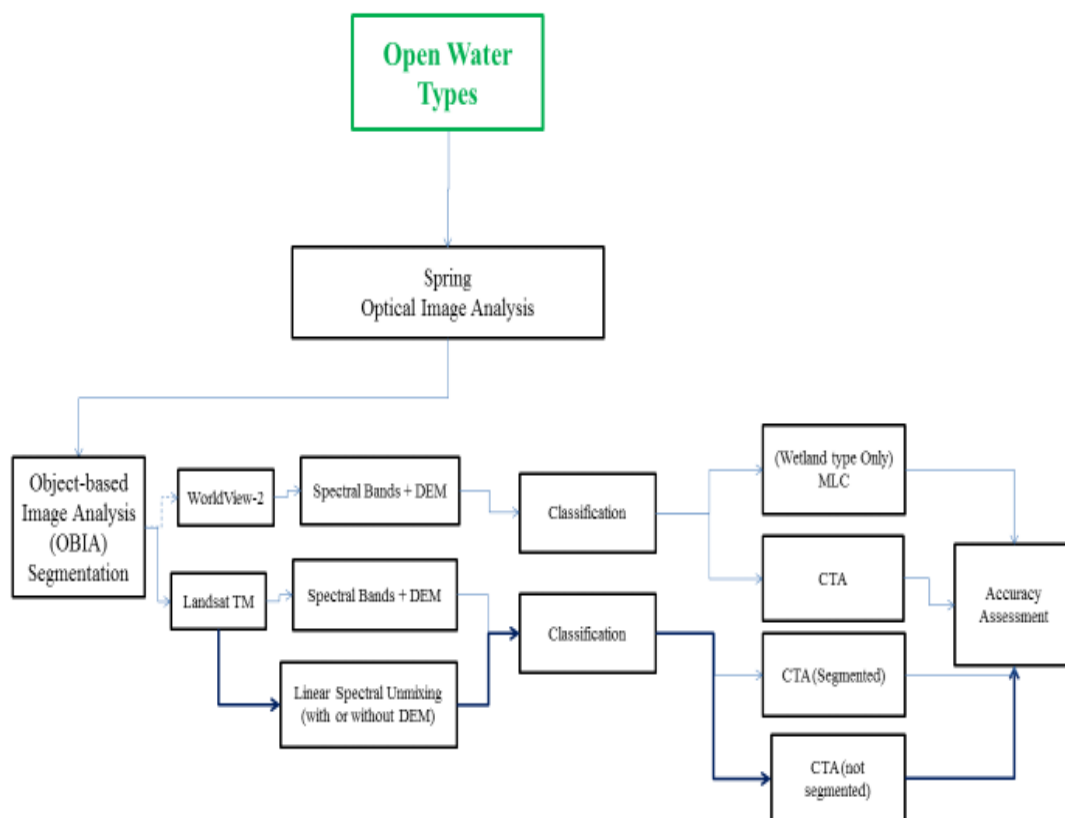


Figure 4.8. A workflow of the methods used to segment, classify and map Open Water Type using optical and radar imagery.

4.4 Methods to segment, classify, and map Inundation Extent using optical imagery

Figure 4.9 provides a work flow for the methods used to segment, classify and map inundation extent.

4.4.1 Field analysis

In spring and summer 2010 transects of 50 m or greater (relating to the resolution of the Landsat TM imagery) were assessed from uplands to the visual marker of wetness (e.g. presence of water) in a direction approximately perpendicular to the wetland edge.

Volumetric soil water content (VWC %), the ratio of water volume to total volume, was measured using a HydroSense Soil Water Measurement System (Campbell Scientific Inc., Canada) at 1 m increments along the transects. The Inundation Extent (wet extent) was assessed as the first occurrence of 100% VWC. 100% VWC would be expected once the probes were inserted into standing water. This was repeated for 48 VWC transects in the spring of 2010 (30 into marshes, 11 into swamps, 3 into fens (the rarest Wetland Type) and 6 into bogs. In the spring of 2011, 117 boundaries were mapped (tracking along the wet boundary at the four sites) and crossing the 48 VWC transects from the previous year. The edge was followed until it could no longer be visually assessed, it became physically impenetrable, or it was at the intersection with a manmade structure (e.g. a road or path). Field data for VWC% is found in Appendix J.

4.4.2 Semi-variogram analysis of VWC

Semi-variogram analysis was conducted to determine the range of spatial dependence of these field data along a given transect and to use that information in selection of data for statistical analysis against the remote sensing data. VWC showed spatial dependence along some transects, but not for others (land cover dependent).

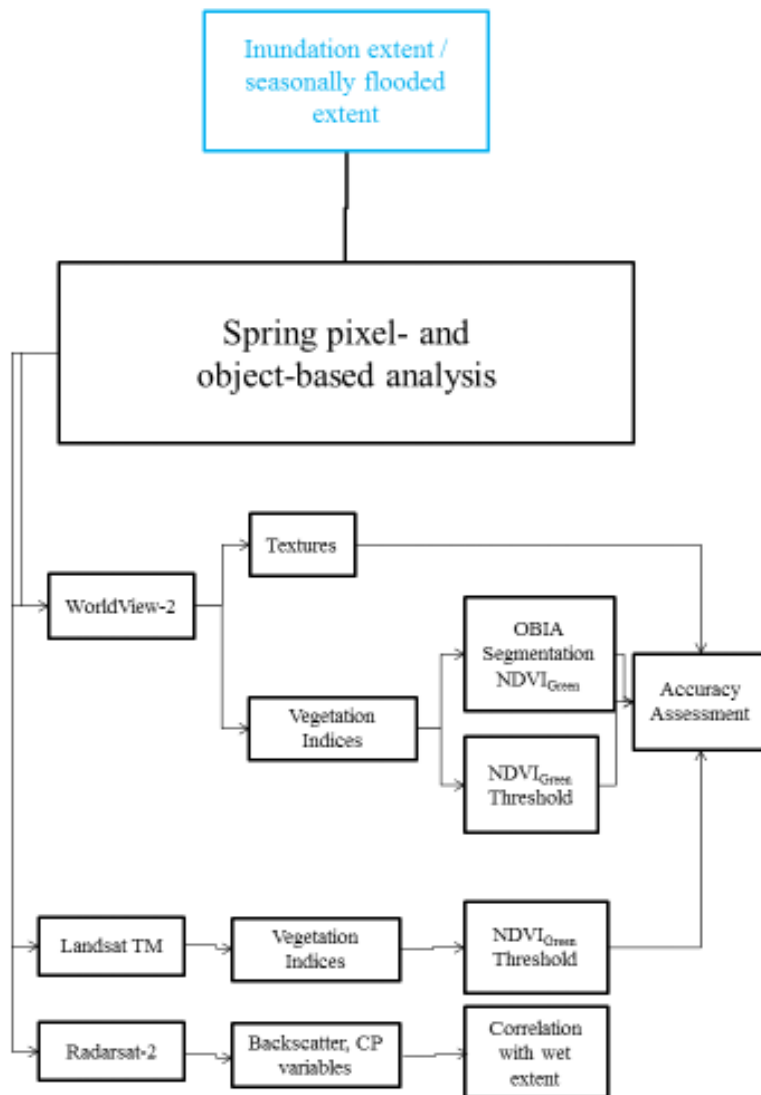


Figure 4.9. A workflow of the methods used to segment, classify and map Inundation Extent using optical and radar imagery.

The semi-variogram range of VWC varied from 6 m representing a portion of a partial transect of cedar forest to dead tree swamp to 50 m representing a full transect of open field to marsh. Transects exhibiting low spatial dependence in measured VWC were considered more than transects exhibiting high spatial dependence for statistical analysis against image data, to maintain the assumption of independence for the reference data.

4.4.3 Pixel-based image processing

The approach taken for image detection of inundation extent was to extract high resolution image parameters deemed to have potential for detection of the water-vegetation edge, including vegetation indices and texture metrics. A WorldView-2 pan-sharpened image (spatial resolution of approximately 0.46 m) was initially developed by merging the high resolution PAN image with the low resolution multi-spectral images (approximately 1.8 m), after which a subset of the study area was used for the following processes. Vrabel (2000) showed that sharpened images have increased utility of vegetation indices over those derived from the original low resolution imagery. In this research principal components analysis of the spectral bands was conducted and the PAN band was substituted for PC1, which generally represents overall image brightness similar to the PAN band (Welch and Ehlers, 1987).

GLCM texture metrics (after Haralick, and Fu, 1983) were extracted including: Contrast, Correlation, Entropy and Homogeneity (Baraldi and Parmiggiani, 1995). They were selected as each measures different aspects of the imagery (e.g. Homogeneity measures the image uniformity; Contrast measures the opposite of Homogeneity (or the heterogeneity) and detects edges well; Entropy measures the randomness within the image; Correlation measures the linear dependency of neighbouring pixels (Baraldi and Parmiggiani, 1995)). However, scatterplots of field measured % VWC compared with texture values showed no discernible relationships, and image texture was not explored further for detecting inundation extent.

It has been shown in the literature that vegetation structure and composition can be related to the wetness, or wetness gradient of the underlying soil (Gitelson and Merzlyak,

1997; Campos *et al.*, 2012; Wang *et al.*, 2012; Zhou Demin *et al.*, 2012; Delgado and Marin, 2013). Vegetation indices derived from multi-spectral band ratios are important and commonly used tools for measuring vegetation health and structure. Fourteen vegetation indices were calculated using the pan-sharpened WorldView-2 imagery, including NDVI, NDVI_{Blue}, NDVI_{Green}, WdVI, TVI, TTVI, RVI, PVI, PVI1, PVI2, PVI3, NRVI, EVI, EVI2. They were selected because they have been shown to be sensitive to soil moisture gradients and/or vegetation gradients (Li and Liu, 2004; Mutanga and Skidmore, 2004; Wu *et al.*, 2007; Wang *et al.*, 2008). In plotting each against field-measured VWC, it was revealed that NDVI_{green} had the best relationship. The plots were used to determine a threshold value of NDVI_{green} values that corresponded to 100% VWC. NDVI_{Green} has not previously been used in detection of the wet extent of wetlands, habitat, or wetland type. It was developed as a way to estimate plant chlorophyll (Gitelson and Merzlyak, 1997), which changes throughout a plants lifespan and as it reacts to stressors (such as soil moisture levels). However, as shown later in Section 5.4, its response to wet extent in the study wetland of this research was very distinct.

The range of NDVI_{green} values was subsequently used to derive a boundary that represented the wet extent (100% VWC) for each image for each wetland complex. An attempt was also made to see if the same NDVI_{Green}/VWC relationship could be found using objects that were segmented from the WorldView-2 NDVI_{Green} derived. In addition, the same object- and pixel-based analyses were conducted using the Landsat data with inputs including NDVI_{Green} and the unmixed fraction maps. Radarsat-2 backscatter was also compared to field-measured VWC to see if there was a relationship between these variables. In the literature, HH polarisation has generally been found to be better correlated with soil moisture than VV polarisation (Dobson and Ulaby, 1988; Lang and Kasischke, 2008),

however, at shallower incidence angle, soil moisture was found to be less influential on all polarisations (HH, HV, VH, VV) (McNairn *et al.*, 2002).

4.5 GIS analysis of derived imagery and existing LIO layers

All processing of GIS variables was completed using thematic maps created in this research, existing data layers found in the OMNR's LIO and using ArcMAP 10.0 software (ESRI). One of the main requirements of the collaboration with the OMNR was to determine if the data existing in the LIO were sufficient to map these attributes.

The following attributes required some degree of GIS analyses including Number of Wetland Types, Diversity of Surrounding Habitat, Proximity to Other Wetlands, Wetland Size, Hunting/Recreation Areas, Proximity to Human Areas, Ownership Patterns, Wetland Basin Size, and Rarity of Wetland and Rarity of Wetland in Landscape. Analyses included combining thematic layers, making measurements, buffering, counting, and measuring hydrologic surface connections and distance of connections. The methods implemented were relatively simple and straightforward for each attribute type and therefore a workflow figure is not provided. The following paragraphs list the layers that were used per attribute.

4.5.1 Number of Wetland Types for the Biological component

The thematic maps developed in the above-noted analysis were used as input to determine the Number of Wetland Types present in each wetland complex.

4.5.2 Diversity of Surrounding Habitat for the Biological component

The layers of Wetland Type derived from this research were combined with existing layers from the LIO that included: contours, water bodies, and a 2011 AAFC Crop Type

Map of Canada from Agriculture Canada. The presence of the surrounding habitat was assessed by taking a 1.5 km straight line distance (buffer) surrounding each wetland boundary within the wetland complex and around the boundary of each wetland complex.

4.5.3 Proximity to Other Wetlands for the Biological component

These hydrological surface connections were assessed by measuring these above-ground surface water paths up to 4 km from the boundaries of the study-site wetland complexes to other wetlands/wetland complexes using the Wetland Type thematic map derived from this research, the OMNR water bodies layer that provides large lakes and ponds information, the rivers layer, and the OMNR wetland layer.

4.5.4 Wetland Size for the Biological component

The Wetland Size was determined by using the 2013 OMNR wetland layer as the Wetland Type layer derived in this research was a subset of the entire complex.

4.5.5 Hunting Pattern mapping for the Social component

In the field in 2010, GPS waypoints were taken when hunting blinds were located by chance. These data, along with existing LIO layers of trap lines, trapper cabins, recreation access points, traditional land use areas and trails present were used to assess intensity of hunting usage at each wetland complex.

4.5.6 Ownership Patterns for the Social component

Data from the LIO of Land Ownership, Crown Land – MNR Non-Freehold Disposition Public, Crown Land – MNR Unpatented Public, Crown Land Use Policy Atlas,

Crown Leased Land, and Traditional Land Use Area were combined to determine a percentage of ownership for the wetland areas in each wetland complex study site.

4.5.7 Wetland Basin Size for the Hydrologic component

The attribute Inundation Extent (see Sections 2.9.4; 4.4) was the best indicator of the ‘true’ size of the wetland in terms of its ability to attenuate floods. The size of the catchment basin and catchment basin upstream of the wetland area were derived from the LIO watershed layer. The size of the other detention areas within the basins were derived from the existing LIO wetland layer and from water bodies and rivers layers.

4.5.8 Rarity of Wetlands and Rarity in Landscape for the Special Feature component

These attributes were assessed by comparing the derived Wetland Type attribute layer, the existing OMNR wetland layer and using the site district and site region layers.

Objective 2 Methods: Compare and relate the scores determined for each of these attributes to the field-evaluated OWES scores

4.6 Compare the scores derived from the geo-spatial analysis to the OWES field-based scores

The second objective of this research was to compare the geo-spatial derived attributes’ scores to the field-based OWES database of wetland “scores” (from field evaluations) to determine if these geo-spatial methods can be related to, and/or integrated with the existing system. Using the results derived from methods presented above, a score was determined using the scoring methods provided in section 2.9.1 to 2.9.13 for each attribute and compared to the OWES score for the same attribute.

Objective 3 Methods: Review of temporal remote sensing data in classification of wetland attributes and analysis of attribute changes over the long term.

4.7 Review of temporal remote sensing data in classification of wetland attributes and analysis of attribute changes over the long term

Wetlands are dynamic and assessing them during one season only or at one time within one season only may limit or skew results. This section outlines methods that were used to map the temporal change of attributes between seasons and inter-annually to determine how the accuracy values or scoring results changed between seasons. This was completed for Wetland Type, VCFs, Open Water Types and Inundation Extent. The methods that were used to: 1) collect validation data and 2) process and analyze imagery are already listed in the corresponding sections above (section 4.1 to 4.4).

The second portion of the temporal analysis evaluated how change can occur over longer terms (decadal) by analysing the Landsat 5 TM imagery (i.e., the only imagery available at this temporal scale). This was specifically done for Anthropogenic Disturbance, which can be assessed through land use change analysis.

4.7.1 Wetland Type, VCFs, and Open Water Types

Classifications using OBIA and CTA with spring, summer, fall and combined WorldView-2 imagery were completed for these attributes as described in sections 4.1 – 4.3 and following Figures 4.2, 4.6 and 4.7. Accuracy was assessed and the best season for imagery acquisition was determined. Statistical comparison of the accuracies was conducted using McNemar's test (McNemar 1947), which is non-parametric and based on the classifiers' error matrices, determining if column and row frequencies are equal (null

hypothesis) (de Leeuw *et al.* 2006; Gao *et al.* 2006). This test has been previously used to compare accuracies of two or more classifications (Dingle Robertson and King, 2011; Duro *et al.*, 2012).

4.7.2 Inundation Extent

The spring and summer 2010 and 2011 field data were plotted on line graphs to determine if there was a spatial difference in VWC measured in the field between seasons, and the seasonal difference in wetland wet extents where VWC = 100%. Next, thresholds for the summer WorldView-2 imagery were developed in the same manner as the spring imagery as outlined in section 4.4. Finally, a comparison was made to determine if the distance between the wet extents (Inundation Extent) matched the distance between the threshold-derived extents in the imagery.

4.7.3 Anthropogenic Disturbance

A change in biomass can be an indicator of anthropogenic disturbance, and this can be assessed using remotely sensed imagery. Figure 4.10 provides the workflow for this attribute. Landsat 5 TM images from 2010 and from the year in which the original field-based OWES evaluations (Table 3.1) were completed (or the closest-date, best quality, non-cloudy imagery were compared. Land cover fraction analyses have been shown to indicate change based upon climatic or human influences (Adams *et al.*, 1995; Schmid *et al.*, 2005; Olthof and Fraser, 2007; Melendez-Pastor *et al.*, 2010) and were therefore selected to assess change through time in the wetlands of this research.

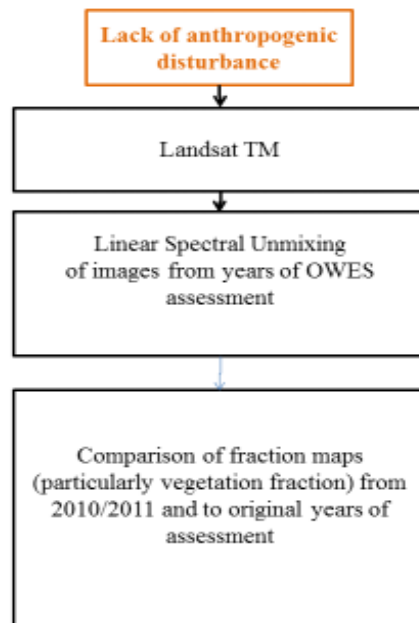


Figure 4.10. A workflow of the methods used to segment, classify and map Anthropogenic Disturbance using optical imagery.

Each image was converted to Top-of-Atmosphere radiance using radiometric calibration coefficients (after Chandler *et al.*, 2009) and the images were then relatively calibrated using pseudo-invariant features (PIFs, Pax-Lenney *et al.*, 2001; Dingle-Robertson & King, 2011) with the newer image (2010) as the master. These calibrated images were subsequently unmixed using 3 manual and 5 automatically selected EMs (Methods Section 4.1.3) and the derived fraction maps (especially the vegetation fraction) were compared for differences using RGB image display to determine if changes caused by humans could be observed.

5.0 Results

This chapter presents the results for the three research objectives. It follows the same format as the methods described in the previous chapter and starts by presenting the results of mapping the selected OWES attributes for one season (spring). The chapter then presents the results of scoring these attributes and the relationships of these scores to the field-evaluated OWES scores. Finally, this chapter reports the results from the analysis of seasonal and decadal temporal dynamics of select attributes. Table 5.1 summarizes the key findings in the structural order of this chapter. The majority of the methods testing was focussed on the attribute Wetland Type, and consequently that section is larger than the others.

Table 5.1. Summary of the key findings of the results in structural order of this chapter.

Attribute	Imagery type or method	Results
<i>Objective 1: Map the selected OWES attributes for one season (spring)</i>		
Wetland Type	Optical	CTA was better than MLC for all classes
		WorldView-2 imagery provided higher accuracies than Landsat 5 TM imagery
		Landsat 5 TM imagery was less useful than WorldView-2 imagery except for a few classes (e.g. Fen or Swamp)
	Radar (includes all seasons)	Spring, steep incidence angle HH, HV images showed best separation for Wetland Types
		Addition of HH, HV images to optical imagery and the DEM improved classification accuracy of the Swamp class
		Addition of CP variable images to optical imagery and the DEM improved the classification accuracy of the Fen class
		The summation of the summer co- and cross-pol pedestal minima showed separation between three distinct groupings of classes
VCFs	Optical	WorldView-2 imagery provided higher accuracies than Landsat 5 TM imagery, but accuracy values were not suitable for operational use

	Radar (includes all seasons)	Spring HH, HV imagery showed good separation of Fen and Swamp plant types, and summer imagery had good separation of Marsh plant types Classification of HH, HV images and CP variables, and combined with optical imagery and the DEM did not improve overall accuracies
Open Water Type	Optical	Three Open Water Type classes were discriminated in a generalized manner across wetlands Spring Landsat 5 TM imagery had higher overall accuracies than spring WorldView-2 imagery
Inundation Extent	Optical & Radar	NDVI _{Green} corresponded well with VWC (%) Pixel-based processing was better than object-based analyses; boundary detail was obscured using OBIA Landsat 5 TM and Radarsat-2 data derived variables were not related to spring VWC (%)
Number of Wetland Types	GIS analysis of derived thematic maps and existing LIO layers	Attribute could be derived using data available in LIO
Diversity of Surrounding Habitat	GIS analysis of derived thematic maps and existing LIO layers	Attribute could be derived using data available in LIO
Proximity to Other Wetlands	GIS analysis of derived thematic maps and existing LIO layers	Attribute could be derived using data available in LIO
Wetland Size	GIS analysis of derived thematic maps and existing LIO layers	Attribute could be derived using data available in LIO
Hunting Pattern	GIS analysis of derived thematic maps and existing LIO layers	Attribute has the potential to be derived
Ownership Patterns	GIS analysis of derived thematic maps	Attribute has the potential to be derived

	and existing LIO layers	
Wetland Basin Size	GIS analysis of derived thematic maps and existing LIO layers	Attribute could not be derived with existing data
<i>Objective 2: Compare and relate the scores determined for each of these attributes to the OWES scores</i>		
Comparative GIS analyses of derived thematic maps and existing LIO layers to determine OWES wetland scores	Same scores for all sites	Diversity of Surrounding Habitat, Wetland Size, Proximity to Other Wetlands
	Same scores for most sites	Rarity of Wetlands and Rarity in Landscape (excluding Westport Bog)
	Higher scores	Open Water Type
	Lower scores	Number of Wetland Types, Wetland Types
	Scores could not be derived	VCFs, Hunting Patterns, Ownership Patterns and Wetland Attenuation Factor
<i>Objective 3: Review of temporal remote sensing data in classification of wetland attributes and analysis of attribute changes over the long term</i>		
Wetland Type	Optical Imagery	Summer imagery improved overall accuracies for two of four sites
		Combining spring, summer, and/or fall imagery in segmentation did not improve overall classification accuracies for three of four sites
		Overall accuracy using summer Landsat 5 TM imagery was not better than for spring
VCFs	Optical Imagery	Summer WorldView-2 imagery did not improve accuracies for 3-form and for VCF classifications
		Combining summer and fall WorldView-2 imagery improved 3-form classification accuracies by ~10%
		Combining spring, summer and/or fall WorldView-2 imagery did not improve the overall classification accuracies for VCFs
Open Water Type	Optical Imagery	Summer WorldView-2 imagery did not improve accuracies for Open Water Type classification
		Combining spring, summer and/or fall WorldView-2 imagery did not improve the overall classification accuracies for the Open Water Type, but some individual classes did improve
		Summer Landsat 5 TM imagery improved UA for some classes
Inundation Extent	Optical Imagery	Seasonal and annual differences in wet extent highlighted the need for multiple season and/or

		inter-annual mapping of wetlands; a single map derived within a long period of time is not representative
		Boundaries representing 100% VWC were well delineated using summer NDVI _{Green}
Anthropogenic Influence	Optical Imagery	In some areas of three study sites, vegetation fractions have decreased since 1984. In a few small areas of marsh, the vegetation fractions have increased since 1984.
		Known changes that were initiated through Anthropogenic Disturbance can be observed using vegetation fraction maps

Objective 1 Results: Map the selected OWES attributes using imagery from for one season

5.1 Wetland Types

5.1.1 Segmentation and classification of Wetland Type using optical and radar imagery

Segmentation and classification analyses were initially tested using Loch Garry imagery and then subsequently extended to the other four sites. The Loch Garry spring 2010 WorldView-2 image and the unaltered 10 m DEM were segmented and the objects that best visually matched lake boundaries, channels, forested areas, and wetland areas were created with a segmentation scale parameter value of 45, shape parameter value of 0.1 and compactness parameter value of 0.75 (see Methods section 4.1.2). As an example of the segmentation results, Figure 5.1A is a CIR composite of the spring Loch Garry image showing the segmented objects using these parameters; in Figure 5.1B the red outline shows the objects forming the boundary of a known fen; Figure 5.1C shows the objects that follow a known water channel; and Figure 5.1D shows the objects following the shoreline of the lake, Loch Garry. Segmentation results using the same parameters were applied to imagery of the other three sites and are found in Appendix D, Figures D1 through D3.

While the main goal for this attribute was to identify generalized classes of Bog, Fen, etc., it was found in the field that many areas were not homogenous. Figure 5.2A (subset of Figure 5.1B) shows there are several segmented objects within a known fen. In the field, the fen graded from swamp (outside the boundary, Figure 5.2B) to less dense treed fen (Figure 5.2C) to mostly grassy fen (Figure 5.2D).

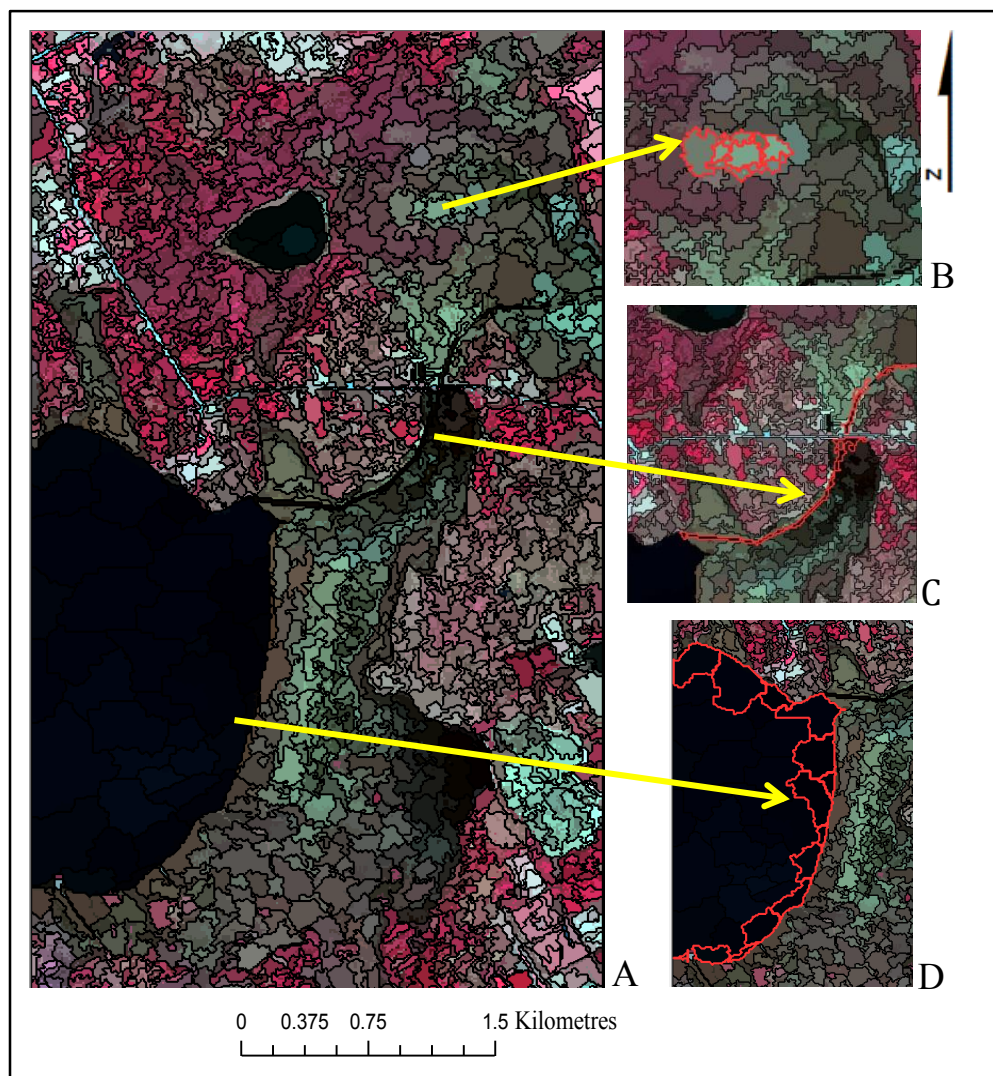
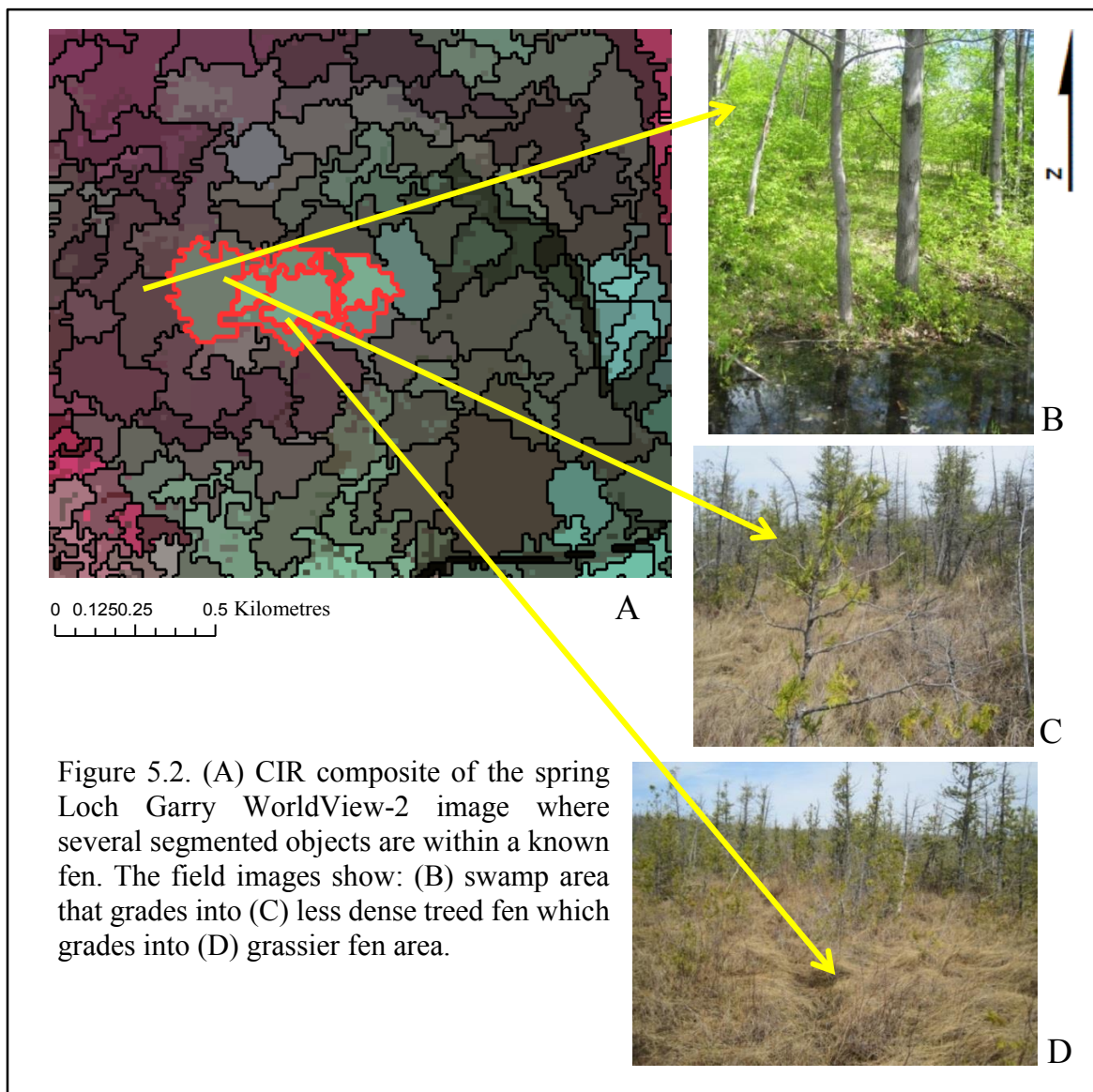


Figure 5.1. (A) CIR composite of the spring 2010 Loch Garry WorldView-2 image showing the created objects using scale value of 45, shape value of 0.1 and compactness value of 0.75; and in red (B) objects that make up the boundaries of a known fen; (C) objects that form a known channel; and (D) objects that mimic the shoreline of Loch Garry.



While these Fen subclasses were not required for this general OWES attribute, understanding the differences and recognizing the patterns within fens overall aided in the analysis of confusion between the classes (e.g. if a validation point in the treed fen area was confused with swamp).

Figure 5.3 is an example of scale parameter testing for Westport Bog. Figure 5.3A highlights an area of detail (bog lagg, Figure 5.4) without segmentation; for the balance of the images all shape and compactness parameter values are 0.1 and 0.75, respectively.

Figures 5.3B through 5.3D show the image segmented with a scale values of 45, 40 and 50, respectively. The yellow outlines highlight the objects that make up the bog lagg. It can be seen that with a scale parameter of 45 the overall lagg shape is maintained, whereas with a larger scale value the objects include surrounding (non-lagg) areas. With the smaller scale parameter values (e.g. 40) non-lagg areas were also included. The green circles in Figure 5.3 show an erroneously incorporated non-lagg feature (e.g. shadow) at all scale values. . While this still indicates that physically different features may be combined in individual objects for any scale parameter selected, overall the scale parameter value of 45 best created objects that depicted Wetland Types and other features in the landscape. It was found that the optimal scale value of 45 found for Loch Garry was also appropriate for the other sites (e.g. see Appendix D, Figures D1 and D3).

As with the segmentation analyses, the spring 2010 WorldView-2 Loch Garry imagery was selected for testing classifications, including MLC applied to the segmented objects. Figure 5.5 presents the spring Loch Garry 7-class map derived using MLC. The classes included Water, Fen, Marsh Swamp, Forest, Short Vegetation and Impervious (Road). Swamp is located around the mid-size lake in the north with some swamp along the shorelines of Loch Garry (both sides). Marsh, located to the northeast and centre of the image, were well classified and Fen areas, such as the large shoreline fen on Loch Garry and the smaller fen east of the small lake in the north were also well classified. Short Vegetation were correctly assigned to agricultural areas and follow typical rectangular field shapes, specifically in the southeast. Impervious (Roads) are located throughout the map and followed a linear pattern with some smaller (cottage/farm) sites located next to the roads. Extensive field knowledge of this site gives confidence that the major spatial entities representing each class are well classified and there are no large areas where one class has

been erroneously classified. There were, however, questionable areas classified as Marsh, which were observed as swamp in the field (red circles).

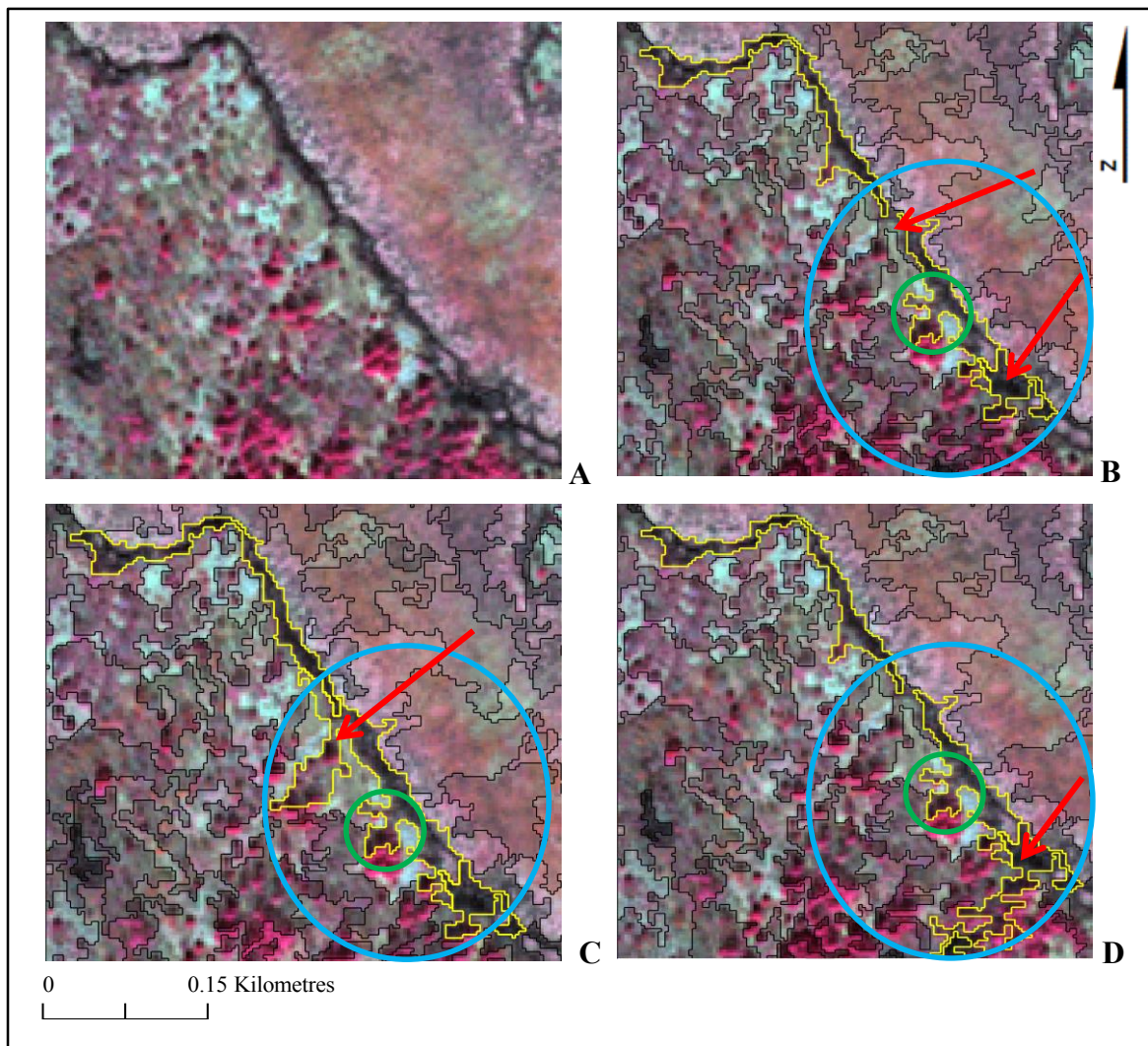


Figure 5.3. Example of the effects of different scale parameter values on segmentation of objects for known features. A) WorldView-2 spring CIR composite sub set of Westport Bog. Yellow outlines in B through D highlight bog lagg objects created with scale values of 45, 40, and 50 respectively. Important features such as the bog lagg are well defined using a scale value of 45, whereas objects for larger and smaller scale values include non-lagg areas (blue circles and red arrows; erroneously incorporated non-lagg at all scales are circled in green). All shape and compactness values were maintained at 0.1 and 0.75, respectively).



Figure 5.4. Lagg at Westport Bog. Yellow circle highlights presence of vegetation showing that the bog is not necessarily a simple linear water feature but a transition zone between the bog and upland.

Table 5.2A is the error matrix for this 7-class MLC. Samples in the error matrix represent one pixel per object (Figure 4.2) to avoid spatial autocorrelation, but this approach limited potential sample size. In terms of PA (Methods Section 4.1.5), Swamp was confused with Forest and with Marsh. The following classes had moderate confusion (2 to 3 samples): Marsh with Swamp and Short Vegetation with Forest. The following classes had slight confusion (1 to 2 samples): Fen with Swamp; and Impervious with Short Vegetation. For UA, the following classes had confusion: Forest with Short Vegetation and Swamp; Swamp with Fen, and Marsh; and Short Vegetation with Impervious.

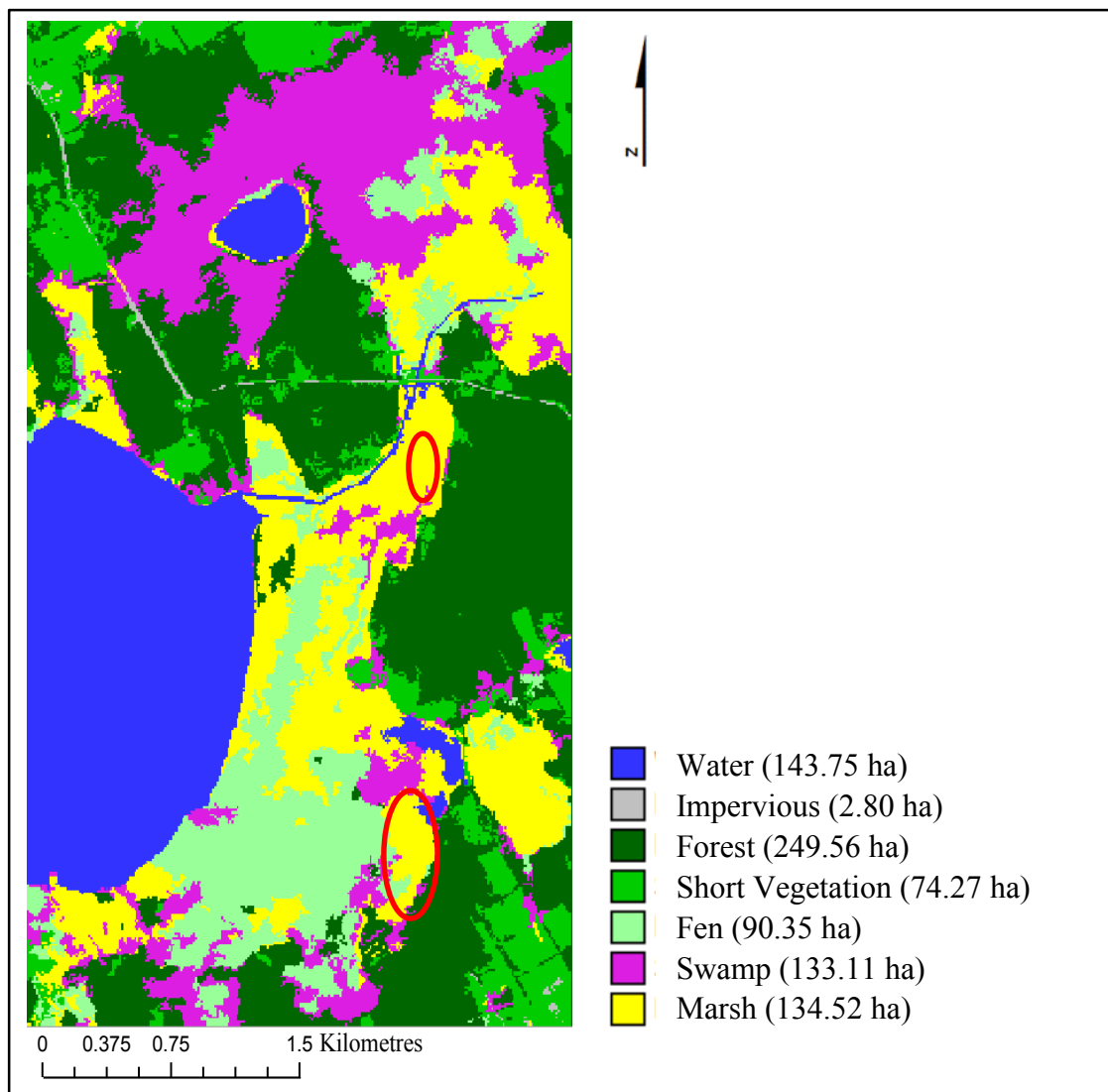


Figure 5.5. MLC Thematic map of Loch Garry developed from spring 2010 WorldView-2 and DEM images segmented (scale value = 45; shape value = 0.1; compactness value = 0.75). Red circles show areas of erroneously classified Marsh.

Table 5.2A. Error matrix for the spring 2010 Loch GarryWorldView-2 and DEM object-based MLC (7-classes).

		Reference Samples							
		Water	Imper- vious	Forest	Short Vegetation	Fen	Swamp	Marsh	Total
Classified Samples	Water	6	0	0	0	0	0	0	6
	Impervious	0	3	0	0	0	0	0	3
	Forest	0	1	11	2	0	1	0	15
	Short Vegetation	0	3	0	5	0	0	0	8
	Fen	0	0	0	0	4	0	0	4
	Swamp	0	0	0	0	1	3	2	6
	Marsh	0	0	0	0	0	3	2	5
	Total	6	7	11	7	5	7	4	47*

*Total reference samples. Additional samples were added for Impervious and Short vegetation.

Table 5.2B provides the accuracy statistics for this 7-class MLC. Overall accuracy was 72.3 % with a kappa (k) = 0.67.

Table 5.2B. Accuracy statistics (%) for the spring 2010 Loch GarryWorldView-2 and DEM OBIA MLC (7-classes).

Overall Accuracy (%):	72.3		
Kappa:	0.67		
Class Name:	PA (%)	UA (%)	Kappa
Water	100.0	100.0	1.00
Impervious	42.9	100.0	1.00
Forest	100.0	73.3	0.65
Short Vegetation	71.4	62.5	0.56
Fen	80.0	100.0	1.00
Swamp	42.9	50.0	0.41
Marsh	50.0	40.0	0.34
Average	69.6	75.1	

The average PA was 69.6% and the average UA was 75.1%. The Swamp class had the poorest accuracy. Water was the best class as expected, due to its distinctly low and uniform reflectance in all WorldView-2 spectral bands. Water, Forest, and Fen had greater than 75% accuracy, which is a common threshold for utility in operation mapping (Foody, 2002). The average UA was above 70%.

To increase accuracy, the three Upland classes were aggregated into one class to obtain these 5-classes. Table 5.3A is the error matrix for the 5-class classification. In terms of PA confusion was evident for the following class groups: Water with Marsh; Fen with Upland and Swamp; and Fen and Marsh. For UA, the following classes were confused: Upland with Fen, and Swamp; and Fen with Swamp and Marsh.

Table 5.3A. Error matrix for the spring 2010 Loch Garry WorldView-2 and DEM object-based MLC (5-classes).

		Reference Samples					Total
		Water	Upland	Fen	Swamp	Marsh	
Classified Samples	Water	4	0	0	0	0	4
	Upland	0	15	1	1	0	17
	Fen	0	0	3	1	1	5
	Swamp	0	1	1	3	0	5
	Marsh	1	0	0	2	3	6
	Total	5	16	5	7	4	37

Table 5.3B. Accuracy statistics (%) for the spring 2010 Loch Garry WorldView-2 and DEM object-based MLC (5-classes).

Overall Accuracy (%):	75.7		
Kappa:	0.67		
Class Name:	PA (%)	UA (%)	Kappa
Water	80.0	100.0	1.00
Upland	93.8	88.2	0.79
Fen	60.0	60.0	0.76
Swamp	42.9	60.0	0.76
Marsh	75.0	50.0	0.60
Average	70.3	71.7	

Table 5.3B lists the accuracy statistics for this classification. The overall accuracy was 75.68% with a kappa = 0.67. The average PA increased to 70.3%, but the average UA decreased to 71.7%. As for the 7-class classification, Water was most accurate. Swamp and Marsh improved in accuracy, but Fen decreased in accuracy. In the 5-class classification Fen was confused with Upland. This could be related to the combination of short grass areas with the forested areas to create the Upland class (for which the overall spectral response may be similar to that for the treed/grassy fen areas). This highlights the need to, if possible, delineate wetland areas first, then mask out non-wetland areas and classify only those areas within a given wetland.

Due to the small validation set(s) there is a degree of imprecision expected (potentially large confidence intervals) with these data sets. However, field knowledge supports these classification results, as larger areas were not erroneously classified. As the intent of aggregation of non-wetland classes was to produce higher accuracy for the wetlands classes, the aggregated 5-class set was used for the following analyses.

Table 5.4 provides the CTA classification accuracies for the spring 2010 WorldView-2 imagery plus DEM using the GINI algorithm. The site with the highest accuracy was Loch Garry (86.5%), which was markedly higher than the MLC overall accuracy for the same wetland. Figure 5.6A presents the Loch Garry 5-class CTA classification next to the 5-class MLC map (Figure 5.6B). The site with the lowest overall accuracy was Marlborough Forest (70.0%). For wetland types, Fen had the highest average PA and UA (PA = 90.0%; UA = 75.0%) while Bog had the lowest average PA (65.93%) and UA (50.3%). Results for other CTA tests using the entropy and gain ratio tree-creation algorithms were poorer and can be found in Appendix E, Figure E1. In relation to the overall literature for Wetland Type classification, these results were comparable, as they fell with the typical overall accuracies of 71% to 92%.

For both techniques, areas that were well classified included the water channel in the centre, the small lake to the northwest, and the shoreline of Loch Garry, etc. CTA appears to have performed better for the swamp areas around the lake in the north of the map and particularly the areas at the edge of the upland in the southeast (red circles) which were observed in the field. Similarly, the representation of Fen along the small lake shoreline in the CTA map is believed to be more accurate than the Upland and Marsh classes in the MLC map. Access to those areas was limited, however the vegetation was similar to what was observed beside a man-made boardwalk, and observed while canoeing (black dashed lines). In terms of total area per Wetland Type, the CTA map had more classified Swamp and Fen and less Marsh and Upland. In relation to the percent cover that was measured during the field-based OWES evaluation, the CTA method came closer to approximating the values of the subset area on the whole, with Fen cover representing 12% (CTA), 10% (MLC), and 14% (field), respectively. Swamp cover was 32% (CTA), 17% (MLC) and 40% (field),

respectively. Marsh was under estimated by both methods, being 8% (CTA), 11% (MLC), and 46% (field), respectively.

Figure 5.7A is the classification tree created using the 5-class training sites and the GINI algorithm. The first major split (Band 4 (NIR) < 8 DN) accounted for 97.18% of Class 1 (Water) and is represented in Figure 5.8B. The next branch is a decision where DEM > 71.5 m ASL and accounts for 93.25% of the Upland class (Figure 5.7E). Both of these are logical and expected as water has very low NIR reflectance compared to other land cover types and upland is usually at higher elevation than wetland. Literature using these techniques for wetlands is lacking, thus these results are relatively new and direct comparisons to previous studies not possible. As an example of a broader land cover classification, Baker *et al.* (2006) showed similar initial splits with elevation and NIR in classifying Agriculture, Wetland, Riparian, Forest and Rangeland using Landsat ETM+ imagery, however, the first major split was not NIR as found in this research, but elevation due to the wider elevation range of that study. Also included in their CTA were the Tasselled Cap variables of Brightness, Wetness, Greenness and % hydric soils, so a direct comparison with this research is difficult. Also not given was the amount of pixels contributing to the class. Much of the other literature using CTA for broader land cover classification does not provide the actual decision trees for analysis or comparison.

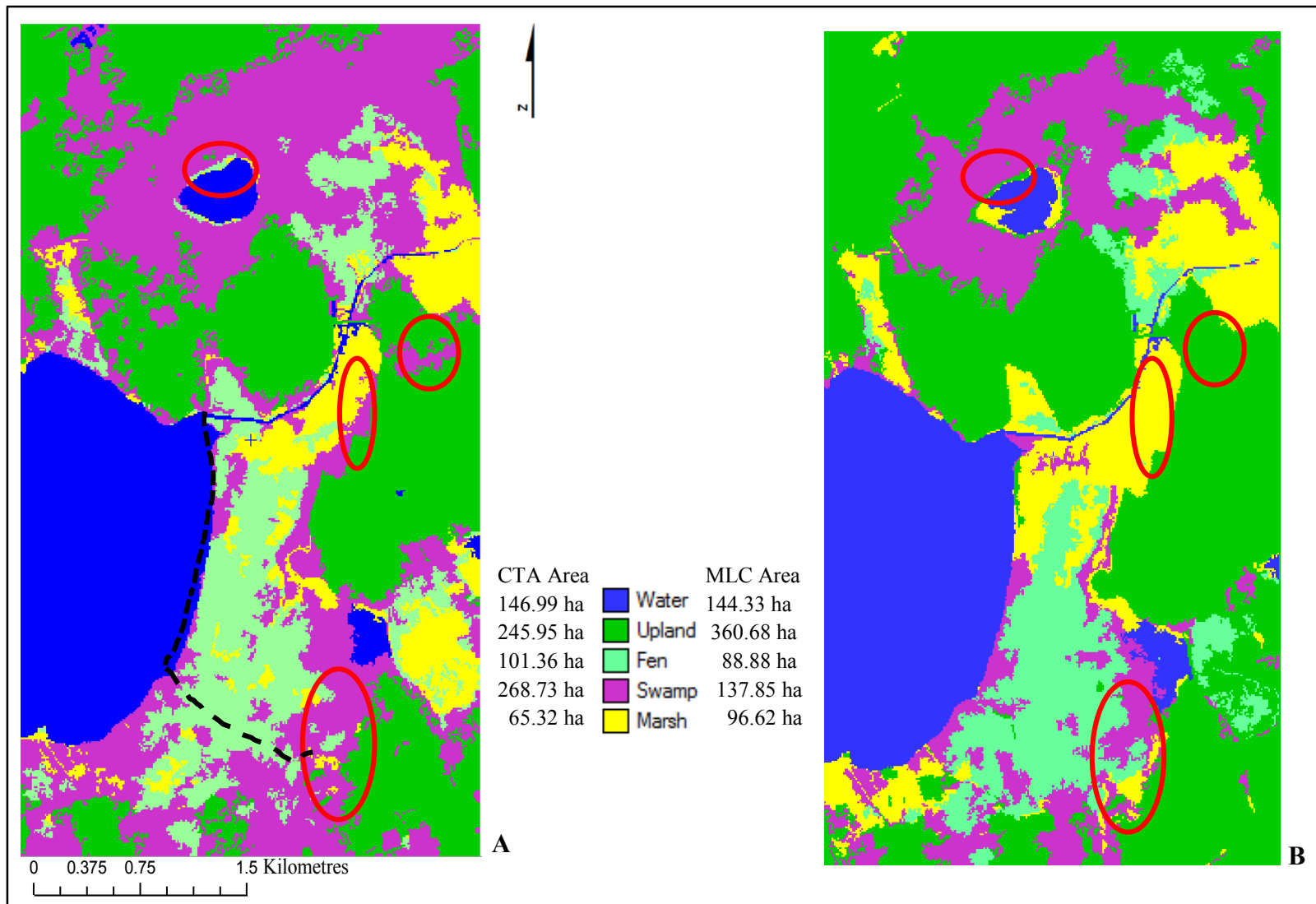


Figure 5.6. 5-class thematic maps of Loch Garry derived from object-based classification of spring 2010 WorldView-2 image and DEM data. A) CTA; B) MLC. Red circles show areas that were well-classified using CTA as compared to MLC. Black dashed lines shows route travelled in the field on foot and by canoe to visually inspect areas with limited access.

Table 5.4. Accuracy statistics for 5-class CTA (GINI algorithm) of segmented spring 2010 WorldView-2 imagery and DEM at all study sites.

	Overall Accuracy (%)	Kappa	Water		Upland		Fen		Bog		Swamp		Marsh		Average	
			PA (%)	UA (%)	PA (%)	UA (%)	PA (%)	UA (%)	PA (%)	UA (%)	PA (%)	UA (%)	PA (%)	UA (%)	PA (%)	UA (%)
Loch Garry	86.49	0.82	100.0	100.0	81.25	100.0	80.0	100.0	n/a	n/a	100.0	58.33	75.0	100.0	87.3	91.7
Marlborough Forest	70.00	0.60	83.3	100.0	60.0	64.29	100.0	50.0	n/a	n/a	83.33	71.43	63.6	70.0	78.1	71.1
					Short Upland		Tall Upland									
Westport Bog	72.50	0.65	100.0	75.0	50.0	100.0	75.0	66.67	77.78	63.64	n/a	n/a	63.6	77.78	73.3	76.6
					Upland		Fen		Tall Bog		Short Bog					
Mer Bleue Bog	73.17	0.64	100.0	100.0	77.78	93.33	n/a	n/a	60.0	27.27	60.0	60.0	62.5	100.0	72.1	76.1
Average Accuracy (%)			Water		Upland		Fen		Bog		Marsh		Swamp			
			95.8	93.7	68.8	84.8	90.0	75.0	65.9	50.3	80.0	61.3	66.9	86.9		

Within the first two branches, over 90% of the contributing pixels for the Water and Upland classes are accounted for, while the data representing the three wetland classes are represented by the subsequent splits. Figure 5.7C and 5.7D are the location in the tree where the majority of the Fen and Swamp class are accounted for (over 83.4% and 81.92%, respectively). The main discriminating variable for fen and swamp is topography, and most of the fens in the study (particularly at Loch Garry) were at a lower elevations than the swamps. This is supported in the Canadian Wetlands Classification System, (National Wetlands Working Group, 1997), which shows that most Fen classes are found at lower elevations, in basins, channels, adjacent to lakes or ponds, etc. The Marsh class is comprised of pixel contributions from several smaller contributing end nodes (underlined in blue). These occur at end nodes where the final decisions are determined by blue image DN values and then, in some cases, with corresponding NIR values.

Table 5.5A is the error matrix for this CTA classification. In terms of PA, fewer classes had confusion than for the MLC, and confusion was only evident for Upland with Swamp, Fen with Swamp, and Marsh with Swamp. For UA, only Swamp was confused with Upland, Fen and Marsh, which was less than the four classes that showed UA confusion for the MLC. Table 5.5B shows the accuracy statistics derived from this error matrix.

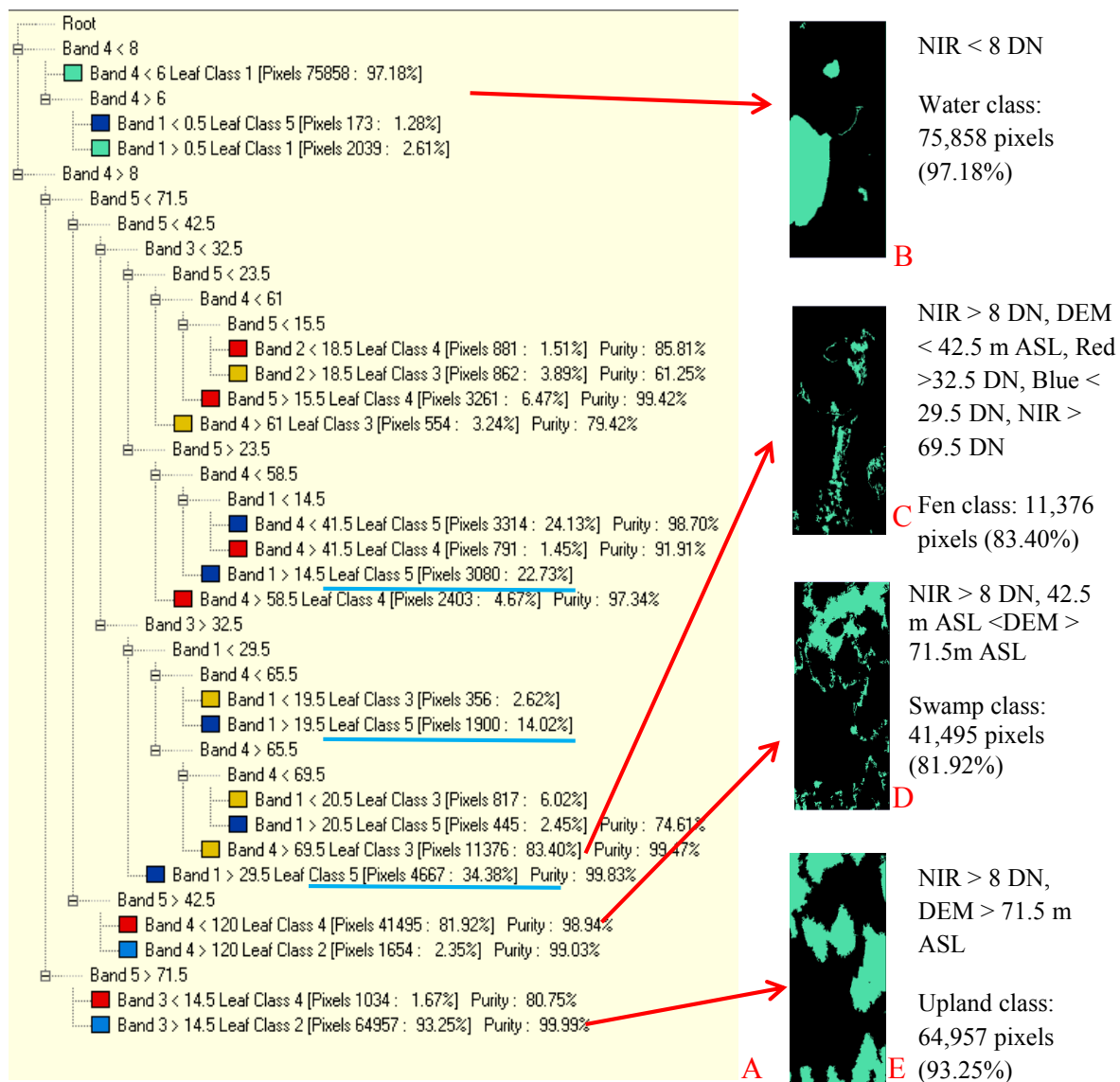


Figure 5.7. A) 5-Class GINI classification tree using spring 2010 WorldView-2 imagery and the DEM for Loch Garry. B through E) are maps representing the leaves (end nodes) where class contributions are greater than 80%. In these maps, green represents the assigned pixels, and black represents the unassigned (or previously assigned) pixels. Blue underlines represent the contributing end nodes for Marsh class.

Table 5.5A. Error matrix for the spring 2010 Loch Garry WorldView-2 and DEM object-based GINI CTA (5-classes).

		Reference Samples					Total
		Water	Upland	Fen	Swamp	Marsh	
Classified Samples	Water	5	0	0	0	0	5
	Upland	0	13	0	0	0	13
	Fen	0	0	4	0	0	4
	Swamp	0	3	1	7	1	12
	Marsh	0	0	0	0	3	3
	Total	5	16	5	7	4	37

The overall accuracy was 86.5% with kappa = 0.82. This was an increase of more than 10% accuracy over the MLC. Water was again the best class, and Swamp was the worst class (UA only). Overall, the class accuracies were higher than those of the MLC, with all classes (except Swamp) having greater than 75% accuracy. The average PA was 87.3% and the average UA was 91.7%.

Table 5.5B. Accuracy statistics (%) for the spring 2010 Loch Garry WorldView-2 and DEM object-based GINI CTA (5-classes).

Overall Accuracy (%):	86.5		
Overall:	0.82		
Class Name:	PA (%)	UA (%)	Kappa
Water	100.0	100.0	1.00
Upland	81.3	100.0	1.00
Fen	80.0	100.0	1.00
Swamp	100.0	58.3	0.49
Marsh	75.0	100.0	1.00
Average	87.3	91.7	

Similar results for the CTA GINI classification of the other three study sites can be found in Appendix F, Figures F1 to F6 and Tables F1A & B to F3A & B.

5.1.2 Results from OBIA using spring 2010 Landsat 5 TM imagery for Wetland Type

Segmentation was evaluated for the Loch Garry site using the Landsat TM imagery and the DEM with a scale value of 10, a shape value of 0.1 and compactness value of 0.5. As expected, segmented objects aligned with the shoreline of Loch Garry, and the outlines of farms fields, and some wetland areas. Objects were not created for the water channel, but that channel was incorporated into objects of the surrounding land cover. Such detail was lost due to the coarser nature of the original imagery. See Appendix G, Figures G1A - D for examples of this segmentation.

All details regarding LSU and the development of the fraction maps are found in Appendix G. Two sets of fraction maps were created: 1) 3 manually selected EMs (vegetation, moisture, bare); and 2) 5 automatically generated EMs (three bare, vegetation and moisture). Analyses of the residual maps showed that values were closer to zero for the five EM fraction maps, indicating higher unmixing precision. Therefore, they were subsequently used in segmentation and classification.

Segmented objects created using a scale value of 10, shape value of 0.1 and compactness value of 0.5 were mostly meaningless as many crossed Wetland Type boundaries or were not representative of known shapes (e.g. farm fields, see Appendix D for examples). Consequently, smaller scale and compactness values were tested. Figure 5.8A

shows the segmented fraction maps for the Mer Bleue Bog study area in a false colour composite (EM 5 (moisture) in blue, EM 2 (green vegetation) in green and EMs 1, 3 and 4 (bare) in red display channels) using a scale value of 2, shape value of 0.1 and compactness value of 0.1. The resulting objects represent known boundaries (e.g. bog boundary) or shapes (e.g. farm fields, see yellow highlights, centre and right in image). The DEM was then included in the segmentation process resulting in the objects in Figure 5.8B. Again, the land cover spatial features are apparent (yellow highlights) and there are smaller objects that suggest topographic contours (blue circles). Similar results for the other three study sites can be found in Appendix G, Figures G10 through 12.

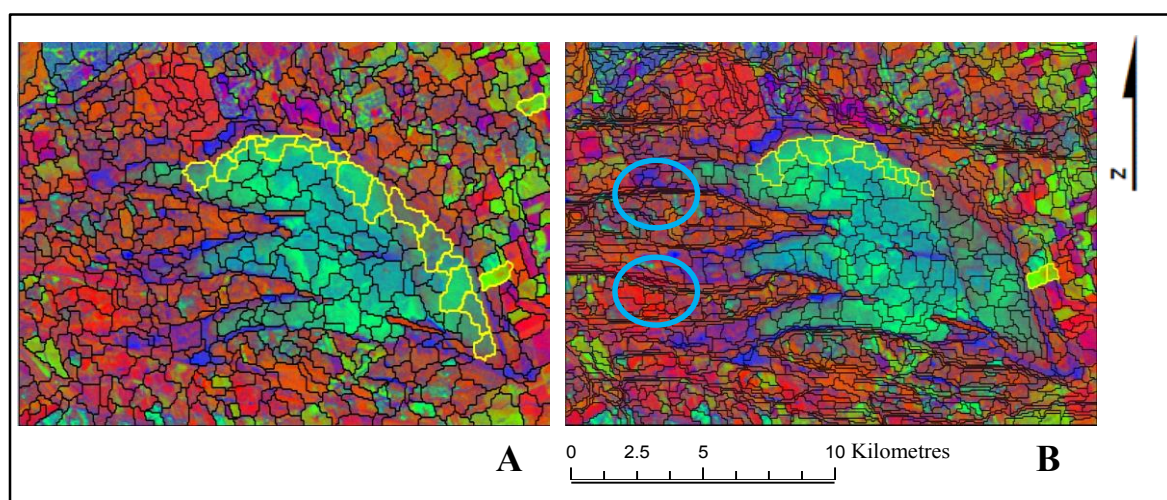


Figure 5.8. (A) Mer Bleue Bog study site segmented fraction map images (5 EMs, no DEM) derived from spring 2010 Landsat 5 TM imagery (scale value = 2; shape value = 0.1; compactness value = 0.1). Yellow highlighted objects represent land cover spatial features. (B) Includes the DEM in the segmentation process (same parameter values). Blue circles show areas where finer objects were segmented due to the addition of the DEM data.

Table 5.6 provides a summary of the overall accuracies for the various combinations of data to classify Wetland Type at all four sites using spring imagery and CTA. In general, the overall accuracies ranged from <40% to a maximum of 78%. Loch Garry, Mer Bleue Bog and Marlborough Forest were completed using an April 2010 image and Westport Bog was processed using a March 2010 image due to extremely poor quality April and May 2010 images (Westport Bog falls within another swath of Landsat 5 TM imagery). Yellow shading highlights the highest accuracy per site. The highest accuracies were obtained using fraction maps classified at pixel level (i.e., not segmented objects). In all cases, the accuracies were higher using the fraction maps as compared to the original (not unmixed) data.

Table 5.6. Wetland Type accuracies (%) per combination of data type and segmentation (yes/no) for spring Landsat TM imagery. The highest accuracy per site is highlighted in yellow.

	Data	5 fraction maps				Original bands			
	DEM?	No	Yes	No	Yes	No	Yes	No	Yes
	Segmented?	No	No	Yes	Yes	No	No	Yes	Yes
Loch Garry		45	54	56	59	40	59	48	56
Mer Bleue Bog		60	74	47	43	65	60	54	54
Marlborough Forest		78	69	63	52	71	69	61	74
Westport Bog		65	72	47	57	55	60	55	52

Although object-based classification produced poorer overall accuracy than pixel based classification, for three of the sites the overall accuracies improved with the addition of the DEM to the segmentation process (Loch Garry, Mer Bleue Bog and Westport Bog). However, no sites had overall accuracies that were acceptable for operational purposes (Foody, 2002), or that matched the spring WorldView-2 CTA accuracies.

Table 5.7 is an example of detailed class-level accuracies for the eight tests of data type at Marlborough Forest. They can be compared to the results for the original Landsat TM data. Overall, the highest accuracies were obtained using 5 EMs without segmentation and without the DEM (overall accuracy = 78.3%; kappa = 0.72). The addition of the DEM did not improve overall accuracy except for the segmented original band data. Segmenting the fraction map images and subsequently classifying them with the GINI CTA (with or without the DEM) did not improve the overall classification accuracy results, and produced poor results across all classes. Thus, pixel-based classification of unmixed fraction maps for Wetland Type was found to be the best approach for spring Landsat TM imagery.

Marsh had the lowest accuracy across all data types (average PA = 37.5%; average UA= 28.1%). It was the only class that benefitted from segmentation of the fraction maps (Table 5.7, test 5 where Marsh values are highlighted in teal) and segmentation of the original band data (Table 5.7, test 4 highlighted in green). The poor overall results are related to the small spatial extent of marsh occurrences in relation to the pixel size of the Landsat imagery. Additionally, this imagery was acquired in April when marsh vegetation (reeds, grasses, etc.) is mostly senescent and yellow and water is dominant. The error matrices show that Marsh was sometimes confused (1 to 3 samples) with Water and confused with the other classes in the other tests (1 to 2 samples) (see Appendix G, Tables G5 to G12 for error matrices).

Fen was well classified using all data configurations, as were Water and Upland. However, test 4 also shows that Fen UA was improved for Fen class using the segmented

data (highlighted in teal). Swamp was generally most accurate with pixel-based classification and without the DEM (highlighted in pink). However, in two cases, the Swamp class improved with the addition of the DEM to the original band data (tests 2 and 4 highlighted in yellow).

Figure 5.9 shows the Marlborough Forest 5-class GINI CTA map derived using the test 5 configuration. It can be seen that the known water areas are well defined, particularly Roger Steven's pond and the channel (Steven's Creek) to the east of it (red circles). Fen areas correspond to the known fen at the centre of the image (black circle). Swamp areas are seen throughout the image with Marsh classified areas corresponding to smaller marsh patches located to the southeast, through the centre of the image and surrounding the water bodies. Table 5.8 is the error matrix for this classification.

For PA confusion was evident for: Upland with Marsh and Fen; and Swamp with Marsh and with Fen. For UA, Water was confused with Marsh; Upland with Fen and Marsh; and Swamp with Marsh and Fen. Similar classifications' thematic maps for the other three sites can be found in Appendix G (Figure G11 to G13).

Figure 5.10 provides a comparison between the best and the worst overall classifications (tests 5 and 8, respectively) with the original spring 2010 Landsat 5 TM CIR image given for reference. It can be seen that the test 8 map does not have the detail found in the test 5 map (black arrows). In the field, this area was not a homogenous area of Upland, but Upland interspersed with wet patches.

Table 5.7. Accuracy statistics (%) for Wetland Type CTA classifications using the spring 2010 Landsat TM data and the DEM, original and unmixed, segmented and not segmented, at Marlborough Forest. Highest accuracy was achieved for test 5 (orange highlight). Other highlights of the best and worst results for some classes are described in the text.

Test #	Type of Classification	Overall Accuracy (%)	Overall Kappa	Water		Upland		Fen		Swamp		Marsh		Average	
				PA (%)	UA (%)	PA (%)	UA (%)								
1	Original 6 bands (not segmented, no DEM)	71.7	0.64	83.3	100.0	66.7	100.0	85.7	75.0	81.8	75.0	42.9	27.3	72.1	75.5
2	Original 6 bands (not segmented, with DEM)	69.6	0.61	83.3	100.0	66.7	83.3	85.7	85.7	72.7	80.0	42.9	25.0	70.3	74.8
3	Original 6 bands (segmented, no DEM)	60.9	0.50	100.0	85.7	66.7	76.9	71.4	71.4	45.5	71.4	28.6	16.7	62.4	64.4
4	Original 6 bands (segmented, with DEM)	73.9	0.66	83.3	100.0	80.0	75.0	71.4	71.4	63.6	87.5	71.4	50.0	74.0	76.8
5	5 member fraction maps (not segmented, no DEM)	78.3	0.72	100.0	85.7	86.7	100.0	100.0	77.8	72.7	72.7	28.6	33.3	77.6	73.9
6	5 member fraction maps (not segmented, with DEM)	69.6	0.61	100.0	85.7	73.3	84.6	85.7	75.0	54.5	75.0	42.9	30.0	71.3	70.0
7	5 member fraction maps (segmented, no DEM)	63.4	0.53	83.3	35.7	66.7	71.4	85.7	100.0	45.5	100.0	42.9	42.9	64.8	70.0
8	5 member fraction maps (segmented, with DEM)	52.1	0.38	33.3	33.3	73.3	61.1	71.4	83.3	54.5	75.0	0.0	0.0	46.5	50.6
Averaged UA and PA (%) across all variations of Landsat TM classifications for Wetland Type (an indicator of which classes were well-classified regardless of configuration of data)				83.3	78.3	75.5	81.6	82.1	80.0	61.4	79.6	37.5	28.1		

Table 5.8. Error matrix for the spring 2010 Marlborough Forest Landsat 5 TM GINI CTA of the 5 EM derived fraction maps, no segmentation, no DEM.

		Reference Samples					
		Water	Upland	Fen	Swamp	Marsh	Total
Classified Samples	Water	6	0	0	0	1	7
	Upland	0	11	1	0	1	13
	Fen	0	1	6	1	0	8
	Swamp	0	0	0	6	2	8
	Marsh	0	3	0	4	3	10
	Total	6	15	7	11	7	46

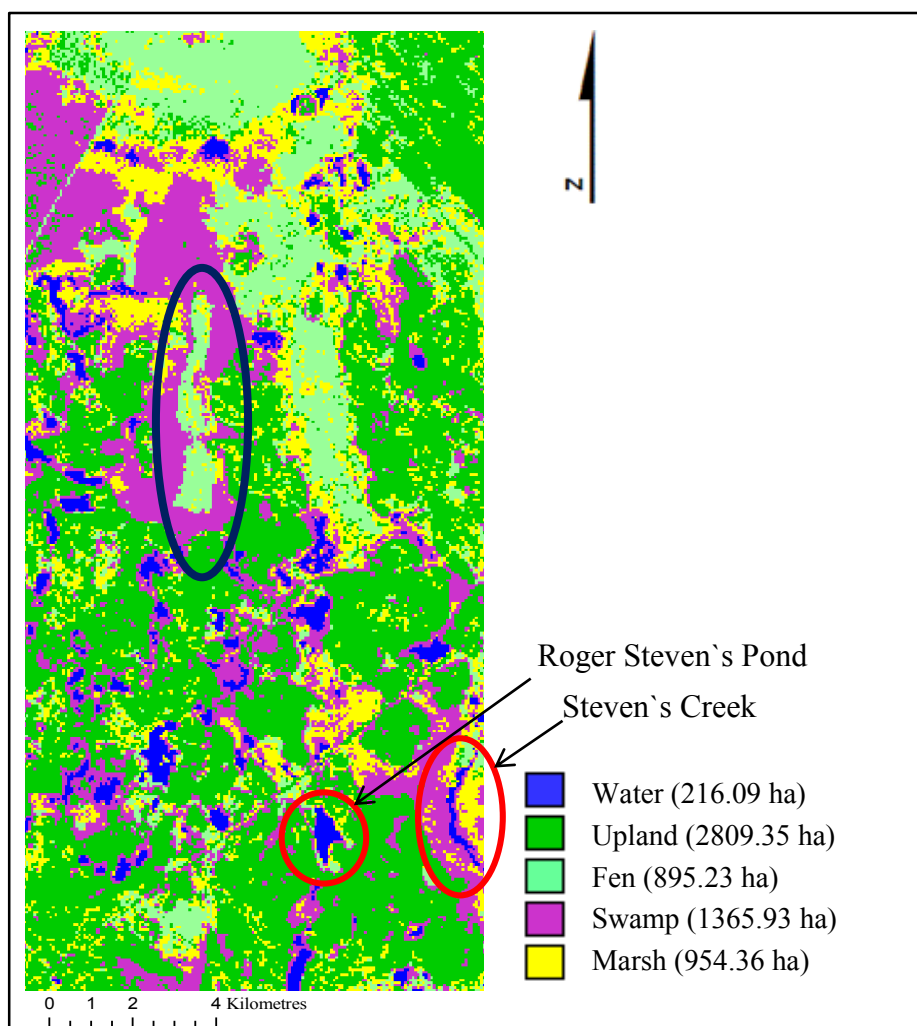


Figure 5.9. 5-Class pixel based GINI CTA map for Marlborough Forest derived using Landsat TM imagery acquired in April 2010. Red circles highlight known water bodies (Roger Stevens Pond and Steven's Creek). Black circle highlights known Fen area.

The test 8 map (Figure 5.10C) shows erroneously classified patches of Marsh that were not observed in the field (red arrows). These results demonstrate that pixel-based classification of Landsat data is preferable over object-based classification if the goal is to retain detail and map small areas of a given Wetland Type.

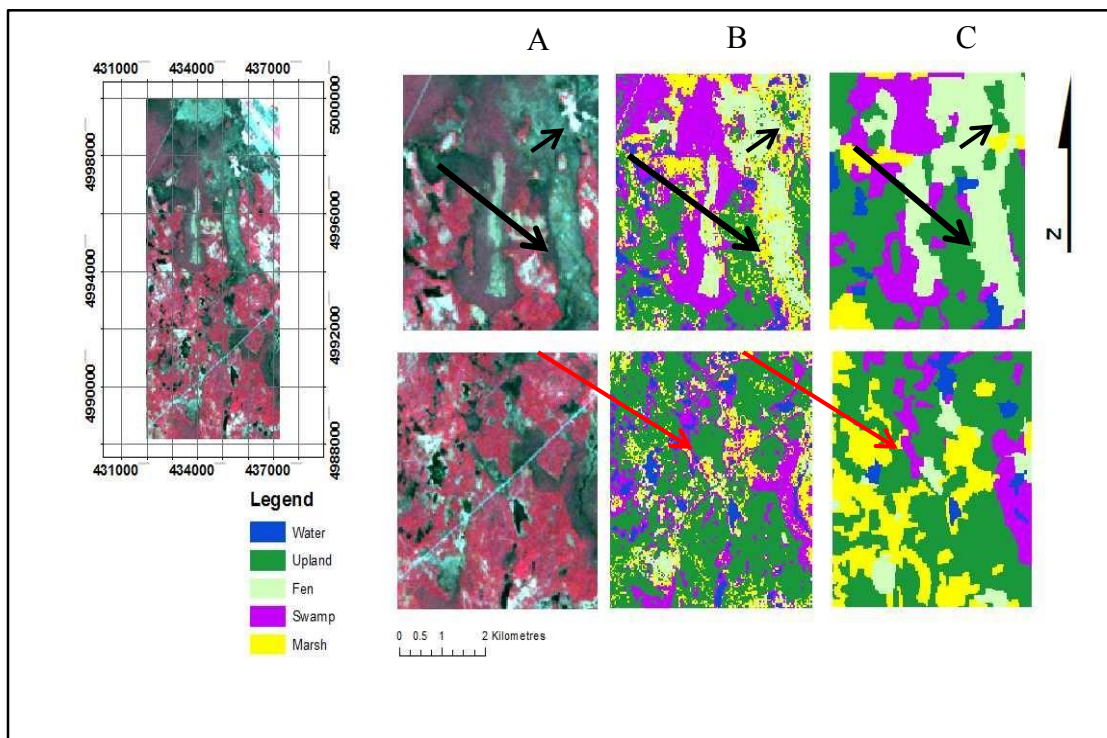


Figure 5.10. Comparison between the best (test 5) and worst (test 8) classification of Marlborough Forest using CTA with spring 2010 Landsat 5 TM imagery. Column A provides CIR sub sets of the overall Marlborough Forest image, with Columns B and C showing the corresponding subsets of the test 5 and test 8 maps, respectively. The black arrows point to areas where detail present in the pixel-based test 5 is not present in the object-based test 8 classification. The red arrows show the excessive amounts of Marsh that were erroneously classified in test 8.

5.1.3 Radarsat-2 image processing, classification and analyses for Wetland Type

The following section provides the detailed results of the various analyses using the Radarsat-2 imagery for Wetland Type mapping. Because of the nature of this analysis, and

for clarity, the analysis of other seasons (summer and fall) are included here (as opposed to section 5.7 with the optical imagery).

HV and HH images were extracted at field validation locations for Water, Upland (separated into Coniferous, Deciduous and Short Grass), Fen, Bog, Marsh and Swamp (at least five classes depending upon the complex), at all complexes (4), for all seasons of data (3), and for all incidence angles (ranging from steep to shallow (18.4° to 48.0° , respectively)). Figure 5.11 shows a comparison for the sample data for three generalized classes (Water, Upland and Wetland) for summer 2010 Loch Garry Radarsat-2 imagery (spring imagery was not acquired at this site). It can be seen that Water is distinct from the other two classes and there is overlap between Wetland and Upland. This is not surprising as Water would be expected to have the lowest backscatter response due to specular scattering away from the antenna, while the vegetated areas would have higher backscatter relating to vegetation-water double bounce interactions and volume scattering within the canopy. There would also be an increase in depolarisation with increasingly complex vegetation canopies such as from short Bog or Fen, to taller Swamp or Upland (Evans *et al.*, 1988; Boerner *et al.*, 1998; McNairn *et al.*, 2002; Touzi *et al.*, 2004), which was evident in the increasing pedestal heights for these land covers, respectively. Further analyses of these graphs were focused on the wetland classes to evaluate their relative separation.

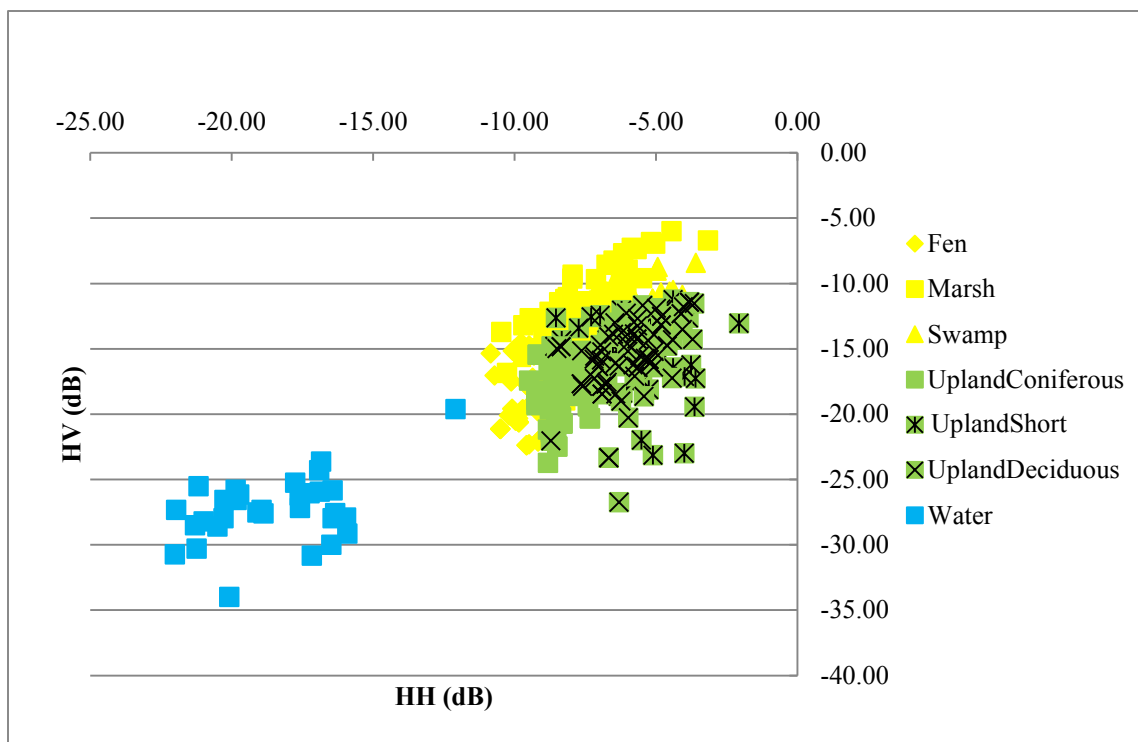


Figure 5.11. Loch Garry summer 2010 Radarsat-2 backscatter for Wetlands (yellow), Uplands (green) and Water (blue) at steep incidence angles (29.1° – 30.9°).

Figure 5.12 shows the spring steep and shallow incidence angle backscatter values for Marlborough Forest. For the shallower incidence angle (46.8° - 48.0°), the backscatter values of the three classes overlap (Figure 5.12B) and the separation is not as distinct as for steeper angles (18.4° - 20.4° , Figure 5.12A). Bog was not included as it did not occur in Marlborough Forest. In the literature, it has been found that steep incidence angle imagery is often best for differentiation between vegetation types. In vegetated areas that are flooded, and in wetland forests or swamps, there is increased backscatter due to trunk-water double-bounce scattering and volume scattering among branches and other vegetation such as reeds, and grasses (Leckie and Ranson, 1998; Baghdadi *et al.*, 2001; Lu and Kuown, 2008). This was confirmed in this research as a result of differences in vegetation structure in Fens, which was comprised of short grass and sedge meadows with little water visibility compared

to Marshes which, in spring, typically had short young green growth as well as senescent, broken and horizontally lying (from snow load) reeds masking some of the water, and Swamps with open, bare canopies and large flooded areas.

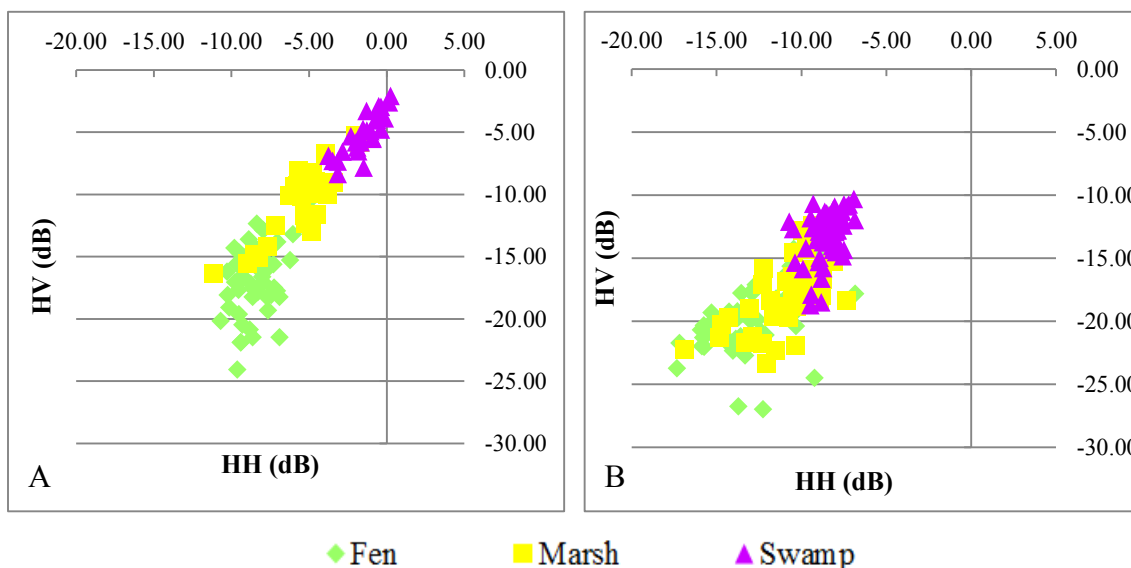


Figure 5.12. Marlborough Forest spring 2010 Radarsat-2 backscatter for Fen (Green), Marsh (Yellow) and Swamp (Purple) at A) steep (18.4° - 20.4°), and B) shallow (46.8° - 48.0°) incidence angles.

Figure 5.13 shows spring steep incidence angle backscatter values for all Wetland Types (including Bog) across all sites. When comparing between each pair of Wetland Types (Figure 5.13) the backscatter separation during the spring is apparent. Swamp is distinct as shown, for example, with Marsh (Figure 5.13A). This is because in swamp there is increased volume scattering in bare tree canopies and increased double-bounce scattering from bare trunks/branches and surrounding water. There would also be increased depolarisation of the signal in swamp due to these multiple scattering interactions. There is more overlap between Marsh and Fen (Figure 5.13B) as expected based upon the similarities of the structure of vegetation (sedges, reeds, etc.). The most overlap is apparent for Bog and Fen (Figure 5.13C), however, there is some separation at HV values of -20.00 dB and HH values of

approximately -10.00 dB. Bog and Fen have the most similar types of vegetation. Typically, in the literature Bog has been shown to have lower HH backscatter (Li and Chen, 2005; Henderson and Lewis, 2008), however, the structure and vegetation present at both Bog and Fen sites were similar in terms of scattering properties with respect to C-Band. Both had smooth canopies with short vegetation, albeit at Bogs vegetation was mostly comprised of small bushes while Fens were typically grassy meadows. At this measurement and observation scale, the differences between these types of canopies may be negligible.

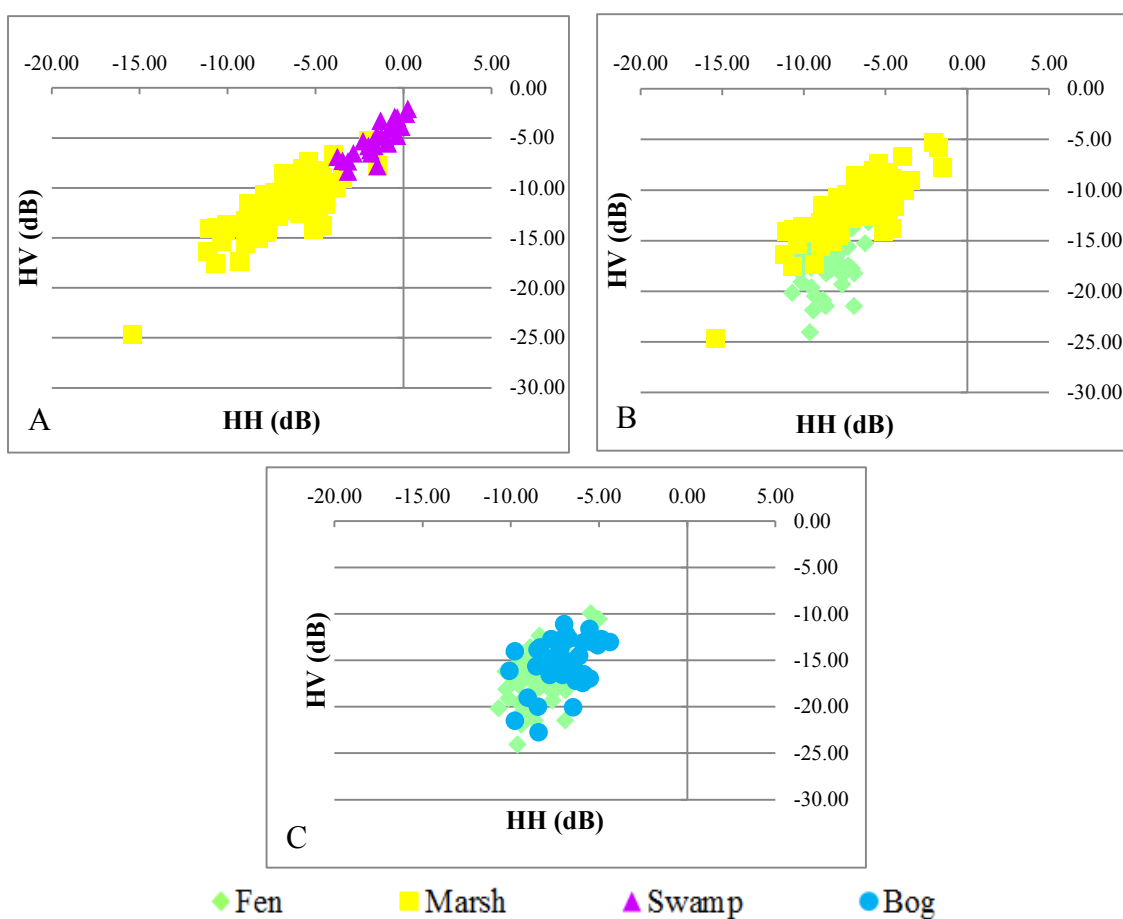


Figure 5.13. All sites spring 2010 Radarsat-2 backscatter for Fen (Green), Marsh (Yellow), Swamp (Purple), and Bog (blue) at steep (18.4° - 27.6°) incidence angles with A) Marsh compared to Swamp; B) Marsh compared to Fen; and C) Fen compared to Bog.

Overall, from the above analyses, the best separation between Wetland Type classes based upon backscatter was found using spring steep angle imagery. These results were expected to lead to good overall classification of Wetland Type. Classifying backscatter images for Wetland Type using CTA (segmented or not segmented), or pixel-based MLC did not produce higher accuracies than those achieved for the optical plus DEM data. The addition of HH and HV images to the optical imagery analysis did not improve the overall results and caused large areas to be erroneously classified. For example, in Mer Bleue Bog, large areas of the bog were erroneously classified as Marsh; in Marlborough Forest, large areas (various land cover types) were erroneously classified as Fen. Table 5.9 illustrates this for Marlborough Forest classified using CTA and the following input data: 1) object-based classification of WorldView-2, DEM and HH, HV images; 2) object-based classification of WorldView-2 and DEM; and 3) pixel-based Landsat TM 5 EM fraction maps (no DEM). The only class improvement evident using HH, HV data was for Swamp.

Figure 5.14 provides a visual comparison of these classifications. In the north part of the map, detail is lacking in an over-classified Fen area (black circle). The WorldView-2/DEM derived map also over-estimated the amount of fen present there. In Figure 5.14A there is an erroneous indication of Marsh (red circle) that is not present in Figure 5.14B. There is more linear detail between farm fields in the northeast corner on Figure 5.14A than there is in Figure 5.14B, however both do not capture Steven's Creek (blue circle) as Figure 5.14C does. The pixel-based classification of fraction images derived from the coarser resolution Landsat TM spring imagery (Figure 5.14C) had the most detail of the three maps.

Table 5.9. Marlborough Forest CTA accuracies (%) utilizing the segmented WorldView-2 imagery (four spectral bands), the DEM, HH and HV images, and Landsat 5 TM unsegmented 5 EM fraction images. Orange highlights the class (Swamp) that improved with the addition of the HH, HV images.

Data Used	Overall Accuracy (%)	Kappa	Water		Upland		Fen		Swamp		Marsh		Average	
			PA (%)	UA (%)	PA (%)	UA (%)								
WorldView-2, DEM, and HH, HV images	62.5	0.51	100.0	40.0	83.3	62.5	45.5	62.5	83.3	71.4	53.3	66.7	73.1	60.6
WorldView-2 and DEM	70.0	0.60	83.3	100.0	60.0	64.3	100.0	50.0	60.0	64.3	63.6	70.0	73.4	69.7
Landsat 5 TM 5 EM fraction images (unsegmented; no DEM)	78.3	0.72	100.0	85.7	86.7	100	100	77.8	72.7	72.7	28.6	33.3	77.6	73.9

In terms of area of each Wetland Type, there was more Fen classified in the combined optical/radar imagery and the radar images alone (Figures 5.14A and B, respectively), as compared to the optical imagery alone which had greater area of Swamp and Marsh classified.

Polarimetric signatures were generated from training data for Water, Upland, Fen, Bog, Swamp and Marsh across all four sites, at two incidence angles (steep and shallow) and for three seasons. Polarimetric signature outputs included polarimetric signature graphs, and the minimum and maximum co- and cross-pol orientation and ellipticity angle statistics. Table I1 in Appendix H provides the signature location references and location details of the training sites for all of the sample signatures along with the accompanying polarimetric signature graphs. Typically there are four types of models expected for polarimetric signatures (Figure 2.5). Polarimetric signatures, elliptical and orientation angles are statistics rather than images.

The following provides examples of typical and atypical response curves for Water, Fen, Bog, Swamp and Marsh using spring data. In addition, one fall signature is shown to illustrate whether fall data could be used given spring data were not available. The majority of the accompanying photographs were taken in spring (April 2010) with some from the summer (July/August 2010). A comparison of the maximum co- and cross-pol orientation (ψ) and ellipticity angles (χ) for spring steep incidence angle data follows these graphical analyses.

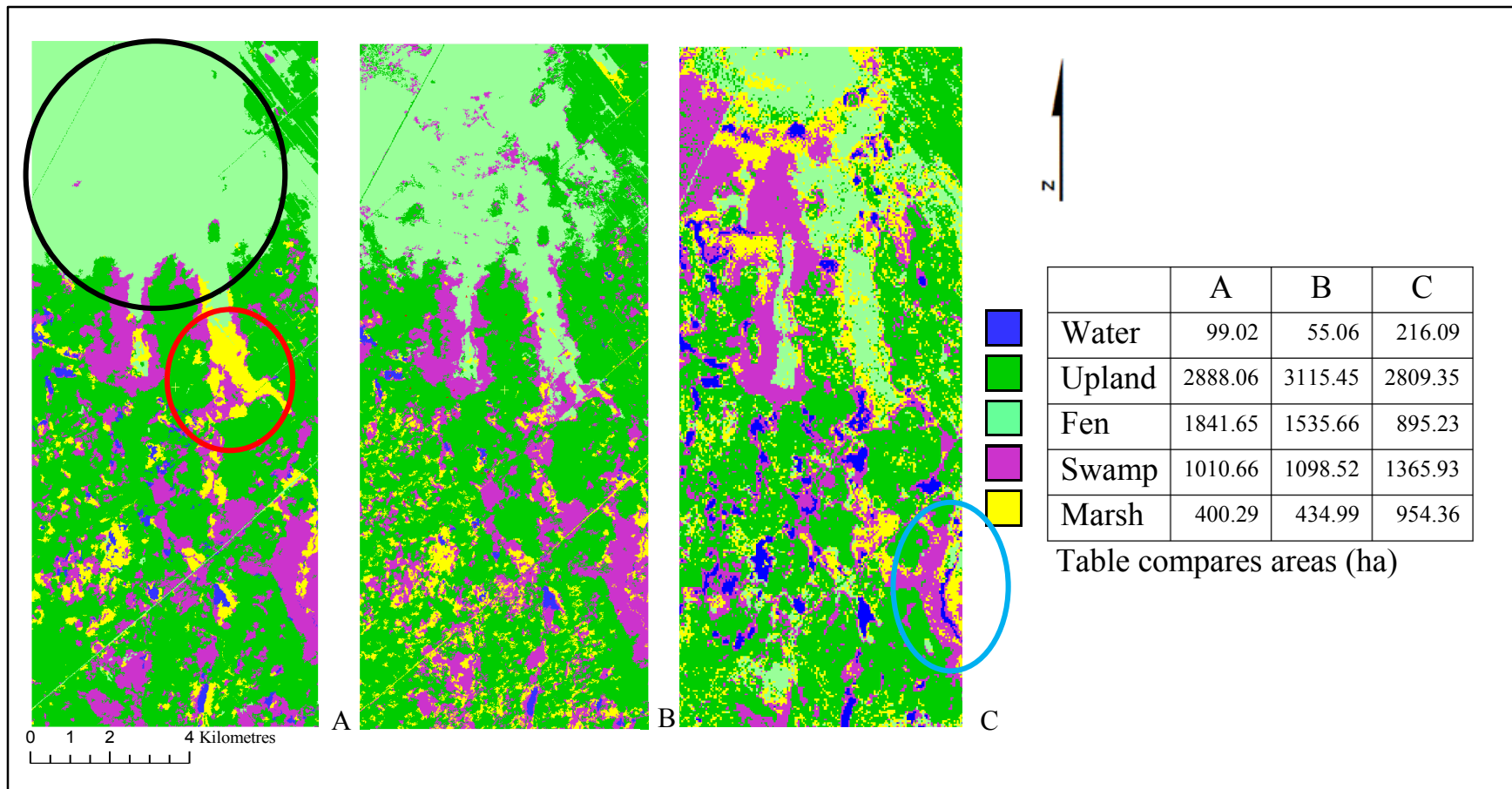
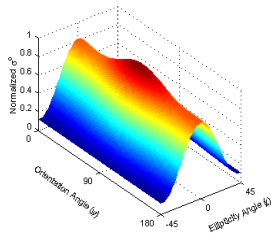


Figure 5.14. Comparison of 5-class CTA Wetland Type thematic maps using A) WorldView-2 optical imagery, DEM and HH and HV images; B) WorldView-2 optical imagery and DEM only; and C) Landsat TM unsegmented fraction maps.

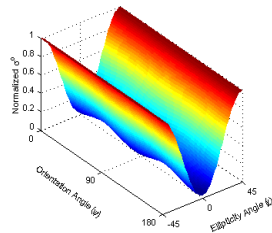
For Water, polarimetric signatures were derived from spring imagery at two samples sites in each of Westport Bog, Marlborough Forest (also at two incidence angles) and from fall imagery at two sample sites in Mer Bleue Bog. All Water training sites were selected based upon reference imagery. Three of the derived Water signatures indicated typical surface scattering for both co- and cross-pol data (both sample sites at Westport Bog and one site at Marlborough Forest) and four of the water samples showed a mixture of single and double bounce scatterers (both fall data sites in Mer Bleue Bog and one spring data site at Marlborough Forest). The presence of emergent vegetation that has developed throughout summer is the probable cause of multiple scattering mechanisms detected in the fall imagery. There had not yet been snowfall to flatten the vegetation, nor had the vegetation decomposition process had much time to break down summer vegetation.

Figure 5.16 provides examples of two of the spring polarimetric signatures derived for Water. Figure 5.16A represents expected surface scattering as seen in Figure 5.15A, such as water at Westport Bog in April. The Westport Bog CIR composite shows dark water with little or no emergent vegetation and/or wave action. Figure 5.15B, in Marlborough Forest represents a more atypical polarimetric signature for water, showing a response typically found in presence of multiple scatterers (e.g. a mix of single and double bounce scatterers such as vegetation stems, trunks, water surface, etc.

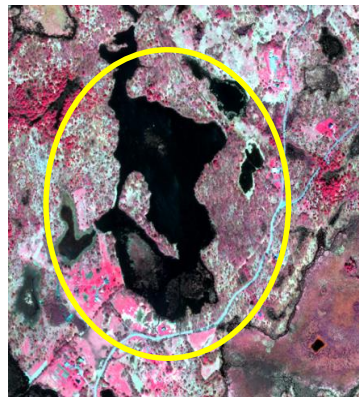
Spring Water Polarimetric Signatures



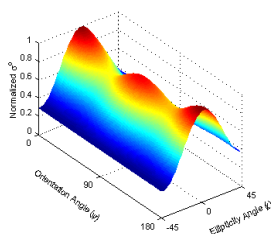
Co-pol



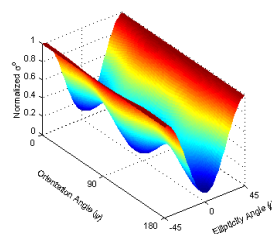
Cross-pol



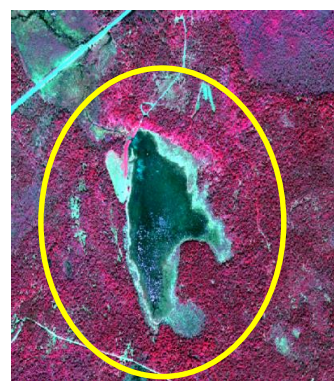
A) Westport Bog, April 2010



Co-pol



Cross-pol



B) Marlborough Forest, March 2010

WorldView-2 CIR composites; April 28
and May 17, 2010, respectively.

Figure 5.15. Polarimetric signatures for (A) typical water (surface scattering) at Westport Bog; and (B) atypical water (double-bounce model (double-bounce scattering)) at Marlborough Forest. Yellow circles on the CIR composites show the area from which training data were extracted.

The Marlborough Forest WorldView-2 image was acquired on May 17, whereas the Radarsat-2 image is from March 29. As 2010 was a drought year, and March was unseasonably warm there was no snow cover from the beginning of March (Environment Canada, 2013). The presence of emergent vegetation would not be as dominant in March, as it is in May. However, there could be dead vegetation present from the previous year, which may be causing this odd scattering response not typically expected for water.

Marsh signatures were acquired at three training areas in each of Marlborough Forest, Westport Bog, and Mer Bleue Bog radar imagery acquired at steep and shallow

incidence angles (Marlborough Forest) in spring (Westport Bog and Marlborough Forest) and fall (Mer Bleue Bog). The polarimetric signatures generally indicate the presence of multiple scatterers. In spring, water and dead vegetation from the previous season, and new emergent growth would be expected. Figure 5.16 provides representative examples of the multiple scatterer signatures obtained for Marsh.

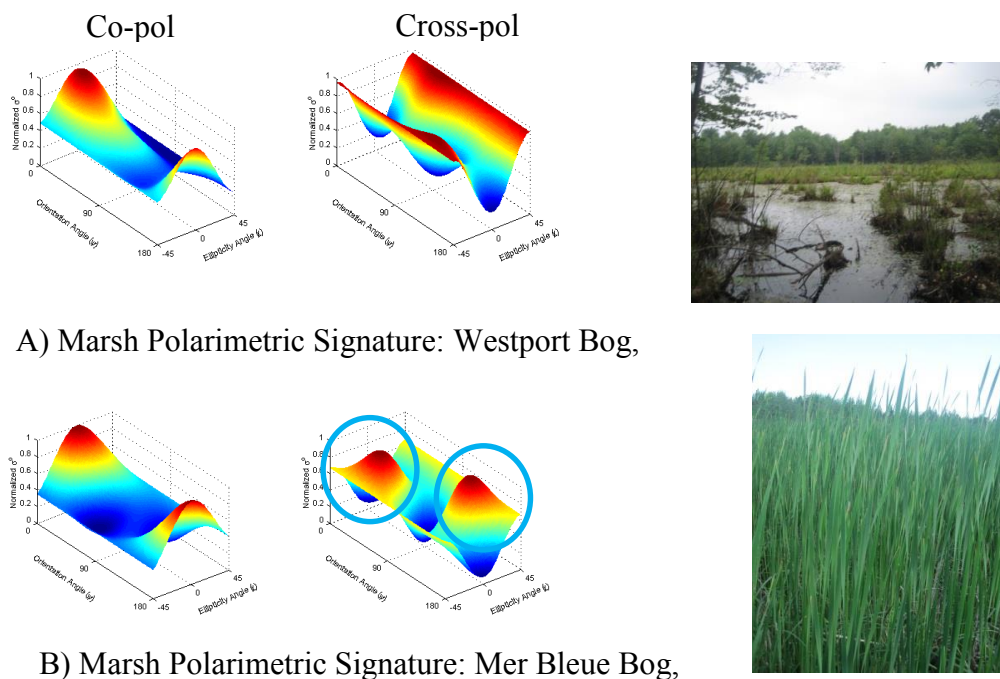


Figure 5.16. Representative polarimetric signatures for Marsh A) in the spring, (Westport Bog); and B) in the fall (Mer Bleue Bog).

All of the Marsh cross-pol signatures from the training areas for Mer Bleue Bog in November data had peaks (blue circles)). The accompanying photograph is from the summer. The training area was a large homogenous cattail marsh. In November there could be water and dead cattails as potential scatterers. Local precipitation data did not show a particularly wet fall (Environment Canada, 2013). The first snowfall of 2011 was on November 17 (image acquired on November 10); therefore this is not related to snow. These

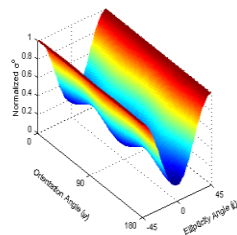
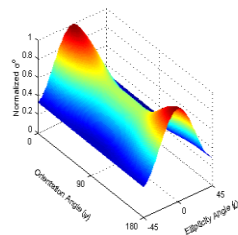
peaks were also apparent to a lesser degree in the cross-pol signatures derived from the Marlborough Forest April imagery which was acquired at a shallow incident angle.

Swamp was confirmed in the field at Loch Garry and Marlborough Forest, and as spring Loch Garry Radarsat-2 imagery were not acquired, only Marlborough Forest was assessed. For Marlborough Forest, image availability for both March 29 (steep incidence angle) and April 10 (shallow incidence angle) provided a comparison opportunity. The polarimetric signatures for both dates generally indicated multiple scatterers, however peaks were apparent in the cross-pol signatures. These peaks are more apparent where the canopy is open and the signal penetrates to a water surface which can be interpreted as double-bounce scattering. Figure 5.17 provides examples of the multiple scatterer signatures obtained for the Swamp sites. The odd peaks are circled in blue (Figure 5.17B2) showing that at a shallow incidence angle where water is present in an open canopy, multiple scattering occurred, including significant double bounce.

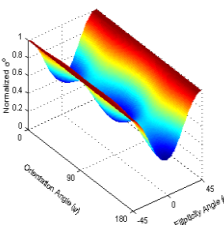
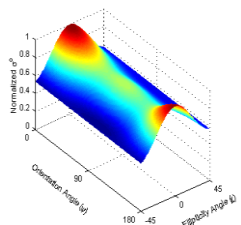
Fen was observed at Loch Garry and Marlborough Forest but as stated above, only Marlborough Forest imagery was available. Spring Fen polarimetric signatures follow the multiple scatterer model, typically showing one broad peak for co-pol and multiple troughs for cross-pol, and indicating grasses, water, and in some cases, shrubs. Figures 5.18A1 and A2 show little difference in the signatures between incidence angles for a large meadow grassy fen at the Marlborough Forest site.

Co-pol

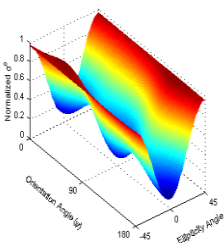
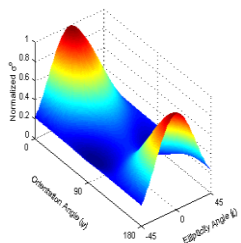
Cross-pol



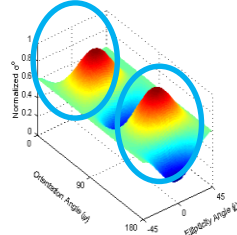
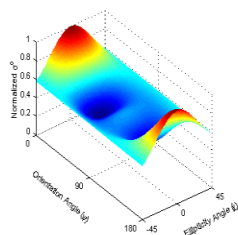
A1) Swamp Polarimetric Signature: Marlborough Forest, March (Steep Incidence Angle)



A2) Swamp Polarimetric Signature: Marlborough Forest, April (Shallow Incidence Angle)



B1) Swamp Polarimetric Signature: Marlborough Forest, March (Steep Incidence Angle)



B2) Swamp Polarimetric Signature: Marlborough Forest, April (Shallow Incidence Angle)

Figure 5.17. Polarimetric signatures for (A1 & B1) Swamp at steep (18.4° - 20.4°) incidence angles and (A2 & B2) at shallow (46.8° - 48.0°) incidence angles at Marlborough Forest in the spring 2010.

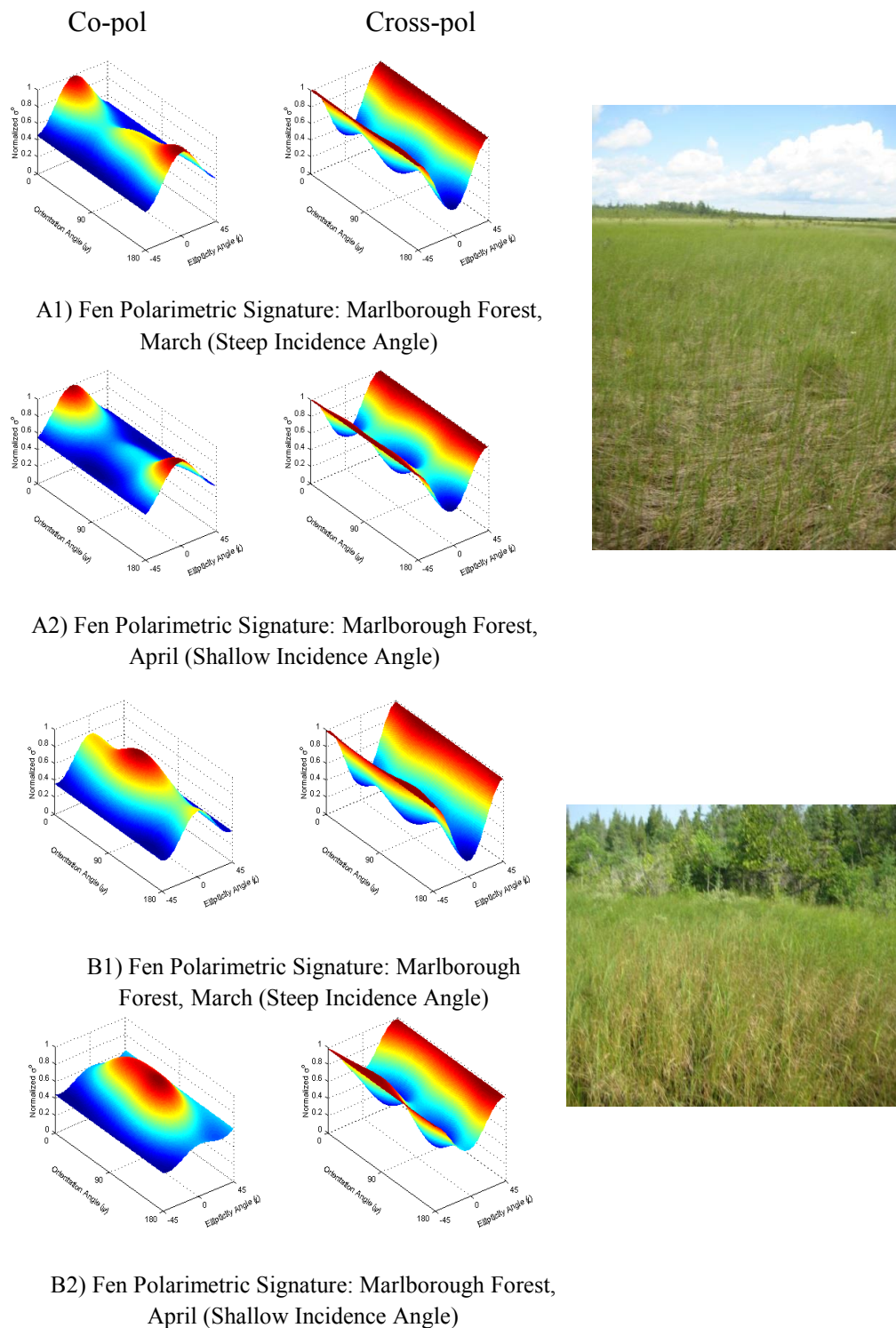


Figure 5.18. Polarimetric signatures for (A1 & B1) Fen at steep incidence angles and (A2 & B2) at shallow incidence angles at Marlborough Forest in the spring 2010.

Bog was observed at Mer Bleue Bog and Westport Bog and polarimetric signatures were obtained for these during the spring (Westport Bog) and the fall (Mer Bleue Bog) at steep incidence angles. The results obtained for the fall imagery are similar to those for spring, indicating that fall imagery might be useful as a substitute for, or in tandem with spring imagery. The signatures for both bogs and seasons mostly follow a surface scatterer model (e.g., Figure 5.19A, Mer Bleue Bog fall site #2), with one site (Figure 5.19B, Westport Bog spring site #3) mimicking a multiple scatterer model.

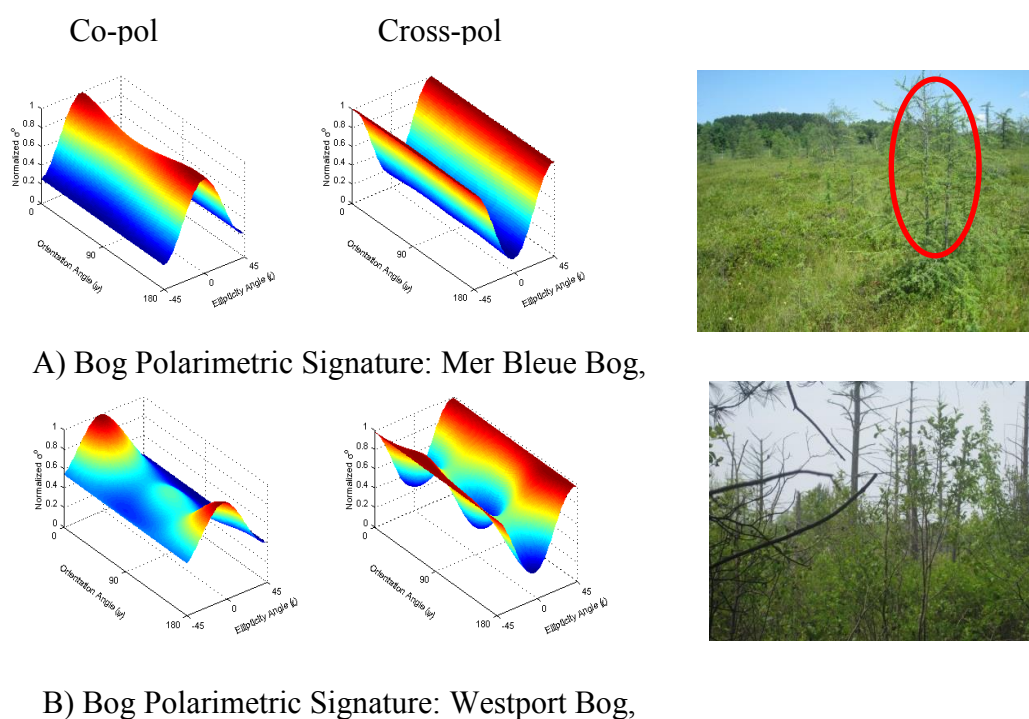


Figure 5.19. Polarimetric signatures for Bog in the fall (A, Mer Bleue Bog) and in the spring (B, Westport Bog) at steep incidence angles. Red circle highlights presence of sporadic tamarack.

The taller canopy of trees at Westport Bog could be responsible for the multiple scattering response. The other bog sites were comprised mostly of short shrubs that had a continuous, smooth canopy with minor, sporadic seedlings/trees (e.g., Figure 5.20B, red circle).

Table 5.10 lists the maximum, minimum and average co- and cross-pol pedestal heights per land cover across all four sites for spring/fall (merged to obtain pedestal heights for all Wetland Types), and summer and Figures 5.20 A-D are their respective graphical representations. In general in the literature, as pedestal height increases, diffuse scattering increases and depolarization increases (Evans *et al.*, 1988; Boerner *et al.*, 1998; McNairn *et al.*, 2002; Touzi *et al.*, 2004). Therefore, it would be expected that areas with increasing backscatter, caused by increased volume or multiple surface scattering, would have increasing pedestal heights (McNairn *et al.*, 2002). By manipulating the data together in simple mathematical terms such as summation, it would be expected that differences between scatterer groupings would be enhanced (in a manner similar to a simple vegetation index ratio of NIR/R), especially with the summer data when the differences between the groups are more pronounced. Water and Marsh areas would have contributions of non-depolarised surface scattering, whereas Swamp and Upland would have greater depolarised response and volume and multiple scattering from within the canopies and from trunk-water double bounce (Evans *et al.*, 1988; Boerner *et al.*, 1998; McNairn *et al.*, 2002; Touzi *et al.*, 2004).

Table 5.10. Minimum, maximum and average co- and cross-pol pedestal heights from training areas from the steep incidence angle spring/fall and summer imagery.

			Water	Upland	Fen	Bog	Marsh	Swamp
Spring	Co-pol	Minimum	0.08	0.15	0.11	0.14	0.10	0.12
		Maximum	0.41	0.64	0.45	0.39	0.46	0.32
		Average	0.21	0.45	0.30	0.28	0.22	0.24
	Cross-pol	Minimum	0.03	0.07	0.07	0.07	0.06	0.10
		Maximum	0.25	0.51	0.30	0.27	0.41	0.23
		Average	0.10	0.34	0.18	0.18	0.17	0.17
Summer	Co-pol	Minimum	0.04	0.31	0.20	0.16	0.02	0.28
		Maximum	0.25	0.42	0.47	0.33	0.37	0.44
		Average	0.16	0.37	0.36	0.26	0.19	0.37
	Cross-pol	Minimum	0.01	0.16	0.15	0.10	0.02	0.20
		Maximum	0.09	0.29	0.34	0.21	0.32	0.34
		Average	0.05	0.25	0.26	0.17	0.20	0.26

Spring/fall co- and cross-polarized pedestal values had similar minimum values (0.08 – 0.15, and 0.03 to 0.10, respectively) and maximum values (0.32 to 0.64 and 0.23 to 0.51, respectively) for all classes. Average pedestal height ranged from 0.21 to 0.45 and 0.10 to 0.34, for co- and cross-pol data, respectively (Figures 5.20 A and C).

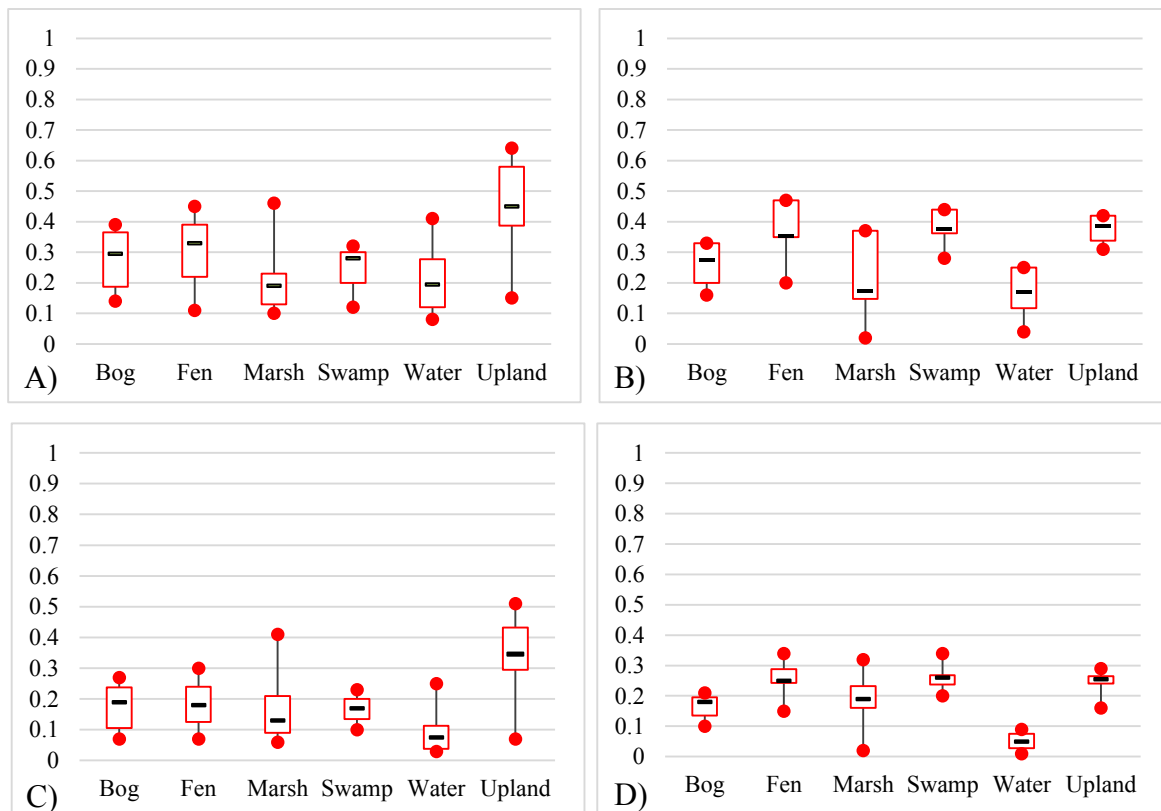


Figure 5.20. (A & C) Spring/fall co- and cross-pol pedestal maximum and minimum heights; (B&D) Summer co- and cross-pol pedestal maximum and minimum heights. Black dashes represent the median. Pedestal height is normalized to 1.00 (vertical axis); land cover type (horizontal axis).

There are notable differences between land cover types for summer pedestal height ranges and averages. The most apparent is in the co-polarized pedestal heights where three groups emerge (Water/Marsh ‘Group 1’ with the lowest values; Swamp/Upland ‘Group 2’ with moderate values; Fen/Bog ‘Group 3’ with the highest values). Manipulations of the

summer pedestal heights were attempted to see if these relationships could be enhanced; they included taking the summation, difference, and the cross-pol: co-pol ratio. Summation of the pedestal heights provided the greatest enhancement of the difference between minima and averages for the land cover types. Appendix I provides the original spring and summer co- and cross-pol data, and the other enhancements. Table 5.11 and Figure 5.21 show the summation of the maximum, minimum and average co- and cross-pol pedestal heights per land cover across all four scenes for summer.

Table 5.11. Minimum, maximum and average summed co- and cross-pol pedestal heights for samples extracted from the steep incidence angle summer imagery.

			Group 1		Group 2		Group 3	
			Water	Marsh	Fen	Bog	Upland	Swamp
Summer	Summed Co- and Cross- polarisation	Minimum	0.05	0.04	0.35	0.26	0.47	0.48
		Maximum	0.32	0.64	0.77	0.53	0.69	0.78
		Average	0.21	0.39	0.61	0.42	0.62	0.63

The minimum values for each of the three groups were distinct; the average values were less distinct as Fen, Uplands and Swamp averages were very close (0.61, 0.62 and 0.63), as were Marsh and Bog (0.39 and 0.42). The maxima overlapped between all groups. Figure 5.22 graphically shows the minimum pedestal height split between the three groups. In the literature pedestal height has been used as an indicator of the number and type of scatterers present, and the degree to which the signal is depolarized. The land covers with the least number of expected scatterers would be Marsh and Water, as both only have the contributions of water and some emergents (in the case of Marshes, usually large continuous homogenous areas of cattails) and there would be minimal depolarisation. Analysis of some the Marsh polarimetric signatures showed double-bounce (that would indicate more

scatterers then expected), while from the polarimetric signatures, Fen seemed to be generally the Wetland Type with more single surface scattering behaviour.

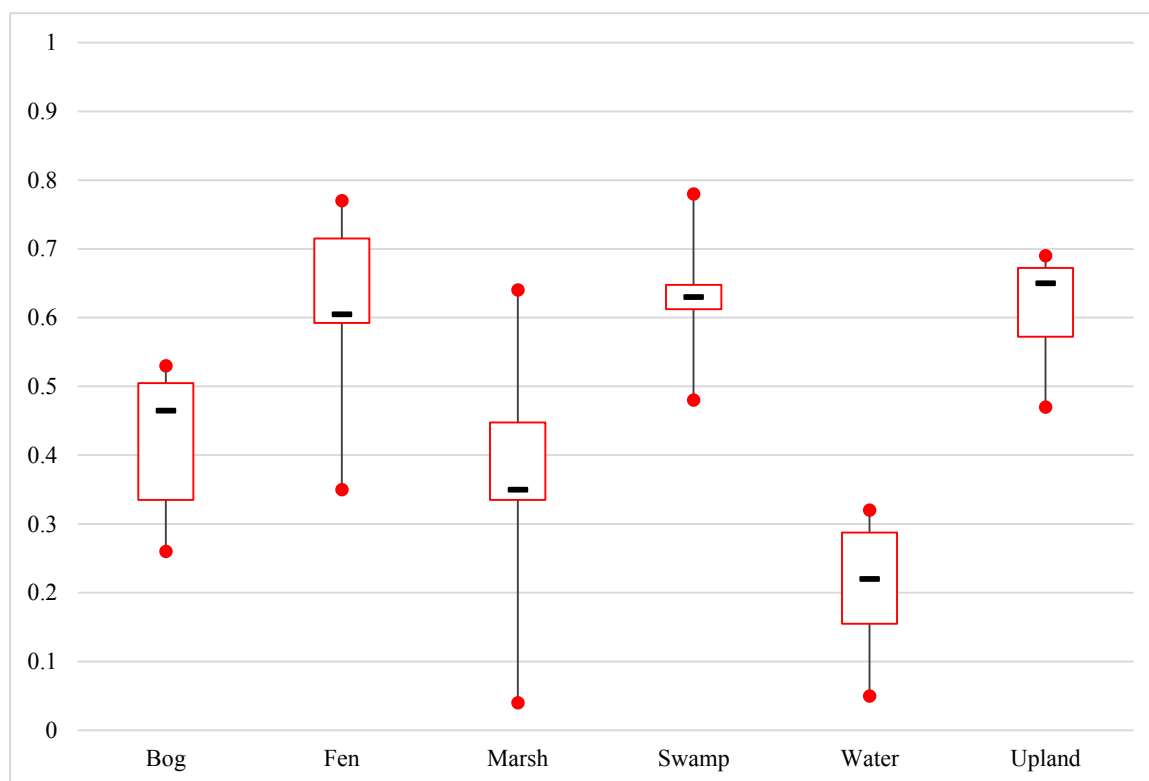


Figure 5.21. The summation of the summer co- and cross-pol minimum pedestal heights (lower red dots) and maximum heights (upper red dots). Black dashes represent the median. Pedestal height was normalized to 1.00 (vertical axis). Group 1 is Bog and Fen, Group 2 is Marsh and Water and Group 3 is Swamp and Upland as described in the text.

Fen and Bog would be expected to have the least number of types of contributing scatterers, which in these cases and based upon their pedestal heights was confirmed. Upland and Swamp should have the more types of contributing scatterers, including volume scatterers with the addition of some trunk-water double-bounce scatterers, as well as the greatest amount of depolarisation; this was borne out in these data. The pedestal heights were averaged across all sample sites, and are representative of the generalized scattering response of the Wetland Types, more so, it appears, than what was determined through the visual analysis of the polarimetric signature graphs.

Entropy, anisotropy and alpha components were derived from the Loch Garry summer Radarsat-2 image and used in pixel-based MLC and CTA classifications as well as in object-based segmentation (in addition to WorldView-2 imagery and the DEM) and classification to see if they improved mapping accuracies for Wetland Type. They were also used in a Wishart unsupervised classification. Figure 5.22A shows the spring WorldView-2 CIR composite and Figures 5.22B - D show the three CP components. Apart from being noisy, it can be seen in the entropy image that low values (e.g. water, red circle) indicate that there was no significant mixing of scattering mechanisms and a low degree of randomness.

Alpha identifies the dominant scattering mechanism; as expected low values (dark areas in the created image) occurred for water bodies (Loch Garry, and the small lake to the North) indicating surface scattering. The brighter areas (red arrows) along the shoreline were where there was fen and a large dead coniferous swamp, both indicating double bounce and multiple scatterers. Fen should have mostly surface scattering with some contributions from volume scattering and double-bounce scattering, as the Fen in this area contained sporadic tamarack, woody vegetation and some more open water presence in comparison to the Fens in Marlborough Forest, which were mostly grassy meadows. Swamp in this area included significant proportions of dead coniferous trees, and therefore volume, multiple and double-bounce would be expected, resulting in high alpha values and bright tones in the alpha image.

Anisotropy provides an indication of the mixing between the second and third scattering mechanisms, higher values (brighter tones in the anisotropy image produced) indicating that the second mechanism is dominant. It does not make sense that areas with

low entropy and one expected dominant scattering mechanism (red circles) would also have high anisotropy, indicating a second scattering mechanism is present. As the image was acquired in mid-summer, and these areas are in open water about 1 km from shore, the second mechanism may be Bragg scattering from surface waves, although this was not verifiable.

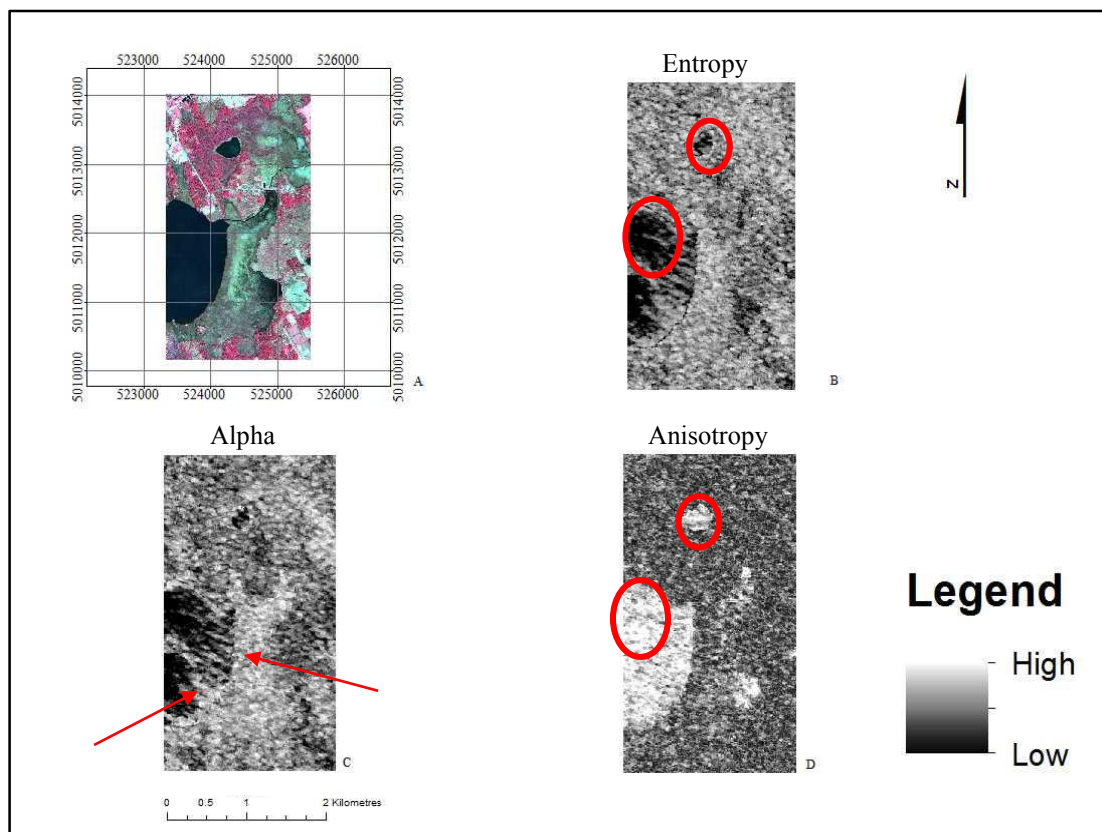


Figure 5.22. A) WorldView-2 CIR composite and CP variables of B) entropy, C) alpha and D) anisotropy derived from summer 2010 Loch Garry Radarsat-2 imagery.

Table 5.12 provides the overall accuracy results of the classifications for Wetland Type at Loch Garry using spring and summer WorldView-2 imagery (four spectral bands), the DEM, and summer CP variables in Wishart, MLC, and CTA classification, respectively. Overall, it was found that the Wishart unsupervised and MLC classifications using the CP variables alone did not provide good discrimination amongst the Wetland Types. Combining

CP variables with optical and DEM data, improved overall accuracy for the summer season for Loch Garry, but did not improve the overall accuracy over optical imagery alone for the best season (spring) (for Loch Garry or for the other three sites). Fen class (orange highlight) improved in accuracy over all seasons.

5.1.4 Summary of main findings for Wetland Type

The following are the main findings from the optical analyses:

- Optimal segmentation parameters determined for WorldView-2 were scale value of 45, shape value of 0.1 and compactness value of 0.75; and for Landsat 5 TM imagery (original data and LSU) were scale value of 2, shape value of 0.1 and compactness value of 0.1;
- CTA was on classification of test site had higher accuracy than MLC for almost all classes;
- 5-classes (Water, Upland, Fen, Swamp and Marsh) using merged non-wetland terrestrial classes had higher accuracy than 7-classes (Water, Forest, Short Vegetation, Impervious (Roads), Fen, Swamp and Marsh);
- WorldView-2 imagery provided a higher accuracy than Landsat 5 TM imagery for this type of classification; and
- Landsat 5 TM imagery was not as useful as WorldView-2 imagery except for a few classes (e.g. Fen or Swamp), with poorer results for Marsh due to spatial resolution and extent of the imagery.

Table 5.12. Accuracies (%) for Loch Garry utilizing the WorldView-2 imagery (four spectral bands), the DEM, summer CP variables images for a Wishart unsupervised, MLC, and CTA classifiers. Orange highlight shows that the Fen improved with the addition of the CP variables.

	Overall Accuracy (%)	Overall Kappa	Water		Upland		Fen		Swamp		Marsh		Average	
			PA (%)	UA (%)	PA (%)	UA (%)								
WorldView-2 and DEM only (spring; object-based; CTA)	86.5	0.82	100.0	100.0	81.3	100	80.0	100	100.0	58.3	75.0	100	87.3	91.7
WorldView-2 and DEM only (summer; object-based; CTA)	70.3	0.59	60.0	100.0	100.0	88.9	40.00	50.0	28.6	40.0	75.0	42.9	60.7	64.4
Wishart Unsupervised (summer; pixel-based)	35.1	0.26	100.0	83.3	14.3	50.0	16.7	25.0	66.7	66.7	16.7	33.3	42.8	41.7
CP variables & MLC; (summer; pixel-based)	39.5	0.26	50.0	60.0	45.5	33.3	80.0	44.4	42.9	37.5	28.6	40.0	49.4	43.0
WorldView-2, DEM, and CP variables (summer; object-based; CTA)	83.3	0.79	100.0	100.0	63.6	87.5	100.0	100.0	100.0	55.6	71.43	100	87.0	88.6

The following are the main findings from the radar analyses:

- Spring, steep (18.4° - 27.6°) incidence angle backscatter images showed better separation between Wetland Type classes than spring, shallow (46.8° - 48.0°) incidence angle, or summer and fall HH, HV images;
- OBIA and CTA classification of HH, HV images alone, or combined with optical imagery and a DEM did not improve overall accuracies but the accuracy of the Swamp class improved;
- The summation of the summer co- and cross-pol pedestal minima showed good distinction amongst groupings of classes (Water/Marsh ('Group 1'; Swamp/Upland 'Group 2'; and Fen/Bog 'Group 3), which related directly to the signal depolarisation of the waves and types of scatterers present; and
- OBIA and CTA classification using CP variables alone, or combined with optical imagery and a DEM improved overall accuracies for one season for one site, and did not have a higher accuracy than the best season optical results; however the accuracy of the Fen class improved overall.

5.2 VCFs

The OWES categorizes VCFs as 14 dominant classes (Figure 3.8). A form must represent approximately 25% of the vegetation community to be recorded. VCFs can be present in various numbers and types within a given Wetland Type. Many of the same

methods applied for Wetland Type were applied to VCFs and the results are summarized (to avoid repetition) in the following sections.

5.2.1 VCF classification using OBIA and 2010 spring WorldView-2 imagery

The optimal OBIA parameter values for VCF were: scale value = 25; shape value = 0.1; and compactness value = 0.75. Figure 5.23 provides an example of the objects that were created using these parameters. Yellow outlines show objects that represent specific vegetation communities and they are accompanied by corresponding field photographs.

Using the segmented WorldView-2 and DEM data, CTA was implemented for both the VCF class types and the number of forms (0 – 3 forms (Class A); 4-5 forms (Class B); > 6 forms (Class C); see Section 2.9.2 for details). Table 5.13 provides the accuracy analysis for Number of Forms. Westport Bog had the highest overall accuracy (70.1%); Marlborough Forest had the lowest accuracy (53.1%). The classes with the best and worst overall results were Class A and Class B with an average of 57% and 59% PA and UA, respectively. Class C had very high PA (average of 93.8%) but extremely poor UA (average of 29.4%).

Figure 5.24 provides a visual representation of the highest accuracy results for the Number of Forms classification (Westport Bog). Figure 5.24A shows the entire Westport Bog area classified as classes A, B, and C. Class A (1 to 3 forms) has the largest spatial extent and is distributed throughout the map. The large patch of Class B in the southwest (black circle) is a forested area observed in the field, which is comprised of mixed deciduous and coniferous species.

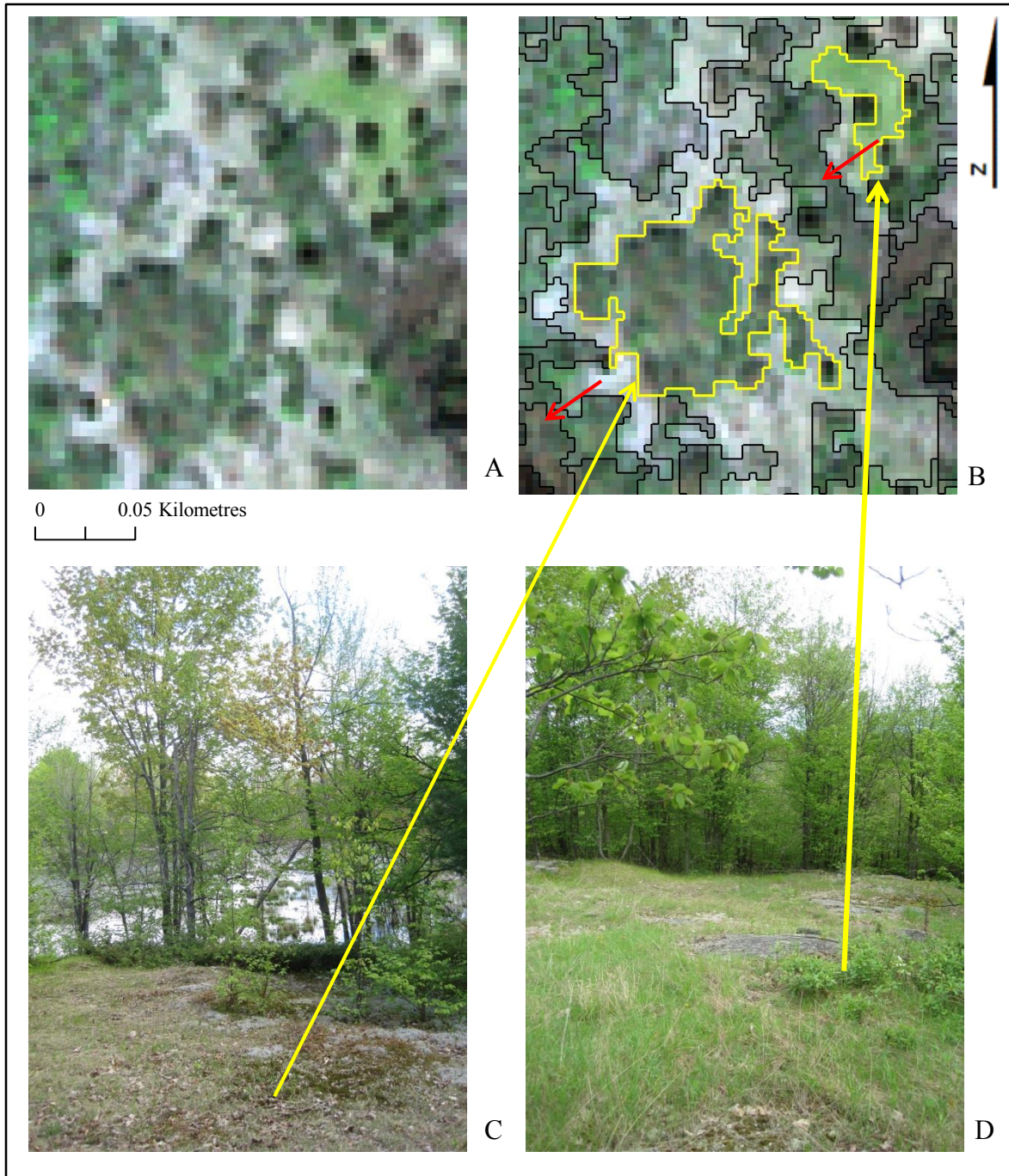


Figure 5.23. A) Spring 2010 WorldView-2 true colour composite of Westport Bog; B) WorldView-2 and DEM segmented imagery (scale = 25, shape = 0.1; compactness = 0.75) with yellow outlines of objects representing vegetation communities; C) field photograph of open, bare rock/lichen covered rock that grades to shrubs/saplings, a small tree stand and then water; and D) grassier open community surrounded by a deciduous forest stand. Yellow arrows point to locations of photos. Red arrows indicate the view direction of the photos.

Table 5.13. CTA accuracies (%) for Number of VCFs for the four sites. Input data were: segmented spring WorldView-2 imagery (four spectral bands) and the DEM. Classes A, B and C represent 1 to 3, 4 to 5, and 6 or more forms, respectively.

	Overall Accuracy (%)	Kappa	A		B		C		Average	
			PA (%)	UA (%)	PA (%)	UA (%)	PA (%)	UA (%)	PA (%)	UA (%)
Loch Garry	60.0	0.37	50.0	83.3	63.6	53.9	75.0	50.0	62.9	62.4
Marlborough Forest	53.1	0.13	54.3	76.0	41.7	27.8	100.0	33.3	65.3	45.7
Westport Bog	70.1	0.46	71.4	79.0	66.7	80.0	100.0	20.0	79.4	59.7
Mer Bleue Bog	65.7	0.39	68.2	79.0	58.3	77.8	100.0	14.3	75.5	57.0
Average Accuracy (%)			61.0	79.3	57.5	59.9	93.8	29.4		

As highlighted in Figure 5.24B, the bog area shows a predominance of Class C representing six or more forms, which corresponds to field observations. The bog communities in Westport Bog consist of both open and treed bogs with multiple species present (see Section 3.1 for descriptions). Along the edges of the bog are areas of 1 to 3 forms (Class A, red) which are representative of the lagg area circled in blue circle that is dominant around this particular bog and were observed in the field.

Table 5.14 provides the VCF classification accuracies for the four study sites. The overall accuracy for three of the wetlands was similar (Loch Garry, Mer Bleue Bog and Westport Bog), but it was much poorer for Marlborough Forest. The classification results for both VCF type and Number of Forms, and particularly the consistency across the sites suggested that further investigation using summer imagery was warranted (see Section 5.7).

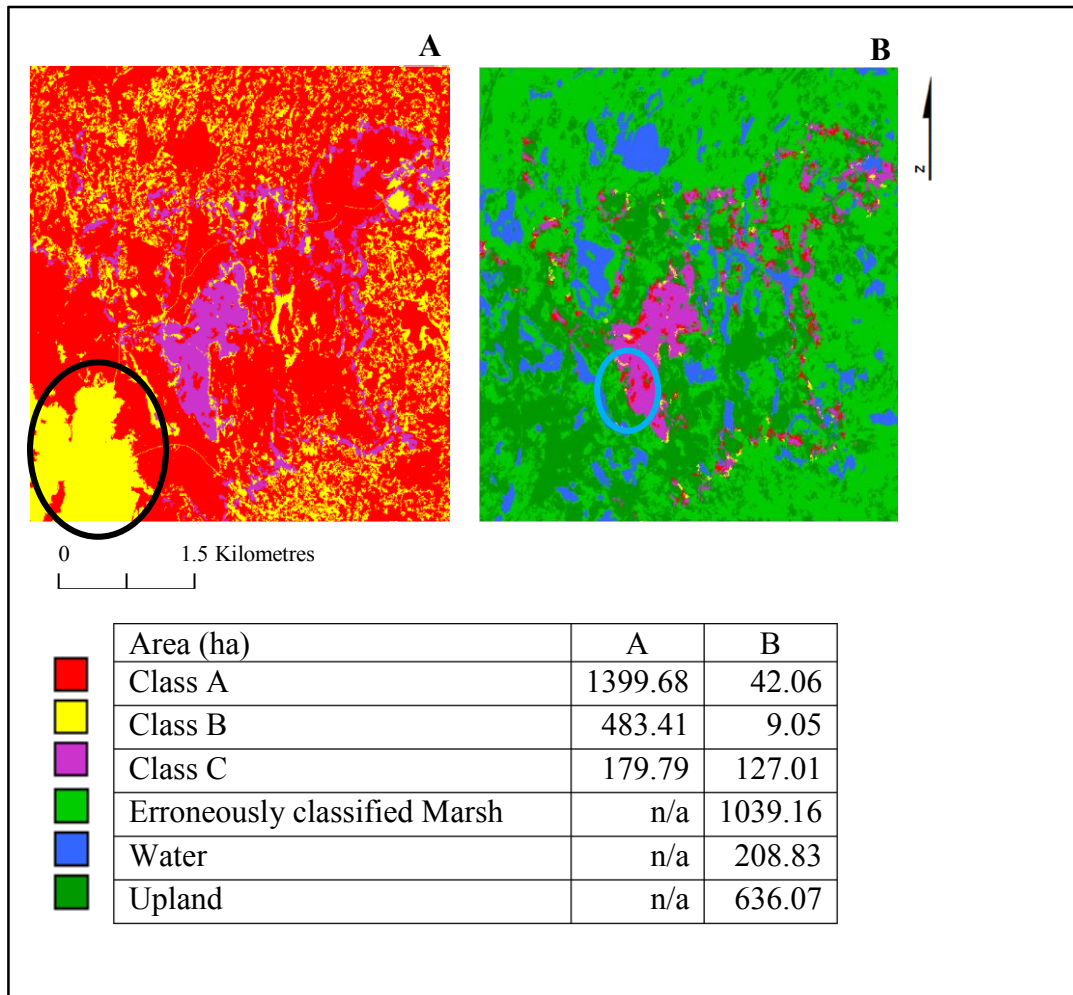


Figure 5.24. A) Number of VCFs (Class A: 1-3; B: 4-5; C: > 6) classification of Westport Bog; B) the same area with an Upland and Water Mask. The Marsh class of the Wetland Type classification (Appendix F, Figure F6) was considerably over-classified, and thus it has been masked as well.

These attribute types are related to the types of vegetation present, and in the spring would be at the earliest point of their seasonal lifecycle; in the summer the physical differences between the vegetation would be more apparent.

5.2.2 VCF classification using OBIA and 2010 spring Landsat 5 TM imagery

Small scale values produced objects that were visually more representative of VCFs than larger values, however, values less than 2 did not produce further significant reduction in object sizes. From these analyses, it was decided that the optimal segmentation parameter values for delineation of objects that represented observed groupings of VCFs were: scale value = 2, shape value = 0.1 and compactness value = 0.1. Based upon the results for Wetland Type classification, CTA classifications using the unsegmented fraction maps (5 EMs) plus DEM, and the segmented original spectral band data plus DEM were implemented for comparison (Table 5.15). In general, the VCF classifications were very poor, which was expected at this spatial resolution. For the three-form classification, the sites with the highest overall accuracies were Marlborough Forest and Westport Bog. While Westport Bog was also well classified using the WorldView-2 imagery, Marlborough Forest had the poorest accuracies with that imagery. The best results for each site type for this attribute (3 form) were obtained using the segmented original Landsat bands plus DEM. Kappa values for all tests were very low and in some cases negative, which indicate these results are no different than from a random assignment of the classes. Since all combinations of the available Landsat data and DEM did not produce acceptable results, it was decided that further investigation using the summer imagery would not be completed.

Table 5.14. CTA accuracy statistics for the VCFs including accuracies (%) for the four sites. Input data were the segmented spring WorldView-2 imagery (four spectral bands) and the DEM (see Section 2.9.2 for descriptions of each class).

	Overall Accuracy (%)	Kappa	C (Coniferous Dominant)		DC/DH (Dead Dominant)		GC (Herb Dominant)		H (Hardwood Dominant)		Other		(Split/ Additional Other Class) Emergent Dominant		Split/ Additional Other Class) Shrub Dominant		Average	
			PA (%)	UA (%)	PA (%)	UA (%)	PA (%)	UA (%)	PA (%)	UA (%)	PA (%)	UA (%)	PA (%)	UA (%)	PA (%)	UA (%)	PA (%)	UA (%)
Loch Garry	68.8	0.60	62.5	55.6	83.3	83.3	80.0	66.7	60.0	85.7	66.7	50.0	n/a	n/a	n/a	n/a	70.2	57.0
Marlborough Forest	44.9	0.32	45.5	41.7	40.0	20.0	33.3	28.6	42.8	75.0	n/a	n/a	54.5	60.0	50.0	50.0	44.4	39.4
Westport Bog	67.7	0.58	n/a	n/a	n/a	n/a	100.0	62.5	54.5	66.7	100.0	100.0	44.4	80.0	85.7	60.0	75.4	61.6
Mer Bleue Bog	68.6	0.58	100.0	60.0	n/a	n/a	100.0	50.0	66.7	80.0	n/a	n/a	100.0	75.0	50.0	70.0	80.9	55.9
Average Accuracy (%)			69.3	52.4	61.6	51.6	78.32	51.9	56.0	76.84	83.35	75.0	66.3	71.7	61.9	60.0		

Table 5.15. Summary of the Landsat CTA accuracy statistics for the 3 form (A, B, C) and VCFs providing accuracies (%) for the four sites. Loch Garry, Mer Bleue Bog and Marlborough Forest were processed using an April 2010 image and Westport Bog was processed using a March 2010 image. Yellow shading highlights the highest accuracy per site.

	5 fraction maps not segmented with DEM				Original bands segmented with DEM			
	3 Forms		VCF		3 Forms		VCF	
	Accuracy (%)	Kappa	Accuracy (%)	Kappa	Accuracy (%)	Kappa	Accuracy (%)	Kappa
Loch Garry	36.00	0.08	43.75	0.30	36.00	0.06	34.37	0.18
Mer Bleue Bog	34.29	-0.02	54.29	0.37	40.00	0.17	34.28	0.18
Marlborough Forest	48.98	0.05	38.77	0.24	65.31	0.29	46.94	0.33
Westport Bog	20.59	-0.08	44.12	0.31	64.71	0.26	35.29	0.21

5.2.3 VCF classification using Radarsat-2 data

It was very difficult to get a consistent set of sample sites (e.g., 5 sites with combinations of VCF classes H, LS, DS, GC, M, NE; see Appendix B, Table B1) because of the overall diversity in the community forms across eastern Ontario. Thus, it was difficult to compare “similar” community forms between sites because they were, in many cases, not that similar. Because of the nature of this analysis, and for clarity, the analysis of other seasons (summer and fall) are included in this section.

HV and HH images were derived and samples were extracted at field validation locations for some of the VCFs (where there were several sites of same/similar types, sampled across eastern Ontario at all complexes (4), for all seasons of data (3), and for all incidence angles (ranging from steep to shallow (18.4° to 48.0°)). The training areas for VCFs were limited across eastern Ontario (e.g. often 1 or 2 sites) making these results fairly

qualitative and subjective. It was decided to stratify the analysis by Wetland Type, and plant types/groups (e.g. sedge, cattail, hardwood, etc.; not specifically the VCFs of the OWES, but similar and based upon field surveys) using backscatter. It was found that separation of particular plant types/groups could be obtained for some Wetland Types. Figure 5.25 provides a representation of the plant types/groups found in bogs (Mer Bleue Bog and Westport Bog) for spring and fall imagery. In general there is little separation between bog plants, except for treed bogs (green circle). This concurs with the literature as treed wetland areas typically have greater backscatter due to volume scattering, and greater depolarisation (Leckie and Ranson, 1998; Henderson and Lewis, 2008).

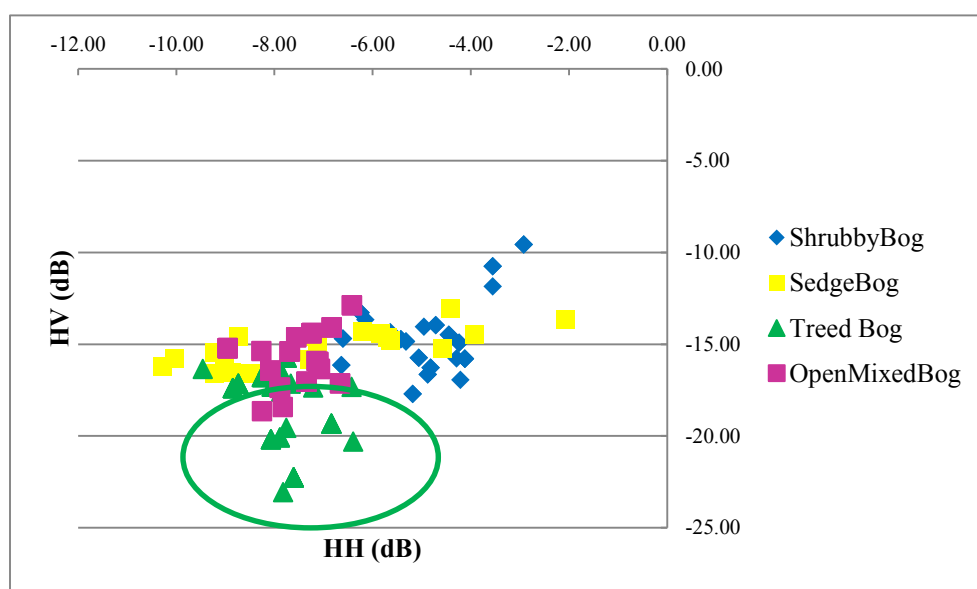


Figure 5.25. Spring step incidence angle backscatter for different bog plant types/groups. The only noticeably separate plant type/group is treed bogs (green circle).

Figure 5.26 shows the different plant types/groups found in marshes in summer. The separation between the three vegetation types for marsh is apparent. There is some overlap

between the free floaters (e.g. duckweed, pondweed, etc.) and the shrubby/cattails communities (purple and blue) which might be related to the mixture of these plant types/groups and scattering properties. The cattail sites were homogeneous, smooth and dense; the free floater site consisted of a large mat of free floating plants, and the shrubby/cattails sites consisted of low shrubs, robust emergents, and narrow leaved emergents.

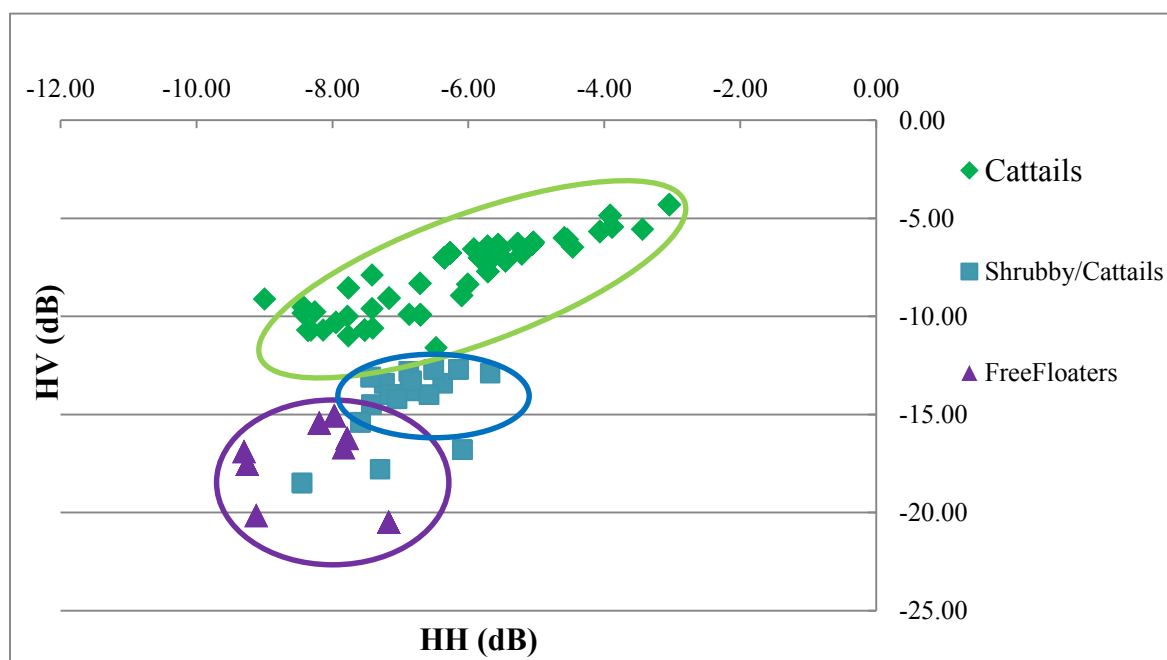


Figure 5.26. Comparison of backscatter obtained for different plant types/groups at marshes. There is distinct separation between all three plant types using summer imagery.

Figure 5.27 shows the separation in backscatter between plant types/groups in fens during the spring. There appears to be some overlap between the low shrub and sedge communities, again, due to mixing of these two groups. Low shrub communities appear to

cluster at a specific range of HH, HV values (e.g. HH between -8 to -10 dB and HV between -15 to -20 dB).

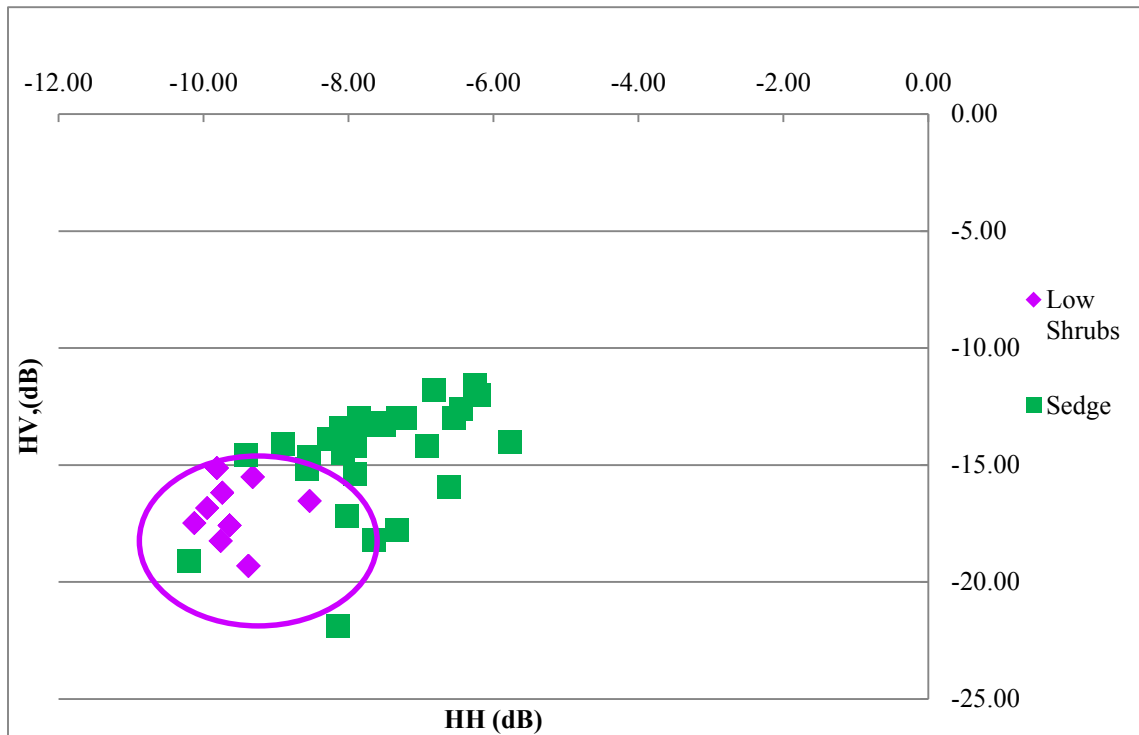


Figure 5.27. Comparison of backscatter obtained for different plant types/groups at fens. There is separation between the two groups using spring imagery. HH and HV values derived from summer imagery acquired at steep incidence angles.

Figure 5.28 provides the backscatter results for hardwood and mixed swamps during spring. There is distinct separation between them related to the presence of conifers in the mixed swamps that were not present in the hardwood swamps. This is particularly noticeable in spring when the hardwood swamp deciduous foliage has not yet flushed, therefore there would a contribution from double-bounce scattering with trunk-water interactions.

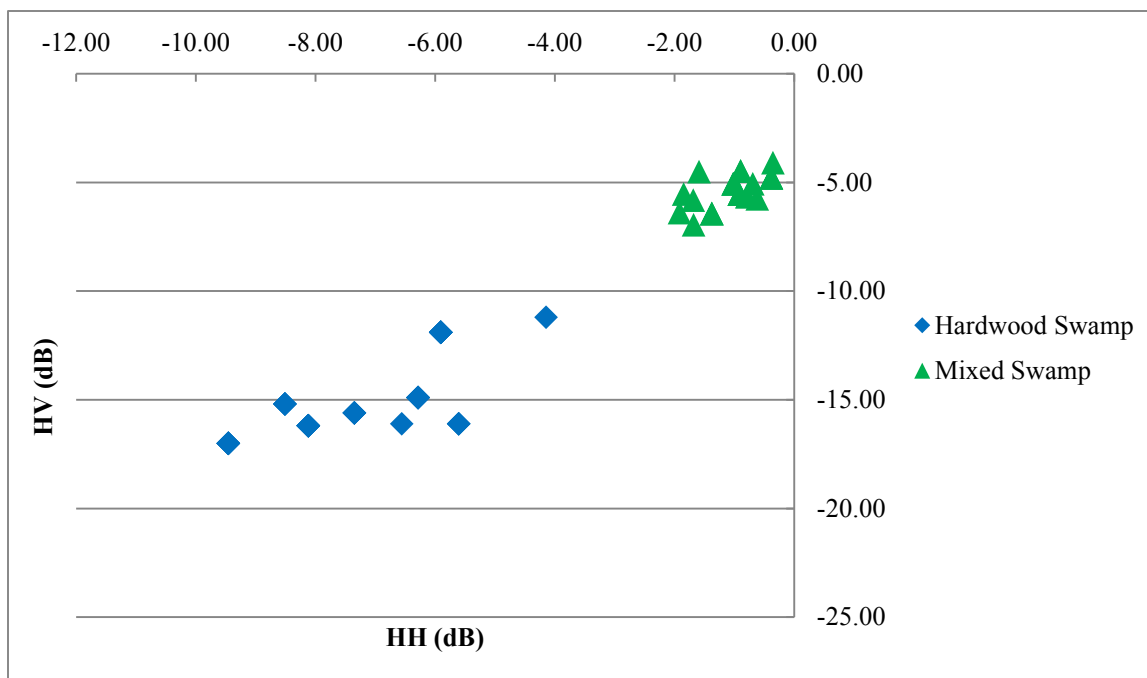


Figure 5.28. Comparison of backscatter obtained for different plant types/groups at swamps during spring. There is separation between hardwood and mixed swamp communities.

Additional analysis, segmentation, and classification of VCFs, Number of Forms, or plant types, with the backscatter images and the CPs variables provided very poor results and, therefore, they were not presented in this thesis.

5.2.4 Summary of main findings for VCF classification

- Optimal segmentation parameters determined for WorldView-2 were scale value of 25, shape value of 0.1 and compactness value of 0.75; and for Landsat 5 TM imagery (original data and LSU) were scale value of 2, shape value of 0.1 and compactness value of 0.1;

- WorldView-2 imagery provided higher VCF classification accuracy than Landsat 5 TM imagery;
- Separation of particular plant types/groups could be obtained for some Wetland Types with spring backscatter imagery showing good separation for Fen and Swamp plant types and summer imagery provided good separation for Marsh plant types; and
- Object-based CTA using HH, HV images and CP variables alone, and combined with optical imagery and a DEM did not improve overall accuracies or accuracies of individual plant types.

5.3 Open Water Type

There are eight categories of Open Water Types outlined in the OWES manual (Table 3.3). Many of the same methods applied for Wetland Type and VCFs were applied to Open Water Types and the results are given in the following sections.

5.3.1 Open Water Type classification using OBIA and 2010 spring WorldView-2 imagery

The optimal segmentation parameter values were scale value = 25, shape value = 0.1, and compactness value = 0.75. Table 5.16 provides the CTA accuracy results for the four study sites. The site with the highest accuracy was Loch Garry (73.3%), while the poorest was Marlborough Forest (40.0%). In general, the classification results were poor, which could be related to the small amount of reference data. The imagery itself was not useful in

providing additional samples. Only Open Water Types in wetland areas are considered in the OWES and this resulted in the following numbers of reference sample sites: Marlborough Forest (20 sites), Loch Garry (15 sites), Mer Bleue Bog (15 sites) and Westport Bog (20 sites) and by Open Water Type (Type 1 = 20; Type 2 = 7; Type 3 = 8; Type 4 = 4; Type 5 = 9; Type 6 = 6; Type 7 = 2; Type 8 = 6; and 8 that didn't have permanent open water (e.g. some bogs and some swamp)). The small numbers of potential sample locations per site and per class also made selecting samples difficult. Based on this, and since the spring results were so poor, it was decided not to conduct analysis using the summer WorldView-2 imagery, since many of the sample sites would be obscured by vegetation, reducing the sample size further.

Figure 5.29 shows the Open Water Type classification for Loch Garry. The yellow circle shows an area where a boardwalk traverses a mixed coniferous/deciduous swamp. In the spring, the canopy over the boardwalk is open, and around the boardwalk there is ponding and standing water. The red circle highlights ephemeral wetland/ponding found in the spring within mixed hardwood/coniferous forest. Other areas that were well classified based upon field knowledge include the areas around the smaller lake in the north which shows open water presence associated with marsh and fen vegetation that surrounds this lake. The black circle highlights an area where there was ponding, particularly with hummocks of marsh vegetation (reeds and cattails, etc.).

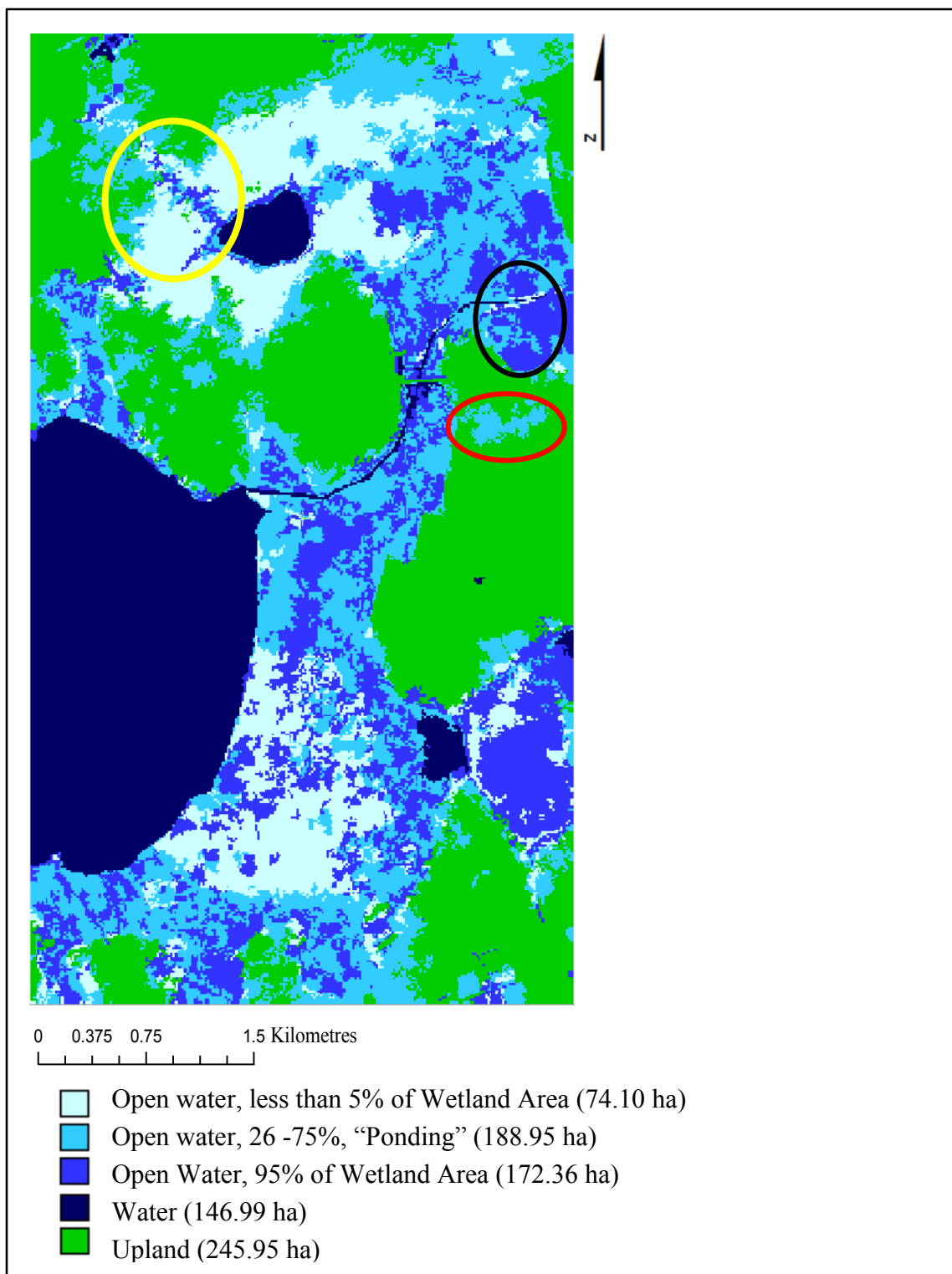


Figure 5.29. Object-based CTA Open Water Type classification of Loch Garry using spring 2010 WorldView-2 imagery and the DEM. The Water and Upland classes are taken from the Wetland Type classification (Section 5.1). Red, yellow and black circles highlight field-assessed areas that were well classified.

Table 5.16. OBIA CTA results for Open Water Type providing accuracies (%) for the four sites. Input imagery included the segmented spring 2010 WorldView-2 imagery (four spectral bands) and a DEM.

	Overall Accuracy (%)	Kappa	Type 1 (Occupies less than 5% of wetland area)		Type 2 (5 to 25% of wetland area, occurring in central area)		Type 5 (26 to 75% of wetland area (occurring with ponding))		Type 8 (Open water occupies more than 95% of wetland area)		Combined (4, and 6 and (when present) (26 to 95 % large central areas)		Average	
			PA (%)	UA (%)	PA (%)	UA (%)	PA (%)	UA (%)	PA (%)	UA (%)	PA (%)	UA (%)	PA (%)	UA (%)
Loch Garry	73.3	0.57	87.5	87.5	n/a	n/a	50.0	100.0	100.0	50.0	n/a	n/a	79.2	79.2
Marlborough Forest	40.0	0.26	50.0	33.3	100.0	33.3	12.5	33.3	40.0	66.7	50.0	50.0	50.5	43.3
Westport Bog	50.0	0.32	33.3	40.0	60.0	37.5	0.00	0.00	33.3	100.0	80.0	66.7	51.7	61.0
Mer Bleue Bog	73.3	0.57	87.5	100.0		57.1	n/a	n/a	n/a	n/a	0.0	0.0	62.5	52.4
Average Accuracy (%)			64.6	65.2	86.7	42.6	20.8	44.4	57.7	72.2	43.3	38.9		

5.3.2 Open Water Type OBIA classification using 2010 spring Landsat 5 TM imagery

The optimal segmentation parameter values were scale = 25, shape = 0.1, and compactness = 0.75. Table 5.17 shows the accuracy of Open Water Type classifications produced using Landsat 5 TM spring data with the same data configurations as noted for the VCF classifications.

Table 5.17. OBIA CTA results for Open Water Type providing accuracies (%) per site for the four sites. Input data included 5 fraction maps not segmented and the original segmented data both including the DEM. Yellow highlights the best results per class.

Wetland Complex	5 fraction maps not segmented with DEM		Original bands segmented with DEM	
	Open Water		Open Water	
	Accuracy (%)	Kappa	Accuracy (%)	Kappa
Loch Garry	53.0	0.10	93.0	0.87
Mer Bleue Bog	73.3	0.56	73.3	0.56
Marlborough Forest	45.0	0.32	60.0	0.48
Westport Bog	60.0	0.00	53.3	0.36
Average (%)	57.8		69.9	

Overall accuracies were higher for the Landsat TM data compared to the WorldView-2 data. Figure 5.30 provides a comparison for Loch Garry of the WorldView-2 derived thematic map (overall accuracy, 73%) and the two best Landsat TM derived thematic maps (overall accuracies of 80% (not shown in Table 5.17; derived using three EM fraction maps with the DEM) and 93%, respectively). Detail in the maps decreases from left to right (Figure 5.30A to C). For example, the detail around the boardwalk is lost in the

Landsat derived images (yellow circles). The results in terms of area of each Open Water Type were significant and there were no consistencies between them.

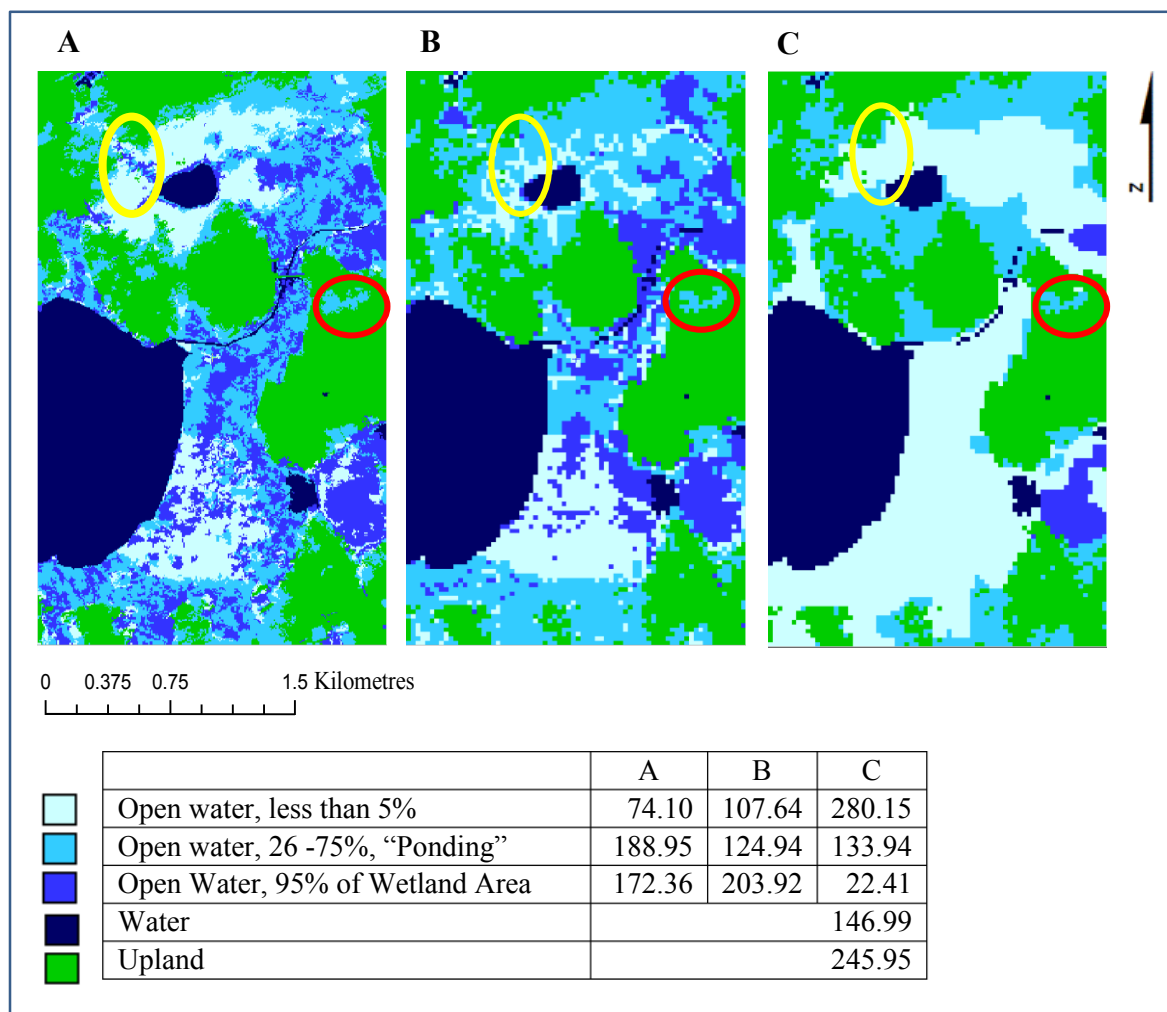


Figure 5.30. Loch Garry Open Water Type CTA classification. A) spring WorldView-2 imagery and DEM; B) Landsat TM imagery (3 EM fraction maps with DEM not segmented; and C) Landsat TM imagery (original bands and a DEM segmented). Water and Upland classes are from the WorldView-2 5-Class Wetland Type classification (Section 5.1). Yellow circles show detail lost at the Landsat scale around a boardwalk. Red circles show an ephemeral wetland captured in all three classifications.

Figure 5.30B shows more ‘ponding’ (medium blue) just to the north side of the small pond as compared to Figure 5.30A. This area corresponds to a treed swamp and the ponding shown in Figure 5.30B could be related to the 38.1 mm of rain received in the 7 days prior to Landsat image acquisition (April 13) (Environment Canada, 2013). In the following 12 days until WorldView-2 image acquisition there was an additional 16.1 mm of rain (last precipitation event on April 17) and the temperature was warm (average daily maximum of 15°C) resulting in drying (Environment Canada, 2013). The ‘ponding’ (medium blue) in Figure 5.30B could be more accurate than Figure 5.30C (the highest accuracy map, 93%) as validation sites in that area were captured along the narrow portion showed ponding around the boardwalk (detail in Figure 5.30A).

5.3.3 Summary of main findings for Open Water Type

- Optimal segmentation parameters determined for WorldView-2 were scale value of 25, shape value of 0.1 and compactness value of 0.75; and for Landsat 5 TM imagery (original data and LSU) were scale value of 2, shape value of 0.1 and compactness value of 0.1;
- Three Open Water Type classes (Type 1: Open Water, less than 5% of wetland area; Type 5: Open Water, 25% to 75% of wetland area, ‘ponding’; and Type 8: Open Water, 95% of wetland area) were discriminated in a generalized manner with average accuracies (%) across all four sites of: Type 1: PA = 76.0%, UA = 89.3%;

Type 5: PA = 83.3%, UA = 66.4%; and Type 8: PA=86.7%, UA=70.0% (Type 5 and 8 were not present in Mer Bleue Bog).

- Spring Landsat 5 TM imagery produced higher overall classification accuracies for Open Water Types than spring WorldView-2 imagery.

5.4 Inundation Extent

5.4.1 Pixel-based analysis of spring 2010 WorldView-2 imagery vegetation index relationships with VWC thresholds as an indicator of Inundation Extent

Vegetation indices were calculated from the WorldView-2 sharpened images, and compared to field measured VWC (%) on scatterplots. A relationship between measured VWC with vegetation indices was visualized from these graphs and assessed, but based upon the nature of the field data (e.g. strong autocorrelation in some transects; see Section 4.4.2) it was decided that statistical relationships (e.g. R^2 values; ranging from ~0.3 to 0.8) could be misleading. Overall, amongst all vegetation indices evaluated, the “best” relationship was with $NDVI_{Green}$, which could be related to the yellowness of the grasses/emergents in wetlands (particularly in the spring). In addition, $NDVI_{Green}$ also displayed a threshold relationship with 100% VWC. For example, at Mer Bleue Bog (Figure 5.31) $NDVI_{Green}$ ranged from about -0.025 to 0.075 where VWC was 100% or greater. Thus, pixels in this range were extracted from the $NDVI_{Green}$ image to map saturated areas. In contrast, NDVI did not produce clear relationships as NDVI values within a small range (about 0.25-0.35) corresponded to VWC across the full range from 0-100% (Figure 5.32).

Figure 5.31 shows an example subset of the 12 transects for Mer Bleue Bog and $NDVI_{Green}$. Although $NDVI_{Green}$ varies within the upland portion of the transects due to diverse land cover (e.g. open fields, shrubby fields, trees, etc.) and the nature of the slope (non-existent to more prominent), $NDVI_{Green}$ values at the 100% VWC were within the same range for all 12 transects. VWC over 100% were related to the factory calibration of the HydroSense instrument and its 10 pre-set soil types; the instrument was not calibrated to particular soils in the eastern Ontario area. Nor were each site's variability in salinity, percent organic matter or other differences taken into consideration. The VWC are relatively comparable, however, as the same instrument was used with the same prong length for all transects.

Figure 5.33 is an example of the applied $NDVI_{Green}$ threshold boundary applied to spring 2010 Worldview-2 imagery for Mer Bleue Bog. Figure 5.33B shows pixels in orange that had $NDVI_{Green}$ values in the range of -0.025 to 0.07, the selected range associated with saturated soils. Figure 5.33C is a subset of that image and shows where some of the spring 2010 field transects (yellow lines) meet the edges of the derived boundary (red circle). While several of the transects (yellow lines) intersect the orange wet extent, others do not. It was difficult to assess overall accuracy for these data with only twelve points of reference/validation. For Mer Bleue Bog spring imagery, approximately nine of the 12 transects encountered 100% VWC at the $NDVI_{Green}$ derived boundary.

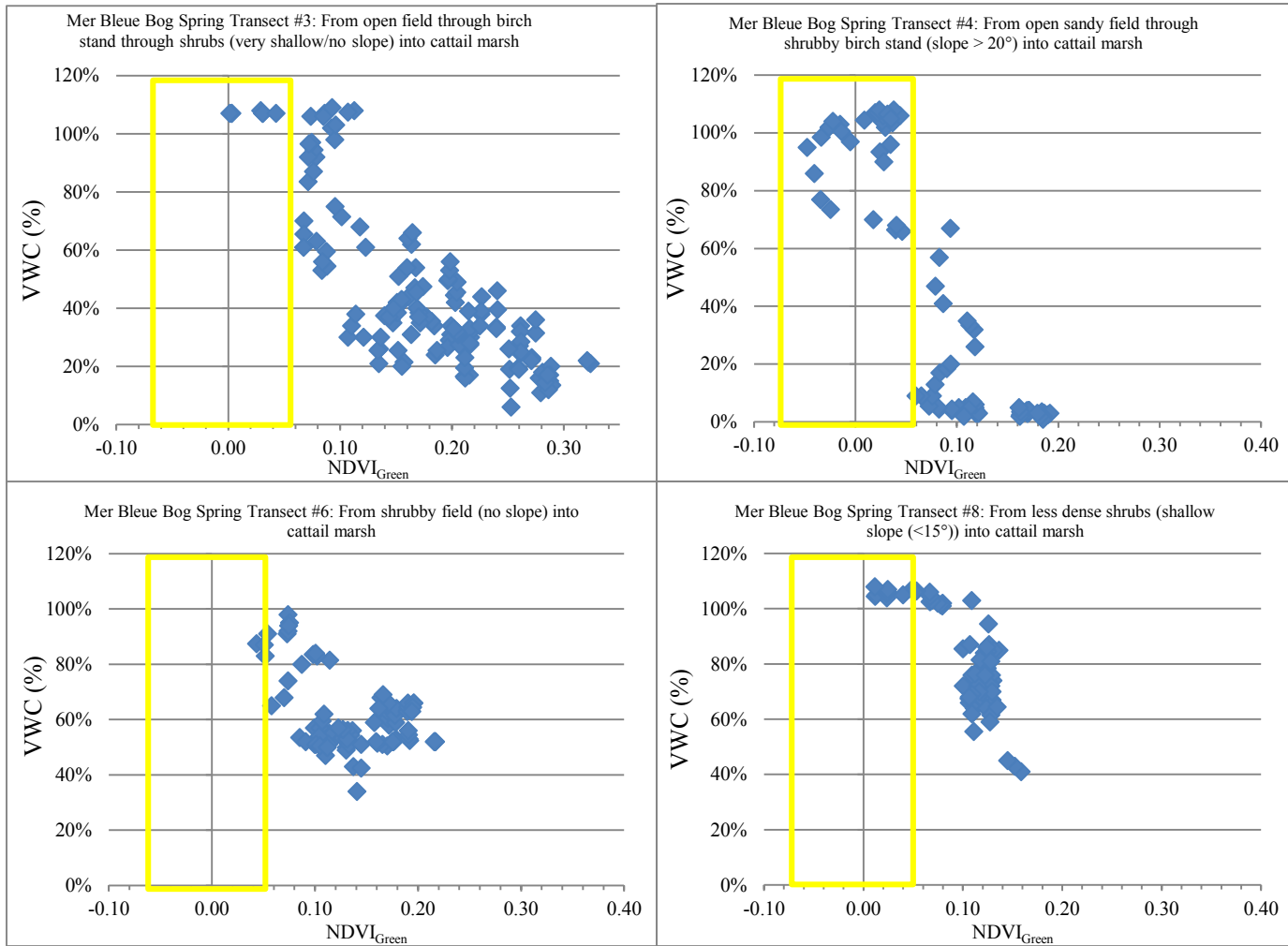


Figure 5.31. Four examples of field measured VWC (%) compared to NDVI_{Green} derived from spring 2010 WorldView-2 imagery for Mer Bleue Bog. Yellow areas give an approximation of the NDVI_{Green} threshold range that relates to 100% or greater VWC.

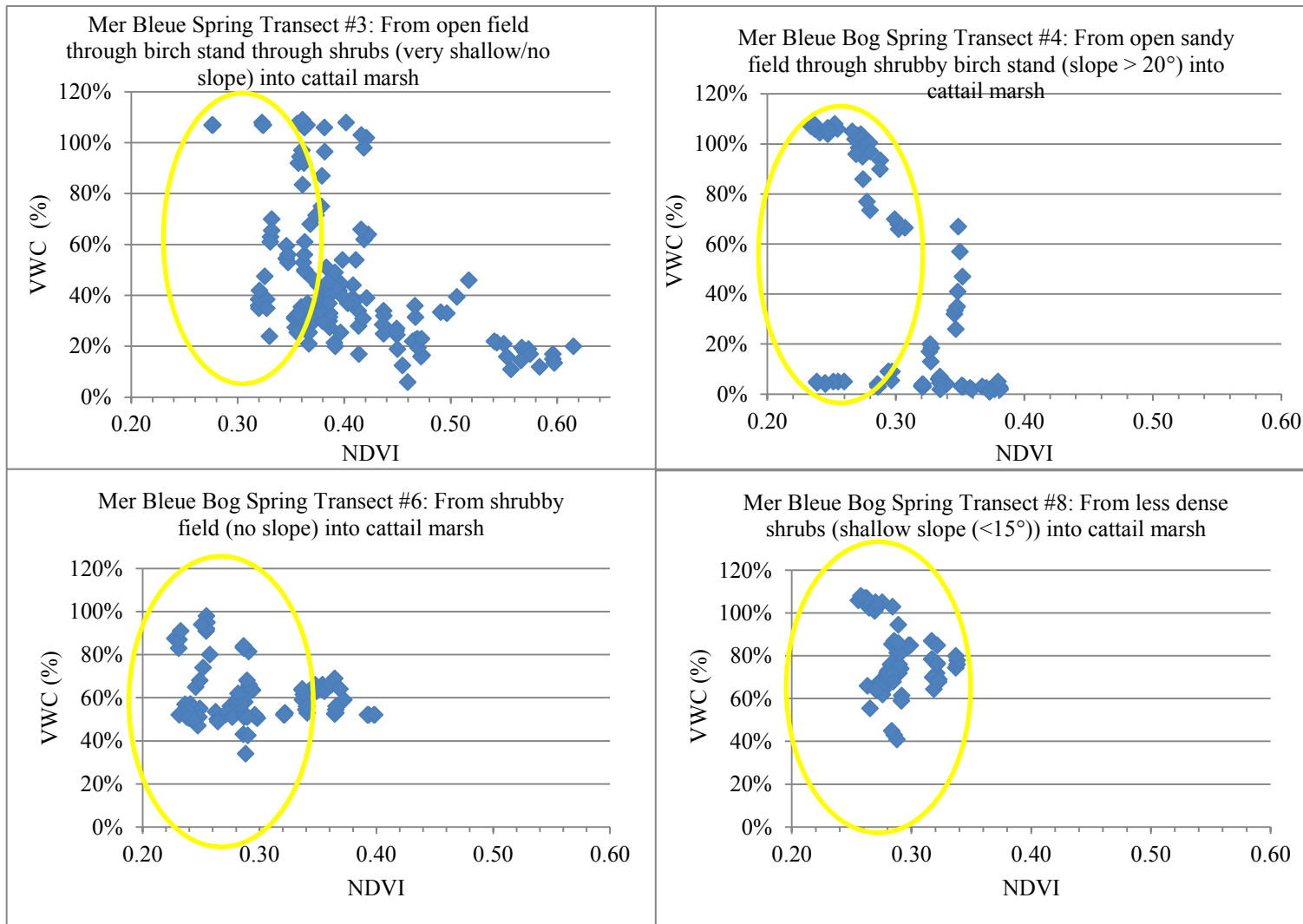


Figure 5.32. Four examples of field measured VWC (%) compared to NDVI derived from spring 2010 WorldView-2 imagery for Mer Bleue Bog. Yellow circles show overlap of NDVI values at varying moisture. There are not distinct ranges/separation at the high (100% or more) end of the VWC as found for $NDVI_{Green}$.

In spring 2011, wet extents were delineated by walking along the 100% VWC edge measured with the Hydrosense probe (blue lines in Figure 5.33 C, D). The orange 2010 NDVI_{Green} boundary matches well with this field-measured wet extent on the north side of the Mer Bleue Bog ridges, but not as well on the south side (green circle, Figure 5.33D). The ridges on the north side have an abrupt topography and thus the saturated zone was confined while the slope on south side transitioned smoothly. 2011 was a wetter year than 2010 (especially after the drought that occurred during the 2010 winter) so it would be expected that the wetland wet extents in spring 2011 would be expanded compared to 2010.

To determine if the same NDVI_{Green} threshold relationship with VWC occurred using OBIA, the NDVI_{Green} image was segmented (alone and with the DEM) using the following parameter values: scale value = 45; shape value = 0.1; compactness value = 0.75. The resulting objects did not align with the field-measured boundaries and because of the segmentation, the boundary was underestimated (contracted and sporadic) compared to the pixel-based boundary. Figure 5.34 is an example of the threshold boundaries created with the objects. Using the same range for NDVI_{Green} of -0.025 to 0.075, fewer areas were highlighted as saturated (pink or green, Figure 5.34C).

Pixel-based analysis and OBIA were also conducted using the Landsat data (using the NDVI_{Green} image) and Radarsat-2 data (using backscatter and the CP variables). None of these variables showed a relationship with field-measured VWC or wet extents.

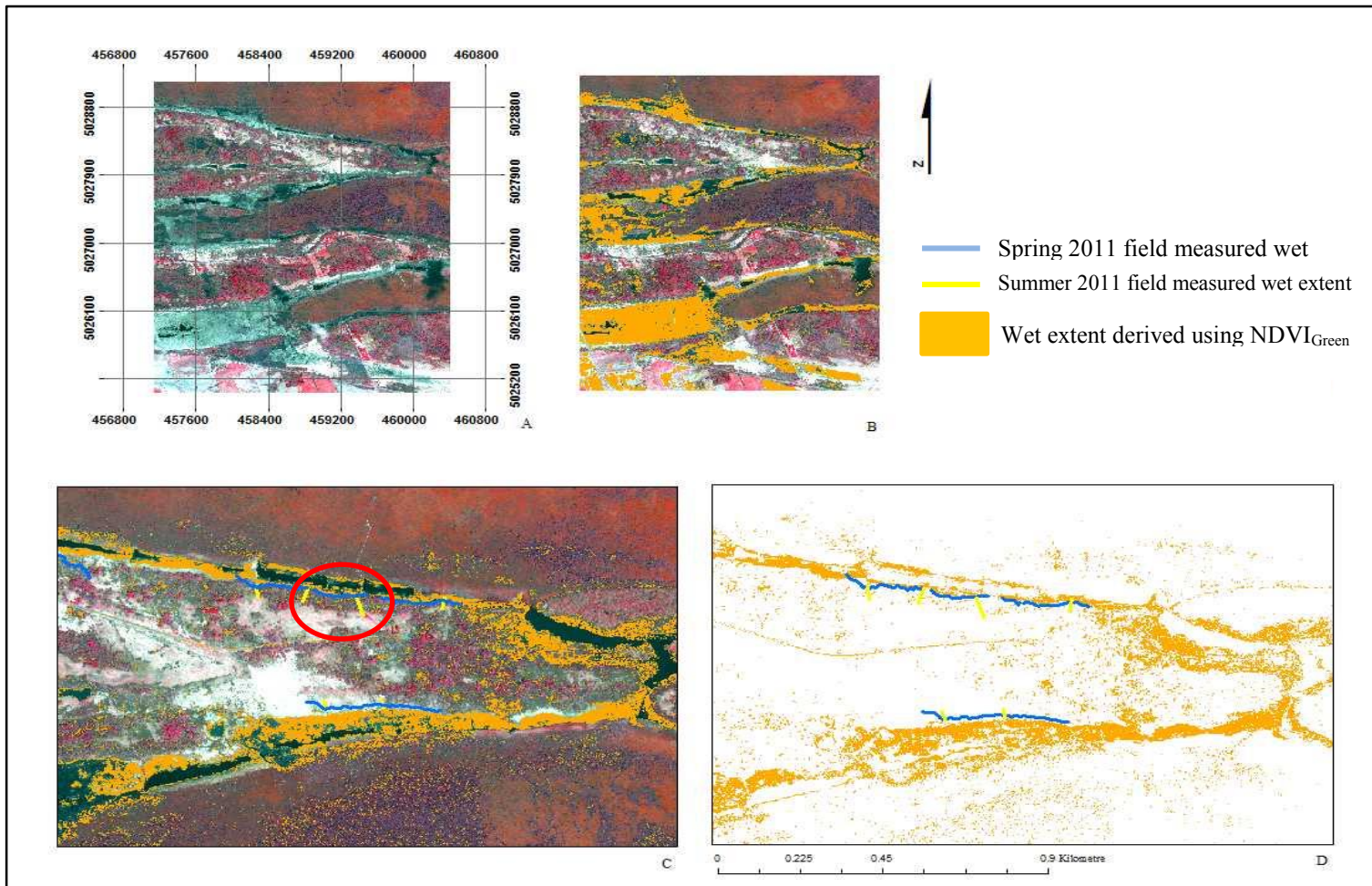


Figure 5.33. A) Spring 2010 WorldView-2 CIR composite of Mer Bleu Bog; B) orange is the 100% saturated boundary derived from the $NDVI_{Green}$ range of -0.025 to -0.075; C) is a close up showing yellow transects measured in 2010 meeting with the orange boundary (red circle); and D) the blue saturated lines mimicking the derived boundary on the north side. but being slightly off on the south side.

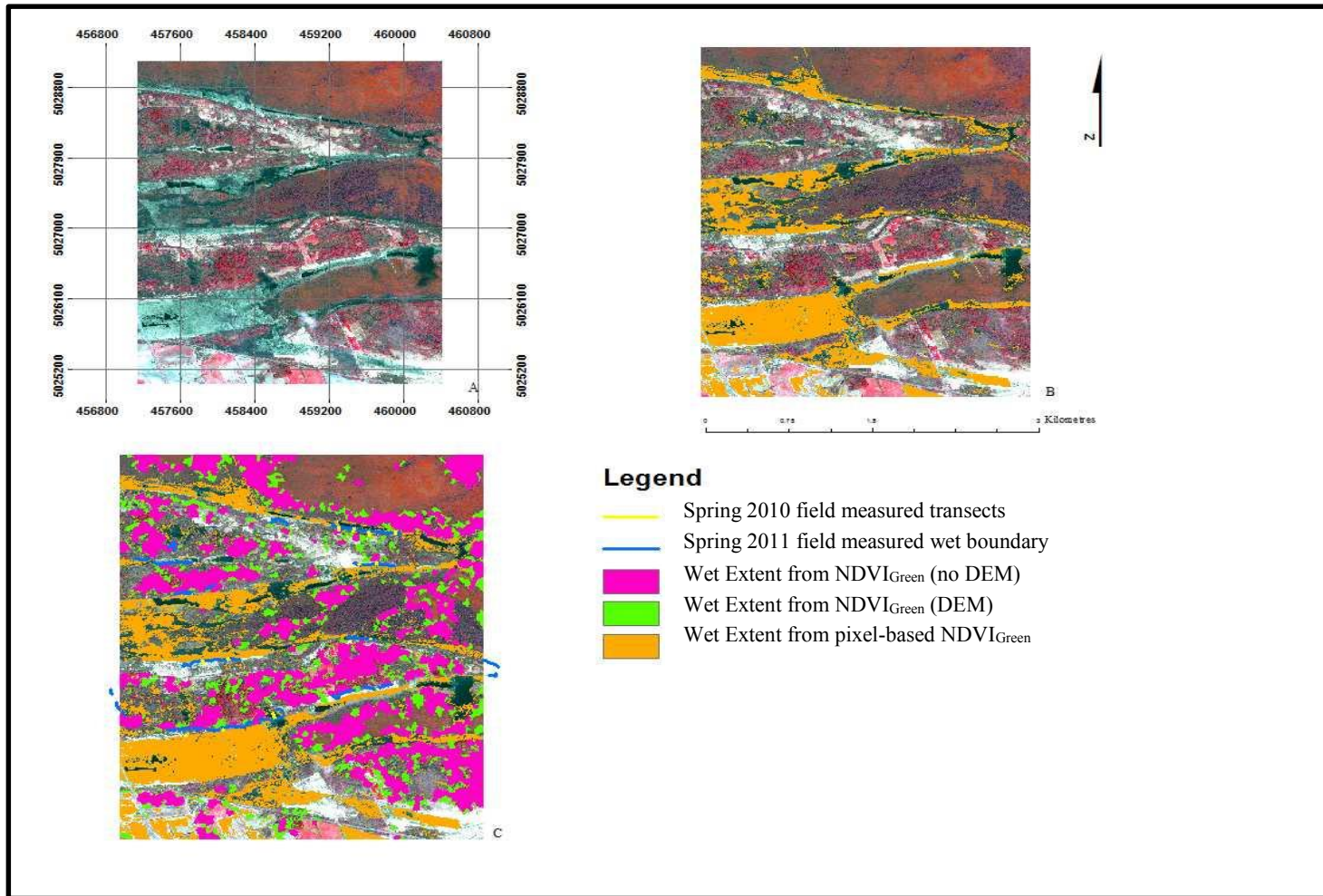


Figure 5.34. A) CIR composite of the WorldView-2 spring image of Mer Bleue Bog; B) orange is the 100% saturated boundary derived from the pixel-based NDVI_{Green} threshold range of -0.025 to 0.075; C) shows the 100% saturated boundaries (pink and green) derived from the segmented imagery.

5.4.2 Summary of main findings for Inundation Extent

- From amongst 14 vegetation indices evaluated, spring $NDVI_{Green}$ corresponded best with VWC (%), and in particular, it showed a consistent range of values related to wet extents;
- Pixel-based processing was better than OBIA, which lost and underestimated boundary detail; and
- Landsat 5 TM and Radarsat-2 data derived variables did not show relationships with spring VWC (%).

5.5 GIS analysis of derived imagery and existing LIO layers for selected OWES attributes

5.5.1 Number of Wetland Types

The Number of Wetland Types determined from the spring WorldView-2 OBIA/CTA classification maps is listed in Table 5.18 for each of the study sites. For Loch Garry, the same Number of Wetland Types were assessed with both methods, however, there was a difference in Wetland Type as Bog was assessed during the 1985 OWES field evaluation and Fen was assessed in 2010 for this research based on observations in the field of fen vegetation (Section 3.1).

Table 5.18. Number and type of wetlands from OWES evaluations and from the image classification of this research.

Wetland Complex	OWES Number of Wetland Types	OWES Wetland Types	Image derived Number of Wetland Types	Image derived Wetland Types
Loch Garry	3	Bog Marsh Swamp	3	Fen Marsh Swamp
Marlborough Forest	4	Fen Bog Marsh Swamp	3	Fen Marsh Swamp
Mer Bleue Bog	3	Bog Marsh Swamp	2	Marsh Bog
Westport Bog	3	Bog Fen Marsh	2	Marsh Bog

This concurred with the subsequent image-based classification. Perhaps because the Loch Garry watershed is hydrologically isolated, it was classified as bog in the earlier OWES field evaluation. The difference is not critical for scoring purposes in this area.

For Marlborough Forest (section 3.1), all four wetland types were included in the 1991 OWES field evaluation. However, a bog area delineated was visited in the spring and summer of 2010 and no identifying bog characteristics or vegetation were observed there, nor anywhere else in Marlborough Forest. This wetland complex is not hydrologically isolated, so this area is most likely not bog. The field and image-based classification of this research did not identify bog areas in this wetland complex, and hence it is believed that none currently exists.

For Mer Bleue Bog, the 1983 OWES evaluation includes Swamp, whereas the field observations and image-based classifications of this research did not identify Swamp. These results concur with others in this well-studied wetland complex (see Baghdadi *et al.*, 2001; Touzi *et al.*, 2007; Millard and Richardson, 2013).

For Westport Bog, the 1983 OWES field evaluations included fen while fen characteristics and vegetation were not observed in the field, nor classified from imagery during this research.

The OWES field evaluations were completed by expert investigators on the dates listed in Table 3.1. There were no investigations during the spring; nor was there a repeat visit the following year as in this research. For determining Wetland Type, there should not be any limitations by visiting the field in the summer only. Additionally, the field evaluators may have had hydrological information (e.g. the confusion between bog and fen at Loch Garry). However, the surveys of the vegetation present in Loch Garry were completed in field in 2010 and 2011 with fully illustrated guide books. What would need to be determined is whether or not the presence of fen-indicator species would indicate Fen OR if the overall general hydrologic condition of the area would supersede the vegetation present and indicates Bog.

5.5.2 Diversity of Surrounding Habitat

Table 5.19 lists the results from assessing the surrounding habitat in a buffer of 1,500 m around each of the four wetland complexes. This was completed using the 2011 AAFC

Crop Type Map of Canada from Agriculture Canada, and Wetland Type thematic maps, contour maps and water bodies' maps from LIO.

Table 5.19. Land cover types within 1.5km of the wetland complex boundaries: OWES field evaluation and those derived from the land cover maps created or obtained for this research.

Wetland Complex	Surrounding land covers and forms determined during the OWES field-based evaluations	Surrounding land covers and forms types derived from various geospatial data sources
Loch Garry	Not listed on the available paper field evaluation	Row crops, pasture, coniferous forest, deciduous forest, pits/quarries, developed land, open lake, creeks
Marlborough Forest	Row crops, pasture, abandoned agriculture land, deciduous forest, coniferous forest, pits/quarries, fence rows, creeks	Row crops, pasture, abandoned agriculture land, deciduous forest, coniferous forest, open lakes, creeks, developed land
Mer Bleue Bog	Row crops, pasture, abandoned agriculture land, deciduous forest, coniferous forest, urban/cottage development, pits/quarries, fence rows, undulating terrain, creeks	Row crops, pasture, deciduous forest, coniferous forest, urban/cottage development, undulating terrains, creeks
Westport Bog	Row crops, pasture, abandoned agriculture land, deciduous forest, coniferous forest, open lake/deep river, fence rows, undulating terrain, creeks	Row crops, pasture, deciduous forest, coniferous forest, open lake/deep river, creeks, developed land, undulating terrain

For the three wetland complexes with OWES data, the numbers of surrounding land cover types were (OWES field evaluation; geospatial data of this research): Mer Bleue Bog (11, 7)1983; Marlborough Forest (8, 8)1991, however, they were not the same types; Westport Bog (9, 8)1983. The most common land cover or form identified in the OWES, but not found using the geospatial data was fence rows. Although different land cover types

were assessed in some cases by the OWES and this research, in general, the number of types was similar for each wetland complex.

Figure 5.35 shows the land cover diversity of the 1,500 m area around Marlborough Forest wetland subset as extracted from the Wetland Type map created in this research and the 2011 AAFC Crop Type Map of Canada, which has an overall accuracy of 82%. This layer is also available for 2012 and is being developed for 2013, with the intent to continue production so the dynamic nature of crops in Ontario can be assessed. Similar figures were created for the other complexes and can be found in Appendix K.

5.5.3 Proximity to Other Wetlands

Table 5.20 compares the geospatial method using the existing OMNR wetland layer, the OMNR water bodies layer and the WorldView-2 image-derived Wetland Type layer with the OWES field-based evaluations of hydrological proximity (based upon surface water, Section 2.9.3) of the wetlands of interest to other wetlands in the same area.

Figure 5.36 is a depiction of stream surface connections to other wetlands in the area around Loch Garry wetland complex at 500 m, 1,000 m, 1,500 m and 4,000 m. This provides an example of how the surface connections were determined using the existing data in the LIO. Similar figures were also created for this variable for the other three wetland complexes and can be found in Appendix K.

Table 5.20. Hydrological Proximity to Other Wetlands as measured during the OWES evaluation and derived from geospatial data.

Wetland Complex	Proximity to Other Wetlands: OWES field-based evaluation	Proximity to Other Wetlands: image derived method
Loch Garry	No indication in field based documentation	Hydrologically connected by surface water to other wetlands (different dominant type), or to open lake or deep river within 1.5 m.
Marlborough Forest	Hydrologically connected by surface water to other wetlands (same dominant type) within 0.5km	Hydrologically connect by surface water to other wetlands (same dominant type) within 0.5km
Mer Bleue Bog	No wetland within 1.5 km	No wetland within 1 km
Westport Bog	Hydrologically connected by surface water to other wetlands (different dominant type) or open water within 1.5 km	Hydrologically connected by surface water to other wetlands (different dominant Wetland Type), or open lake or deep river within 1.5 km.

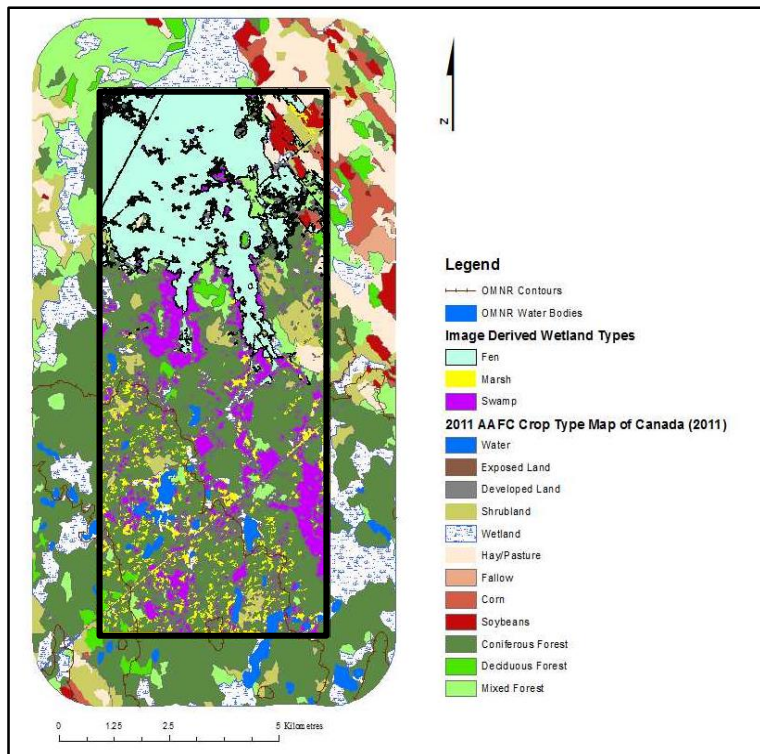


Figure 5.35. The Diversity of Surrounding Habitat surrounding the Marlborough Forest wetland subset (black boundary). The data layers include the WorldView-2 image derived Wetland Type layer, the 2011 AAFC Crop Type Map of Canada (2011); the OMNR water bodies layer, and the OMNR contour layer.

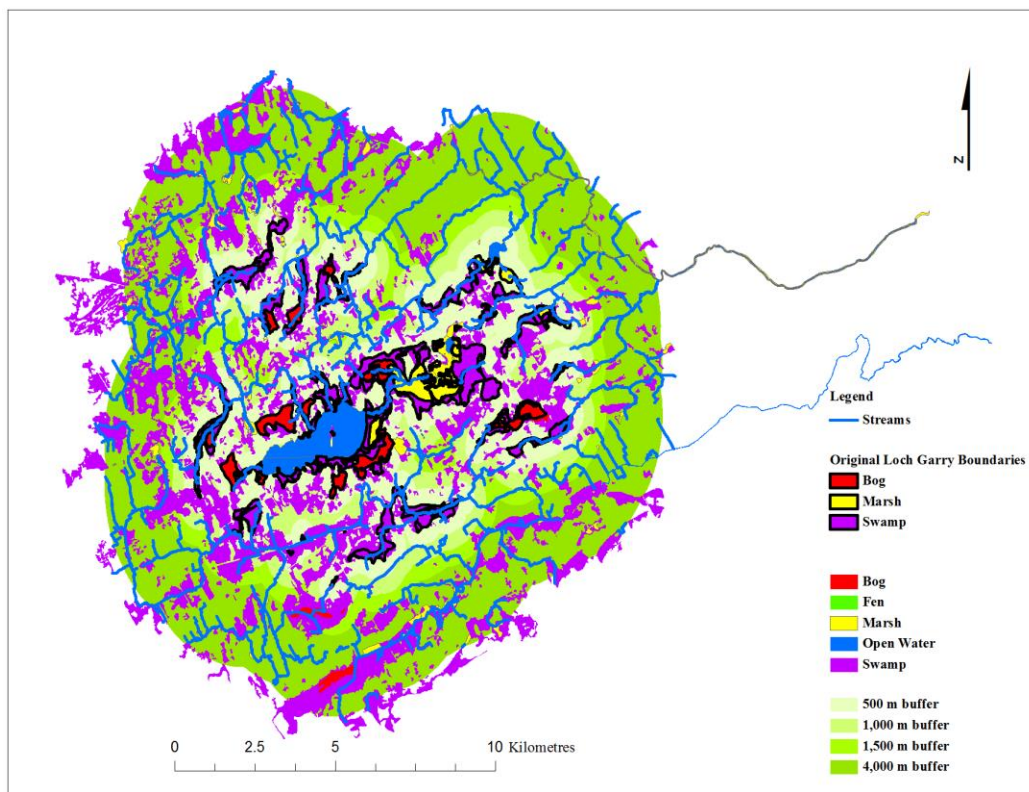


Figure 5.36. Hydrological proximity of the Loch Garry wetland complex to surrounding wetlands. The data layers include the OMNR Wetland Type layer, the OHN watercourses layer; the OMNR water bodies layer, and original Loch Garry boundary layer.

5.5.4 Hunting Pattern mapping

The intensity of hunting usage at each wetland complex was assessed during the OWES field evaluations and an attempt was made to determine hunting intensity in this research using available geospatial data. For eastern Ontario (particularly for the four wetlands of interest) there was little or no coverage that related to hunting (e.g. bear management area, crown game preserves, trapper lines, trapper cabins, among others). More

detailed coverage with these data layers occurred to the west and north of the four wetlands. Figure 5.37 shows the possible layers along with the wetlands of this research. Westport Bog is the most westerly and very few of the data points are present there. For the category of Recreation Use (of which Hunting Patterns is a component) the traditional land use layer provides information regarding lookouts and bird watching sites which may allow for determination of that category.

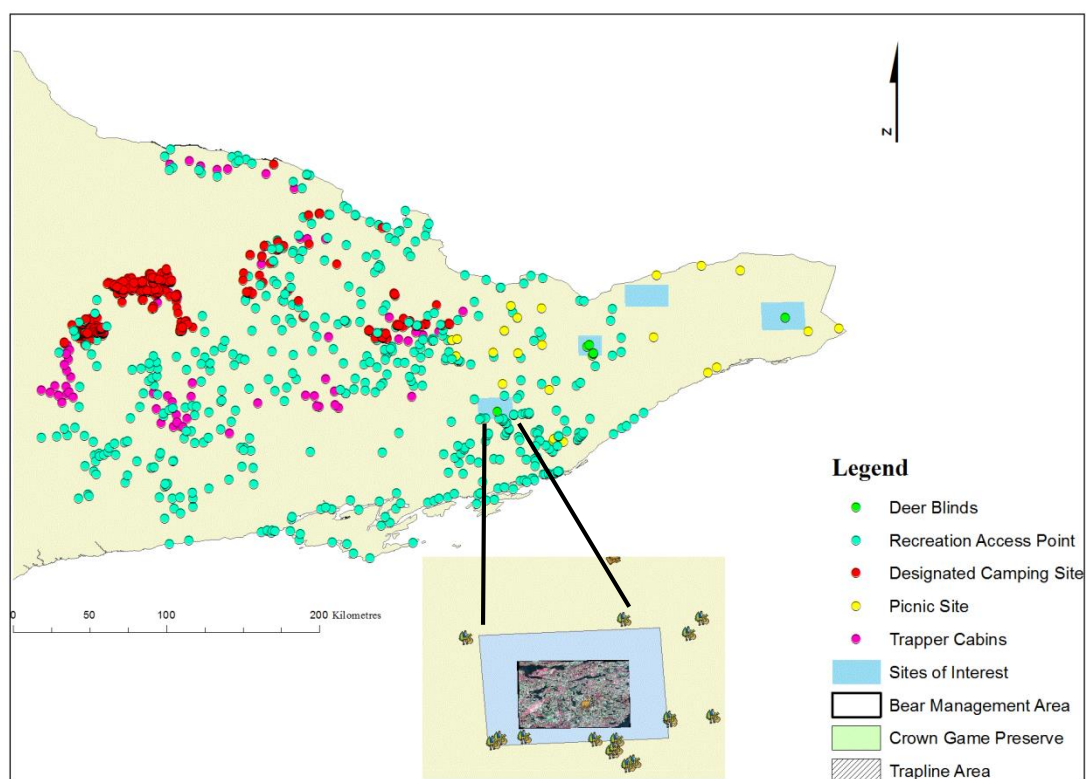


Figure 5.37. Hunting layers available through the LIO and one field observed attribute (deer blinds). Very little coverage is available in far eastern Ontario. Further to the west and north the coverage is denser which may allow for mapping of the intensity of hunting use in those areas.

5.5.5 Ownership Patterns for the Social category

All of the following data layers from the LIO had no data for the sites of interest in eastern Ontario: all the conservation layers (including authority and use), cottage residential area and site, all the crown leased land layers, and the federal land layers. The land ownership layer does not provide coverage for Loch Garry, Mer Bleue Bog and Marlborough Forest, but there is partial coverage of Westport Bog, (but only one type of land ownership (private) and not enough to determine an overall pattern or score for that area). These layers, once again, may prove useful for mapping of this attribute in other areas where there is more data coverage. Property parcel layers available from Teranet (<http://www.teranet.ca/>, 2013) were examined, but only provide Municipal Property Assessment Corporation (MPAC) assessment numbers and property address data, which do not give an indication of ownership. If the type of ownership (e.g. private or crown) is indicative of particular assessment numbers (e.g. particular number pre-fixes, etc.) then a determination of private versus public land based upon these might be possible. That information was not available, but may be at a governmental level.

5.5.6 Wetland area and basin area measurements for Wetland Attenuation Factor

The Wetland Type layer from the LIO was used to calculate the size of the wetland (in terms of its ability to attenuate floods). As the Wetland Type classifications in this research were completed on sub-sets of the complexes of interest, these data were not useful for this method. Therefore, it was necessary to use the existing LIO wetland layer. It was attempted to assess the size of the catchment basin on the whole, and the portion of the

catchment basin upstream of the wetland area from the LIO quaternary watershed layer. The data limitations and required assumptions resulted in this not being suitable for further investigation with the available data. Data that were required include a wetland basin layer, and an appropriate catchment basin with the upstream/downstream locations of all wetland basins located in those catchment layers. Without this data the wetland attenuation factor cannot be calculated.

5.5.7 Rarity of Wetlands and Rarity in Landscape for the Special Feature category

The rarity of a given Wetland Type and its rarity within the landscape are dependent upon the location of the wetland, the ecodistrict in which it is located, and the individual wetland's proportions to the overall wetland area. The four wetland complexes fall within three ecodistricts (5E-11, 6E-11, and 6E-12). For two of the districts (6E-11, and 6E-12) which include Loch Garry, Mer Bleue Bog and Marlborough Forest, wetlands are common. The rarity of each type of wetland within these ecodistricts indicates that fen and bog are the rarest, and marsh is slightly rare, while Swamp is common. Ecodistrict 5E-11 is listed in the Northern OWES Manual and includes Westport Bog (although it is the southernmost study site of this research). Marsh is not considered rare at this site; Fen is the rarest and Swamp and Bog are equally and moderately rare.

5.5.8 Summary of main findings of the GIS analysis of maps created in this research and existing LIO layers for OWES attributes

- It was possible to use existing LIO thematic layers and a Land Cover/Wetland Type map created in this research to derive the Number of Wetland Types, Diversity of Surrounding Land Covers, Proximity of Surrounding Wetlands, and Rarity of Wetlands and Rarity in the Landscape;
- Due to lack of appropriate data, it was not possible to use existing LIO thematic layers to assess Ownership Pattern or Hunting Pattern for the wetlands of this research. However, existing data for other areas in southern Ontario may make this possible; and
- It was not possible to assess Wetland Attenuation Factor because of a lack of existing basin data.

Objective 2 Results: Compare OWES attribute scores and scores derived from the geo-spatial data of this research

5.6 Comparative analyses of wetland attribute scores derived from geo-spatial data, and OWES scores

As entire wetland complexes were not assessed using the image based analysis (only a subset), some of the comparisons to the field scores are skewed. In some cases the existing OMNR wetland layer is used. The following section relates the attributes derived in this

research to scores that can then be compared with OWES scores that were determined using the field evaluations.

5.6.1 Wetland Type

The fractional area of each Wetland Type was calculated from the thematic maps produced in Section 5.1.2 in order to determine the overall score (Table 5.21).

Table 5.21. OWES Wetland Type field observed fractional areas and scores (columns 2, 3); Wetland Type mapping fractional areas and scores (columns 4, 5).

Wetland Complex	OWES Wetland Type as % of total wetland area	OWES field-derived score	Fractional area of Wetland Type (from WorldView-2 derived Wetland Map)	Wetland map derived score
Loch Garry	Unknown	15	Fen: $1.01\text{km}^2/4.35\text{km}^2$ = $0.23 * 6 = 1.39$ points	9
			Swamp: $2.69\text{km}^2/4.35\text{km}^2$ = $0.62 * 8 = 4.96$ points	
			Marsh: $0.65\text{km}^2/4.35\text{km}^2$ = $0.15 * 15 = 2.25$ points	
Marlborough Forest	Bog = 0.3% Fen= 1.7% Swamp = 89.4% Marsh = 8.6%	13	Fen: $15.36\text{ km}^2/30.69\text{ km}^2$ = $0.50 * 6 = 3$ points	8
			Swamp: $10.98\text{ km}^2/30.69\text{ km}^2$ = $0.36 * 8 = 2.88$ points	
			Marsh: $4.35\text{ km}^2/30.69\text{ km}^2$ = $0.14 * 15 = 2.10$ points	
Mer Bleue Bog	Bog = 69% Swamp = 29% Marsh = 2%	7	Bog: $8.74\text{ km}^2/ 10.69\text{km}^2$ = $0.82 * 3 = 2.46$ points	6
			Marsh: $2.45\text{ km}^2/10.69\text{ km}^2$ = $0.22 * 15 = 3.45$ points	
Westport Bog	Bog = 17% Marsh = 55% Swamp = 28%	15	Bog: $0.83\text{ km}^2/ 11.80\text{ km}^2$ = $0.07 * 3 = 0.21$ points	14
			Marsh: $10.98\text{ km}^2/ 11.80\text{ km}^2$ = $0.93 * 15 = 13.95$ points	

The Wetland Type thematic maps produced lower wetland fractional area and lower total scores than the OWES data, indicating that the distribution of wetland types within the subset (total wetland size used) is not the same as the distribution outside of the subset. Additionally, the percentages of the Wetland Types derived from the thematic maps were found to be similar the OWES proportions with the exception of Marlborough Forest, which had a much higher percentage of Swamp in the OWES evaluation (and similar overall wetland size, although portions of two other wetland complexes were included (see Section 3.1).

5.6.2 VCFs and Number of VCF

Based upon the current method of scoring for these classes, it is not possible to assign a score to the image-classified VCFs and Number of VCFs. The image classification thematic maps provide the dominant vegetation form, and not the composition of the community. For example, all dead coniferous/dead hardwood (DC/DH) dominant areas were classified as DC/DH regardless of the other VCFs present. However, these maps can be used to estimate the number and configuration of the dominant VCF in a given area; i.e., to identify areas have 1 to 3, 4 to 5, or 6 or more VCFs. In practice, the thematic map could be broken down into given areas or zones and a count could be made of the numbers of each of the three categories. However, it would not be possible to know the vegetation composition within these categories, which is required for the current OWES scoring method for at least one instance.

5.6.3 Open Water Type

Table 5.22 provides the results of the scores for Open Water Type. In general, the scores derived from the image classified thematic maps were higher than those for the OWES field evaluations. Only one wetland complex, Mer Bleue Bog, had the same water type (Type 1, less than 5% of the area is open water) assessed using both methods. The water types assessed for this research were confirmed in the field and with reference imagery. Additionally, the spring field work completed in this research may have enabled a better survey of the Open Water Types present compared to summer, when the OWES field evaluations were completed. In summer, some water may have dried up or vegetation may have obscured certain water bodies (e.g. ponding (type 5); open water (types 2 and 4)), particularly if viewed from an oblique angle in the field.

Table 5.22. Scores derived for Open Water Types were based upon the image-derived thematic map and compared to those listed in the OWES field evaluations. See Section 2.9.3 for type descriptions.

Wetland Complex	OWES Open Water Type	OWES Open Water Type score	Image-derived dominant Open Water Type	Image-derived Open Water Type score
Loch Garry	Type 4	20	Type 5	30
Marlborough Forest	Type 3	14	Type 5	30
Mer Bleue Bog	Type 1	8	Type 1	8
Westport Bog	Type 3	14	Type 4	20

5.6.4 Number of Wetland Types

The OWES score for the Number of Wetland Types was compared to that found using the derived Wetland Type thematic maps (Table 5.23). In general, the geospatially

derived scores were lower than the OWES scores because the geospatial method mapped fewer Wetland Types within each wetland complex. However, as stated in Section 5.5.1, these types mapped using image classification were confirmed in the field during two different seasons (spring and summer) and for two years.

Table 5.23. OWES and thematic map scores derived for the Number of Wetland Types.

Wetland Complex	OWES field evaluated score	Wetland type map derived score
Loch Garry	20	20
Marlborough Forest	30	20
Mer Bleue Bog	20	13
Westport Bog	20	13

5.6.5 Diversity of Surrounding Habitat

Based upon the information found in Figure 5.35, both the OWES and geospatial methods scored the maximum of 7 points per complex. There were minor differences in terms of number and type of land cover, but in general it was determined that by using the geospatial data, the Diversity of the Surrounding Habitat can be feasibly assessed.

5.6.6 Proximity to Other Wetlands

Table 5.24 lists scores determined for this attribute in the OWES and using geospatial data. The geospatial data allow the same determinations to be made in terms of the surface water hydrological connectivity at these four sites.

Table 5.24. Scores for the hydrological Proximity to Other Wetlands as measured in the field and derived from geospatial data.

Wetland Complex	Proximity to Other Wetlands: OWES	OWES Score	Proximity to Other Wetlands: geospatially derived method	Geo-spatially-based score
Loch Garry	No indication (determination of score based upon score given in 1983(10 max score) and converted to present day scoring system)	8	Hydrologically connected by surface water to other wetlands (different dominant Wetland Type), or open lake or deep river within 1.5 km.	8
Marlborough Forest	Hydrologically connected by surface water to other wetlands (same dominant type) within 0.5km	8	Hydrologically connected by surface water to other wetlands (same dominant type) within 0.5km	8
Mer Bleue	No wetland within 1.5 km	0	No wetland within 1 km	0
Westport Bog	Hydrologically connected by surface water to other wetlands (different dominant type) or open water within 1.5 km	8	Hydrologically connected by surface water to other wetlands (different dominant Wetland Type), or open lake or deep river within 1.5 km.	8

5.6.7 Wetland Size for the Biological component

The scores obtained for the biological attributes (see section 2.9.8) assessed from the geospatial data in this research were summed and, based upon that amount and the physical size of a wetland, a general score was given for the Wetland Size. Table 5.25 lists these

results. Interspersion was not measured, and VCF could not be assigned a score. The OWES scores included these attributes' scores and Interspersion and VCF scores from the OWES were added to the geospatially derived Wetland Size score for the first comparison (column 3 and 5). The second comparison removed the scores for Interspersion and VCF from both (column 4 and 6). It can be seen that, in general, the size scores evaluated for Loch Garry, Marlborough Forest and Westport Bog were similar to those that were assessed during the field evaluations.

As noted above, for certain categories the geospatially derived scores were the same as the OWES scores (e.g. Diversity of Surrounding Habitat, Proximity to Other Wetlands) for Open Water Type, the geospatial method produced larger scores than the OWES and for Number of Wetlands the geospatial method produced lower scores. Overall, the final scores that were assigned for Wetland Size were the same for all the complexes, the maximum allowable amounts when including Interspersion and VCF.

Table 5.25a. Scores for the Wetland Size attribute evaluated in the OWES.

Wetland Complex	Area of the wetland (km ²)	OWES summation of Biological Component	OWES summation of Biological Component (No Interspersion or VCF)	OWES Wetland Size score (with Interspersion and VCF)
Loch Garry	12.81	70	40	50
Marlborough Forest	10.99	72	37	50
Mer Bleue Bog	22.68	42	46	50
Westport Bog	3.56	64	25	50

Table 5.25b. Scores for the Wetland Size attribute derived from geospatial data.

Wetland Complex	Area of the wetland (km ²)	Geospatial results: summation of Biological Component	Geospatial Results: summation of Biological Component (No Interspersion or VCF)	Geospatial Wetland Size score (with Interspersion and VCF)
Loch Garry	12.81	74	46	50
Marlborough Forest	10.99	73	43	50
Mer Bleue Bog	22.68	34	40	50
Westport Bog	3.56	62	25	50

5.6.8 Hunting Pattern method and Ownership Patterns for the Social component and Wetland Attenuation Factor for the Hydrologic component

As it was found that the geospatial data available were not sufficient to determine scores for these categories there is no comparison to the existing field based OWES scores.

5.6.9 Rarity of Wetland Type and Rarity in Landscape for the Special Feature category

The Rarity of Wetland Type and Rarity within the Landscape are dependent upon the location of the wetland. Table 5.26 shows that scores derived using the geospatial data and the OWES scores are sometimes the same and sometimes different, depending on the Wetland Type assigned. For example, OWES lists the presence of Bog at Loch Garry which has a higher value of rarity (80 points), while the geospatial results that determined the same area was Fen has a lower value of rarity (60 points).

Table 5.26. Rarity of Wetland Type and Rarity of Wetlands in the Landscape observed from OWES and geospatial data.

Wetland Complex	Individual wetland OWES score	Individual wetland geospatial score	Rarity Within the Landscape	Rarity of the Wetland Type				Total OWES score*	Geospatial score (Maximum 80)
				Marsh	Swamp	Fen	Bog		
Loch Garry	20	20	0	30	0	60	0	20	80
Marlborough Forest	20	20	0	30	0	60	0	20	80
Mer Bleue Bog	20	20	0	30	0	0	80	20	80
Westport Bog	5	30	0	0	10	30	10	20	20

*20 is the original maximum for the category (OWES, 1981) and therefore is similar to the current maximum score of 80 (OWES, 2002).

5.6.10 Summary of main findings for the comparison of attribute scores derived from geo-spatial data to OWES scores

- The same scores as in the OWES were derived for Diversity of Surrounding Habitat, Wetland Size (when including field-assessed Interspersion and VCF), and Proximity to Other Wetlands;
- Similar scores to those in the OWES were derived for Rarity of Wetlands and Rarity in Landscape for the Special Feature category, the exception being Westport Bog;
- Open Water Type scores were higher than OWES scores;
- The scores for Number of Wetland Types and Wetland Types were lower than OWES scores; and
- Scores could not be derived for VCF, Hunting Pattern, Ownership Pattern and Wetland Attenuation Factor.

Objective 3 Results: Review of temporal remote sensing data in classification of wetland attributes and analysis of attribute changes over the long term.

5.7 Assessing seasonal and inter-annual differences in the OWES attributes

This section outlines the results of multi-season and inter-annual imagery for mapping Wetland Type, VCFs, Open Water Type and Inundation Extent.

5.7.1 Temporal analysis for Wetland Type

The same segmentation parameter values found to be optimal for the spring imagery were also found to be optimal for the summer and fall imagery: scale value = 45; shape value = 0.1; and compactness value = 0.75. Table 5.27 summarizes the object-based (imagery and DEM) CTA results for the four sites using the segmented summer imagery, and the combined two-season and three season results for Mer Bleue Bog. Using summer imagery, the overall classification accuracy for two sites (Mer Bleue Bog and Marlborough Forest) increased over that achieved using spring imagery (73.2% to 80.0%, and 70.0% to 75%, respectively). For the other two sites (Loch Garry and Westport Bog) the overall classification accuracy using summer imagery decreased (86.5% to 70.3% and 72.5% to 68.8%, respectively). For both of these classifications, water accuracies (both UA and PA) declined. The Loch Garry summer imagery water bodies show specular reflectance (see Figure 5.38A) and at Westport Bog (Figure 5.38B) the water bodies which were clear and dark in spring had vegetation cover in summer. These conditions could be responsible for the decline in the water class accuracies and, for the Loch Garry classification, general confusion amongst all classes.

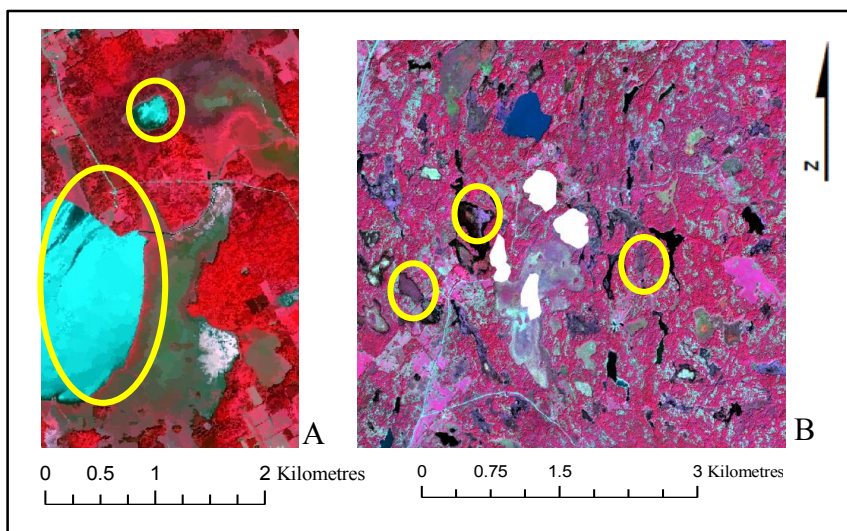


Figure 5.38. WorldView-2 CIR composites of A) Loch Garry in the summer showing specular reflectance of water and B) Westport Bog with vegetation present (yellow circles).

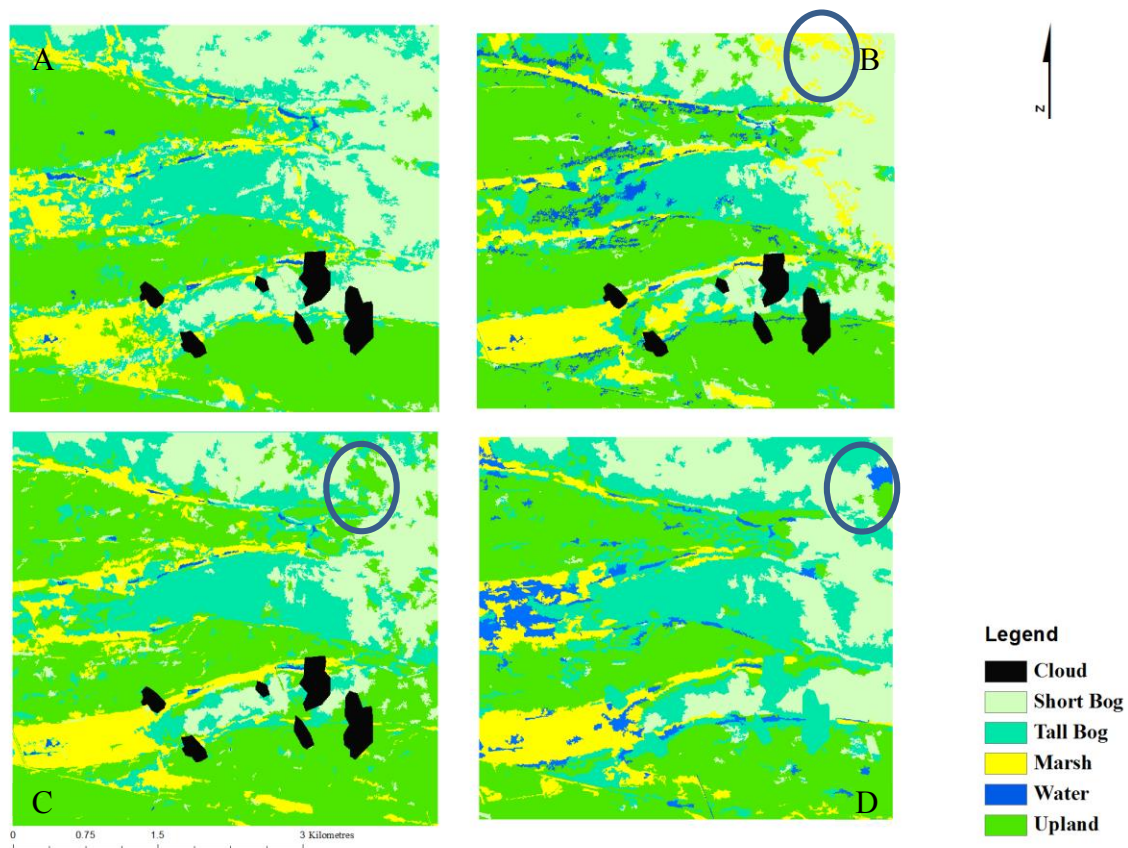
Using summer imagery instead of spring imagery, accuracies for Fen were lower for Loch Garry and higher for Marlborough Forest. Accuracies for Bog were generally higher, while for Swamp, they were the same or lower, and for Marsh they were lower at all four sites. Utilizing a combination of spring and summer imagery in segmentation and classification did not increase the overall accuracies for three of the four sites. Only Mer Bleue Bog improved overall, but the Tall Bog class UA was lower (62.5% for summer imagery alone compared to 54.6% for spring plus summer). Using a combination of three seasons of images (spring, summer and fall) at Mer Bleue Bog did not significantly (statistically) change the overall classification accuracies from those for the spring-summer combination.

Figure 5.39 is a comparison between the spring, summer and combined spring-summer Wetland Type maps for Mer Bleue Bog. Areas of illogical class assignment are found on all three maps (black circles). As outlined in Figure 5.39B (summer) there are areas of excessive water which were not present in the field, and erroneously classified areas of Marsh located within the Bog. For Figure 5.39C (spring and summer) there is a large portion of Upland assigned where Tall Bog (treed bog) was observed in the field. Overall, there is more Upland classified in areas of Bog on the combined season map than for either the spring or summer maps; the overall accuracy is higher for the combined imagery but there are large erroneously classified areas.

The same segmentation parameter values found to be optimal for the spring imagery were also found to be optimal for the summer and fall imagery: scale value = 2; shape value = 0.1; and compactness value = 0.1. The highest accuracy results for the spring Landsat TM 5 spring classifications were achieved using the 5 EM fraction maps (various combinations of segmented and not segmented imagery, plus/minus DEM), and these were initially assessed for summer imagery. Poor results for these data required further processing of the other data inputs (3 EM fraction maps, and original band data, plus/minus DEM). Table 5.28 lists the overall accuracies for: the best spring result, the summer result using the same configuration of data as spring and the best summer result.

Table 5.27. OBIA CTA accuracy statistics for the Wetland Type class accuracies (%) for the four sites using the various combinations of seasonal data.

Wetland Complex	Season	Ove. Acc. (%)	Kappa	Water		Upland		Fen		Bog		Swamp		Marsh		Average	
				PA (%)	UA (%)	PA (%)	UA (%)	PA (%)	UA (%)	PA (%)	UA (%)	PA (%)	UA (%)	PA (%)	UA (%)	PA (%)	UA (%)
Loch Garry	Spring	86.5	0.82	100.0	100.0	81.3	100.0	80.0	100.0	n/a	n/a	100.0	58.3	75.0	100.0	87.3	91.7
	Summer	70.3	0.59	60.0	100.0	100.0	88.9	40.0	50.0	n/a	n/a	28.6	40.0	75.0	42.9	60.7	64.4
	Combined	86.5	0.82	100.0	100.0	93.8	100.0	80.0	100.0	n/a	n/a	57.1	66.7	100.0	57.1	86.2	84.8
Marl-borough Forest	Spring	70.0	0.60	83.3	100.0	60.0	64.3	100.0	50.0	n/a	n/a	83.3	71.4	63.6	70.0	73.4	69.7
	Summer	75.0	0.66	83.3	100.0	80.0	70.6	100.0	100.0	n/a	n/a	83.3	83.3	54.6	60.0	80.3	82.8
	Combined	62.5	0.50	66.7	66.7	66.7	66.7	100.0	66.7	n/a	n/a	83.3	45.5	36.4	66.7	70.6	62.4
						Short Upland		Tall Upland									
Westport Bog	Spring	72.5	0.65	100.0	75.0	50.0	100.0	75.0	66.7	77.8	63.6	n/a	n/a	63.6	77.8	73.3	76.6
	Summer	68.8	0.61	50.0	75.0	80.0	50.0	100.0	75.0	85.7	100.0	n/a	n/a	37.5	50.0	70.6	70.0
	Combined	50.0	0.38	0.00	0.00	80.0	30.8	33.3	67.7	85.7	75.0	n/a	n/a	50.0	57.1	49.8	46.1
						Upland		Fen		Tall Bog		Short Bog					
Mer Bleue Bog	Spring	73.2	0.64	100.0	100.0	77.8	93.3	n/a	n/a	60.0	27.3	60.0	60.0	62.5	100.0	72.1	76.1
	Summer	80.0	0.74	100.0	83.3	76.2	100.0	n/a	n/a	83.3	62.5	100.0	50.0	66.7	100.0	85.2	79.2
	Fall	58.7	0.45	100.0	100.0	52.8	68.8	n/a	n/a	83.3	27.7	60.0	100.0	33.3	75.0	65.8	74.3
	Spring/Summer	87.0	0.82	100.0	100.0	85.7	94.7	n/a	n/a	100.0	54.6	80.0	100.0	77.8	100.0	88.7	89.9
	Spring/Fall	69.6	0.59	100.0	83.3	71.4	83.3	n/a	n/a	66.7	36.4	80.0	57.1	44.4	100.0	72.5	72.0
	Summer/Fall	73.9	0.66	100.0	100.0	57.1	100.0	n/a	n/a	100.0	40.0	100.0	71.3	66.7	85.7	84.8	79.4
	Combined (3 season)	84.8	0.80	100.0	100.0	81.0	100.0	n/a	n/a	100.0	54.6	100.0	71.3	66.7	100.0	89.5	85.2



	Spring	Summer	Spring & Summer	Fall
Short Bog	471.65	397.56	326.15	366.79
Tall Bog	401.65	294.61	425.91	493.02
Marsh	194.77	210.79	204.45	190.16
Water	9.08	63.46	5.96	81.13
Upland	703.21	857.53	861.47	692.84

Figure 5.39. Comparison of A) spring B) summer; C) combined spring & summer; and D) fall only Wetland Type classifications as derived from segmented WorldView-2 imagery and a DEM at Mer Bleue Bog. Blue circles highlight areas of illogical class assignment. Table provides area (ha) per class

For three of four sites, the unsegmented imagery produced higher classification accuracy than the segmented imagery. Overall, the accuracies declined using the 5 EM fraction maps derived from the summer imagery. The 3 EM fraction maps derived from the summer imagery improved those results, but they did not surpass the spring results for the sites except for Loch Garry. The difference between the results was captured by the 3 ‘bare’ fractions in the 5 EM spring data more so than the single ‘bare’ class in the 3 EM summer data. In spring this variability would be due to greater exposure of woody vegetation components and ground in areas of deciduous vegetation, whereas in the summer, such areas may be covered by short or treed vegetation.

Table 5.28. Landsat TM 5 CTA accuracies (%) A) best spring result; B) summer results using same configuration of data; and C) best summer results.

Wetland Complex	A) Best spring result				B) Summer result using same data configuration as spring	C) Best summer result			
	<i>Data</i>	<i>DEM ?</i>	<i>Seg?</i>	<i>%</i>		<i>%</i>	<i>Data</i>	<i>DEM ?</i>	<i>Seg?</i>
Loch Garry	5 EM	Yes	Yes	59	62	3 EM	No	No	70
Marlborough Forest	5 EM	No	No	78	60	Orig Data	No	No	71
Mer Bleue Bog	5 EM	Yes	No	74	41	3 EM	Yes	No	76
Westport Bog	5 EM	Yes	No	72	57	3 EM	No	Yes	67

The site with the highest overall accuracy for summer was Mer Bleue Bog (76%) and the site with the lowest overall accuracy was Westport Bog (67%).

The best Marlborough Forest summer classification was produced using the original band data (no DEM), but its accuracy was not as high as the best spring classification (5EMs, no DEM). This was different from the WorldView-2 Wetland Type classifications for this site where overall accuracies were higher for summer data. For Loch Garry, the overall accuracies were higher in summer while for the WorldView-2 classifications spring accuracy was higher. Summer accuracy at Mer Bleue Bog and Westport Bog was slightly lower than spring.

Summary of main findings for temporal analyses for Wetland Type:

- WorldView-2 summer imagery produced higher overall classification accuracies for two of four sites; the remaining two sites' summer imagery had factors that may have contributed to the lower accuracies (e.g., specular reflectance and vegetation growth in water); the poorest class in spring classifications (Marsh), improved significantly using summer imagery;
- Combining multi-season imagery in the segmentation and classification process did not improve overall accuracies for three of four sites; Mer Bleue Bog classification accuracies did improve with the combination of two seasons (spring and summer) of imagery;
- Landsat 5 TM summer imagery produced lower overall classification accuracies for three of four sites; only the accuracy for Loch Garry improved for the summer; and

- Regardless of season, the best (three out of four for either season) Landsat 5 TM Wetland Type classifications were pixel-based, produced using unmixed fraction maps, either with 5 EMs and spring imagery or 3 EMs and summer imagery.

5.7.2 Temporal analyses for VCFs

The optimal parameter values for VCFs were: scale value = 25; shape value = 0.1, and compactness value = 0.75. Table 5.29 provides the multi-season Worldview-2 CTA accuracy results for the number of VCF for Mer Bleue Bog (selected because spring, summer and fall imagery had been acquired for that site). Appendix L contains the accuracy results for the other 3 sites.

The highest overall accuracy was achieved using the combined summer 2010 and fall 2011 imagery (74.3%). The lowest overall accuracy (54.3%) was obtained using the spring 2010 and fall 2011 imagery. For individual seasons, spring provided the highest overall accuracy (65.7%) while summer produced the lowest overall accuracy (57.1%). From the multi-season results, it is evident that summer and fall imagery represent a better combination than spring-summer or spring-fall, even though spring imagery was the best individually. The error matrices for the summer and fall classifications show similar UA and PA for all classes (Table 5.30B and C, respectively), while the spring error matrix is different with more correctly assigned reference samples for Class B; (Table 5.30A). With the combination of summer and fall, correct class assignment improves for both Classes A and B over the classifications for either season individually (Table 5.30E). In contrast,

combining spring and fall imagery reduced the accuracies of Classes A and B (Table 5.30D) from the classifications using either season individually.

Low kappa values indicate that for the majority of these classifications were only moderately better than random class assignment (Congalton and Green, 1995; Foody, 2002). Additionally, the UAs for Class C for all combinations of data were very low. The spatial variability, and spectral similarity of the forms, especially in the summer, in the visible to NIR portion of the spectrum contribute to these results. These results could also be related to the small sample size of the reference and validation data (35 sites in total), and especially for class C (1 validation site).

Table 5.31 provides the accuracy results for the individual VCF classes for Mer Bleue Bog using the variety of combinations of seasonal data. Spring imagery produced the highest overall accuracy (68.8%) while summer imagery produced the lowest (54.3%). This was not expected as it was thought that unique vegetation signatures would be more apparent in the summer after a period of vegetation growth. There could be more variability among the forms in the spring in leaf-off as opposed to summer when vegetation is green and reflectance similarities in the visible and NIR may be too great. None of the combinations of seasonal imagery produced higher accuracies than any of the contributing individual seasons. Appendix L contains the accuracy results for the other 3 sites.

Table 5.29. CTA accuracy statistics (%) for the Number of VCFs for the combinations of seasonal imagery for Mer Bleue Bog. Class A, B, and C represent 1 to 3, 4 to 5 forms, and 6 or more forms, respectively (Section 2.9.2).

Season and/or combination of seasons	Overall Accuracy (%)	Kappa	Class A		Class B		Class C		Average	
			PA (%)	UA (%)						
Spring	65.7	0.39	68.2	79.8	58.3	77.8	100.0	14.3	75.5	57.3
Summer	57.1	0.19	68.2	71.4	33.3	44.4	100.0	20.0	67.2	45.3
Fall	60.0	0.25	68.2	71.4	41.7	55.6	100.0	20.0	70.0	49.0
Combined Spring/Summer	65.7	0.40	72.7	84.2	50.0	75.0	100.0	12.5	74.2	57.2
Combined Spring/Fall	54.3	0.22	54.5	75.0	50.0	50.0	100.0	14.3	68.2	46.4
Combined Summer/Fall	74.3	0.54	72.7	88.9	75.0	75.0	100.0	20.0	82.6	61.3
Combined (3 season)	65.7	0.39	72.7	80.0	50.0	85.7	100.0	12.5	74.2	59.4

Table 5.30. CTA error matrices for the Number of VCFs for A) spring; B) summer; C) fall; D) spring/fall; E) summer/fall for Mer Bleue Bog. Class A, B, C representing 1 to 3, 4 to 5, and 6 or more forms, respectively (Section 2.9.2).

A-Spring		Reference Samples			
		Class A	Class B	Class C	Total
Classified Samples	Class A	15	4	0	19
	Class B	2	7	0	9
	Class C	5	1	1	7
	Total	22	12	1	35
B-Summer		Reference Samples			
		Class A	Class B	Class C	Total
Classified Samples	Class A	15	6	0	21
	Class B	5	4	0	9
	Class C	2	2	1	5
	Total	22	12	1	35
C-Fall		Reference Samples			
		Class A	Class B	Class C	Total
Classified Samples	Class A	15	6	0	21
	Class B	4	5	0	9
	Class C	3	1	1	5
	Total	22	12	1	35
D-Spring/Fall		Reference Samples			
		Class A	Class B	Class C	Total
Classified Samples	Class A	12	4	0	16
	Class B	6	6	0	12
	Class C	4	2	1	7
	Total	22	12	1	35
E-Summer/Fall		Reference Samples			
		Class A	Class B	Class C	Total
Classified Samples	Class A	16	2	0	18
	Class B	3	9	0	12
	Class C	3	1	1	5
	Total	22	12	1	35

Summary of main findings for temporal analyses for VCFs:

- Using summer WorldView-2 imagery alone for classification of the 3-category Number of VCF classes or for individual VCFs did not improve overall accuracies over spring imagery;
- Combining summer and fall WorldView-2 imagery improved the accuracies for the Number of VCF classes by approximately 10%; and
- Multi-season WorldView-2 imagery did not improve the overall accuracies of individual VCF classifications.

Table 5.31. CTA accuracy statistics (%) for the VCFs for the combinations of seasonal WorldView-2 imagery for Mer Bleue Bog.

Season	Overall Accuracy (%)	Kappa	C (Coniferous Dominant)		GC (Herb Dominant)		H (Hardwood Dominant)		NE, RE, BE (Emergent Dominant)		LS or TS (Shrub Dominant)		Average	
			PA (%)	UA (%)	PA (%)	UA (%)	PA (%)	UA (%)	PA (%)	UA (%)	PA (%)	UA (%)	PA (%)	UA (%)
Spring	68.6	0.58	100.0	60.0	100.0	50.0	66.7	80.0	100.0	75.0	50.0	70.0	80.9	55.9
Summer	54.3	0.41	66.7	28.6	33.3	16.7	50.0	100.0	100.0	60.0	50.0	63.6	60.0	53.8
Fall	62.9	0.50	66.7	33.3	66.7	33.3	75.0	75.0	66.7	100.0	50.0	77.8	65.0	63.9
Combined Spring/Summer	57.1	0.47	100.0	30.0	100.0	42.9	58.3	77.8	100.0	75.0	28.6	80.0	77.4	61.1
Combined Spring/Fall	54.3	0.43	100.0	27.3	100.0	37.5	58.3	100.0	33.3	50.0	35.7	71.4	65.5	57.2
Combined Summer/Fall	62.9	0.49	66.7	33.3	66.7	40.0	66.7	72.7	33.3	100.0	64.3	75.0	59.5	64.2
Combined (3 season)	51.4	0.40	100.0	23.1	100.0	50.0	66.7	80.0	33.3	33.3	21.4	100.0	64.3	57.3

5.7.3 Temporal analyses for Open Water Type

The optimal parameter values for Open Water Types were: scale value = 25; shape value = 0.1, and compactness value = 0.75. Table 5.32 provides the accuracy results for the Open Water Type classifications at Mer Bleue Bog (Other sites' accuracy results are located in Appendix L). Although overall accuracy was the highest with the spring imagery (73.3%), by utilizing combined summer and fall imagery, the highest average PA and UA accuracies were obtained (69.4% and 73%, PA and UA, respectively). This is because of improved results for the Open Water Type classes 4, 6, and 7. These three Open Water Types represent areas (of different percentages) of open water in the central portion of the wetland (Section 2.9.3). In the spring and summer imagery these areas could be confused with Type 2 which is also comprised of a central area of open water (but a smaller portion). In the spring with less green vegetation present, these areas may appear similar, whereas with in summer, green vegetation and differences become more pronounced.

Table 5.32. CTA accuracy statistics (%) for the Open Water Types for Mer Bleue Bog for the combinations of seasonal WorldView-2 imagery.

Season	Overall Accuracy (%)	Kappa	Type 1		Type 2		Combined (4, 6, 7 when present)		Average	
			PA (%)	UA (%)	PA (%)	UA (%)	PA (%)	UA (%)	PA (%)	UA (%)
Spring	73.3	0.57	87.5	100.0	100.0	57.1	0.0	0.0	62.5	52.4
Fall	58.3	0.34	75.0	100.0	100.0	20.0	0.0	0.0	58.3	40.0
Combined Spring/Fall	58.3	0.28	75.0	85.7	100.0	20.0	0.0	0.0	58.3	35.2
Combined Summer/ Fall	66.7	0.42	75.0	85.7	100.0	33.3	33.3	100.0	69.4	73.0
Combined (3 season)	66.7	0.43	87.5	100.0	100.0	25.0	0.00	0.00	62.5	41.7

As the best result using spring Landsat 5 TM imagery was obtained using the segmented original bands and a DEM, summer imagery was also tested using this data

configuration. The same segmentation parameter values found to be optimal for the spring imagery were also found to be optimal for the summer and fall imagery: scale value = 2; shape value = 0.1; and compactness value = 0.1.

Table 5.33 provides the results of the Open Water Type classifications using spring and summer Landsat 5 TM data for Loch Garry (highest accuracy result). Although both seasons produced the same overall accuracies, the average PA and UA for summer imagery were higher (96% and 95%, respectively). This is related to the accuracy for Open Water Type class 8, which was well classified using the summer imagery but poorly classified using the spring imagery. Table 5.34 is the error matrix for the spring classification. Type 8 represents areas where more than 95% of the wetland is open water. Type 5 represents areas where 26 to 75% of the wetland is open water but occurs in a ‘ponding’ pattern. In the spring, the validation sample for Type 8 was classified as Type 5.

Table 5.33. CTA accuracy statistics for the Open Water Types providing accuracies (%) for seasonal Landsat TM 5 imagery for Loch Garry.

Season	Overall Accuracy (%)	Kappa	Type 1		Type 5		Type 8		Average	
			PA (%)	UA (%)	PA (%)	UA (%)	PA (%)	UA (%)	PA (%)	UA (%)
Spring	93.3	0.87	100	100	100	85.7	0.0	0.0	66.7	61.9
Summer	93.3	0.88	87.5	100	100	85.7	100	100	95.8	95.2

Table 5.34. Error matrix for the Landsat TM 5 Open Water Type classification (3 classes).

		Reference Samples			
		Type 1	Type 5	Type 8	Total
Classified Samples	Type 1	8	0	0	8
	Type 5	0	6	1	7
	Type 8	0	0	0	1
	Total	8	6	1	15

The general dryness of the 2010 spring is evident in the larger extents assigned to OWT classes (in Figure 5.40) with lower proportions of open water in comparison to the summer thematic map. In contrast, as June of 2010 was wetter than normal (Figure 5.41), mapped Open Water Type classes generally have higher proportions of open water. Similar to the spring imagery there is no relation between the areas of classified Open Water Types for any of the classifications.

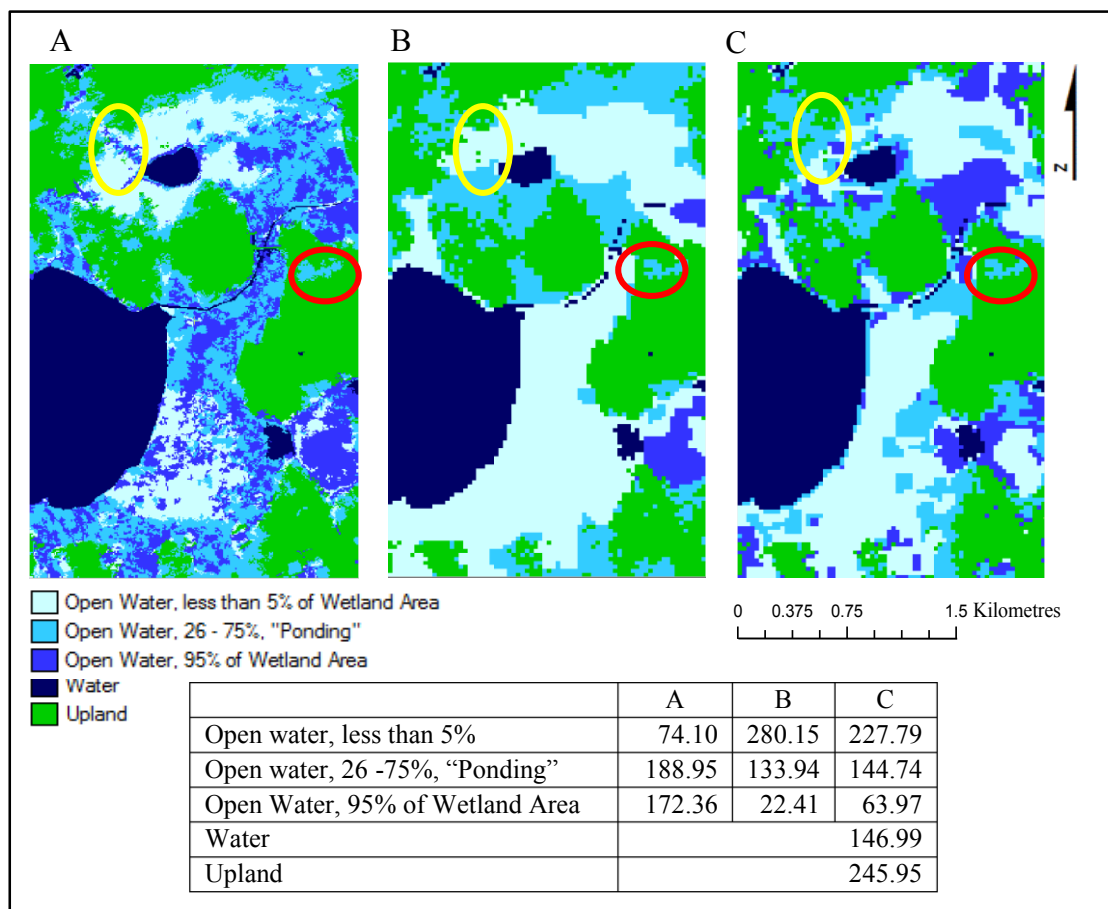


Figure 5.40: Loch Garry Open Water Type classification A) spring WorldView-2 imagery, DEM and CTA analyses; B) spring Landsat TM imagery (original bands segmented with DEM and CTA analyses); and C) summer Landsat TM imagery (original bands segmented with DEM and CTA analyses) Water and Upland class are from WorldView-2 5-Class Wetland Type classification.

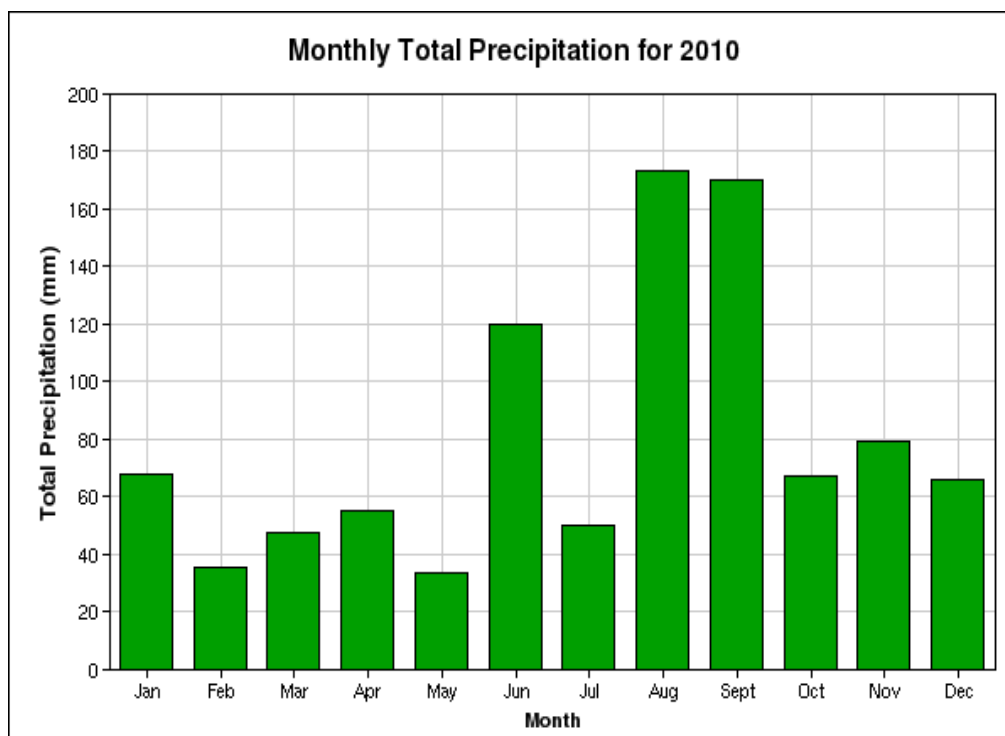


Figure 5.41. Monthly total precipitation for Ottawa-McDonald Cartier Airport, revealing the drought (less precipitation) that occurred before the spring imagery were acquired (February, March for April acquisition) and the greater accumulation that occurred before the summer imagery were acquired (June for July acquisition (Environment Canada, 2013).

Summary of main findings for temporal analyses for Open Water Types:

- Using summer WorldView-2 imagery alone for Open Water Type classification did not improve overall accuracies;
- Combining multi-season WorldView-2 imagery did not improve the overall accuracies for the Open Water Type classifications, but some individual classes did improve; and
- Using summer Landsat 5 TM imagery improved the UA and PA of some classes.

5.7.4 Temporal analyses for Inundation Extent

Comparison was made of the field measured VWC transects that were completed in the spring to those completed in the summer of 2010. In general, in spring, 100% VWC occurred at a greater extent (further upslope) than in summer. This would be expected in a normal year when spring is wetter than summer, however, this was not expected in 2010, where spring measurements occurred after a winter drought. In a few cases 100% VWC occurred further into the wetland in the spring than in summer (e.g. a contracted saturated boundary), which was expected for 2010. Figure 5.42 provides an example of these different scenarios. Figure 5.42A is an example of a transect where the wet extent (100% VWC) for spring expanded past the summer wetland boundary. Figure 5.42B is an example where the saturated extent in summer was further upslope than in spring. This contracted spring extent occurred on transects in three marshes (two cattail marshes and one beaver dam marsh) and the bog example in Figure 5.42B (a lagg). It is believed that these particular features were influenced by the spring drought of 2010 (see Figure 5.41) and by the influx of precipitation in June 2010.

Figure 5.43 provides an example of the 2011 field measured wet extents as compared to the 2010 field measured transects. This example shows that (at the edge of a cattail marsh) the 2010 spring and summer transects went further into the wetland until 100% VWC was measured in comparison to the 2011 spring and summer wet extents.

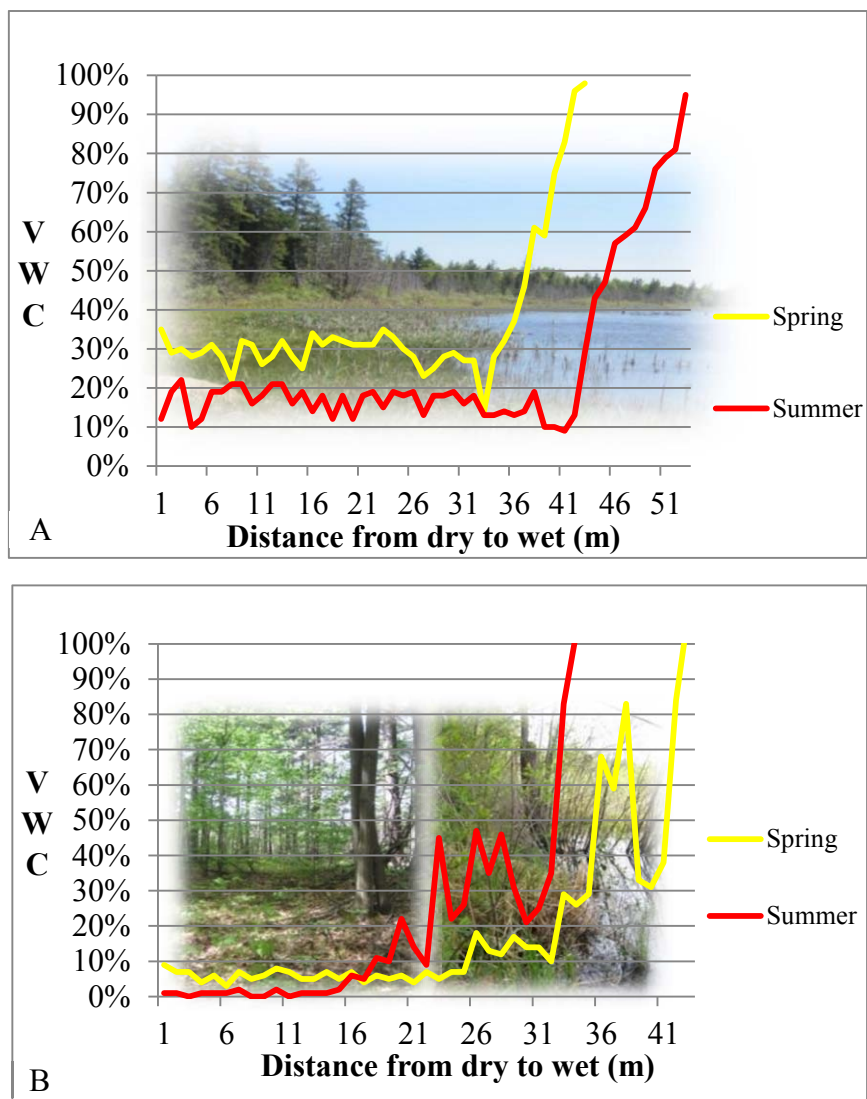
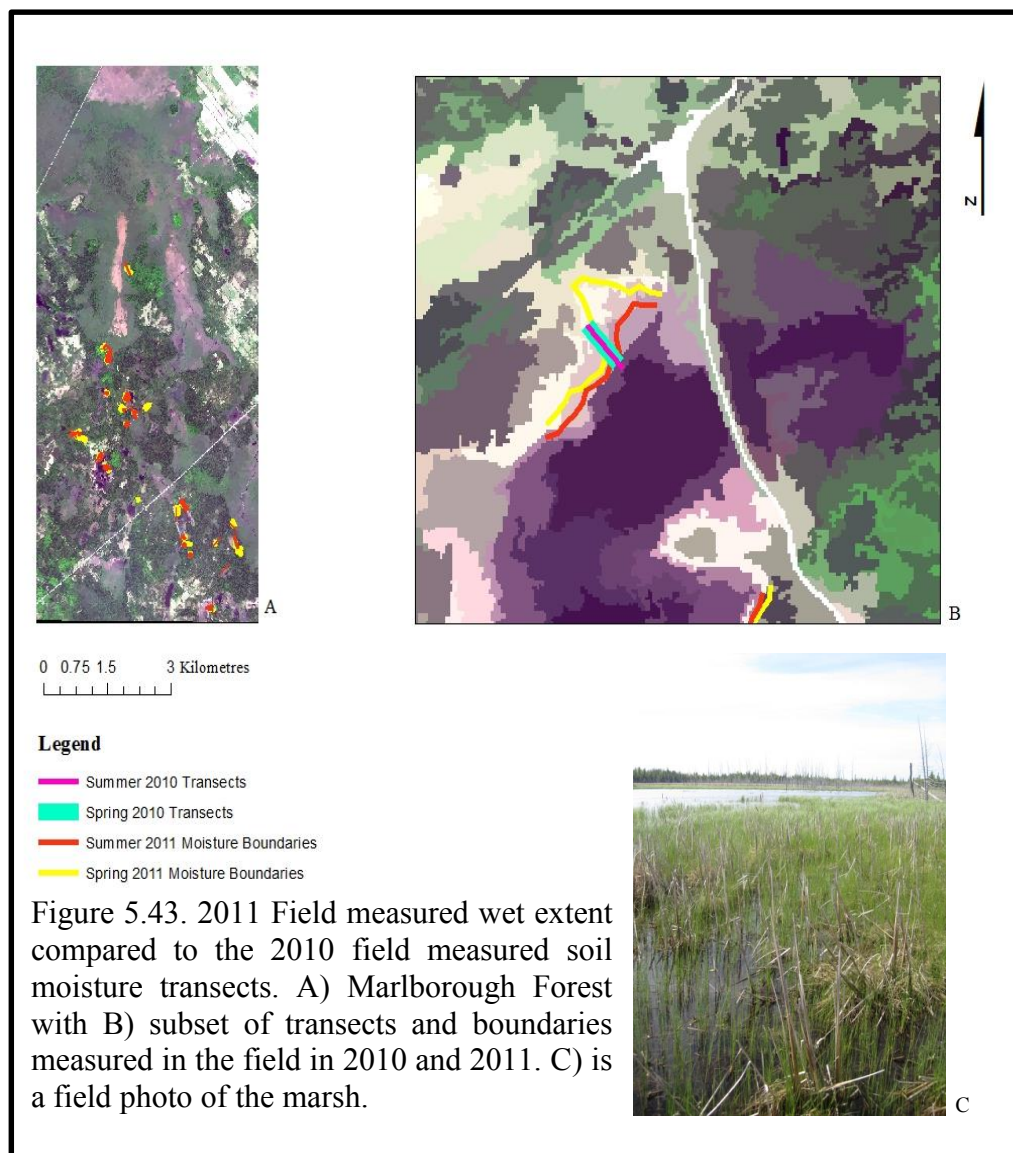


Figure 5.42. Spring and summer field measured VWC transects measured at A) Marlborough Forest, where spring had a larger wet extent than B) Westport Bog, where summer had larger wet extent.

This is expected, as in the first 6 months of 2011 there were 547 mm precipitation, whereas in 2010 there were 360.2 mm of precipitation between January and June (with 120 mm in June 2010, (Environment Canada, 2013)).



The same spring WorldView-2 pan-sharpened $NDVI_{green}$ analysis as described in Section 5.4, was applied to summer imagery. Figure 5.44 is an example of some of the derived wet extents at Mer Bleue Bog for the summer of 2010. It can be seen that summer transects from dry upland to 100% VWC meet with the $NDVI_{Green}$ derived wet extent (100%

VWC) boundary. This is similar to the spring analysis and indicates that $NDVI_{Green}$ is a good indicator of the wet extent in both seasons (see Figure 5.33).

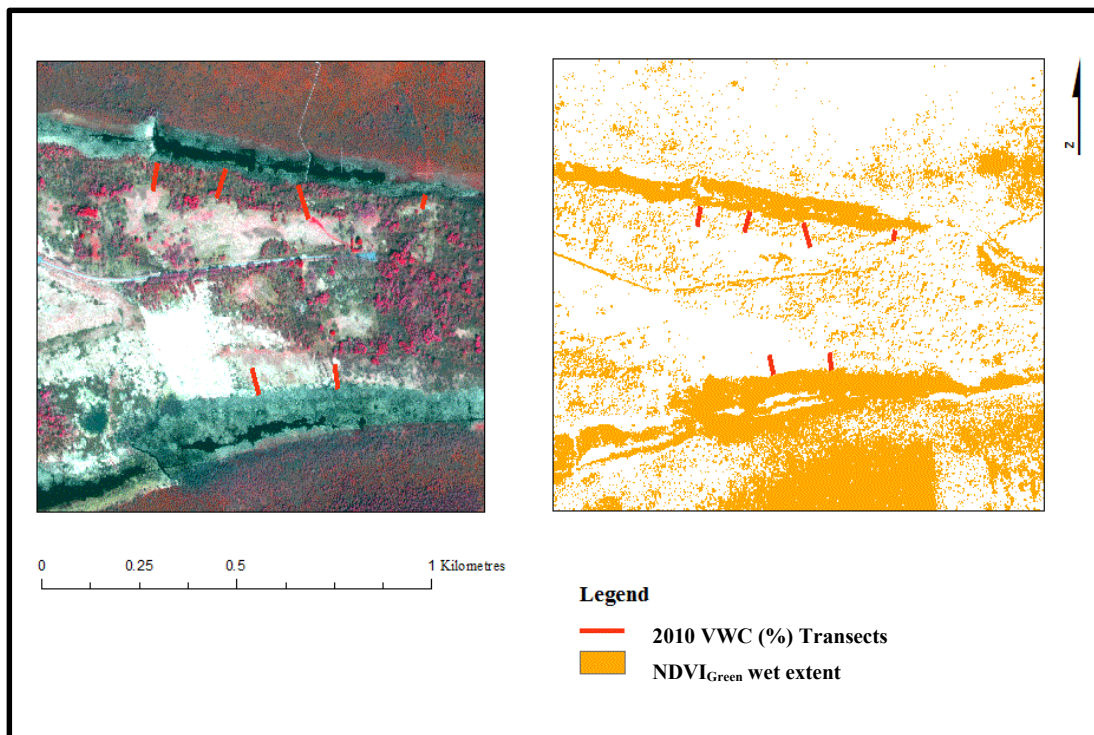


Figure 5.44. A) Summer WorldView-2 CIR composite of a section of Mer Bleu Bog; B) orange is the 100% saturated boundary derived from the $NDVI_{Green}$ threshold with the red lines representing the transects measured in the summer of 2010.

A summer 2011 field-measured wet extent was not completed and therefore cannot be compared to the 2010 individual transects or the 2011 spring wet extent. It appears that seasonal differences are relative in their relation to VWC and, while the threshold values change slightly from season to season (e.g. spring Mer Bleu Bog threshold values were -0.025 to 0.075 whereas summer $NDVI_{Green}$ threshold values were 0.00 to 0.075), a boundary

that represents a wetland wet extent can be derived using either spring or summer NDVI_{Green} images.

Summary of main findings for temporal analyses for Inundation Extent:

- Seasonal and annual differences in wet extent highlighted the need for multiple season and/or inter-annual mapping of wetlands to determine an overall average extent for scoring; and
- Boundaries representing 100% VWC (a wetland wet extent) were well delineated using either spring or summer NDVI_{Green} images derived from WorldView-2 imagery.

5.8 Two-date temporal comparison of fraction maps as an indicator of Anthropogenic Influence.

Landsat 5 TM imagery acquired on the nearest non-cloudy dates to the original field based OWES evaluations (Loch Garry and Mer Bleue Bog, 1983; Westport Bog, 1985; and Marlborough Forest, 1991; see Table 3.1) and the 2010 summer images were converted to Top-of-Atmosphere (TOA) radiance (Methods section 4.7) and then relatively calibrated (older image to 2010 image) using PIFs (see Appendix M for calibration details and graphs). These calibrated images were subsequently unmixed using three and five automatically selected EMs (Background 2.8.2). The resultant fraction maps were then compared using RGB image display and simple image differencing.

Figure 5.45 provides a visual example of the three fractions derived for Loch Garry using July 1984 Landsat 5 TM imagery and July 2010 Landsat 5 TM imagery. In Figure 5.45A, there are similarly high vegetation fraction values for both years (light grey/white areas) in the upland and throughout the wetland complex. There are some small areas (purple circles) where the vegetation fraction was higher in 2010 than in 1984. These particular areas are mostly marsh. The total precipitation accumulated until July 2010 was 360.8 mm and the lake water level was 89.082 m ASL (Environment Canada, 2013; Loch Garry Lake Association, 2013). The total precipitation accumulated to July 1984 was 450 mm (historic lake water levels are unavailable). There was more precipitation accumulated to the date of image acquisition in 1984 than in 2010. It has been found that with an increase in mean water levels there is often a decrease in above-ground biomass in freshwater marshes (McKee and Mendelssohn, 1989), although this is not possible to confirm using these data.

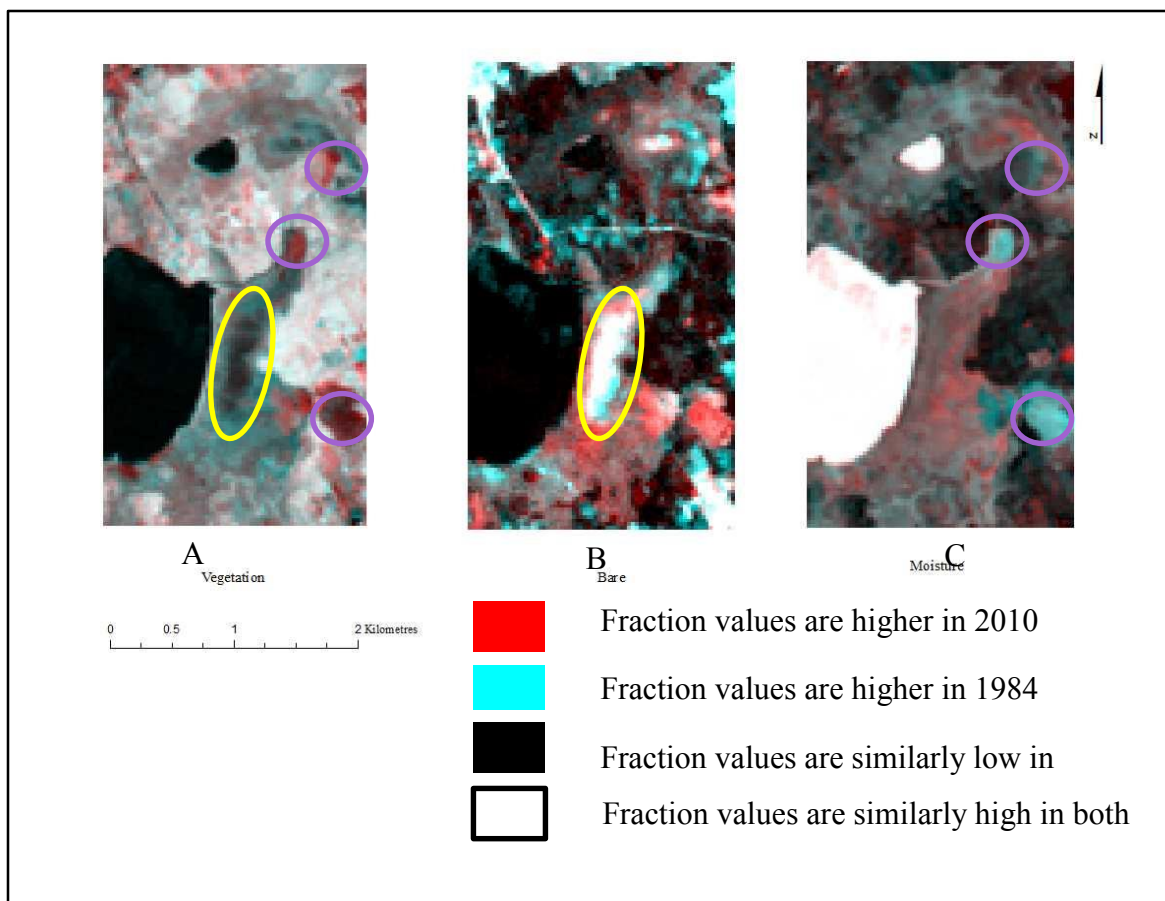


Figure 5.45. Fraction images from 1984 and 2010 for Loch Garry. Yellow circle highlights an area which, for both years, appears as bare with low vegetation values. Purple circles highlight areas where the vegetation fraction was higher in 2010, and the moisture fraction was higher in 1984. (Red display = 2010; Green display = 1984; and Blue display = 1984).

Around the edge and just below the yellow circle the 1984 vegetation fractions are slightly higher than in 2010; within the yellow circle the fractions for both years were similarly low. The Wetland Type classifications indicate these areas to be Fen (Figures 5.6). The Open Water Type classification with the highest accuracy (93%) shows this area to be < 5% open water (Figure 5.31C). Neither of these classifications indicates that the area within the yellow circle is bare as indicated by the high bare fraction within the yellow circle.

Unfortunately it was extremely difficult to physically enter this area, so field verification was not conducted.

Overall vegetation fraction maps derived for Westport Bog, Mer Bleue Bog and Loch Garry showed higher historical vegetation fraction values than the 2010 derived fraction maps. Marlborough Forest vegetation fractions were not higher in 1991 than in 2010 but, similar to 1984, 1991 was a wetter year (524.5 mm accumulated to July) than 2010, which could lower above-ground biomass.

It is difficult to determine if the comparison of the historical vegetation fraction map to the current day fraction map for each site provides much insight into overall anthropogenic influence, and whether or not the differences in vegetation fractions were related to anthropogenic disturbance or simply due to annual differences in precipitation. Known differences were identified as land cover change at Westport Bog. There was abundant vegetation in July 2010 in what appears to be a lake in July 1984. Figure 5.46 highlights this increase (yellow circle); however, the site was inaccessible for field visit (to determine if the lake was filled or if it was the development of floating vegetation in 2010, which again could be related to the water levels, weather, and date of image acquisition (September 11, 2010)). The yellow arrows in Figure 5.46 point to an area that had vegetation cover in 1984, but was water in 2010. It is known that that particular water body had been purposefully dammed in the past, and that the overall area had become a small lake for recreational purposes (fishing) with a central portion developing into wetland. This type of change would be considered Anthropogenic Disturbance within the current OWES.

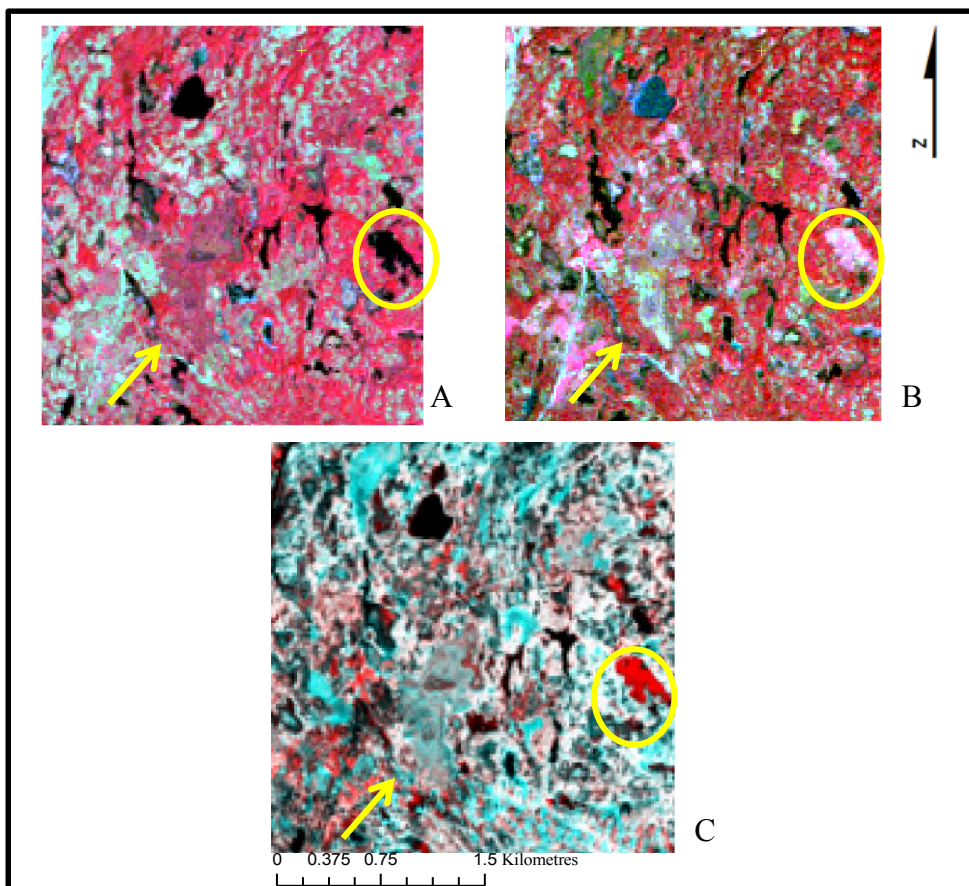


Figure 5.46. A) 1984 CIR composite of Landsat TM image; B) 2010 CIR composite of Landsat TM image; and C) temporal composite (Red display = 2010; Green display = 1984; and Blue display = 1984) of vegetation fractions derived from the previous two images. The yellow circle highlights the change from water body to vegetation; and the yellow arrow points to a flooded area.

5.8.1 Summary of the main findings for the two-date temporal comparison of fraction maps

- Differences between two years of the vegetation, bare and moisture fraction maps can be assessed using simple RGB image display;
- The vegetation fractions were higher historically (1984) in some areas of three of the four study sites. In a few small areas of marsh, vegetation fractions were lower in

1984. This could relate to the increased amount of precipitation received in 1984, which may have benefited some vegetation, but decreased above-ground biomass in marsh areas; and

- Known changes that were initiated through Anthropogenic Disturbance can be observed using vegetation fraction maps as seen at Westport Bog with the flooding of an area for recreational purposes.

6.0 Discussion and conclusions

This chapter discusses the results in two sub-sections: 1) the contributions of the research to the overall understanding of wetlands, wetland dynamics, and using remote sensing and GIS to evaluate and assess wetlands; and 2) the technical successes and contributions of the remote sensing and GIS methods used in this research. Recommendations are given with regards to the best data types, types of analyses, and data processing. The limitations are presented and future directions for this type of research are provided. Finally the chapter presents the conclusions of the research.

6.1 Findings and contributions of this research

6.1.1 Contributions of the research to wetland and remote sensing science

Wetlands (in general, and for specific wetland attributes) require examinations that use a variety of spectral, spatial, and temporal resolution data, and a top-down, overview perspective that considers many possible combinations of information. Evaluating wetlands using only one type of data, or one season, or at one site only provides information that is pertinent to that particular site at that time. This research shows that an overview perspective can emphasize the inherent differences between wetlands across a regional area; highlight the benefits and limitations of particular imagery types; illustrate accuracy differences due to different seasonal assessments; and reveal the unique issues with utilizing remote sensing and GIS methods within an existing wetland management program. Many studies continue to focus on only one (or two) of these aspects of wetland mapping (e.g. differences between

locations, in season, in spectral type, or spatial resolution of imagery, and/or differences in methodology).

The research investigated four sites and three seasons for two years, and looked at change over decades, using three types of imagery (coarse and fine resolution optical and radar imagery). Many of the outcomes were dependent on the type of imagery used, the spatial resolution of the imagery (coarse or fine), the season of image acquisition (spring, summer, fall or combination), and/or particular site location (e.g. on the Canadian Shield as compared to highly fragmented farmland). The omission of any of the variables would have resulted in different outcomes. For example, if only three of the four sites were considered and Westport Bog site was omitted, the lower accuracies and misclassifications that resulted for the Wetland Type classifications (e.g. of Marsh on the shield landscape) would not be apparent. Similarly, if Mer Bleue Bog site was omitted the improvements in accuracy seen using summer (and combined) imagery would also have been missed (and would also be the case if only spring imagery were used). Additionally, using only high resolution imagery for all the wetland attributes would omit the improved accuracies for Open Water Type classifications using coarse resolution imagery. Omitting SAR imagery would overlook the increases in individual class accuracies (e.g. Swamp class improving with HH, HV images; or Fen class improving with CP variable images).

From these in-depth analyses it was found that there were significant differences in overall and specific class related accuracies for all fourteen variables depending upon time of year, location, and/or data used (alone, or in combination). Similar results to some of

those found in this research have been found previous studies. In general, Wetland Type accuracies in the literature using a variety of methods and data range from 71 to 92% (Bernier *et al.*, 2003; Rogers and Kearney, 2004; Li and Chen, 2005; Racine *et al.*, 2005; Wright and Gallant, 2007; Touzi *et al.*, 2007; Grenier *et al.*, 2007; Durieux *et al.*, 2007; Castaneda and Ducrot, 2009; Kwoun and Lu, 2009; Jiao *et al.*, 2011; Dronova *et al.*, 2011; Ricaurte *et al.*, 2012). However, almost all of these studies were conducted in one or two wetlands, whereas this research evaluated capabilities for Wetland Type classification over a region in four distinctly different wetland complexes, showing that accuracy is context and site dependent. Particularly in relation to this research, differences in Wetland Type class accuracies were found in Mwita *et al.* (2013) for four distinct wetland sites across Kenya and Tanzania (using single season Landsat and a DEM). These differences reveal the importance of having several different wetland sites of interest to be able to compare and understand the spatial variation of the attribute of interest.

The improvements found when combining seasonal imagery, particularly for Mer Bleue Bog in this research, have also been demonstrated in the literature (Pope *et al.*, 1997, Baghdadi *et al.*, 2001; Racine *et al.*, 2005; Ghioca-Robrecht *et al.*, 2008; Bourgeau-Chavez *et al.*, 2010; Dribault *et al.*, 2012; Bourgeau-Chavez *et al.*, 2013; Evans and Costa, 2013). However, many of these studies revolved around the combination of multiple SAR image types with fewer concerning optical imagery. Particularly, Ghioca-Robrecht *et al.* (2008) found that multi-temporal QuickBird imagery could improve classifications from 41% to 90% PA and from 17 to 91% UA. In the research presented in this thesis, in combining the

WorldView-2 spring and summer imagery, the improvements found for Mer Bleue Bog were not found for the other three sites, although some of the issues in this research could relate to the problems found with other summer imagery where there were haze or clouds or strange reflectance especially for water.

The most similar research to this work, with a similar number of components but only investigating one variable, Wetland Type, was Grenier *et al.* (2007) who utilized both summer optical (Landsat) and spring Radarsat1 data in an object-based segmentation and classification of five Wetland Types at two sites in Quebec, Canada. They had comparable differences to this research in overall accuracies between the two sites and between Wetland Type classes at each site independently.

In this research, Marsh consistently had the poorest UA, PA, and average accuracies. It often had odd spectral response (see Figure 5.16, polarimetric signatures), and was misclassified (see Figure 5.14), or in CTA, over-classified, as leftover pixels were assigned to Marsh class (see Figure 5.7). There appear to be two possible reasons for this, including vegetation types such as grasses or shrubs that are similar in other wetland types such as Fen and Swamp, and water levels affecting classifications, vegetation presence, etc. These results are similar to other studies such Grenier *et al.* (2007) in which radar and optical imagery (Landsat ETM+) were combined in classification of wetlands that were geographically close to this study (Quebec, Canada). Their Marsh class had the highest commission error (40%) of all wetland classes. They related this to confusion with a “shallow water” class, which was not a specific class of this research. Millard and

Richardson (2013) used different imagery types in a study of Mer Bleue Bog. Their Marsh class had lower average PA and UA, but it was not classified as poorly as Fen. Conversely, in this research, Fen and Bog typically had the best accuracies (as described above) and these were also similar to Grenier *et al.* (2007) and Millard and Richardson (2013) for Bog. Other researchers had higher accuracies with different data types at different locations (Pope *et al.*, 1997, (ENVISAT at Chesapeake Bay Wetlands) and Lang and Kasischke, 2008, (Radarsat-2 imagery at Gagetown, New Brunswick)).

Remote sensing and GIS can be used to assess attributes of wetlands and to produce usable, accurate thematic maps (e.g. Wetland Type), or to support wetland management for scoring. This was not surprising as successes using remote sensing to assess individual wetland attributes/classes have been found in the literature (see Table 2.5). This and prior research also revealed that it is not possible to use remote sensing and GIS to assess every wetland attribute as they are currently assessed in field-based evaluation systems such as the OWES.

For example, for the OWES categorization of biodiversity, the Number of VCFs could not be accurately mapped using the data and methods of this research. Stow *et al.* (2004) also stated that it was not possible to develop a predictive model for such variables because current GIS models “do not adequately emulate field-based methods.”

Remote sensing methods may be developed that can emulate the field-based process, whether in sample design, mapping of vegetation, water or land cover patterns, etc. The problem is that visible-NIR-SWIR-radar remote sensing data are constrained to

representations of reflectance of incident radiation and do not include mapping of many of the other physical attributes of the wetland that are included (although sometimes subjectively) in field-based data. In addition, multiple spatial and compositional configurations of land cover may result in similar reflectance or backscatter at a given scale of analysis, leading to reduced classification precision using remotely sensed data. In this research, it was shown that it was possible to map certain groups of wetland plant types/groups and produce a map of the configuration of the number of VCFs. Rather than seeing that as a failure or an inability to categorize specific VCFs as represented in the OWES, it should be investigated whether that product can be incorporated into the management system in replacement of, or in combination with the existing field-based methodology.

To integrate a remote sensing approach with the field based approach, current methods of measurement and scoring should be reviewed. This would entail an adjustment of the existing management documents and processes, but could enable a functional, repeatable, and cost-effective framework to monitor and manage wetlands. As an example, remote sensing/GIS could be used as an initial means to conduct quick evaluations, produce maps of expected attribute values for those attributes known to have appropriate accuracy, and to aid in sampling design for subsequent field evaluation. Such data could also be used in more frequent temporal monitoring than has occurred with the field-based OWES. Change analysis on a periodic basis (e.g., every five years), could be conducted to determine

if and where significant reflectance change has occurred and if further field investigation is warranted.

6.1.2 Technical successes and contributions

This research had success with several of the OWES attributes under each of the three research objectives: (1) acceptable attribute mapping accuracies were achieved for several attributes; 2) derived scoring values were similar to OWES evaluated scores; and 3) from temporal analysis of remote sensing data, the best single season and multiple seasons for imagery acquisition were determined, and it was determined that long term analysis using archival imagery is valuable and can reveal attribute changes that are missing from the periodic or single field assessments of the current OWES. The following is a detailed discussion of these technical successes and contributions. Table 6.1 lists the highest accuracies obtained for each of the four wetland sites for Wetland Type, Number of VCFs, and Open Water Types, as a reference for the discussion of these results in relation in the literature. The highest Wetland Type accuracies in this research were achieved using spring WorldView-2 and DEM data, ranging from 72% to 89%. These results concurred with the majority of the literature, including studies that used other methods and imagery types, However, other studies used coarser resolution and/or spectrally different data at single study sites (Touzi *et al.*, 2007; Dronova *et al.*, 2012); multiple sites closely related within one watershed and radar data (Racine *et al.*, 2005); synthetic data (Rogers and Kearney, 2004), or distinctly different wetlands in other parts of the world (Wright and Gallant, 2007; Castaneda and Ducrot, 2009; Dronova *et al.*, 2011). Often, previous studies are comparable

to this research in one or two elements (e.g., use of radar backscatter in multiple polarizations) but are different in other elements, such as the nature of the wetland environments, or the processing and classification methods. Or they do not give full information in accuracy assessment. For example, Li and Chen (2005), for three sites, reported individual class accuracies ranging from 71% to 92% for Marsh, Fen, Bog, Swamp, but did not report overall accuracies. Grenier *et al.* (2007), with two sites, presented 80% overall accuracy at a broader Wetland-non-Wetland level, and overall accuracies of 67% and 76% for specific Wetland Types. Additionally, for those studies with more sites, this research achieved higher overall accuracies for Wetland Type classifications (10% higher than in Grenier *et al.*, 2007; 8% higher than in Li and Chen, 2005). Therefore, in comparison with studies in simpler or different environments, or studies of individual wetlands, the results presented in this research are positive, given the complexity of each site and given that they apply across four different wetland complexes.

The highest accuracies for VCF type and Number of VCFs in this research ranged from 44 to 71% and were less than the range of 76 to 96% found throughout the literature. However, some of these studies only looked at one or two sites. For example, Hess *et al.* (2003) had accuracies of 78 to 91% for flooded and non-flooded classification, and for specific flooded herbaceous class (63-65%) for one site using L-band data. Atkinson and Treitz (2012) using IKONOS imagery and four ecological classes at two sites, achieved accuracies ranging from 69 to 79%. Wang *et al.* (2012), using a time-series of ten 32m pixel Beijing-1 images for one site, classified seven classes with accuracies ranging from 81 to

90%. The ranges presented in this research are positively comparable as four study sites were assessed in this research as opposed to one or two sites. Jiang *et al.* (2012) classified four vegetation classes at one lake in China using multiple data types (Landsat and radar) for overall accuracies of 78 to 90%; however they had over 900 reference data samples. Such a large sample size for classification and validation may have improved the results of that research, or at the least provided higher precision in error analysis, however such a sampling or acquisition scheme would not be logistical or realistic for multiple sites in a regional wetland evaluation system. The highest Open Water Type accuracies in this research ranged from 60 to 93%. There was no comparable literature found on classification of water classes such as those in this research. Other studies generally focus on the temporal variation of surface water patterns and relationships between backscatter and soil moisture (Bartsch *et al.*, 2008; Sass and Creed, 2008; Campos *et al.*, 2012; Watts *et al.*, 2012) the second of which was attempted in this research, but had very poor results and therefore were not included.

Given the operational nature of the OWES and the need to develop capacity for geomatics-based mapping and evaluation of wetlands, a reasonable question to ask would be: “To aid development of such a program, what optimal data set should be used in the initial stages to provide the greatest potential for successful mapping of Wetland Type, VCFs and Open Water Type?” Table 6.2 provides the best single data sets based on this research for these attribute groups.

Table 6.1. List of the highest accuracies obtained for Wetland Type (Bog, Fen, Marsh, Swamp); VCFs (overall accuracy only); # of VCFs (A = 3 or less forms, B = 4 -5 forms, C = 6 or more); and Open Water Types (refer to Table 2.7 for Type definitions). OA (%) is Overall Accuracy and, under each individual class, PA (%) / UA(%) are presented. Definitions of codes of data types and seasons are: WV (WorldView-2); L(Landsat TM-5); R2 (Radarsat-2); DEM (DEM); 5EM (5 Automatically selected EM); 3EM (3 manually selected EM); HH & HV (HH and HV backscatter) CP (Cloude-Pottier components); SU (Summer); SP(Spring); F(Fall); and where seasons were combined, '/' means both/all were used. All of the best accuracies were obtained using some form of OBIA and CTA, or pixel-based CTA alone (for EM classifications).

	Wetland Type				VCFs	# of VCFs				Open Water Types			
	OA %	Fen	Marsh	Swamp	OA %	OA %	A	B	C	OA %	1	5	8
Data Combination	SP-WV/DEM	SU-WV/DEM/CP	SP-WV/DEM	SU-WV/DEM/HH/HV	SP-WV/DEM	SU-WV/DEM				SU-L/ 3EM/DEM/NO OBIA			
Loch Garry	86.5	100/100	75/100	100/100	69	60	50/83	64/54	75/50	93	88/100	100/67	100/100
	OA %	Fen	Marsh	Swamp	OA %	OA %	A	B	C	OA %	1	5 Combined	8
Data Combination	SP-L/5EM/No OBIA	SP-L/5EM/No OBIA	SU-WV/DEM	SP-WV/DEM/HH/HV	SP-WV/DEM	SP-WV/DEM				SP-L/Original Bands/DEM			
Marlborough Forest	78	100/78	80/71	83/71	45	53	54/76	41/28	100/33	60	50/33	67/50	60/60
	OA %	Short Bog	Tall Bog	Marsh	OA %	OA %	A	B	C	OA %	1	5	8
Data Combination	SP/SU – WV /DEM		SU-WV/DEM	SP/SU – WV/DEM	SP-WV/DEM	SP-WV/DEM				SU-L/3EM/DEM/NO OBIA			
Mer Bleue Bog	87	80/100	84/63	78/100	68	74	73/89	75/75	100/20	76	83/71	85/80	50/100
	OA	Bog	Marsh	OA	OA	A	B	C	OA	1	Combined	8	

	%			%	%				%			
Data Combination	SP-WV/DEM	SP-WV/DEM/HH/HV	SU-WV-DEM	SU-WV/DEM	SP-WV/DEM				SU-L/3EM/DEM/NO OBIA			
Westport Bog	72	89/73	80/50	68	71	71/79	67/80	100/20	67	17/50	93/76	55/60

Table 6.2. Recommendations for selection of data based upon the majority results presented in this research.

	Wetland Type	VCFs	# of VCFs	Open Water Types
Data Combination	SP-WorldView-2/ DEM / Radarsat-2 CP & HH/HV	SP-WV/DEM		SU-Landsat and DEM
Overall Priority List				
Data Combination	<ol style="list-style-type: none"> 1. Spring WorldView-2 2. DEM 3. Radarsat-2 CP & HH/HV 4. Summer Landsat 			

This is followed by the best data set overall, given a single data set was to be used for all of these attribute groups. Also from this research and supported by the literature, each data set in Table 6.2 should be used with OBIA and CTA or a similar decision tree classifier.

6.1.3 OBIA segmentation for object creation

The importance of optimal segmentation parameter selection continues to be an ongoing technical aspect of interest for research using OBIA (Dragut *et al.*, 2010; Marpu *et al.*, 2010). As many of the current studies utilize eCognition software to create objects, additional, supportive evidence of the ‘correct’ scale (shape and compactness) values for particular imagery types is important.

Optimal segmentation values were determined for WorldView-2 imagery for the attributes: Wetland Type, VCFs and Open Water Types. The scale value ranged from 25 to 45. These values were similar to other wetland studies of Wetland Types that used eCognition-based OBIA applied to high resolution optical imagery. Examples include: Dissanka *et al.* (2009) using Quickbird with a scale parameter value of 50; Wang *et al.* (2011) using IKONOS and scale parameter values of 20 and 25; Barker and King (2012) using 50 cm pixel Digital Orthophotos with a scale parameter value of 300 to first delineate wetlands, and then a value of 20 to segment within wetland vegetation and logs as specific turtle habitat features; and in research that used WorldView-2 imagery, Heumann (2011), who first segmented general land cover classes with a scale value of 25 and then segmented specific coastal vegetation classes using a scale value of 10.

This research found a similar range of segmentation scale values delineated objects that visually represented spatial entities in the landscapes of the wetland study areas using WorldView-2 images; however, they were determined using only four bands and without pan-sharpening. It was difficult to find any study that used only the red, green, blue, and NIR bands of WorldView-2 imagery. Part of the novelty of WorldView-2 imagery is the additional four bands, however eight-band imagery is costly, and the additional four bands are generally highly correlated (redundant) with the four bands used in this research. Achieving similar results as other 8-band studies using only four bands for segmentation parameter selection is a benefit of this research.

Optimal segmentation parameter values were also determined for Landsat 5 TM imagery (original data, and fraction images) for Wetland Type, VCFs and Open Water Types and ranged with scale values of 2 to 10. In the literature, general object segmentation parameter values using eCognition and multi-resolution segmentation for Landsat imagery range from 5 to 10 for similar features to the Wetland Types (Marsh, Swamp, etc.) and or VCFs such as (submerged, emergent, open water, aquaculture, etc.) of the study areas of this research (Kozak *et al.*, 2008; Dingle Robertson and King, 2011; Dronova *et al.*, 2011; Ruan and Ustin, 2012), but these were for single study sites (Dronova *et al.*, 2011; Ruan and Ustin, 2012); or for broader level land cover types such as Wetland, Urban, etc. (Dingle Robertson and King, 2011). In particular, the segmentation parameter values in this research for fraction images are similar to Fernandez-Manso *et al.* (2009) who used Landsat 7 ETM+ data both as pixel level inputs and as fraction maps inputs to a multi-level multi-resolution

segmentation to map fire severity levels. These similar ranges of segmentation values add to the body of OBIA literature relating scale parameter to image type. No other studies were found that used fraction images with OBIA for wetland analysis. This research showed that segmentation of fraction maps creates objects that are visually related to Wetland Types, agricultural fields, and other landforms.

This research also found that CTA is better than MLC for almost all classes in object-based classification. Typically, comparative studies use MLC for pixel-based analysis, and compare its output to that for other classifiers (e.g. nearest neighbour, decision tree, RFs, support vector machine (SVM), among others (see Duro *et al.*, 2012; Hantson *et al.*, 2012; Stein *et al.*, 2013; Lewis *et al.*, 2013). Accuracies found in the literature for CTA are sometimes higher than MLC (e.g., from 1% to 10% higher (Wei *et al.*, 2008; Na *et al.*, 2009; Hladik *et al.*, 2013), but the differences are often not statistically significant (Dingle Robertson and King, 2011, Duro *et al.*, 2012). In this research, the difference between object-based CTA and object-based MLC accuracy was 10%. It was difficult to find a study that used MLC with objects. The results of this research were, however, similar to Li *et al.* (2012) who found that pixel-based CTA (59%) had slightly higher accuracies than pixel-based MLC (56%) using a combination of ALOS PALSAR L-band HH, HV and derived textural images for land cover classification.

Immitzer *et al.* (2012) found object-based RF classification of tree species using 8-band WorldView-2 imagery to be higher overall than pixel based classification (78% versus 72%). RF has become more widely used in part due to its insensitivity to small sample size

(Immitzer *et al.*, 2012). However, in the determination of important data inputs RF can give same (or higher) priority to highly correlated data (e.g. prioritizing them first) rather than ignoring correlated data, and shifting the prioritization to the other variables (Millard and Richardson, 2013). In the research presented here, fewer input variables were used (e.g. four WorldView-2 bands and a DEM), and typically the spectral bands are correlated, negating the need for a classifier such as RF. The simple CTA method provided insight as to what data information (e.g. the blue band or the DEM) was important for assigning pixels or objects to classes, which will aid in the selection of imagery types or other data types for these types of classifications.

WorldView-2 imagery provided higher accuracies and more detailed thematic maps than Landsat 5 TM imagery for Wetland Type and VCF classifications. Most of the literature generally shows higher accuracies, or increased detail using higher resolution imagery (e.g. De Roeck *et al.*, 2007; Grenier *et al.*, 2008; Veettil, 2012). For Wetland Type classifications, Landsat 5 TM imagery may not be useful without added data (e.g. radar variables or other GIS data) except for a few classes (e.g. Fen or Swamp) and not at all useful alone for VCF classifications.

Landsat 5 TM imagery had higher classification accuracies than WorldView-2 imagery for Open Water Types. Several studies have shown that Landsat 5 TM imagery is useful for mapping water and water bodies (e.g. Tulbure and Broich, 2013; Yang *et al.*, 2013; Zhang *et al.*, 2013 among others). WorldView-2 imagery is often used for bathymetric and coastal water applications, but studies showing the configuration of water on land (water

patterns) are limited. Based on the results of this research, it is believed that excessive detail was captured with the WorldView-2 classifications resulting in mis-classification of Open Water Type; the coarseness of the Landsat 5 TM imagery minimized the detail and captured the generalized configuration of the water and land cover.

Overall for this research, using only the original Landsat TM bands (not segmented) resulted in the lowest overall accuracies. The difference from the literature is that a combination of OBIA and fraction images did not produce the highest accuracies for any of the classifications. Pixel-based classification of fraction images or object-based classification of the original bands produced the highest overall accuracies for Wetland Type, VCFs and Open Water Type. This could be due to the complex and dynamic nature of wetlands as compared to simple, relatively homogenous low, moderate and high burned areas found in Fernandez-Manso *et al.* (2009).

6.1.4 Radar analysis

Radar image analyses were completed to obtain an understanding of the potential contributions of non-optical imagery at different spatial and temporal resolutions, broadening the overview perspective. While this research showed that particular radar-derived variables could support classification, radar generally added noise and reduced overall accuracies over optical imagery alone. However, there were some successes for some classes using HH, HV analysis, pedestal height analysis, and when combining radar variables with optical variables.

Spring, steep (18.4° - 27.6°) incidence angle HH and HV images showed better separation between Wetland Type classes than spring shallow (46.8° - 48.0°) incidence angle, and any angle summer and fall HH, HV images. This is because for Swamps and treed Bogs, there was increased penetration at steep angles, increased volume scattering from branches within crowns, and double-bounce scattering between bare trunks and the water surface (more particularly for Swamps) resulting in increased depolarisation of the signal. Consequently, they were more distinct from shorter, more uniformly vegetated wetlands such as Fens, Marshes and non-treed Bogs in the steep spring imagery than in shallower angle imagery. This concurs with the majority of the literature that have found that detection of flooded vegetation is better achieved with steep incidence angle imagery (Raney, 1998; Baghdadi *et al.*, 2001; McNairn *et al.*, 2002; Li *et al.*, 2007; Westra *et al.*, 2010). In one example study of Mer Bleue bog, Baghdadi *et al.* (2001) used airborne C-band quad-pol SAR data to observe differences in wetland vegetation for three seasons, and found that there was greater separation at steeper incidence angles than shallower incidence angles.

Classification of HH and HV images using object-based CTA, and combined with optical imagery and a DEM did not improve overall accuracies over the accuracies obtained with the optical imagery alone. However, individual class accuracies for Swamp improved with the addition of either spring or summer HH and HV images at Loch Garry (Summer, 100% each UA and PA), and Marlborough Forest (Spring, 83% and 71%, respectively). These values match and surpass similar Wetland Type accuracies found in the literature ranging from 71 to 92% (Table 2.5). It is not surprising that HH and HV images enhanced

this Wetland Type as HH has often been shown to be sensitive to vegetation structure in a variety of studies with different satellite types and locations and for other non-wetland vegetation (such as agriculture) (Pope *et al.*, 1997; Lang and Kasischke, 2008; Henderson and Lewis, 2008; Schmitt and Brisco, 2013).

The seasonal differences in this research could be related to the fact that many of the Swamp areas at Loch Garry were comprised of dead coniferous trees, therefore contributing scattering mechanisms would include strong trunk-water double-bounce and increased volume scattering from the branches and the live understory in both spring and summer. At Marlborough Forest, many of the Swamp areas were hardwood dominated. In spring leaf-off conditions, like the Loch Garry dead coniferous swamps, there would be strong trunk-water double-bounce scattering along with volume scattering from crown branches and new understorey vegetation growth. This resulted in high backscatter, making them more distinct than with optical imagery alone. This research found that spring radar imagery (as just described) from March and April provided the best discrimination between Swamp and other Wetland Types. Kandus *et al.* (2001) found leaf-off imagery (May and August, Argentina) best distinguished types of Forest, Marshes and Rushes. Lang *et al.* (2008) found better discrimination for flooded forest during the leaf-off period in North Carolina.

For particular plant types (VCFs) within wetlands, the best season for discrimination was spring for Swamp and Fen vegetation types, and summer for Marsh vegetation. This could be related to the combined presence in Swamps of standing water and bare deciduous, dead coniferous or sparse live coniferous in spring, and to flooded Fen meadows in spring,

resulting in signal interaction with both the woody vegetation and water surface, resulting in increased double-bounce and volume/multiple scattering. For Marshes, however, spring conditions are typically comprised of vegetation (e.g. cattails) that has been crushed and flattened by snow, while in summer the long upright stocks produce increased volume scattering that distinguishes them from more uniform Fens and Bogs that are dominated by surface scattering (Kandus *et al.*, 2001; Baghdadi *et al.*, 2001; Li *et al.*, 2007; Henderson and Lewis, 2008). There was overlap between the different vegetation types for Bog using spring imagery, concurring with Baghdadi *et al.* (2001) and Li *et al.* (2007) who showed overlap between forested bog and non-forested bog classes in spring and summer data and for co-pol data in fall. The overall results obtained by Baghdadi *et al.* (2001) (ranging from 73% with June and July data to 86% in October) were similar to those obtained in this research using optical imagery alone. However, as Baghdadi *et al.* (2001) did not include optical imagery in their research a direct comparison is not possible. Overall, the accuracies did not meet the general published accuracies for specific vegetation community forms or plant types. It is not known if a lack of reference data for training and validation, and/or the variability of the vegetation community forms are the cause for this.

In the literature pedestal height has been an input variable for classifications or used in correlation analysis against other biophysical or image variables such as leaf area index (LAI), textures (Kovacs *et al.*, 2013) or percent residue cover (McNairn *et al.*, 2002). It has been used to determine differences between surface cover types such as oil-covered and oil-free sea surfaces (Nunziata *et al.*, 2011), snow pack differences (Sokol *et al.*, 2003), and

landslide surfaces (Czuchlewski *et al.*, 2003). Theory and empirical literature shows that as pedestal height increases, diffuse scattering and depolarization increase (Evans *et al.*, 1988; Boerner *et al.*, 1998; McNairn *et al.*, 2002; Touzi *et al.*, 2004). Therefore, it would be expected that areas with increasing backscatter, as is seen with different Wetland Types caused by increased volume/multiple surface scattering or increased double-bounced scattering due to flooding, would have increasing pedestal heights (McNairn *et al.*, 2002). By manipulating the data together in simple mathematical terms such as summation, it was expected that differences between scatterer groupings would be enhanced.

In this research, the summation of the summer co- and cross-pol pedestal minimums showed good separation between three distinct groupings of classes (water/marsh ('Group 1'; swamp/upland 'Group 2'; and fen/bog 'Group 3), which relates directly to the depolarisation of the waves and types of scatterers present; with increasing surface roughness and canopy structure there is an increase in depolarisation and number/types of scatterers (e.g. dominant surface scattering versus multiple/volume and double-bounce scattering).

There were no studies that used both the co- and cross-pol pedestal height information, or combined the information, for Wetland Type or wetland plant types/groups discrimination. While the research presented here was successful in revealing the three distinct groups through the manipulation of the pedestal height information, it was not successful in producing thematic maps that could be quantitatively assessed with this information.

Using object-based CTA with CP variables, and combining them with optical imagery and a DEM did not increase overall accuracies over those obtained with optical imagery alone for Wetland Type with the exception of the Fen class for summer imagery of Loch Garry (100% PA and UA, respectively) and spring imagery of Marlborough Forest (100% and 78%, PA and UA, respectively). Scattering for Fen is expected to be mostly surface scattering with small contributions from volume scattering in shrub vegetation and double-bounce scattering where there are sporadic trees (e.g., tamarack in the Loch Garry Fen) and open water. The Fens at Marlborough Forest were mostly grassy meadow Fens. In the literature, it was found that CP components could distinguish between Wetland Type classes such as Upland, Wetland, Forest and Shrub (Sartori *et al.*, 2011) or that higher alpha values showed more double bounce scattering in flooded vegetation compared to lower alpha values in non-flooded areas. Higher and lower were quantified in a range of $+20^{\circ}$ to -20° with higher positive results ($+14^{\circ}$ to $+20^{\circ}$) relating to double-bounce, and lower negative results (-4° to -20°) relating to surface scattering (Schmitt and Brisco, 2013). The results found in this research were the same as in Touzi *et al.* (2007), in that CP components alone were not useful for discriminating wetland vegetation, but they were useful in improving the Fen class using a coarser resolution imagery type (Radarsat-2, in this research of approximately 8 m, as compared to Convair-580 in Touzi *et al.*, 2007, of approximately 64 cm in azimuth per 5 m in range (Touzi *et al.*, 2004)).

6.1.5 Vegetation index thresholding for wet extent mapping

This research found that $NDVI_{Green}$ derived through pixel-based processing of WorldView-2 imagery corresponded well with field-measured VWC (%) and allowed for a spring inundation extent to be derived. The vegetation at the Upland/Wetland ecotone is a combination of vegetation composition and structure from both areas (Cronk and Fennessy, 2001; Mitsch and Gosselink, 2007). Due to the generally flat topography of the study areas, in times of flooding such as spring snow melt, Upland areas adjacent to the wetland may be flooded and the vegetation would be stressed, while in times of drought Wetland vegetation would be stressed. $NDVI_{Green}$ was originally developed as a way to estimate plant chlorophyll (Gitelson and Merzlyak, 1997), which changes throughout a plant's lifespan and as it reacts to stressors (such as soil moisture levels). Because of the unique combination of Upland and Wetland vegetation it would be expected that the values of $NDVI_{Green}$ in those areas would be unique. There was no research in the literature that had used $NDVI_{Green}$ to assess soil moisture or surface wetness, however De Benedetto *et al.* (2013) utilized a green ratio index (NIR/Green) derived from WorldView-2 imagery to assess the response of tomato crops to different water treatments. $NDVI_{Green}$ was selected for this research on this basis, but it was admittedly speculative, as it was not known *a priori* that it would produce such distinctive results compared to the other vegetation indices evaluated.

6.1.6 GIS thematic map analyses and scoring

A large portion of this research required manipulation of existing data, particularly data available in the LIO. Based on the results achieved, it should be possible to derive

OWES attributes such as the number of Wetland Types, Diversity of Surrounding Habitat, Proximity of Surrounding Wetlands, Rarity of Wetlands, and Rarity in the Landscape. LIO data did not exist for the study sites with respect to Ownership and Hunting Pattern, but they do exist elsewhere in southern Ontario, so such assessments should be possible. For ownership patterns, property parcel layers available from Teranet (www.teranet.ca, 2013) were examined, but they only provide Municipal Property Assessment Corporation (MPAC) assessment numbers and property address data, which do not give an indication of ownership. If the type of ownership (e.g. private or crown) is indicative of particular assessment numbers (e.g. particular number pre-fixes, etc.) then a determination of private versus public land based upon these data might also be possible. It was not possible to determine wetland area and basin area measurements for Wetland Attenuation Factor using the derived and existing thematic layers.

Similar simple data manipulation is common in the literature (e.g. Beazley *et al.*, 2005; Connor and Gabor, 2006 among others). Findlay (2005), using regression, attempted without success to statistically predict the OWES scores directly from thematic information (and underlying derived predictor variables) available from the LIO. He concluded that there measurement error in the geo-spatial data was probably too large to derive predictive relationships for the different attributes. He also stated that the landscape variables were not the most important ones in terms of contribution to the overall wetland score, being simple land cover classes such as: Coniferous Swamp, Deciduous Swamp Areas, Forest Area, Forest Edge, Water Edge, per cent Agricultural, and per cent Open Water. They were

extracted from existing thematic maps and other geospatial data and not newly derived maps from high resolution imagery as in this research. This research selected attributes that contribute highly to the OWES score (e.g. Chisholm *et al.*, 1997) for a given wetland and variable(s) were extracted from the newly derived maps and/or from existing LIO data. These were related directly to OWES scores without using surrogates, nor modelling such as regression. For example, Number of Wetland Types was determined by counting the classified Wetland Types in the derived Wetland Type thematic maps and/or the existing OMNR wetland thematic map, etc. These were compared directly to the OWES field based assessment for the same attribute. Based on this, it is concluded that some of the existing LIO thematic layers could be used to map certain OWES attributes.

Scores derived from thematic information for Diversity of Surrounding Habitat, Wetland Size (when including OWES evaluated Interspersion and VCF scores), and Proximity to Other Wetlands were the same as those assessed during the OWES evaluations. Similar scores to the OWES were derived for Rarity of Wetlands and Rarity in Landscape for the Special Feature component using geospatial data, except for Westport Bog.

The 14 attributes of this research were selected because they contribute most to the overall OWES wetland score and had potential to be assessed using remote sensing and GIS. For five of the 14 attributes these scores can be assessed from existing data, without costly field work, and the existing database could be updated using the data available in the LIO.

6.1.7 Temporal analyses

The choice of season (or a combination of seasonal imagery) was important for mapping particular classes (e.g. Wetland Type, VCFs and Open Water Type) and seasonal variability was inconsistent between sites. Many studies in the literature have used multi-date or multi-season imagery analysed together, or analysed separately as individual images to discriminate between Wetland Types and VCFs (Baghdadi *et al.*, 2001; Racine *et al.*, 2005; Ghioca-Robrecht *et al.*, 2008; Bourgeau-Chavez *et al.*, 2010; Dribault *et al.*, 2012; Bourgeau-Chavez *et al.*, 2013; Evans and Costa, 2013). There have been a variety of outcomes, but in general, improved accuracies have been shown when using multi-date versus single date imagery. When discriminating between seasons, Baghdadi *et al.* (2001) found that fall (October) data were best for wetland class discrimination. Racine *et al.* (2005) found that summer (June) imagery was best for a 10-class classification. Bourgeau-Chavez *et al.* (2010) found that neither July nor August imagery was good for mapping wetland flooded condition. In this research, summer WorldView-2 Wetland Type classifications improved overall accuracies over spring classifications for two of four sites. It was difficult to determine if this was the case for all four sites as the remaining two sites' summer imagery was substandard (haze present/ acquisition issues). Landsat 5 TM summer imagery overall Wetland Type accuracies were better than spring for some sites, especially for the poorest class, Marsh. This could be related to the growth and difference of vegetation within each wetland type from spring to summer. Using summer WorldView-2 imagery

alone for Open Water Type, 3-form and VCF classifications did not improve overall accuracies.

Combining multi-season imagery did not improve Wetland Type overall accuracies for three of four sites, and combining multi-season WorldView-2 imagery did not improve the VCF overall accuracies. However, for Wetland Type, Mer Bleue Bog classification accuracies did improve with the combination of spring and summer imagery, and combining summer and fall WorldView-2 imagery improved the overall accuracies for the number of VCFs by approximately 10%.

In the field, there were seasonal and annual differences in wet extents which could be related to accumulated precipitation, topographical constraints and time-of-year of the measurements. These differences highlight the need for multiple season and/or inter-annual mapping of wetlands to determine an overall average inundation extent. Inundation dynamics are well-studied and assessed using multiple season imagery (Bourgeau-Chavez *et al.*, 2005; Lang and Kasischke, 2008; Rebelo *et al.*, 2009; van der Velde *et al.*, 2009; Gala and Melesse, 2012; Zhang *et al.*, 2012; Chen *et al.*, 2013; Kuenzer *et al.*, 2013) with the highest R^2 values of 0.96 between image variables and continuous field variables such as soil moisture or per cent area inundated, and the highest overall accuracies in classification of inundation types of 100%. In particular, some of these studies modelled radar backscatter against field-measured soil moisture, or percent area inundated (e.g., Lang and Kasischke, 2008), while others used temporal data to classify inundation classes (e.g., Bourgeau-Chavez *et al.*, 2005) for classes of dry, saturated, standing water, and flooded, achieving

accuracies of 70% in mapping change over time). This research showed that boundaries representing 100% VWC (a wetland wet extent) can be mapped using either spring or summer NDVI_{Green} derived from WorldView-2 imagery, which has not been reported in the literature. A possible reason for this relationship could be that NDVI_{green} responds to vegetation structure and stress found at the Wetland/Upland ecotone. However, a quantitative assessment of accuracy of this boundary was difficult to conduct using the validation data collected in the field.

In terms of long term landscape dynamics and vegetation change due to anthropogenic factors, this research found that vegetation fractions were higher historically (1984) for three of the four sites. In a few small areas of Marsh, vegetation fractions were lower in 1984. The cause of this difference is unknown. In the literature, vegetation fractions have been used to assess vegetation change in a variety of land cover types, successfully showing both vegetation degradation and regeneration (Sabol *et al.*, 2002; Hostert *et al.*, 2003; Sunderman and Weisberg, 2011; Dubovyk *et al.*, 2012) with overall accuracies of 85 to 89%. A specific example for coastal wetland vegetation change is Yang *et al.* (2013) who assessed the abundance of land cover types using fraction images derived from Landsat TM images for four time periods (1987, 2004, 2005 and 2006). They were able to relate changes in the green fraction to increases of low vegetation cover, or decreases in high vegetation cover related to Hurricane Katrina damage.

Review of the change type (e.g. natural or anthropogenic) can only be made if changes or causes of changes (e.g. hurricane, infestation) are known. For example, known

anthropogenic disturbance such as flooding of an area for recreational purposes in Westport Bog could be observed comparing vegetation fraction images, but field information was necessary in order to determine that the changes were anthropogenic.

The literature has shown that these types of comparisons work well over time, and this research also shows that these kinds of changes in LSU fraction images can be observed in the eastern Ontario region. These results contribute to the accumulating body of evidence showing that LSU applied to moderate resolution sensor data such as Landsat can provide approximations of sub pixel land cover proportions. The long temporal archive of Landsat and its large spatial coverage, allow for land cover change and trend analysis using LSU over a region such as eastern Ontario to be conducted at low cost. This is an attractive approach for an operational wetland evaluation system such as the OWES, because it serves as an alternative to costly acquisition of a temporal series of many higher resolution images for wetland and surrounding areas monitoring.

6.2 Recommendations

While this research shows that an overview perspective from a top-down, investigative approach can reveal the inherent differences of wetlands across a regional area, it is understandable that such an endeavour is time-consuming and cost-prohibitive, from a staffing and data perspective. Table 6.3 outlines recommendations for the OMNR to follow based upon the outcomes of this research. Figure 6.1 provides a workflow for implementing these methods for the first six attributes in Table 6.3.

Table 6.3. Recommendations for OMNR to utilize results from this research.

Action	Attribute	MMU based upon imagery	Method	General Literature	Imagery	Cost
Can start now	Open Water Type classification	3 x 3 pixels or 0.81 ha; can be used across southern Ontario	LSU with CTA	Not confirmed in literature	Landsat TM-5	Free
	Anthropogenic Disturbance	3 x 3 pixels or 0.81 ha; can be used across southern Ontario	LSU with temporal vegetation fraction images	Similar accuracies/ uses seen in literature	Landsat TM-5	Free
	Number of Wetland Types	Depending upon data availability, OMNR data can be used across southern Ontario (AAFC Crop Type Map available for whole area)	Count and score with OMNR Wetland Layer	Simple count and score	Data layers in LIO	Free
	Diversity of Surrounding Areas		Buffering with OMNR Wetland Type layer and most recent AAFC Crop Type Map of Canada	In literature	Data layers in LIO	Free
	Proximity to other Wetlands		Analysis with OMNR Wetland Type layer and waterbodies layers	In literature	Data layers in LIO	Free

Can start soon	Wetland Size	3 x 3 pixels; less than 1 hectare dependent upon coverage of Quickbird data	NDVI _{Green} thresholding	Not in literature/ needs investigation with Quickbird data	Ontario Quickbird 2005* needs testing to see if similar results to this research using WorldView-2	Free
	Ownership Patterns	Dependent on Terranet data.	Assess Terranet data	In literature, Tapsuwan <i>et al.</i> (2012)	Terranet layers and OMNR Wetland Layer	Possibly free
Requires more research	VCFs/Number of VCFs	Need to assess ways to improve upon Number of VCFs classification, whether that is incorporating more data types, or seasonal data (such as fall data), or using other methods in literature (Table 2.5).				
	Hunting Patterns	Look at gathering more local hunter information into a GIS to get a better idea of use				
	Wetland Basin Size	Further investigation to creating a wetland basin layer that gives wetland position based upon the use of high resolution DEMs				

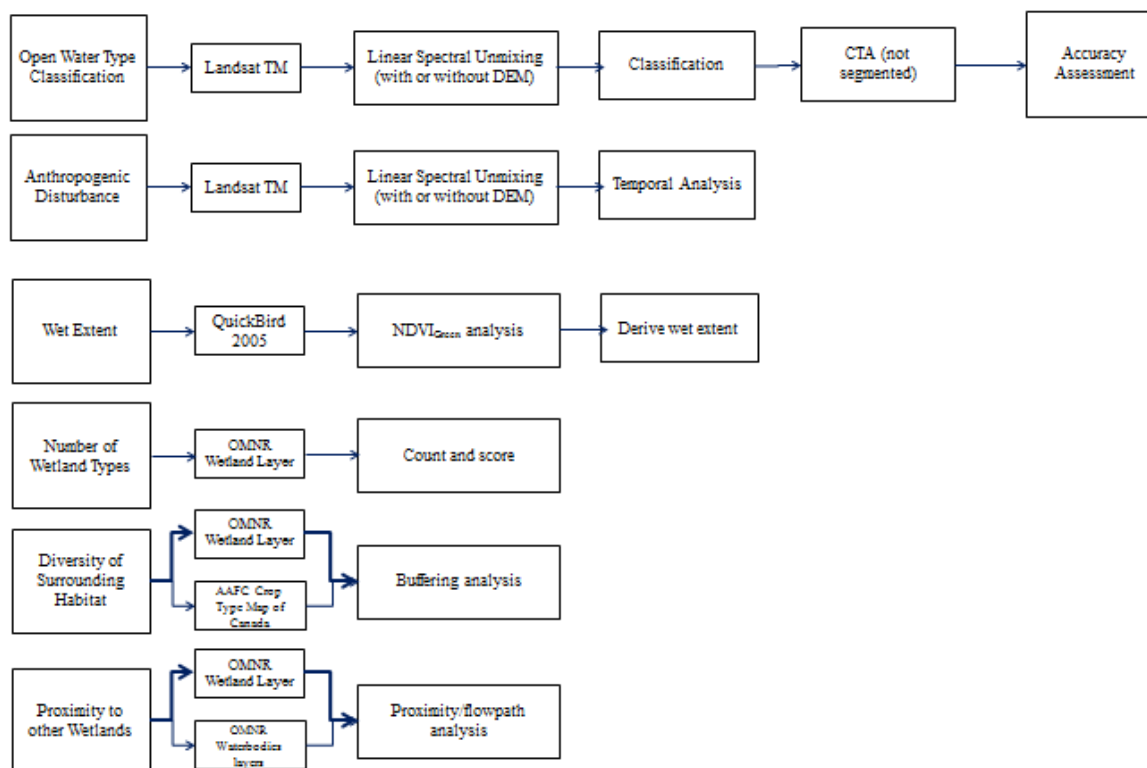


Figure 6.1. Workflow for six OWES attributes that can be implemented immediately or with some investigation (Wet Extent with existing QuickBird data).

As Landsat imagery is currently available at no cost, it is recommended to obtain spring images to assess Open Water Type configurations using OBIA with the original band data, and CTA. Additionally, further comparisons of current vegetation fraction images to historical vegetation fraction images can be made to understand the historical and ongoing changes occurring within, and around wetlands in southern Ontario. Vegetation fraction analysis will aid current OMNR monitoring efforts through the understanding of vegetative disturbance and growth and have been shown to within the literature (Sabol *et al.*, 2002; Hostert *et al.*, 2003; Sunderman and Weisberg, 2011; Dubovyk *et al.*, 2012).

Existing QuickBird data (4 band, 60cm) now available in the OMNR LIO could be assessed with the $NDVI_{Green}$ methods to map wet extents at the time of imagery acquisition. This could provide an estimate of overall wetland size, to be further augmented in the future with other purchases of high-resolution multi-spectral imagery. This has not been previously reported in the literature, however, therefore more evaluation may be needed. Three attributes, Number of Wetland Types, Diversity of Surrounding Habitat, and Proximity to Other Wetlands can be assessed using data available in the LIO.

6.3 Overall limitations of this research

The greatest overall limitation to this research was the size of the reference and validation data set obtained in the field. Wetlands are very challenging to access, which make obtaining field-based validation sets difficult. Part of the difficulty of obtaining a large validation set, was the attempt to obtain field data at four sites. However, by having four dispersed and unique sites, this research showed that there was variability in classifications of the attributes that were site specific, and this would not have been apparent with only one

or two sites as in most other previous studies. In research studies, a balance is necessary between the need for comprehensive validation sets and understanding of spatial differences across regions. It is difficult to recommend a specific proportion for each. In the literature there are variations in terms of number of study sites, number of images or types of data used, number and types of attributes investigated, number and types of variables investigated, and number and spatial representativeness of reference data sites (Pope *et al.*, 1997; Baghdadi *et al.*, 2001; Bernier *et al.*, 2003; Rogers and Kearney, 2004; Li and Chen, 2005; Racine *et al.*, 2005; Grenier *et al.*, 2007; Durieux *et al.*, 2007; Touzi *et al.*, 2007; Wright and Gallant, 2007; Ghioca-Robrecht *et al.*, 2008; Castaneda and Ducrot, 2009; Kwoun and Lu, 2009; Jiao *et al.*, 2011; Dronova *et al.*, 2011; Ricaurte *et al.*, 2012). Henderson and Lewis (2008) noted that as more studies are published there is less consistency between results. However, this balance is particularly important when trying to develop methods that can be utilized in a system like the OWES that covers a large geographical region. This research addressed the relative lack of scope in most previous wetland studies by: 1) studying four quite different wetland complexes across a large region, each with its own set of environmental and ecological conditions (as opposed to 1-2 wetlands (often not wetland complexes) in most studies; 2) evaluating the potential for mapping and monitoring of 14 common attributes used in an operational wetland evaluation system (as opposed to 1-3 attributes typical of most studies); 3) evaluating two types of remote sensing data, optical and radar, and their integration together and with DEM information; 4) integrating spatial scale through the use of sensor data with different pixel sizes and coverages, as well as the use of subpixel analysis applied to moderate resolution imagery; and 5) integrating temporal information and temporal scale through analyses of seasonal impacts on classification accuracy and multi-decadal vegetation dynamics. Thus,

the main limitation of this research in relation to other studies is that, given its much larger scope, it was difficult to obtain in-depth reference data in large sample sizes.

Limitations with the multitude of data and differences of space, time and spectral size and response were that statistical associations (if any) through measurement and observational scale were not analyzed. For example, Michishita *et al.* (2012) used a nine image time series of Landsat-5 TM and MODIS from July 2004 to October 2005 to characterize the trends in LSU fraction images over time, and to statistically compare the trends between the two scales of imagery. They were able to determine the statistical correlation of the trends per fraction type between the two pixel sizes. This research was not able to do this for any of the attributes. These relationships between imagery types and scales are important in terms of facilitating cost-effectiveness in development of multi-scale evaluation framework; e.g. using coarser resolution, larger extent and potentially free imagery for mapping of certain attributes and to guide more detailed sampling and analysis in selected areas using fewer higher resolution/smaller extent images that are higher cost per unit area. The broad scope of the research limited the capability for exhaustive analyses of any one particular attribute, data type, or methodology.

During the implementation of this research several new methodological directions were initially proposed and evaluated in the literature, but could not be incorporated into this research due to timing issues. For example, quantitative methods for segmentation parameter selection were proposed (e.g. ESP, Dragut *et al.*, 2010; Marpu *et al.*, 2010), after segmentation analysis for this research was completed in 2009. It may be prudent in the future to investigate such methods and incorporate them for a more robust segmentation parameter selection.

Regardless of these general limitations, this research made some new and significant findings regarding wetlands, wetland management and remote sensing, and various technical aspects of wetland attribute mapping.

6.4 Further research directions

There are two key directions recommended for further research with regards to wetland and remote sensing science. First, further insight into how wetlands differ in space and time is needed. The spatial and temporal differences found in this research for wetlands and wetland attributes were also found (albeit at smaller scope) in the literature (Pope *et al.*, 1997; Baghdadi *et al.*, 2001; Racine *et al.*, 2005; Ghioca-Robrecht *et al.*, 2008; Bourgeau-Chavez *et al.*, 2010; Dribault *et al.*, 2012; Bourgeau-Chavez *et al.*, 2013; Evans and Costa, 2013). Therefore, it should be apparent that limiting the time and/or space and/or spectral size and resolution components of analysis will only limit the overall outcomes. Until consistent results can be found for these components (as a hypothetical example - all wetlands swamps should be assessed in spring using a combination of optical and radar data), a broader overview perspective with a top-down approach to analysis should be taken. Additionally, the issues with Marsh (poor results, misclassification, low accuracies etc.) should be a focus of future research. The types of data used in this research were different from the data types used in most of the literature, and this may have influenced the poor results for Marsh found here (Lang and Kasischke, 2008; Henderson and Lewis, 2008; Schmitt and Brisco, 2013). However, similar poor results for Marsh were found for other wetlands within the same geographic region (e.g. Grenier *et al.*, 2007 in Quebec, Canada) and for the same wetland (Millard and Richardson, 2013, at Mer Bleue Bog) albeit with

different methods and data types. This could be an indication of regionally specific issues related to Marsh vegetation (e.g. water/vegetation interactions, snowpack interactions, etc.)

For remote sensing analyses to be a successful replacement of (or a supplement to) field-based components of wetland evaluation systems, adaptations to existing methods should be made. Recent advances in deriving landscape metrics and landscape structure from remote sensing derived thematic maps have been made. For example, Hou and Walz (2013) derived landscape metrics such as landscape diversity, edge contrast index and fragmentation metrics to assess biodiversity utilizing imagery developed from thematic maps derived from five-band RapidEye imagery for forest/agriculture/mixed-use landscapes in Germany. Investigation into the replacement of existing field-based indicators with image/thematic map derived metrics is important.

6.4.1 Technical research directions

Further investigation into object-segmentation with LSU fraction images is warranted. The poor accuracy obtained in this research was different from the literature with similar segmentation parameters. Future research should attempt to evaluate variety of complex land covers in general, using OBIA and LSU.

Further research is also warranted in the ability of HH, HV images, pedestal height values and CPs to either discriminate between individual Wetland Types such as Swamp and Fen, VCFS, plant types/groups and/or combinations of classes within, and from those attributes. One future endeavour would be to separate the imagery by Wetland Type and try to specifically classify each Wetland Type by particular wetland plant types/communities.

Pedestal height images should be created to be classified based upon the co- and cross-pol pedestal height data manipulation completed in this research. This research also

showed that the addition of some of these variables to the optical imagery variables improved certain classes. Further research should incorporate a methodology that determined the importance of these variables (e.g. RFs) and uses these variables to produce more accurate thematic classification layers.

6.5 Conclusions

The research in this thesis presented methods to assess 14 wetland attributes selected from the OWES using multiple spectral, spatial and temporal data types. The results support a top-down investigative tactic, which does not focus on one particular aspect, but takes a broad approach for wetlands analysis. This perspective can reveal spatial and temporal consistencies and inconsistencies through analysis of multi-spectral and multiple spatio-temporal data types.

In general, current wetland literature focuses on one (or two) aspects, but in order to be comprehensive, all (or as many as possible) components should be considered. However, a limitation of this approach is that, when multiple attributes are considered, an intensive examination of every attribute cannot be made. Additionally, with a large and varied spatial extent, validation set size suffers and this must also be taken into consideration when attempting to complete a comprehensive project such as this.

This research also showed that if remote sensing methods are to be incorporated into pre-existing evaluation systems, changes to some of the attributes' current methods must be made. This will reduce the reliance on field-based methods, which cannot be conducted spatially or temporally with any frequency, and make use of remote methods of mapping, which are cost-effective and repeatable.

Some of the technical methods that were derived and tested in this research can be utilized in conjunction with the existing evaluation system, and some require further investigation into the repeatability of the results and the availability of other data sources. For example, boundaries representing 100% soil moisture content (a wetland moisture boundary) can be derived using either spring or summer NDVI_{Green} images derived from WorldView-2 imagery. Further investigation into the usability of this method with available QuickBird data is needed. Also as an example, this research was successful in deriving the three distinct groups (Marsh/Water; Bog/Fen; Swamp/Upland) by manipulating the polarimetric radar pedestal height information. Further investigation into the utility of this information is needed.

In general, this research has shown that it is possible to carry out diverse and complex analysis and mapping of the spatial and temporal characteristics of wetland attributes using remotely sensed data, existing geo-spatial data, and currently available processing and analysis methods.

7.0 References

- Adam, E., Mutanga, O., and D. Rugege. 2010. Multispectral and hyperspectral remote sensing for identification and mapping of wetland vegetation: a review. *Wetlands Ecology and Management* 18: 281-295.
- Adams, J.B., Sabol, D.E., Kapos, V., Almeida Filho, R., Roberts, D.A., Smith, M.O., and A.R. Gillespie. 1995. Classification of multispectral images based on fractions of endmembers: application to land-cover change in the Brazilian Amazon. *Remote Sensing of Environment* 52: 137-154.
- Adamus, P.R. 1995. Validating a habitat evaluation method for predicting avian richness. *Wildlife Society Bulletin* 23: 743-749.
- Adamus, P.R., and Stockwell, L.T. 1983. Critical review and evaluation concepts, v. 1 of method for wetland functional assessment: Washington, D.C., U.S. Department of Transportation, Federal Highway Administration Report no. FHWA-IP-82-23, 176p.
- Aguilar, M.A., Saldana, M.M., and F.J. Aguilar. 2013. GeoEye-1 and WorldView-2 pan-sharpened imagery for object-based classification in urban environments. *International Journal of Remote Sensing* 34: 2583-2606.
- Alcaraz, D., Paruelo, J., and J. Cabello. 2006. Identification of current ecosystem functional types in the Iberian Peninsula. *Global Ecology and Biogeography* 15: 200–212.
- Allen, J., Lu, K. S., and T. D. Potts. 2002. A GIS-based analysis and prediction of land-use change in a coastal tourism destination area. *IN* M. I. Miller, J. Auyong, and N. P. Hadley (eds.) *Proceedings of the 1999 International Symposium on Coastal and Marine Tourism: Balancing Tourism and Conservation*. April 26–29, 1999, Vancouver, British Columbia, Canada. Washington Sea Grant Program and School of Marine Affairs, University of Washington, Seattle, Washington; Oregon Sea Grant College Program, Oregon State University, Corvallis, Oregon; and Oceans Blue Foundation, Vancouver, British Columbia, Canada.
- Anderson, J.E., and J.E. Perry. 1996. Characterization of wetland plant stress using leaf spectral reflectance: implications for wetland remote sensing. *Wetlands* 16: 477-487.
- Anderson, J.R., Hardy, E.E., Roach, J.T., and R.E. Witmer. 1976. A land use and land cover classification system for use with remote sensor data. US Geological Survey Professional Paper 964. United States Department of the Interior. US Government Printing Office. Washington. 41p.
- Anfinsen, S.N., Jensen, R., and T. Eltoft. 2007. Spectral clustering of polarimetric SAR data with Wishart-derived distance measures. *Proc. POLINSAR*. 3rd International Workshop on Science and Applications of SAR Polarimetry and Polarimetric Interferometry, Frascati, Italy; 22-26 January, 2007.

- Apte, C., and S. Weiss. 1997. Data mining with decision trees and decision rules. *Future Generation Computer Systems* 13: 197-210.
- Artigas, F. J. and J. Yang. 2006. Spectral discrimination of marsh vegetation types in the New Jersey Meadowlands, USA. *Wetlands* 26: 271-277.
- Asner, G.P. 1998. Biophysical and biochemical sources of variability in canopy reflectance. *Remote Sensing of Environment* 64: 234-253.
- Atkinson, D.M., and P. Treitz. 2012. Arctic ecological classifications derived from vegetation community and satellite spectral data. *Remote Sensing* 4: 3948-3971.
- Baker, C., Lawrence, R., Montagne, C., and D. Patten. 2006. Mapping wetlands and riparian areas using Landsat ETM+ imagery and decision-tree-based models. *Wetland* 26: 465-474.
- Baghdadi, N., Bernier, M., Gauthier, R., and I. Neeson. 2001. Evaluation of C-band SAR data for wetlands mapping. *International Journal of Remote Sensing* 22: 71-88.
- Baker, C., Lawrence, R.L., Montagne, C., and D. Patten. 2007. Change detection of wetland ecosystems using Landsat imagery and change vector analysis. *Wetlands* 27: 610-619.
- Baldwin, D.J.B., Desloges, J.R., and L.E. Band. 2000. Physical Geography of Ontario. *IN* A.H Perera, D.L. Euler and I.D. Thompson (eds). *Ecology of a Managed Terrestrial Landscape: Patterns and Process of Forest Landscapes in Ontario*. Vancouver; British Columbia: University of British Columbia Press. (13-29) 336p.
- Banks, S.N. King, D.J., Merzouki, A., Duffe, J., and S. Solomon. 2011. Assessing Radarsat-2 polarimetric SAR for mapping shoreline cleanup and assessment technique (SCAT) classes in the Canadian Arctic. *IN* Proceedings of the 32nd Canadian Symposium on Remote Sensing, June 13-16, 2011, Sherbrooke, Quebec, Canada.
- Baraldi, A., and F. Parmiggiani. 1995. An investigation of the textural characteristics associated with Gray Level Co-occurrence Matrix statistical parameters. *IEEE Transactions on Geoscience and Remote Sensing* 33: 293-304.
- Barker, R., and D.J. King. 2012. Blanding's Turtle (*Emydoidea blandingii*) potential habitat mapping using aerial orthophotographic imagery and object based classification. *Remote Sensing* 4: 194-219.
- Bartoldus, C.C. 1999. A comprehensive review of wetland assessment procedures: A guide for wetland practitioners. Environmental Concern Inc., St. Michaels, MD. 196p.
- Bartsch, A., Kidd, R.A., Pathe, C., Scipal, K., and W. Wagner. 2007. Satellite radar imagery for monitoring inland wetlands in boreal and sub-arctic environments. *Aquatic Conservation Marine and Freshwater Ecosystems* 17: 305-317.

- Beazley, K., Smandych, L., Snaith, T., MacKinnon, F., Austen-Smith, P., and P. Duinker. 2005. Biodiversity considerations in conservation system planning: map-based approach for Nova Scotia, Canada. *Ecological Applications* 15: 2192–2208.
- Beeri, O., and R.L. Phillips. 2007. Tracking palustrine water seasonal and annual variability in agricultural wetland landscapes using Landsat from 1997 to 2005. *Global Change Biology* 13: 897-912.
- Begley, A.J.P., Gray, B.T., and C.A. Paszkowski. 2012. A comparison of restored and natural wetlands as habitat for birds in the prairie pothole region of Saskatchewan, Canada. *The Raffles Bulletin of Zoology* 25: 173-187.
- Behera, M.D., Chitale, V.S., Shaw, A., Roy, P.S. and M.S.R. Murthy. 2012. Wetland monitoring, serving as an index of land use change – a study in Samaspur wetlands, Uttar Pradesh, India. *Journal of the Indian Society of Remote Sensing* 40:287-297.
- Belluco, E., Camuffo, M., Ferrari, S., Modenese, L., Silvestri, S., Marani, A., and M. Marani. 2006. Mapping salt-marsh vegetation by multispectral and hyperspectral remote sensing. *Remote Sensing of Environment* 105: 54-67.
- Benz, U.C., Hofmann, P., Willhauck, G., Lingenfelder, I., and M. Heynen. 2004. Multi-resolution, object-oriented fuzzy analysis of remote sensing data for GIS-ready information. *ISPRS Journal of Photogrammetry & Remote Sensing* 58: 239- 258.
- Berberoglu, S., Yilmaz, K.T., and C. Özkan. 2004. Mapping and monitoring of coastal wetlands of Çukurova Delta in the Eastern Mediterranean region. *Biodiversity and Conservation* 13: 615-633.
- Berendes, T.A., Kuo, K.S., Logar, A.M., Corwin, E.M., Welch, R.M., Baum, B.A., Pretre, A., and R.C. Weger. 1999. A comparison of paired histogram, maximum likelihood, class elimination, and neural network approaches for daylight global cloud classification using AVHRR imagery. *Journal of Geophysical Research* 104: 6199-6213.
- Bernier, M., Ghedira, H., Gauthier, Y., Magagi, R., Rilion, R., De Seve, D., Ouarda, T.B.M.J., Villeneuve, J.P., and P. Buteau. 2003. Remote sensing and classification bogs in Quebec using RADARSAT-1 images. *Canadian Journal of Remote Sensing* 29: 88-98.
- Boerner, W.M., Mott, H., Luneburg, E., Livingstone, C., Brisco, B., Brown, R.J. and J.S. Paterson. 1998. Polarimetry in radar remote sensing: basic and applied concepts. *IN* R.M. Henderson and A.J. Lewis, Eds. *Principles and applications of imaging radar: manual of remote sensing*, vol. 2. 3rd edition. New York: John Wiley and Sons, Inc. 896 p.

- Bourgeau-Chavez, L.L., Kowalski, K.P., Carlson Mazur, M.L., Scarbrough, K.A., Powell, R.B., Brooks, C.N., Huberty, B., Jenkins, L.K., Banda, E.C. Galbraith, D.M. Laubach, Z., and K. Riordan. 2013. Mapping invasive *Phragmites australis*, in the coastal Great Lakes with ALOS PALSAR satellite imagery for decision support. *Journal of Great Lakes Research* 39: 66-77.
- Bourgeau-Chavez, L.L., Riordan, K., Powell, R.B., Miller, N., and M. Nowels. 2010. Improving wetland characterization with multi-sensor, multi-temporal SAR and optical/infrared data fusion. *IN G. Jedlovec* (ed). *Advances in Geoscience and Remote Sensing*. Open Access Book: Intech: 742p.
- Bourgeau-Chavez, L.L., Smith, K.B., Brunzell, S.M., Kasischke, E.S., Romanowicz, E.A., and C.J. Richardson. 2005. Remote monitoring of regional inundation patterns and hydroperiod in the Greater Everglades using synthetic aperture radar. *Wetlands* 25: 176-191.
- Brady, N. and R. Weil. 2002. *The Nature and Properties of Soils*. 13th Edition, Prentice Hall. Upper Saddle River, New Jersey. 960p.
- Breiman, L. 2001. Random forests. *Machine Learning* 45: 5-32.
- Brenner, J.C., Christman, Z., and J. Rogan. 2012. Segmentation of Landsat Thematic Mapper imagery improves buffelgrass (*Pennisetum ciliare*) pasture mapping in the Sonoran Desert of Mexico. *Applied Geography* 34: 569-575.
- Brinson, M. 1993. A hydrogeomorphic classification for wetlands. *Wetlands Research Program Technical Report WRP-DE-4*. US Army Corps of Engineers. 101p.
- Broseth, H., and H.C. Pedersen. 2000. Hunting effort and game vulnerability studies on a small scale: a new technique combining radio-telemetry, GPS and GIS. *Advances in Applied Ecological Techniques* 37: 182-190.
- Burnett, C., and T. Blaschke. 2003. A multi-scale segmentation/object relationship modelling methodology for landscape analysis. *Ecological Modelling* 168: 233-249.
- Campos, J. C., Sillero, N., and J.C. Brito. 2012. Normalized difference water indexes have dissimilar performances in detecting seasonal and permanent water in the Sahara-Sahel transition zone. *Journal of Hydrology* 464-465: 438-446.
- Carletti, A., De Leo, G.A., and I. Ferrari. 2004. A critical review of representative wetland rapid assessment methods in North America. *Aquatic Conservation: Marine and Freshwater Ecosystems* 14: S103-S113.
- Castaneda, C., and D. Ducrot. 2009. Land cover mapping of wetland areas in an agricultural landscape using SAR and Landsat imagery. *Journal of Environmental Management* 90: 2270-2277.

- Castaneda, C. and J. Herrero. 2008. Assessing the degradation of saline wetlands in an arid agricultural region in Spain. *Catena* 72: 205-213.
- Chandler, G., Markham, B. L., and D.L. Helder. 2009. Summary of current radiometric calibration coefficients for Landsat MSS, TM, ETM+ and EO-1 ALI sensors. *Remote Sensing of Environment* 113: 893-903.
- Chen, Y., Huang, C., Ticehurst, C., Merrin, L., and P Thew. 2013. An evaluation of MODIS daily and 8-day composite products for floodplain and wetland inundation mapping. *Wetlands* 33: 823-835.
- Chisholm, S., Davies, C., Mulamoottil, G., and D. Capatos. 1997. Predictive models for identifying potentially valuable wetlands. *Canadian Water Resources Journal* 22: 249-267.
- Chiu, W-Y., and I. Couloigner. 2006. Modified fuzzy c-means classification technique for mapping vague wetlands using Landsat ETM+ imagery. *Hydrological Processes* 20: 3623-3634.
- Cloude, S.R., and E. Pottier. 1996. A review of target decomposition theorems in radar polarimetry. *IEEE Transactions on Geoscience and Remote Sensing* 34: 498-518.
- Cloude, S.R., and E. Pottier. 1997. An entropy based classification scheme for land applications of polarimetric SAR. *IEEE Transactions on Geoscience and Remote Sensing* 35: 68-78.
- Congalton, R.G., and K. Green. 1993. A practical look at the sources of confusion in error matrix generation. *Photogrammetric Engineering and Remote Sensing* 59: 641-644.
- Connor, K.J., and S. Gabor. 2006. Breeding water bird wetland habitat availability and response to water-level management in Saint John River floodplain wetlands, New Brunswick. *Hydrobiologia* 567: 169-181.
- Conservation Ontario, 2009. <http://www.conservation-ontario.on.ca/> Date last updated: 2009. Date last accessed: November 2013.
- Cronk, J., and M. S. Fennessy. 2001. *Wetland Plants: Biology and Ecology*. London: CRC Press, Taylor & Francis Group. 462p.
- Czuchlewski, K.R., Weissel, J.K., and Y. Kim. 2003. Polarimetric synthetic aperture radar study of the Tsaoiling landslide generated by the 1999 Chi-Chi earthquake, Taiwan. *Journal of Geophysical Research* 108: 7-2 – 7-10.
- Dahl, T.E., and M.D. Watmough. 2007. Current approaches to wetland status and trends monitoring in prairie Canada and the Continental United States of America. *Canadian Journal of Remote Sensing* 33: S17-S27.

- Davidson, N.C., and C.M. Finlayson. 2007. Earth observation for wetland inventory, assessment and monitoring. *Aquatic Conservation: Marine and Freshwater Ecosystems* 17: 219-228.
- Davranche, A., Lefebvre, G., and B. Poulin. 2010. Wetland monitoring using classification trees and SPOT-5 seasonal time series. *Remote Sensing of Environment* 114: 552-562.
- De Benedetto, D., Castrignano, A., Diacono, M., Rinaldi, M., Ruggieri, S. and R. Tamborrino. 2013. Field partition by proximal and remote sensing data fusion. *Biosystems Engineering* 114: 372-383.
- De Busk, W.F., Newman, S., and K.R. Reddy. 2001. Spatio-temporal patterns of soil phosphorus enrichment in Everglades water conservation area 2A. *Journal of Environmental Quality* 30: 1438-446.
- De Leeuw, M. R. 2009. Performance evaluation of several adaptive speckle filters for SAR imaging. *IN Proceedings of Anais XIV Simposio Brasileiro de Sensoriamento Remoto*, Natal, Brasil, April 25-30, 2009, INPE, 7299-7305.
- Delgado, L.E., and V.H. Marin. 2013. Interannual changes in the habitat area of the black-necked swan, *Cygnus melancoryphus*, in the Carlos Anwandter Sanctuary, Southern Chile: A remote sensing approach. *Wetlands* 33: 91-99.
- De Roeck, E.R., Verhoest, N.E.C., Miya, M.H., Lievens, H., Batelaan, O., Thomas, A., and L. Brendonck. 2008. Remote sensing and wetland ecology: A South African case study. *Sensors* 8: 3542-3556.
- Dewan, A. M. and Y. Yamaguchi. 2009. Using remote sensing and GIS to detect and monitor land use and land cover change in Dhaka Metropolitan of Bangladesh during 1960-2005. *Environmental Monitoring and Assessment* 150: 237-249.
- Dillabaugh, K.A, and D.J. King. 2008. Riparian marshland composition and biomass mapping using Ikonos imagery. *Canadian Journal of Remote Sensing* 34: 143-158.
- Dingle Robertson, L., and D.J. King. 2009. A review of existing wetland evaluation and assessment methods: Remote sensing and GIS methodologies for modelling and mapping wetland variables and functions and available remotely-sensed imagery and geo-spatial datasets. Report for Ontario Ministry of Natural Resources. 111p. Included with this thesis.
- Dingle Robertson L., and D.J. King, 2011. Comparison of pixel- and object-based classification in land cover change mapping. *International Journal of Remote Sensing* 32: 1505-1529.
- Dingle Robertson, L., King, D.J., and C. Davies. 2011. Spatial analysis of wetlands at multiple scales in Eastern Ontario using remote sensing and GIS. *IN Proceedings of*

the 32nd Canadian Symposium on Remote Sensing, June 13-16, 2011, Sherbrooke, Quebec, Canada.

- Di Sabatino, A., Coscieme, L., Vignini, P., and B. Cicolani. 2013. Scale and ecological dependence of ecosystem services evaluation: Spatial extension and economic value of freshwater ecosystems in Italy. *Ecological Indicators* 32: 259-263.
- Dissanka, M., Bernier, M., and S. Payette. 2009. Object-based classification of very high resolution panchromatic images for evaluating recent change in the structure of patterned peatlands. *Canadian Journal of Remote Sensing* 35: 189-215.
- Dobson, M.C., and F. T. Ulaby. 1988. Active microwave soil moisture research. *IEEE Transactions on Geoscience and Remote Sensing* GE24: 23-36.
- Dragut L., Tiede, D., and S. R. Levick. 2010. ESP: A tool to estimate scale parameter for multiresolution image segmentation of remotely sensed data. *International Journal of Geographical Information Science* 24: 859-871.
- Dribault, Y., Chokmani, K., and M. Bernier. 2012. Monitoring seasonal hydrological dynamics of minerotrophic peatlands using multi-date GeoEye-1 very high resolution imagery and object-based classification. *Remote Sensing* 4: 1887-1912.
- Dronova, I., Gong, P., Clinton, N.E., Wang, L., Fu, W., Qi, S. and Y. Liu. 2012. Landscape analysis of wetland plant functional types: The effects of image segmentation scale, vegetation classes, and classification methods. *Remote Sensing of Environment* 127: 357-368.
- Dronova, I., Gong, P., and L., Wang. 2011. Object-based analysis and change detection of major wetland cover types and their classification uncertainty during the low water period at Poyang Lake, China. *Remote Sensing of Environment* 115: 3220-3236.
- Du P., Zhang, W., and H. Sun. 2010. Multiple classifier combination for hyperspectral remote sensing image classification. *IN J.A. Benediktsson, J., Kittler, and F. Roli (eds.) Proceedings of the 8th International Workshop, MCS 2009, Reykjavik, Iceland, June 10-12, 2009. 538p.*
- Dubovyk, O., Menz, G., Conrand, C., and A. Khamzina. 2012. Object-based cropland degradation identification: a case study in Uzbekistan. *IN Earth Resources and Environmental Remote Sensing/GIS Applications III, Daniel L. Civco, Manfred Ehlers, Shahid Habib, Antonino Maltese, David Messinger, Ulrich Michel, Konstantinos G. Nikolakopoulos, Karsten Schulz (eds). Proc. of SPIE Vol. 8538.*
- Ducks Unlimited Canada. 2013. Canadian Wetland Inventory. <http://maps.ducks.ca/cwi/>. Date last updated: 2013. Date last accessed: November 2013.
- Durieux, L., Kropáček, J., De Grandi, G.D., and F. Achard. 2007. Object-oriented and textural image classification of the Siberia GBFM radar mosaic with MERIS imagery

- for continental scale land cover mapping. *International Journal of Remote Sensing* 28: 4175-4182.
- Duro, D.C., Franklin, S.E. and M. G. Dube. 2012. A comparison of pixel-based and object-based image analysis using selected machine learning algorithms for the classification of agricultural landscapes using SPOT-5 HRG imagery. *Remote Sensing of Environment* 118: 259 – 272.
- Dyukarev, E.A., Pologova, N.N., Golovatskaya, E.A., and A.G. Dyukarev. 2012. Forest cover disturbances in the South Taiga of West Siberia. *Environmental Research Letters* 6: 1-9.
- Eastern Ontario Model Forest (EOMF). 2006. “Ontario’s Living Legacy”. “Forest Coverage by Age”, State of Eastern Ontario’s Forests. National Resources Canada. Date last modified: 2004-2006. Date of extraction: March-June 2007.
- Environment Canada, 1987. Wetland distribution and conversion in Southern Ontario. Working Paper No. 48. Inland waters and lands directorate.
- Environment Canada. 2005. A national ecological framework for Canada. State of the Environment Infobase. http://www.ec.gc.ca/soer_ree/English/Framework/default.cfm. Date last updated: April 2005. Date last accessed: October/November 2008.
- Environment Canada. 2013. Precipitation Data. <http://climate.weather.gc.ca/>. Date last updated: November 2013. Date last accessed: November 2013.
- Evans, T.L., and M. Costa. 2013. Landcover classification of the Lower Nhecolandia subregion of the Brazilian Pantanal wetlands using ALOS/PALSAR, RADARSAT-2 and ENVISAT/ASAR imagery. *Remote Sensing of Environment* 128: 118-137.
- Evans, D.L., Farr, T.G., and J.J. van Zyl. 1988. Radar polarimetry: analysis tools and applications. *IEEE Transactions on Geoscience and Remote Sensing* 26: 774-789.
- Fernandez-Manso, O., Quintano, C., and A. Fernandez-Manso. 2009. Combining spectral mixture analysis and object-based classification for fire severity mapping. *Investigacion Agraria: Sistemas y Recursos Forestales* 18: 296-313.
- Fernandez-Ordonez, Y., Soria-Ruiz, J., and B. Leblon. 2009. Forest inventory using optical and radar remote sensing. *IN Jedlovec* (ed). *Advances in Geoscience and Remote Sensing*. Open Access Book: Intech: 742p.
- Ferone, J-M., and K.J. Devito. 2004. Shallow groundwater-surface interactions in pond-peatland complexes along a Boreal Plain topographic gradient. *Journal of Hydrology* 292: 75-95.
- Filippi, A.M., and J.R. Jensen. 2006. Fuzzy learning vector quantization for hyperspectral coastal vegetation classification. *Remote Sensing of Environment* 100: 512-530.

- Findlay, S. 2005. Predicting Ontario Wetland Evaluation Scores using remote-sensed information. Report for Ontario Ministry of Natural Resources. 26p.
- Flanders, D. M., Hall-Beyer, M., and J. Pereverzoff. 2003. Preliminary evaluation of eCognition object-based software for cut block delineation and feature extraction. *Canadian Journal of Remote Sensing* 29: 441-452.
- Flinn, K.M., Lechowicz, M.J., and M.J. Waterway. 2008. Plant species diversity and composition of wetlands within an upland forest. *American Journal of Botany* 95:1216-1224.
- Foley, J. A., DeFries, R., Asner, G.P., Barford, C., Bonan, G., Carpenter, S.F., Chapin, F.S., Coe, M.T., Daily, G.C., Gibbs, H.K., Helkowski, J.H., Holloway, T., Howard, E.A., Kucharik, C.J., Monfreda, C., Patz, J. A., Prentice, I. C., Ramankutty, N., and P. K. Snyder. 2005. Global consequences of land use. *Science* 309: 570-574.
- Foody, G.M. 2002. Status of land cover classification accuracy assessment. *Remote Sensing of Environment* 80: 185-201.
- Freeman, A. and S.L. Durden. 1998. A three-component scattering model for polarimetric SAR data. *IEEE Transactions on Geoscience and Remote Sensing* 36: 963-973.
- Frick, A., Steffenhagen, P., Zerbe, S., Timmermann, T., and K. Schulz. 2011. Monitoring of the vegetation composition in rewetted peatland with iterative decision tree classification of satellite imagery. *Photogrammetrie-Fernerkundung-Geoinformation* 3: 109-122.
- Friedl, M.A., and C.E. Brodley. 1997. Decision tree classification of land cover from remotely sensed data. *Remote Sensing of Environment* 61: 399-409.
- Frieswyk, C.B., and J.B. Zedler. 2007. Vegetation change in great lakes coastal wetlands: deviation from the historical cycle. *Journal of Great Lakes Research* 33: 366-380.
- Gala, T.S., and A.M. Melesse. 2012. Monitoring prairie wet area with an integrated Landsat ETM plus, RADARSAT-1 SAR and ancillary data from LiDAR. *Catena* 95: 12-23.
- Gao, B-C. 1996. NDWI – A normalized difference water index for remote sensing of vegetation liquid water from space. *Remote Sensing of Environment* 58: 257-266.
- Gao, J. 2008. Mapping of land degradation from ASTER data: a comparison of object-based and pixel-based methods. *GIScience and Remote Sensing* 45: 149-166.
- Ghioca-Robrecht, D.M., Johnston, C.A., and M.G. Tulbure. 2008. Assessing the use of multiseason QuickBird imagery for mapping invasive species in a Lake Erie coastal marsh. *Wetlands* 28: 1028-1039.

- Gitelson, A.A., and M.N. Merzlyak. 1997. Remote estimation of chlorophyll content in higher plant leaves. *International Journal of Remote Sensing* 18: 2691-2697.
- GLWCAP. 2012. Great Lakes Wetlands Conservation Action Plan Highlights Report 2005–2010. Peterborough, Ontario. 36p.
- Gofman, E. 2006. Developing an efficient region growing engine for image segmentation. IBM Haifa Research Laboratories. *IEEE ICIP 2006*: 2413-2416.
- Govender, M., Dye, P.J., Witkowski, E.T.F., and F. Ahmed. 2009. Review of commonly used remote sensing and ground-based technologies to measure plant water stress. South African Water Research Commission. Review Paper.
- Government of Canada. 1991. Federal Policy on Wetland Conservation. Ottawa, Canada
- Grenier, M., Demers, A-M., Labrecque, S., Benoit, M., Fournier, R.A., and B. Drolet. 2007. An object-based method to map wetland using RADARSAT-1 and Landsat ETM images: test case on two sites in Quebec, Canada. *Canadian Journal of Remote Sensing* 33: S28-S45.
- Hantson, W., Kooistra, L., and P.A. Slim. 2012. Mapping invasive woody species in coastal dunes in the Netherlands: a remote sensing approach using LiDAR and high-resolution aerial photographs. *Applied Vegetation Science* 15: 536-547.
- Haralick, R.M. and K-S Fu. 1983. Pattern Recognition and Classification. *IN* J.E. Estes and G.A. Thorley (eds). *Manual of Remote Sensing: Second Edition*. Falls Church, Virginia. The Sheridan Press. (793- 801). 2440p.
- Hardisky, M.A., Daiber, F.C., Roman, C.T. and Klemas, V. 1984. Remote sensing of biomass and annual net aerial primary productivity of a salt marsh. *Remote Sensing of Environment* 16: 91–106.
- Harris, A., Bryant, R.G., and A.J. Baird. 2005. Detecting near-surface moisture stress in *Sphagnum* spp. *Remote Sensing of Environment* 97: 371-381.
- Harvey, K.R., and G.J.E. Hill. 2003. Mapping the nesting habitats of saltwater crocodiles (*Crocodylus porosus*) in Melacca Swamp and the Adelaide River wetlands, Northern Territory: an approach using remote sensing and GIS. *Wildlife Research* 30: 365-375.
- Hay, G.J., Blaschke, T., Marceau, D.J., and A. Bouchard. 2003. A comparison of three image-object methods for the multiscale analysis of landscape structure. *ISPRS Journal of Photogrammetry & Remote Sensing* 57: 327-345.
- Henderson, F.M., and A.J. Lewis. 2008. Radar detection of wetland ecosystems: a review. *International Journal of Remote Sensing* 29: 5809-5835.

- Hess, L.L., Melack, J.M., Novo, E.M.L.M, Barbosa, C.C.F., and M. Gastil. 2003. Dual season mapping of wetland inundation and vegetation for the central Amazon basin. *Remote Sensing of Environment* 87: 404-428.
- Heumann, B. W. 2011. An object-based classification of mangroves using a hybrid decision tree-support vector machine approach. *Remote Sensing* 3: 2440-2460.
- Hills, G.A. 1959. A Ready Reference to the Description of the Land of Ontario and its Productivity: A Compendium of Maps, Charts, Tables, and Brief Comments. Division of Research, Ontario Department of Lands and Forests, Maple, One. 142 pp. *IN Ontario Wetland Evaluation System: Southern Manual*. 2002. Ontario Ministry of Natural Resources. NEST Technical Manual TM-002. MNR Warehouse #50254-1. 178p.
- Hills, G.A. 1961. The Ecological Basis for Land-use Planning. Research Report No. 64. Research Branch, Ontario Department of Lands and Forests, Maple, One. (Reprinted in 1966 with updated maps). *IN Ontario Wetland Evaluation System: Southern Manual*. 2002. Ontario Ministry of Natural Resources. NEST Technical Manual TM-002. MNR Warehouse #50254-1. 178p.
- Hladik, C., Schalles, J., and M. Alber. 2013. Salt marsh elevation and habitat mapping using hyperspectral and LiDAR data. *Remote Sensing of Environment* 139: 318-330.
- Hogg, A.R., and K.W. Todd. 2007. Automated discrimination of upland and wetland using terrain derivatives. *Canadian Journal of Remote Sensing* 33: S68-S83.
- Hogg, A.R., and J. Holland. 2008. An evaluation of DEMs derived from LiDAR and photogrammetry for wetland mapping. *The Forestry Chronicle* 84: 840-849.
- Horitt, M.S., Mason, D.C., Cobby, D.M., Davenport, I.J., and P.D. Bates. 2003. Waterline mapping in flooded vegetation from airborne SAR imagery. *Remote Sensing of Environment* 85: 271-281.
- Hostert, P., Roder, A., Hill, J., Udelhoven, T., and G. Tsiourlis. 2003. Retrospective studies of grazing-induced land degradation: a case study in central Crete, Greece. *International Journal of Remote Sensing* 24: 4019-4034.
- Hou, W., and U. Walz. 2013. Enhanced analysis of landscape structure: Inclusion of transition zones and small-scale landscape elements. *Ecological Indicators* 31: 15-24.
- Howie, S.A., and I. Tromp-van Meervald. 2011. The essential role of the lagg in raised bog function and restoration: a review. *Wetlands* 31: 613-622.
- Hruby, T., Granger, T., Brunner, K., Cooke, S., Dublanica, K., Gersib, R., Reinelt, L., Richter, K., Sheldon, D., Wald, A., and F. Weinmann. 1998. Methods for assessing wetland functions. Volume I. Riverine and Depressional Wetlands in the Lowlands of

- Western Washington. Publication No 99-115 Olympia, WA: Washington State Department of Ecology.
- Hudon, C., Gagnon, P., and M. Jean. 2005. Hydrological factors controlling the spread of common reed (*Phragmites australis*) in the St. Lawrence River (Québec, Canada). *Ecoscience* 12: 347-357.
- Immitzer, M., Atzberger, C., and T. Koukal. 2012. Tree species classification with random forest using very high spatial resolution 8-band WorldView-2 satellite data. *Remote Sensing* 4: 2661-2693.
- Jensen, J. R. 2005. *Introductory Digital Image Processing: A Remote Sensing Perspective*. New Jersey: Pearson Prentice Hall. 526p.
- Jiang, H., Zhao, D., Cai, Y., and S. An. 2012. A method for application of classification tree models to map aquatic vegetation using remotely sensed images from different sensors and dates. *Sensors* 12: 12437-12454.
- Jiao, Z., Woodcock, C., Schaaf, C.B., Tan, B., Liu, J., Gao, F., Strahler, Al., Li, X., and J. Wang. 2011. Improving MODIS land cover classification by combining MODIS spectral and angular signatures in a Canadian boreal forest. *Canadian Journal of Remote Sensing* 37: 184-203.
- Joshi, C., De Leeuw, J., Skidmore, A.K. van Duren, I.C., and H. van Oosten. 2006. Remotely sensed estimation of forest canopy density: a comparison of the performance of four methods. *International Journal of Applied Earth Observation and Geoinformation* 8: 84-95.
- Ju, W., and J.M. Chen. 2005. Distribution of soil carbon stocks in Canada's forest and wetlands simulated based on drainage class, topography and remotely sensed vegetation parameters. *Hydrological Processes* 19: 77-94.
- Kandus, P., Karszenbaum, H., Pultz, T., Parmuchi, G., and J. Bava. 2001. Influence of flood conditions and vegetation status on the radar backscatter of wetland ecosystems. *Canadian Journal of Remote Sensing* 27: 651-662.
- Karim, F., Kinsey-Henderson, A., Wallace, J., Arthington, A.H., and R.G. Pearson. 2012. Modelling wetland connectivity during overbank flooding in a tropical floodplain in north Queensland, Australia. *Hydrological Processes* 26: 2710-2723.
- Karszenbaum, H., Kandus, P., Martinez, M., Le Toan, T., Tiffenberg, J., and Parmuchi, M.G. 2000. ERS-2, RADARSAT SAR backscattering characteristics of the Paraná River Delta wetland, Argentina. European Space Agency, Special Publication SP-461.
- Kasischke, E.S., Melack, J.M., and M.C. Dobson. 1997. The use of imaging radars for ecological applications – a review. *Remote Sensing of Environment* 59: 141-156.

- Kavzoglu, T., and P.M. Mather. 2003. The use of back propagating artificial neural networks in land cover classification. *International Journal of Remote Sensing* 24: 4907-4938.
- Keddy, C. 1995. The conservation potential of the Frontenac Axis: Linking Algonquin Park to the Adirondacks. *The Canadian Parks and Wilderness Society, Ottawa Valley Chapter*. 59p.
- Kent, B.J., and J. Nystrom Mast. 2005. Wetland change analysis of San Dieguito Lagoon, California, USA: 1928 – 1994. *Wetlands* 25: 780–787.
- Khoshgoftaar, T.M., and E.B. Allen. 2001. Controlling overfitting in classification-tree models of software quality. *Empirical Software Engineering* 6: 59-79.
- Kim, J., Grunwald, S., Rivero, R.G., and R. Robbins. 2012. Multi-scale modeling of soil series using remote sensing in a wetland ecosystem. *Soil Science Society of America Journal* 76: 2327-2341.
- Klemas, V. 2011. Remote sensing techniques for studying coastal ecosystems: an overview. *Journal of Coastal Research* 27: 2-17.
- Kovacs, J.M., Jiao, X., Flores-deSantiago, F., Zhang, C., and F. Flores-Verdugo. 2013. Assessing relationships between Radarsat-2 C-band and structural parameters of a degraded mangrove forest. *International Journal of Remote Sensing* 34: 7002-7019.
- Kozak, J., Estreguil, C., and K. Ostapowicz. 2008. European forest cover mapping with high resolution satellite data: the Carpathian case study. *International Journal of Applied Earth Observation and Geoinformatics* 10: 44-55.
- Kuenzer, C., Guo, H., Huth, J., Leinenkugel, P., Li, X., and S. Dech. 2013. Flood mapping and flood dynamics of the Mekong Delta: ENVISAT-ASAR-WSM based time series analyses. *Remote Sensing* 5: 687-715.
- Kwoun, O., and Z. Lu. 2009. Multi-temporal RADARSAT-1 and ERS backscattering signatures of coastal wetlands in southeastern Louisiana. *Photogrammetric Engineering and Remote Sensing* 75: 607-617.
- Laba, M., Downs, R., Smith, S., Welsh, S., Neider, C., White, S., Richmond, M., Philpot, W., and P. Baveye. 2008. Mapping invasive wetland plants in the Hudson River National Estuarine Research Reserve using QuickBird satellite imagery. *Remote Sensing of Environment* 112: 286-300.
- Laliberte, A.S., Rango, A., Havstad, K.M., Paris, J.F., Beck, R.F., McNeely, R., and A.L. Gonzalez. 2004. Object-oriented image analysis for mapping shrub encroachment from 1937 to 2003 in southern New Mexico. *Remote Sensing of Environment* 93: 198-210.

- Lang, M.W., and E.S. Kasischke. 2008. Using C-band synthetic aperture radar data to monitor forested wetland hydrology in Maryland's coastal plain, USA. *IEEE Transactions on Geoscience and Remote Sensing* 46: 535-546.
- Lang, M.W., Townsend, P.A., and E.S. Kasischke. 2008. Influence of incidence angle on detecting flooded forests using C-HH synthetic aperture radar data. *Remote Sensing of Environment* 112: 3898-3907.
- Leckie, D.G., and K.J. Ranson. 1998. Forestry applications using imaging radar. *IN* R.M. Henderson and A.J. Lewis, Eds. *Principles and applications of imaging radar: manual of remote sensing*, vol 2. 3rd edition. New York: John Wiley and Sons, Inc. 896 p.
- Lee, H., Bakowsky, W., Riley, J., Bowles, J., Puddister, M., Uhlig, P., and S. McMurray. 1998. Ecological land classification for southern Ontario: First approximation and its application. Ontario Ministry of Natural Resources, South-central Science Section, Science Development and Transfer Branch. SCSS Field Guide FG-02. 225p.
- Lee, J., Grunes, M., and G. de Grandi. 1999. Polarimetric SAR speckle filtering and its implication for classification. *IEEE transactions on Geoscience and Remote Sensing* 37: 2363-2373.
- Lee, J-S., and E. Pottier. 2009. *Polarimetric radar imaging: From Basics to Applications*. Boca Raton: Taylor and Francis Group, LLC. 414p.
- Lee, K.H., and R.S. Lunetta. 1995. Wetlands detection methods *IN* *Wetland and Environmental Applications of GIS*. Eds. J.G. Lyon and J. McCarthy. New York: CRC Lewis Publishers. 373p.
- Lewis, D., Phinn, S., and L. Arroyo. 2013. Cost-effectiveness of seven approaches to map vegetation communities – a case study from northern Australia's tropical savannas. *Remote Sensing* 5: 377-414.
- Li, G., Lu, D., Moran, E., Dutra, L., and M. Batistella. 2012. A comparative analysis of ALOS PALSAR L-band and RADARSAT-2 C-band data for land-cover classification in a tropical moist region. *ISPRS Journal of Photogrammetry and Remote Sensing* 70: 26 – 38.
- Li, J., and W. Chen. 2005. A rule-based method for mapping Canada's wetlands using optical, radar and DEM data. *International Journal of Remote Sensing* 26: 5051-5069.
- Li, R., and J. Liu. 2004. Estimating wetland vegetation biomass in the Poyang Lake of central China from Landsat ETM data. *IEEE*. 4590-4593.
- Li, X., Gar-On Yeh, A., Wang, S., Liu, K., Liu, X., Qian, J., and X. Chen. 2007. Regression and analytical models for estimating mangrove wetland biomass in South China using Radarsat images. *International Journal of Remote Sensing* 28: 5567-5582.

- Liao, J., and Q. Wang. 2009. Wetland characterization and classification using polarimetric Radarsat-2 data. *IN* eds. H. Guo and C. Wang. Proc. of SPIE Vol. 7841. Sixth International Symposium on Digital Earth: Data Processing and Applications.
- LiDAR. 2008. LiDAR for stream and wetland assessment. LIDARcomm www.lidarcomm.com. Date last accessed: October/November 2008.
- Lillesand, T.M., Kiefer, R.W., and J.W. Chipman. 2008. Remote Sensing and Image Interpretation. Hoboken: John Wiley & Sons, Inc. 756p.
- Loch Garry Lake Association. 2012. <http://www.lochgarrylakeassociation.ca/>. Date last updated: 2012. Date last accessed November 2013.
- Lodge, T.E., Hillestad, H.O., Carney, S.W., and R.B. Darling. 1995. Wetland Quality Index (WQI): A method for determining compensatory mitigation requirements for ecologically impacted wetlands. *IN* Fennessy, M.S., A.D. Jacobs, and M.E. Kentula. 2004. Review of Rapid Methods for Assessing Wetland Condition. EPA/620/R-04/009. U.S. Environmental Protection Agency, Washington, D.C.
- Lu, S., Oki, K., Shimizu, Y., and K. Omasa. 2007. Comparison between several feature extraction/classification methods for mapping complicated agricultural land use patches using airborne hyperspectral data. *International Journal of Remote Sensing* 28:936-984.
- Lu, Z., and O-I. Kwoun. 2008. Radarsat-1 and ERS InSAR analysis over southeastern coastal Louisiana: Implications for mapping water-level changes beneath swamp forests. *IEEE Transactions on Geoscience and Remote Sensing* 46: 2167-2184.
- Lynch-Stewart, P. 1994. A coming of age: Policy for wetland conservation in Canada. North American Wetlands Conservation Council (Canada). Report No. 93-1. 57p.
- Lyon, J.G. 2001. Wetland Landscape Characterization. Chelsea: Ann Arbour Press. 135p.
- Marceau, D.J. 1999. The scale issue in social and natural sciences. *Canadian Journal of Remote Sensing* 25: 347-356.
- Marceau, D.J, and G.J. Hay. 1999. Scaling and modeling in forestry: Applications in remote sensing and GIS. *Canadian Journal of Remote Sensing* 25: 342-346.
- Marechal, C., Pottier, E., Hubert-Moy, L., and S. Rapinel. 2012. One year wetland survey investigations from quad-pol RADARSAT-2 time-series SAR images. *Canadian Journal of Remote Sensing* 38: 240-252.
- Marpu, P.R., Neubert, M., Herold, H., and I. Niemeyer. 2010. Enhanced evaluation of image segmentation results. *Journal of Spatial Science* 55: 55-68.

- Marti-Cardona, B., Tran, T.D., Blade-Castellet, E., and J. Dolz-Ripolles. 2010. ASAR/ENVISAT images for the calibration of wind hydrodynamic effect on Donana wetlands. IAHS-AISH publication 352: 459-463.
- McCoy, R.M. 2005. Field methods in remote sensing. The Guildford Press. New York: New York. 157p.
- McKee, K.L., and I.A. Mendelssohn. 1989. Response of a freshwater marsh plant community to increased salinity and increased water level. *Aquatic Botany* 34: 301-316.
- McNairn, H., Duguay, C., Brisco, B., and T.J. Pultz. 2002. The effect of soil and crop residue characteristics on polarimetric radar response. *Remote Sensing of Environment* 80: 308-320.
- McNemar, Q. 1947. Note on the sampling error of the difference between correlated proportions or percentages. *Psychometrika* 12 : 153-157.
- Melendez-Pastor, I., Navarro-Pedreno, J., Gomez, I, and M. Koch. 2010. Detecting drought induced environmental changes in a Mediterranean wetland by remote sensing. *Applied Geography* 30: 254-262.
- Melesse, A.M., Oberg, J., Nangia, V., Beeri, O., and D. Baumgartner. 2006. Spatiotemporal dynamics of evapotranspiration at the Glacial Ridge prairie restoration in northwestern Minnesota. *Hydrological Processes* 20: 1451-1464.
- Meneguzzo, D. M., Liknes, G.C. and M.D. Nelson. 2013. Mapping trees outside forest using high-resolution aerial imagery: a comparison of pixel- and object-based classification approaches. *Environmental Monitor Assessment* 185: 6261-6275.
- Mertes, L.A.K., Smith, M.O., and J.B. Adams. 1993. Estimating suspended sediment concentrations in surface waters of the Amazon River wetlands from Landsat images. *Remote Sensing of Environment* 43: 281-301.
- Michishita, R., Jiang, Z., Gong, P., and B. Xu. 2012. Bi-scale analysis of multitemporal land cover fractions for wetland vegetation mapping. *ISPRS Journal of Photogrammetry and Remote Sensing* 72: 1-15.
- Millard, K., and Richardson, M. (2013). Wetland mapping with LiDAR derivatives, SAR polarimetric decompositions and LiDAR-SAR fusion using a random forest classifier. *Canadian Journal of Remote Sensing* 39: 1-18 (pagination not final).
- Milton, G.R., and R. Hélie. 2003. Wetland inventory and monitoring partnering to provide a national coverage. *IN Wetland Stewardship in Canada: Contributed papers from the conference on Canadian wetlands stewardship*. February 2003, Ottawa, ON. ed.

- C.D.A. Rubec. North American Wetlands Conservation Council (Canada), Ottawa. Report 03-2. 21-30.
- Mita, D., DeKeyser, E., Kirby, D., and G. Easson. 2007. Developing a wetland condition prediction model using landscape structure variability. *Wetlands* 27: 1124-1133.
- Mitsch, W.J., and J.G. Gosselink. 2007. *Wetlands*. Hoboken: John Wiley & Sons 582 p.
- Moffett, K.B., and S.M. Gorelick. 2013. Distinguishing wetland vegetation and channel features with object-based image segmentation. *International Journal of Remote Sensing* 20: 1332-1354.
- Morrice, J.A., Danz, N.P., Regal, R.R., Kelly, J.R., Niemi, G.J., Reavie, E.D., Hollenhorst, T., Axler, R.P., Trebitz, A.S., Cotter, A.M., and G.S. Peterson. 2008. Human influences on water quality in Great Lakes coastal wetlands. *Environmental Management* 41: 347-357.
- Munyati, C. 2000. Wetland change detection on the Kafue Flats, Zambia, by classification of multitemporal remote sensing image dataset. *International Journal of Remote Sensing* 21: 1787-1806.
- Murphy, P.N.C., Ogilvie, J., Connor, K., and P.A. Arp. 2007. Mapping wetlands: a comparison of two different approaches for New Brunswick, Canada. *Wetlands* 27: 846-854.
- Murphy, P.N.C., Ogilvie, J., and P.A. Arp. 2009. Topographic modelling of soil moisture conditions: a comparison and verification of two models. *European Journal of Soil Science* 60: 94-109.
- Muster, S., Heim, B., Abnizova, A., and J. Boike. 2013. Water body distributions across scales: a remote sensing comparison of three arctic tundra wetlands. *Remote Sensing* 5: 1498-1523.
- Mutanga, O., Adam, E., and M.A. Cho. 2012. High density biomass estimation for wetland vegetation using WorldView-2 imagery and random forest regression algorithm. *International Journal of Applied Earth Observation and Geoinformation* 18: 399-406.
- Mutanga, O., and A.K. Skidmore. 2004. Narrow band vegetation indices overcome the saturation problem in biomass estimation. *International Journal of Remote Sensing* 25: 3999-4014.
- Mwita, E., Menz, G., Misana, S., Becker, M., Kisanga, D., and B. Boehme. 2013. Mapping small wetlands of Kenya and Tanzania using remote sensing techniques. *International Journal of Applied Earth Observation and Geoinformation* 21: 173-183.

- Na, X., Zhang, S., Zhang, H., Li, X., Yu, H., and C. Liu. 2009. Integrating TM and ancillary geographical data with classification trees for land cover classification of marsh area. *China Geographical Science* 19: 177-185.
- Nagabhatia, N. Wickramasuriya, R., Prasad, N., and C. M. Finlayson. 2010. A multi-scale geospatial study of wetlands distribution and agricultural zones, and the case of India. *Tropical Conservation Science* 3: 344-360.
- National Wetlands Working Group. 1988. Wetlands of Canada. Ecological Land Classification Series No. 24. Sustainable Development Branch, Environment Canada, Ottawa, Ontario, and Polyscience Publications Inc., Montreal, Quebec. 452p.
- National Wetlands Working Group. 1997. The Canadian Wetland Classification System, Second Edition. Eds. B.G. Warner and C.D.A. Rubec. Wetlands Research Centre, University of Waterloo, Waterloo, Ontario. 68p.
- Neville, R.A., Nadeau, C., Levesque, J., Szeredi, T., Staenz, K., Hauff, P., and G.A. Borstad. 1998. Hyperspectral imagery for mineral exploration: comparison of data from two airborne sensors. *IN Proc. of SPIE Vol. 3438*. Part of the SPIE Conference on Imaging Spectrometry IV, San Diego, California, July, 1998.
- NRCAN.gc.ca/earth-sciences/node/2163. 2008. Polarisation Signatures. Natural Resources of Canada. Date last modified: 2008-02-06. Date last accessed: November 2013.
- NRVIS. 2002. Natural Resources and Values Information System (NRVIS): Digital Land Management Tool (computer file). The Ontario Ministry of Natural Resources. Toronto, Ontario.
- Nunziata, F., Migliaccio, M., and A. Gambardella. 2011. Pedestal height for sea oil spill observation. *IET Radar Sonar Navig* 5: 103-110.
- Odum, E. P. and G. W. Barrett. 2005. *Fundamentals of Ecology*, 5th ed. Belmont: Thomson Brooks/Cole. 598p.
- O'Hara, C.G., King, J.S., Cartwright, J.H., and R.L. King. 2003. Multitemporal land use and land cover of urbanized areas within sensitive coastal environments. *IEEE Transactions on Geoscience and Remote Sensing* 41: 2005-2014.
- Olthof, I., and R.H. Fraser. 2007. Mapping northern land cover fractions using Landsat ETM+. *Remote Sensing of Environment* 107: 496-509.
- OMNR. 2013. Ontario Ministry of Natural Resources website. Biodiversity: Wetlands. http://www.mnr.gov.on.ca/en/Business/Biodiversity/2ColumnSubPage/STDPROD_070619.html. Date last modified: August 29, 2012. Date last accessed: November 2013.

- Ontario Wetland Evaluation System: Southern Manual. 2002. Ontario Ministry of Natural Resources. NEST Technical Manual TM-002. MNR Warehouse #50254-1. 178p.
- Ontario Wetland Evaluation System: Southern Manual. 2013. Ontario Ministry of Natural Resources. 283 p.
- Ouyang, Z-T., Zhang, M-Q., Xie, X., Shen, Q., Guo, H-Q., and B. Zhao. 2011. A comparison of pixel-based and object-oriented approaches for VHR imagery for mapping saltmarsh plants. *Ecological Informatics* 6: 136-146.
- Ozesmi, S.L., and M.E. Bauer. 2002. Satellite remote sensing of wetlands. *Wetlands Ecology and Management* 10: 381-402.
- Paola, J.D., and R.A. Schowendgerdt. 1995. A detailed comparison of back propagation neural-network and maximum likelihood classifiers for urban land-use classification. *IEEE Transactions on Geoscience and Remote Sensing* 33: 981-996.
- Papas, P., and J. Holmes. 2007. The index of wetland condition: Review of wetland assessment methods. State of Victoria Department of Sustainability and Environment. 24p.
- Papastergiadou, E.S., Retalis, A., Apostolakis, A., and Th. Georgiadis. 2008. Environmental monitoring of spatio-temporal changes using remote sensing and GIS in a Mediterranean wetland of northern Greece. *Water Resource Management* 22: 579-594.
- Pavelsky, T.M., and L.C. Smith. 2008. Remote sensing of hydrologic recharge in the Peace-Athabasca Delta, Canada. *Geophysical Research Letters* 35: 1-5.
- Pax-Lenney, M., C.E. Woodcock, S.A. Macomber, S. Gopal and C. Song. 2001. Forest mapping with a generalized classifier and Landsat TM data. *Remote Sensing of Environment* 77: 241-250.
- Phillips, R.L., Beeri, O., and E.S. DeKeyser. 2005. Remote wetland assessment for Missouri Coteau Prairie glacial basins. *Wetlands* 25: 335-349.
- Pietroniro, A., and R. Leconte. 2005. A review of Canadian remote sensing and hydrology, 1999-2003. *Hydrological Processes* 19: 285-301.
- Pope, K.O., Rejmankova, E., Paris, J.F., and R. Woodruff. 1997. Detecting seasonal flooding cycles in Marshes of the Yucatan Peninsula with SIR-C Polarimetric Radar Imagery. *Remote Sensing of Environment* 59: 157-166.
- Poulter, B., Christensen Jr., N.L., and P. N. Halpin. 2006. Carbon emissions from a temperate peat fire and its relevance to interannual variability of trace atmospheric greenhouse gases. *Journal of Geophysical Research* 111: 1-11.

- Pu, R., and S. Landry. 2012. A comparative analysis of high spatial resolution IKONOS and WorldView-2 imagery for mapping urban tree species. *Remote Sensing of Environment* 124: 516-533.
- Quattrochi, D.A., and M.F. Goodchild. 1997. *Scale in remote sensing and GIS*. Boca Raton: CRC Press LLC. 432p.
- Quinlan, J.R. 1993. Decision trees and decision making. *IEEE Transactions on Systems, Man, and Cybernetics* 20: 339-346.
- Quinton, W.L., Hayashi, M., and A Pietroniro. 2003. Connectivity and storage functions of channel fens and flat bogs in northern basins. *Hydrological Processes* 17: 3665-3684.
- Racine, M-J., Bernier, M., and T. Ouarda. 2005. Evaluation of RADARSAT-1 images acquired in fine mode for the study of boreal peatlands: a case study in James Bay, Canada. *Canadian Journal of Remote Sensing* 31: 450-467.
- Ramsar Convention Secretariat, 2006. *The Ramsar Convention Manual: A guide to the Convention on Wetlands (Ramsar, Iran, 1971)*, 4th ed. Ramsar Convention Secretariat, Gland, Switzerland. 114p.
- Ramsey, E. W. 1998. Radar remote sensing of wetlands *IN Remote Sensing Change Detection: Environmental Monitoring Methods and Applications*. Eds. R.S. Lunetta and C.D Elvidge. Chelsea: Sleeping Bear Press, Inc. 318p.
- Raney, R.K. 1998. Radar fundamentals: technical perspective. *IN R.M. Henderson and A.J. Lewis, Eds. Principles and applications of imaging radar: manual of remote sensing, vol 2. 3rd edition*. New York: John Wiley and Sons, Inc. 896 p.
- Rebelo, L.-M., Finlayson, C.M., and N. Nagabhatla. 2009. Remote sensing and GIS for wetland inventory, mapping and change analysis. *Journal of Environmental Management* 90: 2144-2153.
- Reuter, H.I., Hengl, T., Gessler, P., and P. Soille. 2009. Preparation of DEMs for geomorphic analysis. *IN T. Hengl and H.I. Reuter, Eds. Geomorphometry: Concepts, software, applications and developments in soil science. Vol. 33*. Amsterdam: Elsevier. 772p.
- Ricaurte, L.F., Jokela, J., Siqueira, A., Nunez-Avellaneda, M., Marin, C., Velazquez-Valencia, A., and K.M. Wantzen. 2012. Wetland habitat diversity in the Amazonian piedmont of Columbia. *Wetlands* 32: 1189-1202.
- Rivero, R.G., Grunwald, S., and G.L. Bruland. 2007. Incorporation of spectral data into multivariate geostatistical models to map soil phosphorus variability in a Florida wetland. *Geoderma* 140: 428-443.

- Rivero, R.G., Grunwald, S., Binford, M.W., and T.Z. Osborne. 2009. Integrating spectral indices into prediction models of soil phosphorus in a subtropical wetland. *Remote Sensing of Environment* 113: 2389-2402.
- Roberts, J.W., Tesfamichael, S., Gebreslasie, M., van Aardt, J., and F.B. Ahmed. 2007. Forest structural assessment using remote sensing technologies: an overview of the current state of the art. *Southern Hemisphere Forestry Journal* 69: 183-203.
- Rogan, J., Franklin, J., and D.A. Roberts. 2002. A comparison of methods for monitoring multitemporal vegetation change using Thematic Mapper imagery. *Remote Sensing of Environment* 80: 143-156.
- Rogers, A.S., and M.S. Kearney. 2004. Reducing signature variability in unmixing coastal marsh Thematic Mapper scenes using spectral indices. *International Journal of Remote Sensing* 25: 2317-2335.
- Roth, E., Olsen, R., Snow, P., and R. Sumner. 1996. Oregon freshwater wetland assessment methodology. 2nd Edition. Oregon Division of State Lands, Salem, OR.
- Ruan, R., and S. Ustin. 2012. Mapping of freshwater lake wetlands using object-relations and rule-based inference. *China Geographical Science* 22: 462-471.
- Rundquist, D.C., Narumalani, S., and R.M. Narayanan. 2001. A review of wetlands remote sensing and defining new considerations. *Remote Sensing Reviews* 20: 207-226.
- Sabol, D.E., Gillespie, A. R., Adams, J.B., Smith, M.O., and C.J. Tucker. 2002. Structural stage in Pacific Northwest forests estimated using simple mixing models of multispectral images. *Remote Sensing of Environment* 80:1-16.
- Sartori, L. R., Imai, N.N., Mura, J.C., Leao de Moraes Novo, E., and Silva, T.S.F. 2011. Mapping macrophyte species in the Amazon floodplain wetlands using fully polarimetric ALOS/PALSAR data. *IEEE Transactions on Geoscience and Remote Sensing* 49: 4717-4728.
- Sass, G.Z., and I.F. Creed. 2008. Characterizing hydrodynamics on boreal landscapes using archived synthetic aperture radar imagery. *Hydrological Processes* 22: 1687-1699.
- Satyanarayana, B., Azwan Mohamad, K., Idris, I.F., Husain, M-L., and F., Dahdouh-Guebas. 2011. Assessment of mangrove vegetation based on remote sensing and ground-truth measurements at Tumpat, Kelantan Delta, east coast of peninsular Malaysia. *International Journal of Remote Sensing* 32: 1635-1650.
- Schmid, T., Koch, M., and J. Gumuzzio. 2005. Multisensor approach to determine changes of wetland characteristics in semiarid environments (Central Spain). *IEEE Transactions on Geoscience and Remote Sensing* 43: 2516-2525.

- Schmitt, A., and B. Brisco. 2013. Wetland monitoring using the curvelet-based change detection method on polarimetric SAR imagery. *Water* 5: 1036-1051.
- Schooley, R.L., and L.C. Branch. 2007. Spatial heterogeneity in habitat quality and cross-scale interactions in metapopulations. *Ecosystems* 10: 846-853.
- Schwanghart, W., and T. Heckmann. 2012. Fuzzy delineation of drainage basins through probabilistic interpretation of diverging flow algorithms. *Environmental Modelling and Software* 33: 106-113.
- Shimabukuro, Y.E., and J.A. Smith. 1991. The least-squares mixing models to generate fraction images derived from remote sensing multispectral data. *IEEE Transactions on Geoscience and Remote Sensing* 29: 16-20.
- Silva, T.S.F., Costa, M.P.F., Melack, J.M., and E.M.L.M. Novo. 2008. Remote sensing of aquatic vegetation: theory and applications 140: 131-145.
- Slatton, K.C., Crawford, M.M., and L-D. Chang. 2008. Modeling temporal variations in multipolarized radar scattering from intertidal coastal wetlands. *ISPRS Journal of Photogrammetry & Remote Sensing* 63: 55-577.
- Smith, A.M. S., Strand E.K., Steele C.M., Hann, D.B., Garrity, S.R., Falkowski, M.J., Michael, J., and J.S. Evans. 2008. Production of vegetation spatial-structure maps by per-object analysis of juniper encroachment in multitemporal aerial photographs. *Canadian Journal of Remote Sensing* 34: S268-S265.
- Smith, K.A., Ball, T., Conen, F., Dobbie, K.E., Massheder, J., and A. Rey. 2003. Exchange of greenhouse gases between soil and atmosphere: interactions of soil physical factors and biological processes. *European Journal of Soil Science* 54: 779-791.
- Smith, R.D., Ammann, A., Bartoldus, C., and M.M. Brinson. 1995. An approach for assessing wetland functions using hydrogeomorphic classification, reference wetlands and functional indices. Wetland Research Program Technical Report WRP-DE-9. US Army Corps of Engineers, Waterways Experiment Station. Vicksburg, MS. 88p.
- Sokol, J., McNairn, H., and T.J. Pultz. 2004. Case studies demonstrating the hydrological applications of C-band multipolarized and polarimetric SAR. *Canadian Journal of Remote Sensing* 30: 470-483.
- SOLRIS. 2003. Southern Ontario Land Resource Information System. Methodology development for wetland and ephemeral water mapping using remote sensing and spatial modelling techniques. The Ontario Ministry of Natural Resources and Ducks Unlimited Canada. 96p.
- SOLRIS. 2008. Southern Ontario Land Resource Information System. Phase 2 – Data Specifications Version 1.2. Ian Smyth. The Ontario Ministry of Natural Resources. 17p.

- Southern Ontario Wetland Conversion Analysis, SOWCA. 2010. Southern Ontario Wetland Conversion Analysis Final Report March 2010. Ducks Unlimited Canada. 51p.
- Stavrakoudis, D.G., Theocharis, J.B., and G.C. Zalidis. 2011. A boosted genetic fuzzy classifier for land cover classification of remote sensing imagery. *Remote Sensors* 4: 3948-3971.
- Stein, B.R., Zheng, B., Kokkinidis, I., Kayastha, N., Seigler, T., Gokkaya, K., Gopalakrishnan, R. and W.H. Hwang. 2013. An efficient remote sensing solution to update the NCWI. *Photogrammetric Engineering and Remote Sensing* 76: 537-547.
- Stevens, C.E., Paszkowski, C.A., and A.L. Foote. 2007. Beaver (*Castor canadensis*) as a surrogate species for conserving anuran amphibians on boreal streams in Alberta, Canada. *Biological Conservation* 134: 1-13.
- Stow, N., Pond, B., and R. Jahncke. 2004. Evaluation of a Wetland Rapid Assessment Technique for Northern Ontario. 14 p.
- Stuart, N., Barrett, T., and C. Place. 2006. Classifying the Neotropical savannas of Belize using remote sensing and ground survey. *Journal of Biogeography* 33: 476-490.
- Sunderman, S.O., and P.J. Weisberg. 2011. Remote Sensing approaches for reconstructing fire perimeters and burn severity mosaics in desert spring ecosystems. *Remote Sensing of Environment* 115: 2384-2389.
- Tapswan, S., MacDonald, D.H., King, D., and N. Poudyal. 2012. A combined site proximity and recreation index approach to value natural amenities: an example from a natural resource management region of Murray-Darling basin. *Journal of Environmental Management* 94: 69-77.
- Thiesing, M.A. 2001. An evaluation of wetland assessment techniques and their applications to decision making. US Environmental Protection Agency. 10p.
- Thompson, I.D. 2000. Forest Vegetation of Ontario. *IN* A.H Perera, D.L. Euler and I.D. Thompson (eds). *Ecology of a Managed Terrestrial Landscape: Patterns and Process of Forest Landscapes in Ontario*. Vancouver; British Columbia: University of British Columbia Press. (54-73) 336p.
- Tian, J., and D.-M. Chen. 2007. Optimization in multi-scale segmentation of high-resolution satellite images for artificial feature recognition. *International Journal of Remote Sensing* 20: 4625-4644.
- Touzi, R. 2007. Speckle effect on polarimetric target scattering decomposition of SAR imagery. *Canadian Journal of Remote Sensing* 33: 60-68.

- Touzi, R., Boerner, W.M., Lee, J.S., and E. Luneburg. 2004. A review of polarimetry in the context of synthetic aperture radar: concepts and information extraction. *Canadian Journal of Remote Sensing* 30: 380-407.
- Touzi, R., Deschamps, A., and G. Rother. 2007. Wetland characterization using polarimetric RADARSAT-2 capability. *Canadian Journal of Remote Sensing* 33: S56-S67.
- Touzi, R., *et al.* 2010. Polarimetric Workstation, **PWSv5r5.3**, November 2010. Downloaded from: <http://www.nrcan.gc.ca/earth-sciences/geography-boundary/remote-sensing/synthetic-aperture-radar/1929> Date of Last Access: November 2013.
- Toyra, J., and A. Pietroniro. 2005. Towards operational monitoring of a northern wetland using geomatics-based techniques. *Remote Sensing of Environment* 97: 174-191.
- Tufford, D.L., McKellar, H.N. Jr., and J.R. Hussey. 1998. In-stream nonpoint source nutrient prediction with land-use proximity and seasonality. *Journal of Environmental Quality* 27: 100-111.
- Tulbure, M.G., and M. Broich. 2013. Spatiotemporal dynamic of surface water bodies using Landsat time-series data from 1999 to 2011. *ISPRS Journal of Photogrammetry and Remote Sensing* 79: 44-52.
- Turner, M.G., R.H. Gardner and R.V. O'Neill. 2001. *Landscape Ecology in Theory and Practice: Pattern and Process*. New York: Springer. 401p.
- Ulaby, F.T., Haddock, T.F., and R.T. Austin. 1988. Fluctuation statistics of millimeter-wave scattering from distributed targets. *IEEE Transactions on Geoscience and Remote Sensing*. 26: 268-281.
- Vaiphasa, C., Skidmore, A.K., and W.F. de Boer. 2006. A post-classifier for mangrove mapping using ecological data. *ISPRS Journal of Photogrammetry & Remote Sensing* 61: 1-10.
- van der Velde, R., Su, Z., Ek, M., Rodell, M., and Y. Ma. 2009. Influence of thermodynamic soil and vegetation parameterizations on the simulation of soil temperature states and surface fluxes by the Noah LSM over a Tibetan plateau site. *Hydrologic Earth Systems Science* 13: 759-777.
- van Horssen, P.W., Schot, P.P., and A. Barendregt. 1999. A GIS-based plant prediction model for wetland ecosystems. *Landscape Ecology* 14: 253-265.
- van Zyl, J. J., Zebker, H. A., & Elachi, C. (1987). Imaging radar polarisation signatures: Theory and observation. *Radio Science* 22: 52-543.
- Veettil, B.K. 2012. A comparative study of urban change detection techniques using high spatial resolution images. *IN Proceedings of the 4th GEOBIA*, May 7 – 9, 2012, Rio de Janeiro, Brazil 29p.

- Vrabel, J. 2000. Multispectral imagery advanced band sharpening study. *Photogrammetric Engineering and Remote Sensing* 66: 73-79.
- Waddell, P., Moore, T., and S. Edwards. 1998. Transportation, land use and air quality: making the connection. 1998 ACSE Conference, Portland, Oregon – May 1998. 1-10.
- Waleska, S., Rodrigues, P., Walfir, P., and M. Souza-Filho. 2011. Use of multi-sensor data to identify and map tropical coastal wetlands in the Amazon of Northern Brazil. *Wetlands*. 31: 11-23.
- Wang, L., Dronova, I., Gong, P., Yang, W., Li, Y., and Q. Liu. 2012. A new time series vegetation-water index of phenological-hydrological trait across species and functional types for Poyang Lake wetland ecosystem. *Remote Sensing of Environment* 125: 49-63.
- Wang, X., Wang, K., and B. Zhou. 2011. Object-based classification of IKONOS data for endemic *Torreya* mapping. *Procedia Environmental Sciences* 10: 1887-1891.
- Wang, Z., Hong, J., and G. Du. 2008. Use of satellite imagery to assess the trophic state of Miyum Reservoir, Beijing, China. *Environmental Pollution* 155: 13-19.
- Watts, J.K., Kimball, J.S., Jones, L.A., Schroeder, R., and K.C. McDonald. 2012. Satellite microwave remote sensing of contrasting surface water inundation changes within the Arctic-Boreal region. *Remote Sensing of Environment* 127: 223-236.
- Wei, W., Zhang, X., Chen, X., Tang, J., and M. Jiang. 2008. Wetland mapping using subpixel analysis and decision tree classification in the Yellow River delta area. *The International Archives of the Photogrammetry, Remote Sensing and Spatial Information Sciences*. Vol. XXXVII. Part B7. Beijing 2008. 667-670.
- Welch, R. and W. Ehlers, 1987. Merging multiresolution SPOT HRV and Landsat TM data. *Photogrammetric Engineering & Remote Sensing* 53: 301-303.
- Westra, T., De Wulf, R., Van Coillie, F., and S. Crabbe. 2010. Optimal ENVISAT advanced synthetic aperture radar image parameters for mapping and monitoring Sahelian floodplains. *Journal of Applied Remote Sensing* 4: 1-17.
- Wilbanks, T.J. 2006. How scale matters: Some concepts and findings. IN *Bridging Scales and Knowledge Systems: Concepts and Applications in Ecosystem Assessment*. Reid, W.V., F. Berkes, T.J. Wilbanks, and D. Capistrano. Island Press, Washington, D.C. 21-35.
- Wilcox, D.A. 1995. Wetland and aquatic macrophytes as indicators of anthropogenic hydrologic disturbance. *Natural Areas Journal* 15: 240-248.

- Wilcox, D.A., Kowalski, K.P., Hoare, H.L., Carlson, M.L., and H.N. Morgan. 2008. Cattail invasion of sedge/grass meadows in Lake Ontario: Photointerpretation analysis of sixteen wetlands over five decades. *J. Great Lakes Res.* 34: 301-323.
- Wright, C., and A. Gallant. 2007. Improved wetland remote sensing in Yellowstone National Park using classification trees to combine TM imagery and ancillary environmental data. *Remote Sensing of Environment* 107: 582-605.
- Wu, H., and Z-L. Li. 2009. Scale issues in remote sensing: a review on analysis, processing and modeling. *Sensors* 9: 1768-1793.
- Wu, J. and O.L. Loucks. 1995. From balance of nature to hierarchical patch dynamics: a paradigm shift. *The Quarterly Review of Biology* 70: 439-466.
- Wu, J., Wang, D., and M.E. Bauer. 2007. Assessing broadband vegetation indices and QuickBird data in estimating leaf area index of corn and potato canopies. *Field Crops Research* 102: 33-42.
- Xu, H. 2006. Modification of normalised difference water index (NDWI) to enhance open water features in remotely sensed imagery. *Int. J. Remote Sens.* 27: 3025-3033.
- Yan, Y., Zhao, B., Chen, J., Guo, H., Gu, Y., Wu, Q., and B. Li. 2008. Closing the carbon budget of estuarine wetlands with tower-based measurements and MODIS time series. *Global Change Biology* 14: 1690-1702.
- Yang, L., Homer, C., Brock, J., and J. Fry. 2013. An efficient method for change detection of soil, vegetation, and water in the Northern Gulf of Mexico wetland ecosystem. *International Journal of Remote Sensing* 34: 6321-6336.
- Yu, Q., Gong, P., Clinton, N., Biging, G., Kelly, M., and D. Schirokauer. 2006. Object-based detailed vegetation classification with airborne high spatial resolution remote sensing imagery. *Photogrammetric Engineering and Remote Sensing* 72: 799-811.
- Zambon, M., Lawrence, R., Bunn, A., and S. Powell. 2006. Effect of alternative splitting rules on image processing using classification tree analysis. *Photogrammetric Engineering & Remote Sensing* 72: 25-30.
- Zhang, H., Li, D., Li, L., and A. Shi. 2011. Wetland landscape pattern analysis with remote sensing images in Ximen Island special marine protected area. *IN U. Michel, D.L. Civco, eds. Proceedings of SPIE* 8181.
- Zhang, S.L., Shi, J.C., and Y.J. Dou. 2012. A soil moisture assimilation scheme based on the microwave land emissivity model and community land model. *International Journal of Remote Sensing* 33: 2770-2797.

- Zhang, X., Pan, D., Chen, J., Zhan, Y., and Z. Mao. 2013. Using long time series of Landsat data to monitor impervious surface dynamics: a case study in the Zhoushan Islands. *Journal of Applied Remote Sensing*. 7: 15p.
- Zhao, D., Jiang, H., Yang, T., Ying, C., Xu, D., and S. An. 2012. Remote sensing of aquatic vegetation distribution in Taihu Lake using an improved classification tree with modified thresholds. *Journal of Environment Management* 95: 98-107.
- Zhou, D., Gong, H., and Z. Liu. 2008. Integrated ecological assessment of biophysical wetland habitat in water catchments: linking hydro-ecological modelling with geo-information techniques. *Ecological Modelling* 214: 411-420.
- Zhu, L., Zhao, X., Lai, L., Wang, J., Jiang, L., Ding, J., Liu, N., Yu, Y., Li, J., Xiao, N., Zheng, Y., and G.M. Rimmington. 2013. Soil TPH concentration estimation using vegetation indices in an oil polluted area of eastern China. *PLOS One*. 8: 12p.

8.0 Appendices

APPENDIX A. Wetland Attenuation Factor scoring method.

WETLAND ATTENUATION COMPLETE SCORING METHOD (after OWES, 2002)

EVALUATION:

If the wetland is a complex including isolated wetlands, apportion the 100 points according to area. For example, if 10 ha of a 100 ha complex is isolated, the isolated portion receives the maximum proportional score of 10. The remainder of the wetland is then evaluated out of 90.

Step 1: Determination of Maximum Score

- _____ Wetland is located one of the defined 5 large lakes or 5 major rivers (Go to Step 4)
 _____ Wetland is entirely isolated (i.e. not part of a complex) (Go to Step 4)
 _____ All other wetland types (Go through Steps 2, 3 and 4B)

Step 2: Determination of Upstream Detention Factor (DF)

- (a) Wetland area (ha) _____
 (b) Total area (ha) of upstream detention areas
 (include the wetland itself) _____
 (c) Ratio of (a):(b) _____
 (d) Upstream detention factor: (c) x 2 = _____
 (maximum allowable factor = 1)

Step 3: Determination of Wetland Attenuation Factor (AF)

- (a) Wetland area (ha) _____
 (b) Size of catchment basin (ha) upstream of wetland
 (include wetland itself in catchment area) _____
 (c) Ratio of (a):(b) _____
 (d) Wetland attenuation factor: (c) x 10 = _____
 (maximum allowable factor = 1)

Step 4: Calculation of final score

- (a) Wetlands on large lakes or major rivers 0
 (b) Wetland entirely isolated 100
 (b) All other wetlands -- calculate as follows:

Initial score 100*
 Upstream detention factor (DF) (Step 2) _____
 Wetland attenuation factor (AF) (Step 3) _____
 Final score: $[(DF + AF)/2] \times \text{Initial score} =$ _____

*Unless wetland is a complex with isolated portions (see note above).

APPENDIX B. Field data including sites and photographs.

Table B1. (Digitally included with this thesis) List of Surveyed Wetland Types, VCF, VCF Categorizations and Open Water Types

Tables B2 -5. Descriptions with photographs of the examples of wetland class training sites by wetland complex for Wetland Type classification and the associated Open Water Type

Tables B6 -9. Descriptions with photos of the examples of training sites by wetland complex for VCF classification and VCF Number of Forms categories (A, 1 – 3 forms; B 4 -5 forms, and C, 6 of greater forms)

Table B2. Examples of Wetland Type and Open Water Type classes at Loch Garry. Red circles highlight areas in photographs where site is actually located.

Class	Location (Vegetation Plot (VP))	Photo	Field notebook description	Vegetation present	Open Water Type
Fen	VP 102		Meadow fen; very sporadic trees (e.g. tamarack/cedar)	sweet gale/ dwarf birch pitcher plants sphagnum rushes / sedge flatleaf bladderwort	0
Fen/Swamp ecotone (referenced as Fen)	VP 101		More fen than swamp	tamarack dwarf birch wire sedge	0

Swamp	VP 109			Mixed forest swamp (very dry (but with man-made boardwalk going through))	maple/ash/ elm white pine/ cedar/ spruce/ hemlock/ balsam fir/tamarack tall ferns brown mosses	1
Swamp	VP 99			Dead tree swamp	dead coniferous cedar ferns sphagnum tall grasses wild calla	5

Marsh	VP 85		Giant marsh; cattail dominated	cattails	5
Marsh	VP 96		Marsh OR Fen	ferns sphagnum tall grasses wild calla duckweed	5

Table B3. Examples of Wetland Type and Open Water Type classes at Marlborough Forest.

Class	Location (Vegetation Plot (VP))	Photo	Field notebook description	Vegetation present	Open Water Type
Fen	VP 38			Grassy fen sedges	0
Fen	VP 4			Grassy fen pitcher plant sedge	0

Swamp	VP2			Hardwood swamp	black ash poison ivy sphagnum sedge	0
Swamp	VP 18			Hardwood swamp	maple ferns sedge	2

Marsh	VP 49		Cattail marsh	cattails	3
Marsh	VP 36		Open water marsh (Roger Stevens Pond)	sedges cattails yellow pond lily	8

Table B4. Examples of Wetland Type and Open Water Type classes at Mer Bleue Bog.

Class	Location (Vegetation Plot VP))	Photo	Field notebook description	Vegetation present	Open Water Type
Bog	VP 148		Open bog area with very sporadic tamarack saplings/ some very minor birch saplings	tamarack saplings leatherleaf / labrador tea sphagnum cotton grass	0
Bog	VP 118		Dominant cotton grass area of bog	leatherleaf sphagnum cotton grass	0

Treed Bog	VP 123			Forested bog	tamarck /white pine leatherleaf/ blueberry sphagnum	0
Treed Bog	VP 150			Treed bog (mixed treed; more birches present plus now maple saplings); coniferous species are much taller;	birch/ maple tamarack / black spruce / red pine / white pine leatherleaf / labrador tea / bog laurel sphagnum	0

Marsh	VP 140		Cattail marsh	cattails	1
Marsh	VP 144		Beaver pond marsh; lots of variety of vegetation	speckled alder sweet gale spotted joe-pye weed Canada bluejoint wild calla duckweed	6

Table B5. Examples of Wetland Type and Open Water Type classes at Westport Bog. Red circles highlight areas in photographs where site is located.

Class	Location (Vegetation Plot (VP))	Photo	Field notebook description	Vegetation present	Open Water Types
Open Bog	VP 63		Meadow bog; grasses; and ferns and cotton grass shrubs	cotton grass ferns short grass	0
Open Bog	VP 79		Bog off of Norwood/Grady Roads; on the north side of the road (point is taken road side); typical bog lagg then shrubby bog material	willow sphagnum cottongrass	1

Treed Bog	VP 72			Shrubby/treed bog; on other side of the bog lagg	maple saplings tamarack dead coniferous (looks like pine) willow sphagnum tall grasses	0
Treed Bog	VP 77			Treed/sapling bog (long peninsula crossing transect (marsh to bog))	maple saplings willow sphagnum tall grasses	0

Bog Lag/Marsh Vegetation	VP 70			Bog lagg	Serviceberry ferns tall grasses wild calla duckweed	6
Marsh	VP 75			Open grassy marsh with less shrubs	cattails rushes tall grasses	5

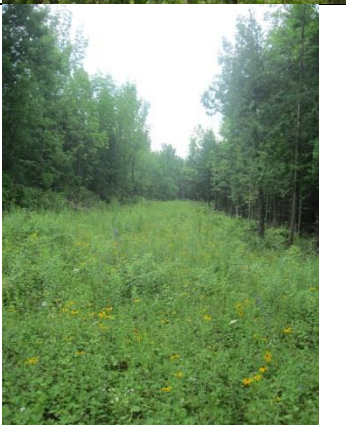
Marsh	VP 78		Free floating plants	duckweed waterhyacinth	8
-------	-------	--	----------------------	---------------------------	---

Tables B6-9. Descriptions with photographs of the examples of training sites by wetland complex for VCF classification and VCF Number of Forms categories (A, 1 – 3 forms; B 4 -5 forms, and C, 6 of greater forms)

Table B6. Examples of VCFs at Loch Garry. Red circles highlight areas in photographs where site is located.

Vegetation Plot		Photograph	All VCF Codes	VCF Category for Classification	VCF Number of Forms Category
VP 97	Swamp		DC/DH, GC, M, NE, BE, FF	DC/DH	C

VP 105	Swamp		H, C, LS, GC, M, NE	H	C
VP 102	Fen		LS, GC, M, NE, SU	Other (Shrubs)	B

VP 104	Fen/Swamp Ecotone			C, TS, LS, GC, M, BE	C	C
VP 92	Upland (Open Meadow)			GC	GC	A

VP 85	Marsh			RE	Other (emergents)	A
-------	-------	--	--	----	----------------------	---

Table B7. Examples of VCFs at Marlborough Forest. Red circles highlight areas in photographs where site is located.

Vegetation Plot	Wetland Type	Photograph	All VCF Codes	VCF category for classification	VCF Number of Forms category
VP 2	Swamp		H, LS, DS, GC, M, NE	H	C
VP 14	Swamp		DC/DH, NE, RE, F	DC/DH	B

VP 18	Swamp/Marsh			GC, NE	GC	A
VP 45	Swamp			C, DC/DH, TS, NE	C	B

VP 49	Marsh			RE	Other (emergents)	A
VP 38	Fen			NE	Other (emergents)	A

Table B8. Examples of VCFs at Mer Bleue Bog.

Vegetation Plot	Wetland Type	Photograph	All VCF Codes	VCF category for classification	VCF Number of Forms category
VP 144	Marsh		TS, LS, GC, NE, BE, FF	Other (Shrubs)	C
VP 147	Marsh/Bog Ecotone		C, LS, GC, R	C	B

VP 137	Marsh/Upland Ecotone		TS, LS, NE, RE	Other (shrubs)	B
VP 146	Marsh		RE,F	Other (emergents)	A
VP 120	Treed Bog		C, LS, M	C	A

Table B9. Examples of VCFs at Westport Bog.

Vegetation Plot	Wetland Type	Photograph	All VCF Codes	VCF category for classification	VCF Number of Forms category
VP 70	Marsh		NE, BE, FF, F	Other (emergents)	B
VP 75	Marsh		GC, NE	GC	A

VP 78b	Marsh			Other (Floating)	F	A
VP 72a	Bog			H, GC, NE, BE, FF	H	B

VP 72b	Bog			H, C, DC/DH, TS, M, NE	C	C
--------	-----	--	--	------------------------------	---	---

APPENDIX C. Training separabilities for Loch Garry spring, summer and combined imagery and segmentation scale parameter values of 25, 45 and 75.

Table C1. Bhattacharyya Distance assessed for five MLC tests using Loch Garry spring (scale parameter value of 45)

Average Separability	1.951148			
Minimum Separability	1.835126			
Maximum Separability	2.000000			
Signature Pair with Minimum Separability	Fen, Marsh			
	Water	Upland	Fen	Swamp
Upland	1.999996			
Fen	2.000000	1.969085		
Swamp	2.000000	1.964282	1.908866	
Marsh	1.999036	1.951109	1.835126	1.883982

Table C2. Bhattacharyya Distance assessed for five MLC tests using Loch Garry summer (scale parameter value of 45)

Average Separability	1.943182			
Minimum Separability	1.838589			
Maximum Separability	1.999964			
Signature Pair with Minimum Separability	Upland, Swamp			
	Water	Upland	Fen	Swamp
Upland	1.994557			
Fen	1.999676	1.838589		
Swamp	1.999964	1.985812	1.908898	
Marsh	1.999103	1.918417	1.889967	1.896818

Table C3. Bhattacharyya Distance assessed for five MLC tests using Loch Garry combined spring & summer (scale parameter value of 45)

Average Separability	1.991326			
Minimum Separability	1.972173			
Maximum Separability	2.000000			
Signature Pair with Minimum Separability	Swamp, Marsh			
	Water	Upland	Fen	Swamp
Upland	2.000000			
Fen	2.000000	1.997011		
Swamp	2.000000	1.991802	1.976136	
Marsh	1.999977	1.991239	1.984919	1.972173

Table C4. Bhattacharyya Distance assessed for five MLC tests using Loch Garry spring (scale parameter value of 25)

Average Separability	1.936777			
Minimum Separability	1.792341			
Maximum Separability	2.000000			
Signature Pair with Minimum Separability	Fen, Marsh			
	Water	Upland	Fen	Swamp
Upland	1.999991			
Fen	2.000000	1.965079		
Swamp	2.000000	1.951085	1.895145	
Marsh	1.998813	1.940842	1.792341	1.824469

Table C5. Bhattacharyya Distance assessed for five MLC tests using Loch Garry spring (scale parameter value of 75)

Average Separability	1.964748			
Minimum Separability	1.886956			
Maximum Separability	2.000000			
Signature Pair with Minimum Separability	Fen, Marsh			
	Water	Upland	Fen	Swamp
Upland	1.999998			
Fen	2.000000	1.973094		
Swamp	2.000000	1.976596	1.903817	
Marsh	1.999654	1.973235	1.886956	1.934127

APPENDIX D. Results from Wetland Type segmentations for Marlborough Forest, Mer Bleue Bog and Westport Bog.

Figures D1 – 3. Examples of segmentation results using the tested segmentation parameters (scale value = 45, shape value = 0.1, compactness value = 0.75) for Marlborough Forest, Mer Bleue Bog, and Westport Bog.

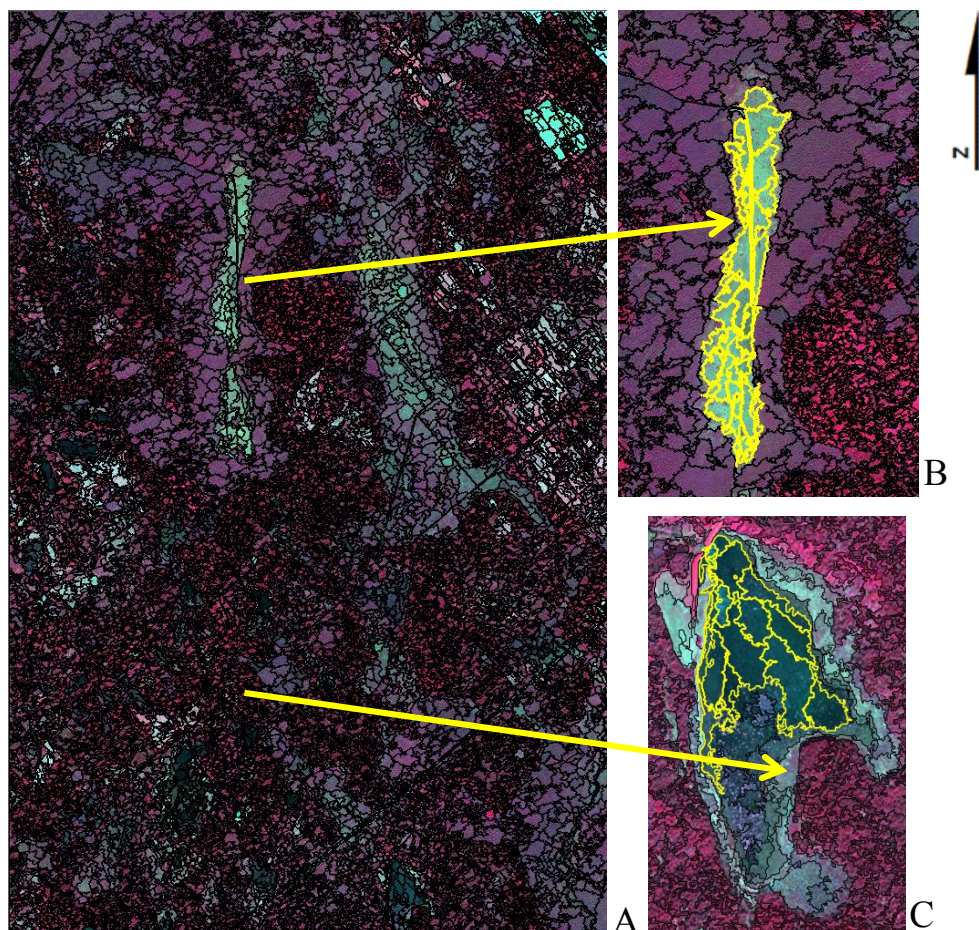


Figure D1. A) CIR composite of the spring 2010 Marlborough Forest WorldView-2 image showing the created objects using scale value of 45, shape value of 0.1 and compactness value of 0.75; and in yellow B) objects that make up the boundaries of a known fen; and C) objects that mimic the shoreline of pond Roger Steven's Pond.

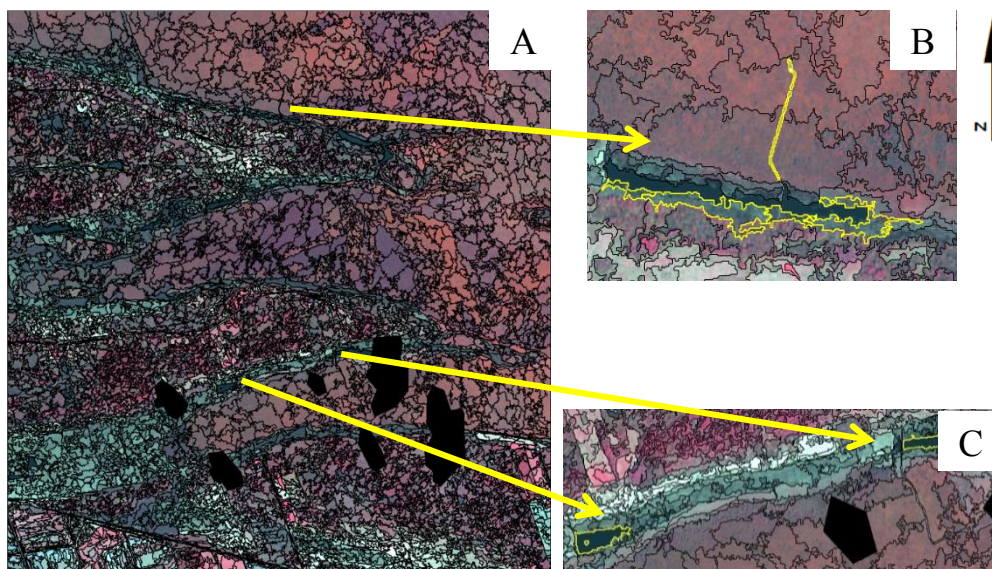


Figure D2. A) CIR composite of the spring 2010 Mer Bleue Bog WorldView-2 image showing the created objects using scale value of 45, shape value of 0.1 and compactness value of 0.75; and in yellow (B) irregular objects that make up marsh areas; linear feature is research boardwalk ; and (C) objects that mimic the shoreline of known water bodies.

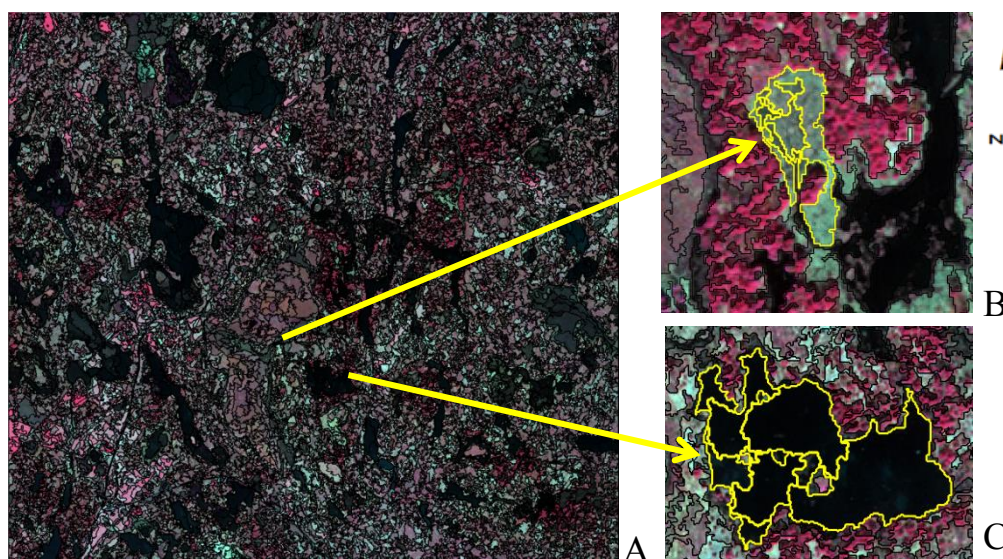


Figure D3. A) CIR composite of the spring 2010 Westport Bog WorldView-2 image showing the created objects using scale value of 45, shape value of 0.1 and compactness value of 0.75; and in yellow (B) irregular objects that make up marsh areas; and (C) objects that mimic the shorelines of known water bodies.

APPENDIX E. Results from CTA testing of GINI, Gain Ratio and Entropy algorithms.

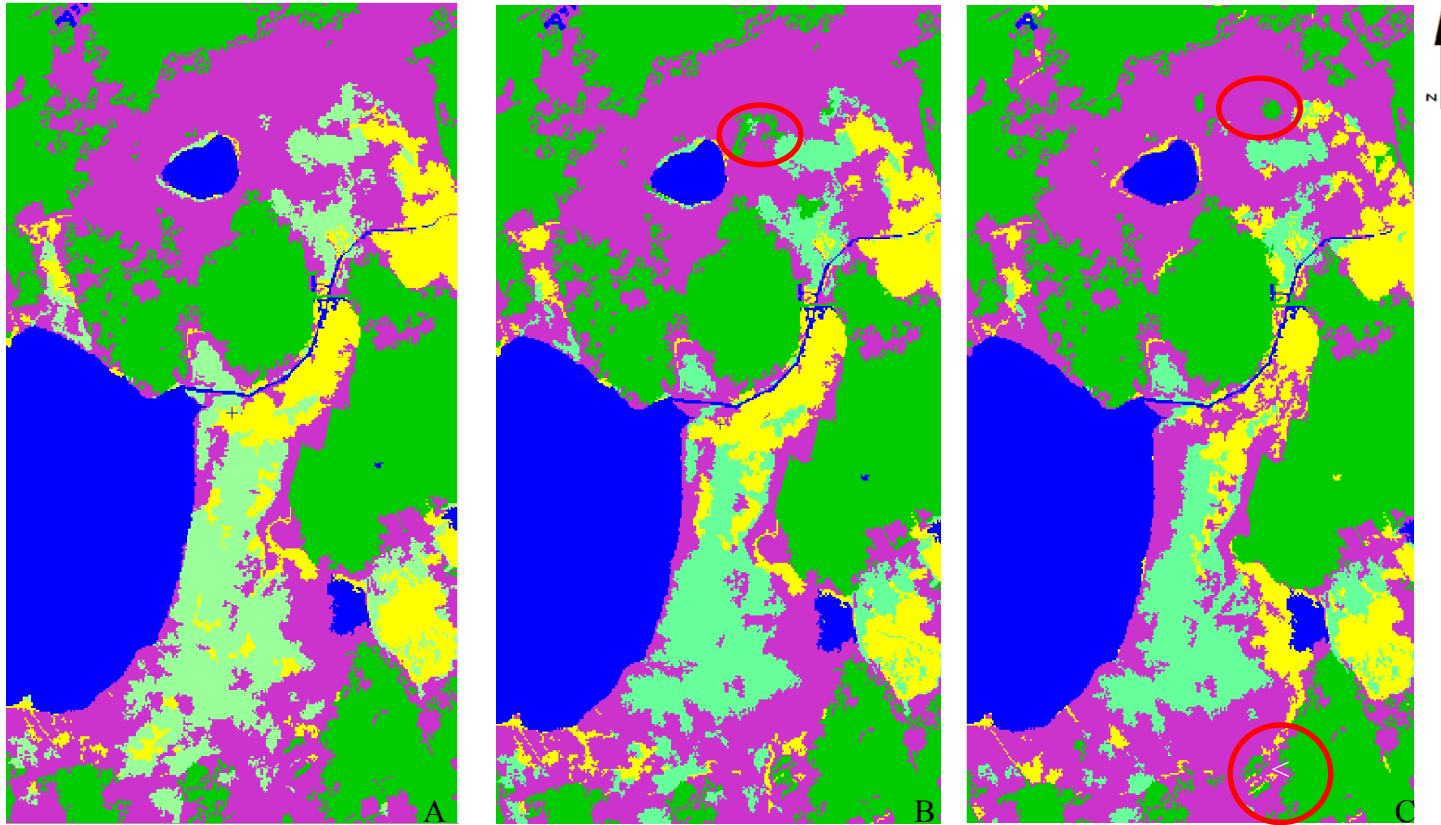


Figure E1. Thematic maps of Loch Garry derived from spring 2010 WorldView-2 image (scale value = 45, shape value = 0.1 and compactness value = 0.75 and classified using A) CTA (GINI) and 5-classes of interest; B) CTA (Entropy) and 5-classes of interest and B) CTA (Gain Ratio) and 5 classes of interest. Red circles show areas that were erroneously classified for Entropy and Gain Ratio CTAs.

- Water
- Upland
- Fen
- Swamp
- Marsh

APPENDIX F. Results from Wetland Type classifications for Marlborough Forest, Mer Bleue Bog and Westport Bog.

Figure F1 – F2. 5-Class GINI classification trees for spring 2010 Marlborough Forest, and Mer Bleue Bog.

Figures F3 – F5. Thematic maps of Marlborough Forest, Mer Bleue Bog and Westport Bog derived from spring 2010 WorldView-2 image and DEM segmented using scale value of 45, shape value of 0.1 and compactness value of 0.75 and classified using GINI CTA and 5-classes of interest.

Tables F1A & B – F3A & B. As) Error matrix for the spring 2010 Marlborough Forest, Mer Bleue Bog and Westport Bog WorldView-2 and DEM object-based GINI CTA (5-classes); and Bs) Accuracy statistics for the spring 2010 Marlborough Forest, Mer Bleue Bog and Westport Bog WorldView-2 and DEM object-based GINI CTA (5-classes).

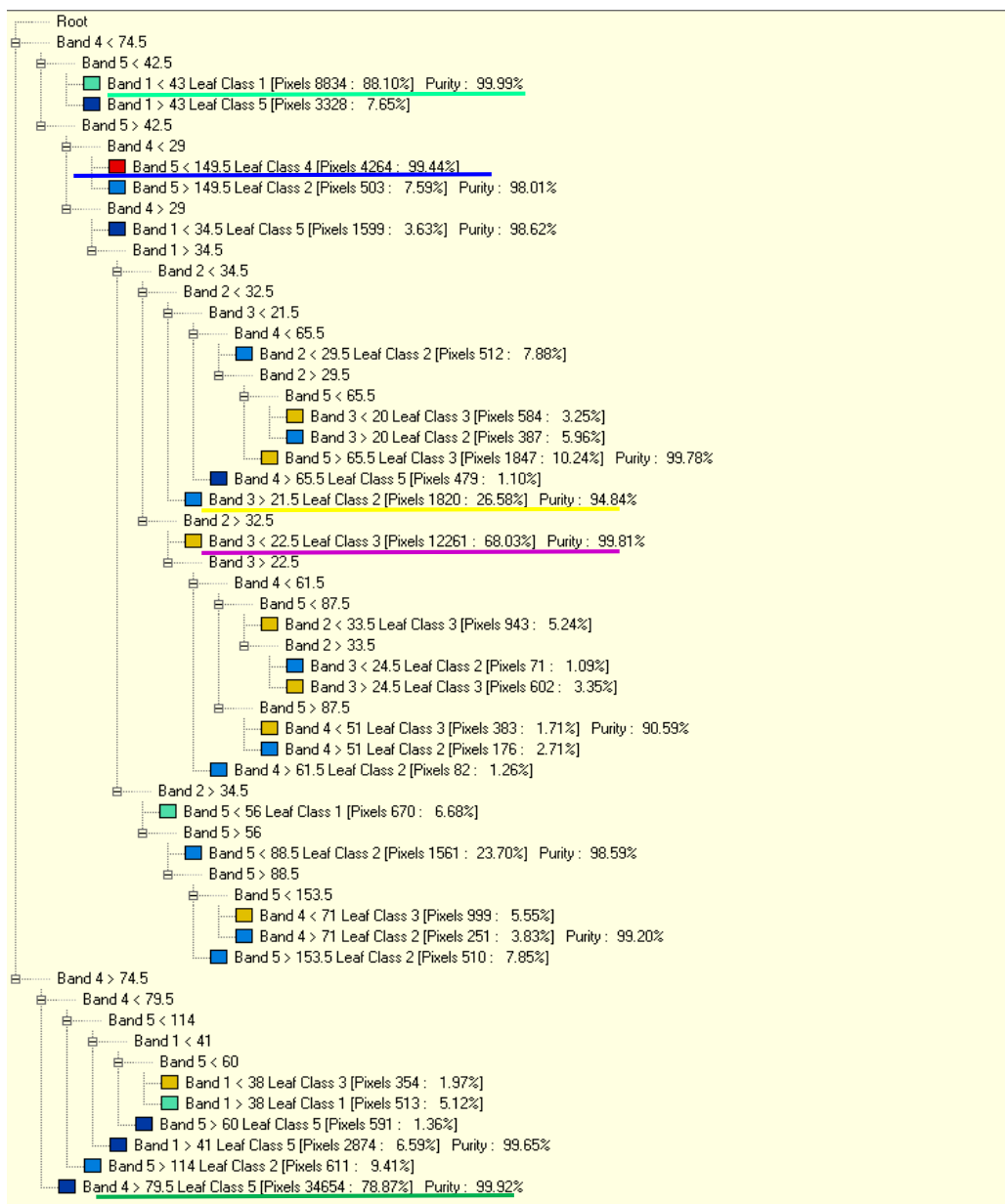


Figure F1. 5-class GINI classification tree for spring 2010 Marlborough Forest segmented WorldView-2 imagery (and DEM). **Leaf Class 1 = Fen**, **Leaf Class 2 = Marsh**, **Leaf Class 3 = Swamp**, **Leaf Class 4 = Water**, and **Leaf Class 5 = Upland**. End nodes with majority pixel contributions underlined in class colour.

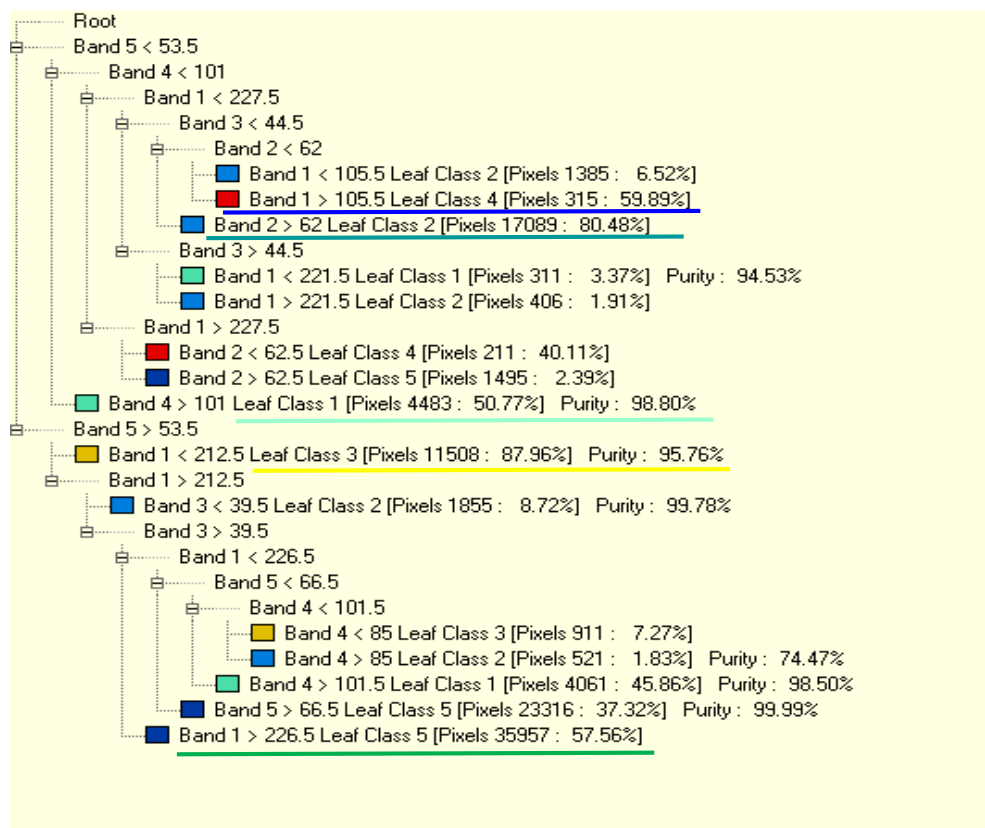


Figure F2. 5-class GINI classification tree for spring 2010 Mer Bleue Bog segmented WorldView-2 imagery (and DEM). **Leaf Class 1 = Short Bog, Leaf Class 2 = Tall Bog, Leaf Class 3 = Marsh, Leaf Class 4 = Water, and Leaf Class 5 = Upland.** End nodes with majority pixel contributions underlined in class colour.

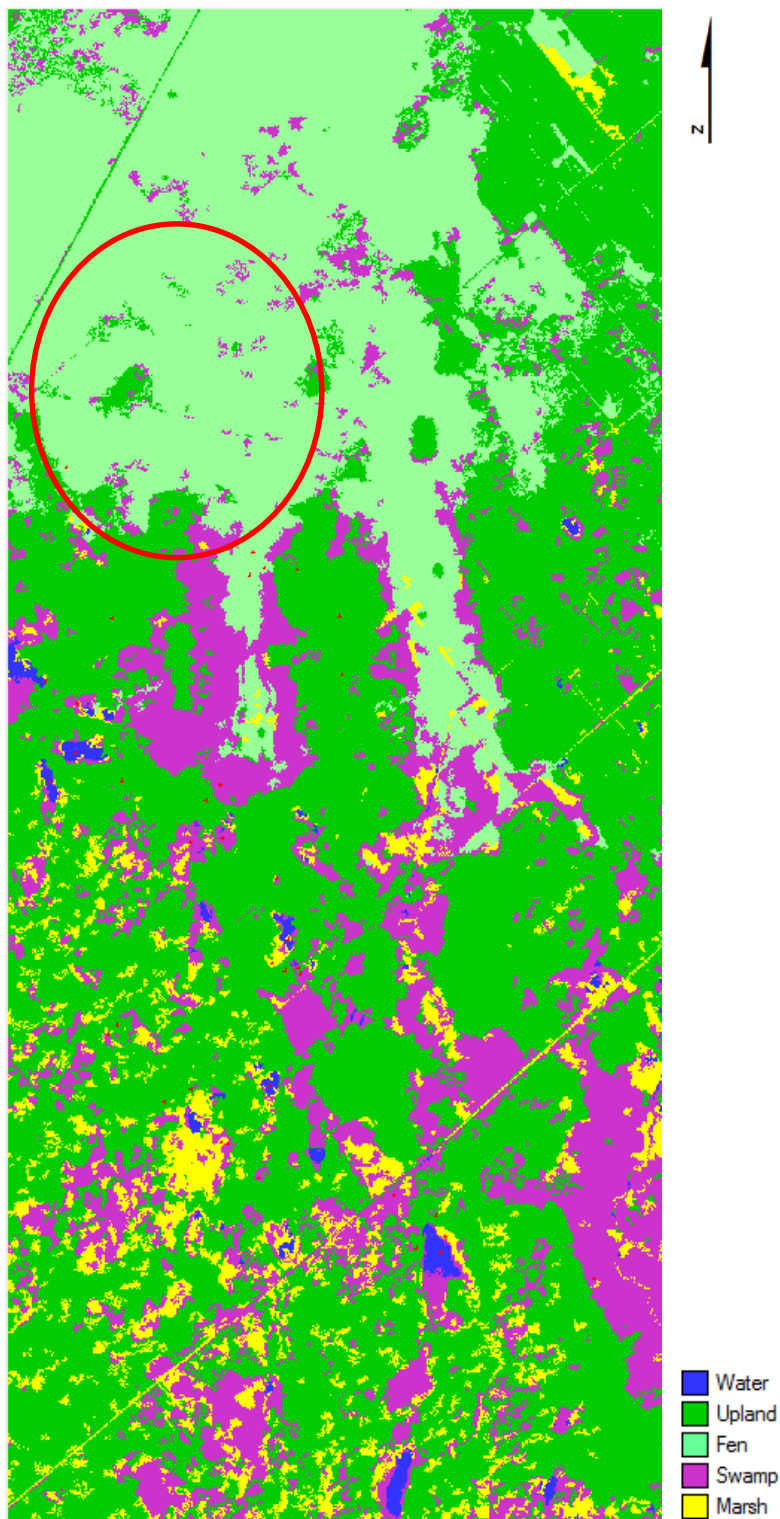


Figure F3. Thematic map of Marlborough Forest derived from spring 2010 WorldView-2 image segmented using scale value of 45, shape value of 0.1 and compactness value of 0.75 and classified using CTA and 5-classes. Red circle highlights over-classified Fen.

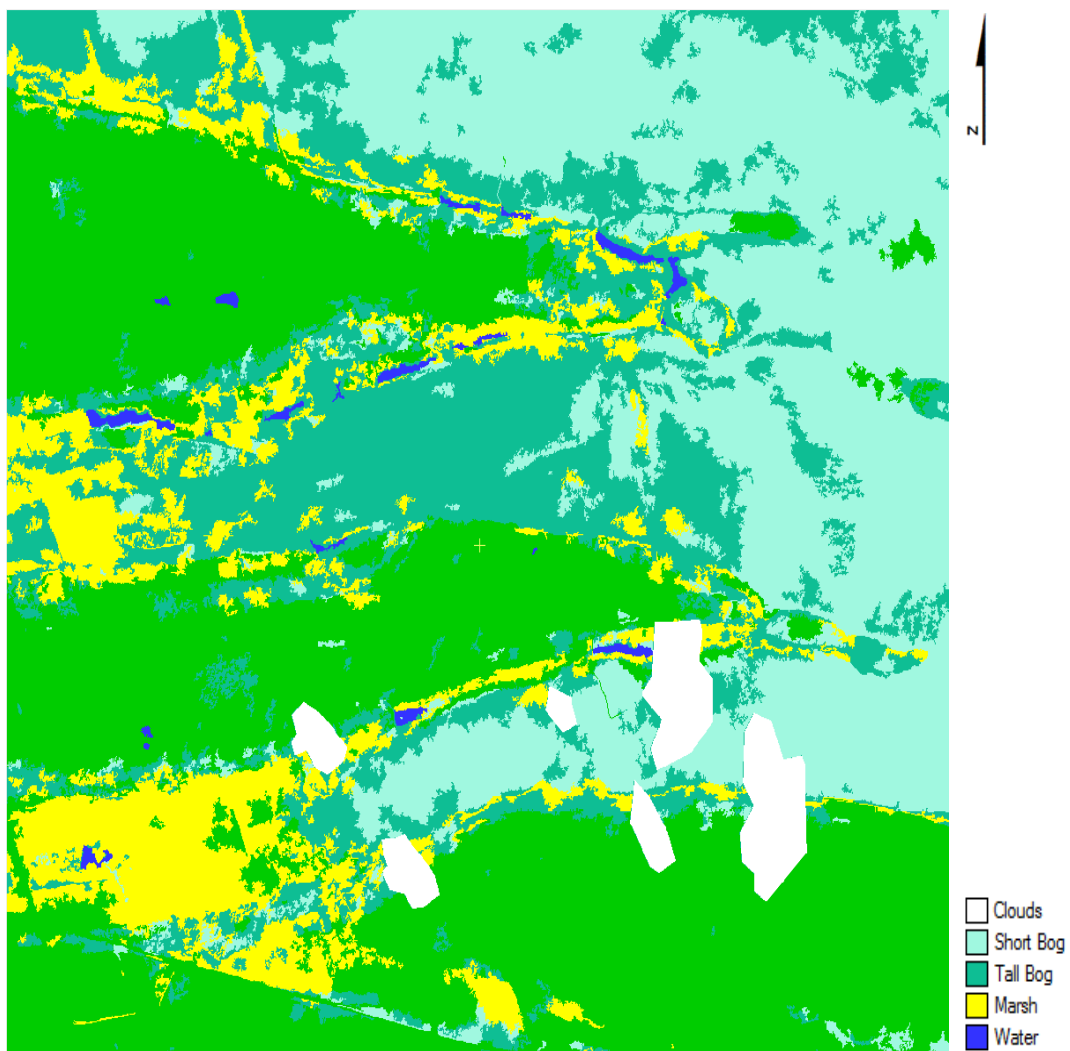


Figure F4. Thematic map of Mer Bleue Bog derived from spring 2010 WorldView-2 image segmented using scale value of 45, shape value of 0.1 and compactness value of 0.75 and classified using CTA and 5-classes.

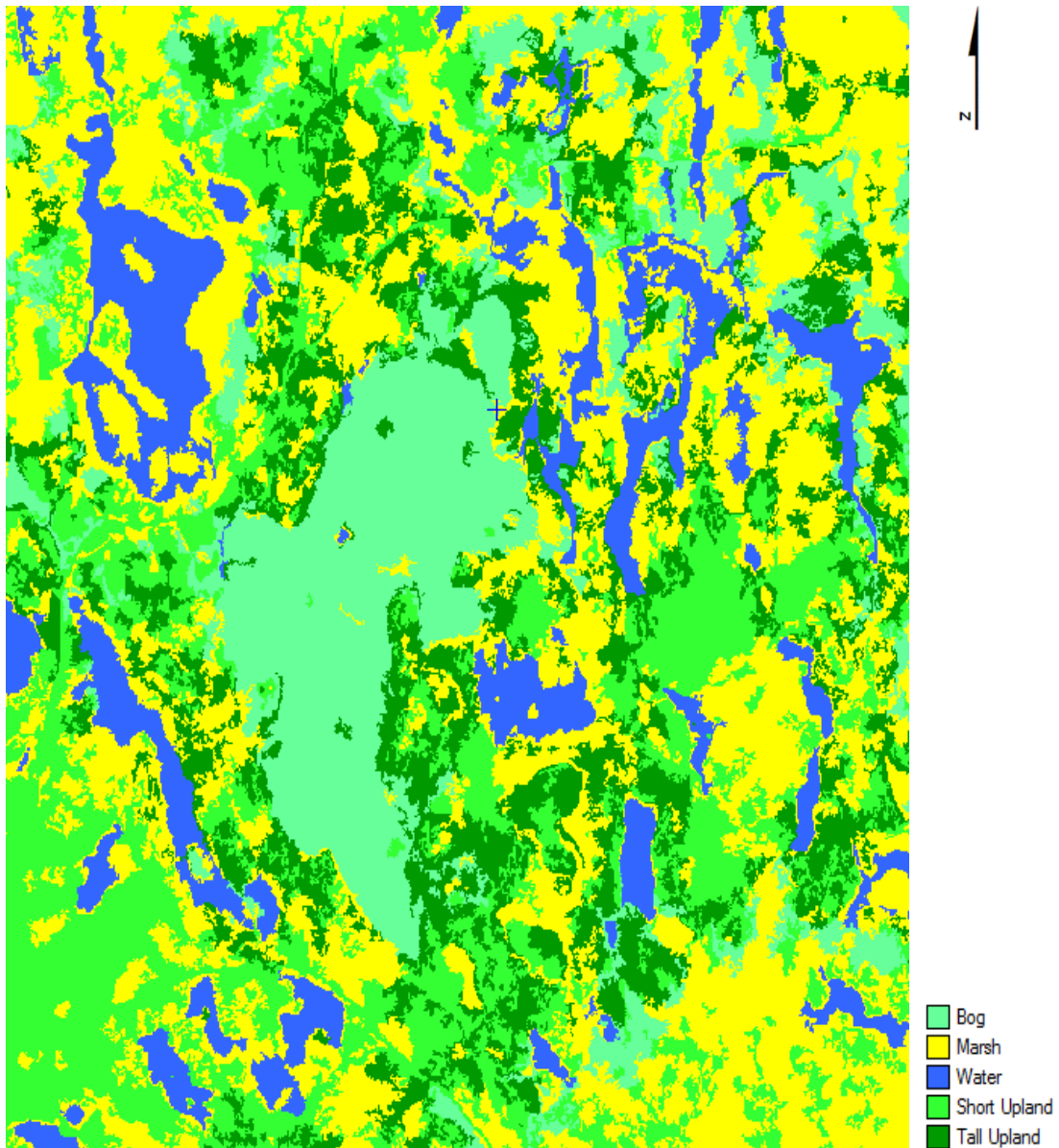


Figure F5. Thematic map of Westport Bog derived from spring 2010 WorldView-2 image segmented using scale value of 45, shape value of 0.1 and compactness value of 0.75 and classified using CTA and 5-classes of interest; the excessive amounts of marsh are mis-classifications.

Table F1A. Error matrix for the spring 2010 Marlborough Forest WorldView-2 and DEM object-based GINI CTA (5-classes).

		Reference Samples					Total
		Water	Upland	Fen	Swamp	Marsh	
Classified Samples	Water	5	0	0	0	0	5
	Upland	1	9	0	1	3	14
	Fen	0	1	2	0	1	4
	Swamp	0	2	0	5	0	7
	Marsh	0	3	0	0	7	10
	Total	6	15	2	6	11	40

Table F1B. Accuracy statistics for the spring 2010 Marlborough Forest WorldView-2 and DEM object-based GINI CTA (5-classes).

Overall Accuracy (%)	70.0		
Kappa	0.60		
Class Name	PA (%)	UA (%)	Kappa
Water	83.3	100.0	1.00
Upland	60.0	64.3	0.43
Fen	100.0	50.0	0.47
Swamp	83.3	71.4	0.66
Marsh	63.6	70.0	0.59
Average	78.0	71.1	

Table F2A. Error matrix for the spring 2010 Mer Bleue Bog WorldView-2 and DEM object-based GINI CTA (5-classes).

		Reference Samples					Total
		Water	Upland	Short Bog	Tall Bog	Marsh	
Classified Samples	Water	5	0	0	0	0	5
	Upland	0	14	0	0	1	15
	Short Bog	0	0	3	2	0	5
	Tall Bog	0	4	2	3	2	11
	Marsh	0	0	0	0	5	5
	Total	5	18	5	5	8	41

Table F2B. Accuracy statistics (%) for the spring 2010 Mer Bleue Bog WorldView-2 and DEM object-based GINI CTA (5-classes).

Overall Accuracy (%)	73.2		
Kappa	0.64		
Class Name	PA (%)	UA (%)	Kappa
Water	100.0	100.0	1.00
Upland	77.8	93.3	0.88
Short Bog	60.0	60.0	0.54
Tall Bog	60.0	27.3	0.17
Marsh	62.5	100.0	1.00
Average	72.1	76.1	

Table F3A. Error matrix for the spring 2010 Westport Bog WorldView-2 and DEM object-based GINI CTA (5- classes).

		Reference Samples					Total
		Water	Short	Tall	Bog	Marsh	
			Upland	Upland			
Classified Samples	Water	6	0	0	0	2	8
	Short Upland	0	3	0	0	0	3
	Tall Upland	0	2	6	0	1	9
	Bog	0	1	2	7	1	11
	Marsh	0	0	0	2	7	9
	Total	6	6	8	9	11	40

Table F3B. Accuracy statistics (%) for the spring 2010 Westport Bog WorldView-2 and DEM object-based GINI CTA (5-classes).

Overall Accuracy (%)	72.5		
Kappa	0.65		
Class Name	PA (%)	UA (%)	Kappa
Water	100.0	75.0	0.71
Short Upland	50.0	100.0	1.00
Tall Upland	75.0	66.7	0.58
Bog	77.8	63.6	0.53
Marsh	63.6	77.8	0.69
Average	73.3	76.6	

APPENDIX G. LSU details for all four sites.

This appendix contains details for image processing with Landsat TM imagery including LSU.

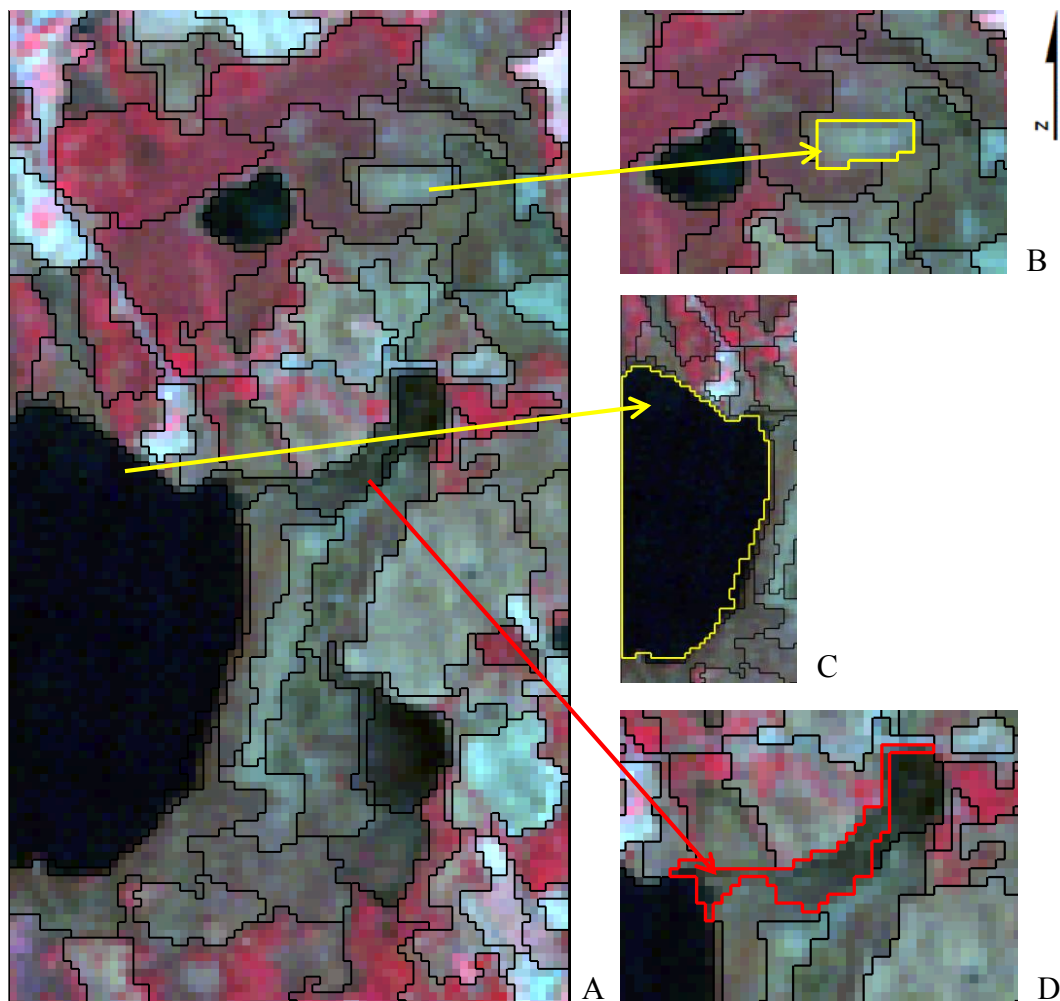


Figure G1. A) CIR composite of the spring 2010 Loch Garry Landsat TM 5 (and DEM) imagery showing the created objects using scale value of 10, shape value of 0.1 and compactness value of 0.5; and in yellow (B) objects that make up the boundaries of a known fen; and (C) objects that mimic the shoreline of the lake Loch Garry; and in red (D) objects that mask a known channel; detail is lost due to coarseness of the imagery.

Table G1. EMs (manually and automatically selected) and the mean spectral values for each of the 6 Landsat TM bands for Loch Garry.

Selection Method	EM	Blue	Green	Red	NIR	MIR(5)	MIR(7)
Manual	Bare	25.2162	34.3784	41.9460	61.2162	116.5405	53.9460
	Green	9.4886	23.6183	21.2061	52.0611	51.1298	21.7786
	Moisture	5.0427	19.3590	14.2222	9.9487	7.7180	4.7180
Automatic	Member 1	31.1111	38.7778	49.0000	72.1111	138.7778	65.2222
	Member 2	8.0000	23.7500	19.2500	73.8750	47.2500	17.6250
	Member 3	39.0000	43.5000	52.5000	58.5000	116.5000	76.5000
	Member 4	4.0000	21.5000	18.5000	11.1667	10.5000	6.0000
	Member 5	16.5000	30.0000	29.0000	94.5000	93.5000	51.5000

Table G2. EMs (manually and automatically selected) and the mean spectral values for each of the 6 Landsat TM bands for Marlborough Forest.

Selection Method	EM	Blue	Green	Red	NIR	MIR(5)	MIR(7)
Manual	Bare	33.6531	40.6225	50.8776	61.9694	122.2449	64.3980
	Green	9.6840	25.1415	22.2594	53.8208	53.3302	22.7453
	Moisture	5.5345	20.1379	17.4310	14.5862	15.0172	8.4483
Automatic	Member 1	79.0000	80.0000	100.0000	97.0000	116.0000	58.0000
	Member 2	37.3000	43.8000	56.9000	72.2000	153.5000	78.5000
	Member 3	11.3333	27.0000	21.7778	85.4444	53.4444	19.6667
	Member 4	30.8889	39.0000	47.8889	52.6667	114.8889	76.1111
	Member 5	4.0000	21.5000	18.8750	13.2500	8.2500	5.1250

Table G3. EMs (manually and automatically selected) and the mean spectral values for each of the 6 Landsat TM bands for Mer Bleue Bog.

Selection Method	EM	Blue	Green	Red	NIR	MIR(5)	MIR(7)
Manual	Bare	40.8888	47.7271	62.5169	70.0266	143.0680	79.1932
	Green	28.5908	28.5908	30.9135	66.9901	72.0012	30.5914
	Moisture	6.5000	22.1087	21.6957	25.6937	37.2609	18.5652
Automatic	Member 1	107.0000	75.0000	92.0000	80.0000	181.0000	117.0000
	Member 2	11.1000	27.7000	23.0000	118.4000	80.5000	26.6000
	Member 3	64.5000	54.5000	63.0000	71.0000	68.5000	33.5000
	Member 4	21.5000	32.5000	39.0000	55.5000	110.0000	96.0000
	Member 5	26.0000	41.6666	45.6666	29.3333	46.3333	26.6666

Table G4. EMs (manually and automatically selected) and the mean spectral values for each of the 6 Landsat TM bands for Westport Bog.

Selection Method	EM	Blue	Green	Red	NIR	MIR(5)	MIR(7)
Manual	Bare	82.7286	64.6286	70.4429	41.2000	16.9571	10.1000
	Green	13.4157	29.5804	34.7490	50.4784	80.4510	38.2784
	Moisture	11.0952	25.1191	24.2857	20.2381	25.5714	12.8095
Automatic	Member 1	113.0000	80.3333	95.3333	68.6667	25.6667	15.6667
	Member 2	23.6000	38.3000	50.4000	67.6000	133.8000	65.9000
	Member 3	6.4444	24.4444	23.1111	56.6667	41.2222	16.6667
	Member 4	81.5000	66.2500	70.2500	35.0000	20.2500	12.7500
	Member 5	1.0000	23.0000	21.0000	17.0000	26.0000	14.0000

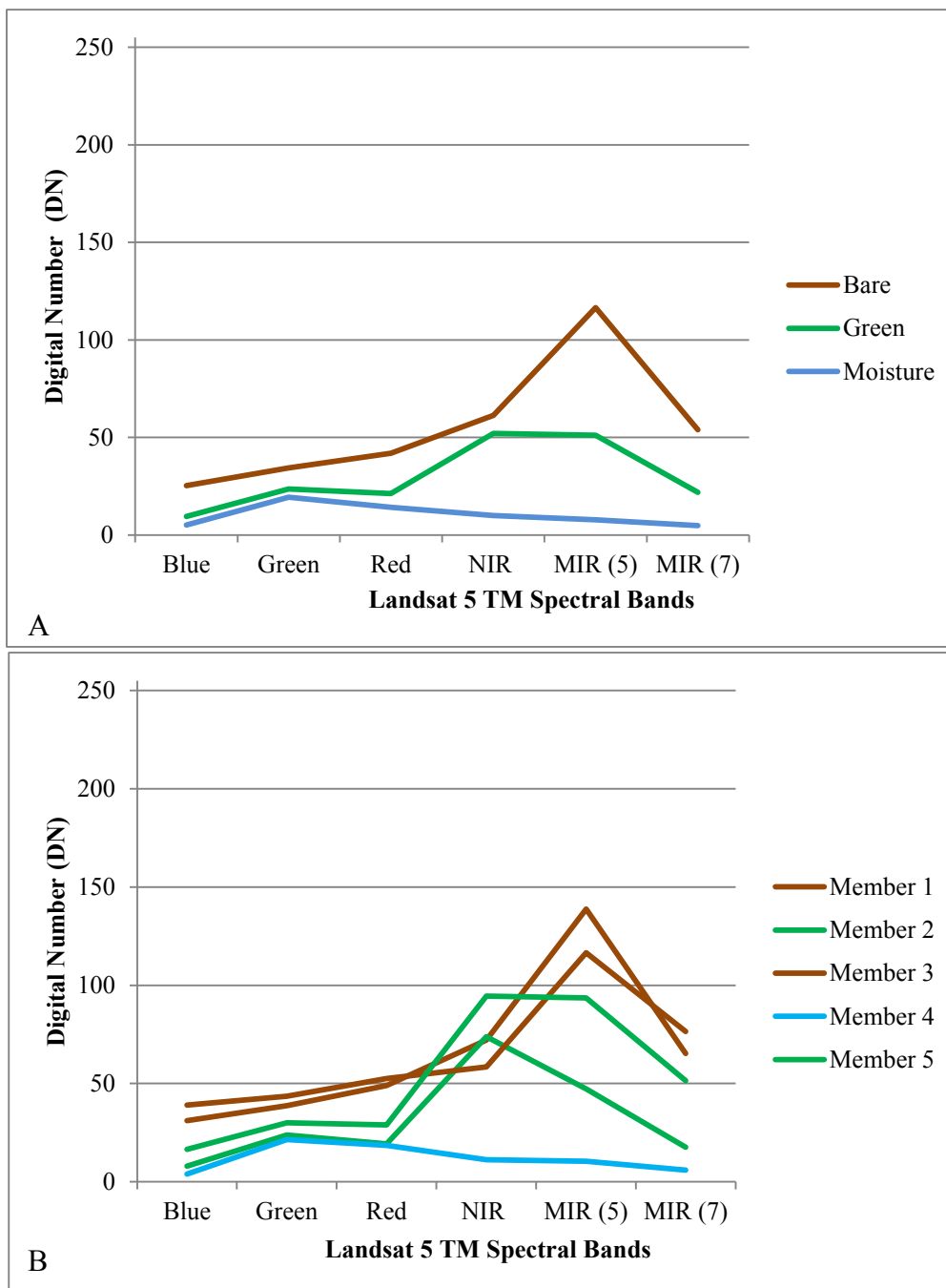


Figure G2. Spectral signature graphs for the automatic and manually selected EMs for Loch Garry Landsat 5 TM spring image. A) Signatures for the three manually selected EMs; and (B) signatures of the five automatically selected EMs.

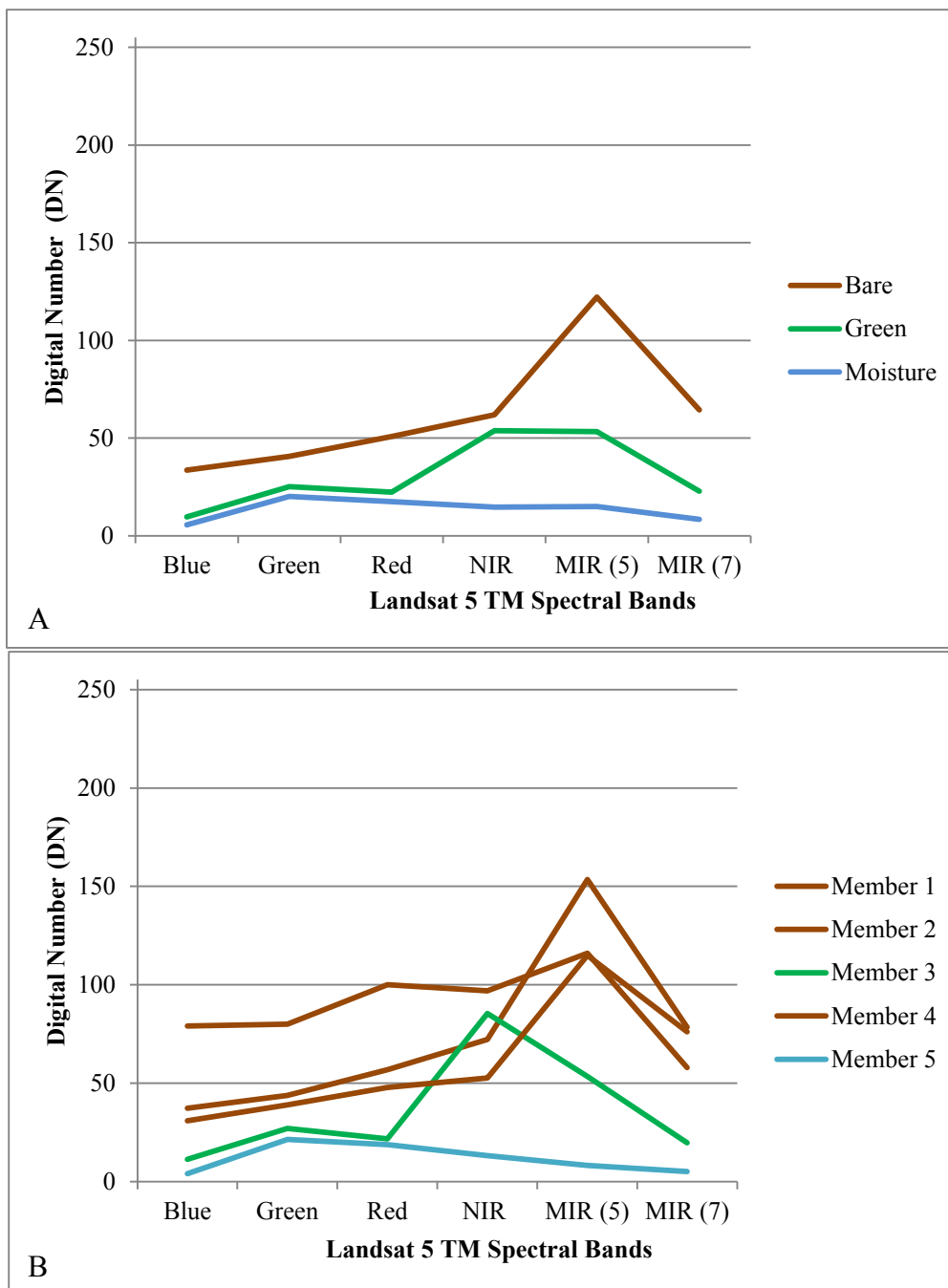


Figure G3. Spectral signature graphs for the automatic and manually selected EMs for Marlborough Forest Landsat 5 TM spring image. A) Signatures for the three manually selected EMs; and (B) signatures of the five automatically selected EMs.

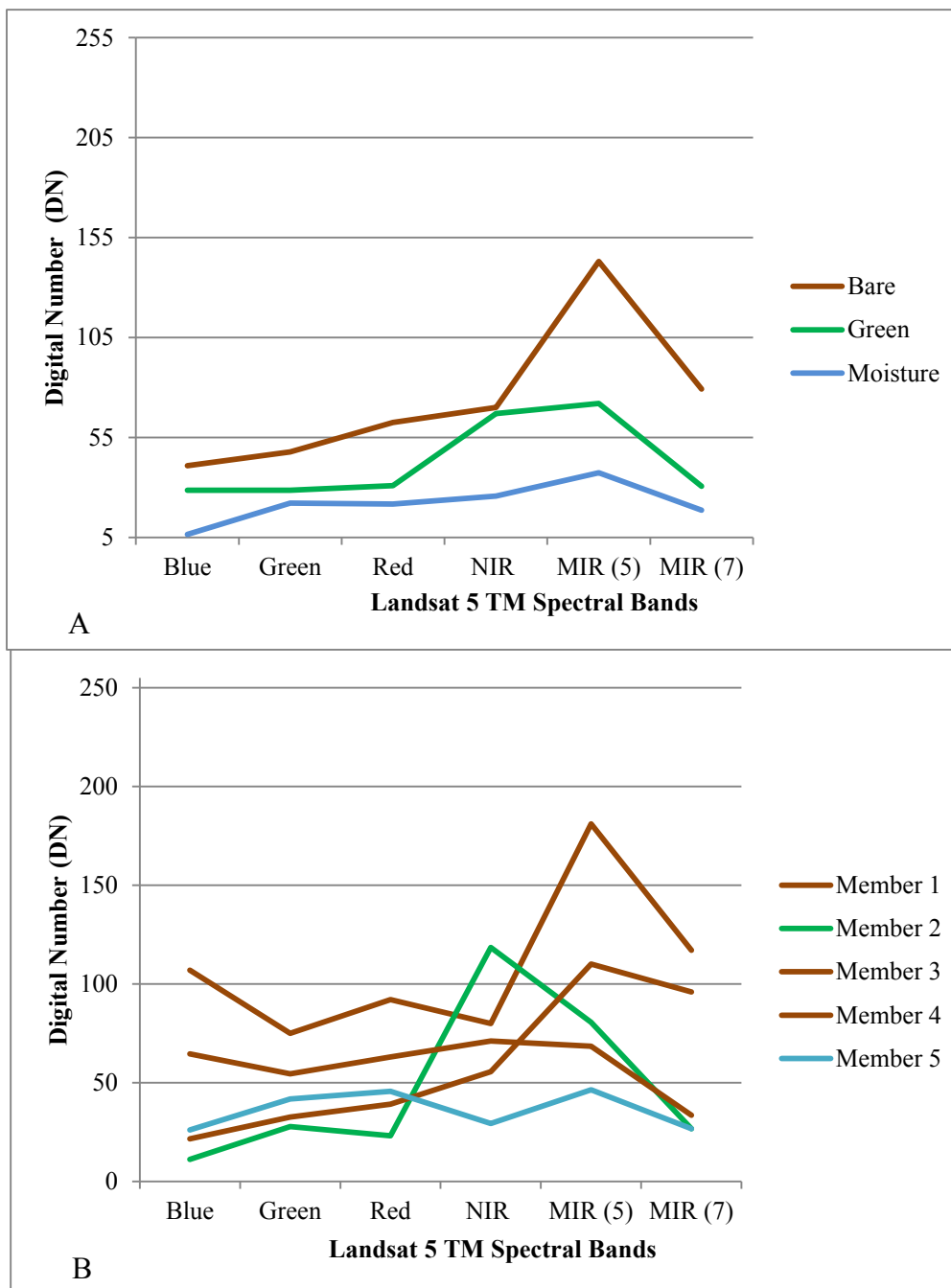


Figure G4. Spectral signature graphs for the automatic and manually selected EMs for Mer Bleue Bog Landsat 5 TM spring image. A) Signatures for the three manually selected EMs; and (B) signatures of the five automatically selected EMs.

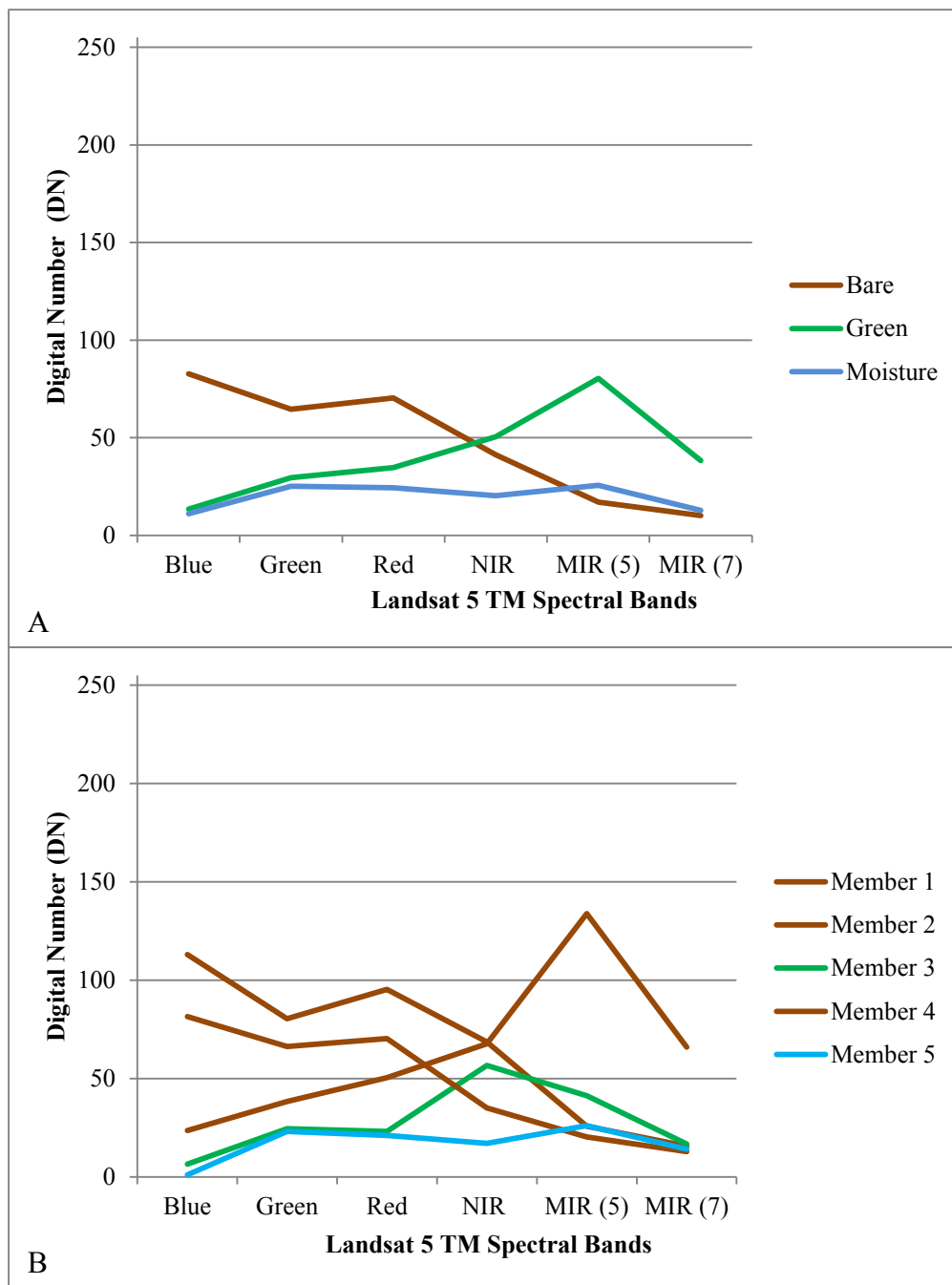


Figure G5. Spectral signature graphs for the automatic and manually selected EMs for Westport Bog Landsat 5 TM spring image. A) Signatures for the three manually selected EMs; and (B) signatures of the five automatically selected EMs.

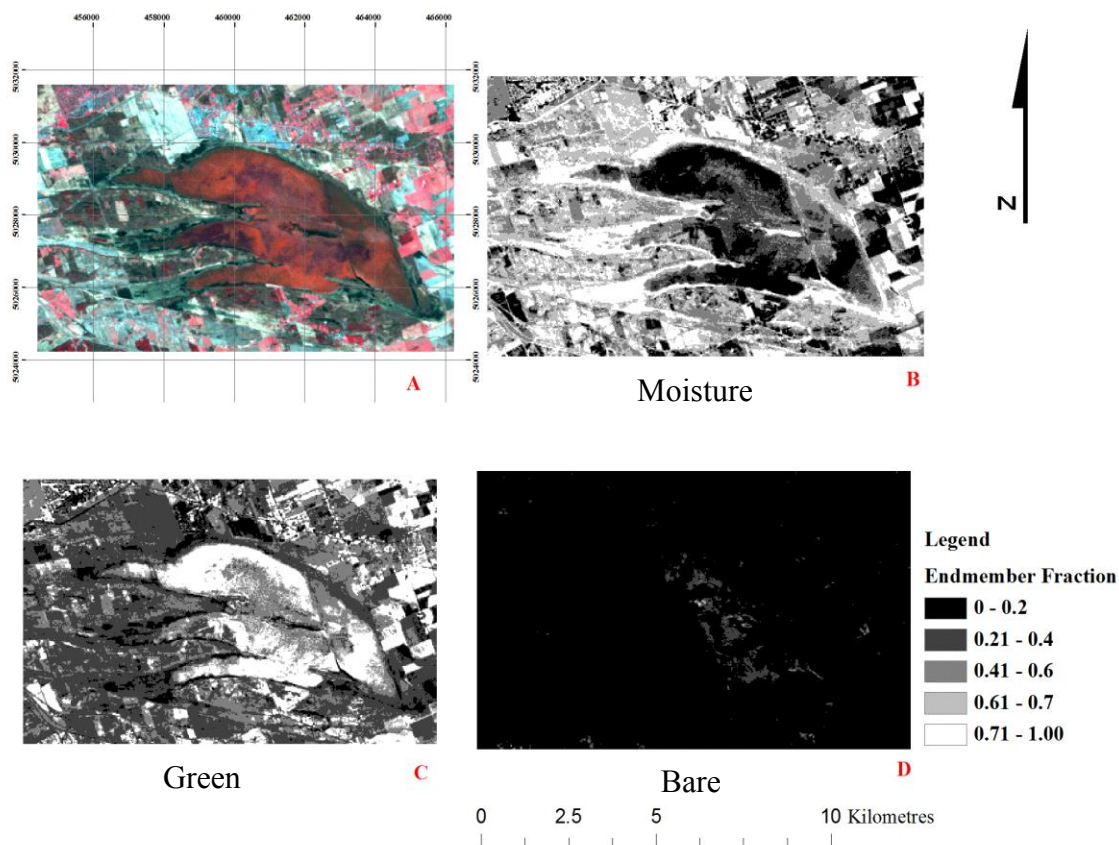


Figure G6. Derived fraction maps in greyscale from the 3 manually selected EMs. The values are the proportion of the pixel that represents that EM. A) CIR composite of Mer Bleue Bog; B through D) are the EM fraction maps.

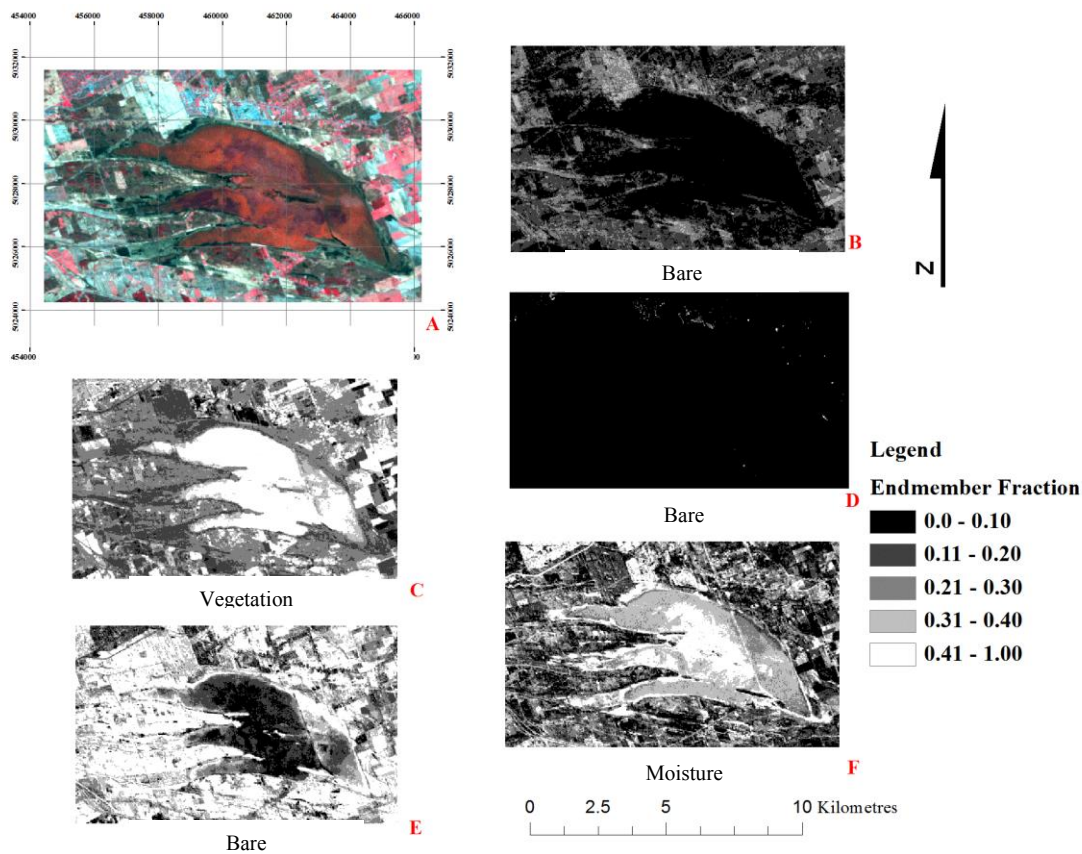


Figure G7. Derived fraction maps in greyscale from the five automatically selected EMs. The values are the proportion of the pixel that represents that EM. A) CIR composite of Mer Bleue Bog; B through F) are the EM fraction maps.

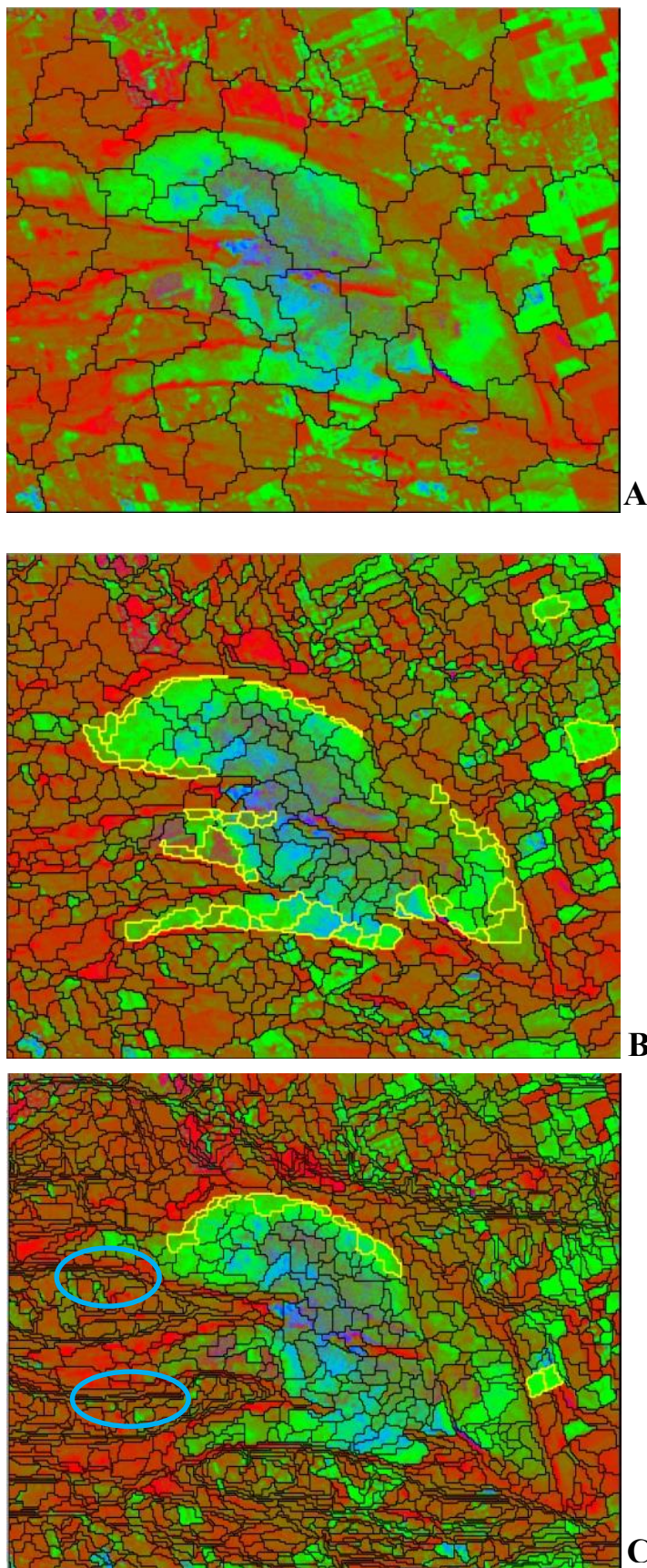


Figure G8. Example of the segmentation parameter testing using the 3 manual EM fraction images. (A) 3-layer composite of Mer Bleue Bog created using three EMs; (moisture in blue; bare in red; and green (vegetation) in green) showing the segmented objects (scale value = 10, shape value = 0.1 and compactness value = 0.5) (B) segmented object (scale value = 2, shape value = 0.1 and compactness value = 0.1) With changing values objects represent meaningful features (e.g. bog boundary and farm fields highlighted in yellow). (C) is the same composite with the addition of the DEM in the segmentation process. The same meaningful features appear (yellow) and include finer objects that mimic the topographic contours (blue circles).

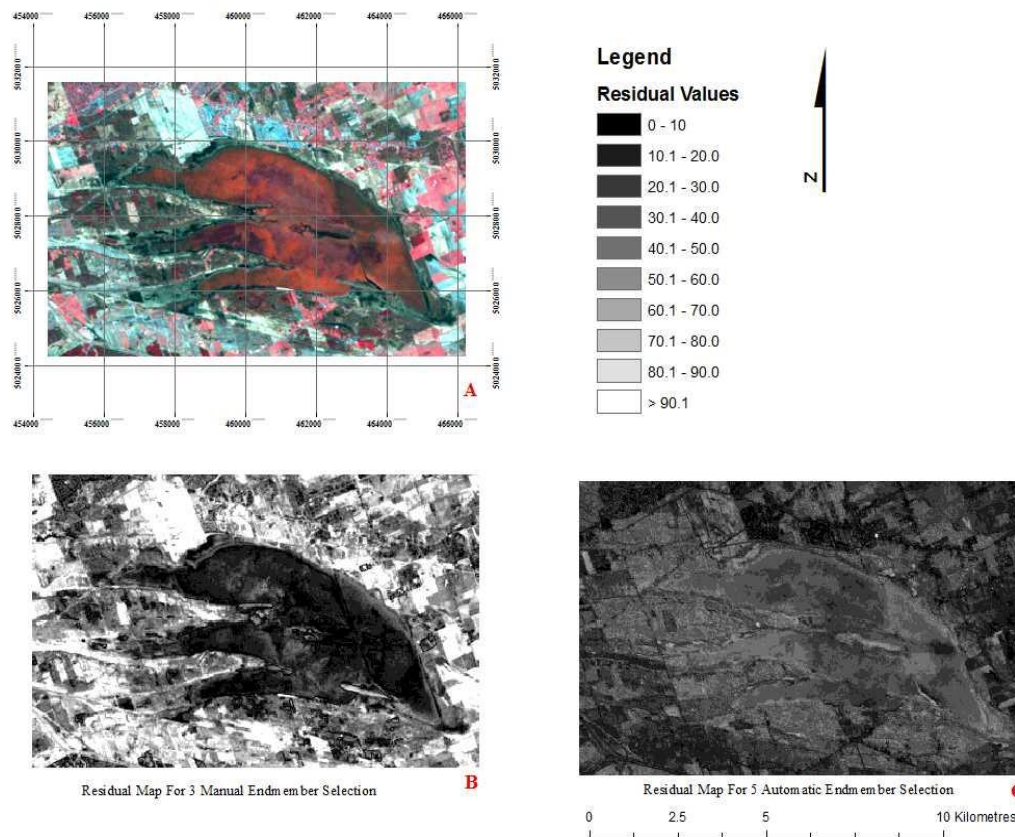


Figure G9. Residual maps for Mer Bleu Bog. Values closer to zero indicate higher unmixing precision, and the fractions are more representative of actual land cover proportions than areas with higher residuals (A) CIR composite of Landsat 5 TM spring image of Mer Bleu Bog. B) and C) are the 3 manual and 5 automatic EM residual maps, respectively.

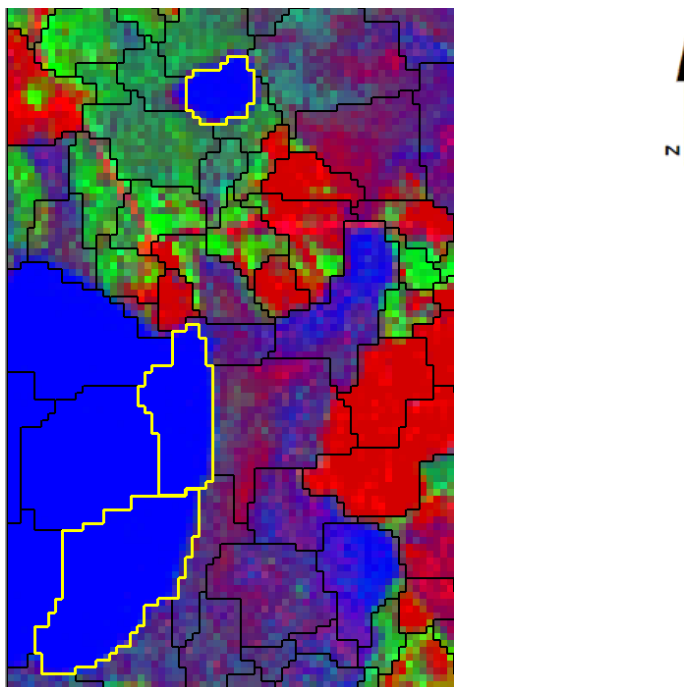


Figure G10. Segmented 5 EM fraction maps (without the DEM, moisture in blue; vegetation in green; and bare in red) derived from spring 2010 Landsat 5 TM Loch Garry imagery (scale value =2; shape value = 0.1; compactness value = 0.1). Yellow highlighted objects represent land cover spatial features.

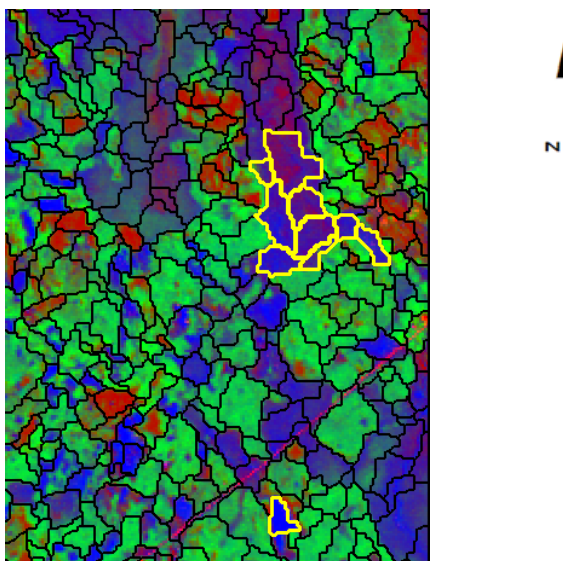


Figure G11. Segmented 5 EM fraction maps (without the DEM, moisture in blue; vegetation in green; and bare in red) derived from spring 2010 Landsat 5 TM Marlborough Forest imagery (scale value =2; shape value = 0.1; compactness value = 0.1). Yellow highlighted objects represent land cover spatial features

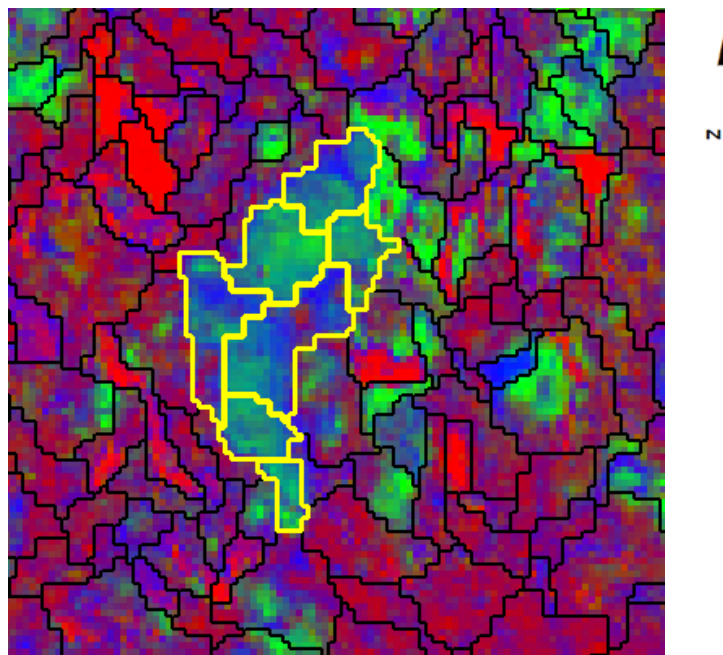


Figure G12. Segmented 5 EM fraction maps (without the DEM, moisture in blue; vegetation in green; and bare in red) derived from spring 2010 Landsat 5 TM Westport Bog imagery (scale value =2; shape value = 0.1; compactness value = 0.1). Yellow highlighted objects represent spatial features (Bog).

Table G5. Error matrix for the spring 2010 Marlborough Forest Landsat 5 TM original 6 bands (not segmented, no DEM) object-based GINI CTA (5-classes).

		Reference Samples					Total
		Water	Upland	Fen	Swamp	Marsh	
Classified Samples	Water	5	0	0	0	0	5
	Upland	0	10	0	0	0	10
	Fen	0	0	6	0	2	8
	Swamp	1	0	0	9	2	12
	Marsh	0	5	1	2	3	11
	Total	6	15	7	11	7	46

Table G6. Error matrix for the spring 2010 Marlborough Forest Landsat 5 TM original 6 bands (not segmented, with DEM) object-based GINI CTA (5-classes).

		Reference Samples					
		Water	Upland	Fen	Swamp	Marsh	Total
Classified Samples	Water	5	0	0	0	0	5
	Upland	0	10	0	0	2	12
	Fen	0	1	6	0	0	7
	Swamp	0	0	0	8	2	10
	Marsh	1	4	1	3	3	12
	Total	6	15	7	11	7	46

Table G7. Error matrix for the spring 2010 Marlborough Forest Landsat 5 TM original 6 bands (segmented, no DEM) object-based GINI CTA (5-classes).

		Reference Samples					
		Water	Upland	Fen	Swamp	Marsh	Total
Classified Samples	Water	6	0	0	0	1	7
	Upland	0	10	2	1	0	13
	Fen	0	0	5	0	2	7
	Swamp	0	0	0	5	2	7
	Marsh	0	5	0	5	2	12
	Total	6	15	7	11	7	46

Table G8. Error matrix for the spring 2010 Marlborough Forest Landsat 5 TM original 6 bands (segmented, with DEM) object-based GINI CTA (5-classes).

		Reference Samples					
		Water	Upland	Fen	Swamp	Marsh	Total
Classified Samples	Water	5	0	0	0	0	5
	Upland	0	12	1	3	0	16
	Fen	0	1	5	0	1	7
	Swamp	0	0	0	7	1	8
	Marsh	1	2	1	1	5	10
	Total	6	15	7	11	7	46

Table G9. Error matrix for the spring 2010 Marlborough Forest Landsat 5 TM 5 EM fraction maps (not segmented, no DEM) object-based GINI CTA (5-classes).

		Reference Samples					
		Water	Upland	Fen	Swamp	Marsh	Total
Classified Samples	Water	6	0	0	0	1	7
	Upland	0	13	0	0	0	13
	Fen	0	0	7	1	1	9
	Swamp	0	0	0	8	3	11
	Marsh	0	2	0	2	2	6
	Total	6	15	7	11	7	46

Table G10. Error matrix for the spring 2010 Marlborough Forest Landsat 5 TM 5 EM fraction maps (not segmented, with DEM) object-based GINI CTA (5-classes).

		Reference Samples					
		Water	Upland	Fen	Swamp	Marsh	Total
Classified Samples	Water	6	0	0	0	1	7
	Upland	0	9	1	1	2	13
	Fen	0	1	6	1	0	8
	Swamp	0	5	0	5	2	7
	Marsh	0	5	0	4	2	11
	Total	6	15	7	11	7	46

Table G11. Error matrix for the spring 2010 Marlborough Forest Landsat 5 TM 5 EM fraction maps (segmented, no DEM) object-based GINI CTA (5-classes).

		Reference Samples					
		Water	Upland	Fen	Swamp	Marsh	Total
Classified Samples	Water	5	2	0	4	3	14
	Upland	0	10	1	2	1	14
	Fen	0	0	6	0	0	6
	Swamp	0	0	0	5	0	5
	Marsh	1	3	0	0	3	7
	Total	6	15	7	11	7	46

Table G12. Error matrix for the spring 2010 Marlborough Forest Landsat 5 TM 5 EM fraction maps (segmented, with DEM) object-based GINI CTA (5-classes).

		Reference Samples					
		Water	Upland	Fen	Swamp	Marsh	Total
Classified Samples	Water	2	0	0	1	3	6
	Upland	0	11	2	3	2	18
	Fen	0	0	5	0	1	6
	Swamp	1	0	0	6	1	8
	Marsh	3	4	0	1	0	8
	Total	6	15	7	11	7	46

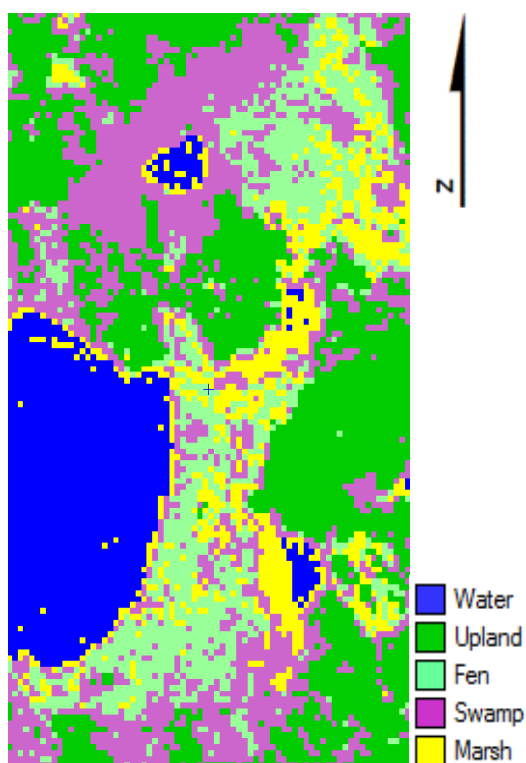


Figure G13. 5-Class GINI CTA classification for Loch Garry using Landsat TM imagery acquired in April

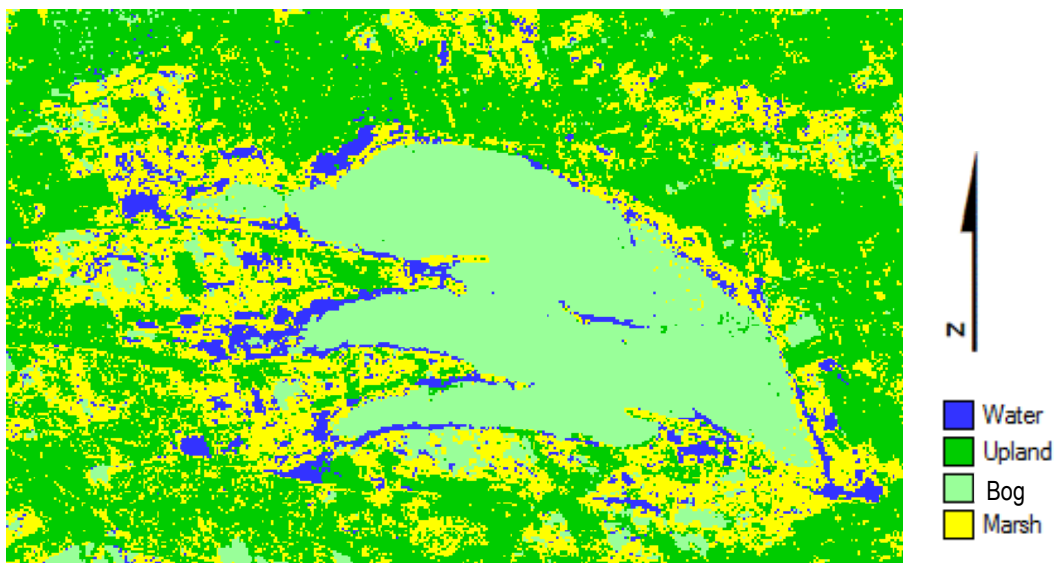


Figure G14. 5-Class GINI CTA classification for Mer Bleue Bog using Landsat TM imagery acquired in April 2010.

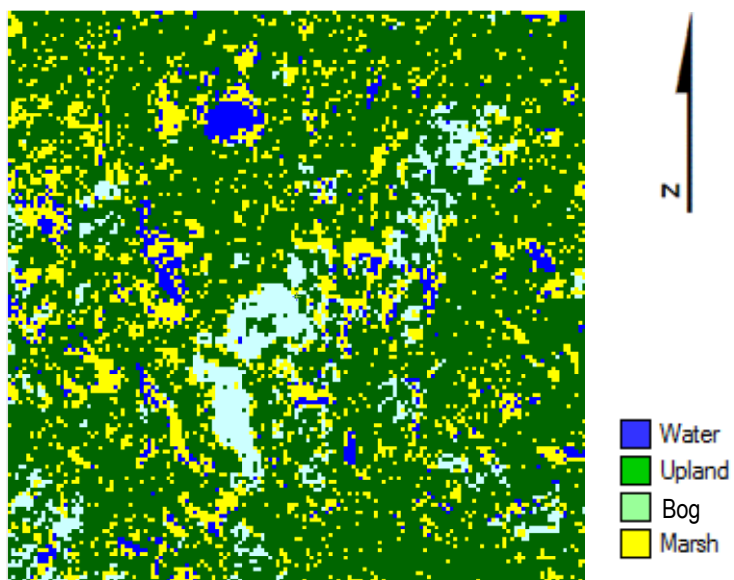


Figure G15. 5-Class GINI CTA classification for Westport Bog using Landsat TM imagery acquired in March 2010.

APPENDIX H. Sites and polarimetric signatures for Bog, Fen, Marsh, Swamp, Water and Upland.

Table H1. Location of sites for polygons selected to derive polarimetric signatures and pedestal heights.

Wetland Complex	Signature	Location	Corresponding reference point (see Table C1)
Loch Garry	Fen 1	East of small lake	VP111
	Fen 2	South of Loch Garry	VP102
	Fen 3	Right on north side of small lake	VP111
	Marsh 1	At canoe entry point	
	Marsh 2	Giant marsh north of road	VP 84
	Marsh 3	Right on small lake	VP108
	Swamp 1	Just north of small lake	VP 109
	Swamp 2	Just north of jut out	VP 99
	Swamp 3	On arm of big lake	VP 90
	Water 1	In small lake	
	Water 2	In big lake	
	Water 3	In smaller lake east of Loch Garry	
	Upland 1	North of small lake (deciduous/mixed stand)	VP110
	Upland 2	South of Loch Garry (coniferous/mixed stand)	VP 94/95
Marlborough Forest	Fen1	Long fen	VP4
	Fen2	Long fen (further north)	
	Fen3	Just south of small lake south of Roger Stevens Pond	VP38
	Marsh1	Just north of Roger Stevens Road	VP47
	Marsh2	North of Roger Stevens Road	VP24
	Marsh3	North of Roger Stevens Road	VP49
	Swamp1	West of long fen	VP16
	Swamp2	South of Rogers Stevens Pond	VP29

	Swamp3	East of small lake	VP 41
	Water 1	Roger Stevens Pond	
	Water 2	Just north of VP17 (Upland)	
	Upland1	Deciduous stand	VP1
	Upland2	Coniferous/mixed stand	VP12
Mer Bleue Bog	Bog1	Off the private boardwalk (north side)	VP118
	Bog2	Off the public boardwalk	VP149
	Bog3	West of the public boardwalk	
	Marsh1	West of private boardwalk	VP114
	Marsh2	Middle arm	VP140
	Marsh3	West of public boardwalk	VP 135
	Water1	Middle arm	
	Water2	West of public boardwalk	
	Upland1	Southern arm	VP134
	Upland2	Northern arm	VP125
Westport Bog	Bog1	Hurlbutt Property – east side of bog	VP64
	Bog2	Hurlbutt Property (around the bog hole)	
	Bog3	Jevons Property – west side of bog	VP72B
	Marsh1	Jevons Property	VP74
	Marsh2	Hurlbutt Property	VP 51
	Marsh3	Down the road	VP78B
	Water	Big lake north of bog	
	Water	Lake northeast of previous lake	
	Upland	Coniferous Jevons Property	VP73
	Upland	Deciduous/mixed stand Hurlbutt Property	VP53

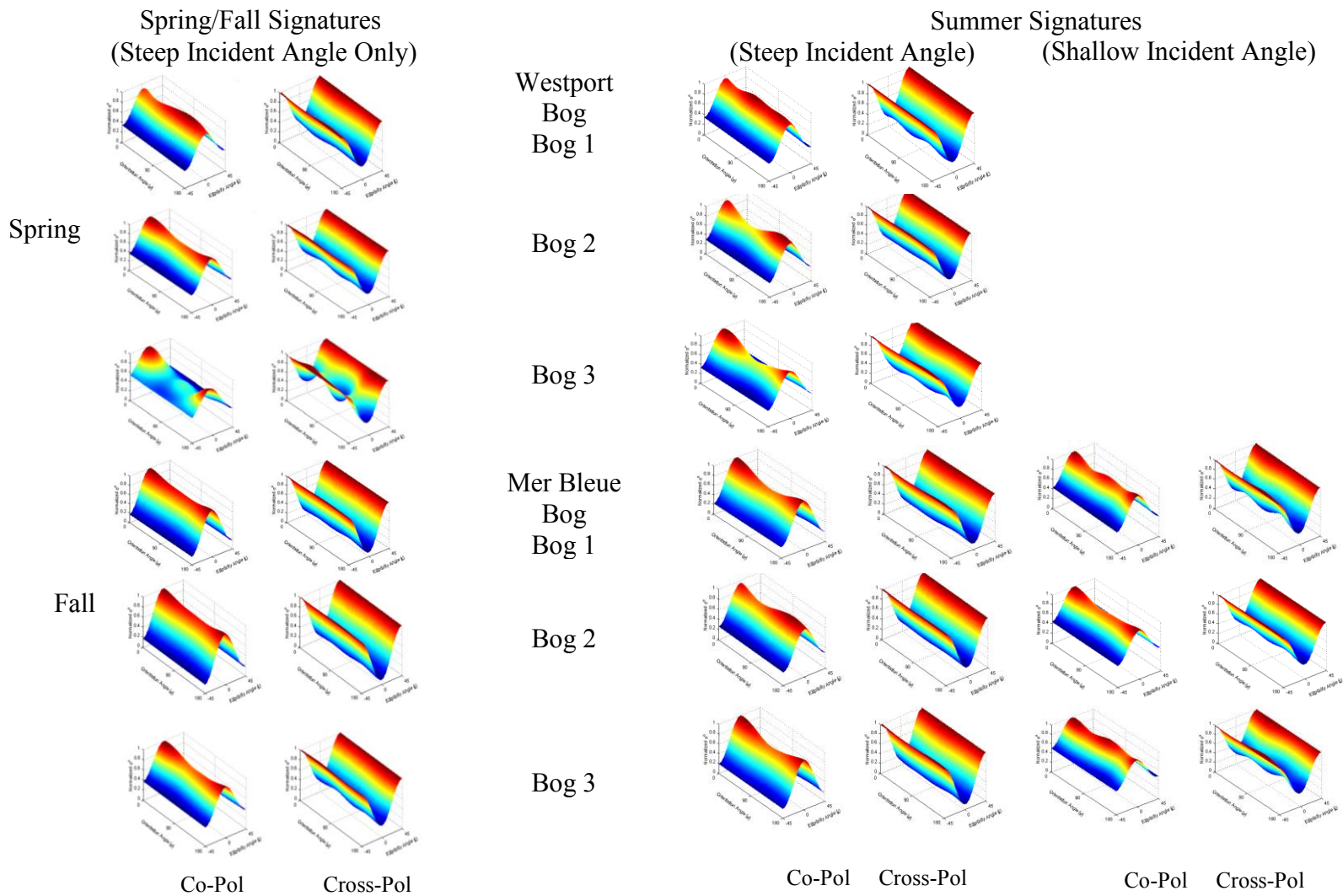


Figure H1. Spring/fall and summer co- and cross-pol signatures for Bog at Westport Bog and Mer Bleue Bog.

Spring Signatures
 (Steep Incident Angle) (Shallow Incident Angle)

Summer Signatures
 (Steep Incident Angle Only)

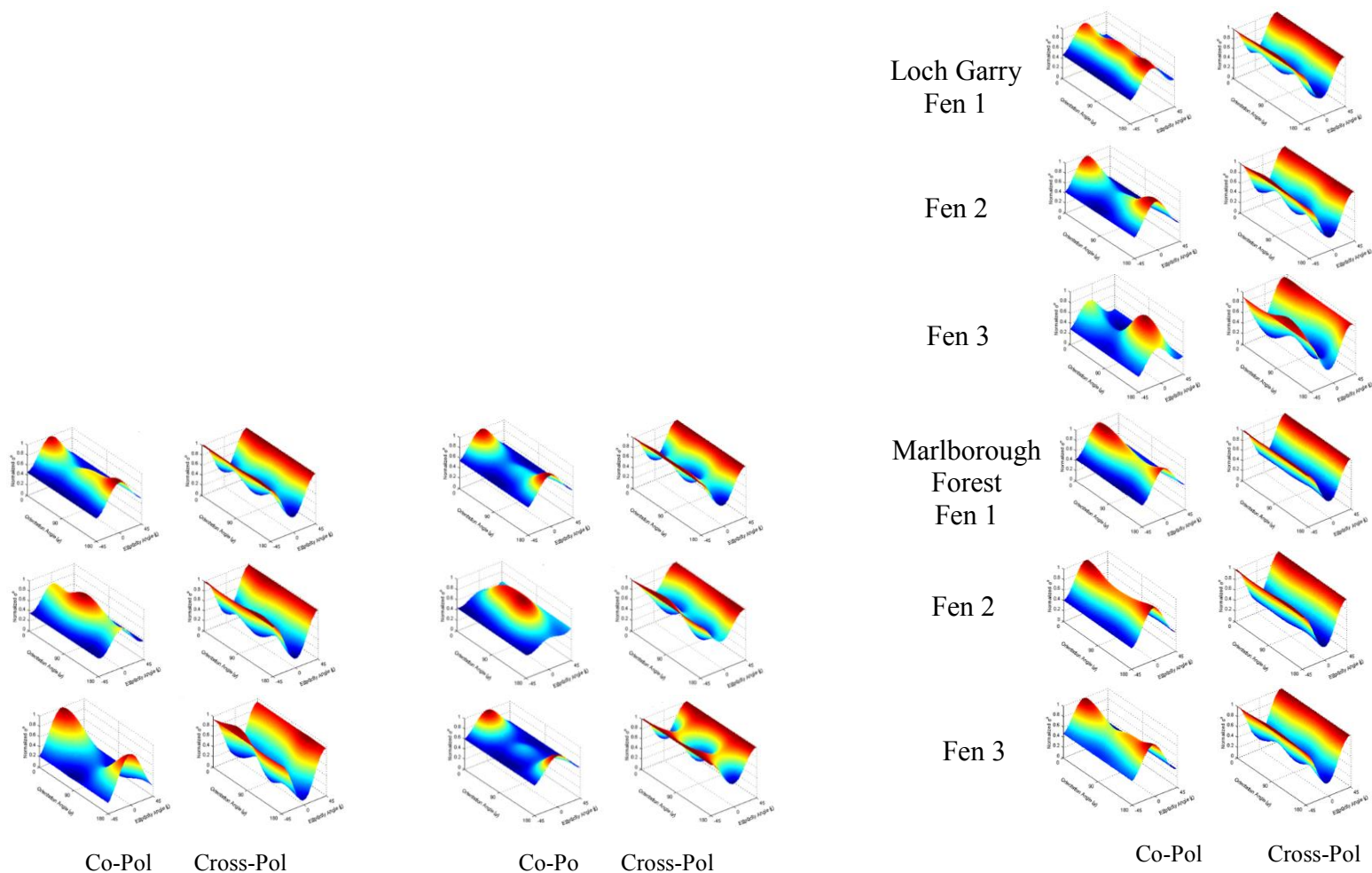
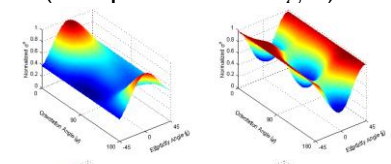


Figure H2. Spring and summer co- and cross-pol signatures for Fen at Loch Garry and Marlborough Forest.

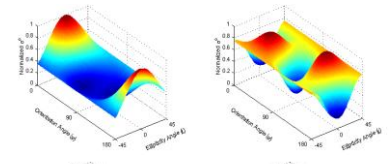
Spring/Fall Signatures
 (Steep Incident Angle) (Shallow Incident Angle)

Summer Signatures
 (Steep Incident Angle)

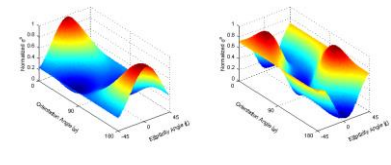
Loch Garry
 Marsh 1



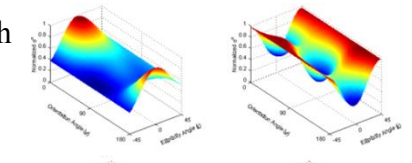
Marsh 2



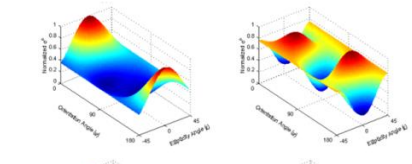
Marsh3



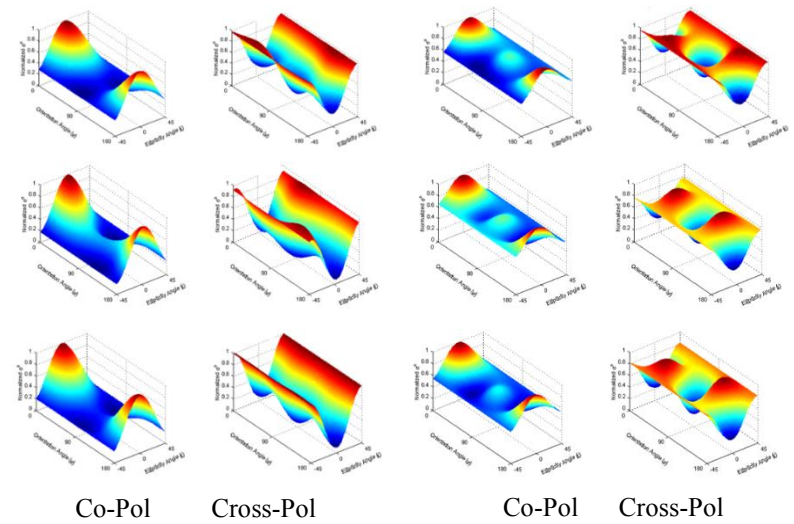
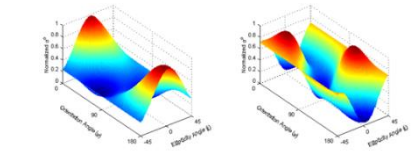
Marlborough
 Forest
 Marsh 1



Marsh 2



Marsh3



Co-Pol Cross-Pol

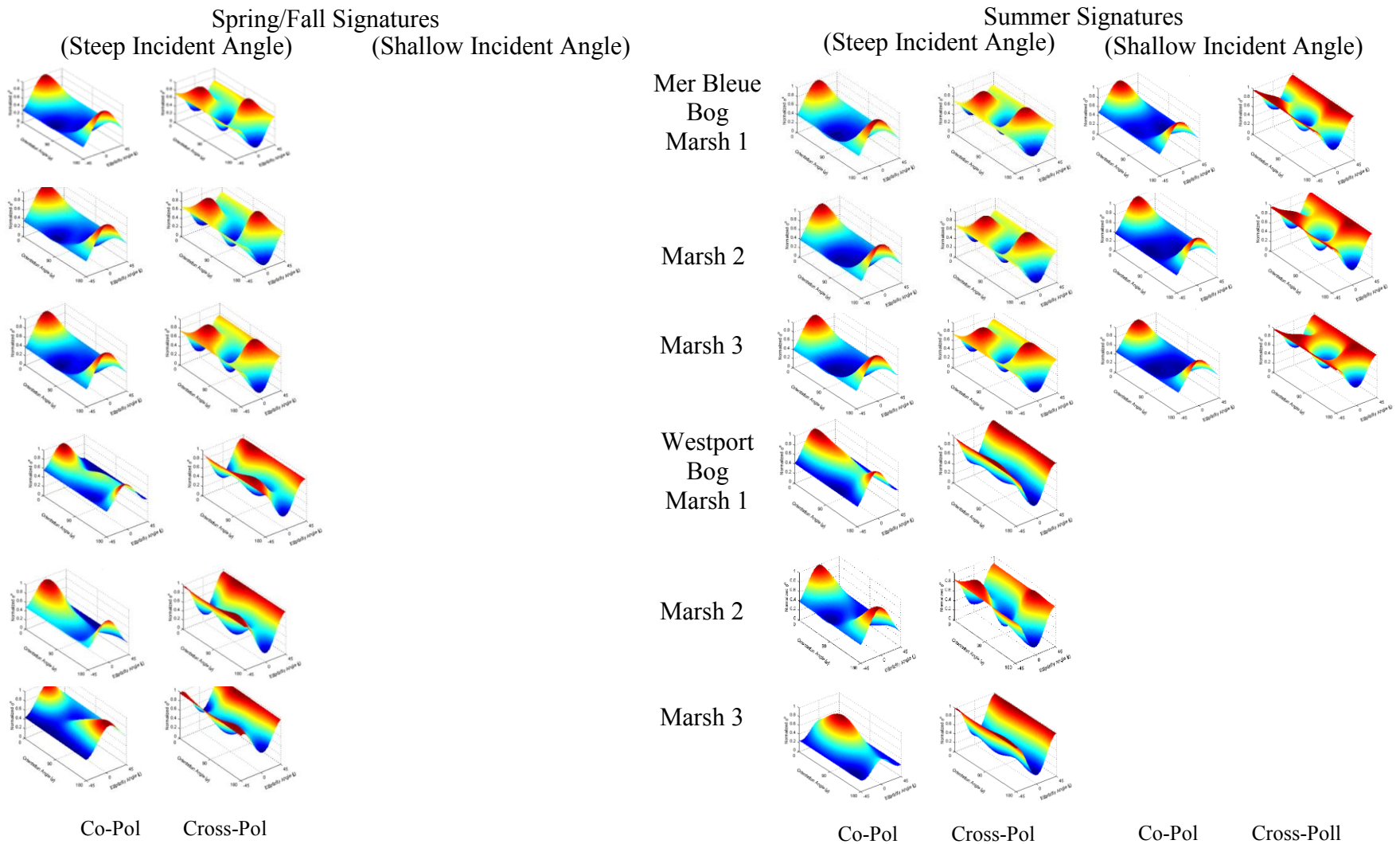


Figure H3. Spring/fall and summer co- and cross-pol signatures for Marsh at Loch Garry, Marlborough Forest, Mer Bleue Bog and Westport Bog.

Spring Signatures
 (Steep Incident Angle) (Shallow Incident Angle)

Summer Signatures
 (Steep Incident Angle Only)

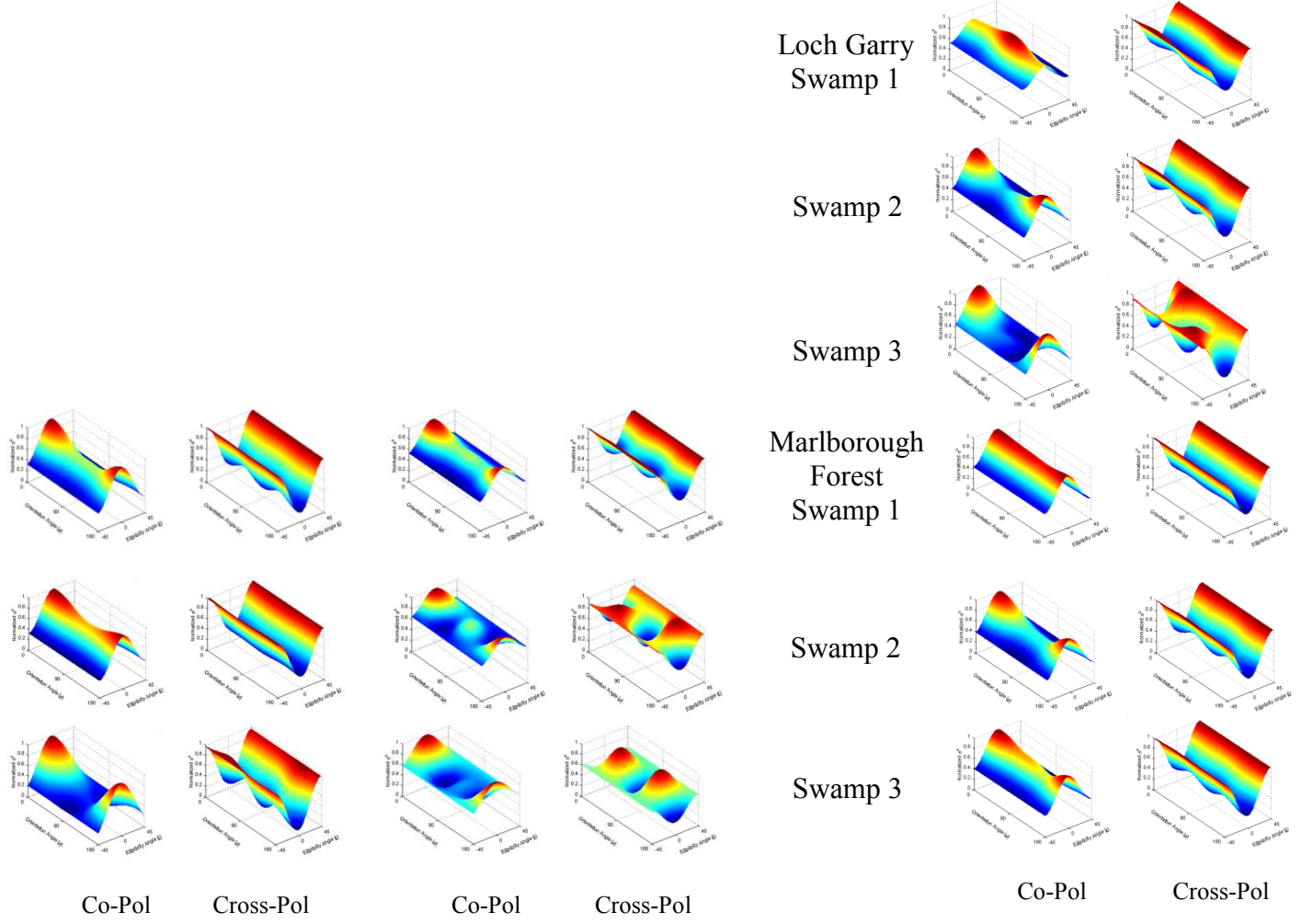
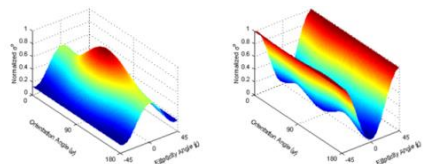


Figure H4. Spring and summer co- and cross-pol signatures for Swamp at Loch Garry and Marlborough Forest.

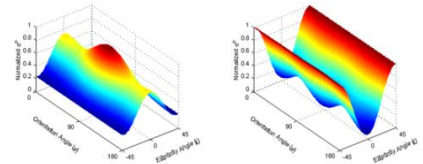
Spring/Fall Signatures
 (Steep Incident Angle) (Shallow Incident Angle)

Summer Signatures
 (Steep Incident Angle)

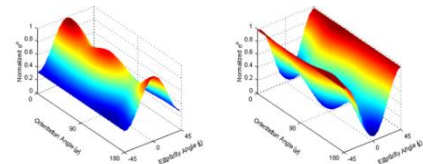
Loch Garry
 Water 1



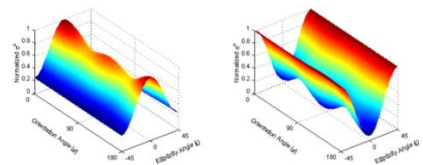
Water 2



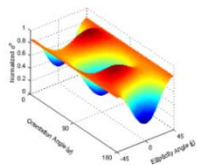
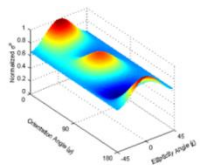
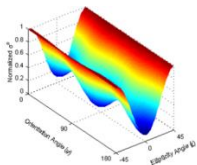
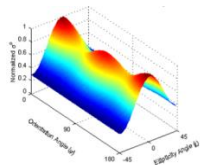
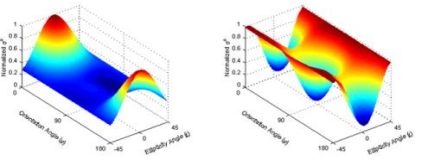
Water3



Marlborough
 Forest
 Water 1



Water 2



Co-Pol

Cross-Pol

Co-Pol

Cross-Pol

Co-Pol

Cross-Pol

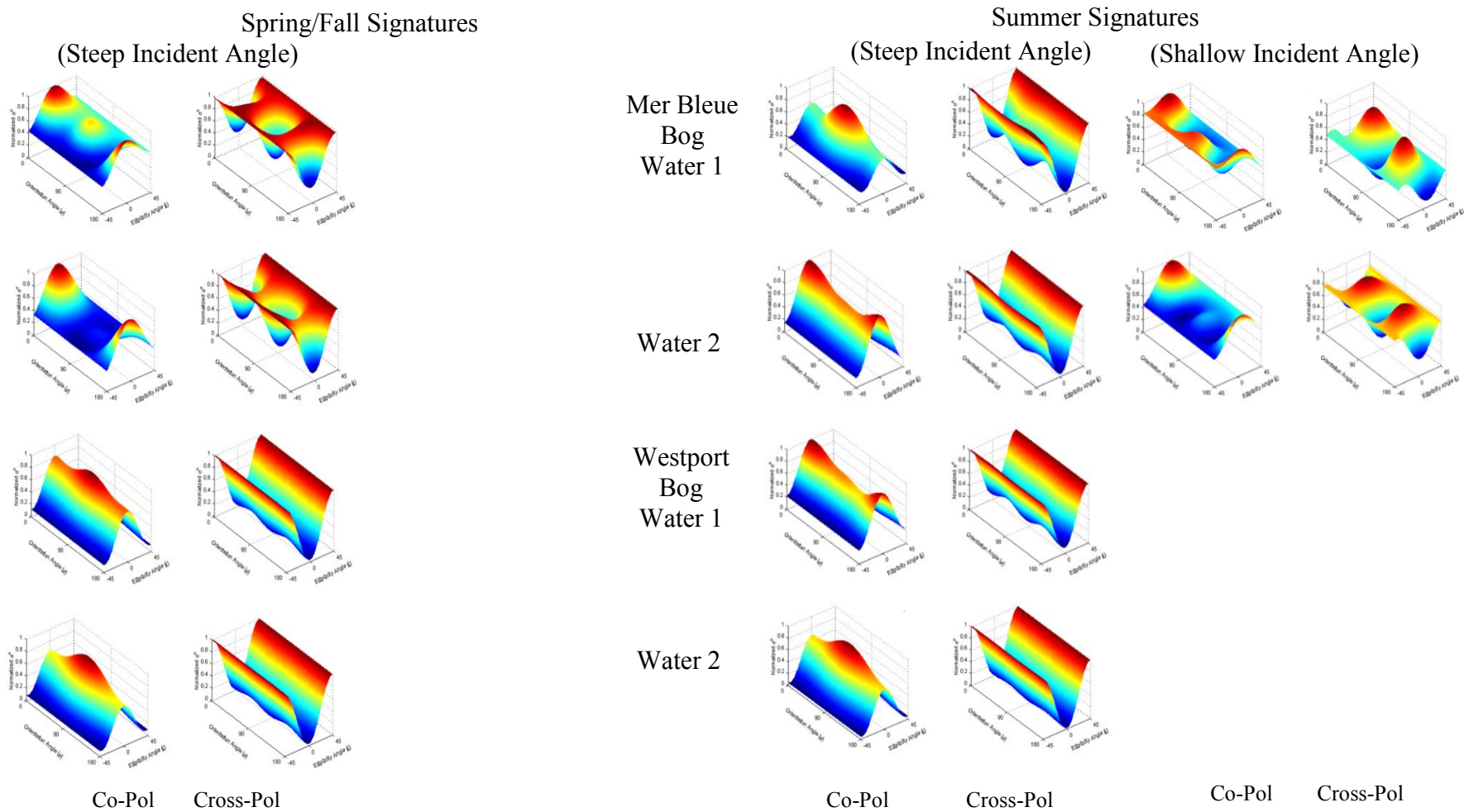
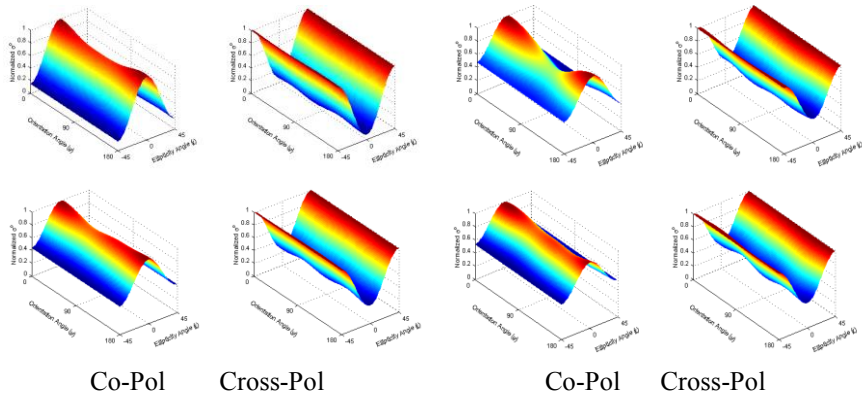


Figure H5. Spring/fall and summer co- and cross-pol signatures for Water at Loch Garry, Marlborough Forest, Mer Bleue Bog and Westport Bog.

Spring/Fall Signatures

(Steep Incident Angle)

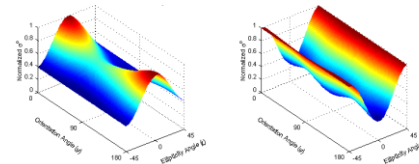
(Shallow Incident Angle)



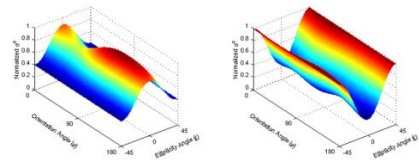
Summer Signatures

(Steep Incident Angle)

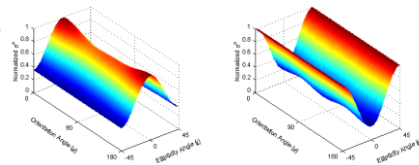
Loch Garry Upland 1



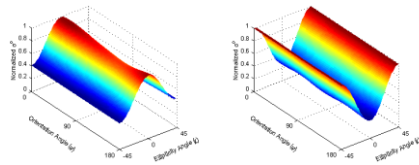
Upland 2



Marlborough Forest Upland 1



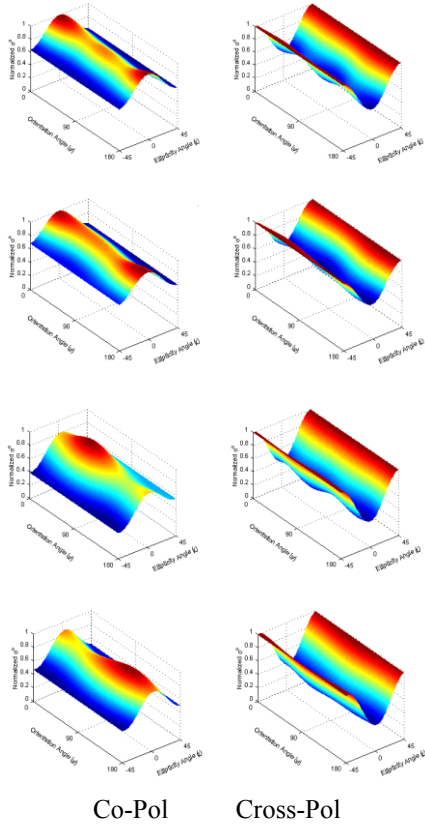
Upland 2



Co-Pol Cross-Pol

Spring/Fall Signatures

(Steep Incident Angle)

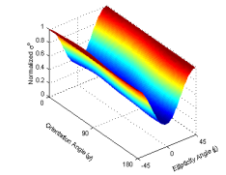
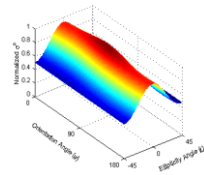
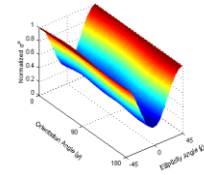
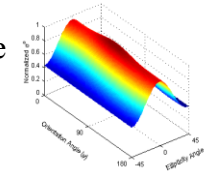


Summer Signatures

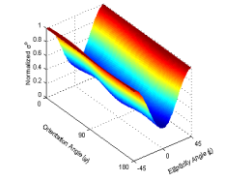
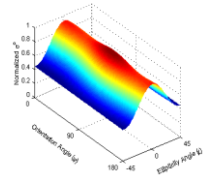
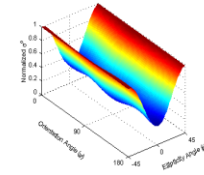
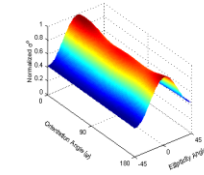
(Steep Incident Angle)

(Shallow Incident Angle)

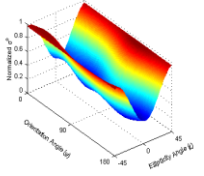
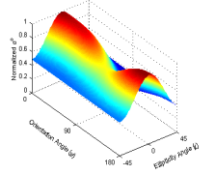
Mer Bleue Bog Upland 1



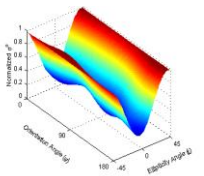
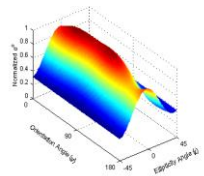
Upland 2



Westport Bog Upland 1



Upland 2



Co-Pol

Cross-Pol

Co-Pol

Cross-Pol

Figure H6. Spring/fall and summer co- and cross-pol signatures for Upland at Loch Garry, Marlborough Forest, Mer Bleue Bog and Westport Bog.

APPENDIX I. Pedestal height analysis for spring and summer radar imagery.

Figure I1-I6. Spring and summer co- and cross-pol pedestal heights and the enhanced (difference, and the cross-pol: co-pol ratio) summer co- and cross-pol pedestal heights.

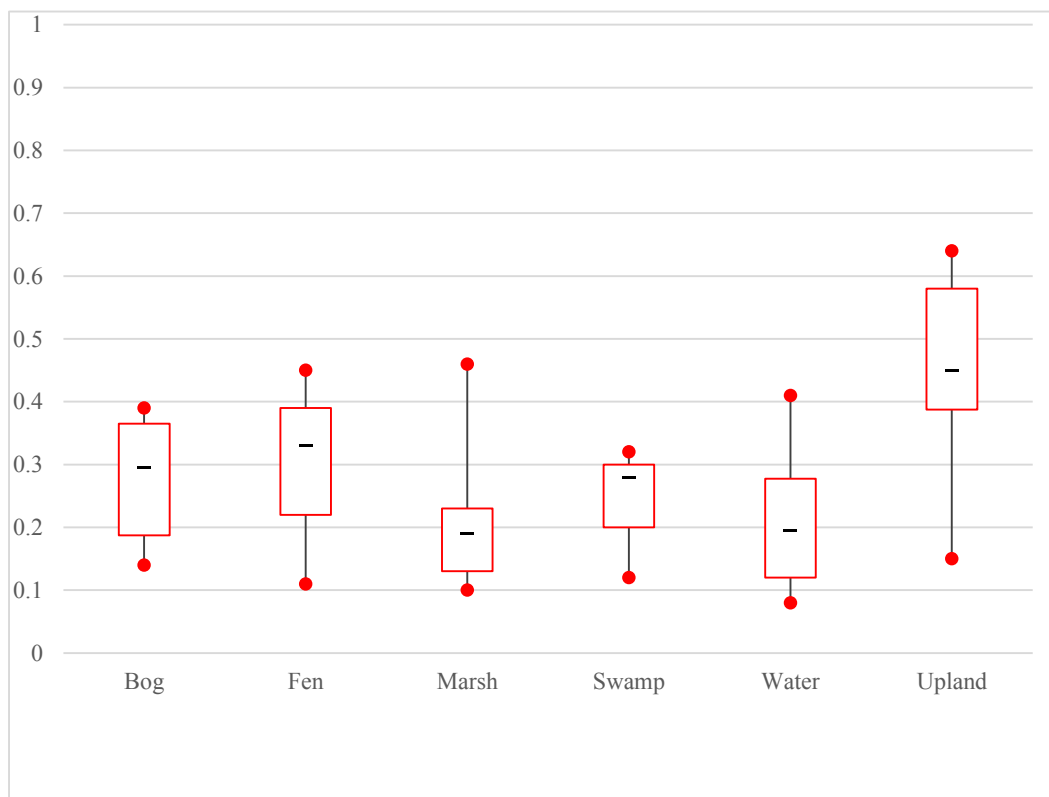


Figure I1. The spring steep incident angle co-pol pedestal minimum, maximum and average heights. Black dashes represent the median. Pedestal height normalized to 1.00 (vertical axis); land cover type (horizontal axis).

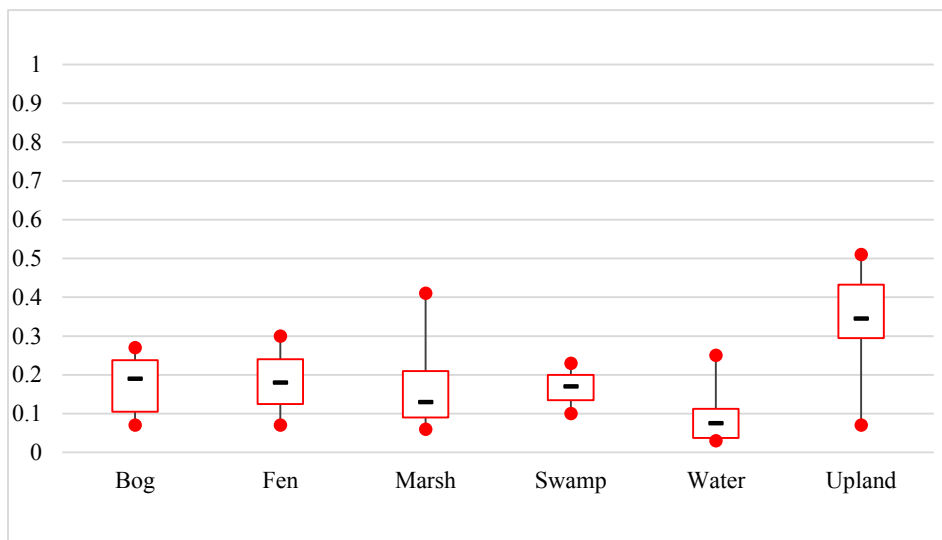


Figure I2. The spring step incident angle cross-pol pedestal minimum, maximum and average heights. Black dashes represent the median. Pedestal height normalized to 1.00 (vertical axis); land cover type (horizontal axis).

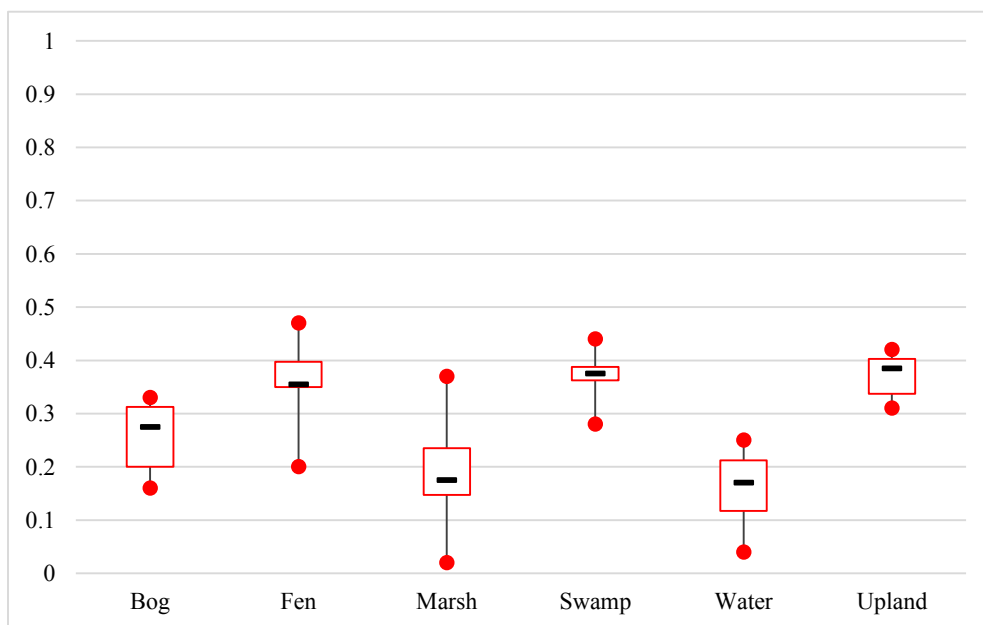


Figure I3. The summer step incident angle co-pol pedestal minimum, maximum and average heights. Black dashes represent the median. Pedestal height normalized to 1.00 (vertical axis); land cover type (horizontal axis).

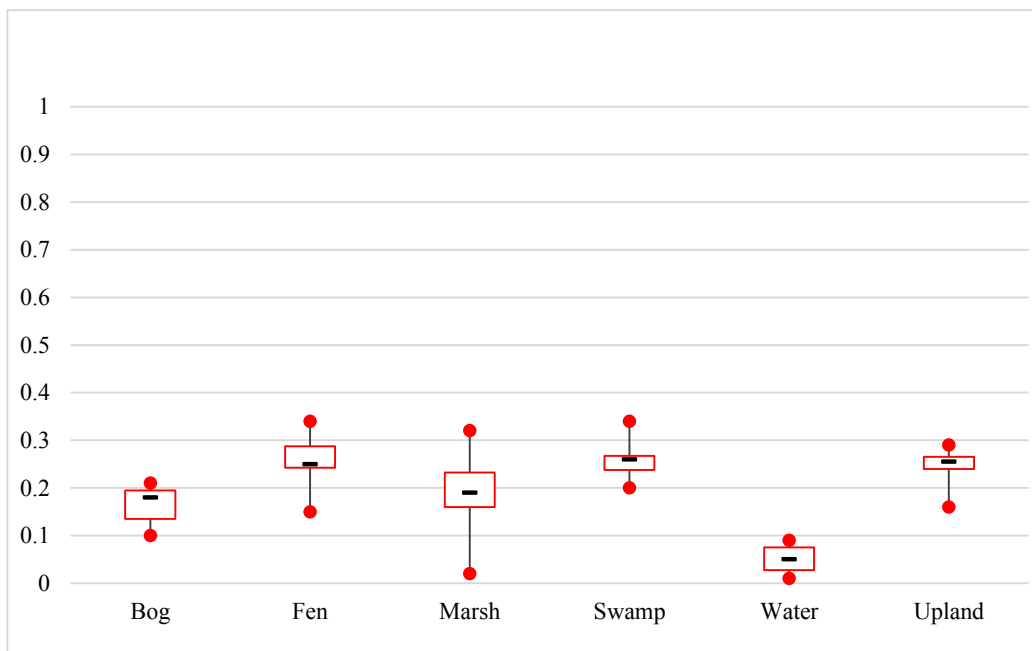


Figure I4. The summer steep incident angle cross-pol pedestal minimum, maximum and average heights. Black dashes represent the median. Pedestal height normalized to 1.00 (vertical axis); land cover type (horizontal axis).

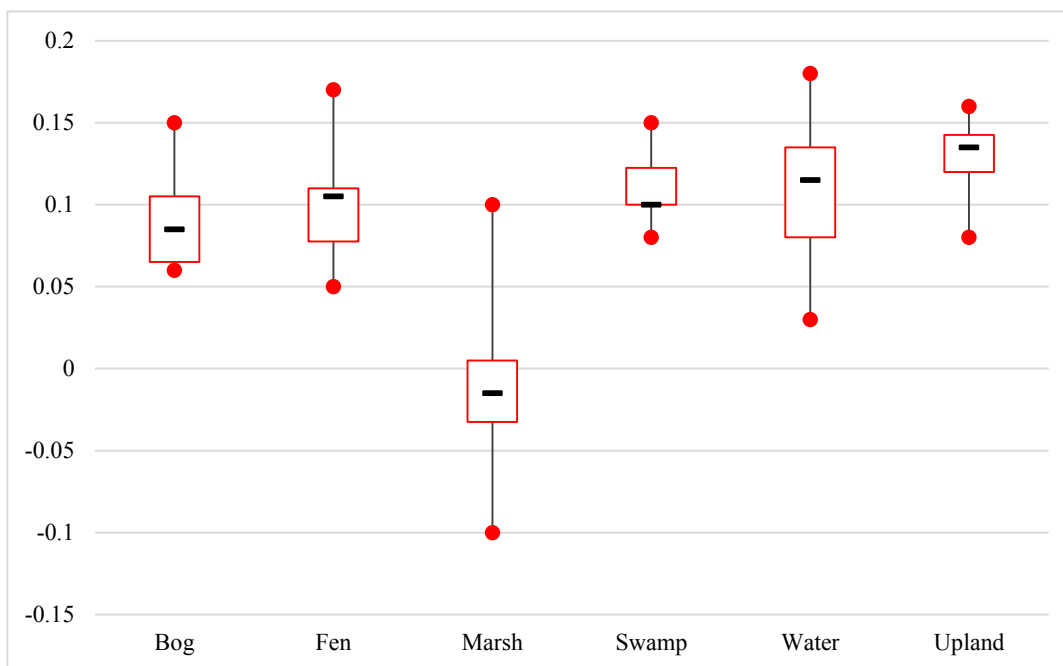


Figure I5. The difference of the summer co- and cross-pol pedestal minimum, maximum and average heights. Black dashes represent the median.

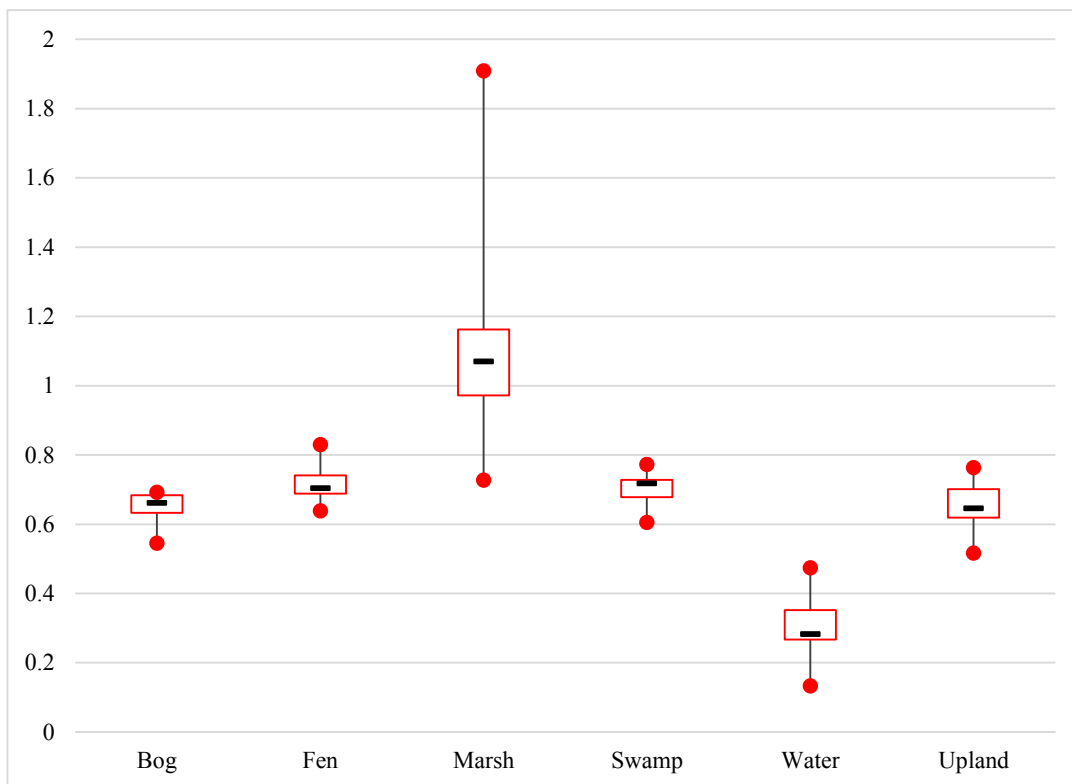


Figure I6. The ratio of the summer co- and cross-pol pedestal minimum, maximum and average heights. Black dashes represent the median.

APPENDIX J. Field-measured VWC% for all four sites and two seasons.

Table J1. (Digitally accompanying this thesis) Field-measured VWC (%) at the four sites for two seasons (spring and summer). This workbook first presents the field measured VWC by Wetland Type (Bog, Fen, Marsh, Swamp) and then by site.

APPENDIX K. GIS analysis for Diversity of the Surrounding Habitat and the Proximity of Other Wetlands attributes for Loch Garry, Mer Bleue Bog and Westport Bog.

Figures K1 – K6. GIS analysis for Diversity of the Surrounding Habitat and the Proximity of Other Wetlands to the wetlands of interest.

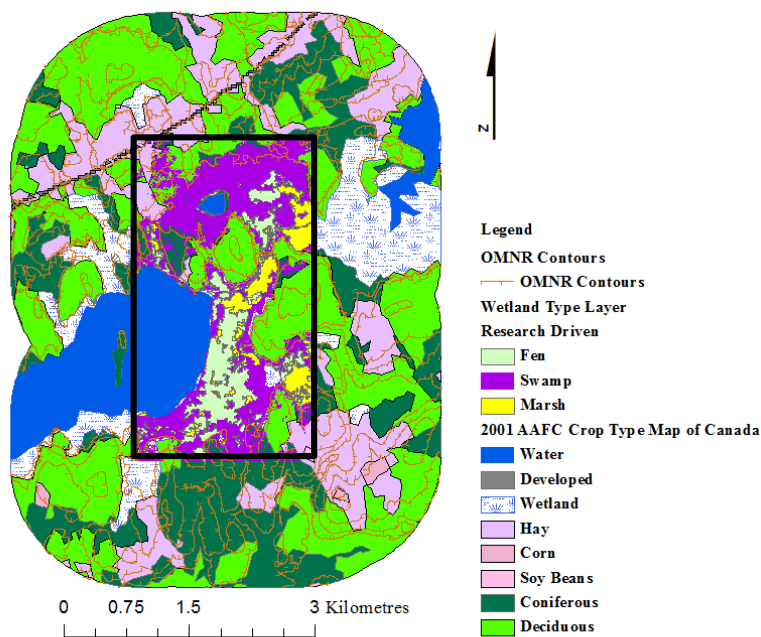


Figure K1. Diversity of the Surrounding Habitat around Loch Garry wetland subset. The data layers include the WorldView-2 image derived Wetland Type layer, the 2011 AAFC Crop Type Map of Canada; the OMNR water bodies layer, and the OMNR contour layer. Black outline is the image-derived subset.

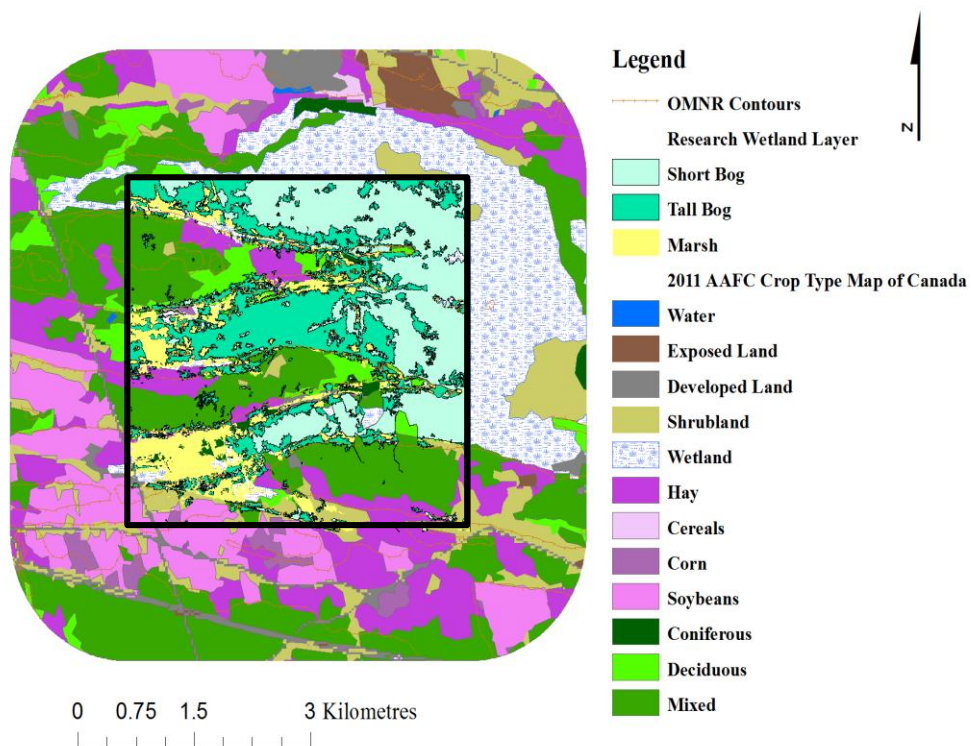


Figure K2. Diversity of the Surrounding Habitat around Mer Bleue Bog wetland subset. The data layers include the WorldView-2 image derived Wetland Type layer, the 2011 AAFC Crop Type Map of Canada; the OMNR water bodies layer, and the OMNR contour layer. Black outline is the image-derived subset.

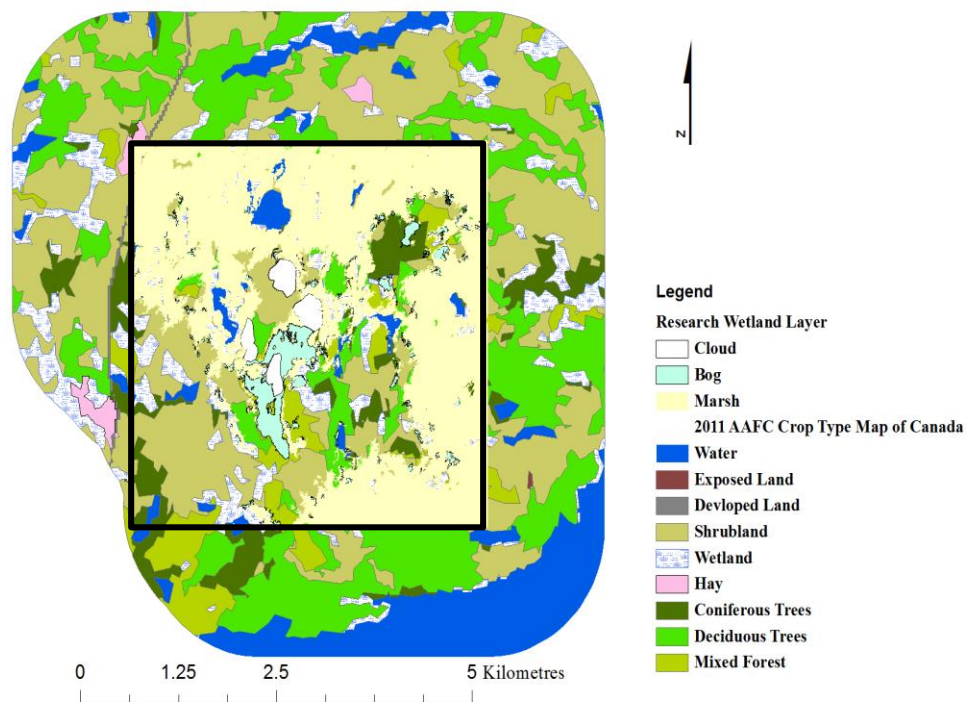


Figure K3. Diversity of the Surrounding Habitat around Westport Bog wetland subset. The data layers include the WorldView-2 image derived Wetland Type layer, the 2011 AAFC Crop Type Map of Canada; the OMNR water bodies layer, and the OMNR contour layer. Black outline is the image-derived subset.

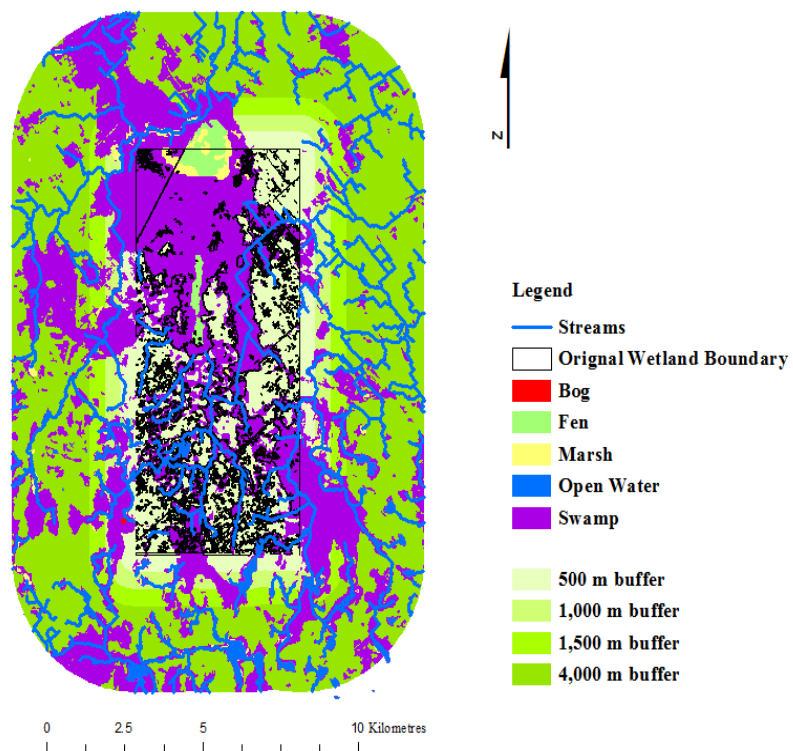


Figure K4. The hydrological Proximity of the Surrounding Wetlands to the Marlborough Forest wetland complex. The data layers include the OMNR wetland type layer, the OHN watercourse layer; the OMNR water bodies layer, and original Marlborough Forest boundary layer.

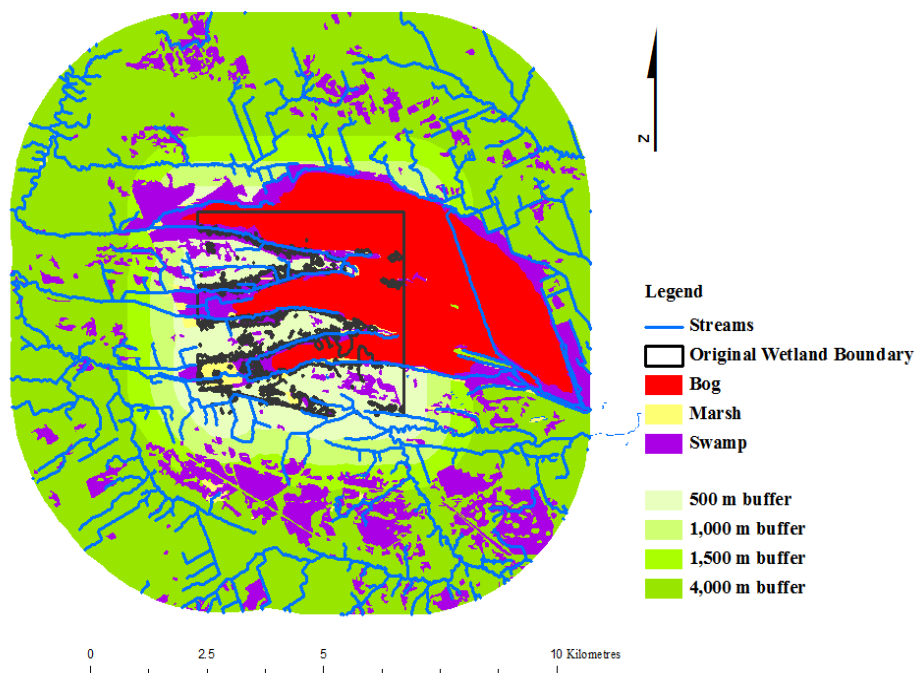


Figure K5. The hydrological Proximity of the Surrounding Wetlands to the Mer Bleue Bog wetland complex. The data layers include the OMNR wetland type layer, the OHN watercourse layer; the OMNR water bodies layer, and original Mer Bleue Bog boundary layer.

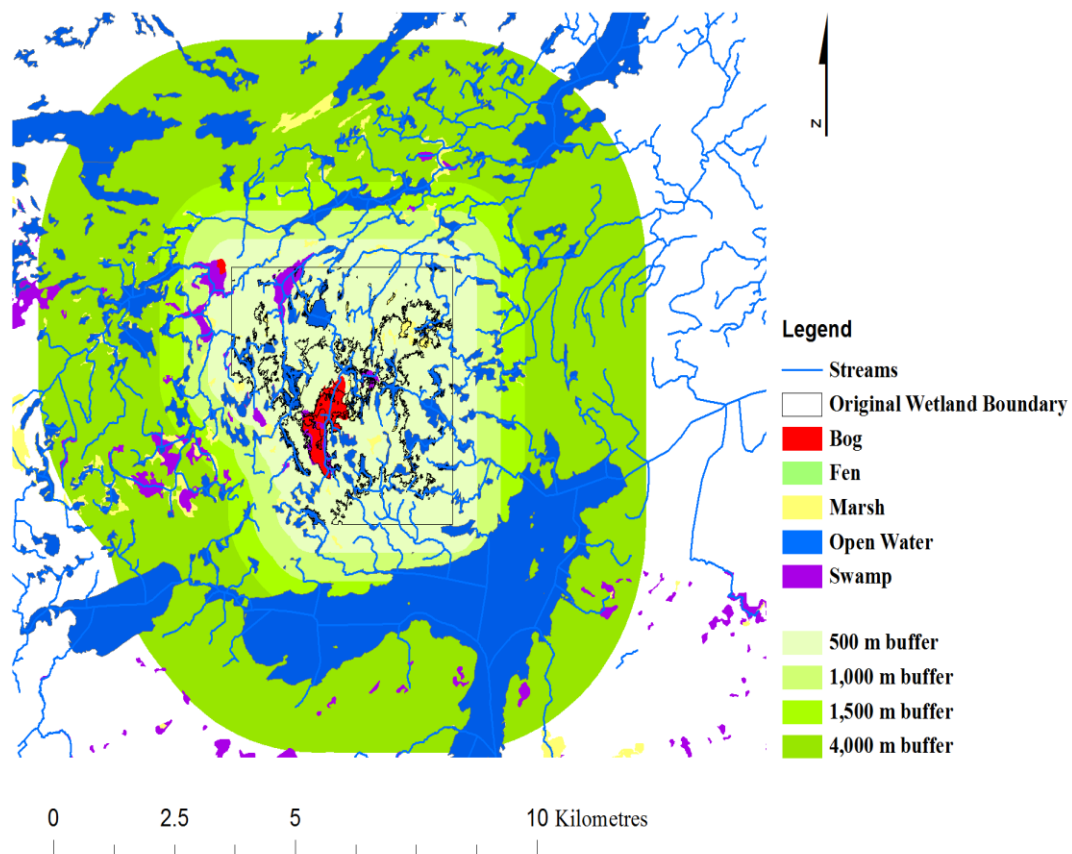


Figure K6. The hydrological proximity of the surrounding wetlands to the Westport Bog wetland complex. The data layers include the OMNR wetland type layer, the OHN watercourse layer; the OMNR water bodies layer, and original Westport Bog boundary layer.

APPENDIX L. Multi-season WorldView-2 CTA results for Number of VCFs, VCFs and Open Water Types for Loch Garry, Marlborough Forest and Westport Bog.

Tables L1 – L3. Multi-season Worldview-2 CTA accuracy results for the Number of VCF for Loch Garry, Marlborough Forest and Westport Bog.

Tables L4 – L6. Multi-season Worldview-2 CTA accuracy results for VCFs for Loch Garry, Marlborough Forest and Westport Bog.

Table L7 – L9. Multi-season Worldview-2 CTA accuracy results for Open Water Types for Loch Garry, Marlborough Forest and Westport Bog.

Table L1. CTA accuracy statistics (%) for the Number of VCFs for seasonal imagery for Loch Garry. Class A, B, and C represent 1 to 3, 4 to 5 forms, and 6 or more forms, respectively (Section 3.2.2).

Season and/or combination of seasons	Overall Accuracy (%)	Kappa	Class A		Class B		Class C		Average	
			PA (%)	UA (%)						
Spring	48.0	0.31	20.0	50.0	63.6	87.5	75.0	50.0	52.9	62.5
Summer	60.0	0.37	50.0	83.3	63.6	53.8	75.0	50.0	62.9	62.4

Table L2. CTA accuracy statistics (%) for the Number of VCFs for seasonal imagery for Marlborough Forest. Class A, B, and C represent 1 to 3, 4 to 5 forms, and 6 or more forms, respectively (Section 3.2.2).

Season and/or combination of seasons	Overall Accuracy (%)	Kappa	Class A		Class B		Class C		Average	
			PA (%)	UA (%)						
Spring	53.1	0.13	54.3	76.0	41.7	27.8	100	33.3	65.3	45.7

Table L3. CTA accuracy statistics (%) for the Number of VCFs for seasonal imagery for Westport Bog. Class A, B, and C represent 1 to 3, 4 to 5 forms, and 6 or more forms, respectively (Section 3.2.2).

Season and/or combination of seasons	Overall Accuracy (%)	Kappa	Class A		Class B		Class C		Average	
			PA (%)	UA (%)						
Spring	70.6	0.46	71.4	78.9	66.7	80.0	100	20.0	79.4	59.6
Summer	58.8	0.37	71.4	93.8	33.3	100.0	100	7.1	68.2	66.7

Table L4. CTA accuracy statistics (%) for the VCFs for the combinations of seasonal WorldView-2 imagery for Loch Garry.

Season	Overall Accuracy (%)	Kappa	C (Coniferous Dominant)		DC (Dead Dominant)		GC (Herb Dominant)		H (Hardwood Dominant)		Other (Emergent/ Shrub Dominant)		Average	
			PA (%)	UA (%)	PA (%)	UA (%)	PA (%)	UA (%)	PA (%)	UA (%)	PA (%)	UA (%)	PA (%)	UA (%)
Spring	68.8	0.60	62.5	55.6	83.3	83.3	80.0	66.7	60.0	85.7	66.7	50.0	70.5	68.3
Summer	28.1	0.18	50.0	33.3	33.3	66.7	0.0	0.0	0.0	0.0	100.0	100.0	36.7	40.0

Table L5. CTA accuracy statistics (%) for the VCFs for the combinations of seasonal WorldView-2 imagery for Marlborough Forest.

Season	Overall Accuracy (%)	Kappa	C (Coniferous Dominant)		DC (Dead Dominant)		GC (Herb Dominant)		H (Hardwood Dominant)		Other (Emergent Dominant)		Other (Shrub Dominant)		Average	
			PA (%)	UA (%)	PA (%)	UA (%)	PA (%)	UA (%)	PA (%)	UA (%)	PA (%)	UA (%)	PA (%)	UA (%)	PA (%)	UA (%)
Spring	44.9	0.32	45.5	41.7	40.0	20.0	33.3	28.6	42.9	75.0	54.5	60.0	50.0	50.0	44.4	45.9

Table L6. CTA accuracy statistics (%) for the VCFs for the combinations of seasonal WorldView-2 imagery for Westport Bog.

Season	Overall Accuracy (%)	Kappa	GC (Herb Dominant)		H (Hardwood Dominant)		NE, RE, BE (Emergent Dominant)		LS or TS (Shrub Dominant)		Ff (Floating Dominant)		Average	
			PA (%)	UA (%)	PA (%)	UA (%)	PA (%)	UA (%)	PA (%)	UA (%)	PA (%)	UA (%)	PA (%)	UA (%)
Spring	55.9	0.43	60.0	27.3	54.5	60.0	44.4	66.7	71.4	83.3	50.0	100.0	56.1	67.5
Summer	67.7	0.58	100.0	62.5	54.5	66.7	44.4	80.0	85.7	60.0	100.0	100.0	76.9	73.8

Table L7. CTA accuracy statistics (%) for the Open Water Types for Loch Garry for seasonal WorldView-2 imagery.

Season	Overall Accuracy (%)	Kappa	Type 1		Type 5		Type 8		Average	
			PA (%)	UA (%)	PA (%)	UA (%)	PA (%)	UA (%)	PA (%)	UA (%)
Spring	73.3	0.59	75.0	100.0	66.7	80.0	100.0	50.0	80.7	76.7
Summer	66.7	0.51	62.5	100.0	66.7	80.0	100.0	33.3	76.4	71.1

Table L8. CTA accuracy statistics (%) for the Open Water Types for Marlborough Forest for seasonal WorldView-2 imagery.

Season	Overall Accuracy (%)	Kappa	Type 1		Type 2		Type 5		Type 7		Type 8		Average	
			PA (%)	UA (%)	PA (%)	UA (%)								
Spring	41.2	0.34	12.5	100	50	50	100	50	100	100	50.0	33.3	62.5	66.7
Summer	40.0	0.26	50.0	33.3	100	33.3	12.5	33.3	50.0	50.0	40.0	66.7	50.5	38.1

Table L9. CTA accuracy statistics (%) for the Open Water Types for Westport Bog for seasonal WorldView-2 imagery.

Season	Overall Accuracy (%)	Kappa	Type 1		Type 2		Combined (4, 6, 7)		Type 8		Average	
			PA (%)	UA (%)	PA (%)	UA (%)	PA (%)	UA (%)	PA (%)	UA (%)	PA (%)	UA (%)
Spring	50.0	0.33	33.3	40.0	60.0	37.5	80.0	66.7	33.3	100.0	51.7	61.1
Summer	50.0	0.37	50.0	60.0	40.0	40.0	80.0	100	33.3	100.0	50.8	75.0

APPENDIX M. Relative calibration data for temporal analysis of Landsat 5 TM vegetation fraction images.

Tables M1 – M4. Lists of locations of PIFs at each of the four sites.

Tables M5 – M6. At-sensor reflectance and Top of Atmosphere reflectance variables for calibration.

Figure M1 – M4. Relative calibration graphs for the four sites using the values for the PIFs obtained at the locations in Table N1 – N4.

Table M1. List of the location and type of PIFs at Loch Garry.

ID	Eastings	Northings	Landcover	Type
1	523438.654	5012094.974	Lake	Dark
2	523714.048	5010865.398	Lake	
3	523376.593	5011245.519	Lake	
4	524167.866	5013250.853	Lake	
5	524136.835	5012157.035	Lake	
6	523388.229	5013774.489	Road	Bright
7	523469.684	5013541.762	Road	
8	523466.775	5013512.671	Road	
9	524879.753	5012640.533	Bridge	
10	523954.532	5012579.822	Driveway	

Table M2. List of the location and type of PIFs at Marlborough Forest.

ID	Eastings	Northings	Landcover	Type
1	434249.698	4992931.604	Lake	Dark
2	434094.034	4991763.287	Lake	
3	434189.560	4992899.672	Lake	
4	436503.417	4996043.778	Lake	
5	434162.102	4993049.099	Lake	
6	432359.899	4988849.562	Road	Bright
7	432868.547	4989238.067	Road	
8	433354.178	4989628.779	Road	
9	434369.587	4990438.163	Road	
10	436405.182	4998480.990	Road	

Table M3. List of the location and type of PIFs at Mer Bleue Bog.

ID	Eastings	Northings	Landcover	Type
1	457605.421	5027559.275	Water	Dark
2	456860.354	5027506.475	Water	
3	459390.382	5028345.510	Water	
4	459959.557	5026683.809	Water	
5	463680.306	5026168.991	Water	
6	460601.516	5030231.224	Bare	Bright
7	456515.732	5026962.431	Bare	
8	455298.710	5026156.919	Bare	
9	459089.431	5031028.504	Road	
10	455942.004	5030911.681	Roof	

Table M4. List of the location and type of PIFs at Westport Bog.

ID	Eastings	Northings	Landcover	Type
1	392616.562	4952195.625	Lake	Dark
2	393480.449	4952420.267	Lake	
3	391982.082	4951981.226	Lake	
4	391981.519	4950873.493	Lake	
5	390216.913	4950094.477	Lake	
6	390341.870	4952766.997	Lake	
7	390631.187	4949846.813	Lake	
8	390328.361	4953050.685	Lake	
9	390058.183	4952906.589	Bright	Bright
10	390209.595	4950330.321	Bright	
11	390238.302	4951470.138	Bright	
12	389274.664	4953567.402	Road	
13	389457.034	4954258.610	Road	
14	392242.129	4954316.023	Road	

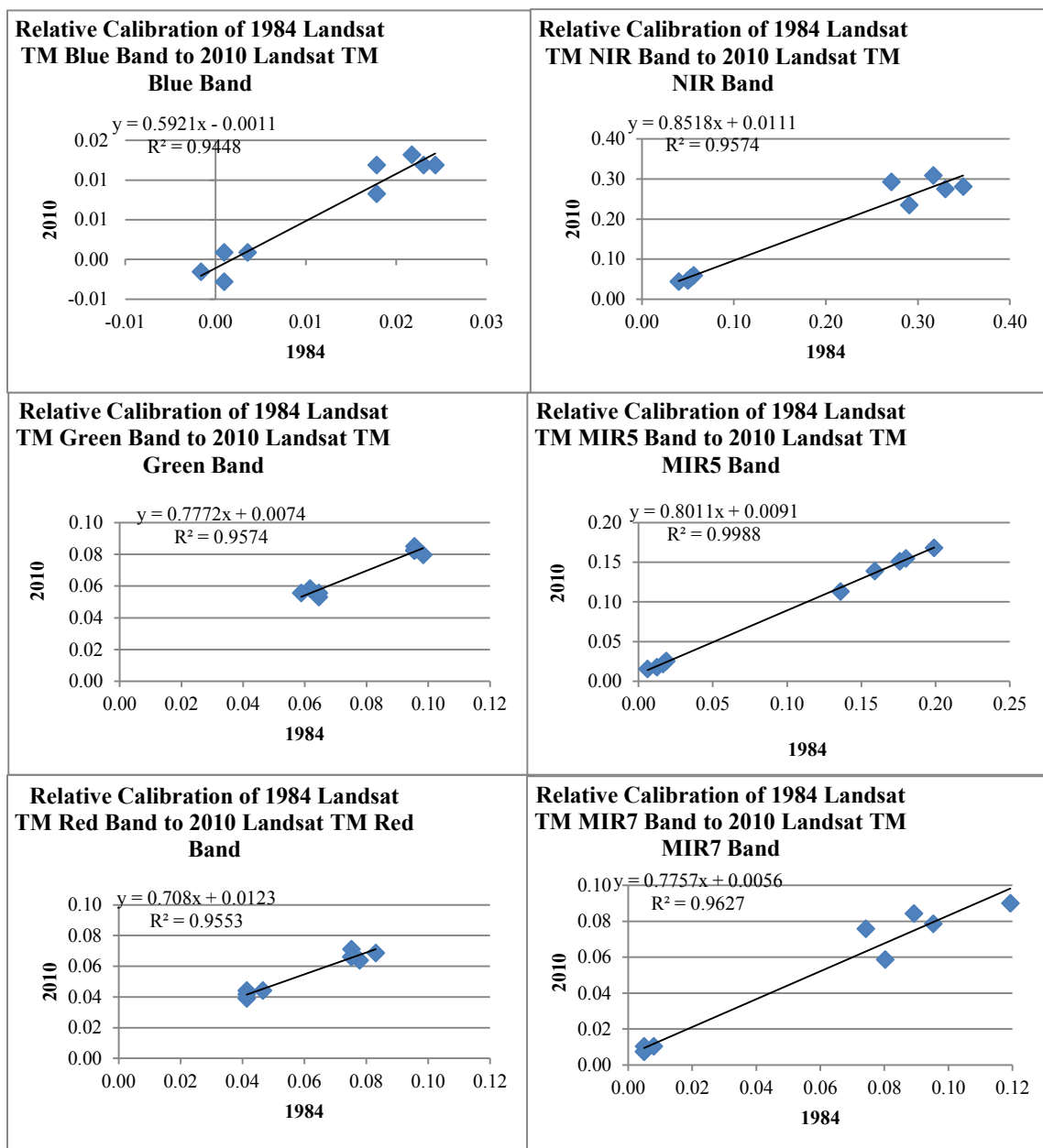


Figure M1. Relative calibration graphs for Loch Garry using the values for the PIFs obtained at the locations in Table M1.

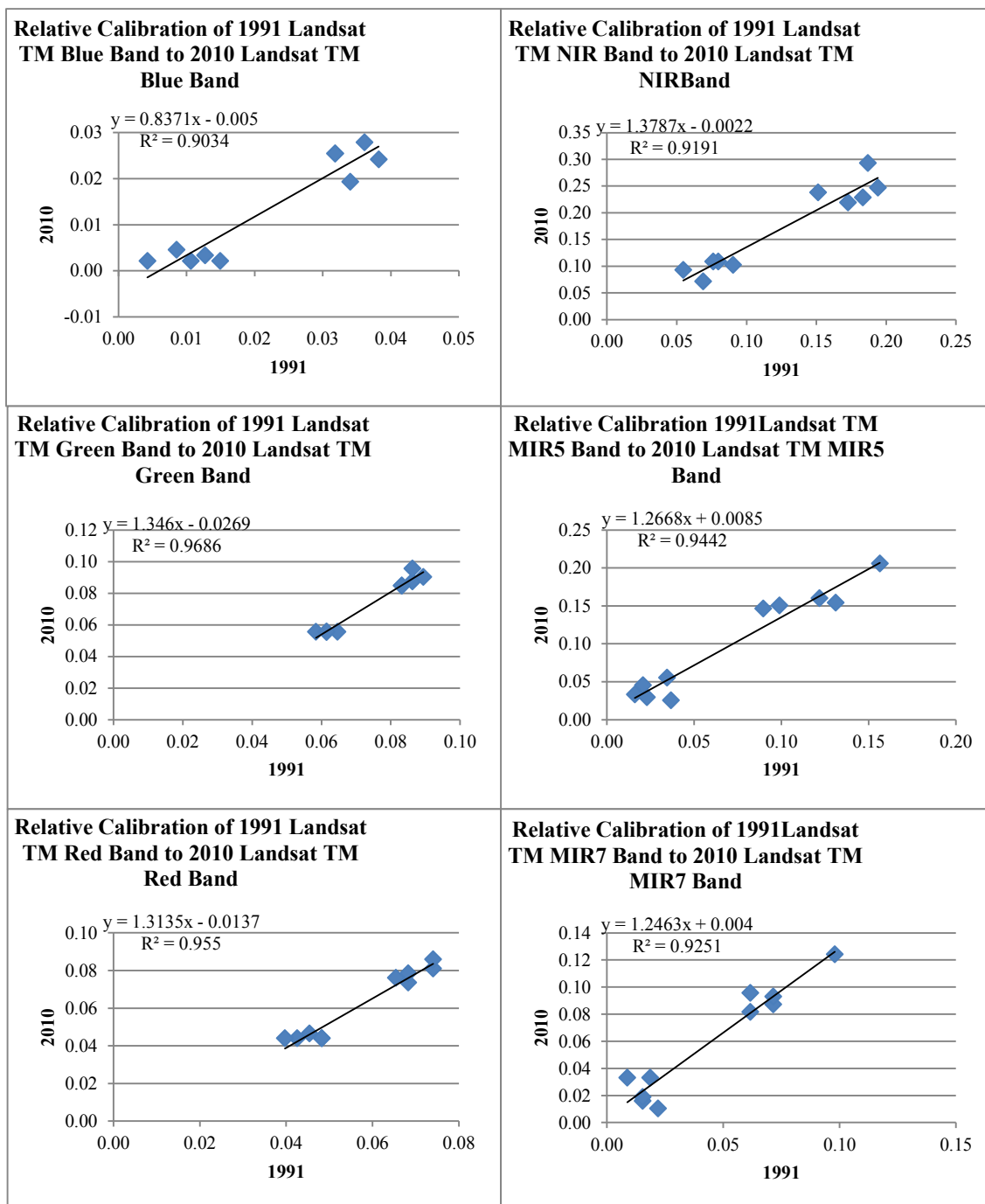


Figure M2. Relative calibration graphs for Marlborough Forest using the values for the PIFs obtained at the locations in Table M2.

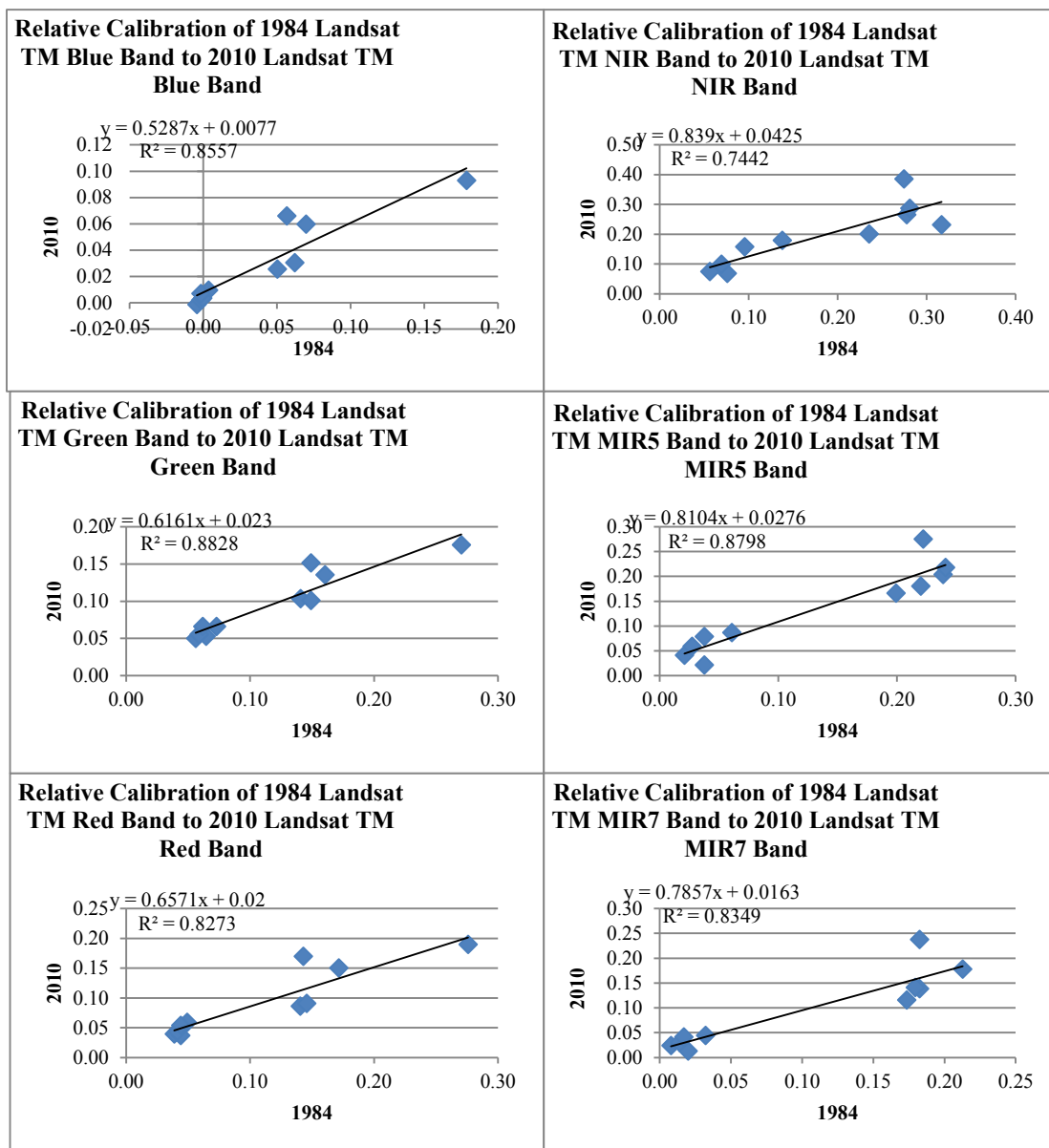


Figure M3. Relative calibration graphs for Mer Bleue Bog using the values for the PIFs obtained at the locations in Table M3.

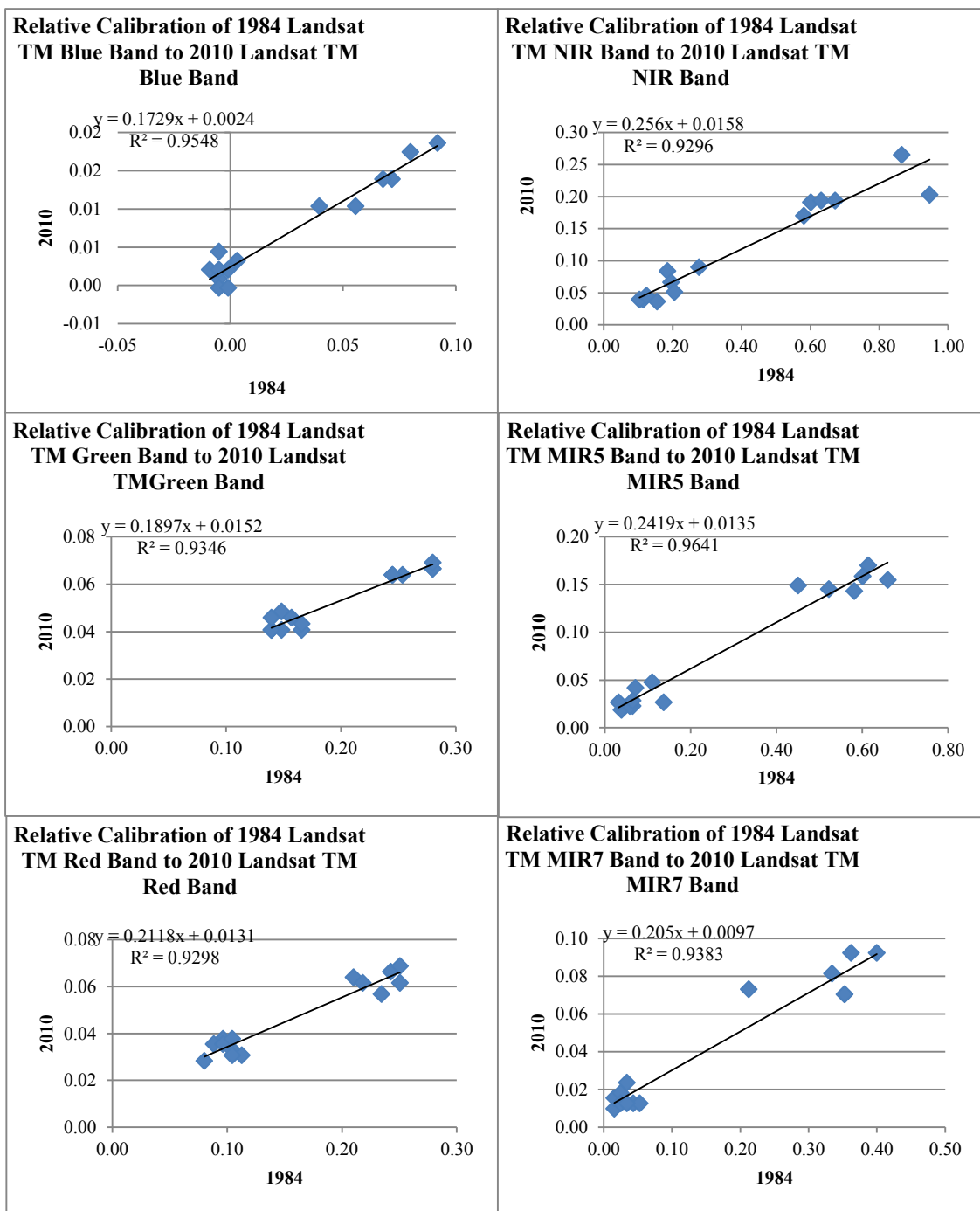


Figure M4. Relative calibration graphs for Westport Bog using the values for the PIFs obtained at the locations in Table M4.

Conversion to at-sensor spectral radiance:

$$L_{\lambda} = G_{rescale} * Q_{cal} * B_{rescale}$$

Where:

$$G_{rescale} = \frac{LMAX_{\lambda} - LMIN_{\lambda}}{Q_{calmax} - Q_{calmin}}$$

$$B_{rescale} = LMIN_{\lambda} - \left(\frac{LMAX_{\lambda} - LMIN_{\lambda}}{Q_{calmax} - Q_{calmin}} \right) Q_{calmin}$$

where

L_{λ} = Spectral radiance at the sensor's aperture, W/m² sr μ m

Q_{cal} = Quantized calibrated pixel value, DN

Q_{calmin} = Minimum quantized calibrated pixel value corresponding to $LMIN_{\lambda}$, DN

Q_{calmax} = Maximum quantized calibrated pixel value corresponding to $LMAX_{\lambda}$, DN

$LMIN_{\lambda}$ = Spectral at-sensor radiance that is scaled to Q_{calmin} , W/m² sr μ m

$LMAX_{\lambda}$ = Spectral at-sensor radiance that is scaled to Q_{calmax} , W/m² sr μ m

$G_{rescale}$ = Band-specific rescaling gain factor, (W/m² sr μ m)/DN

$B_{rescale}$ = Band-specific rescaling bias factor, W/m² sr μ m

Conversion to TOA reflectance:

$$\rho_{\lambda} = \frac{\pi * L_{\lambda} * d^2}{ESUN_{\lambda} * \cos \theta_s}$$

ρ_{λ} = Planetary TOA reflectance

π = ~3.14159

L_{λ} = Spectral radiance at the sensor's aperture W/m² sr μ m

d = Earth-Sun distance astronomical units

$ESUN_{\lambda}$ = Mean exoatmospheric solar irradiance W/m² μ m

θ_s = Solar zenith angle, °

Table M5. Given calibration variables for at-sensor radiance, and Top of Atmosphere (TOA) reflectance corrections (after Chandler *et al.*, 2009)

Landsat TM Band	G _{rescale}	B _{rescale}	ESUN
Blue	0.671339	-2.19	1983
Green	1.322205	-4.16	1796
Red	1.043974	-2.21	1536
NIR	0.876024	-2.39	1031
MIR5	0.120354	-0.49	220
MIR7	0.065551	-0.22	83.44

Table M6: Image specific variables for conversion to TOA reflectance

Image Acquisition Date	Sun Elevation ^o	SIN (Sun Elevation)	Day of Year	d (earth-sun distance)	d ²
Aug 18, 1984	50.59088714	0.77263261	231	1.10205	1.214514
July 10, 1984	57.91035315	0.84721793	192	1.01661	1.033496
Aug 22, 1991	49.04039541	0.75517194	234	1.01145	1.023031
Sept 11, 2010	45.9942987	0.71927067	254	1.00672	1.013485
July 2, 2010	61.80033	0.88130618	183	1.01668	1.033638